

Agents: Boston Electronics, (800)347-5445, TCSPC@boselec.com

**Wolfgang
Becker**



The bh

TCSPC Handbook

Becker & Hickl GmbH



Agents: Boston Electronics, (800)347-5445, TCSPC@boselec.com

Dr. Wolfgang Becker
Tel. +49 / 30 / 787 56 32
FAX +49 / 30 / 787 57 34
<http://www.becker-hickl.com>
email: becker@becker-hickl.com

Becker & Hickl GmbH
Nahmitzer Damm 30
12277 Berlin
Germany
Tel. +49 / 30 / 787 56 32
FAX +49 / 30 / 787 57 34
<http://www.becker-hickl.com>
email: info@becker-hickl.com

2nd Edition, September 2006

This handbook is subject to copyright. However, reproduction of small portions of the material in scientific papers or other non-commercial publications is considered fair use under the copyright law. It is requested that a complete citation be included in the publication. If you require confirmation please feel free to contact Becker & Hickl GmbH.

Preface

Time-correlated single photon counting (TCSPC) is an amazingly sensitive technique for recording low-level light signals with picosecond resolution and extremely high precision. TCSPC originates from the measurement of excited nuclear states and has been used since the late 60s [242, 379]. For many years TCSPC was used primarily to record fluorescence decay curves of organic dyes in solution. Due to the low intensity and low repetition rate of the light sources and the limited speed of the electronics of the 70s and 80s the acquisition times were extremely long. More important, classic TCSPC was intrinsically one-dimensional, i.e. limited to the recording of the waveform of a periodic light signal.

Light sources ceased to be a limitation when the first mode-locked Argon lasers and synchronously pumped dye lasers were introduced. For the recording electronics, the situation changed with the introduction of the SPC-300 modules of Becker & Hickl in 1993. Due to a new analog-to-digital conversion principle these modules could be used at photon count rates almost 100 times higher than the classic TCSPC devices. Moreover, the modules were able to record the photons of a large number of detectors simultaneously. They were thus able to record a photon distribution not only versus the time in a fluorescence decay but also versus a spatial coordinate or the wavelength of the photons. Multi-dimensional TCSPC was born.

Within a few years, more dimensions were added to multidimensional TCSPC. Fast sequential recording was introduced with the SPC-430 in 1995, fast scanning with the SPC-535 in 1997. Time-tag recording was introduced with the SPC-431 in 1996; multi-module TCSPC systems followed in 1999. Since then, the Becker & Hickl TCSPC systems became bigger, faster and more flexible. Recent TCSPC modules, like the SPC-830, can be configured for sequential recording, imaging, or time-tag recording by a simple software command. Multi-module systems, like the SPC-144, can be used for scanning at unprecedented count rates and acquisition speeds.

Nevertheless, TCSPC still has the reputation to be an extremely sluggish technique unable to record any fast changes in the fluorescence or scattering behaviour of a sample. The multi-dimensional features of modern TCSPC are not commonly understood. Thus, many users do not make efficient use of their SPC modules. However, if appropriately used, multi-dimensional TCSPC techniques not only deliver superior results but also solve highly sophisticated measurement problems.

This handbook is an attempt to help existing and potential users understand and make use of the advanced features of modern TCSPC.

After a short introduction into the bh TCSPC devices and associated detector and control modules the principles of advanced TCSPC techniques are described. Based on a short review of classic TCSPC, multi-dimensional TCSPC techniques are explained. These include multi-detector TCSPC, multiplexed TCSPC, sequential recording techniques, scanning techniques, time-tag recording, and multi-module TCSPC techniques. The next chapter describes the architecture of the bh SPC modules. A chapter about detectors gives a review of detector principles and the parameters used to characterise detectors. It describes a number of detectors commonly used for TCSPC and gives advice about getting best performance from them.

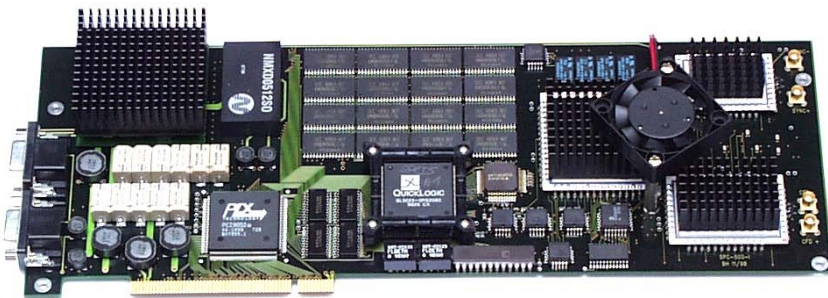
The use of bh SPC devices is described in the next part of the handbook. It includes the installation, wiring diagrams for a number of typical experiments, guidelines for first system setup, and for system optimisation. It describes dead-time, counting loss, and pile-up effects, detector effects, and effects related to the optical system.

A large part of the handbook is dedicated to TCSPC applications. It includes classic applications like measurements of fluorescence and anisotropy decay curves, the application to trans-

sient fluorescence lifetime phenomena, time-resolved laser scanning microscopy, measurement of local environment parameters in tissue, autofluorescence of tissue, and FRET imaging in cells. A chapter about diffuse optical tomography includes breast imaging, static and dynamic brain imaging, and other DOT applications. Picosecond photon correlation, fluorescence correlation spectroscopy, burst-integrated fluorescence lifetime techniques, and photon counting histogram techniques are reviewed in the next sections. The last part of the application section gives an review of other applications like positron lifetime measurement, measurement of barrier discharges, remotes sensing, and metrological applications. The application section includes practical hints about optical systems, detectors, and other technical aspects of the spectroscopy techniques described.

A large chapter describes the operating software of the bh SPC modules. It describes the various operation modes, the system and control parameters, the handling and display of the multidimensional data recorded by the modules, and the associated data file structure.

The handbook ends with a list of more than 350 references of publications related to TCSPC, in particular to applications of the bh SPC devices.



Contents

Introduction	1
General Features of the bh TCSPC Devices	1
Measurement Modes.....	2
SPC Module Types.....	3
Other Photon Counters	9
Light Sources, Detectors and Detector Electronics.....	9
Classic Time-Correlated Single Photon Counting	15
Single-Photon Detection.....	15
Time-Correlated Single Photon Counting.....	15
The Classic TCSPC Architecture	19
Multi-Dimensional TCSPC	23
Multi-Detector TCSPC	24
Multiplexed TCSPC	27
Sequential Recording.....	28
TCSPC Scanning Techniques.....	30
Time-Tag Recording.....	31
Multi-Module TCSPC Systems	33
Architecture of the bh TCSPC Modules.....	35
General Principle	35
CFD and SYNC circuits.....	35
TAC	36
ADC	36
Channel Register	37
Sequencer.....	37
Memory Control.....	37
Recording of single curves	38
Multi-Detector Operation	38
Multiplexed TCSPC	39
Sequential Recording	39
Continuous Flow Mode	40
Scan Modes	40
CNT and ADD Control	41
Time-Tag (FIFO) Mode	41
Detailed Description of Building Blocks.....	42
CFD in the Detector (Start) Channel.....	42
SPC-x00 Versions	42
SPC-x30 Versions	43
CFD in the Synchronisation (Stop) Channel	44
SPC-x00 Versions	44
SPC-x30 Versions	45
Time-to-Amplitude Converter.....	46
Analog-to-Digital Conversion.....	48
ADC Error Correction.....	48
Variable ADC Resolution.....	49
ADC Zoom.....	50
Detectors for TCSPC.....	51
Detector Principles	51
Detector Parameters.....	54
Gain.....	54
Single Electron Response.....	54
Pulse Height Distribution	55
Signal Transit Time.....	56
Transit Time Spread and Timing Jitter	57
Cathode Efficiency.....	58
Dark Count Rate.....	59
Afterpulsing	60
Pre-Pulses.....	61
Description of Selected Detectors.....	63
MCP PMTs	63

Hamamatsu R5600 and R7400 Miniature PMTs	64
H5783 and H5773 Photosensor Modules.....	65
PMH-100 and PMC-100	66
Hamamatsu H7422 and H8632	67
Hamamatsu H7421.....	68
PML-16 Multichannel Detector Head.....	68
Conventional PMTs	68
Single-Photon Avalanche Photodiodes	69
Preamplifiers and Detector Control.....	73
Preamplifiers.....	73
The DCC-100 detector controller	74
Safety Recommendations for Using Detectors	76
Installation of the bh TCSPC Modules.....	79
General Requirements.....	79
Software Installation	79
First Installation	80
Installing the DLL and Lab View Libraries	81
Software Update.....	81
Update from the Web.....	82
Installing New Software Components.....	82
Software Repair.....	83
Removing the TCSPC Package.....	83
Hardware Installation - Single SPC Modules	83
Driver Installation	83
Hardware Installation - Several SPC Modules.....	84
Software Start	84
Module Test Program	85
Installation Problems	86
Starting the SPC Software without an SPC Module	86
Operating the SPC Module.....	89
Detector and Reference Inputs.....	89
Generating the Reference Signal.....	89
Delayed Stop Operation.....	91
Synchronisation to Random Signals	92
Connecting the Detectors.....	93
Single-Detector Systems	93
Multi-Detector Systems.....	95
Using the Experiment Trigger	98
TCSPC Scanning Techniques	99
f(xyt) mode.....	99
Scan Sync In Mode	99
Scan Sync Out Mode.....	100
Scan XY Out Mode.....	101
FLIM Systems for Laser Scanning Microscopes	101
Single-Module TCSPC systems	102
Multi-Module (Parallel Detection) Systems.....	104
Connecting Detectors and Shutters of FLIM Systems.....	105
First Light: Getting Started	108
Recommended System Parameters.....	108
Setup of Standard Fluorescence Lifetime Systems.....	109
Setup of Scanning Systems	111
Multi-Detector Systems.....	115
Setup Procedure for Other TCSPC Applications	116
Optimising a TCSPC System	117
General Recommendations	117
Configuring the CFD and SYNC Inputs	118
Pulse Shaping.....	118
Configuration for Positive Input (SPC-x00 only).....	119
Optimising the CFD Parameters	120
Adjusting the CFD Threshold	120
CFD Zero Cross Level	122

Optimising the SYNC Parameters	123
Adjusting the SYNC and CFD Cable Length	124
Adjusting the TAC Parameters	126
TAC Linearity.....	128
Dead Time	129
Counting Loss.....	131
Dead-Time Compensation	132
Pile-Up Effects	133
Classic Pile-Up.....	133
Inter-Pulse Pile-Up.....	134
Fighting Pile-Up Effects	135
Low Repetition Rate Measurements	135
High Repetition Rate Signals	136
Optimising the Photomultiplier.....	138
Voltage Divider.....	138
Illuminated Area	138
Signal-Dependent Background	139
Dark Count Rate.....	140
Checking the SER of PMTs	140
Quick Test of a PMT.....	141
Optical System.....	142
Lenses	142
Absorptive Colour Filters.....	142
Interference Filters	142
Monochromators and Polychromators	143
Optical Fibres.....	143
Baffles and Aperture Stops	143
Avoiding Optical Reflections.....	144
Fluorescence Depolarisation	144
Re-Absorption.....	145
TCSPC Applications	147
Measurement of Luminescence Decay Curves	147
Monochromator-Based Systems.....	147
Time-Resolved Spectra	149
Filter-Based Systems.....	150
Multi-Spectral Lifetime Experiments	152
Measurement of Time-Resolved Fluorescence Anisotropy.....	154
Lock-in TCSPC.....	157
Transient Fluorescence Phenomena.....	158
Chlorophyll Transients.....	158
Stopped Flow Techniques.....	161
Continuous Flow Mixing Techniques	161
Simultaneous Measurement of Fluorescence and Phosphorescence Decay	162
Time-Resolved Laser Scanning Microscopy	164
Implementing TCSPC in Laser Scanning Microscopes	165
The TCSPC Laser Scanning Microscope	165
TCSPC in Descanned (Confocal) Detection Systems.....	167
TCSPC in Non-Descanned (Direct) Detection Systems	168
Multi-Wavelength FLIM	169
Multi-Module FLIM Systems.....	171
Acquisition Time of TCSPC FLIM	172
Multi-Exponential Decay Functions	175
IRF Recording	176
Biological FLIM Applications	177
Measurement of Local Environment Parameters.....	177
Fluorescence Resonance Energy Transfer (FRET).....	178
Autofluorescence Microscopy of Tissue	183
Internalisation and Conversion of Photosensitisers for Photodynamic Therapy.....	185
Time-Resolved Optical Near-Field Microscopy (SNOM).....	186
Diffuse Optical Tomography	187
Scanning Mammography	190

Static Brain Imaging	192
Dynamic Brain Imaging	193
Other DOT Experiments	195
Muscle and Bone Studies	195
Exogenous Absorbers	195
Fluorescence in DOT	196
Small-Animal Imaging	196
Technical Aspects of DOT	197
Optical Fibres	197
Detectors	197
Autofluorescence of Tissue	199
Single-Point Multi-Wavelength Measurement	199
Autofluorescence Lifetime Imaging	199
Ophthalmic Imaging	200
Picosecond Photon Correlation	203
Antibunching	204
Technical Aspects	205
Fluorescence Correlation Spectroscopy	206
Principle	206
FCS in Live Cells	209
Scanning FCS	209
Correlation of Delayed Detector Signals	210
Fluorescence Correlation down to Picoseconds	211
Practical Tips	212
Time-Resolved Single-Molecule Spectroscopy	219
Burst-Integrated Fluorescence Lifetime (BIFL) Techniques	219
Correlation of Lifetime Fluctuations	221
Identification of Single Molecules	222
Photon Counting Histograms	222
Two-Photon Excitation by Picosecond Diode Lasers	225
Barrier Discharges	226
Positron Lifetime Measurements	227
Ranging Systems	228
Remote Sensing	228
Measurement of Absolute Detector Quantum Efficiency	230
Optical Oscilloscope	230
SPCM Software	233
Configuration of the SPC Main Panel	233
System Parameter Settings	237
Status Information	238
Main	241
Load Panel	241
Save Panel	243
Predefined Setups	245
Multi-File View	246
Convert	247
Converting .sdt Files	247
Converting FIFO Files	248
Send Data to SPCImage	250
Print	250
Sleep policy	250
System Parameters	253
Operation Modes	253
‘Single’ Mode	254
Oscilloscope Mode	255
f(txY) Mode	256
f(t,T) Mode	258
f(t,EXT) Mode	260
fi(T) Mode	262
fi(EXT) Mode	264
Continuous Flow Mode	266

Scan Sync Out Mode.....	270
Sequential Recording in the Scan Sync Out mode	272
Scan Sync In Mode	273
Scan Sync In, Continuous Flow Imaging	277
Scan XY Out Mode (SPC-700/730 only).....	278
Scan Mode Display	279
FIFO Mode	281
FIFO Imaging Mode	285
Control Parameters (Photon Distribution Modes)	288
Stop Condition and Overflow Handling.....	288
Steps.....	289
Cycles and Autosave	289
Accumulate	289
Repeat	289
Trigger	289
Display after each step and each cycle	290
Add / Sub Signal	290
Stepping Device	290
Timing Control Parameters.....	290
Collection Time	290
Repeat Time.....	291
Display Time.....	291
Dead Time Compensation.....	292
CFD Parameters.....	292
SYNC Parameters.....	292
TAC Parameters	293
Data Format	294
Page Control	298
More Parameters.....	299
Parameter Management for Multi-Module SPC systems	299
Display Parameters.....	301
General Display Parameters.....	301
2D Display Parameters	302
3D Display Parameters	302
Displaying Subsets of Multidimensional Data.....	304
Display Parameters for Different Display Windows.....	306
2D Trace Parameters	307
Trace Parameters for 2D Curve Mode.....	307
Trace Parameters for 2D Block Mode	309
Block Info.....	310
Export of Trace Data	310
3D Trace Parameters	311
Window Intervals	313
Time Windows	313
Routing X and Y Windows.....	315
Scan X and Y Windows.....	318
Auto Set Functions	319
Adjust Parameters	321
Production Data.....	321
Adjust Values	321
Display Routines	323
2D Display.....	323
Cursors	323
2D Data Processing.....	324
3D Display	325
Display of Multi-Dimensional Data	325
Cursor and Zoom Functions.....	326
3D Data Processing.....	328
Starting and Stopping a Measurement.....	329
Start	329
Interrupt	329

Stop.....	329
Exit	330
Data file structure	331
Data of the Photon Distribution Modes	331
File Header.....	331
File Information	332
Setup	332
Measurement Description Blocks	333
Data Blocks.....	333
FIFO Files.....	335
Setup Files.....	335
FIFO Data Files (SPC-600/630, 4096 Channel Mode)	335
FIFO Data Files (SPC-600/630 256 Channel Mode)	336
FIFO Data Files (SPC-134, SPC-144, SPC-154, SPC-830).....	337
Trouble Shooting.....	339
How to Avoid Damage	339
Testing the Module by the SPC Test Program.....	340
Test for General Function and for Differential Nonlinearity	340
Test for Time Resolution.....	341
Frequently Encountered Problems.....	341
Assistance through bh.....	347
Routing and Control Signals	348
SPC-600/630	348
SPC-700/730 and SPC-830	349
SPC-134.....	352
SPC-144.....	353
Specifications	355
SPC-600/630	355
SPC-700/730	356
SPC-830.....	357
SPC-130/134	358
SPC-140/144	359
SPC-150/154	360
Absolute Maximum Ratings (for all SPC modules).....	361
References	362
Index.....	377

Introduction

This handbook applies to the Becker & Hickl SPC-130/134, SPC-140/144, SPC-600, SPC-630, SPC-700, SPC-730 and SPC-830 time-correlated single photon counting modules operated by the ‘Multi SPC’ software version 8.43 of the ‘TCSPC Package’ 2.3 or later.

The Multi-SPC Software does not work with the older SPC-3xx, -4xx and -5xx modules. If you have one of these modules please use the SPC Standard Software and the corresponding manual.

General Features of the bh TCSPC Devices

The SPC-130/134, SPC-140/144, SPC-150/154, SPC-600/630, SPC-700/730 and SPC-830 modules contain complete electronic systems for recording fast light signals by time-correlated single photon counting (TCSPC) on single PC boards. The Constant Fraction Discriminators (CFDs), the Time-to-Amplitude Converter (TAC), a fast Analog-to-Digital Converter (ADC) and the Multichannel Analyser (MCA) with the data memory and the associated control circuits are integrated on the board. All boards employ bh’s proprietary multi-dimensional TCSPC technique and fast ADC principle. Count rates in excess of $4 \cdot 10^6$ photons/s can be recorded, resulting in acquisition times in the ms range. The modules are able to record the signals of several detectors or detector channels simultaneously, record fast sequences of optical waveforms, separate the photons excited by several lasers multiplexed at high rate, acquire fluorescence lifetime images in conjunction with fast optical scanners, or store the fluorescence signals of single molecules photon by photon.

Although all bh TCSPC devices are an excellent choice for the traditional fluorescence lifetime experiments they are targeted at advanced applications, such as multi-spectral fluorescence lifetime spectroscopy, single- and multi-wavelength fluorescence lifetime imaging, laser scanning microscopy, fast sequential recording of time-of-flight distributions in diffuse optical tomography, measurement of transient fluorescence lifetime effects in biological systems, and spectroscopy on single molecules, quantum dots and semiconductor nano-structures by FCS, FIDA, and BIFL techniques. There are a number of different TCSPC modules targeting at different applications.

The SPC-600/630 was designed single molecule experiments. The modules have a ‘time tag’ or ‘FIFO’ mode that records the time in the decay curve, the time from the start of the experiment, and the detector number for each individual photon. The mode is used in single-molecule spectroscopy to obtain FCS, FIDA, and BIFL results with a number of detectors detecting in different wavelength intervals or under different angle of polarisation. Moreover, the modules have a ‘continuous flow’ or ‘double-kinetic’ mode that records fast and virtually infinite sequences of fluorescence decay curves. It is used for flow experiments in micro-capillaries, for recording haemodynamic effects in the brain by diffuse optical tomography, and for recording transient fluorescence lifetime effects in biological systems.

The SPC-730 is targeted to fluorescence lifetime imaging, especially in conjunction with confocal and two-photon laser scanning microscopes. Its ‘Scan Sync In’ mode has become a standard technique of fluorescence lifetime microscopy. Now the SPC-730 is more and more being replaced with the more powerful SPC-830 module, see below.

The SPC-830 combines the features of the SPC-730 and SPC-630. It has both the imaging modes and the FIFO mode implemented. It has an extremely fast bus interface, and a memory four time larger than that of the SPC-730. The large memory and the fast readout speed are a

benefit especially in multi-spectral and sequential lifetime imaging applications and single molecule experiments by FCS, FIDA, and BiFL techniques.

The SPC-134, SPC-144 and SPC-154 are compact packages of four fully parallel TCSPC cards. With a saturated count rate of 10 MHz per card, the devices can be operated at total recorded count rates of more than 20 MHz. The SPC-134 has the Continuous Flow mode implemented and targets at diffuse optical tomography. The SPC-144 contains the Scan modes and targets at high-count rate fluorescence lifetime imaging. The SPC-154 has both the Continuous Flow mode and the Scan modes implemented. Moreover, it has an extremely fast bus interface for fast data readout. All SPC-1 modules contain the FIFO (or ‘time tag’) mode. They are therefore used for single-molecule experiments, especially if the correlation of photons at a time scale below 100 ns is required.

The SPC-6 and SPC-7 modules exist in two versions. The -00 and -30 versions differ in the input voltage range and the time resolution. The SPC-x30 modules require negative input pulses. They have an input voltage range from -50 mV to -1 V and an electrical time resolution of <8 ps FWHM or <4 ps RMS. The -00 modules work with positive or negative input signals from ±10 mV to ±80 mV. The electrical time resolution of the SPC-x00 modules is 10 ps FWHM or 5 ps RMS typically. Although the -x00 modules have been discontinued in 1999 they are still fully supported by the current software versions.

All bh SPC systems are designed to work in the reversed start-stop mode. Laser repetition rates of more than 150 MHz can be used, and count rates of more than $4 \cdot 10^6$ photons/s per TCSPC channel can be recorded. In a single recording, results are obtained at data acquisition times down to 1 ms. In conjunction with triggered accumulation transient lifetime phenomena can be recorded down to the time scale of a few microseconds. Furthermore, the SPC modules can be operated as high resolution optical oscilloscopes with a sensitivity at the single photon level.

All functions of the SPC modules are controlled by the ‘Multi SPC Software’. The software provides functions such as set-up of measurement parameters, 2-dimensional and 3-dimensional display of measurement results, mathematical operations, selection of subsets from 4 dimensional data sets, loading and saving of results and system parameters, control of the measurement in the selected operation mode. The Multi SPC Software runs under Windows 2000, Windows NT, and Windows XP and is able to control up to four TCSPC modules simultaneously.

Measurement Modes

In the ‘Single’ mode the intensity versus time (usually a fluorescence decay curve) is measured. In the ‘Oscilloscope’ mode a repetitive measurement is performed and the results are displayed in short intervals.

In the ‘ $f(t,T)$ ’ mode the measurement is repeated in specified time intervals. The results represent the change of the measured waveform (decay curve) over the time. In the ‘ $f(t,EXT)$ ’ mode an external parameter is controlled via the optional step motor controller. The results represent the change of the waveform as a function of the external parameter (usually wavelength or sample displacement).

The ‘ $f_i(ext)$ ’ and ‘ $f_i(T)$ ’ modes record time resolved spectra, see page 262. Up to 8 time independent time windows can be defined on the measured waveforms, and the intensities within these windows are displayed as a function of time or an externally variable parameter.

The ‘ $f(t,x,y)$ ’ mode is used for multichannel measurements with detector arrays and for other applications which control the destination of the photons by an external ‘routing’ signal. Up to

128 decay curves (16384 for the SPC-7 and -8 modules) can be recorded simultaneously and displayed as $f(t,x)$, $f(t,y)$ or $f(x,y)$.

The ‘Continuous Flow’ mode records an unlimited sequence of decay curves or other photon distributions (see page 266). Unlike $f(t,T)$, the Continuous Flow mode is strictly hardware controlled and thus provides an extremely fast and accurate recording sequence. The Continuous Flow mode was originally developed for single molecule detection or DNA analysis in a gel electrophoresis setup. Now the mode is mainly used for dynamic functional brain imaging by optical tomography techniques, stopped flow measurements, measurement of the Kautski effect in living plants, and other applications which require a large number of decay curves to be recorded in short and exactly defined time intervals without time gaps between subsequent recordings. The Continuous Flow mode is available in the SPC-600/630, the SPC-130/134, and the SPC-150/154. For the SPC-150/154 a continuous-flow imaging mode is available, see page 277.

The ‘FIFO’ mode is available in the SPC-600/630, the SPC-830, the SPC-130/134, the SPC-140/144, and the SPC-150/154. This mode is used for single molecule experiments by BIFL, FCS, and FIDA techniques. For each photon the time within the laser pulse sequence, the time from the start of the experiment, and the number of the detector channel that received the photon are recorded. The memory is configured as a FIFO (First In First Out) buffer. During the measurement, the FIFO is continuously read by the device software and the results are stored to the hard disk of the computer. The results are used to calculate fluorescence correlation spectra, fluorescence decay curves, and photon counting histograms over specified time intervals within the measurement interval or as a function of time. Moreover, FIFO data are used to identify bursts of photons emitted by single molecules and to run a fluorescence analysis within the bursts. In the SPC-140/144 and the SPC-150/154 modules FIFO recording can be combined with imaging, see page 285.

The ‘Scan’ modes are used for image recording in the SPC-700/730, SPC-830, SPC-140/144, and SPC-150/154 modules. In the ‘Scan Sync In’ mode the data acquisition is controlled by synchronisation pulses from the scanning device. The mode is used with commercial scanning microscopes to acquire images with pixel dwell time down to 100ns. The ‘Scan Sync Out’ mode sends synchronisation pulses to the scanning device. It is used to control a scanner from the SPC module. Furthermore, the SPC-7 modules have a ‘Scan XY Out’ mode which delivers digital X,Y position signals to an optical scanner. Images with up to 256x256 pixels and 2048x2048 pixels can be recorded with the SPC-7 and SPC-8 modules, respectively. The SPC-8 modules are even able to record steady state images with 4096x4096 pixels. Except for the Sync XY out mode multidetector operation is available in all modes and all modules.

SPC Module Types

SPC-600/630 - the TCSPC General Solution

The SPC-600/630 modules are an excellent choice for the complete range from the traditional fluorescence lifetime and anisotropy decay experiments to photon correlation experiments, and single-molecule spectroscopy by FCS, FIDA and BIFL techniques. Moreover, the SPC-600/630 modules are used to record transient phenomena in the absorption, scattering and fluorescence parameters of a sample.

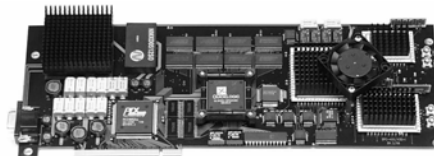


Fig. 1: SPC-630 module

The SPC-600/630 modules combine the features of the older SPC-400/430, SPC-401/431 and SPC-402/432 modules. They use a dual memory structure for simultaneous measurement and data readout, and a FIFO memory structure to produce a continuous data stream containing information about the individual photons.

A ‘Continuous Flow’ mode records decay curves with short collection times and without time gaps between subsequent recordings and saves the results to the hard disk. It was originally designed for single molecule detection in a gel electrophoresis setup, but is now increasingly used for dynamic brain imaging and stopped flow experiments.

The ‘FIFO’ - or time-tag - mode of the SPC-6 modules is used for single-molecule experiments to simultaneously obtain fluorescence decay data with FCS or FIDA data, or record BIFL data. In this mode the device memory is configured as a fast FIFO memory to store the time within the excitation pulse sequence, the time from the start of the experiment and the detector channel for each individual photon. During the measurement, the FIFO is continuously read by the device software and the results are stored to the hard disk of the computer. Due to an extremely fast signal processing circuitry and a large FIFO size burst count rates of more than $4 \cdot 10^6$ photons/s can be recorded for more than 10 ms.

SPC-700/730 - the TCSPC Imaging Solution

The SPC-700/730 modules are a solution to all TCSPC scanning and imaging applications. They combine the features of the older SPC-500/530, SPC-505/535 and the SPC-506/536 modules.

Due to their flexible scanning interface, the SPC-7 modules can be coupled to almost any scanning device. The modules can be synchronised by the frame/line synchronisation pulses or by X/Y signals from free running scanners such as confocal laser scanning microscopes or ultra-fast video-compatible ophthalmic scanners. Furthermore, the SPC-7 modules can actively control a scanning device by sending appropriate synchronisation pulses or X/Y signals. The maximum scanning area is 128 x 128 pixels for the X/Y control modes and 256 x 256 pixels for the modes using synchronisation pulses.

The SPC-700/730 work also for the traditional applications. Fluorescence decay curves, time, resolved fluorescence spectra etc. can be recorded in the same way as with the all other bh SPC modules. Transient lifetime phenomena down to the microsecond time scale can be recorded by triggered sequential recording in the Scan Sync Out mode.

SPC-830 - the High-End Solution

The SPC-830 module is the solution to the complete range from the traditional fluorescence lifetime and anisotropy experiments to photon correlation, confocal and two-photon fluorescence lifetime microscopy and single molecule lifetime, anisotropy and fluorescence correlation, cross-correlation and burst-integrated lifetime experiments.

The SPC-830 combines the functionality of the SPC-630 and the SPC-730 modules. It has a memory four times as large as the SPC-730 and an extremely fast bus interface. It aims at high-end applications that require both high resolution lifetime imaging, single molecule detection and fluorescence correlation spectroscopy (FCS). As the SPC-730, the SPC-830 modules can be coupled to almost any scanning device. The modules can be synchronised by the frame/line synchronisation pulses or

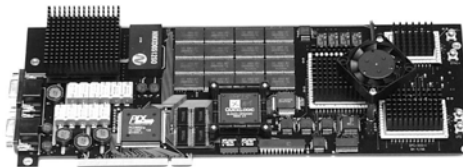


Fig. 2: SPC-730 module

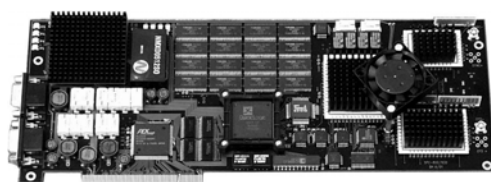


Fig. 3: SPC-830 module

by X/Y signals from free running scanners such as confocal or two-photon laser scanning microscopes or ultra-fast video-compatible ophthalmic scanners. Furthermore, the SPC-830 modules can actively control a scanning device by sending appropriate synchronisation pulses. The scanning applications benefit largely from the large memory of the SPC-830. For single-wavelength detection the maximum scanning area is up to 2048 x 2048 pixels for lifetime images and up to 4096 x 4096 pixels for steady state images. Multi-spectral lifetime data with 16 wavelength channels can be recorded with up to 512 x 512 pixels. Due to the fast bus interface, even large images can be read out and displayed in intervals of less than one second.

The SPC-830 modules can be operated in the FIFO - or time-tag - mode and used for single molecule detection and combined FCS / lifetime experiments. In this mode the device memory is configured as a fast FIFO memory to store the time within the excitation pulse sequence, the time from the start of the experiment and the detector channel for each individual photon. During the measurement, the FIFO is continuously read by the device software and the results are stored to the hard disk of the computer. In the FIFO mode the SPC-830 benefits from its large memory and fast bus interface. The FIFO buffers up to $8 \cdot 10^6$ photons, which is often enough to buffer a complete FCS, FIDA, or BIFL measurement. Moreover, the readout rate is on the order of $4 \cdot 10^6$ photons/s. A sustained count rate close to the maximum useful count rate of the SPC-830 does therefore not overload the FIFO. Another benefit of the SPC-830 is that the time-tag clock can be synchronised with the laser repetition rate. FCS artefacts due to aliasing of the time-tag clock with the laser repetition rate are thus avoided.

Of course, the SPC-830 works also for the traditional fluorescence lifetime experiments. Fluorescence decay curves, time, resolved fluorescence spectra etc. can be recorded the same way as with the all other bh SPC modules. Transient lifetime phenomena down to the microsecond time scale can be recorded by triggered sequential recording in the Scan Sync Out mode.

SPC-134 - The TCSPC Power Package

The SPC-134 is a stack of four completely parallel TCSPC modules. It occupies four adjacent PCI slots. With its four channels and a 40 MHz total saturated count rate the SPC-134 is an extremely powerful solution for all applications which require high count rate and high data throughput. Although the SPC-134 can be used for traditional fluorescence lifetime experiments the typical applications are diffuse optical tomography, stopped flow experiments, single molecule detection by BIFL, and combined FCS/lifetime experiments.

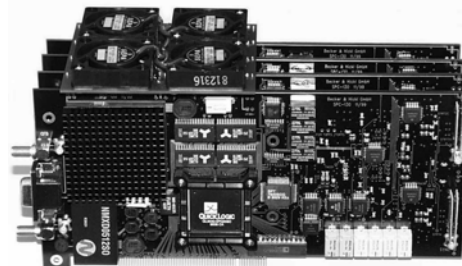


Fig. 4: SPC-134 package

As in the SPC-830, the time-tag clock in the FIFO mode can be synchronised with the laser repetition rate. This not only avoids aliasing artefacts in FCS but also allows the user to synchronise the time-tag clocks of the four channels. Photons in different TCSPC channels can therefore be correlated.

Due to space, power supply and price constraints the SPC-134 channels the routing capability is reduced to 16 detectors per TCSPC channel. However, no compromises have been made for the essential parameters such as count rate, time resolution, or differential nonlinearity. The SPC-134 works in the Single, Oscilloscope, f(t,T), f(t, ext), fi(T), fi(ext) and in the Continuous Flow and FIFO mode.

SPC-144 - The High Speed FLIM Solution

The SPC-144 is a stack of four TCSPC modules for scanning and single-molecule applications. The SPC-144 has full routing capability. It targets at high-throughput fluorescence lifetime imaging (FLIM) and single-molecule spectroscopy. The total saturated count rate is 40 MHz, as for the SPC-134. The time-tag clock in the FIFO mode can be synchronised with the laser repetition rate. This avoids aliasing artefacts in FCS and allows the user to synchronise the time-tag clocks of the four channels and correlate the photons in different TCSPC channels. The latest version of the SPC-144 combines the FIFO mode with scanning and thus simplifies the application to scanning FCS.

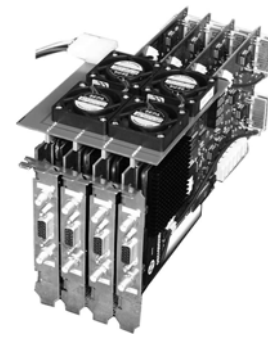


Fig. 5: SPC-144

SPC-154 - The Solution to High Speed FLIM, Dynamic DOT, and Fast Photon Correlation

As the SPC-134 and -144, the SPC-154 is a stack of four parallel TCSPC channels. The total saturated count rate is 40 MHz. The SPC-154 combines the Continuous Flow mode, the Scan mode and the FIFO (time tag) mode of the other SPC-1 modules. Moreover, it allows the user to combine both the Continuous Flow mode and the FIFO mode with scanning. A fast bus interface in combination with a large data memory allows for fast readout of the data in all operation modes. Thus, the SPC-154 is an excellent solution to dynamic diffuse optical tomography, high speed and high-resolution FLIM, high speed sequential FLIM, scanning FCS, and the recording of any other kind of transient effects in fluorescence lifetime or photon migration data.

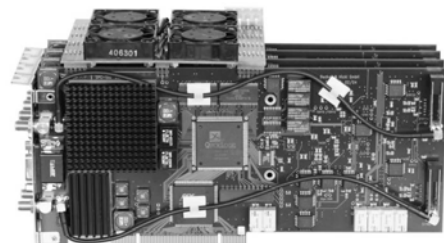


Fig. 6: SPC-154 package

Simple-Tau Systems

The Simple-Tau is a compact stand-alone TCSPC system. It consists of a lap-top PC and an extension box. The box contains an SPC-140 module (a single TCSPC channel of the SPC-144 system), an SPC-150, or an SPC-830 module along with a DCC-100 detector controller. The Simple-Tau comes with a cooled PMC-100-1 detector module. Power supply, gain control, overload shutdown, and current supply for cooling is provided by the DCC-100 card. Because the SPC-140 contains all basic operation modes including FIFO (time tagging) and scan modes the Simple-Tau is a powerful instrument for the whole range of TCSPC applications. The system can be upgraded with additional detectors and routing, or be delivered with other photon counting modules, e.g. the bh MSA-300 and MSA-1000 multichannel scalers.



Fig. 7: Simple-Tau system

SPC-130, SPC-140 and SPC-150 OEM Boards for Industrial Applications

Becker & Hickl deliver TCSPC boards for large-volume industrial applications. The SPC-130 board can be used for traditional fluorescence lifetime experiments, diffuse optical tomography, stopped flow experiments, single molecule detection and combined FCS/lifetime experiments. The SPC-140 and SPC-150 modules have the scan modes im-

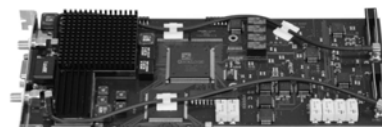


Fig. 8: SPC-150 board

plemented and can be used for fluorescence lifetime imaging, fluorescence correlation, and diffuse optical tomography with a large number of detector channels. The OEM boards have especially overvoltage-hardened signal inputs and are reliable and rugged solutions even under harsh conditions. When ordered in large quantities, the bh OEM modules offer unprecedented price-performance ratio.

A comparison of all bh SPC versions (not including the older SPC-3 to SPC-5 modules) is given in the table next page.

Comparison of bh TCSPC Modules

Features	SPC-600	SPC-630	SPC-700	SPC-730	SPC-830	SPC-134	SPC-144	SPC-154
TCSPC Channels / Module	1	1	1	1	1	4 ⁵⁾	4 ⁵⁾	4 ⁵⁾
Operating Software	multi SPC	multi SPC	multi SPC	multi SPC				
Time Channels /Curve	64, 256, 1024, 4096	64, 256, 1024, 4096	64, 256, 1024, 4096	64, 256, 1024, 4096	1 to 4096 ⁶⁾	64, 256, 1024, 4096	1 to 4096 ⁶⁾	1 to 4096 ⁶⁾
No. of Curves in Memory	64 to 4096	64 to 4096	up to 65536	up to 65536	up to 16·10 ⁶ ⁴⁾	32 to 2048	up to 4·10 ⁶ ⁴⁾	up to 4·10 ⁶ ⁴⁾
Input Voltage Range	10..80 mV	20mV..2V	10..80 mV	20mV..2V	20mV..2V	20mV..2V	20mV..2V	20mV..2V
Time Resol. el., FWHM	11 ps	6 ps	11 ps	6 ps	6 ps	6 ps	6 ps	6 ps
IRF w. MCP PMT, FWHM	30 ps	25 ps	30 ps	25 ps	25 ps	25 ps	25 ps	25 ps
Time / Channel, min.	815 fs	815 fs	815 fs	815 fs				
Dead Time	125 ns	125 ns	150 ns	150 ns	125ns	100 ns	100 ns	100 ns
Saturated Count Rate 1)	8 MHz	8 MHz	6.6 MHz	6.5 MHz	8 MHz	40 MHz total	40 MHz total	40 MHz total
Useful Count Rate 2)	4 MHz	4 MHz	3.3 MHz	3.3 MHz	4 MHz	20 MHz total	20 MHz total	20 MHz total
Memory (MCA)	dual/FIFO	dual/FIFO	single	single	single/FIFO	dual/FIFO	single/FIFO	dual/FIFO
Multi-Detector Operation	yes	yes	yes	yes	yes	16 detectors/channel ⁵⁾	yes	yes
Multi-Module Operation	2, 3 or 4	4 ⁵⁾	4 ⁵⁾	4 ⁵⁾				
Readout during Measurement	FIFO and Cont. Flow	FIFO and Cont. Flow	no	no	FIFO mode	FIFO and Cont. Flow	FIFO mode	FIFO and Cont. Flow
Count Rate Display	yes	yes	yes	yes	yes	yes	yes	yes
Sync Rate Display	no	yes	no	yes	yes	yes	yes	yes
Dead Time Compensation	on/off	on/off	on/off	on/off	on/off	on/off	on/off	on/off
Experiment Trigger	yes	yes	yes	yes	yes	yes	yes	yes
PC Bus Interface	PCI	PCI	PCI	PCI	PCI	4 x PCI	4 x PCI	4 x PCI
Application								
Optical Oscilloscope	X	X	X	X	X	X	X	X
Fluorescence Decay	X	X	X	X	X	X	X	X
Fluorescence Spectra	X	X	X	X	X	X	X	X
ps Photon Correlation		X		X	X	X	X	X
FCS / FCFS, FIDA, BIFL	X	X			X	X	X	X
Opt. Tomography	X	X			X	X	X	X
FLIM, Laser Scanning Microscopy			X	X	X		X	X
Multi-Wavelength FLIM					X		X	X
High Speed FLIM							X	X
Sequential FLIM						(X) ⁶⁾		X
High resolution FLIM, scanning FCS								X

- 1) The saturated count rate is the reciprocal dead time. It is the theoretical maximum for infinite detector count rate.
- 2) The maximum useful count rate is the recorded count rate for 50% counting loss.
- 3) Number of time channels is 1, 4, 16, 64, 256, 1024, or 4096.
- 4) Max. number of curves or pixels depends on number of time channels. 16·10⁶ and 16·10⁶ is for 1 time channel per pixel. Please see 'System Parameters'.
- 5) The SPC-134, SPC-144 and SPC-154 are packages of four parallel SPC-130, SPC-140 or SPC-150 TCSPC modules.
- 6) Modules manufactured later than September 2006

Operation Modes	SPC-600	SPC-630	SPC-700	SPC-730	SPC-830	SPC-134	SPC-144	SPC-155
'Single' Mode	X	X	X	X	X	X	X	X
Oscilloscope Mode	X	X	X	X	X	X	X	X
3D mode, f(t,x,y)	X	X	X	X	X	X	X	X
Sequence, f(t,T)	X	X	X	X	X	X	X	X
Sequence, f(t,ext)	X	X	X	X	X	X	X	X
Spectrum, f(T)	X	X	X	X	X	X	X	X
Spectrum, f(ext)	X	X	X	X	X	X	X	X
Unlimited Sequence, Continuous Flow	X	X				X		X
FIFO (Time-Tag) Mode	X	X			X	X	X	X
FIFO Imaging								X
Imaging, Scan Sync In			X	X	X		X	X
Scan Sync In with Cont. Flow								X
Imaging, Scan Sync Out			X	X	X		X	X
Imaging, Scan XY Out			X	X	X			
Sequence, by Scan Sync Out			X	X	X		X	X
Control Functions								
Routing, Multi-Detector Operation	X	X	X	X	X	x	X	X
Multiplexing	X	X	X	X	X	X	X	X
Page stepping	X	X	X	X	X	X	X	X
Accumulate	X	X	X	X	X	X	X	X
Autosave	X	X	X	X	X	X	X	X
Experiment Trigger	X	X	X	X	X	X	X	X

Other Photon Counters

For photon counting at moderate time resolution and for steady-state applications a number of multichannel scalers are available from bh [24, 25]. Multichannel scaling differs from TCSPC in that it is able to record several photons per signal period. Moreover, count rates on the order of several $100 \cdot 10^6 \text{ s}^{-1}$ can be recorded. The PMS-400, MSA-300, and MSA-1000 multichannel scalers are shown in Fig. 9. The minimum time-channel width of these devices is 250 ns, 5ns, and 1 ns, respectively. In optical spectroscopy, the multichannel scalers are excellent instruments for recording phosphorescence decay curves of organic dyes, luminescence decay curves of rare-earth chelates, and luminescence decay curves of inorganic fluorophores. Other applications are time-of-flight mass spectrometry and LIDAR.



Fig. 9: Photon counters based on multichannel scaling. Left to right: PMS-300 (250 ns per channel), MSA-300 (5 ns per channel), MSA-1000 (1 ns per channel)

Light Sources, Detectors and Detector Electronics

Picosecond Diode Lasers

BH delivers a number of picosecond diode laser modules with wavelengths from the NUV to the NIR [26, 27]. All lasers feature simple +12V power supply, high repetition rate, short pulse width, and an extremely low electrical noise level. The complete driver electronics is integrated in the module. All bh diode laser modules are directly compatible with the bh TCSPC modules.

NUV and Blue Lasers

The BDL-375, -405, -440, and -473 lasers have emission wavelengths of 375nm, 405nm, 440nm and 473 nm, respectively [26]. The typical pulse width is 50 to 90 ps, the average power up to a few mW. All BDL lasers have a fast on/off control input which can be used to multiplex several laser of different wavelength or to shutdown the laser during the beam fly-back in a laser scanning microscope. Moreover, the latest versions of the BDL lasers can be switched between pulsed and CW operation. The lasers are available with beam-profile and astigmatism correction and single-mode fibre coupling (see -smc versions of BDL lasers, Fig. 10 right). A coupling efficiency of more than 60% is achieved. The BDL-SMC lasers are thus excellent excitation sources for fluorescence lifetime imaging in laser scanning microscopes [20, 21, 22].



Fig. 10: Blue and NUV ps diode lasers. BDL-405C (left) and BDL-405-SMC with single-mode fibre coupler (right)

Red and NIR Lasers

The BHL-600 modules are available for wavelengths from 635 nm to 1300 nm [27]. They are optimised for short pulse width. Due to their short pulse width down to 50 ps they can be used for fluorescence excitation from 635 nm to 780 nm and for testing purposes.

The BHLP-700 modules are available for wavelengths from 680 nm to 980 nm [27]. They are optimised to deliver an output power of up to 15 mW (CW equivalent) at 50 MHz repetition rate. As the BDL lasers, the BHLP modules have a fast multiplexing input. The BHLP modules are an excellent choice for photon migration experiments.

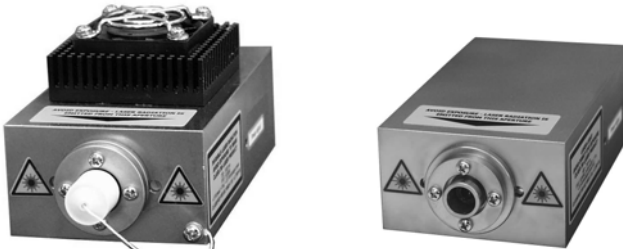


Fig. 11: Red and NIR ps diode lasers. BHLP-700 (left) and BHL-600 (right)

Single-Channel Detectors

A wide variety of PMT and MCP detectors can be used with the SPC modules. The fastest detector currently available is the Hamamatsu R3809U family. Extremely high sensitivity is achieved by the Hamamatsu H7422P-40 and H7422P-50 modules. Both the R3809U and the H7422 are controlled by the DCC-100 detector controller card. The detectors can be purchased via bh together with the appropriate signal and control cables and preamplifiers.

For single-molecule experiments often the Perkin Elmer SPCM-AQR is used. A single SPCM-AQR can be connected to the bh SPC module via an attenuator and an A-PPI pulse inverter, see Fig. 18. Up to eight SPCM-AQRs can be connected to one SPC module via an HRT-82 router. Other SPAD modules, such as the id-100-20 of idQuantique or the PDM 50CT of MPD can be connected similarly.

For standard TCSPC applications often the bh PMH-100 detector head is used. This device contains a fast, small PMT, the high voltage generator and a preamplifier with overload detection in a 32x38x92mm housing. The PMH-100 is powered directly from the SPC module, i.e. no high voltage power supply is required.

The bh PMC-100 is a cooled version of the PMH-100. It is available with an NIR-sensitive cathode. Both the PMH and the PMC have an exceptionally stable timing response function at high count rates, see [46].

For multichannel measurements, e.g. spectrally resolved lifetime measurements, the bh PML-16 detector head is available [18]. An overview about detectors for photon counting and their characterisation is given in [28, 46] and in chapter ‘Detectors for TCSPC’ of this manual. The PMH-100, PMC-100, and PML-16C detectors are shown in Fig. 12.



Fig. 12: Left to right: PMH-100 module, PMC-100 cooled PMT module, PML-16 sixteen-channel PMT module with internal routing electronics

PML-Spec and MW-FLIM 16-Channel Spectral Detection Modules

The PML-Spec consists of a bh PML-16 sixteen-channel PMT module [18] and a polychromator. With a bh TCSPC module 16 wavelength channels are recorded simultaneously. Typical applications of the PML-Spec are single-point autofluorescence measurements of biological tissue and multi-spectral time-resolved laser scanning microscopy. The MW-FLIM system is a spectral detection module optimised for direct (non-descanned) detection in multi-photon laser scanning microscopes.

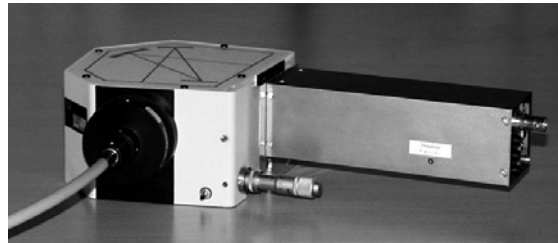


Fig. 13: PML-SPEC 16-channel spectral detection unit

DCC-100 Detector Control Module

The bh DCC-100 module [19] was designed to control detectors in conjunction with bh photon counters. It can be used to drive the cooler and control the gain of the PMC-100, the PML-16C, the Hamamatsu H7422, H5783, H6783 or similar photosensor modules from the software. The gain of MCPs and PMTs can be controlled via an FuG HCN-14 high-voltage power supply. In conjunction with bh preamplifiers, overload shutdown of the detectors is achieved. High-current digital outputs are available for shutter or filter control. The DCC-100 is a PCI module for IBM compatible computers. It works under Windows 2000, NT, and XP.

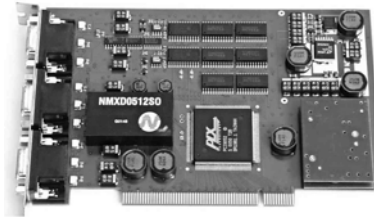


Fig. 14: DCC-100 detector controller. Provides power supply, cooling control, gain control, shutter control and overload shutdown for two detectors

Preamplifiers

For TCSPC experiments with most PMTs and MCPs preamplifiers are recommended. For safe operation of MCPs and PMTs the HFAC-26 (26 dB, 1.6 GHz) and the HFAH amplifiers (26 dB, 1.6 GHz or 40dB, 500 MHz) with current sensing are available. These amplifiers indicate overload conditions in the detector by a LED and by a TTL signal. For multidetector

measurements the HFAM-26 with eight amplifier channels is available. Other amplifiers are the ACA-2 and ACA-4 devices with gains from 10 dB to 40 dB and a bandwidth up to 2 GHz.

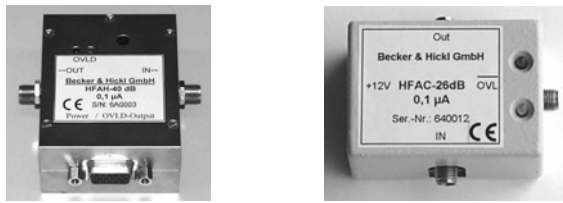


Fig. 15: HFAH series and HFAC series preamplifiers

Routing Devices for Multi-Detector Operation

The HRT-41 and HRT-81 routers are used to connect up to four (or eight) individual PMTs or MCPs to one bh SPC module. To connect up to eight Perkin Elmer SPCM-AQR APD modules the HRT-82 is available. With the HRT devices, all detector channels work simultaneously and the detected photons are ‘routed’ into individual memory blocks. Please individual manual [17] or data sheets.



Fig. 16: HRT-41 (left) and HRT-81 (right) routers. The routers connect several detectors to a single TCSPC module

Reference Photodiodes

To generate the synchronisation signal for SPC modules from a laser pulse sequence fast photodiode modules are available. The bh PHD-400 and the bh PDM-400 use fast PIN photodiodes. If high sensitivity is required the bh APM-400 avalanche photodiode modules are recommended. All photodiode modules are powered directly from the SPC card or from a DCC-100 detector controller.



Detector, Shutter and Beam Splitter Assemblies for TCSPC Microscopy

Photon counting detectors, especially MCP-PMTs, can easily be damaged or destroyed by overload. Even when an MCP or PMT is switched off the cathode performance is impaired temporarily if the cathode is exposed to a high light intensity [211]. Especially in microscopy applications the microscope lamp - usually a mercury, xenon or halogen lamp - is a potential source of detector damage. A simple operator error can destroy one or several detectors. BH deliver detector/shutter/beamsplitter assemblies for one, two, and four detectors. The assemblies contain a field lens for efficient light transfer in the non-descanned beam path of two-photon laser scanning microscopes. The assemblies can also be used with fibre adapters at the inputs. They can be used with a wide variety of detectors, including the R3809U, the H7422, the PMH-100, the PMC-100, and the PML-16C. Although primarily developed for laser scanning microscopes, the detector assemblies can be used for any application in which detector overload cannot be reliably excluded. Please see [29].



Fig. 17: Detector assemblies. Left to right: One R3809U MCP with shutter, two R3809U with shutter and beamsplitter, the PMH-100 with shutter and beamsplitter, four PMH-100 with three beamsplitters

Cables and Adapters

To connect signals from different detectors to the bh SPC modules a wide variety of cables and adapters are available. This includes attenuators and inverting transformers for TTL signals (e.g. from SPCM-AQR avalanche photodiode modules), power splitters, attenuators, cables, and various adapters, see Fig. 18. Since 2001 all bh SPC modules are delivered with an extended set of cables and adapters.



Fig. 18: Left to right: A-PPI pulse inverter, 1:2 and 1:4 power splitters, attenuator, cable with SMA connectors, SMA-to-SMA adapters, SMA-to-BNC adapter

Step Motor Controller

For driving a monochromator or scanning a sample the STP-340 step motor controller is available. The STP-340 drives up to two unipolar 4 phase motors with up to 1 A phase current. The electrical and mechanical drive parameters are set via a configuration file. The control of the STP-340 is included in the SPC software.

Data Analysis for TCSPC Imaging Data

The ‘SPCImage’ software [20, 21, 22, 23] is available for fluorescence decay analysis of TCSPC Imaging data obtained in the ‘Scan’ modes of the SPC-700/730 or SPC-830. The program performs single, double and triple exponential decay analysis in the individual pixels of the image. The fluorescence lifetime, lifetime components of multi-exponential decay functions, amplitudes of lifetime components, or ratios of these parameters are displayed as colour of the image, see Fig. 19. Thus, images of local environment parameters such as pH, oxygen or ion concentrations, of the FRET intensity, of the distance and fraction of interacting proteins, bound and unbound fluorophores can be produced. Please see [20, 21, 22, 23], and chapter ‘Time-Resolved Laser Scanning Microscopy’ of this handbook.

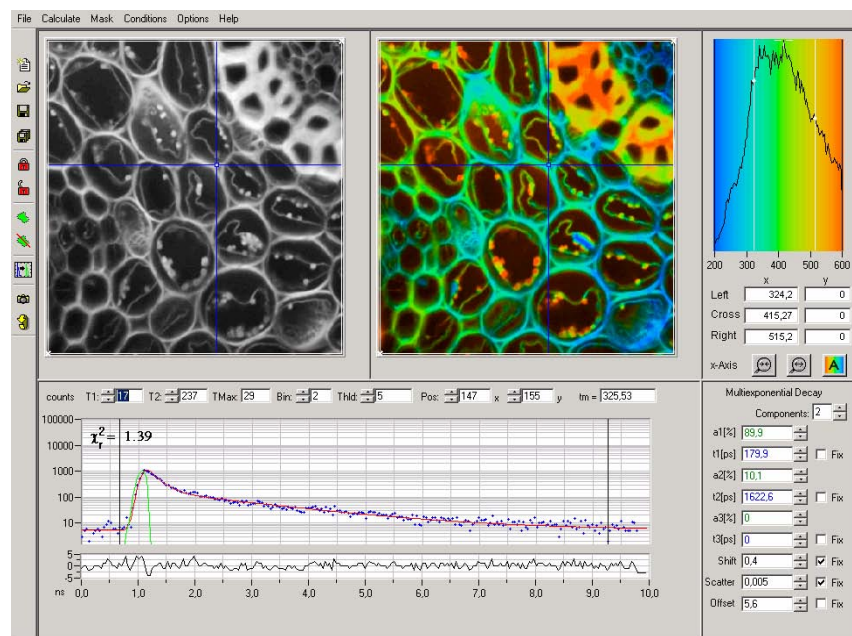


Fig. 19: SPCImage FLIM analysis software

Classic Time-Correlated Single Photon Counting

Single-Photon Detection

Photon counting techniques consider the detector signal a random sequence of pulses corresponding the detection of the individual photons. Fig. 20, left shows the output pulses of a R5900 PMT for a photon detection rate of 10^7 photons per second. The figure left shows the pulses at a time scale of 1 ns per division. The same signal of the same PMT at a time scale of 100s is shown right.

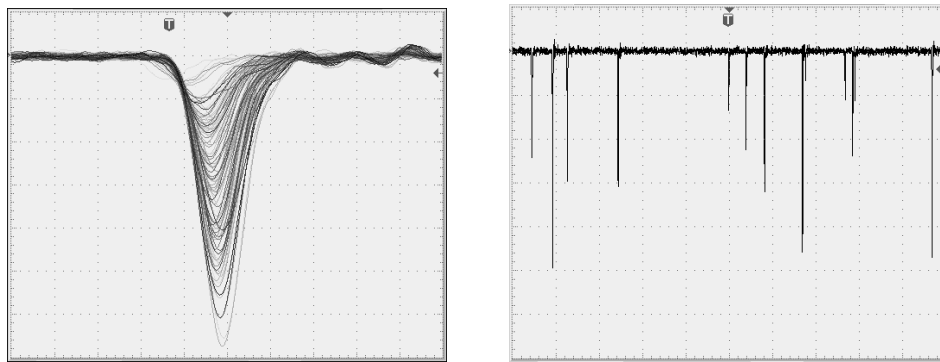


Fig. 20: Single-photon pulses delivered by a R5900 PMT (left, 1 ns / div) and output signal of the PMT at a photon detection rate of 10^7 s⁻¹ (right, 100 ns / div). Operating voltage -900V, signal line terminated with 50 Ω.

The individual single-photon pulses have a duration of less than 2 ns. Therefore, the detector signal is a random sequence of single-photon pulses rather than a continuous waveform (Fig. 20, right). The light intensity is represented by the density of the pulses, not by their amplitude. Obviously, the intensity of the light signal is obtained best by counting the pulses in subsequent time channels.

Photon counting has a number of advantages over analog recording techniques. Fig. 20, left, shows that the single photon pulses have a considerable amplitude jitter. The amplitude jitter - or ‘gain noise’ - is a result of the random amplification process in the PMT. It is present in all high-gain detectors. In analog techniques the gain noise contributes to the noise of the measurement. Photon counting results are free of gain noise. Also electronic noise does not contribute to the result as long as its amplitude is smaller than that of the photon pulses. Photon counting techniques therefore obtain a shot-noise-limited signal-to noise ratio down to the background count rate of the detector.

Another unique feature of photon counting results from the fact that the arrival time of a photon pulse can be determined with high precision. The bandwidth of a photon counting experiment is limited only by the transit time spread of the pulses in the detector, not by the width of the pulses. The transit-time distribution is usually an order of magnitude narrower than the width of the single-photon pulses. For the same detector, photon counting therefore obtains a significantly higher time-resolution than any analog recording technique. This feature is more or less inherent to all photon counting techniques, but is found in extreme form in time-correlated single photon counting, or TCSPC.

Time-Correlated Single Photon Counting

Time-correlated single photon counting, or TCSPC, is based on the detection of single photons of a periodic light signal, the measurement of the detection times, and the reconstruction of the waveform from the individual time measurements [46, 265, 379]. TCSPC makes use of

the fact that for low-level, high-repetition rate signals the light intensity is usually low enough that the probability to detect more than one photon in one signal period is negligible. The situation is illustrated in Fig. 21.

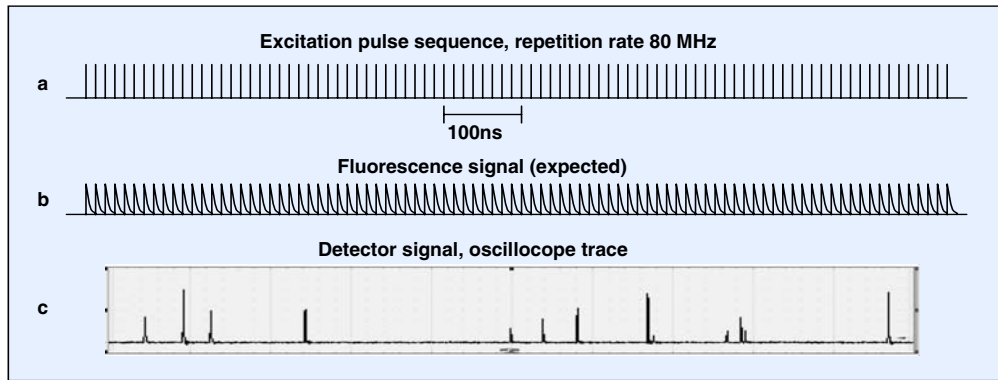


Fig. 21: Detector signal for fluorescence detection at a pulse repetition rate of 80 MHz

Fluorescence of a sample is excited by a laser of 80 MHz pulse repetition rate (a). The expected fluorescence waveform is (b). However, the detector signal measured by an oscilloscope has no similarity with the expected fluorescence waveform. Instead, it consists of a few pulses randomly spread over the time axis (c). The pulses represent the detection of single photons of the fluorescence signal. Please note that the photon detection rate of (c) is about 10^7 s^{-1} , which is on the order of the maximum possible detection rate of most detectors. Thus, the fluorescence waveform (c) has to be considered a probability distribution of the photons, not anything like a signal waveform. Moreover, Fig. 21 shows clearly that the detection of a photon in a particular signal period is a relatively unlikely event. The detection of several photons in one signal period is even less likely. TCSPC therefore neglects the detection of several photons per signal period. The principle is shown in Fig. 22.

As shown above in Fig. 21, the detector signal consists of a train of randomly distributed pulses corresponding to the detection of the individual photons. There are many signal periods without photons, other signal periods contain one photon pulse.

When a photon is detected, the arrival time of the corresponding detector pulse in the signal period is measured. The events are collected in a memory by adding a ‘1’ in a memory location with an address proportional to the detection time. After many signal periods a large number of photons has been detected, and the distribution of the photons over the time in the signal period builds up. The result represents the ‘waveform’ of the optical pulse. (Please note that there is actually no such waveform, only a distribution of the photon probability, see Fig. 21.)

Although this principle looks complicated at first glance, it has a number of intriguing features.

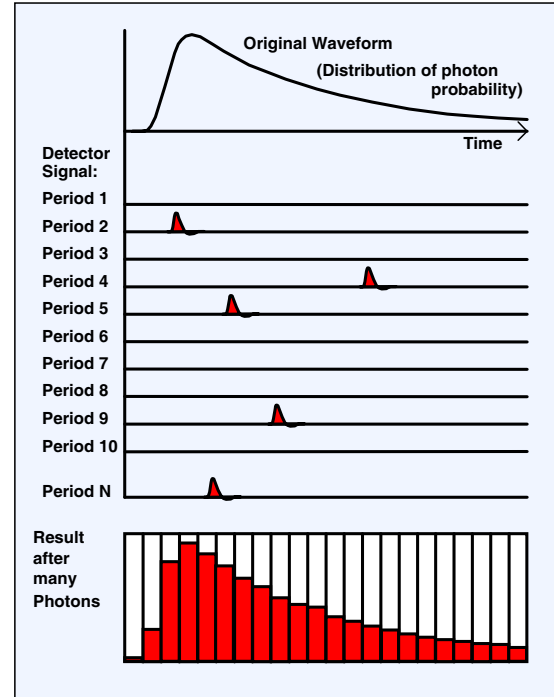


Fig. 22: Principle of TCSPC

Time resolution

The time resolution of an analog signal recording technique is limited by the bandwidth of the detector. The width of the instrument response function cannot be shorter than the ‘single electron response’, SER. The SER is the pulse that the detector delivers for a single detected photon (see Fig. 54, page 54).

The time resolution of TCSPC is not limited by the SER width. Instead, it depends on the accuracy at which the time of the individual photons can be determined. It is thus limited by the width of the transit-time distribution (or transit time spread, TTS) of the detector. For a given detector, the TTS is typically an order of magnitude narrower than the SER. Thus, TCSPC delivers a far better time resolution and signal bandwidth for a given detector than any analog recording technique. The width of the TCSPC instrument response function (IRF) for a number of typical detectors is given below (see also chapter ‘Detectors for TCSPC’).

Conventional photomultipliers	
standard types	0.6 to 1 ns
high speed (XP2020)	200 to 300 ps
Hamamatsu TO8 photomultipliers R5600, R5783 [154]	140 to 200 ps
MCP photomultipliers Hamamatsu R3809 [155]	25 to 30 ps
Single-photon APDs [93, 280, 179]	20 to 500 ps

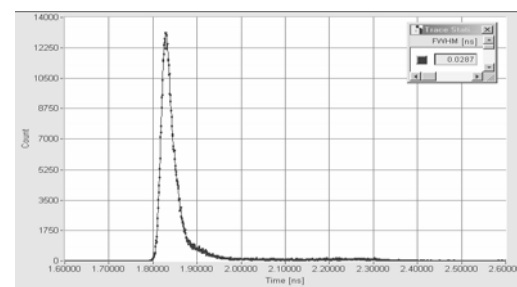


Fig. 23: TCSPC instrument response function for an R3809U MCP PMT, 100 ps / division

The TCSPC IRF for an R3809U MCP PMT [155] is shown in Fig. 23. The width is 29 ps, full width at half maximum (FWHM). For comparison, the SER of this detector is about 300 ps wide. Thus, using the MCP PMT in the TCSPC mode delivers a time resolution and detection bandwidth about 10 times better than using it as an analog detector.

The bandwidth and IRF width should not be confused with the minimum fluorescence lifetime detectable by a particular technique. The fluorescence lifetime is determined by fitting a model (e.g. an exponential function) to the recorded data. Depending on the signal-to-noise ratio of the raw data a lifetime considerably shorter than the IRF width can be determined.

Sample rate

The sample rate, i.e. the density of the signal points on a recorded waveform, must be higher than twice the frequency of the fastest signal component present in the signal. Only if this condition is fulfilled signal parameters, e.g. fluorescence lifetimes, can be recovered without presumptions about the signal shape. Consequently, the time channels into which the photons are recorded must be at least one order of magnitude smaller than the IRF width. TCSPC yields a time-channel width of less than one picosecond, and an effective sample rate of more than 1 THz. This is enough to fully exploit the time resolution of even the fastest detectors.

Gain Noise

Due to the random nature of the gain mechanism in a photomultiplier tube or avalanche photodiode the single-photon pulses have a considerable amplitude jitter, see Fig. 20. For analog recording, this jitter contributes to the noise of the result. TCSPC counts all the pulses with the same weight, independently of their amplitude. Within reasonable limits, the signal-to-noise ratio is therefore not influenced by the gain noise of the detector. Photon counting is also

insensitive to baseline drift and background noise as long as the amplitudes are small compared to the amplitude of the single-photon pulses.

Counting Efficiency

An ideal optical recording technique would record all detected photons with the same weight, an infinitely short IRF, negligible signal background, a time-channel width much shorter than the signal width, and a number of time channels that cover the complete duration of the signal. Under these conditions a single-exponential fluorescence lifetime can be determined with a signal-to-noise ratio, SNR, of

$$SNR = \sqrt{N}$$

from a number, N, of detected photons. This is the same SNR as it is obtained for intensity measurement based on the same number of photons [139, 195]. In a TCSPC device operated at reasonable count rate all detected photons contribute to the result. There is no counting loss due to ‘gating’ as in ‘Boxcar’ devices or gated image intensified CCDs, and no variable weight as in sine-wave modulation techniques [72, 281]. Moreover, TCSPC delivers the shortest possible IRF for a given detector, an extremely small time-channel width, and large number of time channels. Therefore the SNR of TCSPC comes very close to the ideal value [13, 195].

Sensitivity

The sensitivity of the TCSPC technique is limited mainly by the dark count rate of the detector. Defining the sensitivity as the intensity at which the signal is equal to the noise of the dark signal the following equation applies:

$$S = \frac{(Rd * N/T)^{1/2}}{Q}$$

(Rd = dark count rate, N = number of time channels, Q = quantum efficiency of the detector, T = overall measurement time)

Typical values (PMT with multialkali cathode without cooling) are $Rd=300s^{-1}$, $N=256$, $Q=0.1$ and $T=100s$. This yields a sensitivity of $S=280$ photons/second. This value is by a factor of 10^{15} smaller than the intensity of a typical laser (10^{18} photons/second). Thus, when a sample is excited by the laser and the emitted light is measured, the emission is still detectable for a conversion efficiency of 10^{-15} .

Count rate

Depending on the desired accuracy, the light intensity must be not higher than to detect 0.01 to 0.1 photons per signal period (see also ‘Classic Pile-Up’ page 133). If the count rate is higher the detection of several photons per signal period cannot be longer ignored, and signal distortion by ‘pile-up’ occurs. In early times of TCSPC the light sources delivered repetition rates on the order of 10 kHz. Pile-up was therefore a serious limitation. Modern laser light sources deliver pulses with repetition rates of 50 to 100 MHz. For these light sources, the count rate constraint is satisfied even at count rates of several 10^6 photons per second. Such count rates already cause overload in many detectors. Consequently the pile-up effect does not cause major problems in conjunction with high repetition rate laser light sources.

Acquisition time

The TCSPC technique is often believed to suffer from slow recording speed and long data acquisition times. This reputation comes from early fluorescence lifetime spectrometers which indeed needed acquisition times of several minutes or even hours to record a single fluorescence decay curve. The reason was the low repetition rate of the light sources used and the long ‘dead time’ of the electronics of the early 80s. At a repetition rate of a few 10 kHz (typical of the nanosecond flash lamps used) pile-up indeed precluded count rates of more than 1000 photons per second. The acquisition times were correspondingly long. Another limitation was the slow signal processing speed of the electronics. The ‘dead time’ after the detection of a photon was on the order of 10 μ s, which precluded the recording of more than a few 10^4 photons per second.

These limitations do not longer exist in modern TCSPC setups. Modern light sources can be operated at repetition rates of 50 to 80 MHz. Moreover, advanced TCSPC devices employ a new AD conversion principle that results in processing times about 100 times shorter than in the traditional TCSPC setups (see ‘Analog-to-Digital Conversion’, page 48). TCSPC devices from Becker & Hickl have dead times of 100 to 125 ns and are able to record photons at a rate of about $5 \cdot 10^6$ photons per seconds. Fig. 24 shows a fluorescence decay curve of plant tissue recorded within an acquisition time of 100 ms. About 400,000 photons were recorded within this time. Reasonable fluorescence lifetimes can be obtained from 1000 photons, which can be obtained within less than 1 ms. Advanced TCSPC devices can therefore be used for high speed applications such recording of chlorophyll transients, dynamic brain imaging by diffuse optical tomography, spectroscopy of single molecules, or fluorescence lifetime imaging by fast scanning techniques.

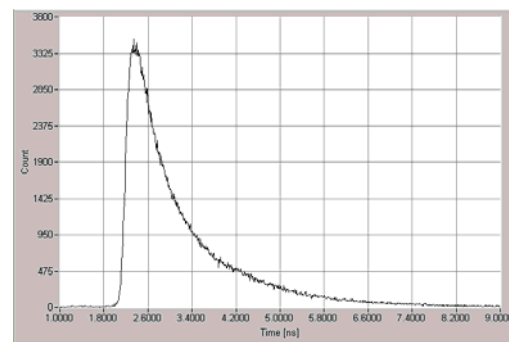


Fig. 24: Fluorescence decay curve of plant tissue, count rate $4 \cdot 10^6$ s $^{-1}$, acquisition time 100 ms.
SPC-140 TCSPC module.

The Classic TCSPC Architecture

The architecture of a classic TCSPC device [90, 265, 379] is shown in Fig. 25.

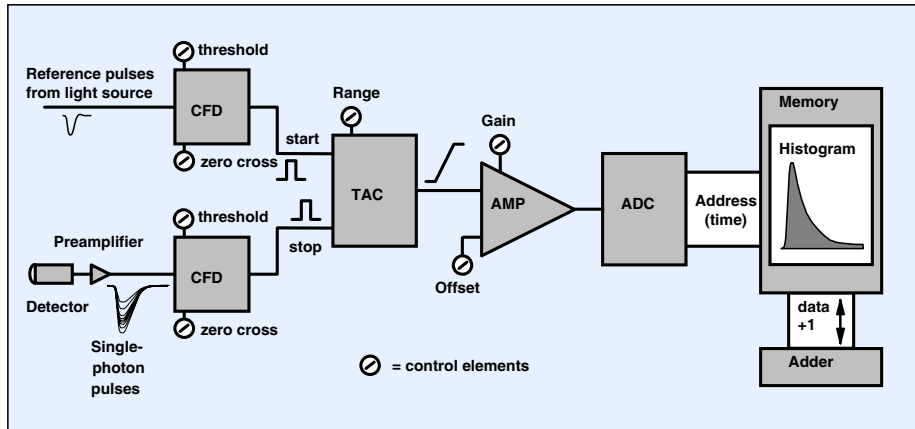


Fig. 25: Architecture of a classic TCSPC device

The detector, usually a PMT, delivers pulses for individual photons of the repetitive light signal. The pulses are detected by a fast discriminator. Due to the random amplification mechanism in the detector, these pulses have a considerable amplitude jitter. If a simple leading-edge discriminator were used, it would trigger when the leading edge of the input pulse reached a defined threshold. Even if the discriminator were infinitely fast, the amplitude jitter would induce a timing jitter of the order of the pulse rise time. Therefore a ‘Constant Fraction Discriminator’, CFD, is used to trigger on the PMT pulses. The CFD triggers at a constant fraction of the pulse amplitude, thus avoiding pulse-height induced timing jitter. Practical implementations of CFDs trigger at the baseline transition of a re-shaped pulse, which is equivalent to constant fraction triggering. The details of constant-fraction triggering are described in chapter ‘Detailed Description of Building Blocks’ page 42.

A second CFD is used to obtain a timing reference pulse from the light source. The reference signal is usually generated by a photodiode, or, in case of ns flashlamps, by a PMT operated at medium gain. Thus also the reference pulses may have some amplitude fluctuation or amplitude drift. The use of a CFD in the reference channel prevents these fluctuations from causing timing jitter or timing drift.

The output pulses of the CFDs are used as start and stop pulses of a time-to-amplitude converter, TAC. The TAC generates an output signal proportional to the time between the start and the stop pulse. Conventional TACs use a switched current source charging a capacitor. The start pulse switches the current on, the stop pulse off. If the current in the start-stop interval is constant, the final voltage at the capacitor represents the time between start and stop. This principle works with remarkable accuracy, and time differences of a few ps can be clearly resolved.

The TAC output voltage is sent through a ‘Biased Amplifier’, AMP. The amplifier has a variable gain and a variable offset. It is used to select a smaller time window within the full-scale conversion range of the TAC.

The amplified TAC signal is fed to the Analog-to Digital Converter, ADC. The output of the ADC is the digital equivalent of the photon detection time. The ADC must work with an extremely high precision. Not only must it resolve the amplified TAC signal into thousands of time channels, but the time channels must also have the same width. Any non-uniformity of the channel width results in a systematic variation of the numbers of photons in the channels, creating noise or curve distortion.

The ADC output is used as an address word for the measurement data memory. When a photon is detected, the ADC output word addresses a memory location corresponding to the time of the photon. By incrementing the data contents of the addressed location the photon distribution over time is built up.

Reversed Start-Stop

The principle described above measures the time from the reference pulse, which is usually a pulse from an excitation light source, to the detection of a photon. Of course, there are many pulse periods in which no photons are detected. In these periods the TAC is started but not stopped. Consequently, there must be a circuit in the TAC that detects the out-of-range condition, and resets the TAC for the next signal period. The frequent start-only events and subsequent resets are no problem at low pulse repetition rates.

However, for light sources of 50 to 100 MHz repetition rate, like titanium-sapphire lasers or pulsed diode lasers, the principle described above is not applicable. The TAC must be reset each 10 or 20 ns, while measuring some rare detection events between the reset pulses. Therefore, high-repetition rate systems work in the ‘reversed start-stop’ configuration [191, 371], see Fig. 26.

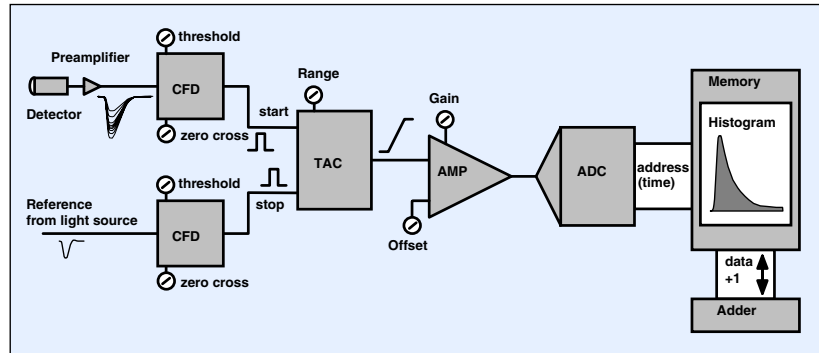


Fig. 26: Reversed start-stop configuration of TCSPC

In the reversed start-stop configuration, the TAC is started when a photon is detected and stopped with the next reference pulse from the light source. Consequently, the TAC has to work only at the rate of the photon detection events, not at the much higher rate of the excitation pulses. In the reversed start-stop mode the TAC output voltage decreases for increasing arrival times of the photons. The reversal of the time axis can be compensated for electronically by inverting the signal in the biased amplifier, by inverting the ADC bits, or simply by reversed readout of the data memory.

The setup shown in Fig. 26 is based on the presumption that the period of the excitation pulses is constant and free of jitter down to the order of 1 ps. If there is a pulse period jitter it adds to the transit time spread of the detector. The reversed start-stop configuration can easily be made insensitive to pulse period jitter by introducing a passive delay line in the reference channel. With an appropriate delay in the reference channel the time of the photon is measured against the laser pulse from which the detected photon originated. This removes the effect of any pulse period change on the timing (see ‘Delayed Stop Operation’ page 91).

The setup shown in Fig. 25 and Fig. 26 is often complemented by passive delay lines in the detector and reference channels, by rate meters that display the start and stop rates, and by a suitable computer interface for data readout [265]. Classic TCSPC setups were usually built from nuclear instrumentation (NIM) modules. The CFDs, the TAC, the biased amplifier, the ADC, and accessories like rate meters or delay lines were individual plug-in modules. The large size of these modules and the large number of cable connection made the devices relatively bulky. The system parameters had to be set by manual controls. The long dead times of the TAC and ADC limited the available count rates. However, the most severe limitation of classic TCSPC is that it is intrinsically one-dimensional, i.e. restricted to the recording of the waveform of the light signal.

Agents: Boston Electronics, (800)347-5445, TCSPC@boselec.com

Agents: Boston Electronics, (800)347-5445, TCSPC@boselec.com

Multi-Dimensional TCSPC

In 1993 bh introduced a new generation of TCSPC devices. It abandoned the NIM technique entirely and integrated all building blocks on a single printed circuit board (PCB). The enormous size reduction became possible by using surface mount PCB technology, hybrid circuits, and field programmable gate arrays (FPGAs). The single-board design relaxed the interconnection problems between the individual building blocks so that the speed of new analog and logic ICs could be fully exploited. The electronic system was optimised as a whole, resulting in time-shared operation of TAC, ADC and memory access. Together with new time-to-digital conversion principles the count rate of TCSPC was increased by two orders of magnitude.

Compared with the very limited capacity of the more or less discrete control electronics of classic TCSPC systems, the use of FPGAs also led to a breakthrough in functionality. Advanced TCSPC devices use a multi-dimensional recording process [46]. They record the photon density not only as a function of the time in the signal period, but also of other parameters, such as wavelength, spatial coordinates, location within a scanning area, the time from the start of the experiment, or other externally measured variables. The general architecture of a TCSPC device with multi-dimensional data acquisition is shown in Fig. 27.

In addition to the time-measurement block of the classic TCSPC technique, multi-dimensional TCSPC contains a channel register and a sequencer logic. The memory is much larger than for a classic TCSPC device. When a photon is recorded its destination in the device memory is controlled by the time-measurement block, by the bits in the channel register, and by the bits generated in the sequencer logic. Consequently, the device builds up a multi-dimensional photon distribution versus the time of the photons in the signal period, versus the data word at the ‘channel’ input, and versus one or several additional data words generated by the sequencer.

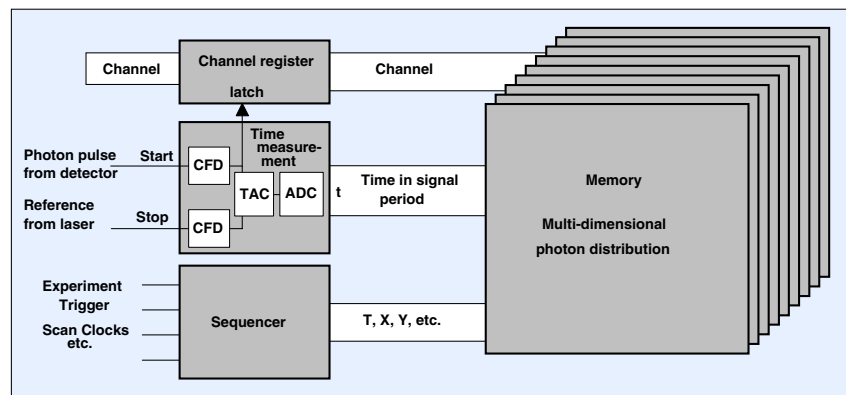


Fig. 27: Multi-dimensional TCSPC architecture

The additional address bits provided by the channel register and the sequencer are often termed ‘routing bits’, and the technique is termed ‘routing’. Depending on the information fed into the ‘channel’ input, a number of advanced signal acquisition principles are available:

- **Classic TCSPC:** If the channel register and the sequencer are not used the device works as a classic TCSPC device. Compared with NIM systems the available count rates are considerably higher.
- **Multi-detector operation:** Several individual detectors or several channels of a multi-anode PMT are used. A ‘router’ generates a ‘channel’ information that indicates which of the detectors detected the current photon. Depending on the optical system, spectral resolution, spatial resolution, or separation of photons of different polarisation can be obtained.
- **Multiplexed detection:** Several lasers of different wavelength, different excitation positions, different samples or different sample positions are multiplexed. The ‘channel’ signal

indicates the number of the particular laser, the sample, or the position in the sample in the moment when the photon was detected.

- Multi-parameter detection: The ‘channel’ information comes from one or several external ADCs. The ADCs deliver data words for externally measured sample parameters, such as temperature, pressure, or electrical or magnetic field strength.
- One or several recording dimensions are added by the sequencer, for example:
- Sequential recording: Controlled by an internal clock oscillator, the sequencer counts through a range of subsequent address words. The result is a sequence of waveform measurements. The individual measurements can be multi-dimensional themselves, due to the capabilities of the ‘channel’ control. The sequence can be recorded at almost any rate. It can be triggered by an ‘experiment trigger’, and a specified number of triggered sequences can be accumulated.
- Scanning: The sequencer synchronises the recording with the action of an external scanner. The sequencer delivers two additional dimensions, X and Y. Synchronisation with the scanner is obtained either by sending to or receiving clock pulses from the scanner. The result is a spatial array of data sets, each of which can be multi-dimensional, due to the capabilities of the ‘channel’ control. TCSPC scanning is able to work at extremely high scan rates, even at pixel rates much higher than the count rate.
- A variation of the TCSPC technique does not build up photon distributions but stores information about each individual photon. This mode is called ‘time tag’, or ‘FIFO’ mode. The memory is configured as a FIFO buffer. For each photon, this method stores the time in the signal period (‘micro time’), the time from the start of the experiment (‘macro time’), and the data word at the channel input. During the measurement, the FIFO is continuously read, and the photon data are transferred into the main memory or to the hard disc of a computer. Most bh TCSPC devices can be configured to build up either multi-dimensional photon distributions or to store the individual photons.

The most frequently used multidimensional recording modes and their combinations are described in the next paragraphs.

Multi-Detector TCSPC

For reasonable operation of a TCSPC device the average number of photons detected per signal period must be less than one, see Fig. 22, page 16. Often a limit of 0.01 photons per signal period is given, but a detection rate up to 0.1 or even 0.2 per signal period can usually be tolerated [46], see Fig. 144, page 134. In any case, the detection of several photons per period remains an unlikely event.

Now consider an array of detectors over which the same photons flux is spread. Because it is unlikely that the complete array detects several photons per period it is also unlikely that several detectors of the array will detect a photon in one signal period. This is the basic idea behind multi-detector TCSPC. Although several detectors are *active simultaneously they are unlikely to deliver a photon pulse in the same signal period*. The times of the photons detected in all detectors can therefore be measured in a single TAC [32, 36, 46].

The principle is illustrated in Fig. 28. The photons of all detectors are combined into a common timing pulse line. Simultaneously, a detector number signal is generated that indicates in which of the detectors a particular photon was detected. The combined photon pulses are sent through the normal time measurement procedure of the TCSPC device. The detector numbers are used as a channel (or routing) signal for multi-dimensional TCSPC, routing the photons from the individual detectors into different waveform memory sections.

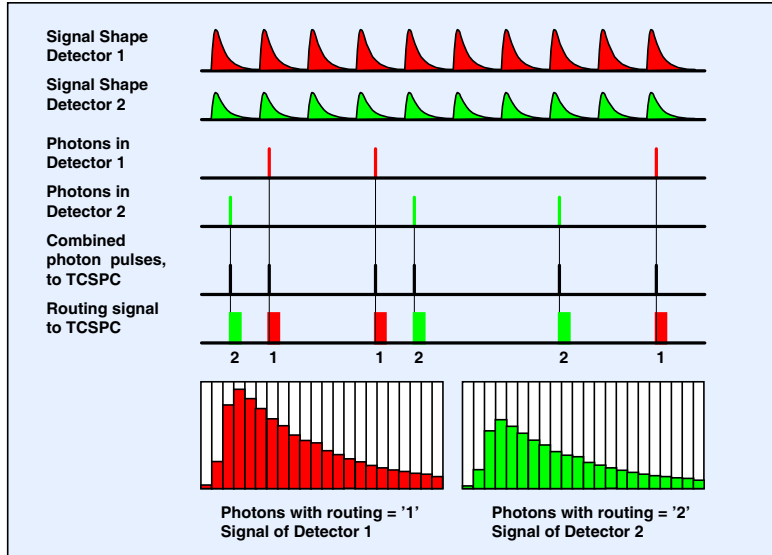


Fig. 28: Principle of TCSPC multi-detector operation. The photon pulses from both detectors are combined, and the times of the pulses are measured in a single TAC. A routing signal indicates which of the detectors detected the current photon. The TCSPC module uses the routing signal to store the photons from different detectors into different memory blocks.

Routing was already used in classic NIM-based TCSPC setups [54, 55, 336]. Each of the detectors had its own CFD. The CFD output pulses were combined into one common TAC stop signal, and controlled the destination memory block in the MCA. Because separate CFDs were used for the detectors, the number of detector channels was limited.

The modern implementation uses a single CFD for all detector channels. A ‘router’ combines the single-photon pulses into one common timing pulse line, and generates a channel signal that indicates at which of the detectors the current photon arrived [32, 36, 46].

A block diagram of the router is shown in Fig. 29. The routing module consists of a number of amplifiers, A_1 through A_n , connected to discriminators, D_1 through D_n , a digital encoder circuit, and a summing amplifier, A_s . The amplifiers, A_1 through A_n , amplify the single-photon pulses of the detectors, typically to several hundred mV. When a detector detects a photon, the corresponding discriminator responds and the subsequent encoder generates a channel byte that indicates which detector detected the photon. Simultaneously, the photon pulse propagates through the summing amplifier, A_s , and appears at the photon pulse output of the routing module.

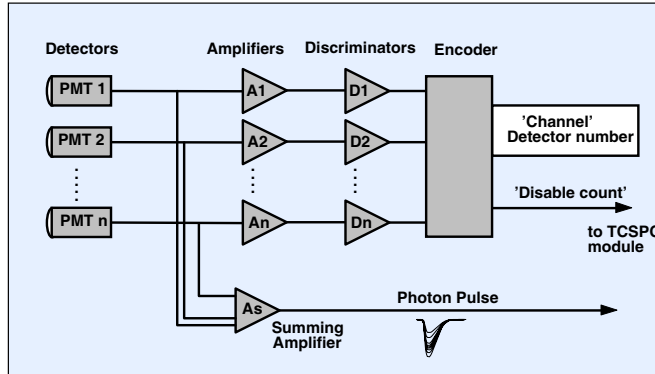


Fig. 29: Routing module for multi-detector TCSPC. For each photon, the routing module delivers the photon pulse and a ‘channel’ signal that indicates in which detector the photon was detected.

The function of the router is based on the assumption that the detection of several photons in *different* detectors within the response time of the amplifiers and discriminators is unlikely. The detection of several photons is, however, not impossible. The encoder is unable to deliver a valid routing information for such events. It does, however, easily detect them. It delivers then a ‘disable count’ signal, which suppresses the recording of the event in the TCSPC module. Because simultaneous recording of several photons is more likely to happen in different detectors than in one a multidetector setup reduces pile-up effects (see section ‘Pile-Up Effects’, page 133).

Fig. 30 shows how the router works in concert with the TCSPC module. The CFD of the TCSPC module receives the single-photon pulse from the router, i.e. the amplified pulse of the detector that detected the photon. When the CFD detects this pulse, it starts a normal time measurement sequence for the detected photon. Furthermore, the output pulse of the CFD loads the ‘channel’ information from the router into the channel register. The latched channel information is used as an additional dimension in the recording process. In other words, it controls the memory block in which the photon is stored. Thus, in the TCSPC memory separate photon distributions for the individual detectors build up. In the simplest case, these photon distributions are single waveforms. However, if the sequencer is used, the photon distributions of the individual detectors can be multidimensional themselves.

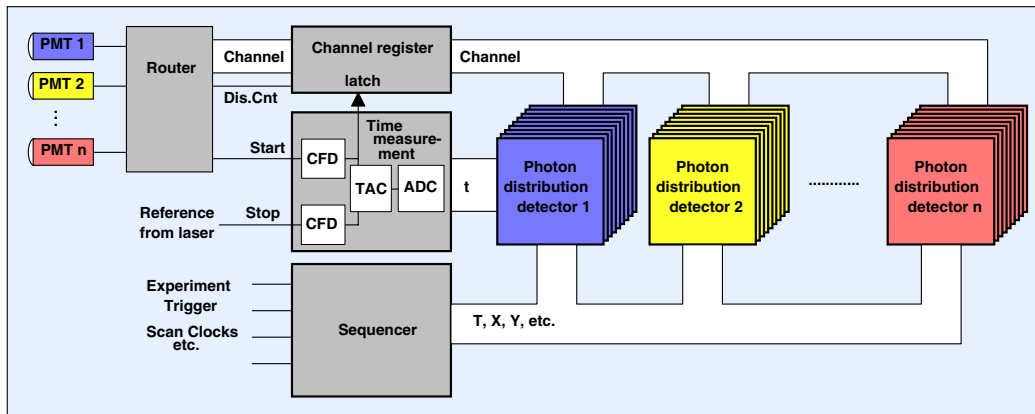


Fig. 30: TCSPC multidetector operation. By the ‘channel signal’ from the router, the photons of the individual detectors are routed into separate memory blocks.

In practice the noise sets a limit to the number of individual PMTs that can be connected to a router. The cables connecting the PMTs to the router must be matched with 50 Ohm resistors. Even with a near-perfect summing amplifier, the noise from the matching resistors would be added to the output signal. Even worse is noise from the environment picked up by the detectors. While resistor noise adds quadratically, noise from the environment is more or less in phase for all detectors and therefore adds linearly. In practice, no more than eight individual PMTs are connected to one routing device.

A higher number of channels can be obtained if a multi-anode PMT is used. In a multi-anode PMT the photon pulses of all channels can be derived from the last dynode. The combination of the pulses works therefore without introducing noise. Using this method, devices with 32 channels and even 64 channels appear feasible. In practice the number of channels is limited mainly by the power dissipation of the routing electronics. Routers for multi-anode PMTs are combined with the PMT tube into a common detector housing. TCSPC multichannel detector heads are currently available for 16 channels [18].

It should be pointed out that the multidetector technique does not use any detector switching or multiplexing. Thus the multi-detector technique can considerably improve the counting efficiency of a TCSPC system. This is especially the case if a fluorescence signal has to be

recorded with spectral resolution. With a single detector several measurements have to be performed one after another, usually by scanning the spectrum by a monochromator. Most of the photons emitted by the sample are then lost. In a multidetector TCSPC system the signals of all wavelength intervals are detected simultaneously and loss of photons is avoided.

Of course, the multidetector technique does not increase the maximum count rate (or the throughput rate) of a TCSPC system. In any TCSPC device there is a small but noticeable loss of photons due to the ‘dead time’ of the processing electronics. The dead time of the bh TCSPC devices is of the order of 100 ns, and for count rates above 1 MHz the counting loss becomes noticeable (see ‘Counting Loss’, page 131). The counting loss for a multi-detector TCSPC system is the same as for a single detector system operated at the total count rate of the detectors of a multi-detector system.

An important and sometimes confusing feature of the multi-detector technique is that the relative counting loss is the same for all channels, independent of the distribution of the rates over the detectors. The reason is that the photons detected by all detectors are processed by the same TCSPC channel so that the counting loss depends on the *overall* count rate. However, the photons appear randomly in the particular detector channels. Therefore the dead time caused by a detection event in one detector on average causes the same relative loss for *all* detector channels. At first glance this behaviour may be considered a drawback. However, in practice it is often rather a benefit because the intensity ratios of the particular detection channels remain unaffected by the counting loss. The intensity ratio is often more important than the absolute intensity.

The multi-detector technique was first implemented in 1993 in the SPC-300 module of Becker & Hickl [32]. Although an amazingly efficient and versatile technique, it was first used widely only when diffuse optical tomography (DOT) began to require a large number of time-resolved detection channels [261, 262]. Typical applications of the multidetector technique are diffuse optical tomography, time-resolved laser scanning microscopy, combined fluorescence cross correlation and fluorescence lifetime experiments, single molecule spectroscopy, and multi-spectral measurement of transient fluorescence lifetime effects.

An alternative to the multi-detector technique is parallel operation of several independent TCSPC channels, which increases the total counting capability at the expense of higher system cost. Please see ‘Multi-Module TCSPC Systems’, page 33.

Multiplexed TCSPC

The routing capability of TCSPC can be used to multiplex several light signals and record them quasi-simultaneously. The principle of multiplexed TCSPC is shown in Fig. 31.

Several optical signals are multiplexed on the microsecond or millisecond time scale. Multiplexing of signals can be accomplished by switching several diode lasers, either electronically or by fibre switches, or by rotating elements in an optical system. The channel signal indicates the current state of the multiplexing in the optical system. Consequently, the photons of the different signals are routed into separate photon distributions.

In most applications fast multiplexing has advantages over consecutive recording of the same signals. One advantage is that sequential recording by the sequencer can still be used at a time scale longer than the multiplexing period. Moreover, slow changes in the sample have the same effect on all multiplexed signals.

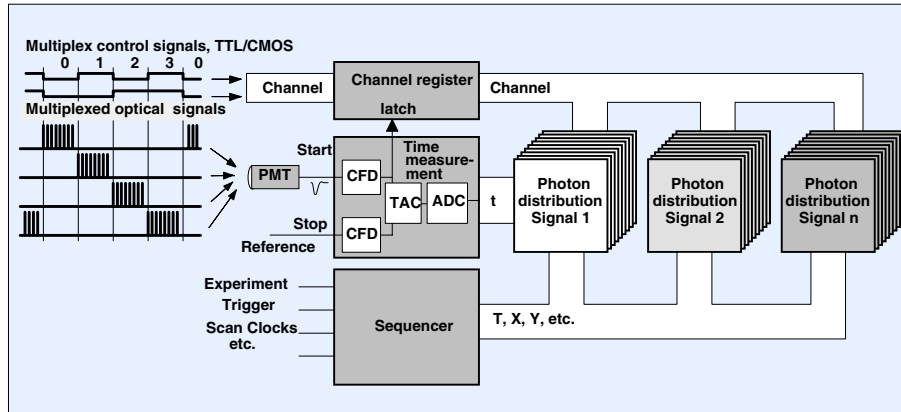


Fig. 31: Multiplexed TCSPC operation. Several signals are actively multiplexed into the detector. The destination in the TCSPC memory is controlled by a multiplexing signal at the ‘channel’ input.

Multiplexing has some similarities to multi-detector operation. However, multiplexing is controlled by a determinate signal from some kind of experimental control device. Moreover, multiplexing usually switches between the signals at a rate much lower than the pulse repetition rate. Consequently, the photons of one signal are recorded for a large number of signal periods before the system switches to the next signal. Multi-detector operation, on the other hand, is random. The destination of a photon in the memory is controlled by a property of the photon itself, e.g. its wavelength or angle of polarisation. Therefore multiplexing can be combined with multi-detector operation. In this case a number of channel-register bits are used for the detector channel information delivered by the router. Other channel bits are used for multiplexing. A multiplexed multi-detector system records the photon distribution over the time in the signal period, the detector channel number, the multiplex-channel number, and one or two additional coordinates determined by the sequencer. The result can be interpreted as a sequence of photon distributions for all combinations of detector and multiplexing channels.

An important application of multiplexed multi-detector systems is diffuse optical tomography (DOT). In DOT several picosecond diode lasers are multiplexed into the input of a fibre switch. The multiplexed lasers are switched consecutively into a large number of optical fibres which deliver the light to the sample. The diffusely transmitted light is recorded by a large number of detectors at different locations at the sample (see ‘Diffuse Optical Tomography’, page 187).

Multiplexed multi-detector systems can also be used to obtain fluorescence decay curves simultaneously for several excitation and several emission wavelengths, see ‘Chlorophyll Transients’, page 158.

Sequential Recording

Sequential recording, also known as ‘double kinetic mode’ [47] or ‘time-lapse recording’, adds one or two additional dimensions to the photon distributions recorded by multi-detector operation and multiplexing. Controlled by its internal clock oscillator, the sequencer switches through a specified number of memory blocks. Each memory block contains the photon distributions of all detectors and multiplexing channels. Sequential recording in a multi-detector system is illustrated in Fig. 32. For sake of simplicity, multiplexing has been omitted.

The sequence may be started by a simple operator command. However, in practice what is to be recorded is usually the response of the investigated system to a stimulation event. The stimulation can be a strong laser pulse, a temperature jump, a change in an electric field applied across the sample, or the switch-on of the excitation source. The recording is then better started by a trigger pulse that coincides with the stimulation. After being started, the sequencer

steps through a defined (usually large) number of memory blocks. Each block contains a full photon distribution over the time in the signal period, t , several detector channels, and (not shown in Fig. 32) several multiplexing channels.

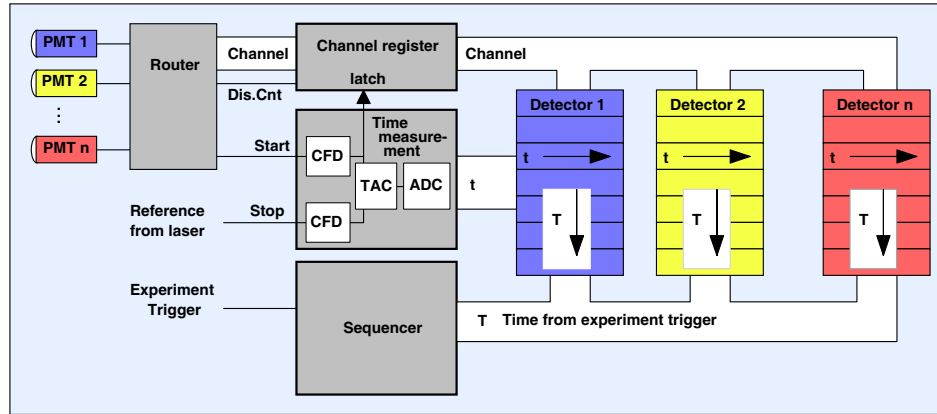


Fig. 32: Sequential recording. Triggered by the experiment trigger, the sequencer switches through a large number of memory blocks. Each block contains the photon distribution over the time in the signal period, t , and over the detector channels.

If the stimulation of the system under investigation is repeatable a large number of triggered sequences can be accumulated. With accumulation, a sufficient number of photons per step is obtained even for sequencing rates faster than the count rate. Because the sequence is controlled by the TCSPC hardware, it is possible to achieve extremely fast and accurate stepping, down to less than a microsecond per data block. Of course, sequential recording can also be achieved by software control of a TCSPC device, and advanced TCSPC devices in fact include operating modes for recording software-controlled sequences. However, modern computers are far from being real-time systems. Stepping faster than 100 ms per step becomes inaccurate, which makes an accumulation of software-controlled sequences impossible.

In some bh TCSPC devices a ‘Continuous Flow’ mode is implemented to record a virtually unlimited number of waveforms. The sequencer of the continuous-flow mode uses two independent data memory banks; see Fig. 33.

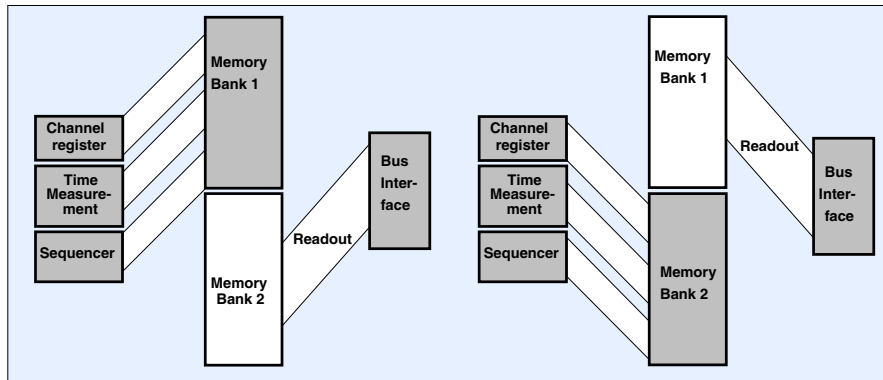


Fig. 33: Unlimited sequential recording by memory bank swapping. When one memory bank is full, the sequencer swaps the banks. While the sequencer writes into one bank, the other bank is read by the computer

After a trigger pulse or a start command by the operator, the sequence starts in the first memory bank. The sequencer switches through the memory blocks of the current bank. Again, each memory block provides space for a full photon distribution versus the time in the signal period, and the detector and multiplexing channel numbers. When the current memory bank is full, the sequencer swaps the memory banks and continues recording. While the measurement

is running in one memory bank, the results of the other bank are read and stored to the hard disk. Thus, a virtually unlimited number of decay curves can be recorded without any time gaps between subsequent steps of the sequence [33].

The 'Continuous Flow' was introduced 1996 with the SPC-430 modules of bh. It was originally developed for DNA analysis and single-molecule detection in a capillary gel electrophoresis setup [33]. Now it is increasingly used for dynamic brain imaging by diffuse optical tomography (DOT) techniques [230, 231, 232], see 'Diffuse Optical Tomography', page 187. The continuous flow mode can be used with a trigger signal that starts either the recording of each bank or the recording of each data block within the current bank. The continuous flow mode, with bank or data block triggering, is therefore also an efficient and convenient technique for slow-scan systems. Trigger pulses from the scanning device synchronise the recording with the scanning, and the data are continuously read from the TCSPC module without stopping the scan.

TCSPC Scanning Techniques

In conjunction with an external optical scanner, the sequencer of the multi-dimensional TCSPC technique can be used to acquire time-resolved images [35, 40, 46, 115]. The principle is shown in Fig. 34.

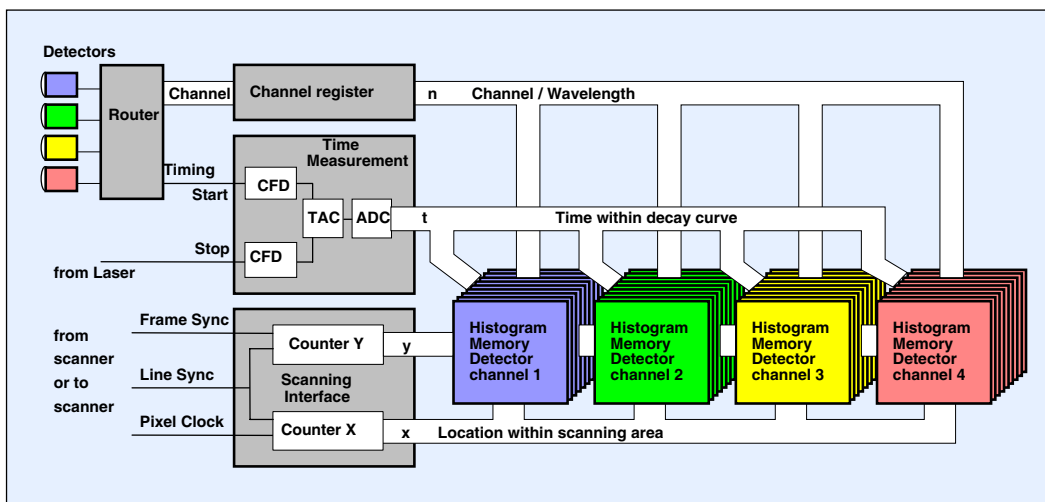


Fig. 34: Image acquisition by synchronising the recording with an external scanner. Data acquisition is synchronised with the scanning via the frame clock, line clock, and pixel clock pulses. For each detector, a stack of images for consecutive times in the laser pulse sequence is built up.

The sequencer is configured as a scanning interface. It contains two counters, X,Y, for the x and y location in the scanning area. Synchronously with the scanning action, the sequencer counts through x and y. Synchronisation is achieved by the scan clock pulses, frame clock, line clock, and pixel clock. The sequencer can work either in an active mode, i.e. control a scanner, or in a passive mode, i.e. be controlled from a free-running scanner.

In the active mode the sequencer runs a time-controlled sequence through the pixels and lines of the image, and sends the frame clock, line clock, and pixel clock pulses to the scanner. The active mode is called 'Scan Sync Out' and is often used for slow-scan imaging in conjunction with piezo scan stages. It is available in the SPC-730, SPC-830, SPC-140, SPC-150 modules and in the SPC-144 and SPC-154 four-channel packages. Another active mode, called 'Scan XY OUT' sends digital position signals to a scanner. The Scan XY OUT mode is available only in the SPC-700/730 modules.

In the passive mode the sequencer receives the clock pulses from the scanner. The passive imaging mode of the sequencer is called ‘Scan Sync In’ mode. It is available in the SPC-730, SPC-830, SPC-140, and SPC-144 modules. The pixel clock is used as the clock for the X counter, the line clock as the clock for the Y counter. The X counter is reset by the line clock, the Y counter by the frame clock. The practical implementation of the scanning interface includes additional prescalers for pixel and line binning, and additional counter control logic for recording selectable parts of a scan area, see ‘Scan Sync In Mode’, page 273.

Both the Scan-Sync-Out and the Scan-Sync-In mode can be combined with multi-detector operation and multiplexing. The maximum size of the image and the number of detector and multiplexing channels depend on the memory space in the TCSPC module.

The Scan-Sync-In mode has become a standard fluorescence lifetime imaging (FLIM) technique in confocal and two-photon laser scanning microscopes [20, 21, 22, 35, 38, 40, 60, 115, 124, 201]. These microscopes use optical beam scanning with pixel dwell times in the microsecond range and below. Several individual detectors or channels of a multi-anode PMT detect the fluorescence in different wavelength intervals.

In the typical applications the pixel dwell time is on the order of a few microseconds. The pixel rate is then higher than the photon count rate. This makes the recording process more or less random. When a photon is detected, the TCSPC device measures the time of the photon in the laser pulse period, t , and determines the detector channel number, n , (i.e. the wavelength, λ , of the photon) and the current beam position, x and y , in the scanning area. These data are used to build up the photon distribution over t , λ , x , and y . The recording is continued over as many frames as necessary to obtain the desired number of photons per pixel.

As shown in Fig. 34, the result can be interpreted as a number of data blocks for different wavelength, each containing a stack of images for different times in the laser pulse sequence.

Of course, the Scan Sync In mode is not restricted to confocal and two-photon laser scanning microscopy or high-speed scanning. Due to the simple interfacing with the scanner, it can be used for other scanning applications as well [315].

Time-Tag Recording

The ‘Time-Tag’ or ‘FIFO’ mode does not build up photon distributions but stores information about each individual photon. For each photon, the time in the signal period, the channel word, and the time from the start of the experiment, or ‘macro time,’ is stored in a first-in-first-out (FIFO) buffer. During the measurement the FIFO is continuously read, and the photon data are stored in the main memory or on the hard disc of a computer.

The structure of a TCSPC device in the time-tag mode is shown in Fig. 35. It contains the channel register, the time-measurement block, a ‘macro time’ clock, and the FIFO buffer for a large number of photons. It has some similarity to the multi-dimensional TCSPC described in the paragraphs above. In fact, most bh TCSPC modules have both the photon distribution and the time-tag mode implemented, and the configuration can be changed by a software command, see ‘FIFO Mode’, page 281. The sequencer then turns into the macro-time clock, and the memory turns into the FIFO buffer.

When a photon is detected, the ‘micro time’ in the signal period is measured by the time-measurement block. Simultaneously the detector channel number for the current photon and often a number of additional bits from external experiment control devices are written into the channel register. The ‘macro time’ clock delivers the time of the photon from the start of the experiment. All these data are written into the FIFO.

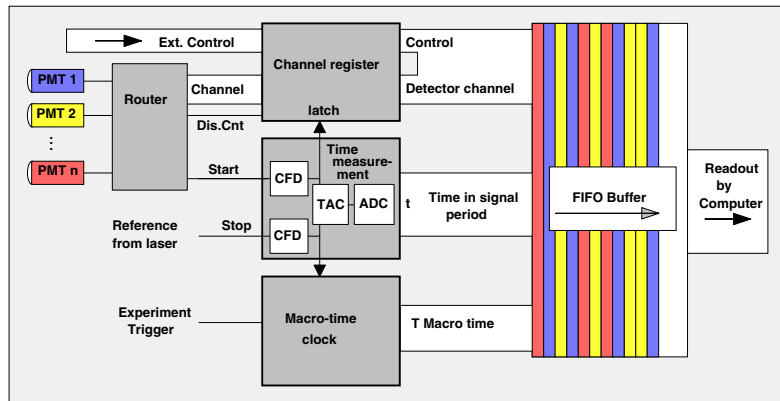


Fig. 35: Architecture of a TCSPC module in the FIFO mode

The output of the FIFO is continuously read by the computer. Consequently, the time-tag mode delivers a continuous and virtually unlimited stream of photon data. It is, of course, imperative that the computer reads the photon data at a rate higher than the average photon count rate. However, modern operation systems are multi-task systems, and it is unlikely that the computer reads the FIFO continuously. Moreover, in typical applications bursts of photons appear on a background of relatively moderate count rate. Therefore the FIFO has to be large enough to buffer the photon data for a sufficient time. In the bh SPC modules FIFO sizes of 64,000 to 8 million photons are used, see ‘Specification’, page 355.

The macro time clock can be started by an external experiment trigger or by a start-measurement command from the operating software. In the SPC-830, SPC-130/134, SPC-140/144 and SPC-150/154 modules the clock signal source of the macro time clock can be selected. The macro time clock can be an internal quartz oscillator, an external clock source, or the reference signal from the laser. Triggering and external clock synchronisation are mandatory for multi-module operation in the time-tag mode, see ‘Fluorescence Correlation down to Picoseconds’, page 211.

In principle, many of the multi-dimensional recording problems described above can also be solved in the time-tag mode. Synchronisation with the experiment can be accomplished via the experiment trigger, the macro time clock, and additional experiment control bits read into the channel register. Transitions of synchronisation pulses transitions from a scanner can be inserted directly, i.e. without an accociated photon, in the data stream (see ‘FIFO Imaging Mode’, page 285). The drawback of the time-tag mode is the large amount of data that has to be transferred into the computer and processed or stored. A single photon typically consumes four or six bytes. A single FLIM or DOT recording may deliver 10^8 to 10^9 photons, resulting in several gigabytes of data. At high count rates the bus transfer rate into the computer may be still sufficient, but the computer may be unable to simultaneously process the data or write them to the hard disc. The transfer rate problem is even more severe for multi-module systems.

The benefit of the time-tag mode is that it delivers absolute photon times. The time-tag mode has therefore become a standard tool of single-molecule spectroscopy. Based on the same time-tag data, combined fluorescence correlation / lifetime spectroscopy (FCS) [43, 45, 127], fluorescence intensity distribution and lifetime analysis (FIDA and FILDA), or the burst-integrated fluorescence lifetime (BIFL) analysis [121, 287] can be performed. The techniques are described on page 222 and page 219, respectively.

The time-tag mode in conjunction with multi-detector capability and MHz counting capability was introduced in 1996 with the SPC-431 and SPC-432 modules of Becker & Hickl. Its large

potential in single molecule spectroscopy began to attract attention only when sufficiently fast computers with large memories and hard discs became available.

Multi-Module TCSPC Systems

The maximum count rate of a single TCSPC channel is limited not only by the counting loss due to the ‘dead time’ of the TCSPC channel, but also by pile-up effects and the counting capability of the detector.

Compared with classic systems, the dead time of advanced TCSPC systems has been considerably reduced. It is however, still on the order of 100 to 150 ns. The fraction of photons lost in the dead time - the ‘counting loss’ - becomes noticeable at detector count rates higher than 10% of the reciprocal dead time (see ‘Counting Loss’, page 131).

Pile-up is caused by the detection of a second photon within one signal period. Because a second photon is more likely to be detected in the later part of a signal period, pile-up causes a distortion of the signal shape (see ‘Classic Pile-Up’, page 133). The pile-up distortion is smaller than commonly believed (see Fig. 144, page 134), and reasonable results can be obtained up to a detector count rate of 10 to 20% of the signal repetition rate. Nevertheless, pile-up sets a limit to the applicable count rate.

The third limitation, the counting capability of the detector, depends on the detector type used, the voltage divider design, and the requirements for IRF stability, long-term gain stability, and detector lifetime. For conventional PMTs the practical limit for TCSPC is of the order of 5 to 10 MHz. For MCP-PMTs the maximum count rate is 200 kHz to 2 MHz, depending on the MCP gain used.

Because of pile-up and detector effects, a breakthrough in the counting capability of TCSPC cannot be achieved by simply making the signal processing electronics of the TCSPC device faster.

The solution to the count-rate problem is multi-module operation. Splitting the light into several detectors connected to independent TCSPC modules proportionally increases the counting capability. Of course, multi-module operation also increases the system cost and can cause space and power supply problems in the host computer. These problems have at least partially been solved with the SPC-134, SPC-144 and SPC-154 four-channel packages of bh. The SPC-134 and SPC-144 packages are shown in Fig. 36.



Fig. 36: Packages of four fully parallel TCSPC channels. SPC-134 (left), SPC-144 (middle) and SPC-154 (right)

With a dead time of 100 ns per TCSPC channel, the total saturated count rate is 40 MHz and useful count rates on the order of 20 MHz can be achieved. All four channels can be used for multi-detector operation. The high count rate and the high number of channels make multi-module TCSPC systems exceptionally useful for diffuse optical tomography [36, 230, 231]

and high count rate applications in laser scanning microscopy [41]. Details are described under ‘Diffuse Optical Tomography’ and ‘Time-Resolved Laser Scanning Microscopy’.

Another application of multi-module systems is in correlation spectroscopy of single molecules. If the photons detected in different detectors are recorded in different modules, the minimum correlation time is no longer limited by the dead time. By synchronising the macro-time clocks of the modules, a correlation down to the macro time clock period is possible. By including the TAC time (micro-time) in the correlation continuous correlation functions from the picosecond to the millisecond scale can be achieved [127], see ‘Fluorescence Correlation down to Picoseconds’, page 211.

Architecture of the bh TCSPC Modules

General Principle

The bh SPC modules contain all the building blocks of TCSPC on a single PCI-compatible PC board. The general principle of the modules is shown in Fig. 37.

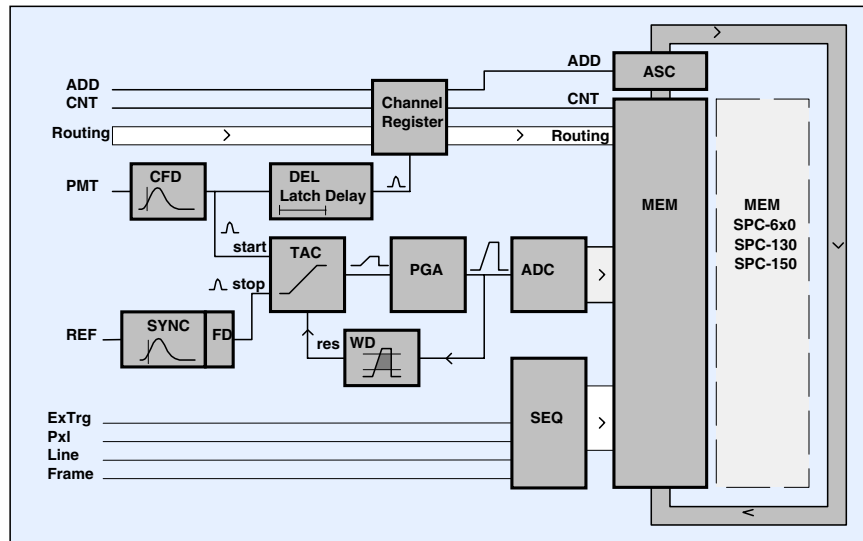


Fig. 37: General principle of the bh TCSPC modules

CFD and SYNC circuits

TCSPC is based on the measurement of the time differences between the single-photon pulses from a detector (or from a number of detectors) and reference pulses. For fluorescence decay measurements the reference pulses are derived from the excitation pulse sequence; in photon correlation experiments the reference pulses are single-photon pulses from a second detector. Accurate time measurement means accurate triggering on the single-photon pulses of the detectors and the reference pulses from the light source. Unfortunately, these pulses are far from being stable. The single-photon pulses have a considerable amplitude jitter due to the random amplification mechanism in the detectors (see Fig. 20, page 15), and the pulse amplitude of the light source may change due to intensity fluctuations. A simple leading edge discriminator cannot be used to trigger on such pulses. The amplitude jitter would introduce a timing jitter of the order of the pulse rise time (Fig. 38, left).

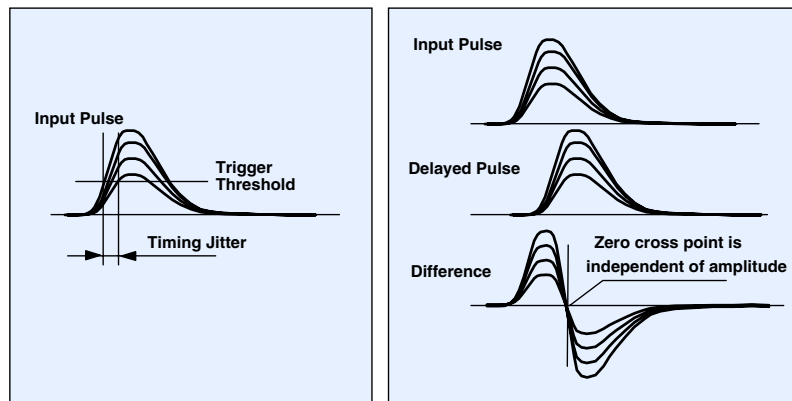


Fig. 38: Leading-edge triggering (left) and constant-fraction triggering (right)

Therefore constant-fraction discriminators (CFDs) are used both at the detector and at the reference input. A CFD triggers at a constant fraction of the pulse amplitude, thus avoiding pulse-height-induced timing jitter. Constant-fraction triggering is achieved by triggering on the zero cross point of the sum of the input pulse and the delayed and inverted input pulse, see Fig. 38, right. Since the temporal position of the crossover point is independent of the pulse amplitude, this timing method minimises the time jitter caused by the amplitude jitter of the detector pulses. Furthermore, the CFD contains a discriminator that rejects input pulses smaller than a selectable discriminator threshold (SPC-x3x) or outside a selected amplitude window (SPC-x0x). The threshold or the amplitude window are adjusted to reject noise from the environment, noise from preamplifiers or small background pulses from the detector.

The general architecture of both CFDs is the same. However, the CFD in the SYNC channel has a selectable frequency divider. Controlled by the software, the internal SYNC frequency can be reduced by a factor of 1...16, see SYNC Parameters, page 292. With the divider set to ratios greater than one several periods of the light signal are recorded. Recording several periods is used to record signals of high repetition rates and to check the time-calibration of a TCSPC module.

TAC

The time-to-amplitude converter, TAC, measures the time of a detected photon from the pulse at the detector input to the next pulse at the reference input. This 'reversed start-stop' method is the key to process high photon count rates at high pulse repetition rates. It reduces the speed requirements to the TAC because its working cycle (start-stop-reset) has to be performed only at the photon detection rate instead of the considerably higher pulse repetition rate, see Fig. 26, page 21.

When the TAC is started by a pulse at the start input, it generates a linear ramp voltage until a stop pulse appears at the stop input. Thus the TAC generates an output voltage depending linearly on the temporal position of the photon. The TAC output voltage is fed to the programmable gain amplifier, PGA. The PGA is used to stretch a selectable part of the TAC characteristic over the complete measurement time window. To increase the effective count rate at high PGA gains, the output voltage of the PGA is checked by the window discriminator WD which rejects the processing of events outside the time window of interest. For details of the TACs of the bh SPC modules, see 'Detailed Description of Building Blocks', page 42.

ADC

The analog-digital converter, ADC, converts the amplified TAC signal into the address of the memory, MEM. The challenge of the analog-to-digital conversion is that it has work with an extremely high accuracy. The ADC has to resolve the TAC signal into 4096 time channels, and the width of the particular channels must be equal within 1% or better. ADC chips are usually specified by a 'non-missing code accuracy' which defines the number of bits for which the ADC characteristic is still monotonous. 12-bit conversion with a channel uniformity of 1% requires a non-missing code accuracy of 19 bits. Although ADCs with such a high accuracy exist, they are far too slow for TCSPC applications. Therefore, in the early TCSPC systems, the ADC was the bottleneck both in terms of speed and channel uniformity.

The breakthrough was achieved by an error correction technique introduced by bh in 1993. The technique is based on a modified 'dithering' process [31, 33, 36]. By adding an auxiliary signal to the ADC input and subtracting the digital equivalent of it from the ADC output the non-uniformity of the ADC channels is averaged out. Thus, an ADC with 12 bit non-missing code accuracy is sufficient to convert the TAC signal. 12-bit ADCs are available with high

speed so that the ADC does not longer limit the available count rate of the TCSPC module. The error correction is described under ‘Analog-to-Digital Conversion’, page 48.

Channel Register

The channel register receives the ‘channel’ data used for multi-detector operation and multiplexing (see also Fig. 28 and Fig. 29). Except for the SPC-130 and SPC-134, the channel data are loaded into the channel register with an adjustable delay. The delay is used for multi-detector operation with an external router. It takes the router a few 10 ns to encode the channel data word. Thus, the channel signal arrives at the TCSPC module after the single-photon pulse. The ‘latch delay’ compensates for the delay in the router and loads the channel data within the time interval when the router delivers a valid channel data word.

Sequencer

The sequencer generates address bits for one or two additional dimensions of the recording process. The sequencer is a block of counters which are driven either by an internal clock signal, by a signal derived from the synchronisation signal of the TCSPC module, or by a number of clock or trigger signals from the external experiment setup. Depending on the clock signals used and on the number and configurations of the counters the sequencer can generate different information:

In the sequential recording modes the sequencer data word is the time from the start of the experiment or the number of experiment trigger pulses received at the ‘experiment trigger’ input. In the scan modes, the sequencer delivers the X and Y coordinates for the currently detected photon. In the FIFO mode the sequencer is used as a ‘Macro Time Clock’. It delivers the Macro Time, i.e. the time from the start of the experiment for the time tagging of the individual photons. Details of the sequencer function are described below under ‘Memory Control’.

Memory Control

In the photon distribution modes the memory of the TCSPC module is used to add the individual photons in a memory location according to the time in the signal period, the detector channel number, the time from the start of the experiment, or other coordinates delivered by the sequencer. In the time-tag (or FIFO) modes the memory buffers the corresponding data for the individual photons. The structure of the memory and the way it is controlled is thus different for different operation modes of the TCSPC module.

Different modules differ considerably in memory size. Moreover, the available range of the ADC resolution, i.e. number of time channels per waveform block, is different. Some values for the number of available waveform blocks are given in the table below.

ADC resolution, channels	Number of waveform blocks (curves) in the device memory				
	SPC-6	SPC-7	SPC-130	SPC-140	SPC-150
4096	64	1024	32	1024	1024
256	1024	16384	512	16384	16384
16	--	--		262,144	262,144
1	--	--		4,194,304	4,194,304
					16,777,216

To get an overview about the number of available waveform channels, detector channels, multiplexing channels, or pixels of a scan we recommend to load the SPCM operating software (available from www.becker-hickl.com) and check the available combinations. Please see ‘Software Installation’, page 79.

Recording of single curves

In the simplest case the SPC module is used as a conventional one-dimensional TCSPC device. Although the architecture shown in Fig. 37 is used the channel data word is ignored, and the sequencer delivers a constant address offset from the beginning of the memory. When a photon is detected the ADC delivers an address proportional to the time of the photon in the signal period. The addressed memory location is read, the data word is incremented in the addition/subtraction circuit, ASC, and the result is written back into the same memory location. After the detection of many photons the waveform of the light signal, e.g. a fluorescence decay curve, is built up.

The adder/subtractor delivers an overflow signal when the memory contents of the addressed memory location has reached a maximum of 65535 counts. In this moment the measurement can be stopped automatically ('stop on overflow' function).

The incrementation of the memory contents can be done by any number from 1 to 255. Of course, count increments greater than one do not improve the sensitivity of a measurement. Values >1 are, however, useful to vary the number of photons for which a 'stop on overflow' is obtained. Different recordings can thus be normalised at their maxima.

By changing the address offset from the sequencer by software, a large number of 'pages' in the memory are available. Consequently, several signals can be recorded one after another and the results be held in different pages of the memory.

Multi-Detector Operation

The addressing of the memory for multi-detector operation is shown in Fig. 39. The router delivers a channel signal that indicates which of the detectors detected the current photon. The detector channel number is loaded into the channel register of the TCSPC device. When a photon is added into the memory the bits of the channel data word are used as higher address bits of the memory address. Thus the memory provides space for as many waveforms as there are detectors. The memory location within one waveform block is determined by the ADC data word, i.e. by the time of the photon in the signal period. The waveform block is determined by the bits in the channel register, i.e. by the number of the detector that detected this photon.

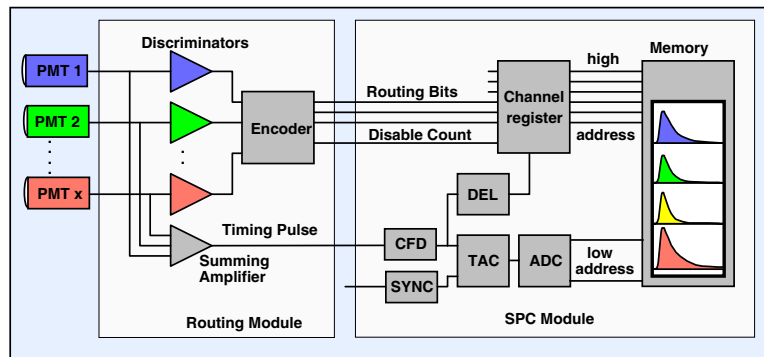


Fig. 39: Memory addressing for multidetector operation

The number of channel bits that are loaded into the channel register can be defined by the parameters 'routing channels x' and 'routing channels y'. Together with the parameter 'ADC resolution' these parameters are used to automatically configure the memory into the right number of waveform blocks and time channels.

Because the discriminators and the encoder of the router need 10 to 20 ns to deliver a valid detector channel number the loading of the data into the channel register must be delayed. The

delay is adjustable by the parameter ‘Delay’, see ‘Page Control’, page 298. The delay of the higher address bits does not conflict with the memory access as long as the delay is shorter than the conversion time in the TAC and the ADC. Only for latch delays greater than 100 ns the memory access is delayed. Because this reduces the maximum count rate unnecessarily large latch delays should be avoided.

At high count rates the probability of detecting several photons in different detector channels within the response time of the router cannot be neglected. Of course, the router is unable to deliver a valid channel data word in this case. It does, however, detect such multi-photon events and activates the ‘disable count’ signal. The ‘disable count’ bit is loaded together with the channel data word. When ‘disable count’ is active the storing of the corresponding photon in the memory is suppressed.

Multiplexed TCSPC

Multiplexing works in the same way as routing. However, the channel bits come from external experiment control electronics. The most frequent application is multiplexing of several diode lasers see ‘Chlorophyll Transients’, page 158, and ‘Diffuse Optical Tomography’, page 187. The channel bits then indicate which of the lasers is active. Multiplexing can, however, also be used for multiplexing several detection light paths (see Fig. 166) or to record photons into a large number of waveform blocks depending on the state of an externally measured signal (see ‘Barrier Discharges’, page 226).

Most of the bh TCSPC modules have 7 or more channel bits. Multiplexing can therefore be used in combination with multi-detector operation. Normally the lower channel bits are used for the detector number from the router, the higher bits for the multiplexing signal.

Sequential Recording

As routing and multiplexing, sequential recording uses higher address bits of the memory. However, for sequential recording these bits are generated by an internal logic block, the sequencer. The number of bits (or accessible memory blocks) is not limited by the number of externally available routing bit lines. The only limitation is the number of address bits of the memory, i.e. the memory size. Within reasonable limits, sequential recording can therefore be combined with multi-detector operation and multiplexing. For sequential recording the sequencer switches through a defined number of subsequent data blocks of the memory. One data block can be a single waveform, a number of waveforms for different detectors, or a number of waveform blocks for multiplexed signals.

Because the switching through the memory blocks is strictly hardware-controlled an extremely accurate sequence is obtained. The start of the sequence can be triggered by an external ‘experiment trigger’. The trigger is normally used to synchronise the start of the sequence with a stimulation event. Triggered sequential recording can be combined with accumulation, i.e. a large number of sequential recording cycles is performed and the data of the individual waveform, routing, or multiplexing data blocks are accumulated. Triggered accumulation does not require a large number of photons to be recorded within a single step of a sequence. It works even at count rates lower than the step rate of the sequence. The recording then becomes a random process, i.e. a detected photon is stored in a memory location according to its time in the signal period, its detector channel, and the current state of the data word delivered by the sequencer. The recording is continued until the desired number of photons per time channel of the waveform has been accumulated. Consequently, triggered sequences can be recorded with times down to about one microsecond per step (see ‘Transient Fluorescence Phenomena’, page 158).

Sequential recording can also be obtained by triggering the individual steps of the sequence. Step triggering is used to synchronise the recording with an experiment control device, i.e. a scan stage or a monochromator drive.

A number of different sequential modes are available in the bh TCSPC modules. The SPC-630, SPC-130/134 and SPC-150/154 have the ‘Continuous Flow’ mode implemented which can be used to record virtually unlimited sequences (see paragraph below).

Special cases of sequential recording are the ‘Scan Sync In’ and ‘Scan Sync Out’ modes of the SPC-730, -830 and SPC-140/144 and -150/154 modules. These modes are actually designed to scan images with fast optical scanners. They can, however, also be used for sequential recording (see ‘Sequential Recording in the Scan Sync Out mode’, page 272).

Continuous Flow Mode

In the SPC-600/630, SPC-130/134 and SPC-150/154 modules a ‘Continuous Flow’ mode is implemented. The mode is designed for sequential recording of a virtually unlimited number of waveforms, or routing/multiplexing blocks. The Continuous Flow mode makes use of the two independent memory banks which are implemented in the SPC-6, SPC-130 and SPC-150 modules.

Subsequent waveforms or waveform blocks are measured in intervals of ‘Collection Time’. The measurement is repeated while the sequencer switches through all memory blocks of one memory bank. When one bank is full the sequencer swaps the memory banks. While the measurement is running in one memory bank, the results of the other bank are read and stored to the hard disk. Thus, a virtually unlimited number of decay curves can be recorded without any time gaps between subsequent curves. The principle is illustrated in Fig. 33, page 29.

The continuous flow mode can also be used with a limited number of sequencer steps. If the number of steps is smaller than the number of waveform blocks of one memory bank the mode can be used for triggered accumulation of a fast sequence.

Scan Modes

In the Scan modes the TCSPC module records the photons into a large two-dimensional array of waveform blocks. A waveform block may contain a single waveform, or a number of waveforms for different detector or multiplexing channels. Each waveform block represents a pixel of the image. The sequencer controls the higher address bits of the memory and thus addresses the individual pixels of the image. Moreover, the sequencer synchronises the recording with the action of an external scanner. The sequencer can be used to control the scanner actively (‘Scan Sync Out’ or ‘Scan XY Out’ modes), or the scanner can be used to control the sequencer (‘Scan Sync In’ mode). Fig. 40 shows how the sequencer switches through the pixels of the image.

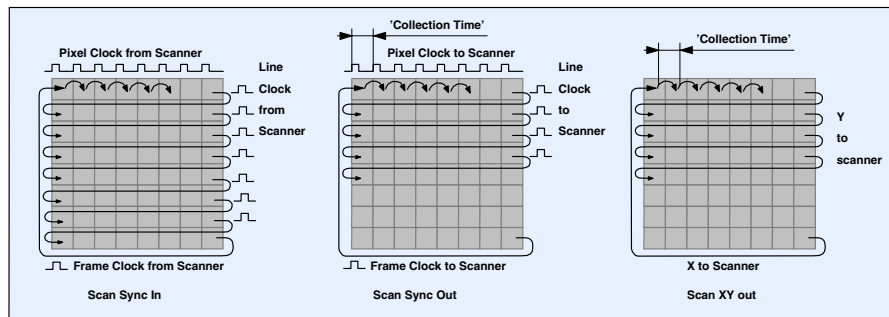


Fig. 40: Sequencer operation in the scan modes. Left: Scan Sync In, Middle: Scan Sync Out, Right: Scan XY Out

In the Scan Sync In mode the sequencer receives scan clock pulses from a scanner. A ‘pixel clock’ sets the waveform block address to the next pixel, a ‘line clock’ pulse to the beginning of the next line, and a ‘frame clock’ pulse to the first pixel of the frame. The pixel dwell time is determined by the scanner. The measurement is started by an operator command or by an experiment trigger pulse. The measurement is stopped after the specified ‘collection time’ has elapsed or the measurement is stopped by the operator. Thus, any number of frames of a repetitive scan can be accumulated.

Dynamic effects in galvanometer mirrors often preclude reasonable recording in the first pixels after a frame or a line flyback. These pixels can therefore be excluded from being recorded by two additional counters. The excluded pixels are defined by the system parameters ‘upper boarder’ and ‘left boarder’.

In the Scan Sync Out mode the sequencer controls the scanner. The pixel dwell time is specified by the parameter ‘collection time’. After each collection time interval the sequencer proceeds to the next waveform block address and sends a pixel clock pulse to the scanner. When the scanner receives this pulse it proceeds to the next pixel. At the end of a line the sequencer sends a line clock pulse which causes the scanner to return to the beginning of the next line. When a frame is completed the sequencer sends a frame clock, which resets the scanner to the first pixel of the image. The number of pixels per line and the number of lines per frame is defined by the system parameters ‘Scan pixels X’ and ‘Scan Pixels Y’. Dynamic effects in the scanner can be reduced by defining a ‘flyback x’ and a ‘flyback y’ time.

The Scan XY Out mode is available only in the SPC-700/730. It is similar to the Scan Sync Out mode except for the scanner control. Instead of sending clock pulses to the scanner the sequencer sends complete data words of the X and Y position. The Scan XY out mode is an easy way to control a scanner. However, the number of pixels is limited by the number of available output lines for the X and Y bits. The largest image is therefore 128 by 128 pixels.

CNT and ADD Control

Additional control over the measurement is possible by the signals CNT and ADD. CNT is a ‘Count Enable’ signal, i.e. a photon is stored only if CNT is ‘1’ in the moment of its detection. The CNT signal is used to suppress photons for which no valid routing information is provided or to confine the recording to externally controlled time intervals.

The ADD signal controls whether a photon is added or subtracted. This allows the user to combine the TCSPC recording with a digital lock-in technique. By using an optical system with light choppers or rotating sector mirrors background or scattering signals can be suppressed [30] (see also ‘Lock-in TCSPC’, page 157).

All external control signals are read via the ‘Channel’ register. The signals are latched at an adjustable delay time after the start pulse. By adjusting this delay it can be assured that every photon be processed with the correct state of the control signals.

Time-Tag (FIFO) Mode

The Time-Tag, or FIFO Mode is used to record information about each individual photon. The mode is available in the SPC-660/630, SPC-830, SPC-130/134, and SPC-140/144 modules. The principle is shown in Fig. 35, page 32. The sequencer delivers the time from the start of the recording, and the memory is configured as a FIFO (first-in-first-out) buffer. For each photon the time in the pulse period (measured by the TAC and the ADC), the time from the start of the recording (delivered by the sequencer), and the channel data word (usually delivered by a router) are stored into the FIFO.

At the output, the FIFO memory is continuously read by the software. The data are written into a buffer in the main memory of the computer and then to the hard disc. Due to the buffering in the FIFO of the SPC module it is not required that the computer reads the data continuously. Even strong bursts of photons can be detected with the maximum count rate of the SPC module as long as the number of photons in the burst does not exceed the size of the FIFO.

For photon numbers larger than the FIFO size but smaller than the size of the buffer in the computer memory the maximum average count rate is determined by the rate the computer is able to read the FIFO. However, if the buffer in the computer memory runs full the count rate is limited by the hard disc speed. The effective rate of the hard disc does not only depend on the hard disc itself but also on background activities and the way the operating system handles the hard disc. Although modern hard discs are very fast the hard disc can limit the average count rate. Some typical values are given in the table below.

Module Type, ADC resolution	FIFO size (photons)	Burst Rate (saturated, photons)	Continuous Rate FIFO to memory (photons)	Continuous Rate FIFO to Hard Disc (photons)
SPC-600/630, ADC Resolution 12bit	$128 \cdot 10^3$	$8 \cdot 10^6 \text{ s}^{-1}$	$400 \cdot 10^3 \text{ s}^{-1}$	$300 \cdot 10^3 \text{ s}^{-1}$
SPC-600/630, ADC Resolution 8 bit	$256 \cdot 10^3$	$8 \cdot 10^6 \text{ s}^{-1}$	$600 \cdot 10^3 \text{ s}^{-1}$	$500 \cdot 10^3 \text{ s}^{-1}$
SPC-830	$8.3 \cdot 10^6$	$8 \cdot 10^6 \text{ s}^{-1}$	$3.5 \cdot 10^6 \text{ s}^{-1}$	$1 \cdot 10^6 \text{ s}^{-1}$
SPC-130	$256 \cdot 10^3$	$10 \cdot 10^6 \text{ s}^{-1}$	$1 \cdot 10^6 \text{ s}^{-1}$	$800 \cdot 10^3 \text{ s}^{-1}$
SPC-140	$2.05 \cdot 10^6$	$10 \cdot 10^6 \text{ s}^{-1}$	$1.5 \cdot 10^6 \text{ s}^{-1}$	$800 \cdot 10^3 \text{ s}^{-1}$
SPC-150	$2.05 \cdot 10^6$	$10 \cdot 10^6 \text{ s}^{-1}$	$4 \cdot 10^6 \text{ s}^{-1}$	$1 \cdot 10^6 \text{ s}^{-1}$

Detailed Description of Building Blocks

CFD in the Detector (Start) Channel

SPC-x00 Versions

The -00 SPC versions have been discontinued in 1999 and replaced with the faster -30 versions. Nevertheless, a large number of -00 SPCs are still in use, and a description of the -00 CFDs appears indicated. The principle of the CFD in the detector (start) channel of the SPC-x00 versions is shown in Fig. 41.

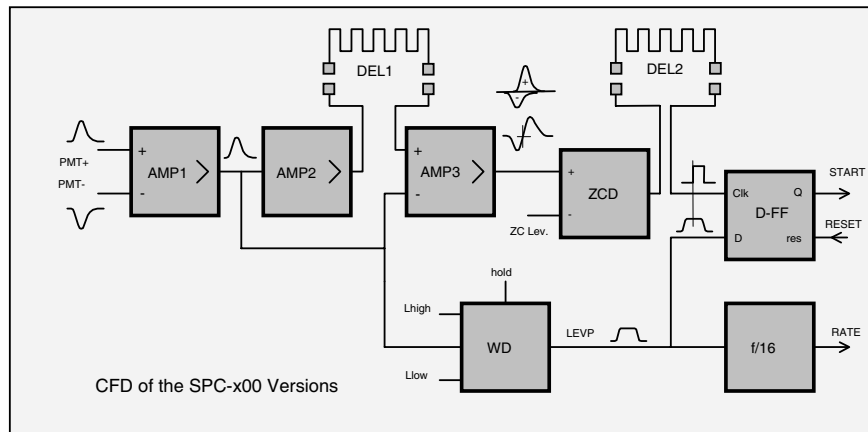


Fig. 41: Principle of the CFD in the detector (start) channel of the SPC-x00 versions

Depending on the polarity of the detector signal, the input pulses are fed to the ‘plus’ or ‘minus’ input of a amplifier, AMP1. The output pulse of AMP1 is fed through another amplifier, AMP2, and a delay line, DEL1, into the negative input of a third amplifier, AMP3. AMP3 generates the difference of the signal from AMP1 and the delayed signal from AMP2. The result is a bipolar pulse which is negative at the beginning, than crosses the baseline and be-

comes positive. The position of the zero cross point does (as long as the amplifiers are in the linear range) not depend on the amplitude of the input pulses.

The zero cross discriminator, ZCD, converts the baseline transition into a pulse edge of a logical (ECL) signal. The zero cross level is adjusted by the reference voltage, 'ZC level', to compensate small DC offsets in the circuit.

A window discriminator, WD, checks the pulse amplitude at the output of AMP1. WD switches its output voltage to 'High' when the lower threshold (CFD limit low) is exceeded. If the amplitude exceeds the upper threshold (CFD limit High) WD switches back to the 'Low' state. Thus WD delivers a 'Level Pulse', LEVP, if the amplitude of the input pulse is in the desired range. The output is switched back to 'Low' after a programmable time, 'CFD Hold'. Please see 'CFD Parameters', page 292.

The LEVP pulse is used to drive the D input of an ultra-fast ECL flip-flop. The clock of the flip-flop is the delayed zero cross pulse from the zero cross trigger ZCT. The flip-flop is set if the rising edge of this pulse is inside the LEVP pulse. Thus the flip-flop is triggered by the zero cross of input pulses that are inside the desired amplitude range. The flip-flop is reset by the TAC when the processing of the current photon pulse is finished.

To measure the count rate in the CFD the frequency divider, f/16, is used. The frequency division is necessary because the subsequent counter/timer circuits are not able to count short pulses as they appear inside the CFD. The frequency divider counts the pulses on the LEVP line. Therefore, the CFD count rate represents the all pulses with amplitudes greater than 'CFD Limit Low'.

The delay lines DEL1 and DEL2 are exchangeable to adapt the CFD to various detectors. DEL1 serves for zero cross shaping. The sum of the delay through DEL1 and the internal delay in AMP2 should be about the rise time of the detector pulses. The internal delay is 0.6...0.8ns; therefore a zero-delay of DEL1 is adequate for fast detectors with rise times below 0.8ns (please see also 'Configuring the CFD and SYNC Inputs').

The second delay line, DEL2, shifts the rising edge of the zero cross pulse into the level pulse, LEVP. Normally the internal delay is sufficient for this purpose, so that DEL2 can be zero. An additional delay is needed only if a detector with a long rise time is used with a short DEL1. In this (unusual) case the zero cross pulse must be shifted to a time after the pulse maximum at the output of AMP1.

SPC-x30 Versions

The CFDs of the SPC-x30 versions are designed for maximum time resolution. The amplifiers of the SPC-x00 CFD were omitted to achieve maximum signal speed at the input of the zero-cross trigger and to reduce the influence of amplifier noise and amplifier nonlinearities. The -30 CFDs require negative input pulses. The required pulse amplitudes are slightly higher than for the -00 CFDs. In the majority of applications this do not cause major problems. PMTs and MCP PMTs deliver negative pulses, and the use of a preamplifier for these detectors is recommended already by detector safety and lifetime considerations. Positive pulses are delivered by a number of actively quenched single-photon avalanche photodiodes (SPADs). The pulses of these detectors can easily be inverted by a passive pulse inverter (A-PPI pulse inverter, Fig. 18). A possible loss in pulse risetime by the inverter has no influence on the timing jitter because the pulses of actively quenched SPADs are free of amplitude jitter. A block diagram of the CFD in the detector channel of the SPC-x30 versions is shown in Fig. 42.

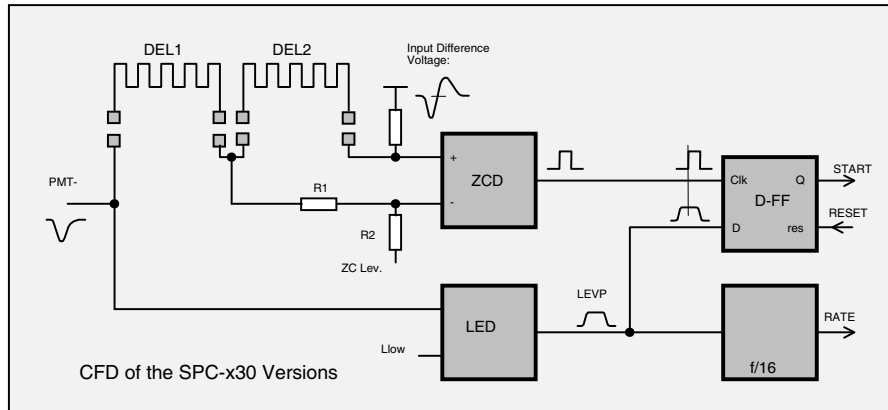


Fig. 42: Principle of the CFD in the detector (start) channel of the -30 SPC versions

The input signal is fed via two delay lines, DEL1 and DEL2, to the positive input of the zero cross discriminator, ZCD. The negative input gets the same signal, but with less delay and a smaller amplitude. The effective difference voltage at the input of ZCD is a bipolar pulse which is negative at the beginning, than crosses the baseline and becomes positive. The temporal position of the zero transition does not depend on the amplitude of the input pulse. The zero cross discriminator picks off the zero cross point and converts it into a positive edge of an ECL (emitter coupled logic) signal. To minimise the timing jitter for a particular detector the delay lines can be replaced and the reference level of the ZCD adjusted (see ‘Configuring the CFD and SYNC Inputs’, page 118).

The amplitude of the input pulses is checked by a leading-edge discriminator, LED. The reference level of the leading edge discriminator is adjustable, see ‘CFD Parameters’, page 292. If the amplitude exceeds the threshold, Llow, the discriminator responds and its output voltage switches to the ‘high’ state. The resulting pulse is used as a D input of the ultra-fast ECL D flip-flop. When a positive edge from ZCT appears inside a pulse from CMP, the D flip-flop is set and a ‘start’ signal for the TAC is generated. The D flip-flop is reset when the conversion in the TAC is finished.

To measure the count rate in the CFD the frequency divider f/16 is used. The frequency division is necessary because the width of the pulses at the output of LED can be as short as 1 ns and the frequency as high as a few 100 MHz. The subsequent counter/timer circuits are not fast enough to count these pulses reliably. Please note that the count rate signal is derived from the leading-edge discriminator, LED. Consequently, the count rate refers to the number of detector pulses which exceed the LED threshold, not to the pulses which caused a zero transition.

CFD in the Synchronisation (Stop) Channel

SPC-x00 Versions

The -00 SPC versions have been discontinued in 1999 and replaced with the faster -30 versions. Nevertheless, a large number of -00 SPCs are still in use; therefore a description of the -00 SYNC circuits appears indicated. The principle of the CFD in the synchronisation (stop) channel of the SPC-x00 versions is shown in Fig. 43.

Depending on the polarity the pulses of the synchronisation detector are fed to the positive or negative input of an amplifier, AMP1. The output pulse of AMP1 is fed through another amplifier, AMP2, and a delay line, DEL1, into the minus input of a third amplifier, AMP3. AMP3 generates the difference of the signal from AMP1 and the delayed signal from AMP2. The result is a bipolar pulse which is negative at the beginning, than crosses the baseline and

becomes positive. The temporal position of the zero transition does (as long as the amplifiers are in the linear range) not depend on the amplitude of the input pulse. The delay line can be replaced to optimise the timing for different input pulse shapes, see ‘Configuring the CFD and SYNC Inputs’, page 118.

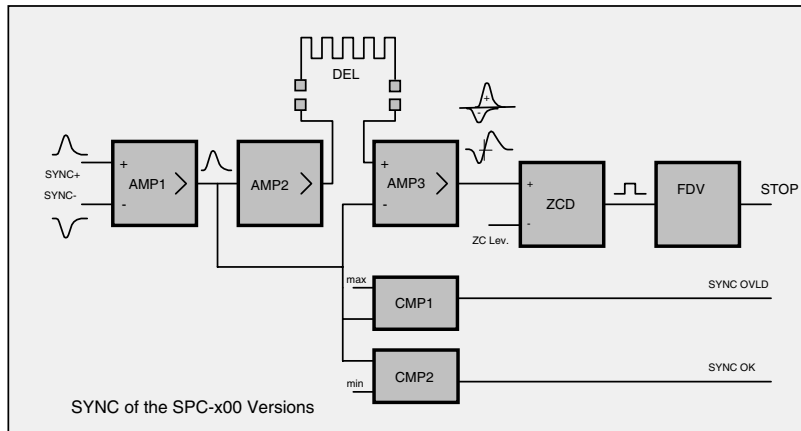


Fig. 43: Principle of the CFD in the synchronisation (stop) channel of the SPC-x00

The zero cross discriminator, ZCD, converts the zero transition into an ECL pulse. The zero cross level can be adjusted by the reference voltage of ZCD to compensate for small DC offsets in the circuit and to minimise the timing jitter. The duration of the pulse is adjustable by the 'SYNC Holdoff' control voltage. 'SYNC Holdoff' is set to a value that allows triggering at the normal SYNC frequency, but suppresses multiple triggering due to ringing or reflections.

The pulse from the zero-cross discriminator, ZCD, is fed into a frequency divider, FDV. The divider ratio can be selected from 1 to 16, see ‘SYNC Parameters’, page 292. The divider ratio determines the number of signal periods recorded.

The output signal of AMP3 is checked by the comparators CMP1 and CMP2. If the amplitude is in the optimum range, CMP1 switches on and the signal 'SYNC OK' becomes active. If the amplitude is too high, CMP2 switches on and 'SYNC OVLD' becomes active.

The delay line, DEL, is exchangeable to adapt the CFD to the pulse shape of the synchronisation pulses. The sum of the delay through DEL1 and the internal delay in AMP2 should be about the rise time of the input pulses. The internal delay is 0.6 to 0.8 ns; therefore a zero-delay line for DEL is adequate for pulse rise times below 0.8 ns. Please see ‘Configuring the CFD and SYNC Inputs’, page 118.

SPC-x30 Versions

The stop (SYNC) CFDs of the SPC-x30 versions are designed for maximum time resolution. The amplifiers of the SPC-x00 CFDs have been omitted to achieve maximum signal speed at the input of the zero cross discriminator. Moreover, a threshold discriminator has been added. The stop channel of the -30 CFDs can therefore be connected to a second PMT in the photon counting mode. Thus, the -30 SPCs can be used for photon correlation experiments with two PMTs in a Hanbury-Brown-Twiss setup [127, 159], see Fig. 218, page 204. As the CFD in the start channel, the -30 stop CFD requires negative input pulses. As described for the start channel, this does not cause major problems in practical setups. A block diagram of the SPC-x30 CFD in the synchronisation (stop) channel is shown in Fig. 44.

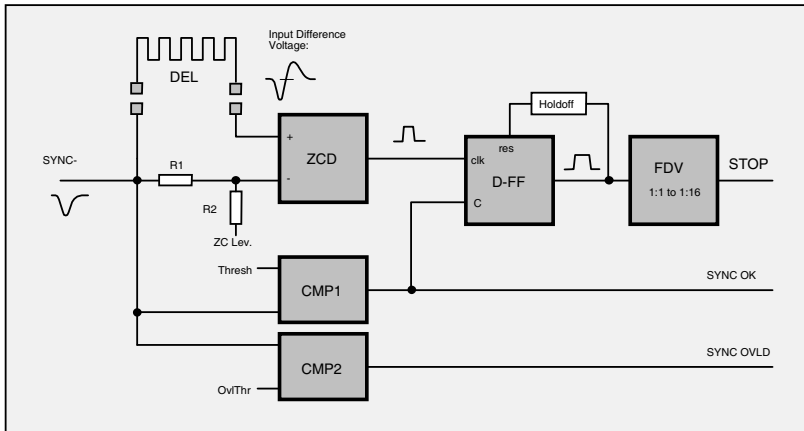


Fig. 44: Principle of the CFD in the synchronisation (stop) channel of the SPC-x30

The input signal is fed via the delay line DEL to the positive input of the zero cross discriminator, ZCD. The negative input gets the same signal, but without delay and with a smaller amplitude. The effective difference voltage at the input of ZCD is a bipolar pulse which is negative at the beginning, than crosses the baseline and becomes positive. The temporal position of the zero transition does not depend on the amplitude of the input pulse. The delay line can be replaced to optimise the timing for different input pulse shapes, (see ‘Configuring the CFD and SYNC Inputs’, page 118). The zero cross comparator picks off the baseline transition and converts it into a positive edge of an ECL signal.

The amplitude of the input pulses is checked by two comparators, CMP1 and CMP2. If the amplitude exceeds a defined threshold (see ‘SYNC Parameters’, page 292), CMP1 responds and delivers a ‘high’ pulse for a few ns. This pulse is used as a D input of the ultra-fast ECL D flip-flop. When a positive edge from ZCT appears inside a pulse from CMP1, the D flip-flop is set and a ‘stop’ signal for the TAC is generated. The flip-flop is reset automatically after the ‘holdoff’ delay.

The output pulses of CMP1 are stretched and used as a ‘SYNC OK’ signal. (Please note that ‘SYNC OK’ means that the stop CFD triggers, but not necessarily that it triggers on the right signal and at the right frequency.) A second comparator, CMP2, switches on if the input amplitude exceeds a fixed maximum value. The pulses are stretched and used to activate a ‘SYNC Overload’ signal.

The pulses from the D flip-flop are fed into a frequency divider, FDV. The divider ratio can be selected from 1 to 16, see ‘SYNC Parameters’, page 292. The divider ratio determines the number of signal periods recorded.

Time-to-Amplitude Converter

The bh TCSPC modules use a TAC (time to amplitude converter) principle to measure the times of the photons. The TAC of the bh modules has been optimised together with the subsequent ADC to obtain high count rates, low differential nonlinearity, and small time channel width. It should be mentioned that there are a number of other time-measurement principles [82, 182, 222] that can be used for TCSPC. Compared with direct time-to-digital conversion (TDC) [82, 182] the circuitry of a TAC/ADC system is relatively complicated. However, the time resolution of a TAC/ADC system is on the order of 1 ps, which is currently about 40 times shorter than for a TDC. The principle of the TAC of the bh TCSPC modules is shown in Fig. 45.

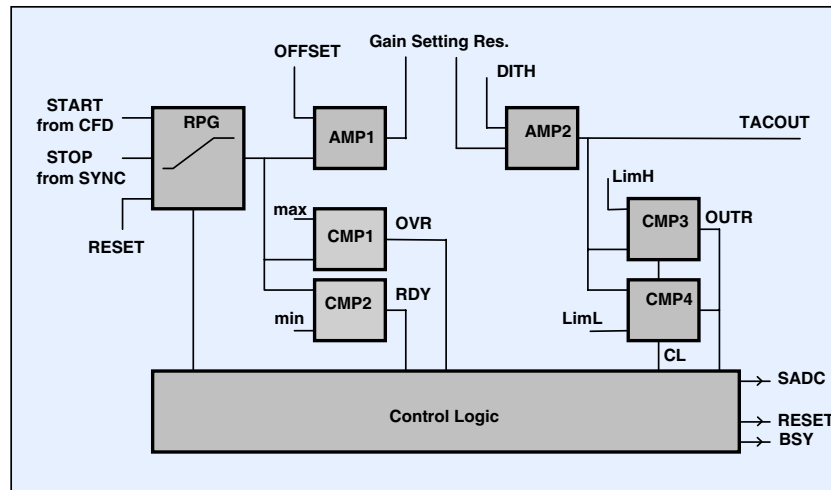


Fig. 45: Principle of the TAC

The TAC contains a linear ramp generator, a biased amplifier with variable gain, several comparators to check the conversion result and the associated control circuitry.

The ramp generator, RPG, is started when a pulse from the CFD in the start channel arrives at the start input of the TAC. Once started, the ramp voltage increases until a stop pulse from the CFD in the stop (Sync) channel arrives at the TAC stop input. After the stop pulse the voltage remains constant until the TAC is reset. The slope of the ramp (and thus the conversion range of the TAC) is variable via the control software, see ‘TAC Parameters’, page 293.

An amplifier, AMP1, adds an adjustable offset voltage to the ramp voltage. A second amplifier, AMP2, has variable gain. The offset and the gain are used to define a smaller conversion time interval within the total range of the ramp generator. Both the offset and the gain of AMP1 are set via the control software, see ‘TAC Parameters’, page 293.

The ‘Dithering’ signal, DITH, is used for the ADC error correction. It shifts the TAC output voltage periodically up and down at the ADC characteristic (see below, ‘ADC Error Correction’).

CMP3 and CMP4 are latched comparators. They check whether the ramp voltage is inside the window selected by ‘TAC Limit L’ to ‘TAC Limit H’ (see ‘TAC Parameters’, page 293). The comparator latch pulse, cl, is generated by the TAC control logic. It is derived from the delayed stop pulse. If the ramp voltage is outside the selected window in the moment of the cl pulse an OUTR (outrange) signal is generated.

If the ramp voltage is inside the selected window (i.e. OUTR not active) the control logic generates the SADC (start ADC) pulse. This pulse starts the ADC and the signal processing in the digital part of the TCSPC module. After about 40 ns the control logic generates a reset signal for the ramp generator. The reset signal remains active until the comparator CMP2 detects the reset of the ramp voltage. The reset signal is also used to reset the CFD.

If the TACOUT amplitude is not inside the selected window the control logic does not generate a SADC pulse but immediately initiates a reset sequence. Thus, no further time is wasted for converting photons with TAC signals outside the selected TAC range.

If the stop pulse from the SYNC does not arrive within the time of the selected TAC range the comparator CMP1 detects an OVR (overrange) condition. To avoid that the TAC is blocked by missing stop pulses the OVR signal initiates a reset sequence.

The bh TCSPC modules have a ‘dead time compensation’ that can (but need not) be used to obtain an intensity-proportional counting result even at extremely high count rates when a substantial fraction of photons is lost in the dead time. The dead-time compensation extends the acquisition time (‘collection time’) by the accumulated dead time during the measurement. To determine the dead time the control logic of the TAC delivers a BSY (‘BUSY’) signal. This signal is used to stop the ‘Collection Time’ timer during the times the TAC is unable to convert a new photon. Thus, the effective collection time increases by the sum of the dead time over the whole measurement, resulting in a linear intensity scale up to count rates on the order of the reciprocal dead time. (See ‘Dead-Time Compensation’, page 132)

The TACs of the SPC-6, -7, and -8 modules differ slightly from the TACs used in the SPC-130/134 and 140/144 modules. The visible difference is that the TAC of the SPC-6, 7 and 8 modules is a module built in hybrid technique while the TACs of the SPC-130/134 and SPC-140/144 are built in standard printed circuit board technique. Moreover, the SPC-1 TACs do not contain the comparators CMP3 and CMP4. Instead, the TAC window is set by comparators in the digital signal processing circuitry of the modules.

Analog-to-Digital Conversion

ADC Error Correction

The high maximum count rate of the bh SPC modules is achieved by a fast flash ADC in conjunction with a proprietary error correction technique [31, 36, 46]. The error correction improves the accuracy of the ADC by several bits without any loss in speed or channel resolution. The error correction is based on a modified ‘Dithering’ process. The technique is essential to the operation of the module. The following description helps to understand the principle of the technique and the side-effects associated with its application.

The AD conversion in the bh modules is based on a modified ‘dithering’ process . Dithering is a technique to enhance the resolution of an ADC by accumulating a large number of samples with a digitally generated noise (the dither signal) added to the input signal. The digital equivalent of the dither signal is later subtracted from the ADC output bytes. In TCSPC the principle of dithering is reversed. The ADC input signal is random, and a determinate dither signal is used. The principle is shown in Fig. 46.

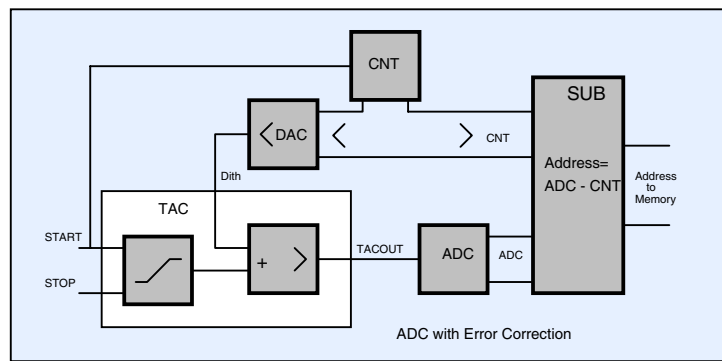


Fig. 46: TAC/ADC principle used in the bh TCSPC modules

A DA converter, DAC, is used to shift the TAC output voltage up and down on the ADC characteristic. The DAC is controlled by a counter that counts the start pulses of the TAC. Consequently the DAC generates a sawtooth voltage that increases by one DAC step at the recording of each photon. The DAC voltage is added to the TAC output voltage. The resulting signal is converted by the ADC. The ADC data word corresponds to the sum of the DAC and

the TAC voltage. To restore the correct address byte for the memory the digital equivalent of the DAC voltage is subtracted from the ADC value in a digital subtraction circuit SUB.

Of course each address byte still contains the unavoidable deviation of the particular ADC step from the correct value. But there is a significant difference to a direct ADC conversion in that the error is now different for different photons - even if these photons appeared at equal times in the signal periods and caused equal TAC voltages. For a large number of photons the non-uniformity of the ADC channels is averaged. The result is that the effective ADC characteristic is smoothed.

For an ideal DAC, the smoothing of the ADC characteristics does not cause any loss in signal detail. In practice, gain and linearity errors of the DAC cause a slight broadening of the recorded signal. The broadening is, however, smaller than 1 or 2 ADC steps or 0.8 to 1.6 ps in the fastest TAC Range, see Fig. 47.

The improvement in conversion accuracy depends on the number of ADC steps, N_{dac} , over which the signal is shifted by the DAC voltage (see system parameter 'Dither Width') and on the distribution of the errors of the ADC characteristic. If there is no correlation between the errors of adjacent ADC step the improvement is $N_{dac}^{1/2}$. However, in practice the errors of flash ADCs are more or less periodical, i.e. near a big ADC step a smaller one occurs and vice versa. In this case the accuracy improvement is considerably larger than $N_{dac}^{1/2}$. In Fig. 47 the differential nonlinearity of an SPC-134 channel is shown for 'Dither Width' = 0 (original ADC characteristics), 'Dither Width' = 1/32 or 7 ADC bits and 1/8 of the conversion range or 9 ADC bits.

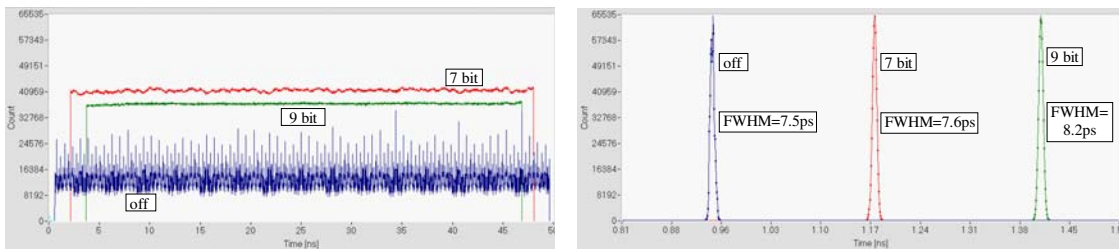


Fig. 47: Left: Unmodulated light recorded without error reduction, and with a counter data width of 7 bit and 9 bit. Right: Corresponding instrument response function of the module (electrical test signal)

The price that has to be paid for the accuracy improvement is that the outer parts of the ADC characteristic cannot be used. The sum of the TAC and the DAC signals is clipped at the ends of the ADC range. The clipped parts are visible as artefacts at both ends of the ADC range. However, except for a few very special applications the loss in conversion range is not essential. With the system parameter 'Dither Width' the shift width can be selected to make an tradeoff between ADC accuracy and useful ADC range.

Variable ADC Resolution

The ADC of all bh SPC modules resolves the TAC voltage into 4096 discrete values. In the photon-distribution modes this yields 4096 time channels per curve. There are, however, applications where such a high number of time channels is not needed. In these cases it is often useful to reduce the number of time channels to decrease the required memory space, to increase the available number of curves or scan pixels in the memory, or to obtain more photons per time channel. Therefore in all bh TSCPC modules a specified number of ADC channels can be combined (binned) into one time channel, see Fig. 48.

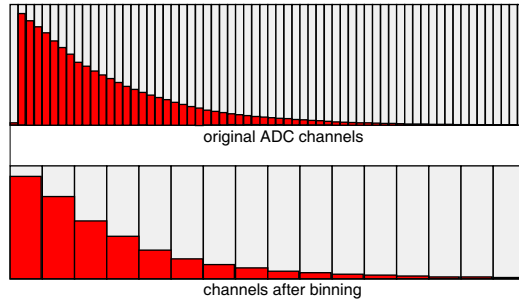


Fig. 48: Variable ADC resolution by binning several ADC channels

All SPC modules can be used with a resolution of 4096, 1024, 256, and 64 time channels. In the SPC-830, SPC-130/134 and SPC-140/144 modules the resolution can further be reduced to 16, 4 and even 1. To work with only one time channel, i.e. discarding the time information at all, may appear useless at first glance. The setting can, however, be used to turn the SPC-830 or SPC-140/144 into extremely sensitive photon counting imagers for scanning applications.

ADC Zoom

Another possibility to reduce the number of time channels is the ‘ADC Zoom’. The ADC zoom feature is implemented in the SPC-830 and the SPC-140/144 modules. It assigns the original ADC channels of a selectable part of the ADC characteristics to a full scale recording with a reduced number of channels. The principle is shown in Fig. 49.

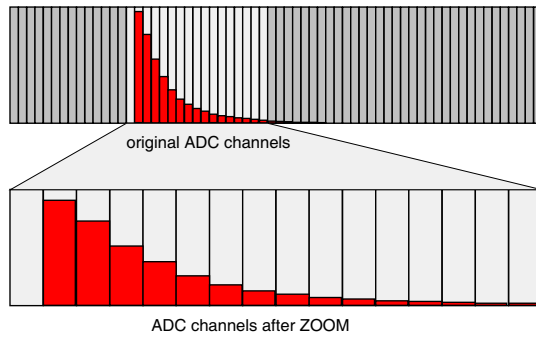


Fig. 49: ADC Zoom

The ADC Zoom feature is useful in imaging and other multi-curve applications if very fast fluorescence decays are recorded with a fast detector. The photons then fill only part of the available conversion range. Zooming this range into a full-scale time axis makes it possible to record a large number of curves (or pixels) at extremely high time resolution.

Detectors for TCSPC

Detectors for photon counting must have sufficient gain to deliver a useful output pulse for a single detected photon. The output pulse must be short enough to resolve the individual photons at high count rate, and the transit time jitter in the detector should be small to achieve a good time resolution. There is wide variety of photomultiplier tubes (PMTs) and photomultiplier modules, and a number of single-photon avalanche photodiode (SPAD) modules that meet these general requirements. However, these devices are far from being ideal photon detectors. Knowledge about the different classes of detectors and their typical performance under practical conditions is therefore important to obtain best results from a TCSPC experiment. The following section gives an introduction into the general principles of detectors and the parameters used to characterise them. Moreover, it describes a number of frequently used detectors and gives advice about selecting the right detector and getting best performance from it.

Detector Principles

The most frequently used detectors for low level detection of light are photomultiplier tubes. A conventional photomultiplier tube (PMT) is a vacuum device which contains a photocathode, a number of dynodes (amplifying stages) and an anode which delivers the output signal [162, 211, 242]. The principle is shown in Fig. 50.

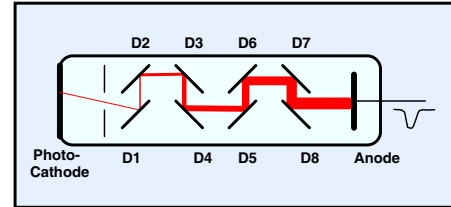


Fig. 50: Principle of a conventional PMT

The operating voltage builds up an electrical field that accelerates the electrons from the photocathode to the first dynode D1, further to the next dynodes, and from D8 to the anode. When a photoelectron hits D1 it releases several secondary electrons. The same happens for the electrons emitted by D1 when they hit D2. The overall gain reaches values of 10^6 to 10^8 . The secondary emission at the dynodes is very fast, therefore the secondary electrons resulting from one photoelectron arrive at the anode within a few ns. Due to the high gain and the short response a single photoelectron yields an easily detectable current pulse at the anode.

A wide variety of dynode geometries has been developed. Some of the designs are in use for more than 50 years [162]. Of special interest for photon counting are the ‘linear focused’ type dynodes, the ‘fine mesh’ and the ‘metal channel’ types [211]. Linear-focused dynodes are designed to obtain similar transit time for different electron trajectories. Thus, linear-focused PMTs have a short transit-time spread and a fast single electron response. A fast response can also be obtained by keeping the pathways of the electrons extremely short. Because fine mesh and metal channel PMTs can be built in extremely small sizes they deliver similar or even faster response than the larger linear focused devices. Moreover, the fine mesh and metal channel design can be combined with an array of anodes to obtain spatial resolution.

A similar gain effect as in the conventional PMTs is achieved in the Channel PMT (Fig. 51, left) and in the Microchannel PMT (Fig. 51, right). These detectors use channels with a resistive coating. A high voltage is applied along the channels. The walls of the channels work as secondary emission targets. The principle can be used in a single macroscopic channel or a microchannel plate (MCP). A microchannel plate contains a large number of channels with a diameter of 3 to 15 μm . Two or three channel plates can be arranged in series to obtain a high gain. Due to the small distance between the photocathode and the first MCP and the small size of the channels the transit time spread of the photoelectrons can be as short as 25 ps [1, 211,

212, 377]. Microchannel PMTs are currently the fastest commercially available single-photon detectors. Moreover, the microchannel plate technique is used to build position-sensitive detectors and image intensifiers.

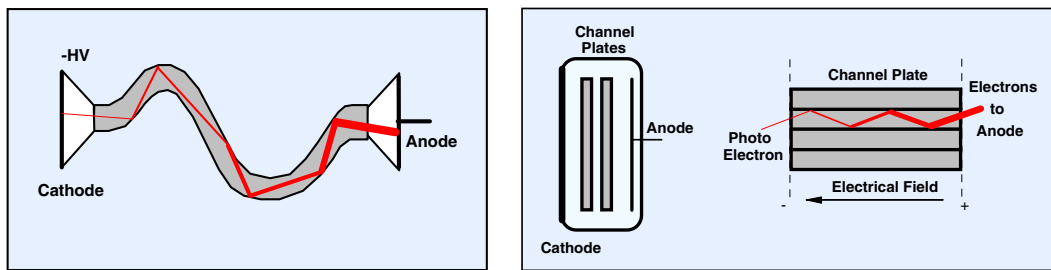


Fig. 51: Channel plate PMT (left) and microchannel PMT (right)

To obtain position sensitivity, the single anode can be replaced with an array of individual anode elements (Fig. 52). By individually detecting the pulses from the anode elements the position of the corresponding photon on the photocathode can be determined. Multi-anode PMTs are particularly interesting in conjunction with the multi-detector capability of the bh TCSPC modules.

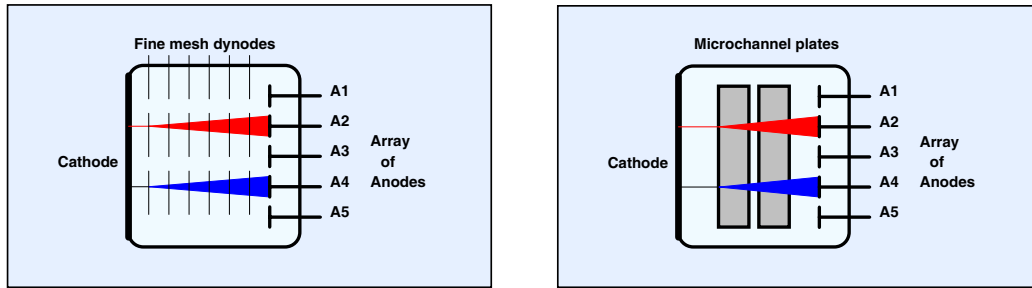


Fig. 52: Multi-anode PMTs for position-sensitive detection. Fine-mesh PMT (left) and MCP-PMT (right)

PMTs use the emission of photoelectrons from a photocathode, i.e. the ‘external photo effect’, as a primary step of detection. The drawback of the external photo effect is that the photoelectrons are emitted in all directions, including back into the photocathode. Therefore the quantum efficiency, i.e. the probability that a photon releases an photoelectron, is smaller than 0.5. The best cathodes reach a quantum efficiency of about 0.4 between 400 and 500 nm [158].

Semiconductor detectors use the ‘internal photo effect’. That means that the photons generate electron-hole pairs inside the semiconductor. Theoretically the internal photo effect works with a quantum efficiency of 1. In practice the quantum efficiency of a good silicon photodiode reaches 0.8 around 800 nm. In photodiodes and photo-conductors an electrical field separates the electrons and holes, so that a photocurrent flows through the device when it is illuminated. Of course, the photocurrent caused by a single electron-hole pair is far too small to be recorded directly. Single photons can therefore be detected only if the semiconductor detector has an internal gain mechanism that does not introduce any thermal noise background. A suitable gain mechanism exists in the ‘avalanche effect’. A photodiode is operated at a reverse voltage so high that the carriers moving through the semiconductor break off new electron-hole pairs from the lattice of the semiconductor material. The avalanche effect is used in standard avalanche photodiodes (APDs) and delivers a stable gain on the order of 10^2 to 10^3 .

A gain of 10^3 is still too low to detect single photons with the time resolution required for TCSPC. Unfortunately, higher gain normally results in instability, i.e. the avalanche becomes self-sustaining and destroys the diode. Nevertheless, photon-induced avalanche breakdown can be used for single photon detection. The reverse voltage of the diode is set several volts above the breakdown voltage. To avoid the avalanche destroying the diode, an active or pas-

sive quenching circuit restores normal operation after each photon [91, 93, 216]. The principle is often termed ‘Geiger mode’, because of the similarity with the Geiger-Müller counter. The principle of a single-photon avalanche photodiode (SPAD) operating in the Geiger mode is shown in Fig. 53.

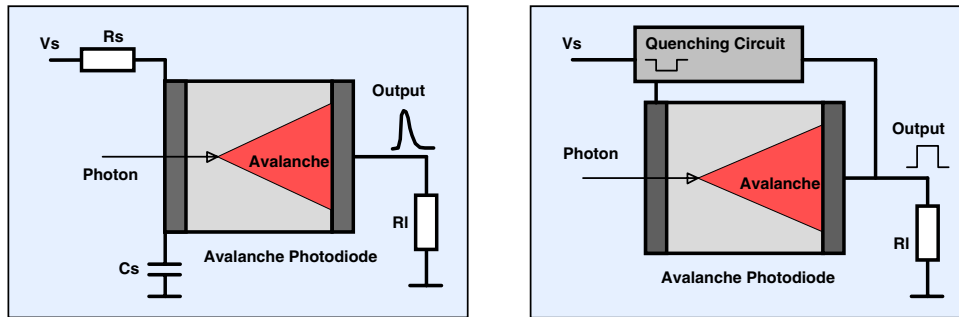


Fig. 53: Single photon avalanche photodiode (SPAD). Left Passive quenching, right active quenching

Passive quenching is obtained by operating the diode via a series resistor, R_s , which is typically a few hundred $k\Omega$. C_s is the stray capacitance of R_s and the diode leads to ground, or an additional capacitor of a few pF. When an avalanche breakdown occurs, C_s is discharged within a time on the order of a nanosecond. The discharge current flows through the diode and the load, producing a correspondingly short output pulse. Simultaneously the voltage across the diode drops below the breakdown voltage and the avalanche stops. The voltage across the diode then increases and eventually reaches the supply voltage. Full recovery of the reverse voltage normally takes several microseconds. Consequently, passive quenching can be used only at count rates far below 1 MHz, and some count-rate dependence of the timing performance and efficiency must be expected.

Active quenching uses an electronic quenching circuit [91, 94, 123, 216]. When a breakdown occurs, the output pulse of the diode triggers the quenching circuit, which reduces the reverse voltage of the diode below the breakdown level for a time of typically 20 to 50 ns. After the quenching pulse the reverse voltage is restored within a few ns, and the diode resumes normal operation. Thus a much higher count rate can be obtained than for passive quenching. Nevertheless, also actively quenched photodiodes often show some count-rate-dependent timing shift and change in efficiency.

APDs suitable for single-photon detection must be free of premature breakdown at the edge of the junction or at local lattice defects. So far, only selected silicon APDs can be operated in the passive or active quenching mode, and only a few SPAD detectors are commercially available [179, 247, 280, 321]. The diameters of active areas are small, typically 20 to 150 μm . For detection in the infrared region the situation is even less favourable. A few TCSPC applications of liquid-nitrogen cooled Ge APDs have been reported [266], but have not resulted in commercially manufactured detectors. InGaAs APDs suffer from strong afterpulsing which has prevented continuous quenched operation so far.

Another problem associated with quenched breakdown operation is light emission from the diode. Light emission can be a problem for correlation experiments and quantum cryptography [213, 356].

Detector Parameters

Gain

The secondary emission coefficient at the dynodes of a PMT depends on the material of the dynodes and the energy of the primary electrons. The gain of a photomultiplier tube therefore changes strongly with the operating voltage. For typical interstage voltages on the order of 100 V the secondary emission coefficient is between 4 and 10 and changes with the 0.7th to 0.8th power of the voltage [162]. For a 10 stage PMT the total gain increases with the 7th or 8th power of the total voltage.

PMTs of the same type but with different cathode materials may differ considerably in gain. The reason is that the cathode material is at least partially involved in the secondary emission process. During the manufacturing process the cathode material spills into the dynode system, with the result that the secondary emission coefficient is changed. Coating the dynodes with the cathode material can even be intentional, because most cathode materials are efficient secondary electron emitters.

High PMT gain is essential for TCSPC applications. A good timing stability can only be obtained if the gain is high enough to obtain single photon amplitudes considerably above the noise of the termination resistor and the subsequent amplifier.

Single Electron Response

The detector output pulse for a single photoelectron is called the ‘Single Electron Response’ or ‘SER’. Some typical SER shapes for PMTs are shown in Fig. 54.

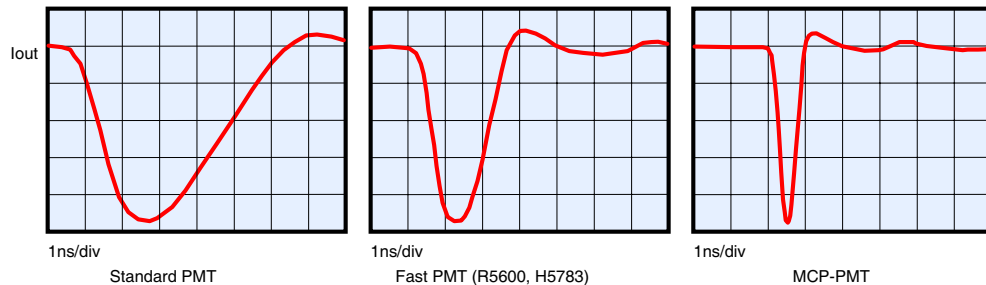


Fig. 54: Single electron response (SER) of different photomultipliers

Due to the random nature of the detector gain, the pulse amplitude varies from pulse to pulse. The pulse-height distribution can be very broad, up to 1:5 to 1:10. The average peak current of the SER is approximately

$$I_{SER} = \frac{G \cdot e}{T_{FWHM}},$$

with G = PMT Gain, $e=1.6 \cdot 10^{-19}$ As, T_{FWHM} = SER pulse width, full width at half maximum. The table below shows some typical values. I_{SER} is the average SER peak current and V_{SER} the average SER peak voltage when the output is terminated with 50Ω . I_{max} is the maximum permitted continuous output current of the PMT.

PMT type	PMT Gain	FWHM	I_{SER}	V_{SER} (50Ω)	I_{max} (cont)
Standard	10^7	5 ns	0.32 mA	16 mV	100uA
Fast PMT	10^7	1.5 ns	1 mA	50 mV	100uA
MCP PMT	10^6	0.36 ns	0.5mA	25 mV	0.1uA

There is one significant conclusion from this table: If the PMT is operated near its full gain the peak current I_{SER} from a single photon is much greater than the maximum continuous output current. Consequently, for steady state operation the PMT delivers a train of random pulses rather than a continuous signal (see also Fig. 20, page 15). Because each pulse represents the detection of an individual photon the pulse density - not the pulse amplitude - is a measure of the light intensity at the cathode of the PMT. Obviously, the pulse density is measured best by counting the PMT pulses within subsequent time intervals. Therefore, photon counting is a logical consequence of the high gain and the high speed of photomultipliers.

Pulse Height Distribution

The secondary emission coefficient at a particular dynode depends on the dynode material and energy of the primary electrons. For typical inter-dynode voltages used in PMTs, the secondary emission coefficient, n , is between 4 and 10. Because the secondary emission is a random process the number of the generated secondary electrons varies from electron to electron. The width of the distribution can be expected at least of the size of the standard deviation, $n^{1/2}$, of a poissonian distribution of the secondary emission coefficient, n . Therefore the single-photon pulses obtained from a PMT have a considerable amplitude jitter. For TCSPC applications it is important that the pulse amplitudes of the majority of the pulses are well above the unavoidable noise background.

Because the gain of a PMT may vary over a wide range, the total width of the distribution may vary for different tubes and different supply voltages. However, despite of the different materials and shapes of the dynodes in different PMTs, the general shape of the distribution is more or less similar.

A pulse amplitude distribution measured for a Hamamatsu H7422P-40 PMT module at different gain is shown in Fig. 55. There is a broad peak at high amplitudes and a secondary peak at low pulse amplitudes. The high amplitude peak contains the regular single-electron pulses. The low-amplitude peak is at least partially related to the light. Its relative height does not appreciably depend on the count rate. It is possibly caused by photoelectrons scattered at the first dynode and reaching the second dynode without amplification. Another source of the small-amplitude peak is photoelectron emission on the first dynode. If the discriminator threshold is set low enough an extremely high peak appears at very low amplitudes. This peak does not originate in the PMT but is caused by electronic noise of the preamplifier and noise pickup from the environment. For some photomultipliers a ‘peak to valley’ ratio is specified, which indicates how much higher the main peak is compared to the valley between the main and the secondary peak.

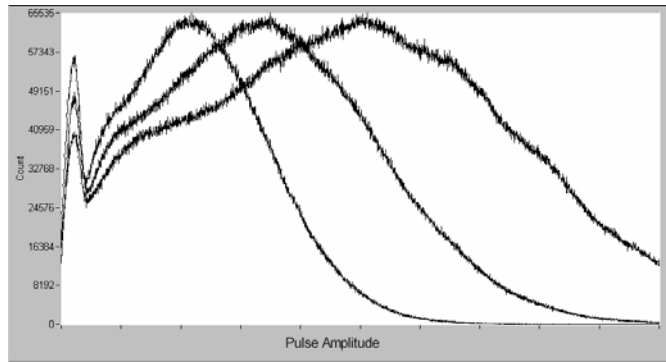


Fig. 55: Pulse amplitude distribution of a H7422P-40 for different gain.

The pulse height distribution at high detector gain often shows a sub-structure (see Fig. 55), probably due to the discrete numbers of secondary electrons emitted at the first dynode.

The shape of the main peak of the amplitude distribution is almost the same for the photon pulses and the dark pulses, see Fig. 56. This is not surprising because the secondary emission process makes no difference between electrons emitted at the cathode thermally or optically. However, the secondary peak at low amplitudes is more pronounced for the dark pulses, probably because some of the thermal electrons are emitted at the dynodes.

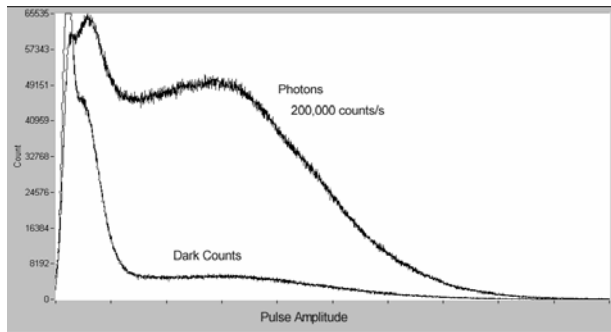


Fig. 56: Pulse amplitude distribution for dark pulses and photon pulses of an R5600P-01 PMT

For reasonable TCSPC operation, a discriminator threshold must be found that rejects the electronic noise background and the pulses in the low-amplitude peak, but counts as many of the regular photon pulses as possible. Moreover, the threshold should be considerably above the electronic noise level so that the smallest detected pulses still have a good signal-to-noise ratio. For photon counting it is therefore essential that a sufficient gain can be achieved within the permissible operating voltage of the PMT.

It is often believed that the width of the pulse amplitude distribution depends on the cathode material. Certainly there are differences in the peak ratios of the main peak and the low-amplitude peak, and in the peak-to-valley ratio. However, the differences are not very large, and the relative width of the main peak does not vary appreciably. It seems that detectors of different cathode type differ mainly in gain, rather than in the shape of the distribution. Consequently, the problem of most PMTs of poor photon counting performance is lack of gain, especially at the first dynode, not so much an odd shape of the amplitude distribution.

Signal Transit Time

The signal transit time in a PMT is almost entirely determined by the transit time of the electrons through the PMT. It is therefore proportional to the reciprocal square root of the supply voltage. Typical transit times for a number of frequently used PMTs are shown in the table below.

Detector	Operating voltage (Gain control voltage)	Transit Time	Transit Time per % Change in operating or gain control voltage
R3809U MCP-PMT	3000 V	< 1 ns	3 ps
R7400 and R5600 TO8 PMTs	900 V	5.4 ns	21 ps
H5773 Photosensor module	(0.9 V)	5.4 ns	21 ps
H7422 PMT module	(0.9 V)	6.5 ns	27 ps
R928 side window PMT	900 V	22 ns	100 ps
XP2020 44 mm linear focused PMT	2500 V	28 ns	140 ps

The transit time has to be taken into account when choosing the cable length in the detector and reference signal path of a TCSPC system (see ‘Adjusting the SYNC and CFD Cable Length 124’). More important than the transit time itself is the variation of the transit time with

the detector supply voltage. To keep the average transit time of a conventional PMT stable within 1 ps a stability of the operating voltage on the order of 0.05% to 0.01% is required.

Transit Time Spread and Timing Jitter

The delay between the absorption of a photon at the photocathode and the output pulse at the anode of a PMT varies from photon to photon. The effect is called ‘transit time spread’, or TTS. There are three major TTS components in conventional PMTs and MCP PMTs - the emission at the photocathode, the variation in the electron transit times, and the timing jitter of the subsequent electronics.

The time constant of the photoelectron emission at a traditional photocathodes is small compared to the other TTS components and usually does not noticeably contribute to the transit time spread. However, high efficiency semiconductor-type photocathodes (GaAs, GaAsP, InGaAs) are much slower and can introduce a transit time spread on the order of 100 to 150 ps.

The photoelectrons are emitted at the photocathode of a photomultiplier at random locations, with random velocities and in random directions. Therefore, the time they need to reach the first dynode or the channel plate is slightly different for each photoelectron (Fig. 57). Since the average initial velocity of a photoelectron increases with decreasing wavelength of the absorbed photon the transit-time spread is wavelength-dependent.

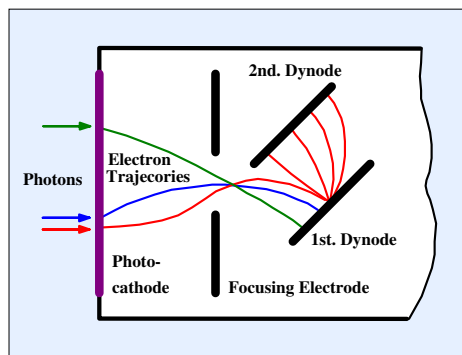


Fig. 57: Different electron trajectories cause different transit times in a PMT

As the photoelectrons at the cathode, the secondary electrons emitted at the first dynodes of a PMT or in the channel plate of an MCP PMT have a wide range of start velocities and start directions. The variation in the time they need to reach the next dynode adds to the transit time spread in the cathode space. The variation of the electron transit times usually delivers the by far largest contribution to the total transit time spread of a PMT.

Another source of timing uncertainty is the timing jitter in the discriminator at the input of a photon counter. The amplitude of the single electron pulses at the output of a PMT varies, which causes a variable delay in the trigger circuitry. Although timing jitter due to amplitude fluctuations can be minimised by constant fraction discriminators it cannot be absolutely avoided. Electronic timing jitter is not actually a property of the detector, but usually cannot be distinguished from the TTS of the detector.

TTS does exist also in single-photon avalanche photodiodes. The main reason of TTS in SPADs is the different depth in which the photons are absorbed. This results in different conditions for the build-up of the carrier avalanche and in different avalanche transit times. Consequently the TTS depends on the wavelength. Moreover, if high count rates are used, the re-

verse voltage may not have completely recovered from the breakdown caused by the previous photon. The result is an increase or shift of the TTS with the count rate.

Cathode Efficiency

Several different definitions are used to specify the efficiency of a PMT cathode.

Often the sensitivity of a PMT is specified in units of ‘cathode luminous sensitivity’. This is the cathode current per lumen incident light from a tungsten lamp operated at a temperature of 2856 K. Because the intensity maximum of the lamp is at about 1000 nm, the luminous sensitivity may not represent the efficiency at a given wavelength. Photocathodes of different spectral sensitivity are therefore not directly comparable. Moreover, the cathode luminous sensitivity does not include the efficiency of the electron transfer from the cathode into the dynode system and the possible loss of photon pulses due to incomplete resolution of the pulse height distribution.

In the test sheets of PMTs, the manufacturers occasionally specify the measured ‘anode luminous sensitivity’ instead of the cathode sensitivity. The anode sensitivity is the cathode sensitivity (including the electron transfer efficiency) multiplied by the gain of the tube. Because almost any gain can be obtained by increasing the supply voltage, the anode luminous sensitivity cannot be used to compare the photon counting performance of PMTs.

The ‘cathode radiant sensitivity’ is the cathode current per watt of incident power at a given wavelength. It is usually given as a plot versus the wavelength. The cathode radiant sensitivity does not include the efficiency of the electron transfer from the cathode into the dynode system or the possible loss of photon pulses due to poor resolution of the pulse height distribution. Nevertheless, the cathode radiant sensitivity is useful for comparing different detectors and different cathode versions.

The most useful parameter for characterising the efficiency of a photon-counting detector is the quantum efficiency. The quantum efficiency, QE , of a photocathode is the probability of the emission of a photoelectron per incident photon. It is directly related to the radiant sensitivity, S :

$$QE = S \frac{hc}{e\lambda} = \frac{S}{\lambda} \cdot 1.24 \cdot 10^{-6} \frac{\text{Wm}}{\text{A}}$$

with h = Planck constant, e = elementary charge, λ = Wavelength, c = velocity of light.

Usually quantum efficiencies given for detectors refer to the emission of a photoelectron or, in avalanche photodiodes, the generation of an electron-hole pair. The ‘detection efficiency’ in PMTs or SPADs is smaller for the reasons mentioned above: Not all photoelectrons cause a detectable anode current pulse in a PMT, and not all electron-hole pairs trigger an avalanche in a SPAD.

The efficiency of the commonly used photocathodes is shown in Fig. 58. The QE of the conventional bialkali and multialkali cathodes reaches 20 to 25 % between 400 and 500 nm. The recently developed GaAsP cathode reaches 45 %. The GaAs cathode has an improved red sensitivity and is a good replacement for the multialkali cathode above 600 nm.

Generally, there is no significant difference between the efficiency of similar photocathodes in different PMTs and from different manufacturers. The differences are of the same order as the variation between different tube of the same type. Reflection type cathodes are a bit more efficient than transmission type photocathodes. However, reflection type photocathodes have non-uniform photoelectron transit times to the dynode system and therefore cannot be used in ul-

tra-fast PMTs. An overview about the spectral characteristics of PMT cathodes is given in [211].

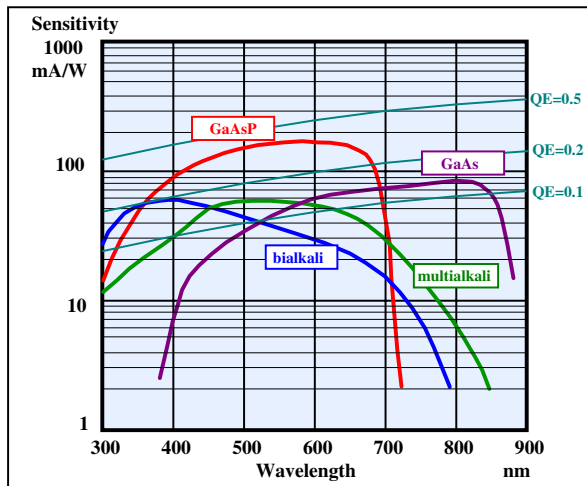


Fig. 58: Sensitivity of different photocathodes, after [211]

The typical efficiency of the Perkin Elmer SPCM-AQR single photon avalanche photodiode (SPAD) modules is shown in Fig. 59 (after [280]). The wavelength dependence follows the typical curve of a silicon photodiode and reaches more than 70% at 700nm. However, the active area of the SPCM-AQR is only 0.18 mm wide, and the diameters of other SPADs are as small as 20 μm . Therefore the high efficiency of a SPAD can only be exploited if the light can be focused into such a small area.

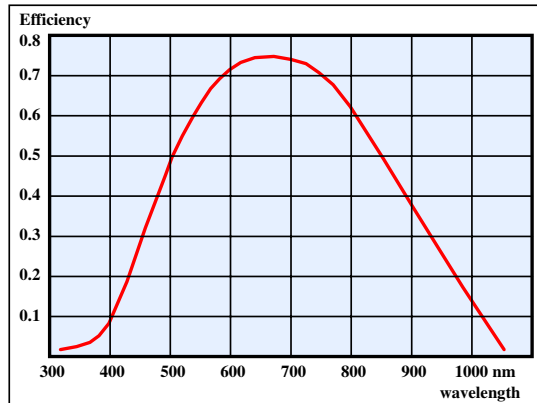


Fig. 59: Quantum efficiency vs. wavelength for a Perkin-Elmer SPCM-AQR SPAD module [280]

Dark Count Rate

The dark count rate of a PMT depends on the cathode type, the cathode area, and the temperature. The dark count rate is highest for cathodes with high sensitivity at long wavelengths. Depending on the cathode type, the dark count rate increases by factor of 3 to 10 for a 10 °C increase in temperature. Therefore, additional heating, i.e. by the voltage divider resistors, amplifiers connected to the output, or by the coils of shutters should be avoided. The most efficient way to keep the dark count rate low is thermoelectric cooling. Because the temperature has a large effect on the dark count rate cooling the PMT or PMT module 5 or 10 °C below the environment is often sufficient.

Exposing the cathode of a switched-off PMT to daylight increases the dark count rate for a longer period of time. For the traditional cathodes the effect is reversible, but full recovery takes several hours, see Fig. 60. Semiconductor cathodes should not be exposed to full daylight at all.

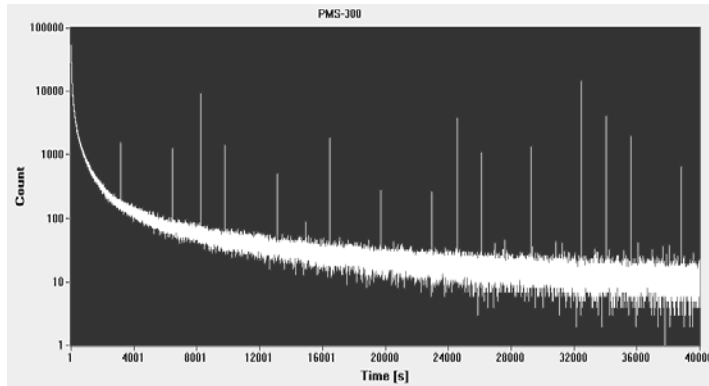


Fig. 60: Decrease of dark count rate (counts per second) of a H5773P-01 photosensor module after exposing the cathode to room light. The better show the decrease of the dark count rate the device was cooled to 5°C.

After extreme overload, e.g. daylight on the cathode of an operating PMT, the dark count rate can be permanently increased by several orders of magnitude. The tube is then damaged and does not recover.

Many PMTs produce random single pulses of extremely high amplitude or bursts of pulses with extremely high count rate. Such bursts are responsible for the peaks in Fig. 60. The peaks may indicate beginning instability in the tube and disappear if the gain is slightly reduced. However, irregular bursts can also originate from scintillation effects by radioactive decay in the vicinity of the tube, in the tube structure itself, by cosmic ray particles or from tiny electrical discharges in the cathode region. Therefore not only the tube, but also the materials in the cathode region must be suspected to be the source of the effect. Generally, there should be some mm clearance around the cathode region of the tube.

Afterpulsing

Photon-counting detectors have an increased probability of producing background pulses within a few microseconds following the detection of a photon. These afterpulses are detectable in almost any conventional PMT. It is believed that they are caused by ion feedback, or, by a smaller amount, by luminescence of the dynode material and the glass of the tube. Afterpulsing exists also in SPADs. Afterpulsing of SPADs is caused by electrons and holes from a previous avalanche. The carriers are trapped in lattice imperfections; the duration of afterpulsing in SPADs therefore depends on the temperature.

Afterpulses are difficult to identify in a standard TCSPC setup. The afterpulses appear within a few microseconds after the detection of a photon. However, TCSPC records only one detector pulse per signal period. An afterpulse is recorded only if it appears in a new signal period and after the dead time caused by the previously detected photon.

The afterpulsing probability versus the time after a regular single-photon pulse can be measured by illuminating the detector by a source of continuous classic light, such as an incandescent lamp or an LED, and recording the detector pulses in the FIFO (time-tag) mode of a TCSPC module. Afterpulsing reveals itself in the autocorrelation function of the photon density over time. For continuous classic light, the autocorrelation function is a horizontal line. Afterpulsing shows up as a peak at times shorter than a few microseconds. An example is shown in Fig. 61.

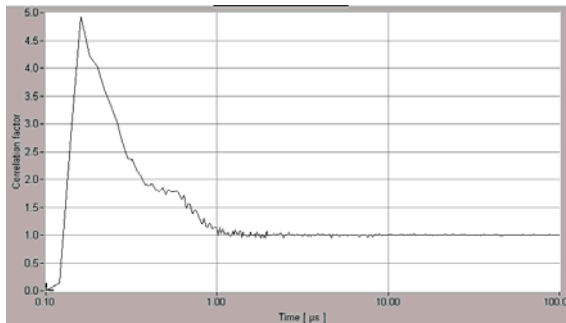


Fig. 61: Afterpulsing of an R5600P-1 PMT. Autocorrelation of the photon density recorded for a continuous light, count rate 10.000 /s.

The height of the afterpulsing peak depends on the count rate. The reason is that the probability of detecting the afterpulse of a previously detected photon is constant, whereas the probability of detecting another photon increases with the count rate. To make the results directly comparable different detectors must be tested at the same count rate.

The density of the afterpulses, as a function of time after a light pulse, can be recorded directly with a multichannel scaler. The PMT is illuminated with light pulses at a pulse period in the μs range, and the PMT pulses are recorded over a time interval of a few microseconds. An example is given in [46].

Afterpulsing can be a problem in high-repetition rate TCSPC applications, especially with Ti:Sapphire lasers or diode lasers, as well as in fluorescence correlation experiments. At high repetition rate, the afterpulses from many signal periods pile up and cause a considerable signal-dependent background. The total afterpulsing rate can easily exceed the dark count rate of the detector by an order of magnitude (see ‘Signal-Dependent Background’, page139). In fluorescence correlation spectra, afterpulsing results in a typical ‘afterpulsing peak’ at times shorter than a few μs (see Fig. 231, page 214). The amount of afterpulsing depends on the PMT gain. It can be reduced, yet not entirely removed, by decreasing the operating voltage of the PMT and using a preamplifier of a correspondingly higher gain.

The average amplitude of the afterpulses is higher than of the regular single-photon pulses. The higher amplitude can result in a number of confusing effects. One of them is that the apparent background of a detector may increase with increasing discriminator threshold. The reason is, of course, not a real increase of the background count rate. Instead, the afterpulsing background remains almost constant while the signal count rate decreases. In extreme cases almost all photon pulses are suppressed, and only afterpulses are recorded, see Fig. 127, page 122.

Pre-Pulses

In some detectors a bump in the TCSPC instrument response function (IRF) appears a few ns before the main peak. The size of the bump depends on the discriminator threshold. Normally the bump can be suppressed or reduced in size by increasing the discriminator threshold. The effect is probably caused by photoelectron emission from the first dynode. The corresponding pulses reach the anode prior to the photons from the cathode, and have a lower amplitude.

Similar effects can arise from an inappropriate zero cross level in a CFD. If the zero cross level is too close to the signal baseline, the zero cross comparator may oscillate and produce a double structure in the IRF. Therefore the CFD parameters should be checked before a PMT is suspected of producing pre-pulses.

In general pre-pulses do not cause major problems in TCSPC measurements. Even if the corresponding peak in the instrument response function (IRF) cannot be suppressed, e.g. because maximum counting efficiency is required, the deconvolution with the actual IRF delivers correct results.

Description of Selected Detectors

MCP PMTs

Best time resolution in TCSPC experiments is currently achieved with MCP PMTs. The Hamamatsu R3809U (Fig. 62) achieves a FWHM below 30 ps [155]. It is available with the conventional bialkali, multialkali, and extended-red multialkali cathodes. Recently R3809 versions with high efficiency GaAs and GaAsP cathodes and versions for the spectral range above 1000 nm have become available.

Typical TCSPC instrument response functions of an R3809U are shown in Fig. 63. At an operating voltage of -3 kV an IRF width of 28 to 30 ps (FWHM) is obtained. The IRF width decreases to about 25 ps if the operating voltage is increased to -3.4 kV. The IRF has a shoulder of about 0.5 ns duration and 1 to 2 % of the peak amplitude, see Fig. 63, right.



Fig. 62: Hamamatsu R3809U
MCP

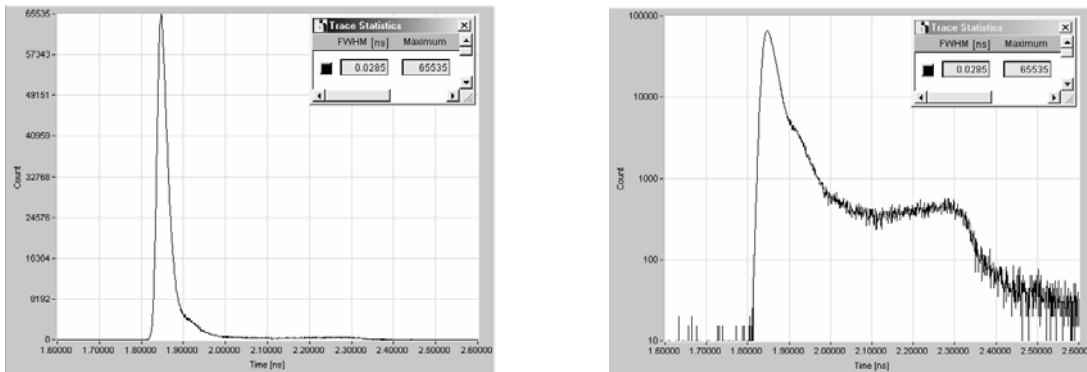


Fig. 63: IRF of an R3809U at -3 kV operating voltage. Linear scale (left) and logarithmic scale (right). Measured with Ti:Sapphire laser and SPC-630 TCSPC module. Time channel width 820 fs, time per division 100 ps.

Unfortunately, MCP PMTs are expensive and can easily be damaged by overload. When used at high count rate, their lifetime is limited due to degradation of the microchannels under the influence of the signal electrons. To provide maximum safety for the detector we recommend to use the bh HFAC-26-01 or HFAH-26-01 preamplifiers (see ‘Preamplifiers’, page 73) and the bh DCC-100 detector controller card (see ‘The DCC-100 detector controller’, page 74). The preamplifier gives a warning when the maximum permitted output current of the detector is exceeded and sends an overload signal to the DCC card. The DCC-100 then shuts down the operating voltage of the detector. In extreme situations the R3809U should be protected by a shutter, see Fig. 17, Fig. 96 and Fig. 111.

The R3809U-50 and -52 have been found almost free of afterpulsing [28, 46]. This makes the detector exceptionally suitable for fluorescence decay measurements over a wide dynamic range. Moreover, the fast and clean IRF makes the R3809U an excellent choice for FRET measurements by TCSPC laser scanning microscopy [40], see ‘Fluorescence Resonance Energy Transfer (FRET)’, page 178.

MCP PMTs are commonly believed to be unable to work at count rates higher than a few 10^4 photons per second. Fig. 64, left, shows the IRF of a Hamamatsu R3809U MCP for count rates of 100 kHz, 1.4 MHz, and 3.3 MHz for an illuminated area of 10 mm^2 . There is indeed a

considerable change in the IRF, with a shift in the first moment of almost 20 ps. The IRF shift is most likely an effect of the saturation of the microchannels. At high detector gain the output of a single microchannel saturates when a single photon enters the input [211]. The recovery time of the channel is in the microsecond range. If a large number of photoelectrons is concentrated on a limited number of microchannels these do not fully recover, and the IRF changes.

A simple extrapolation from the spot area of 10 mm² in Fig. 64, left, to smaller areas shows that the useful count rate can indeed be in the 10-kHz range. On the other hand, a substantially improved IRF stability is obtained for illumination of the full cathode area of 120 mm². IRF curves measured with illumination of the full cathode area are shown in Fig. 64, right. The response remains stable up to more than 3 MHz recorded count rate, with a shift in the first moment of less than 3 ps.

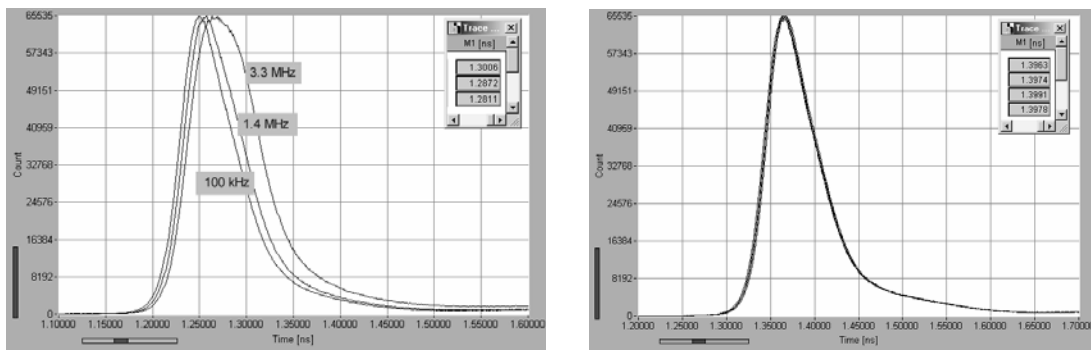


Fig. 64: IRF of an R3809U MCP-PMT for different count rates. Illumination by diode laser, pulse width 50 ps. Operating voltage -3 kV, 20 dB preamplifier gain, CFD threshold 80 mV. Left: Illuminated spot of 2 x 5 mm, recorded count rates 100 kHz, 1.4 MHz, 3.3 MHz. Right: Full cathode area illuminated, recorded count rates 3.3 MHz, 1.8 MHz, 480 kHz, and 25 kHz

These results show that MCP PMTs can be used for count rates close to the maximum useful count rate of currently available TCSPC systems. It should be noted, however, that the output current at a count rate of 3.3 MHz and an operating voltage of 3 kV is considerably higher than the maximum rating of 100 nA specified by the manufacturer. This is certainly not a problem in applications where high count rates appear only temporarily, as in scanning microscopy. The lifetime of the MCP at a continuous count rate of more than 3 MHz is not known.

Hamamatsu R5600 and R7400 Miniature PMTs

The Hamamatsu R7400 and the older R5600 are miniature PMTs in a TO-8 size housing. The R7400 PMTs are the basis of the H5773 and H5783 photosensor modules, see paragraph below. Due to their small size, the tubes yield a fast TCSPC instrument response. The typical IRF width for multialkali and bialkali tubes is between 150 and 180 ps fwhm. Increasing the voltage between the cathode and the first dynode makes the response even faster. It is unknown how far the voltage can be increased without the tube breaking down. A test tube worked stable at 1 kV overall voltage with a cathode-to-dynode voltage 3 times as high as the dynode-to-dynode voltage. The decrease of the response width is shown in Fig. 65.

The metal-channel design of the R5600 and R7400 results in slight periodical variations of the efficiency and the IRF over the active area, see Fig. 66, right. Consequently, either the entire active area should be illuminated or the position of the illuminated spot should be kept stable.

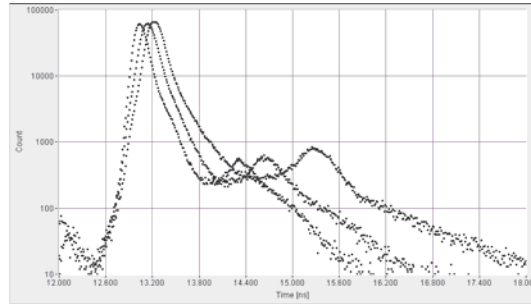


Fig. 65: R5600P-1, -1kV supply voltage: TCSPC response for different voltage between cathode and first dynode. Left to right: 3, 2 and 1 times nominal voltage. Entire cathode area illuminated, time scale 600 ps/div.

The afterpulsing probability of the miniature PMTs is relatively high, especially for the NIR-sensitive versions. However, the afterpulsing ceases after one microsecond and can, as usual, be reduced by operating the tube at reduced gain.

The performance of the R7400 and R5600 tubes with the standard voltage divider is the same as for the Hamamatsu H5773 and H5782 photosensor modules (see below). It is questionable whether the slightly lower price compensates for the inconvenience of building a voltage divider and using a high voltage power supply. Moreover, a R5600 or R7400 with a standard voltage divider does not yield the same high timing stability as the photosensor modules.

H5783 and H5773 Photosensor Modules

H5783 and H5773 are miniature optical sensors containing a TO-8-size PMT together with a high-voltage power supply. The modules are operated from a simple +12 V to +15 V power supply. The operating voltage of the PMT is controlled by a 0 to +0.9 V gain control signal. The modules are available in different cathode and window versions. A 'P' version selected for high gain and good pulse height distribution is available for the bialkali and multialkali tubes.

The typical IRF of an H5773P-0 is shown in Fig. 66. The output pulses were amplified by a HFAC-26-10 preamplifier, and the response to 50 ps pulses from a 650 nm diode laser was recorded by an SPC-730 TCSPC module.

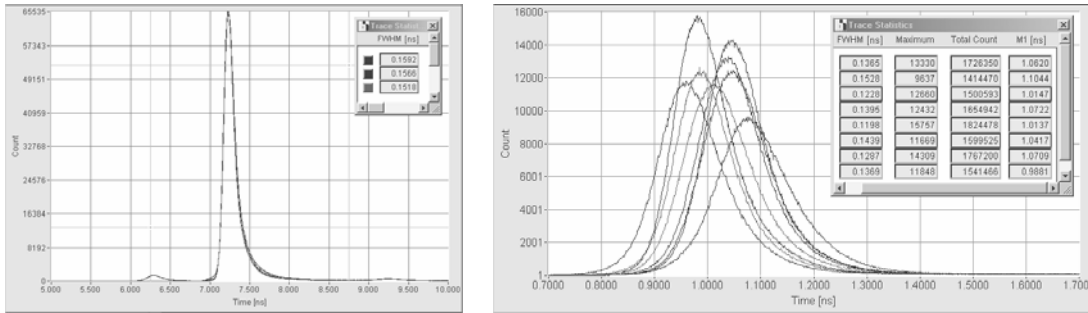


Fig. 66: H5773P-0. Left: TCSPC IRF, time scale 500 ps/div. Gain control voltage 0.9 V, preamplifier gain 20dB, discriminator threshold -100mV, -300mV and -500mV. Right: Variation of the IRF and the efficiency over the cathode area.

The response function has a pre-peak about 1 ns before and a secondary peak 2 ns after the main peak. The pre-peak is caused by low amplitude pulses, probably by photoemission at the first dynode. It can be suppressed by properly adjusting the discriminator threshold. The secondary peak is independent of the discriminator threshold.

The variation of the IRF for an H5773-20 over the active area is shown in Fig. 66, right. The FWHM of the IRF varies from about 120 ps to about 140 ps, and the first moment shifts over 90 ps (see insert). This means that the IRF width for small spots can be substantially shorter than for the full active area. However, the improved resolution can only be exploited if the location of the illuminated spot is kept stable within less than 0.1 mm. If timing stability is important it is probably better to spread the light over the full cathode area. There is also some variation in the efficiency, see total count numbers in the insert of Fig. 66, right.

The H5783 and H5773 photosensor modules have an exceptionally good timing stability at high count rates. A test result for a Hamamatsu H5773P-20 photosensor module is shown in Fig. 67.

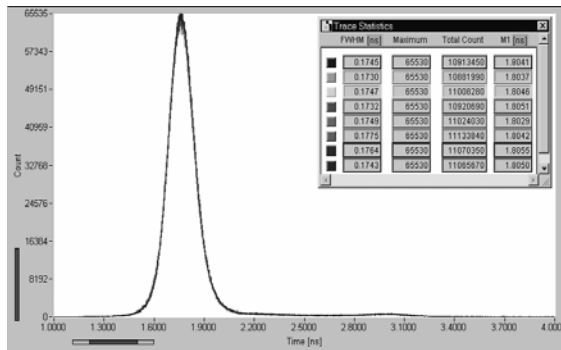


Fig. 67: IRF of an H5773-20 photosensor module for recorded count rates of 30 kHz, 300 kHz, and 4 MHz. The shift between 30 kHz and 4 MHz is <2 ps and not discernible in the IRF curves. Insert: First moments of the curves.

For (recorded) count rates varying from 30 kHz to 4 MHz the shift in the first moment of the IRF is <2 ps and not discernible in the IRF curves. The surprisingly high timing stability may in part be a result of the Cockcroft-Walton voltage-divider design of the H5773 and H5783 modules [157].

Surprisingly, the internal high voltage generator of the H5783 and H5773 does not induce much noise at the output of the modules. Some ripple is detectable, especially at a load impedance of 1 MΩ, but the amplitude is much smaller than the amplitude of the single-photon pulses.

Unfortunately the housings of the H5783 and H5773 modules have a poor RF shielding effect. Apparently there is no low-impedance connection between the internal signal ground and the housing. To obtain reasonable photon counting operation, the modules must be operated in an additional shielding box.

To improve the noise immunity and to provide safety against damage by overload the photosensor modules should be used with an HFAC-26-10 preamplifier. The +12 V supply voltage can be taken from the sub-D connector of the SPC module. The gain control voltage can be obtained from a simple voltage divider. A more comfortable solution is the DCC-100 detector controller of bh [19] (see ‘The DCC-100 detector controller’, page 74). The DCC-100 provides software-controlled gain setting, detector on/off switching and overload shutdown in conjunction with a bh HFAC-26 preamplifier.

PMH-100 and PMC-100

The PMH-100 and PMC-100 detector modules of bh contain H5773 photosensor modules together with a preamplifier. Moreover, the PMC-100 contains a thermoelectric cooler.



Fig. 68: PMH-100 (left) and PMC-100 detector modules

Both the PMH-100 and the PMC-100 have a C mount adapter for simple interfacing to an optical system.

The PMH-100 is operated from the +12 V output at the sub-D connectors of the bh SPC modules. No further power supply or amplifier modules are required. Due to its compact design and the internal preamplifier the PMH-100 features excellent noise immunity.

The PMC-100 is a cooled version of the PMH-100. The PMC-100 requires the DCC-100 detector controller for proper operation. The DCC-100 delivers the current for the peltier cooler and provides an overload shutdown of the detector. Due to the cooling, even the NIR-sensitive versions of the PMC-100 deliver low dark count rates.

The IRF of the PMC and PMH modules is identical with the IRF shown for the H5773 in Fig. 66. Moreover, the PMH-100 and PMC-100 detectors feature the same exceptionally IRF stability at high count rates, see Fig. 66. Due to the high IRF stability and the high NIR sensitivity the PMC-100-20 is currently the best detector for DOT applications.

Hamamatsu H7422 and H8632

The H7422-40, the H7422-50 and the H8632 are high-speed, high-sensitivity PMT modules [158]. The modules feature excellent sensitivity in the red and near-infrared region. They contain an GaAsP or GaAs photomultiplier along with a thermoelectric cooler and a high voltage generator. The resolution in the TCSPC mode is typically 200 to 350 ps [28, 46]. The H7422 comes in different cathode versions for the wavelength range up to 900 nm.

The H7422-40 has a GaAsP cathode and can be used from about 300 nm to 700 nm. The quantum efficiency reaches 40% in the visible range of the spectrum. The H7422-40 is therefore an excellent detector for single-molecule experiments. It is also used in laser scanning microscopy, especially if a system is used both for FLIM and FCS. The IRF measured for three different specimens of the H7422-40 is shown in Fig. 69. The width varies from about 200 ps to 350 ps.

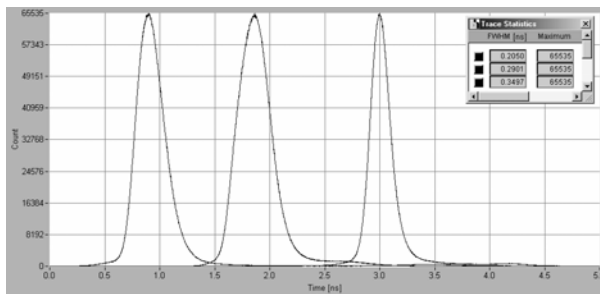


Fig. 69: IRF for three different specimen of the H7422-40. Gain control voltage 0.81 V, preamplifier HFAC-26-1 (20 dB), CFD threshold -150 mV, 650 nm diode laser of 45 ps pulse width, SPC-630 TCSPC module, 500 ps/division

For the wavelength range up to 900 nm the H7422-50 can be used. The timing behaviour is about the same as for the H7422-40. Due to its high NIR sensitivity the H7422-50 is frequently used for diffuse optical tomography.

For the wavelength range up to 1100nm the H8632 is available.

The modules must be handled with care because the cathodes can easily be damaged by overload. Exposure to bright daylight is not allowed even when the devices are switched off. The maximum output current is $2 \mu\text{A}$. Therefore the H7422 and the H8632 should be used with an HFAC-26-1 or -2 preamplifier. Power supply, gain control, overload shutdown and cooling current for H2422 modules is provided by the bh DCC-100 detector controller [19].

Hamamatsu H7421

The H7421 is a TTL output version of the H7422. As the H7422, the modules feature excellent sensitivity in the red and near-infrared region and come in different cathode versions for the wavelength range up to 900 nm. The H7421 can be connected to the SPC boards via an A-PPI pulse inverter and a 20 dB attenuator. The internal discriminator of the H7421 has a fixed threshold. Moreover, the discriminator is not of the constant fraction type. That means that the H7421 has poor time resolution when used in TCSPC applications. The typical IRF width is 600 to 700 ps, and a noticeable dependence of the IRF on the count rate was found [28, 46].

PML-16 Multichannel Detector Head

The bh PML-16 is a 16 channel detector head. It contains a Hamamatsu R5900-L16 multi-anode PMT [156] and the routing electronics for the 16 detector channels. The older PML-16 requires a 1kV power supply. The new PML-16C [18] has an internal high-voltage generator. It is controlled by the DCC-100 card, which provides for power supply, gain control, and overload shutdown.

The channel arrangement of the PML-16 and PML-16C is 1-by-16, the time resolution 150 to 250 ps FWHM [18, 28]. The PML detectors can be connected directly to the SPC-6, -7, -8 -140/144 and -150/154 modules. The photons from the individual detector channels are routed into different blocks of the SPC memory. Thus the measurement yields a separate decay function for each PMT channel. The benefit of the PML-16 compared to single-detector solutions is the dramatically increased detection efficiency. Typical applications are optical tomography, multi-wavelength lifetime microscopy, stopped flow experiments, and classic multi-wavelength fluorescence lifetime experiments. The PML-16 is part of the bh PML-SPEC spectral detection and the bh multi-wavelength MW-FLIM systems [18, 20, 21, 22].



PML-16 Multichannel detector head

Conventional PMTs

Compared to the H5783 and the PMH-100, conventional PMT tubes have poor timing performance and are therefore not recommended for the SPC modules. The least objectionable are short-time PMTs, such as the XP2020, with high gain and single-photon specification. Due to the high gain and output current, these tubes work well without preamplifiers. Nevertheless, preamplifiers should be used to protect the CFD inputs of the SPC module against damage by high-amplitude pulses. The IRF width is about 200 to 350 ps (FWHM), but depends strongly on the wavelength and the illuminated area of the photocathode [46].

Sometimes older PMTs (such as the 56 UVP) were built up with voltage dividers with an extremely high cross current (10 mA and more). We strongly discourage to use such devices. They require high power HV supplies which are extremely dangerous. Furthermore, the detector current can be very high and the PMT is easily damaged at higher light levels. For TCSPC applications a voltage divider current of a few 100 uA is sufficient.

Simple side-window PMTs (R928, R931 etc.) were reported to yield a time resolution below 300 ps FWHM in the TCSPC mode [71, 192, 243]. This is correct - with some serious restrictions. A short response is obtained only if the light is focused into a spot of less than 1 mm on the PMT cathode and the best location on the cathode is selected (see Fig. 70). There is a considerable ‘Colour Delay’, i.e. a change of the delay and the shape of the response as a function of the wavelength. Furthermore, there is usually a long tail in the response with an ugly bump some ns after the main peak. Therefore, we do not recommend to use such tubes for TCSPC. The exception are cases when a complex instrument with side-window PMTs, such as a laser scanning head, has to be upgraded with TCSPC.

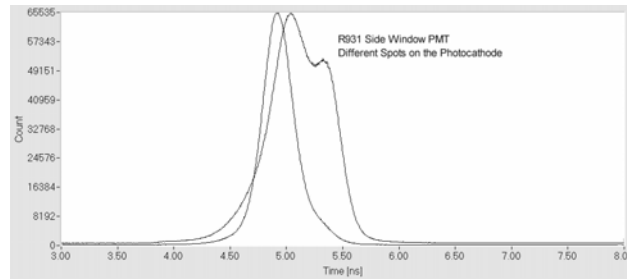


Fig. 70: IRF of an R931 side-window PMT

Single-Photon Avalanche Photodiodes

Single photon operation of standard silicon APDs in simple passive and active quenching circuits has been reported since 1981 [91, 123, 216]. Nevertheless there is currently no off-the-shelf diode for which single-photon operation is guaranteed. For a long time the only commercially available single photon avalanche photodiodes (SPADs) were the SPCM-AQR modules from Perkin Elmer [280]. The SPCM-AQR modules have a high efficiency in the near infrared. They are available in different dark count classes down to 25 counts per second. The output pulses are positive, with TTL/CMOS levels and a pulse width of several 10 ns. The pulses can be coupled into CFD inputs of the bh TCSPC devices via an A-PPI inverting transformer (see Fig. 18) or via a HRT-82 router. Due to their high efficiency and low after-pulsing probability, the SPCM-AQR modules are preferentially used in FCS and single-molecule experiments. Unfortunately the timing performance of the SPCM-AQR varies over a relatively wide range, see Fig. 71.

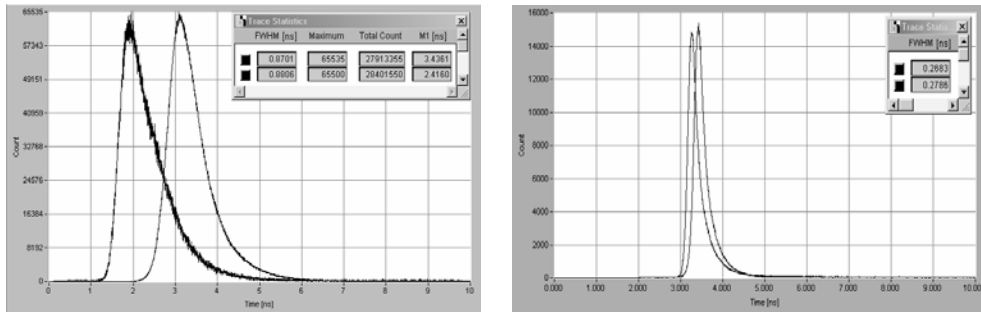


Fig. 71: TCSPC IRF of two SPCM-AQR modules, 1 ns/div. Left: Unselected modules, measured at 650 nm, 50 kHz, and 500 kHz count rate. Right: Module selected for low timing jitter, measured at 496 nm, 50 kHz and 500 kHz count rate.

The IRF of an unselected SPCM-AQR is shown in Fig. 71, left. The pulse width of the laser was about 50 ps, i.e. much shorter than the detector response. The measurements show that

not only was the TTS of the tested detector relatively wide, but also there was a considerable change with the count rate. Fig. 71, right shows the IRF of an SPCM-AQR selected for low timing jitter. The IRF of this module was shorter than 300 ps, and the dependence of the IRF on the count rate was reduced.

In the last years it became possible to manufacture silicon SPADs in standard epitaxial processes as they are used for high-speed CMOS devices. The diodes are characterised by a small thickness of the depletion region. The thin depletion region results in a relatively low breakdown voltage, high time resolution, and low dark count rate. The drawback of the thin depletion region is a reduced quantum efficiency in the near infrared.

Fig. 72 shows IRF recordings for an id 100-20 detector of id Quantique [179] (left) and for a PDM 50 CBT detector of Micro Photon Devices [247]. The test light source was a bh BHL-600 785 nm diode laser of 24 ps pulse width; the signals were recorded by bh SPC-140 TCSPC module. For both detectors the detector count rate was varied from a few 10 kHz up to several MHz.

The three curves for the id 100 (Fig. 72, left) were recorded at detector count rates of 61 kHz, 2.7 MHz, and 8.1 MHz. The recorded pulse width (FWHM) is 49 ps, 48 ps and 45 ps, respectively. Corrected for the laser pulse width, the detector IRF width is 43 ps, 42 ps, and 38 ps. The shape of the IRF is remarkably clean, without any secondary peaks. Compared to a count rate of 61 kHz, the IRF shifts by 13 ps and 27 ps for 2.7 MHz and 8.1 MHz, respectively.

The curves for the PDM 50 CBT were recorded at a detector count rate of 750 kHz, 1.7 MHz, 3.2 MHz, and 4.1 MHz. Surprisingly, the detector tested had a dead time longer than the dead time of the SPC-140 (100 ns). A detector dead time longer than the TCSPC dead time can cause tails and secondary peaks in the recorded response, especially if the end of the dead time interval coincides with a laser pulse. The IRFs of the PDM 50 CBT were therefore recorded by an SPC-150 with the module dead-time adjusted to about 140 ps. The detector then showed a clean response with extraordinary low shift in the first moment. The shift in the first moment is 1.1 ps for 1.7 MHz, 6.5 ps for 3.2 MHz, and 8.8 ps for 4.1 MHz. For count rates of 750 kHz, 1.7 MHz, 3.2 MHz, and 4.1 MHz the recorded pulse width is 43 ps, 47 ps, 64 ps, and 67 ps, respectively.

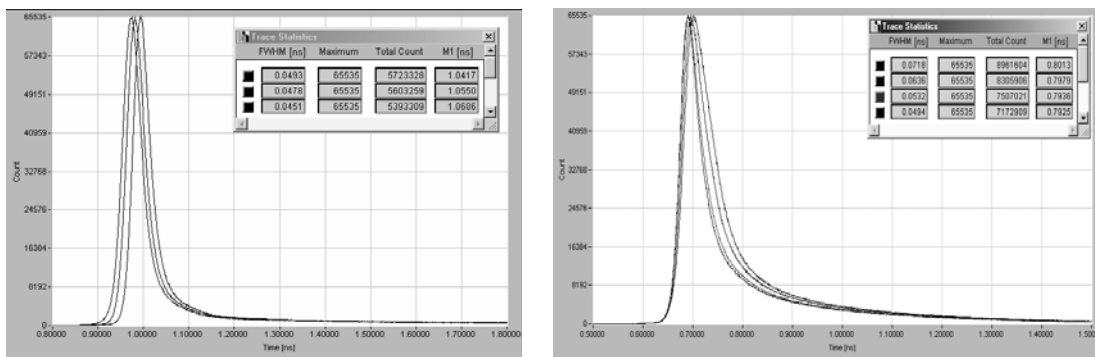


Fig. 72: IRF shapes of epitaxial SPADs. Response to diode laser pulses, wavelength 785 nm, pulse width 24 ps. Time channel width 814 fs, 100 ps / division. Left: id 100-20 at detector count rates of 61 kHz, 2.7 MHz, and 8.1 MHz. Right: PDM 50 CBT at detector count rates of 750 kHz, 1.7 MHz, 3.2 MHz, and 4.1 MHz.

Fig. 73 compares the response of two epitaxial SPADs (id 100-20 of id Quantique [179] and PDM 50 CT of Micro Photon Devices [247]) with the response of an R3809U MCP PMT for a detection wavelength of 785 nm. There is a slow tail in the response measured at 785 nm. This ‘diffusion tail’ is typical of APDs operated at long wavelengths. It is caused by photons which penetrate the depletion layer and generate photons in the neutral regions nearby.

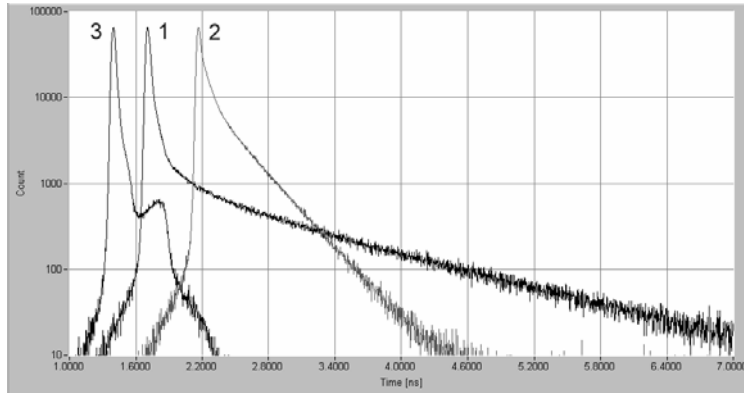


Fig. 73: Response of an id 100-20 SPAD (1), an PDM 50CT SPAD (2), and an R3809U MCP PMT (3). Wavelength 785 nm, optical pulse width 24 ps, time scale 600 ps/div.

The diffusion tails in the SPAD responses are almost single-exponential. The single-exponential profile and the fact that the tail is not present at short wavelength can be a pitfall in fluorescence decay measurements, where the diffusion tail is sometimes mistaken for a fluorescence component.

The dependence of the IRF on the wavelength is shown in detail in Fig. 74. Not only is there a considerable change in the amplitude of the diffusion tail but also a change in the width on the main peak and consequently in the FWHM, see especially Fig. 74, right. Some care is therefore indicated if SPADs are used at variable wavelength.

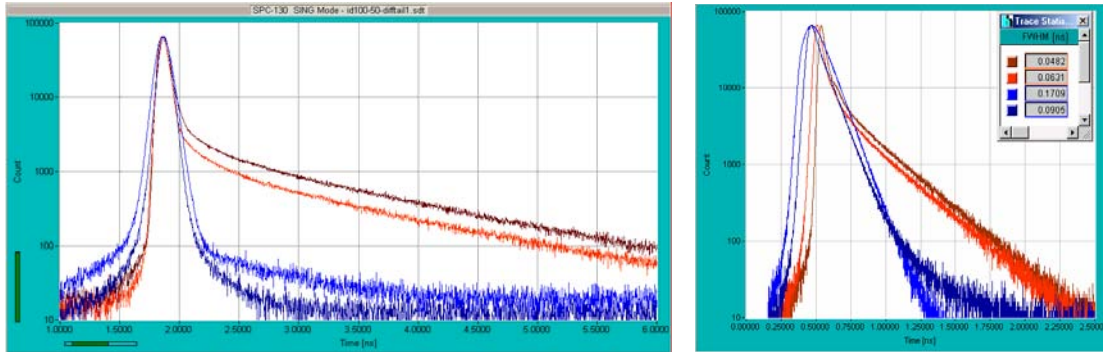


Fig. 74: Wavelength dependence of the IRF of an id 100-50 (left, 500 pd/div) and a PDM 50 CBT SPAD (right, 250 ps/div). 785nm (dark red), 650 nm (red), 446 nm (blue), 405 nm (dark blue)

Agents: Boston Electronics, (800)347-5445, TCSPC@boselec.com

Agents: Boston Electronics, (800)347-5445, TCSPC@boselec.com

Preamplifiers and Detector Control

Preamplifiers

Most MCPs and PMTs deliver pulses of 20 to 50 mV when operated at maximum gain. Although these pulses can easily be detected by the input discriminators of the bh SPC modules a preamplifier can improve the time resolution, the noise immunity, the threshold accuracy and the safety against damaging the SPC input. Furthermore, it can extend the detector lifetime because the detector can be operated at a lower gain and a lower average output current. The strongest argument is, however, that a properly designed preamplifier can be used to protect the detector against overload. The principle is shown in Fig. 75.

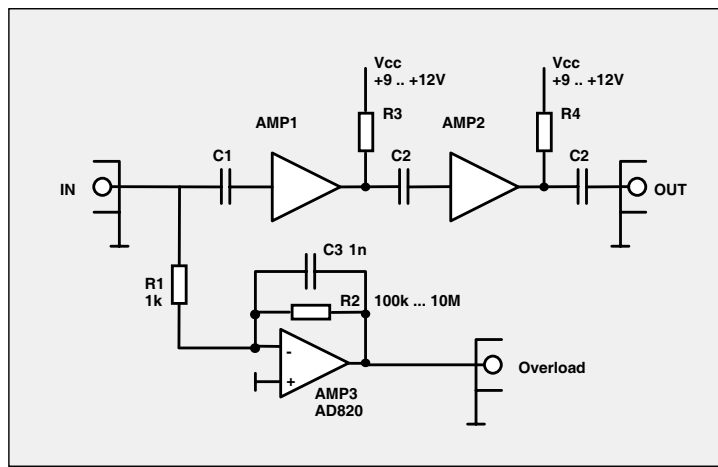


Fig. 75: Preamplifier with overload signal output

AMP1 and AMP2 are AC coupled high-frequency amplifiers as they are used in communication devices. To avoid signal inversion, either two inverting amplifiers are used in series or one non-inverting amplifier is used. Many types of amplifier chips are available, with similar designs but different gains and bandwidths. Depending on the amplifier chips used, AMP1 and AMP2 deliver a total gain between 12 dB and 40 dB, at a bandwidth between 500 MHz and several GHz. The DC component of the detector current is fed into AMP3. AMP3 is an operational amplifier with FET input. It converts the input current into a voltage with a transimpedance determined by R2. The output voltage of AMP 3 is proportional to the detector current. If it becomes too high it activates an overload warning, e.g. turns on a LED or an acoustic signal, or switches off the detector (see below).

The preamplifier shown in Fig. 75 is a much better overload indicator than a rate meter. Monitoring the count rate is not safe because the discriminator threshold can be wrong, or the detector gain may be set too low to obtain any counts. Moreover, the count rate may break down at extreme overload. An inexperienced user may then increase the light intensity even more. In contrast, overload detection via the detector current responds properly in all these situations.

The design principles shown in Fig. 75 are used in the bh HFAC-26 and HFAH-26 preamplifiers. The amplifiers are shown in Fig. 76.



Fig. 76: HFAC-26 (left) and HFAH-26 preamplifiers (right)

Please note that the amplifiers come with different overload thresholds. The recommended overload thresholds for different detectors are:

R3809U MCP PMT	0.1 μ A
R5600 and R7400 Miniature PMTs	10 μ A
H5773 and H5783 Photosensor Modules	10 μ A
H7422-40 and -50 Modules	2 μ A
R928, R931, etc. Side Window PMTs	10 μ A
XP2020 Linear focused PMTs	100 μ A

The recommended Gain is 20 to 26 dB, i.e. 10 to 20. Higher gain is available but requires exceptionally good detector shielding. Because of the noise of the internal high voltage generator gains higher than 20 should not be used for the H5773, H5783, and H7422 photosensor modules.

The DCC-100 detector controller

The DCC-100 module was designed to control detectors in conjunction with bh photon counters [19]. It can be used to control the gain of the Hamamatsu H7422, H5773, H5783, H6783, or similar photosensor modules by software. The gain of MCPs and PMTs can be controlled via the FuG HCN-14 high voltage power supply. In conjunction with bh preamplifiers, overload shutdown of the detectors is provided. Furthermore, the DCC-100 delivers the current for thermoelectric coolers, e.g. for the Hamamatsu H7422 and the bh PMC-100. High current digital outputs are available for shutter control.

The DCC-100 is a PCI module for IBM compatible computers, see Fig. 77. The software of the DCC-100 is included in the TCSPC installation package (please see ‘Software Installation’).

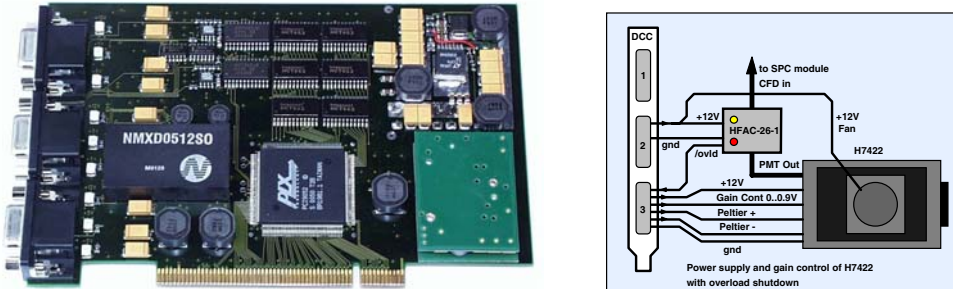


Fig. 77: DCC-100 detector controller. The module controls the gain of PMT modules or the high voltage of PMTs, provides the power supply for thermoelectric cooling, provides overload shutdown of the detector, and drives electromechanical shutters. The connection of a Hamamatsu H7422 PMT module is shown right.

The connection of an H7422 module is shown in Fig. 77, right. The use of the DCC-100 for a number of frequently used detectors and detector configurations is described under ‘Connecting the Detectors’ and ‘FLIM Systems for Laser Scanning Microscopes’.

The block diagram of the DCC-100 is shown in Fig. 78. The DCC-100 contains two detector control blocks and one general purpose power switch block.

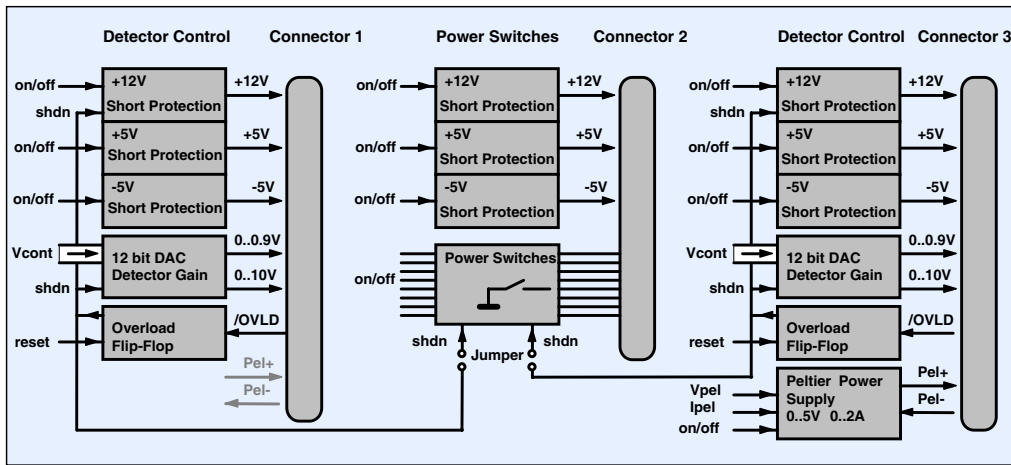


Fig. 78: Block diagram of the DCC-100 detector controller

Detector Control Blocks

The detector control blocks contain power supply outputs for detectors, a digital-to-analog converter (DAC) for detector gain control, and an overload shutdown circuit. The power supply outputs are short-circuit-protected and deliver +12 V, +5 V and -5 V. The outputs can be switched on or off by software. A 12 bit DAC is used to control the gain of the detector. It delivers the 0 to +0.9 V control voltage required for Hamamatsu photosensor modules (H7422, H5783, H5773 etc.) and the bh PMC-100 detector. A 0 to +10 V control voltage is available for FuG high voltage power supplies.

Both detector control blocks have a detector overload shutdown function. The shutdown function works in conjunction with bh HFAC-26 and HFAH-26 preamplifiers, and with the PMC-100 detector module. If the preamplifier or the detector module detects an overload condition it sends an active low overload signal (/ovld) to the DCC-100. This signal sets the overload flip-flop which shuts down the detector control voltage and the +12 V detector power supply. Furthermore, it can be used to deactivate the switches in the power switch block (see below).

High-Current Switch Block

The high-current switch block contains power supply outputs for detectors and preamplifiers and eight high-current MOSFET switches to operate shutters, motors or magnetic actuators.

The power supply outputs are short-circuit-protected and deliver +12 V, +5 V and -5 V. The outputs can be switched on or off by software. The MOSFET switches are able to switch currents up to 2A and voltages up to 20V. One side of each switch is connected to ground, the other side is available at the output connector. The switches are **not** short circuit protected.

The high-current switches can be shut down (i.e. set into the non-conducting state) by one or both overload signals from the detector control blocks. The configuration is set by jumpers on the DCC-100 board, see DCC-100 manual [19].

Power supply for thermoelectric cooler

Current supply for thermoelectric coolers is provided at connector 3 or at connector 1 and 3. If coolers are supplied both from connector 1 and 3 the coolers are connected in series. The configuration is set by jumpers on the DCC board. The cooler driver delivers up to 5 V and 2 A. Both voltage and current can be selected by software. The device automatically controls either

the output voltage or the output current. Voltage control is active as long as the current through the load is smaller than the current limit set by the software. When the current through the load reaches the current limit the device automatically switches to current control. A block diagram is shown in Fig. 79.

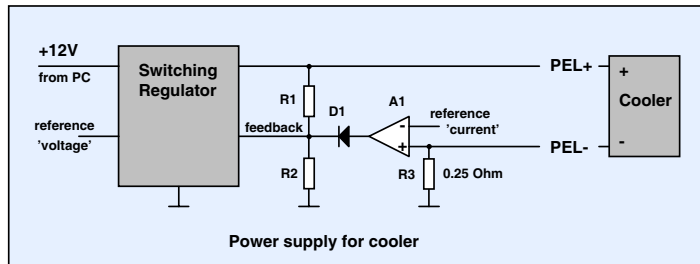


Fig. 79: DCC-100, control of the cooling current

A switching regulator is used to generate the supply current for the cooler. The cooling current flows through the sensing resistor R3. As long as the voltage at R3 is smaller than the reference voltage at A1 ('current' reference) A1 is inactive and the switching regulator works as a normal voltage stabiliser. If the voltage at R3 exceeds the reference voltage at A1, the amplifier becomes active, and, via D1, overwrites the feedback voltage of the switching regulator. This causes the regulator to reduce the output voltage until the voltage at R3 equals the reference of A1.

For more information, please see DCC-100 data sheet and DCC-100 manual, available on www.becker-hickl.com.

Safety Recommendations for Using Detectors

PMTs are operated at a voltage in the range of 800 to 3500 V, and the operating voltage of avalanche photodiodes can be as high as 300 V. Therefore it is necessary to obey the usual safety rules for handling high voltage. An extremely important but often neglected issue is the ground return path to the power supply. A typical situation is illustrated in Fig. 80.

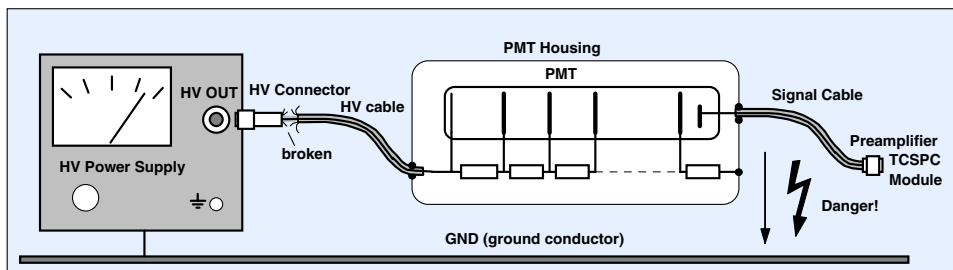


Fig. 80: Effect of a broken ground return path to the high voltage power supply

The cable that connects the voltage divider of the PMT to the high voltage power supply has a broken outer conductor. The inner conductor still connects the 'hot' side of the voltage divider to the high voltage. However, because the outer connector is broken, the current through the voltage divider resistors cannot flow back to the power supply. Therefore the current flows through the preamplifier, the TCSPC module, the computer, and the ground conductor of the power socket back to the power supply. Nothing happens, but the setup is not safe: When the signal cable is disconnected, there is a high voltage between the signal cable and the TCSPC module. Fortunately the resistors in the PMT voltage divider limit the current so that a broken HV cable will probably not deliver a fatal shock; but nevertheless the effect can be surprising.

The setup can easily be made safe by providing an auxiliary ground return path from the PMT housing to the high voltage power supply. Unfortunately, most PMT housings and many power supplies do not provide any connectors for an additional ground connection. Therefore: Do not disconnect the PMT signal cable from the SPC module when the high voltage is switched on, and do not use any cables with broken or unreliable screen or ground connectors.

High voltage safety is not the only reason why a PMT cable should not be connected or disconnected when the high voltage is on. The situation is illustrated in Fig. 81.

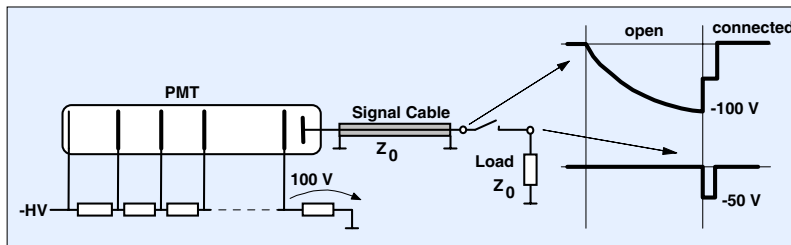


Fig. 81: Discharging a charged PMT signal cable into a resistive load

If the load is unconnected, the output current of the PMT charges the signal cable until the voltage reaches approximately the voltage at the last dynode. This voltage can be as high as several hundred Volts. When the load is connected, the cable discharges into the load. For a load impedance equal to the characteristic impedance of the cable, the amplitude of the resulting pulse is half the voltage to which the cable was charged. The pulse duration is twice the cable transit time. The pulse can be enough to destroy an amplifier or a CFD. Normally the limiter diodes at the input of the amplifier or CFD will prevent a destruction. However a cable discharge will stress the diodes enormously so that an absolute safety is not given. Therefore, be careful and don't tempt fate.

If possible, you can connect a resistor of about $100 \text{ k}\Omega$ from the PMT anode to ground inside the PMT case. This will prevent the cable from being charged and thus provide protection against preamplifier or CFD damage.

Summary: Never connect or disconnect a photomultiplier to the SPC module or a preamplifier when the high voltage is switched on! Never connect a photomultiplier to the SPC module or a preamplifier if the high voltage was switched on before with the PMT output left open! Never use switchable attenuators between the PMT and the SPC! Never use cables and connectors with bad contacts! The same rules should be applied to photodiodes which are operated at internal reverse voltages above 20V.

Agents: Boston Electronics, (800)347-5445, TCSPC@boselec.com

Agents: Boston Electronics, (800)347-5445, TCSPC@boselec.com

Installation of the bh TCSPC Modules

General Requirements

The computer must be a Pentium PC with a graphics card of 1024 by 628 resolution or more. The operating system can be Windows 95, 98, 2000, NT, or XP. For the SPC-6 and -134 modules the computer should have at least 128 Mb memory, for the SPC-730, SPC-830, and the SPC-144 256 Mb are recommended. Although the SPC Software requires only a few Mb hard disk space, much more space should be available to save the measurement results. The data files can be as large as 32 Mb for the imaging modes and several 100 Mb for the FIFO mode. Although not absolutely required, we recommend to use a computer with a speed of at least 1 GHz for convenient working with the SPC. For the SPC-6 and -7 modules a space of two PCI slots is required. The SPC-134, SPC-144 and SPC-154 packages occupy four adjacent PCI slots.

Software Installation

With the introduction of the SPC-830 module in July 2002 the installation procedure was changed. The software comes on a CD that contains all software components commonly used for bh TCSPC systems.

SPCM Application

The SPC-6xx, SPC-7xx, SPC-830, SPC-134 and SPC-144 modules come with the 'Multi SPC' or 'SPCM Software', a comfortable software package that contains all components to operate up to four SPC-6xx, four SPC-7xx, four SPC-830, or one SPC-134 or SPC-144 package. The SPCM software is described under 'Software' in this manual. The SPCM software is free. Updates are available from www.becker-hickl.com.

DCC Application

This application controls the DCC-100 detector controller card that is often used in conjunction with bh SPC modules. For details, please see individual DCC-100 manual [19] or section 'The DCC-100 detector controller' in this manual. If you do not have a DCC-100 in your system you need not install the DCC application. The DCC software is free.

SPCImage Application

SPCImage is the data analysis program for image files obtained in the imaging modes of the SPC-730, SPC-830 and SPC-144. For details, please see SPCImage manual [23]. SPCImage is available on extra order. Installing SPCImage requires a licence keyword.

DLL Libraries and SPC Lab View Drivers

To facilitate the development of user-specific software DLL libraries for the SPC modules, the DCC-100, and the STP-340 Step motor controller are available on extra order. Moreover, Lab View drivers for the SPC modules are available. Installing the DLLs and Lab View drivers requires a licence keyword.

Important note: Before you start into the laborious work of developing your own programs please check whether the problem can be solved by the functions of the Multi-SPC software or by the multi-dimensional recording features of the SPC module. Please do not hesitate to discuss the control problem with bh.

Manuals

The pdf files of the SPC, DCC and SPCImage manuals and the manuals of the DLL libraries are in a ‘manuals’ folder on the CD. The latest versions of the manuals are also available from www.becker-hickl.com.

First Installation

When you put the installation disk into the CD drive the installation procedure starts automatically. If you want to start the procedure on command for whatever reason, start TCSPC_setup_cd.exe from the CD. If the installation is run the first time it comes up with the window shown right.

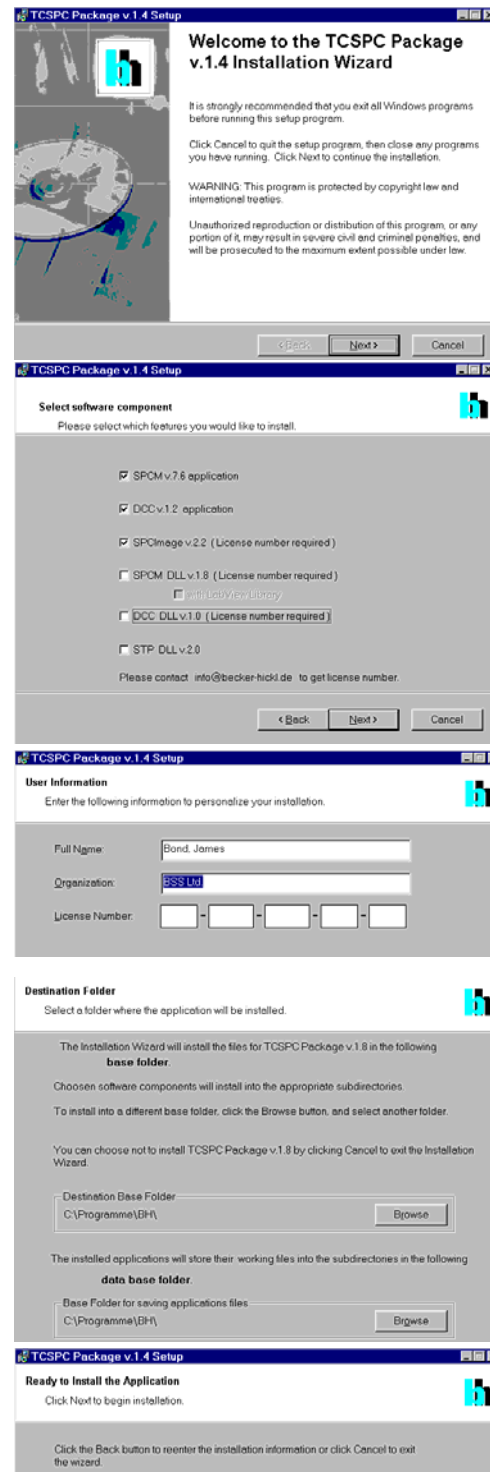
The installation wizard bores you with the usual copyright warnings. We explicitly note that you are allowed

- to install all software features that are not licence-number protected on any computer and in any place you like to.
- to install the key-protected features on several computers within your workgroup for use with all SPC modules you purchased.

The next window allows you to select the software components you want to install. If you have no other modules than the SPC module and do not use it for imaging installing the SPCM application is enough.

If you select features protected by a licence number the next widow asks you for the licence number. Type in your licence number, or, if you cannot find it, please call bh under +49 30 787 56 32 or mail to info@becker-hickl.com. If possible keep the purchase number handy - this simplifies reproducing your licence number.

In the next window you can - but need not - change the directory (‘base folder’) in which the selected software features will be installed. The installation procedure will create individual sub-directories for the selected software components in the selected folder. Moreover, you can define a ‘data base folder’. This folder is used as a working directory, as a default directory for loading and saving data and setup files, and as a source directory for predefined setups.

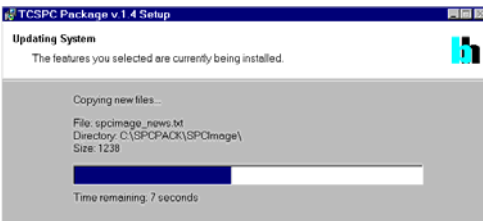


After you confirmed the base directory the installation wizard is ready to install the selected components. You have a last chance to cancel the installation or to go back to the previous step. After clicking on 'Next' the installation goes ahead.

Copying the files will take some 10 seconds for each selected feature. It is not required to re-boot the computer after installation. At the end you get the message 'TCSPC package has been successfully installed'.

If you are using the SPCM and DCC software frequently we recommend to create a shortcut on the desk top.

Note: If software components of the TCSPC package are already installed the next installation of the same version of the package comes up with a different start window. To install additional components or repair a damaged installation please see 'Installing New Features' or 'Software Repair'.



When you have installed the SPC software, please send us an email with your name, address and telephone number. This will help us to provide you with information about new software releases and about new features of your module which may become available in future. We won't use your address to spam you with advertising.

Installing the DLL and Lab View Libraries

DLL and Lab View libraries for the SPC modules can be installed by activating the corresponding buttons in the installation panel, see above. The installation of the libraries requires a licence number. You get this number if you purchase the libraries from bh.

Please note that the DLL and Lab View libraries are only required if you plan to design your own experiment software. They are not required to run the SPCM software.

Please check carefully whether you really need your own experiment software. There is certainly no objection against designing special software for complex instruments dedicated to special applications. However, in many (if not in most) cases software control is only used because the multi-dimensional features of the modules are not understood. In other words, the SPC module is used as a software-controlled classic TCSPC device. Software control then not only causes unnecessary development effort but also results in slow and often inefficient data acquisition. Moreover, problems can arise from undefined processing times due to interrupts, hard disk actions, or other applications running on the same computer. Therefore, please check whether you can solve your control problem by using the multi-dimensional features of the SPC modules. Do not hesitate to contact bh for advice.

Software Update

If you install a newer SPC software version over an older one the installation runs as described under 'First Installation'. Only files are replaced which have a newer date on the CD. This, to a certain extend, avoids overwriting setup files like auto.set (the last system settings) or spc400.ini (hardware configuration). Consequently, you cannot install an older software version in the place of a newer one. If you want to do this (normally there is no reason why you should), run the 'Uninstall' program before installing.

Update from the Web

The latest software versions for all bh modules are available from the Becker & Hickl web site. To install the SPC software from the web, please open www.becker-hickl.com, and click on the ‘Software’ button. On the ‘Software’ page, click on ‘TCSPC Modules’, ‘Operating Software for Windows 95 / 98 / NT4 / 2k / XP’. Then click on ‘Setup’ for SPC-830, SPC-134, SPC-730, SPC-630 (see Fig. 82). Download TCSPC_setup_web.exe and start it. It works the same way as the installation from the CD.

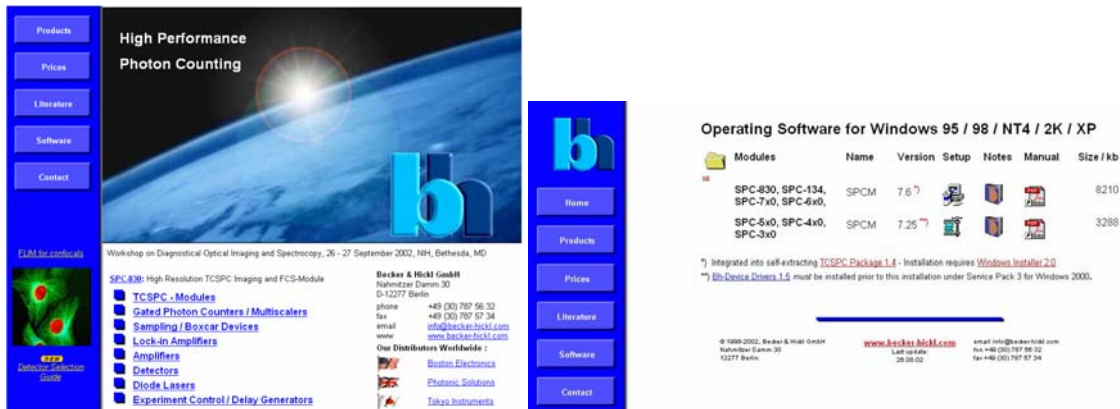


Fig. 82: Downloading the SPCM software from the web

It can - but need not - be required that you have to download the ‘Windows Installer’ from Microsoft. If the setup procedure complains that it is missing, please click on ‘Windows Installer 2.0’.

After installing a new software version we recommend also to download the corresponding manual. Click on ‘Manual’ and download the PDF file. Please see also under ‘Applications’ to find notes about new applications of the bh TCSPC modules.

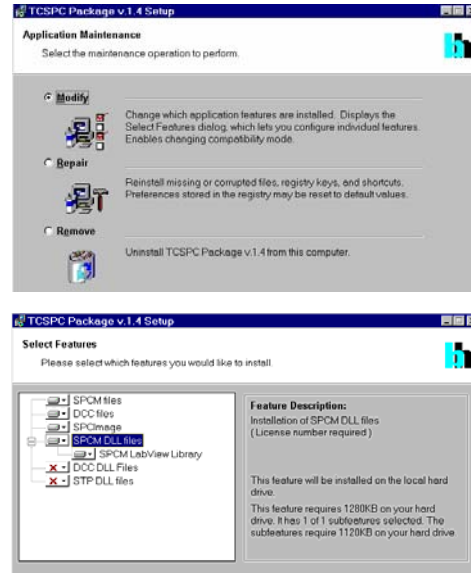
Installing New Software Components

It can happen that you want to add new software components to an existent SPCM installation. In this case the installation procedure recognises the installed components and starts as shown in the figure right.

Chose ‘Modify’ and click on ‘Next’. The next window shows which of the components are installed. To install a new component, click on the field with the ‘X’, and chose ‘Will be installed on local hard drive’. You can also chose ‘Entire feature will be installed on local hard drive’ to install the feature with all available sub-features. If you click on ‘Entire feature will be installed when required’ the feature will be copied from the CD when it is called the first time.

The rest of the installation works as described under ‘First Installation’.

If you have selected a protected feature you will be asked for your licence number. You get the licence number when you purchase the selected component(s). If you have purchased the components but cannot find the licence number, please call bh under +49 30 787 5632 or mail to info@becker-hickl.com.



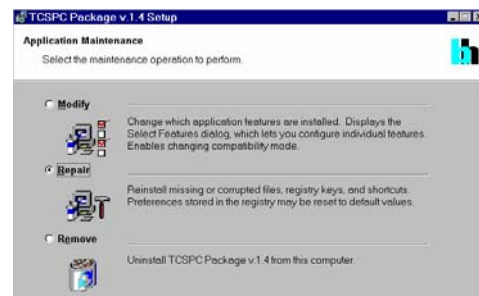
Software Repair

If the TCSPC package has been damaged, e.g. if a file has got lost or corrupted, please start the installation procedure as described above and chose 'Repair'.

The procedure will check your files and, if something is wrong or missing, copy the correct files to the hard disk.

Removing the TCSPC Package

To remove the TCSPC package from your computer, start the installation CD and chose 'Remove'. The 'remove' procedure removes all software components of the package, but not the data and setup files of the measurements.



Hardware Installation - Single SPC Modules

To install the SPC module, switch off the computer and insert the module into a free slot. To avoid damage due to electrostatic discharge we recommend to touch a metallic part of the computer with one hand and then to grasp the module at the metallic back shield with the other hand. This will drain any potentially dangerous charge from you and the module. Then insert the module into a free slot of the computer. Keep the SPC module as far as possible apart from loose cables or other computer modules to avoid noise pick-up.

The SPC-6, SPC-7, SPC-8 and SPC-134 modules have PCI interfaces. Windows has a list of PCI hardware components, and on the start of the operating system, it automatically assigns the required hardware resources to the components of this list. If you have several SPC modules in the computer each module automatically gets its own address range.

Driver Installation

When the computer is started the first time with an SPC module Windows detects the SPC module and attempts to update its list of hardware components. Therefore it may ask for driver information from a disk. When this happens, put the installation CD into the drive and select between 'Win9x' for Windows 95 / 98 and Win2kNT for Windows 2000, Windows NT or Windows XP.

If you don't have the installation disk handy you can download the driver file from the bh web site. Open www.becker-hickl.com and click on 'Software'. On the 'Software' page, click on 'TCSPC Modules', 'Operating Software for Windows 95 / 98 / NT4 / 2k / XP (figure right). Then click on 'BH Device Drivers 1.5' and download the drivers.

Modules	Name	Version	Setup	Notes	Manual	Size / kb
SPC-830, SPC-134, SPC-7x0, SPC-6x0,	SPCM	7.67				8210
SPC-5x0, SPC-4x0, SPC-3x0	SPCM	7.25				3288

*) Integrated into self-extracting TCSPC Package 1.4 - Installation requires Windows Installer 2.0.
**) BH Device Drivers 1.5 must be installed prior to this installation under Service Pack 3 for Windows 2000.

© 1999-2000, Becker & Hickl GmbH
Hanns-Martin-Schleyer-Str. 30
12277 Berlin

www.becker-hickl.com
e-mail: support@becker-hickl.com
tel: +49 (0)30 797 87 32
fax: +49 (0)30 797 87 34

Hardware Installation - Several SPC Modules

Up to four SPC modules of similar type can be operated in one computer by one Multi-SPC application. If you plan to build up a multi SPC configuration you should check that you have a computer with a sufficient number of free PCI slots. Because the SPC-6, SPC-7 and SPC-8 occupy two PCI slots there is space for only two modules in a standard PC. Consequently, operation of more than two SPC-6, -7 or -8 modules requires an industrial PC with more PCI slots.

The SPC-134 and the SPC-144 are packages of four single-width cards which can be inserted in a standard PC. However, the power supply must be strong enough to deliver 3.5 to 4 A at +5V for each module. Although most computers have no problems to power two SPCs, operating the SPC-134 or the SPC-144 can be a problem if the computer itself is a fast, power eating high-end machine.

Problems with the power supply often result from improper power supply cables rather than from the power supply itself. The cable from the power supply to the motherboard often is too long and has insufficient cross section. Thus, there is too much voltage drop on the cable. If less than 4.8 V arrive at the SPC module the DC-DC converters on the module may shut down. You can easily check the situation by measuring the output voltage at the sub-D connector of the SPC-module. There should be more than +4.8 V at pin 1 and -4.9 V to -5 V at pin 6 referred to pin 5 (ground). If the voltage is lower, make the power cables from the computer power supply to the motherboard shorter or use a stronger power supply which (hopefully) has thicker cables. The latest versions of the SPC-134 and -144 have an additional power connector that can be connected to a free floppy-disk power cable. This usually solves any power-supply problems.

The SPC-134 and SPC-144 packages comes with a fan assembly which is plugged onto the four adjacent cards. Please make sure that the assembly is attached correctly and all fans are working. The correct setup is shown in Fig. 83. Working without the fans for an extended period can cause serious damage to the modules and to the computer. Please check the temperature of the computer when the system has been run for the first 30 minutes or so. If necessary, improve the air flow in the computer, e.g. by installing a second fan in the computer case.

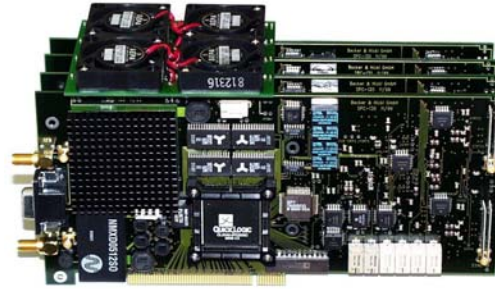


Fig. 83: Fan assembly of the SPC-134 and SPC-144 packages

Software Start

When the module is inserted, switch on, start Windows and start the Multi SPC Software. The initialisation panel shown in Fig. 84, left should appear. The installed modules are marked as 'In use'. The modules are shown with their serial number, PCI address and slot number.

Important: If the SPC module is not found at this stage, e.g. because the driver was not installed, the software starts in an emulation mode (see below, 'Starting the SPC software without an SPC module'). What you see in this mode is generated by the software or loaded from a file - it is not the data recorded by your SPC module!

The software runs a simple hardware test when it initialises the modules. If an error is found, a message 'Hardware Errors Found' is given and the corresponding module is marked red. In

case of non-fatal hardware errors you can start the SPCM main window by selecting ‘Hardware Mode’ in the ‘Change Mode’ panel. Please note that this feature is intended for trouble shooting and repair rather than for normal use.

When the initialisation window appears, click on ‘OK’ to open the main window of the Multi SPC Software. At the first start the software comes up with default parameter settings which may be not appropriate for your measurement problem. Therefore, changes may be required for your particular application. Typical parameter settings are given under ‘Recommended System Parameters’, page 108. The parameters and their mutual dependence, the measurement modes, display modes etc. are described in chapter ‘SPCM Software’, starting on page 233.

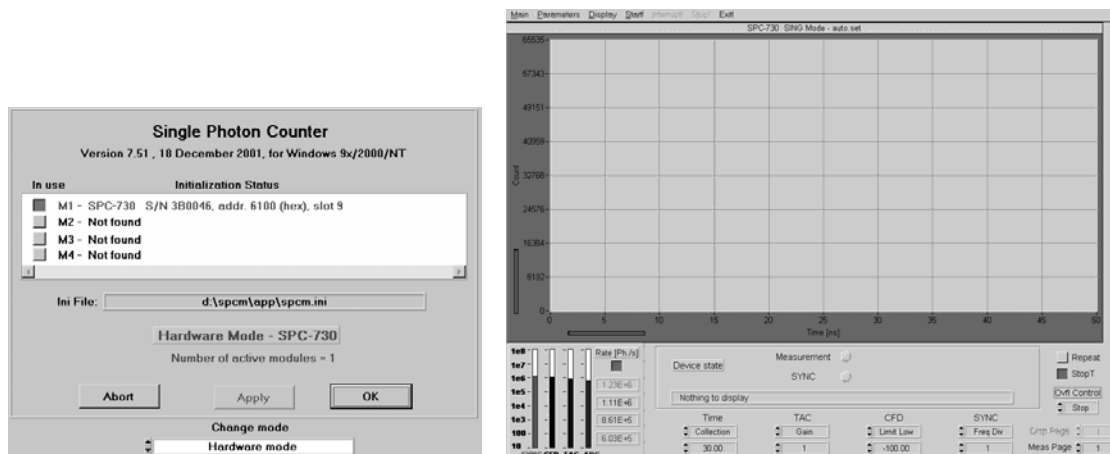


Fig. 84: Starting the SPCM software. Initialisation panel (left) and main panel of SPCM (right)

When you exit the Multi SPC software after changing parameters, the system settings are saved in a file ‘auto.set’. This file is automatically loaded at the next program start. So the system will come up in the same state as it was left before.

Module Test Program

If you suspect any problems with the bus interface, the timing and control circuits or the memory of the SPC module, run the ‘SPC Test’ program delivered with the SPC Standard Software. The main panel of this program is shown right.

Switch on ‘All Parts’, ‘Repeat’ and ‘Break on Error’ and start the test. If the program performs several test loops (indicated by ‘Test Count’) without indicating an error you may be sure that the bus interface, the timing and control circuits and the memory of the module work correctly. Depending on the type of the SPC module and the speed of the computer, it can take some minutes to run one test loop.

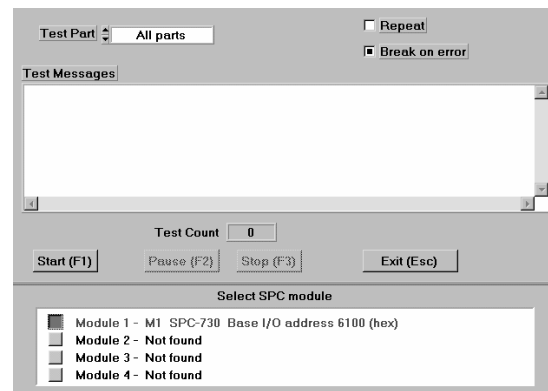


Fig. 85: Module test program

Installation Problems

If there should be any malfunction after installing the SPC it may have one of the following reasons:

- Computer does not start: Module not correctly inserted or connector dirty. Clean connector with ethanol, propanol or acetone, insert module carefully. In terms of mechanical dimensions, computers are anything but precision devices. Sometimes there is some side play in the connector, and mechanical stress can cause contact problems.
- Module not found: Driver not correctly installed.
- Module not found: CMOS setting of the computer is wrong. New PCI devices are not accepted. Set ‘Plug&Play’ ‘off’. Or try with another computer.
- Module not found: Module not correctly inserted or connector dirty. Clean connector with ethanol, propanol or acetone, insert module carefully. In terms of mechanical dimensions, computers are anything but precision devices. Sometimes there is some side play in the connector, and mechanical stress can cause contact problems.
- Module not found: Another driver overwrites the SPC driver. Especially some driver versions of Ocean Optics spectrometers use to overwrite drivers of devices using the same bus interface chip.
- Module found, but measurement does not work. ‘SYNC OK’ light on without SYNC input: Power supply insufficient. Check the voltage at the sub-D connector, see ‘Hardware Installation - Several SPC Modules’.
- If you have problems with the installation that you cannot solve by the hints given above please call +49 / 30 787 56 32 or send an email to info@becker-hickl.com. If the fault looks like a software problem you are welcome to contact our software expert Stefan Smietana directly, +49 / 30 787 56 32, smietana@becker-hickl.com.

Starting the SPC Software without an SPC Module

You can use the Multi SPC Software without an SPC module. In its start window the software will display a warning that the module is not present, see Fig. 86.

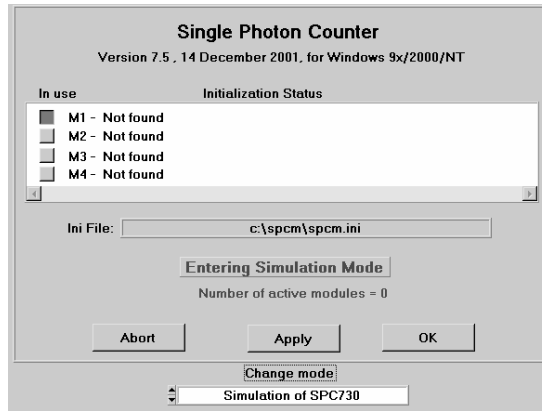


Fig. 86: Startup panel in the simulation mode (without a TCSPC module)

To configure the software for the desired module type, click into the ‘Change Mode’ field and select the module type from the list which is opened. Click on the ‘in use’ buttons for the modules you want to have active. Then click on ‘Apply’, ‘OK’. The software will start in a special mode and emulate the SPC device memory in the computer memory. You can set the

TCSPC system parameters, load, save, process, convert and display data, i.e. do everything except for a real measurement.

Clicking on an .sdt file name in the windows explorer, windows commander, etc., starts the SPCM software automatically.

Agents: Boston Electronics, (800)347-5445, TCSPC@boselec.com

Agents: Boston Electronics, (800)347-5445, TCSPC@boselec.com

Operating the SPC Module

Detector and Reference Inputs

For the basic measurement modes, all SPC modules need two input signals:

- the single photon pulses from the detector
- the synchronisation signal derived from the pulse sequence of the light source

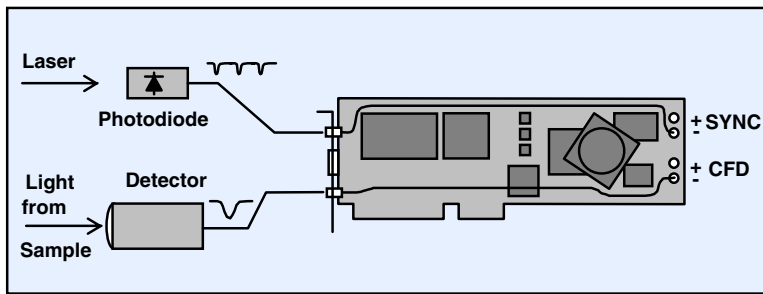


Fig. 87: Basic connections required to operate a TCSPC module

The SPC-x0x modules accept either positive or negative input signals. To select the polarity, plug the cables from the front panel into the appropriate connector on the board. Terminate the unused inputs with the 50 Ohm terminators delivered with the board. After manufacturing both inputs are set to ‘negative’. The pulses at both inputs should be in the amplitude range of 10...80 mV. Due to the finite bandwidth of the input circuitry the amplitudes may be higher if the pulse duration is below 1ns.

The SPC-x3x modules (including the SPC-134 and SPC-144) need negative input pulses at both inputs. The pulses amplitude on both inputs should be in the range of -50 mV to -1 V. If you have positive pulses, please use an A-PPI inverter (see Fig. 18) in front of the input.

The inputs of both the SPC-x0x and the SPC-x3x are protected with diodes that limit input amplitudes to about 1.5 V. The diodes withstand input currents up to 2A (100V from a 50 Ohm source) for times <1us. DC input currents should not exceed 100mA (5V from a 50 Ohm source). Thus, pulses with amplitudes up to some volts will normally not damage the SPC modules. The most likely source of damage are pulses that have both high amplitudes and extremely short rise times. Such pulses can appear at the outputs of PMTs, and if a signal cable from an operating PMT is connected to the input of the SPC module, see ‘Safety Recommendations for Using Detectors’, page 76. It is therefore recommended to connect PMTs to the SPC inputs via preamplifiers.

Generating the Reference Signal

The TCSPC module measures the times of the single-photon pulses of a detector or a number of detectors to the next pulse at the reference, or synchronisation input. The reference pulses are normally derived from the excitation light source.

To derive the synchronisation signal from a laser pulse sequence a fast PIN photodiode with >300 MHz bandwidth can be used. Two simple circuits for positive and negative output pulses are shown in Fig. 88. For the SPC-x30 modules the circuit for negative output should be used. To obtain short pulses the PIN photodiode should be operated close to its maximum reverse voltage, typically 20 to 30 V.

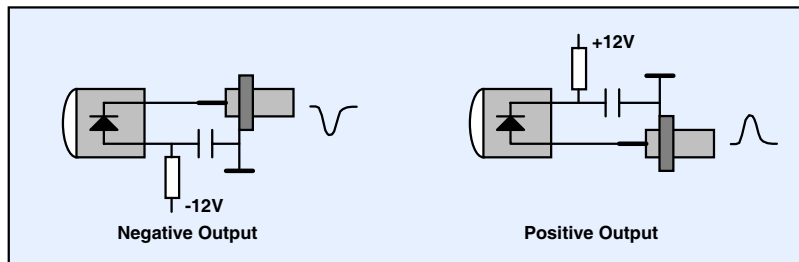


Fig. 88: Using a PIN photodiode for reference signal generation

Complete photodiode modules are available from Becker & Hickl, see Fig. 89. These modules get their +12V supply voltage from the SPC module so that no special power supply is required. For low repetition rates we recommend the PDM-400, for high repetition rates the PHD-400 which incorporates a current indicator for convenient adjusting. Please see www.becker-hickl.com.



Fig. 89: Photodiode modules for reference signal generation

The optimum pulse amplitude for the SPC-x30 modules is between 100 and 500 mV. When a PIN photodiode is used to generate a reference signal from a Titanium:Sapphire laser an unfocused reflex from a glass surface is often enough to obtain enough signal amplitude. If the amplitude is too small focusing the full beam diameter on the diode chip usually solves the problem. In Titanium:Sapphire systems with frequency multiplying the reference signal should be derived from the fundamental wavelength. The pulses at the fundamental wavelength not only have the smallest amplitude fluctuation, they are also in a wavelength range where a silicon photodiode has its efficiency maximum.

Modern Titanium:Sapphire lasers often incorporate a reference photodiode. In general, the signals delivered by the lasers can be used as reference pulses for the SPC modules. The pulses should be checked for pulse amplitude and pulse polarity. (Use an oscilloscope of more than 400 MHz bandwidth, and switch the input to 50Ω .) The amplitude should be higher than 50 mV for reliable synchronisation of the SPC module. If the pulse polarity is positive, and an SPC-x30 module is used, the polarity can be reversed by an A-PPI pulse inverter, see Fig. 18. Problems can arise from noise and line frequency pickup via ground loops. Indications of noise pickup are poor time resolution, or synchronisation at a wrong frequency. Therefore the rate display in the main panel should be switched on and the SYNC rate be checked.

Picosecond diode lasers normally deliver reference pulses that are precisely correlated with the light pulses (see bh BDL, BHL, and BHLP lasers, www.becker-hickl.com). It may be necessary to reverse the pulses with an A-PPI inverter. PIN photodiodes should not be used to generate reference signals from the optical output of diode lasers. A PIN photodiode has a sensitivity of about 0.5 A/W in the NIR region. For wavelengths in the blue or ultraviolet region the sensitivity is lower. A simple comparison with the pulse power of a diode laser shows that almost the full laser power is required to generate a reasonable synchronisation signal [46].

In multi-module systems, e.g. the SPC-134, SPC-144, or in systems containing two SPC-630 or -830 it may be required to distribute a reference signal to several TCSPC modules. For this purpose, only reflection-free power splitters should be used. Suitable splitters for 1:2 and 1:4 signal distribution are available from bh, see Fig. 18. It should, however, be taken into regard that the signal amplitude for 1:2 and 1:4 distribution drops by a factor of 2 and 4, respectively. The loss in amplitude is no problem if the reference signal is obtained from a solid-state laser via a photodiode. In other cases an amplifier may be required.

If a reference signal has to be derived from optical pulses of low peak power an avalanche photodiode (APD) can be used, see bh APM modules, www.becker-hickl.com. The avalanche effect introduces gain noise; therefore an APD should be operated at the lowest gain possible.

There are a few cases where even an APD is unable to generate reference pulses of sufficient amplitude. Typical cases are luminescence decay measurement by ns flashlamps [379], positron lifetime experiments [209], experiments of sonoluminescence [14, 112, 141], the measurement of the decay time of scintillators by radioactive decay, or the measurement of electrical barrier discharges [366, 367] (see ‘Barrier Discharges’, page 226). In these cases it may be required to use a PMT to generate the reference signal. A good choice for reference generation are the Hamamatsu H5773 and H5783 photosensor modules. The modules must be operated at a gain below the single-photon detection level, i.e. with a gain control voltage no higher than 0.7 V [46]. Please note that the maximum output current of 100 µA sets a limit to the possible amplitude and repetition rate of the reference signal.

PMTs or SPADs at the reference (stop) input are also as stop detectors for photon correlation experiments, see ‘Picosecond Photon Correlation’, page 203. The situation differs from the cases described above in that the PMT or SPAD is used as a single-photon detector. The requirements to the single-photon pulses and the way the detector are connected are the same as described for the detectors at the start input.

Delayed Stop Operation

The typical TCSPC setup measures the times of the individual photons of an optical signal that is exited by some kind of pulsed light source. The photon times are measured relative to synchronisation pulses derived from the light source. Modern TCSPC devices are normally optimised for ‘reversed start-stop’ operation, see Fig. 26, page 21. The pulse period of the light source is often considered constant, and the time measurement is performed from the photon to the next laser pulse. For a laser with a constant pulse period on the order of 10 to 50 ns this mode of TCSPC operation delivers satisfactory results.

However, not all lasers can be considered to deliver negligible pulse-period jitter. If the photon times are measured from the photon to the next laser pulse the pulse period jitter adds to the transit-time jitter of the detector. The repetition rate of the excitation pulses may also be variable, i.e. by changing the pulse reduction ratio of a pulse picker or the oscillator frequency of a diode laser. The result is a shift of the recorded photon times with the repetition rate, which is at least inconvenient. Moreover, the pulse period may simply be too long to measure reasonable photon times by stopping with the next pulse.

The problem can easily be avoided by inserting a delay line in the SYNC path of the SPC module, see Fig. 90. The upper part of the figure shows stopping with the next laser pulse. The laser pulse that generated the detected photon is marked black. If the pulse period changes (upper part, left and right) the measured photon time changes correspondingly.

With an appropriate delay in the reference channel the time of the photon is measured against the laser pulse that initiated the detected photon. The measured photon time does not depend on the pulse period, see lower part of Fig. 90. TCSPC with delayed stop operation can even be used to record the shape of entirely random light pulses, see paragraph below.

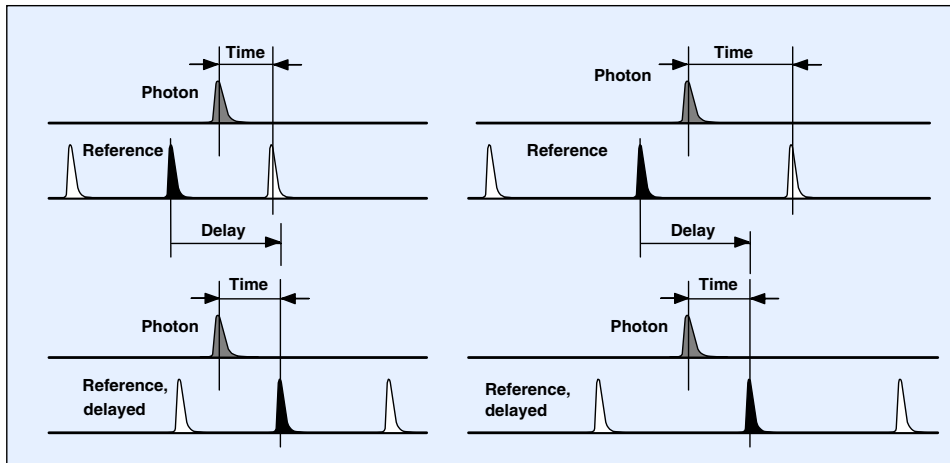


Fig. 90: Upper part: Stop with the undelayed laser pulse, different period of laser pulses. The laser pulse which released the photon is marked black; the measured photon time depends on the laser period. Lower part: Stop with the delayed laser pulse. With an appropriate delay in the reference channel the time of the photon is measured against the laser pulse that generated the photon. The measured photon time does not depend on the signal period.

The required delay can easily be obtained by a cable in the reference (SYNC) path, see Fig. 91. The delay should be approximately the desired measurement time interval, plus the difference in the transit times of the detector and photodiode path. A good reference delay to start with is 15 ns or 3 m cable for an MCP PMT and 25 ns or 5 m cable for TO-8 PMTs, photo-sensor modules, or the bh PMH-100 and PMC-100 detectors. Adjusting the delay cable length is described on page 124.

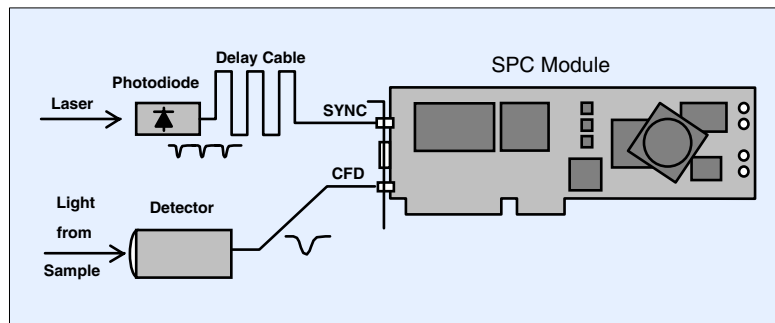


Fig. 91: Delayed stop operation

Synchronisation to Random Signals

There are a few TCSPC applications where the light pulses appear at entirely random times. Typical examples are experiments on electrical barrier discharges, positron lifetime experiment, and sonoluminescence. Because the light pulses are not generated by an external event, such as a laser pulse, an independent timing reference signal does not exist. Nevertheless, TCSPC can be used to record the shape of such signals. The principle is shown in Fig. 92.

PMT 1 is the reference PMT. It is operated at a relatively low gain and receives a strong signal from the sample. Consequently, it delivers a signal roughly corresponding to the true shape of

the optical pulse. These reference pulses are delayed and fed into the SYNC input of the TCSPC module. Even if the pulses vary in amplitude, the constant fraction discriminator of the SYNC channel produces a timing signal that is reasonably correlated with the leading edge of the light pulses.

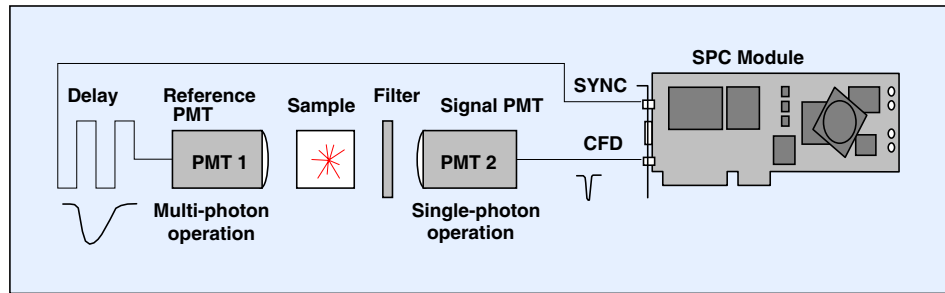


Fig. 92: Recording random light pulses by a TCSPC module

PMT 2 receives the light through a set of filters, a monochromator, or another optical element that transmits only a small fraction of the photons. The gain of PMT 2 is high. Therefore it delivers single-photon pulses. If the intensity at PMT 2 is low enough correct single-photon operation is achieved, and the TCSPC module records the shape of the light pulses emitted by the sample.

Connecting the Detectors

The detectors commonly used with bh TCSPC modules are described under ‘Description of Selected Detectors’, page 63. A detailed discussion of different detectors is given in [46]. It is impossible here to give detailed instructions for any possible single-detector or multi-detector system in any possible application. Nevertheless, the following section gives examples of the most frequently used detector configurations.

Single-Detector Systems

Extremely simple systems can be built with the PMH-100 and PMC-100 detectors and a bh picosecond diode laser. The components and cable connections for a PMH-100 detector are shown in Fig. 93.

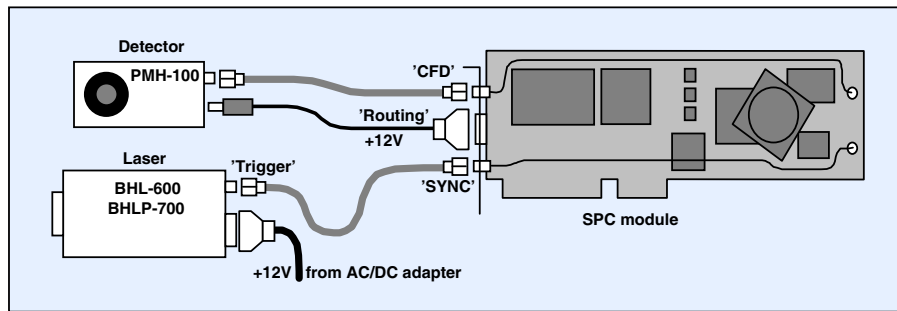


Fig. 93: Connecting the PMH-100 detector

No further components or cable connections are needed. The cables are included in the standard cable set delivered with the SPC module. The drawback of the simple system shown in Fig. 93 is that the detector is switched on all the time when the SPC module is active.

The system shown in Fig. 94 uses a PMC-100 detector that is controlled via a DCC-100 detector controller. The PMC-100 is connected to the DCC-100 via its standard power supply ca-

ble. The cable connects the +12V power supply, the gain control signal, and the power supply for the peltier cooler from the DCC-100 to the PMC-100, and the overload signal of the PMC-100 to the DCC-100. Thus, the operation of the detector is fully controlled via the DCC-100. The photon-pulse output of the PMC-100 is connected directly - without an additional amplifier - to the 'CFD' input of the TCSPC module. The reference signal comes directly from the laser. Any of the bh BDL, BHL, or BHLP lasers can be used. The BDL (NUV and blue) lasers deliver positive pulses and require the A-PPI pulse inverter (see Fig. 18). All cables and the A-PPI are included in the standard cable set delivered with the SPC module and the PMC-100.

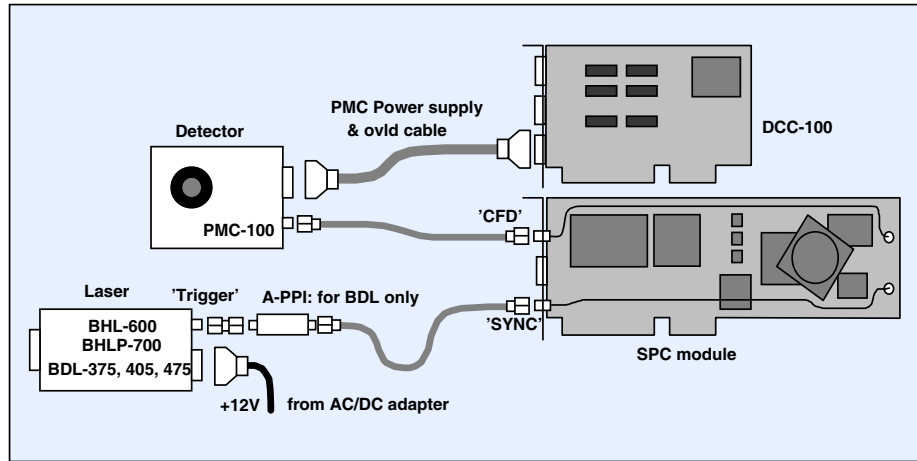


Fig. 94: Connecting the PMC-100 detector to a bh TCSPC system

Fig. 95 shows how a Hamamatsu H7422 module is connected to the same TCSPC system. The +12V power supply, the gain control signal, and the peltier cooler current are delivered by the DCC-100 via the H7422-DCC power supply cable. Because the H7422 does not contain a preamplifier a HFAC-26-2 amplifier is used in the photon pulse path. The overload signal of the HFAC-26 is connected to the DCC-100; the power supply comes from the routing connector of the SPC module.

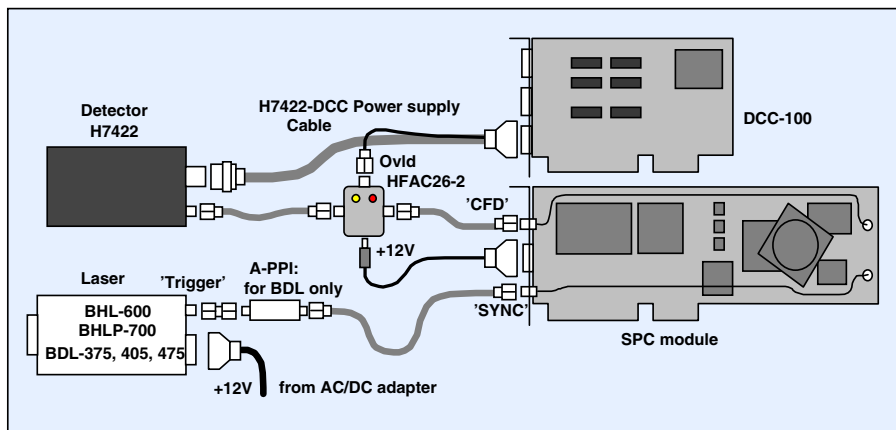


Fig. 95: Connecting a H7422 PMT module to a bh TCSPC system

A TCSPC system with an R3809U MCP PMT is shown in Fig. 96. The high voltage for the R3809U is delivered by an FuG HCN14-3500 power supply. The HCN14-3500 is controlled by a signal delivered by the DCC-100. The single photon pulses of the MCP PMT are amplified by an HFAC-26-01 preamplifier. The overload signal of the HFAC-26 is connected to the DCC-100. If the overload signal becomes active the DCC shuts down the high voltage delivered by the HCN14-3500.

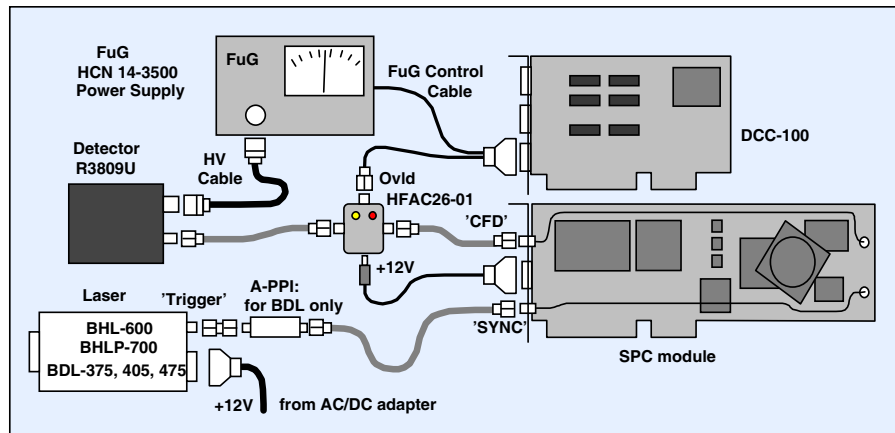


Fig. 96: Operation of an R3809U MCP PMT in a bh TCSPC system

Important: Monitor cables for PCs have the same connectors and generally the same connection scheme as the power supply cables of the PMC-100. However, some monitor cables have not all lines connected, or even have some pins connected in parallel. This can cause malfunctions of the detectors or even damage the DCC-100 module. Therefore, please use only the router and detector cables delivered with the SPC or PMC modules.

The connection of a single SPCM-AQR (SPAD) module to an SPC-x30 module is shown in Fig. 97. The SPCM delivers positive output pulses of about 4 V peak amplitude. Therefore, a 20-db attenuator and an A-PPI pulse inverter are inserted in the detector signal line.

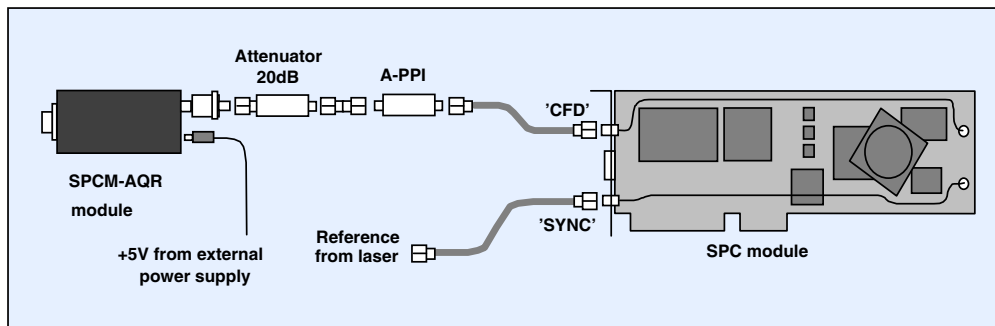


Fig. 97: Connecting an SPCM-AQR detector to an SPC module

Multi-Detector Systems

A TCSPC system with two PMC-100 detectors is shown in Fig. 98. Both detectors are controlled by a single DCC-100 card. The DCC-100 is configured to connect the coolers of both PMCs in series (see DCC-100 manual). The photon pulses of the PMCs are connected to two inputs of an HRT-41 router. The combined photon pulses of the detectors are available at the timing output of the router and are connected into the 'CFD' input of the TCSPC module. The routing signal delivered by the router is connected to the 'Routing' input of the SPC module. Because both the PMC-100 and the HRT41 router have internal preamplifiers the total gain of the PMC-HRT combination is about 100. The high gain can cause problems with the noise of the high-voltage generator of the photosensor modules used in the PMCs. Therefore two 12-dB attenuators are inserted in the photon pulse lines.

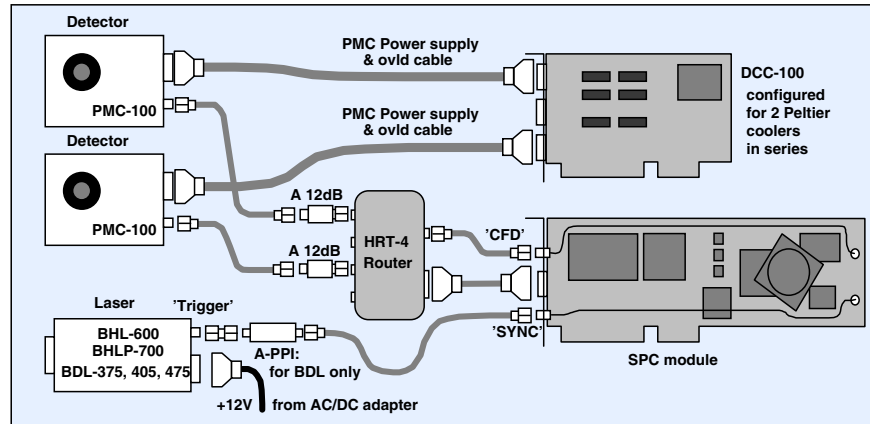


Fig. 98: Dual detector system with two PMC-100 and a HRT-4 router

The setup shown in Fig. 98 can be used with more than two detectors. With a HRT41 router up to four, with an HRT81 router up to eight detectors can be connected to one SPC module. Additional PMCs can be controlled by additional DCC cards. For more than four PMCs it may be convenient to connect the gain control and overload signals of several PMCs parallel and to drive the coolers from an external power supply.

A dual-detector system with two R3809U MCP PMTs is shown in Fig. 99. The R3809U MCP PMTs are used with HFAC-26-01 preamplifiers. The amplified PMT pulses are connected to the HRT-41 router. Attenuators of 10 to 20 dB can (but need not) be inserted to keep the gain within reasonable limits. The amount of attenuation needed depends on the gain of the R3809U PMTs and the environment noise possibly picked up by the detectors.

The overload signals of both preamplifiers are connected parallel by a standard power combiner and fed into the overload input of the DCC-100. The DCC-100 controls an FuG HCN14-3500 high voltage power supply. The high voltage output of the HCN-14-3500 is split into two branches for the two detectors. Thus, the DCC-100 shuts down the high voltage of both detectors if one of the preamplifiers detects an overload condition.

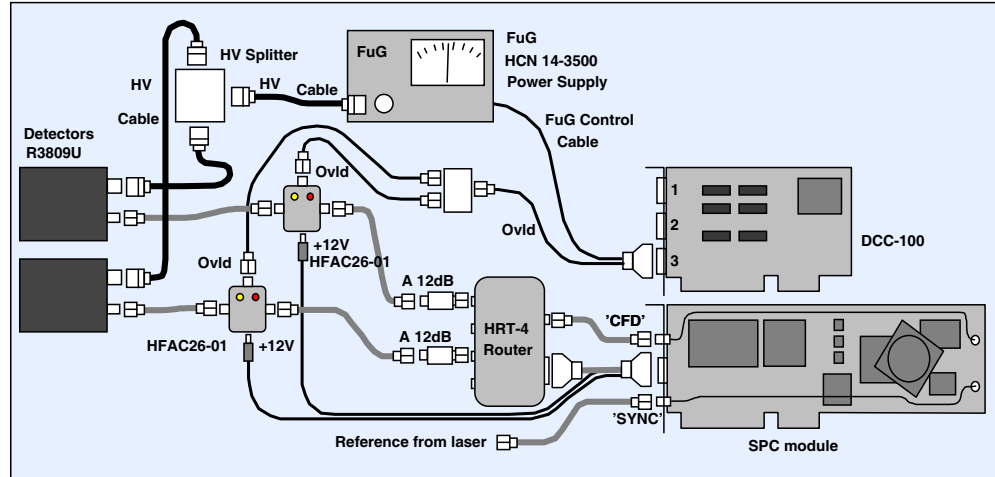


Fig. 99: Dual-detector system with two R3809U MCP PMTs

A number of modifications are possible in this setup. The control cable can be connected also to output 1 of the DCC-100 instead of output 3. Except for the operation of a cooler, both outputs are equivalent. The +12 V power supply of the preamplifiers can also be taken from connector 2 of the DCC-100. However, in this case make sure that the +12 V output of DCC output 2 is switched on in the DCC software panel. It may also be convenient to use individual

high-voltage power supplies for the two detectors, especially if the detectors differ considerably in gain. In this case one high-voltage power supply is controlled from output 1 of the DCC, the other from output 3. If you use two power supplies, please make sure that the overload signals of the two preamplifiers are connected to the correct DCC connector.

Fig. 100 shows a system based on the bh PML-16 16-channel detector head. The routing signal of the PML-16 is connected to the ‘Routing’ connector of the SPC module. The PML-16 gets its ± 5 V power supply via the routing cable. The high voltage of typically -900 to -1000V is delivered by an FuG HCN14-3500 power supply. The high voltage power supply can (but need not) be controlled via a DCC-100 detector controller.

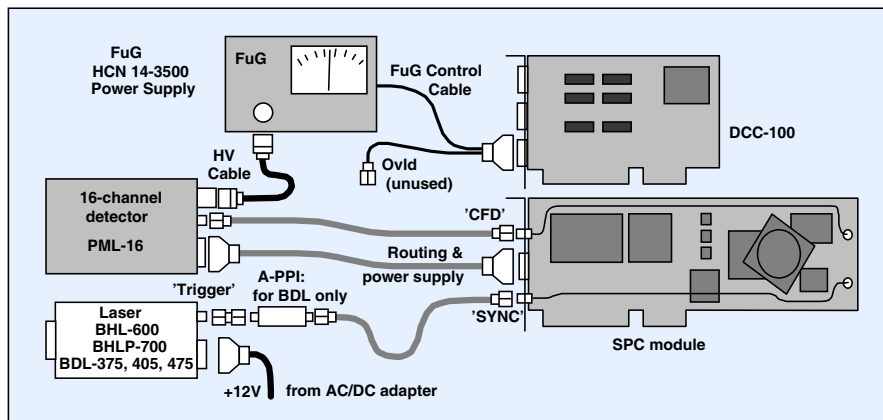


Fig. 100: 16-channel parallel detection system with PML-16

TCSPC systems for single-molecule spectroscopy often use several Perkin Elmer SPCM-AQR detectors. The connection of up to eight SPCM-AQRs to one SPC modules is possible via the HRT-82 router. The principle is shown in Fig. 101.

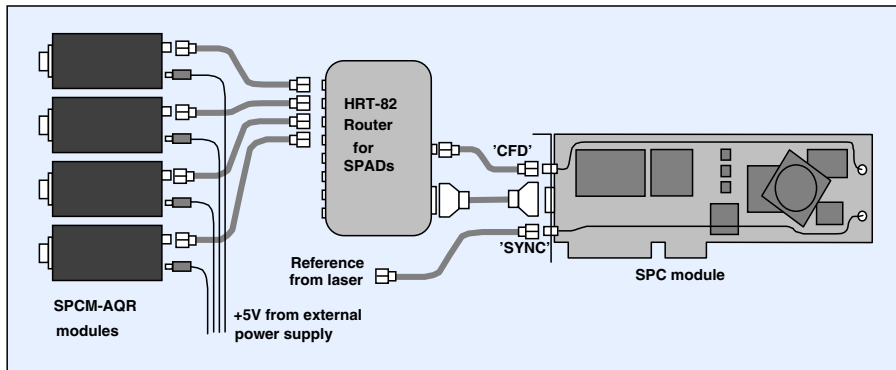


Fig. 101: Connecting several SPCM-AQR modules to one SPC module

The same setup can be used for other SPAD modules delivering TTL pulses, or PMT modules with internal discriminators and TTL output.

Important: Monitor cables for PCs have the same connectors and generally the same connection scheme as the router and the power supply cables of the HRT, PMC and PML modules. However, some monitor cable have not all lines connected, or even have some pins connected in parallel. This can cause malfunction of the routers and detectors or even damage the SPC or DCC modules. Therefore, please use only the router and detector cables delivered with the SPC modules or routers.

Using the Experiment Trigger

The SPC-6, -7, -8 and the SPC-130/134 and SPC-140/144 modules have an ‘Experiment Trigger’ to start a measurement by an externally applied TTL/CMOS trigger signal. The experiment trigger is a simple, but extremely powerful experiment control feature of the bh SPC modules. By using the experiment trigger complex experiment procedures can often be performed in the SPCM standard software, i.e. without the need of special DLL or LabView programming. Moreover, because the experiment trigger is a hardware function the response of the SPC modules to a trigger event is virtually immediate. The trigger can therefore be used for a number of real-time applications that are entirely beyond the capabilities of software control. A few typical applications are:

- Slow Scan applications. A sample is scanned by a step motor assembly or a piezo scan stage, or a spectrum is scanned by a step-motor-driven monochromator. After each step of the scan, the scan controller sends a trigger pulse to the SPC module. Each trigger initiates an individual measurement in the SPC module. The results can be saved in individual files, or written into a number of subsequent ‘pages’ of the memory. Page stepping can either be accomplished by using the page stepping function of the ‘Single’ of $f(txy)$ mode, or the ‘continuous flow’ mode. Moreover, the $f_i(t)$ or $f_i(ext)$ spectrum scan modes can be used to convert the sequence of decay curves directly into time-resolved spectra.
- Measurement of signals that are present only during brief periods of time. A measurement is performed in the Oscilloscope, Single, or $f(txy)$ mode. The measurement is started when the signal is present and continued for a ‘collection time’ corresponding to the typical dwell time of the signal. The results can either be accumulated, stored into subsequent memory blocks, or saved into individual files.
- Sequential recording (‘double-kinetic mode’). Started by the experiment trigger, the SPC module records a hardware-controlled sequence of decay curves. In the ‘continuous flow mode’ or in the ‘Scan Sync Out’ mode the sequence can be as fast as a few μs per curve. To obtain a reasonable number of photons within a collection time this short a large number of triggers sequences can be accumulated (see ‘Chlorophyll Transients’, page 158).
- Starting the measurement synchronously in a multi-modules system.

The experiment trigger input is at pin 13 of the 15 pin sub-D connector. In some SPC modules the experiment trigger shares one pin with the ‘Add/Sub’ signal, see ‘Routing and Control Signals’, page 348. The experiment trigger function is then only available if the system parameter ‘Add/Sub Signal’ is set to ‘add only’. The electrical configuration of the experiment trigger input is shown in Fig. 102.

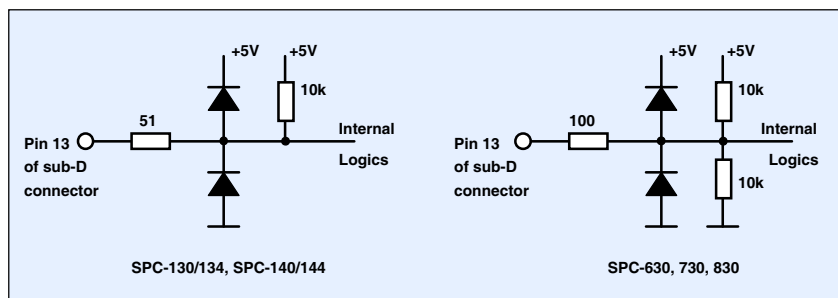


Fig. 102: Experiment trigger input

The $51\ \Omega$ or $100\ \Omega$ series resistor and the diodes are used for overvoltage protection. The $10\ k\Omega$ resistors provide a defined ‘high’ level when the input is open. Thus, the experiment trigger can either be driven from a standard TTL or CMOS gate or by a switch that connects pin 13 to ground. Connecting the input to ground generates a falling, disconnecting it a rising

trigger signal edge. To trigger a measurement by an optical pulse a phototransistor or photodiode can be connected from pin 13 to ground.

If the experiment trigger is used in multi-detector systems a split router cable may be required. Suitable cables are available from bh.

TCSPC Scanning Techniques

f(xyt) mode

Imaging in the ‘f(xyt)’ mode is shown in Fig. 103. Scanning is accomplished by two piezo- or galvanometer-driven mirrors. The excitation spot sweeps over the sample in 128 rows and 128 columns. The x-y position of the spot is used as a routing signal for an SPC-700/730 or SPC-830 module. The routing bits are either taken directly from the scan controller or - if a digital x-y signal is not available - generated by digitising the analog x and y signals by a bh SCAD-2 dual ADC module.

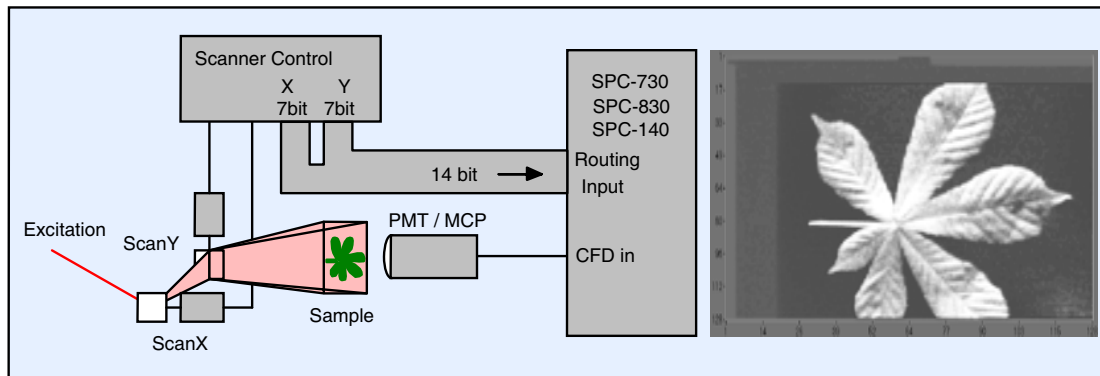


Fig. 103: Imaging in the f(xyt) mode

As long as the scan controller is able to deliver a correct xy position there is practically no limitation of the scanning rate. Subsequent frames of the scan are accumulated automatically, i.e. the data acquisition can be run until a sufficient number of photons have been collected.

Due to the maximum number of 14 routing bits in the SPC-700/730 and SPC-830 the maximum number of pixels is 16,384, or 128 x 128 for a square image. Since the routing inputs of the SPC module are used for imaging the method cannot reasonably be used for multi-detector setups.

Scan Sync In Mode

The ‘Scan Sync In’ mode is implemented in the SPC-700/730, SPC-830 and the SPC-140/144 modules. The TCSPC module receives synchronisation pulses from the scanner. These pulses control the start of a new frame, a new line and a new pixel in the scanning logic of the SPC module. The ‘Scan Sync In’ mode is compatible with almost any laser scanning microscope and with fast ophthalmic scanners.

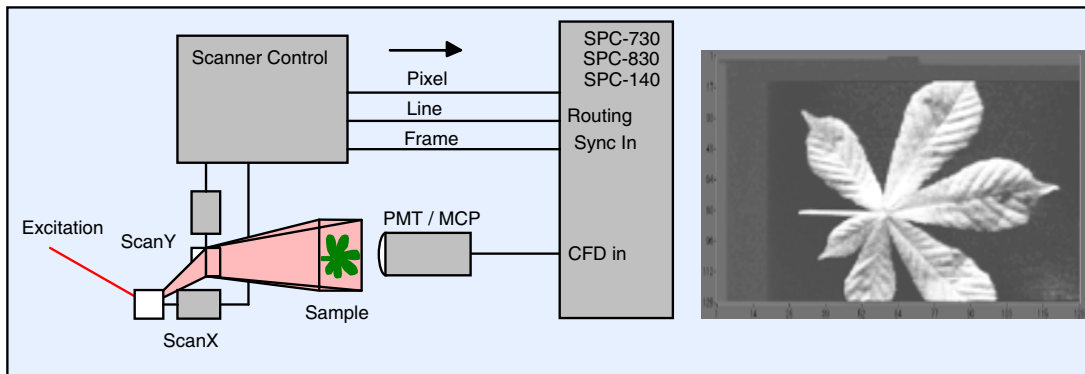


Fig. 104: Imaging in the Scan Sync In mode

The scan rate in the ‘Scan Sync In’ mode is limited only by the speed of the scanner. Subsequent frames of the scan are accumulated automatically, i.e. the data acquisition can be run until a sufficient number of photons have been collected.

Since the scanning logic of the SPC module generates the routing information internally the image size is not limited by the number of routing bits. Therefore, images sizes up to 256x256 can be obtained with the SPC-700/730. In the SPC-830 and SPC140/144 modules images with much higher pixel numbers can be recorded. Some numbers are given in the table below.

ADC resolution, channels	1024	256	64	16	4	1
SPC-700/730	64x64	128x128	256x256	-	-	-
SPC-140	64x64	128x128	256x256	512x512	1024x1024	2048x2048
SPC-830	128x128	256x256	512x512	1024x1024	2048x2408	4096x4096

The ‘Scan Sync In’ mode can be used in conjunction with a multidetector setup and a router, i.e. images from several detectors can be recorded in the same scan.

Scan Sync Out Mode

In the ‘Scan Sync Out Mode’ the SPC module controls the scanning device via Frame, Line and Pixel pulses. The mode is available in the SPC-700/730, SPC-830, and SPC-140/144 modules. These pulses control the start of a new frame, a new line and a new pixel in an external scan controller.

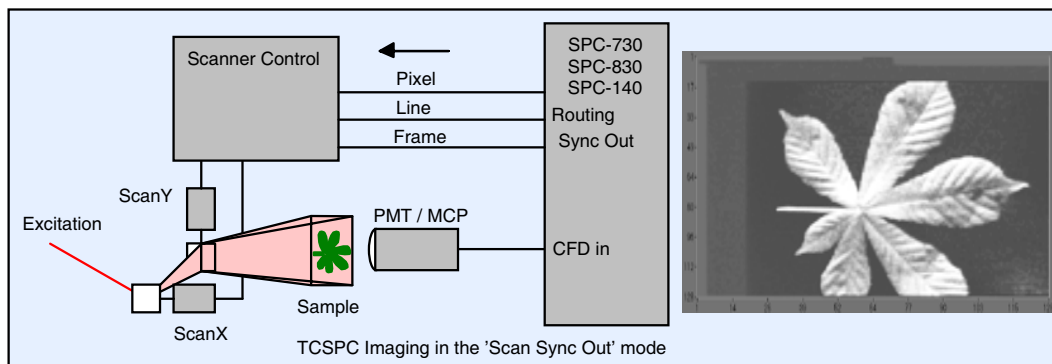


Fig. 105: Imaging in the Scan Sync Out mode

As long as the scan mirrors are able to follow the change of the xy position there is practically no limitation of the scanning speed. Subsequent frames of the scan can be accumulated automatically, i.e. the data acquisition can be run until a sufficient number of photons have been collected.

As for the ‘Scan Sync In’ Mode, the number of pixels is not limited by the number of routing bits. Therefore, images sizes up to 256x256 can be obtained with the SPC-700/730. In the SPC-830 images with much higher pixel numbers can be recorded. The ‘Scan Sync Out’ mode can be used in conjunction with a multidetector setup and a router, i.e. images from several detectors can be recorded in the same scan.

Scan XY Out Mode

The SPC-700/730 module has an additional scan mode that delivers digital position signals to an external scan controller. Controlled by the parameters ‘Scan X’ and ‘Scan Y’ the SPC modules internally scans through all pixels of the image and sends a 14 bit X/Y information to the scanner.

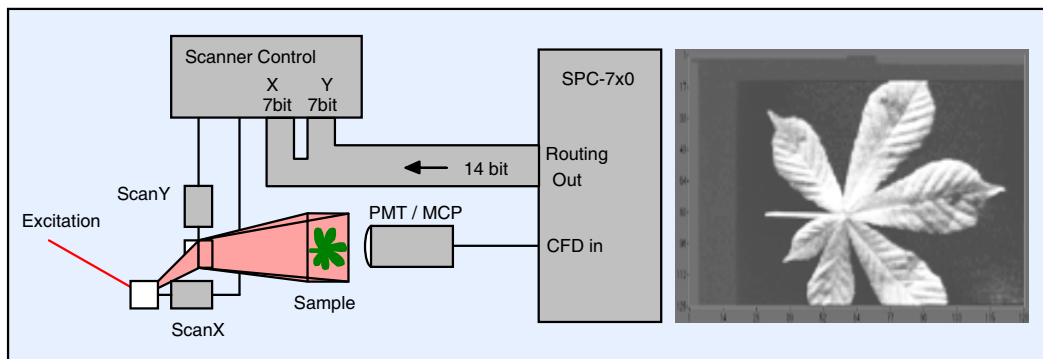


Fig. 106: Imaging in the Scan XY Out mode

As long as the scan mirrors are able to follow the change of the xy position there is practically no limitation of the scan rate. Subsequent frames of the scan can be accumulated automatically, i.e. the data acquisition can be run until a sufficient number of photons have been collected.

For scanners accepting analog input signals the SCDA-2 dual DAC module is available.

Since the routing lines of the SPC-700/730 are used for the XY output to the scanner the ‘Scan XY Out’ mode cannot be used for multidetector operation.

FLIM Systems for Laser Scanning Microscopes

bh deliver a number of FLIM upgrade kits for laser scanning microscopes. Scanning microscopes may differ considerably in the excitation sources used, the detector beam path configuration, and the applications for which they are used. Therefore FLIM kits for one-photon and multiphoton microscopes, single- and dual-detector versions, and multi-spectral detection versions are available. A wide variety of detectors, detector/shutter modules, and beamsplitter modules are available for use at various confocal or direct output ports of the microscope. Moreover, the recording electronics can be based on a single TCSPC module with routing, or on a multi-module TCSPC system. An overview of the FLIM systems available from bh is given below. Individual manuals of the bh FLIM systems for Zeiss [20], Leica [21], and Olympus microscopes [22] are available from www.becker-hickl.com. Applications of the bh FLIM systems are described under ‘Time-Resolved Laser Scanning Microscopy’, page 164.

Single-Module TCSPC systems

FLIM systems based on a single TCSPC module are summarised in Fig. 107.

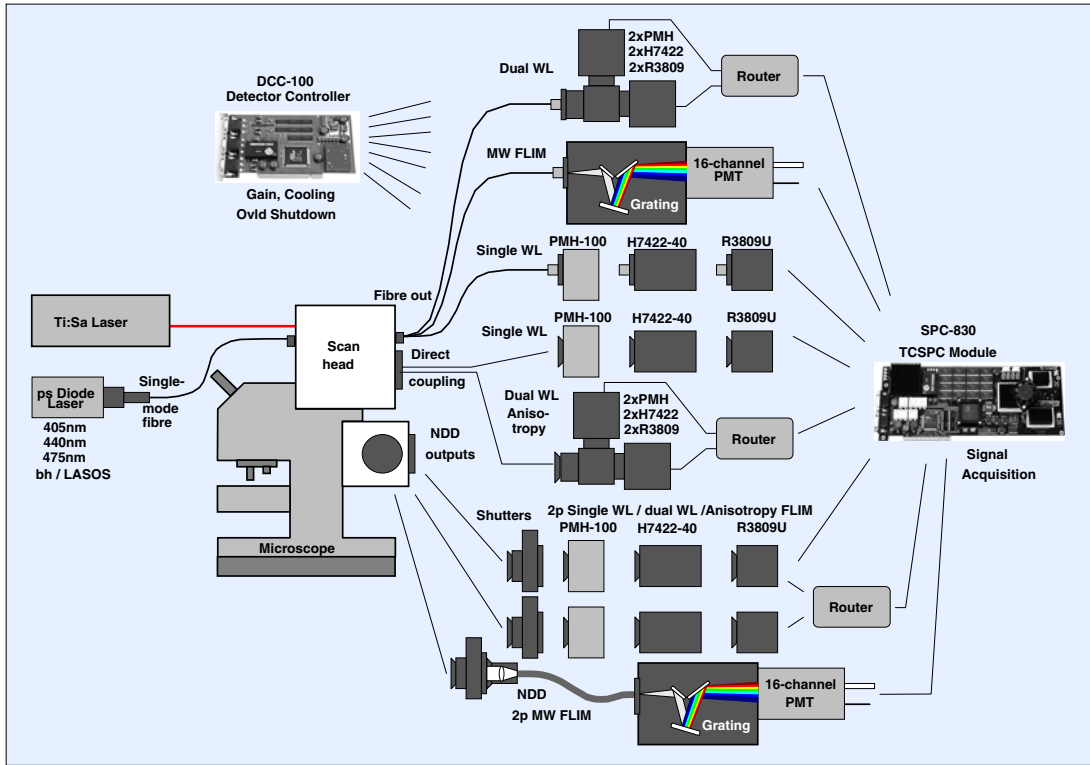


Fig. 107: Different options of bh FLIM systems. Single TCSPC module.

Excitation Source

TCSPC fluorescence lifetime imaging requires a pulses excitation source of high repetition rate.

Two-photon microscopes come with titanium-sapphire lasers. The laser delivers femtosecond pulses at a repetition rate from 78 to 92 MHz. Two-photon microscope therefore do not need any changes in the excitation part. Sometimes the titanium-sapphire laser is equipped with a frequency-doubler and used for one-photon excitation. There is no difference between these cases in terms of TCSPC data recording. However, in contrast to two-photon excitation, one-photon excitation by the frequency-doubled laser does not deliver inherent depth resolution. Therefore descanned (confocal) detection should be used, and a suitable FLIM detection path be provided.

Confocal laser scanning microscopes use gas lasers and steady-state solid-state lasers for excitation. Consequently, to upgrade these systems for FLIM a suitable pulsed excitation source must be added. The bh FLIM kits use bh picosecond diode lasers which are available for wavelengths of 375 nm, 405 nm, 440 nm, 473 nm, and a large number of wavelengths above 635 nm. The lasers are available with beam-profile correction and single-mode fibre couplers (see BDL-405-SM, BDL-440-SM and BDL-475-SM lasers [26]). The laser is attached directly to one of the single-mode fibre inputs of the microscope.

The bh lasers have a TTL input for fast on-off switching. A TTL ‘low’ signal turns the laser off, TTL ‘high’ turns it on. If the microscope delivers a suitable signal the laser on/off control should be used to switch the laser off during the beam flyback, and when the scan is stopped.

Detector Options

Depending on the type of the microscope FLIM detectors can be attached to a confocal fibre output from the scan head, to a direct confocal output of the scan head, or to a non-descanned output port.

Confocal fibre outputs are available for the Zeiss LSM 510, the Olympus FV 1000, and the Biorad Radiance 2000. Direct confocal outputs from the scan head are available for the Leica SP2 and SP5 [21] and for the Olympus FV 1000 [22]. Compared with a fibre output the direct confocal output has the benefit of higher efficiency, absence of pulse dispersion, and of maintaining the polarisation of the fluorescence light. A dual-detector assembly connected to a direct output from the scan head can therefore be used both for dual-wavelength and anisotropy FLIM.

Two-photon microscopes normally have a non-descanned detection path (see ‘TCSPC in Non-Descanned (Direct) Detection Systems’, page 168). The optical ports for non-descanned output are normally located at one side or at the back of the microscope body. The ports have standard optical interfaces, such as c-mount thread or dovetail adapters. The Zeiss LSM 510 NLO two-photon microscope is available with an ‘NDD Switch Box’ that contains a computer-controlled beamsplitter and filter wheel. The box has two outputs; a FLIM detector can be attached to each of them [20].

As indicated in Fig. 107, all non-descanned detection systems are used with a shutter assembly; typical assemblies are shown in Fig. 17. The shutter not only avoids detector damage by the light of the microscope lens, it also contains the field lens required to transfer the fluorescence light efficiently to the detector.

The standard detector for all FLIM systems is the bh PMC-100. It has a typical IRF width of 150 ps. The detector is rugged and delivers a stable IRF up to extremely high count rates. Typical applications are pH imaging, and other ion concentration measurements that use bright fluorophores in high concentration.

The fastest detector is the Hamamatsu R3809U, with a typical IRF width of 25 to 30 ps. The R3809U should be used whenever decay times below 200 ps are to be expected. Typical cases are FRET measurements and autofluorescence of tissue. The short and clean IRF of the R3809U helps to resolve fast decay components of complex decay profiles down to the sub-50 ps range.

In cases when ultimate sensitivity is required the Hamamatsu H7422P-40 can be used. The quantum efficiency of this detector reaches almost 45% at 500 nm. The IRF width is 200 to 350 ps. The H7422P-40 is currently the best compromise for systems that are used both for FLIM and FCS.

Dual-Detector Systems

Dual detector systems can be built with two PMH-100, two R3809U, or two H7422P-40 detectors. An HRT-41 router is used to record the signals of both detectors simultaneously in one TCSPC module. If two detectors are to be connected to a single fibre or a direct confocal output from the scan head a beamsplitter assembly is used.

Non-descanned detection systems should be used with a shutter, as indicated in Fig. 107. If two detectors are connected the non-descanned outputs of an LSM 510 the beamsplitter carousel in the NDD switch box of the microscope is used to split the light. The detectors are then connected to the two outputs of the NDD switch box [20]. For other two-photon microscopes shutter assemblies with beamsplitter units are available.

Multi-Wavelength Detection

For multi-wavelength detection the ‘PML-Spec’ assembly is available. It consists of a polychromator and a bh PML-16 16-channel detector head [18]. The PML-Spec can be attached to a confocal fibre output from the scan head or to the non-descanned output of a two-photon microscope. For confocal detection a single multi-mode fibre is used. The diameter of the fibre can be anywhere from 0.1 to 1 mm. For non-descanned detection the PML-Spec is delivered with a special fibre bundle [18], see Fig. 182, page 170.

TCSPC Module

Single-Module FLIM systems preferably use the SPC-830 TCSPC module. This module provides enough memory space to simultaneously record images in several wavelength intervals or even multi-spectral images. For single-wavelength systems also the SPC-730, SPC-140 or SPC-150 modules can be used.

Detector and Shutter Control

The detectors and shutters are controlled via a DCC-100 detector controller card. In systems with bh picosecond diode lasers the DCC-100 also controls the laser intensity [20, 22, 26].

Multi-Module (Parallel Detection) Systems

Multi-module FLIM systems are used to obtain short acquisition times for samples that deliver high count rates. The different options are summarised in Fig. 108.

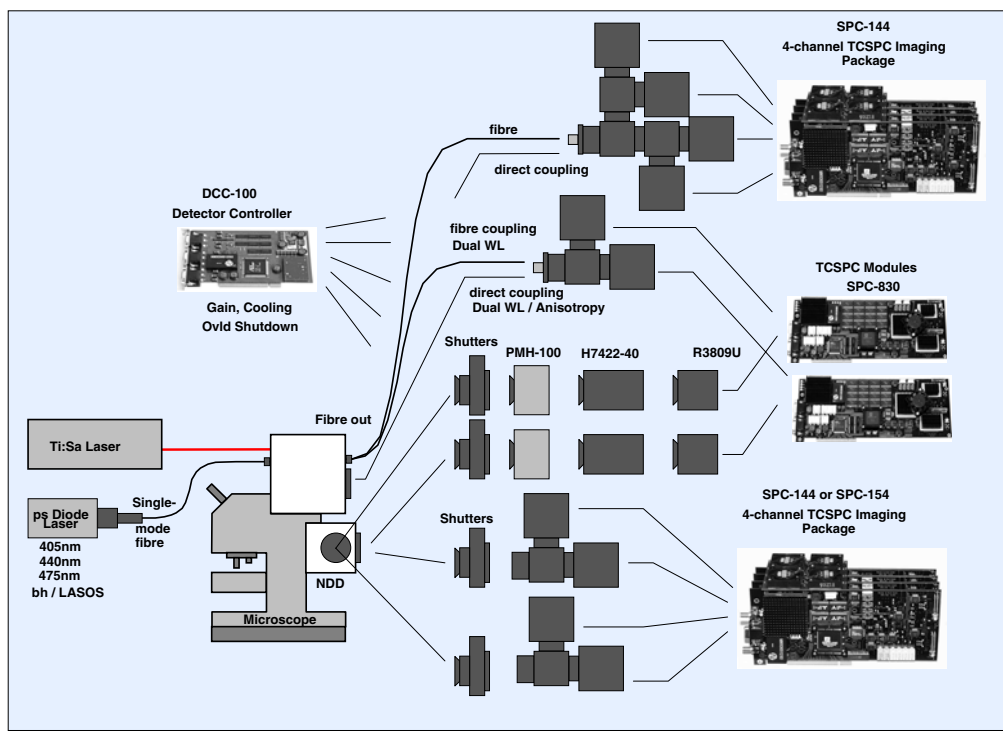


Fig. 108: bh FLIM systems with several parallel TCSPC modules

The detector options are essentially the same as for the single-module setup. In one-photon microscopes the detectors are connected either to a confocal fibre output of the scan head, or to a direct confocal output. One or three external beamsplitter can be used to split the light spectrally and into 0° and 90° polarisation components. The components are detected by two or four detectors.

Direct detectors for two-photon imaging are connected via shutter assemblies. If the microscope has a beamsplitter unit (as the LSM 510 NLO) two detectors can be attached directly. With two additional external beamsplitters the light can be further split and distributed to four detectors.

The detectors of high-count rate systems are normally PMC-100 or H7422-40 modules. For higher time resolution, in principle, the R3809U can be used. If the light is spread over the full detector area count rates of $3 \cdot 10^6 \text{ s}^{-1}$ per detector can be reached (see Fig. 64, page 64). However, the output current at count rates this high is considerably higher than the maximum value specified by Hamamatsu. It is not known how long the R3809U will last if extremely high count rates are used continuously.

The TCSPC systems for multi-module FLIM consist either of an SPC-144 or SPC-154 four-channel package of two SPC-830s.

Connecting Detectors and Shutters of FLIM Systems

Wiring diagrams of typical FLIM systems are shown in the figures below. Fig. 109 shows a single-detector system.

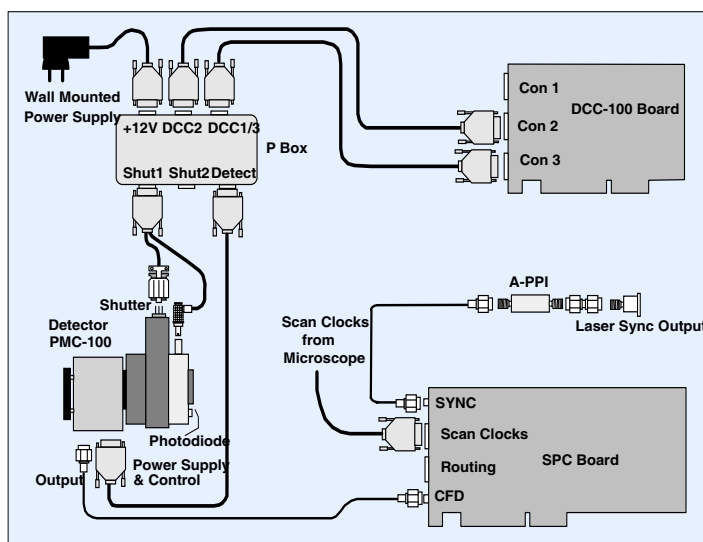


Fig. 109: Wiring Diagram of a single-detector FLIM system. One shutter, PMC-100 detector, SPC-830 TCSPC module. Detector and shutter control via DCC-100 card.

The system uses a PMC-100 detector. The PMC-100 is connected to an optical output of the microscope via a shutter assembly. Both the detector and the shutter are controlled via the DCC-100 detector controller card. A shutter control signal is provided at connector 2 of the DCC-100. The ‘P box’ (power saving box) reduces the current in the shutter coils when the shutter is open and thus avoids heating of the detector by the shutter. Moreover, the box combines the overload signal of the PMC-100 detector with an overload signal from a photodiode in front of the shutter. This prevents unintentional opening of the shutter when strong light is present, e.g. when the microscope lamp is on.

The +12V power supply, the cooling current, and the gain control signal for the PMC-100 is provided at connector 3 of the DCC-100. The cooling circuit of the DCC-100 is configured for ‘one detector’, see DCC-100 manual.

The detector pulses are fed into the CFD input of an SPC-830, SPC-730 or SPC-140 module. The SYNC signal is obtained directly from the laser. In most two-photon microscopes a suit-

able signal is delivered by the Ti:Sapphire laser. The signal is normally positive. Also the bh BDL lasers deliver positive synchronisation pulses. Therefore an A-PPI pulse inverter is inserted in the SYNC line. The scan clock signals of the microscope controller are connected to the upper sub-D connector of the SPC-830 or SPC-730 module.

The system shown in Fig. 110 uses two H7422P-40 detectors and one shutter. The setup is typical of microscopes that have no internal beamsplitter unit, e.g. the Leica SP2 in the multiphoton version with non-descanned (RLD) output. The detector assembly is connected to an optical port of the microscope via a single shutter. An external beam splitter unit distributes the light to the detectors. Both detectors and the shutter are controlled via the DCC-100 detector controller card. A shutter control signal is provided at connector 2 of the DCC-100. The ‘P box’ reduces the current in the shutter coils when the shutter is open and thus avoids heating of the detectors by the shutter. Moreover, the box combines the overload signals from the preamplifiers with an overload signal from a photodiode in front of the shutter.

The +12V power supply, the cooling current, and the gain control signal for the H7422 detectors are provided at connector 1 and connector 3 of the DCC-100. The cooling circuit of the DCC-100 is configured for ‘two detectors’, see DCC-100 manual. One H7422 is connected directly to the DCC-100, the other via the ‘P box’. The output pulses of the detectors are amplified in HFAC-26-2 preamplifiers and fed into two inputs of an HRT-41 or HRT-81 router. As usual, the router is connected to an SPC-830 module via a 15-pin routing cable and an 50- Ω cable. The SYNC signal for the SPC-830 module comes from the laser. The scan clocks of the microscope are connected to the upper sub-D connector of the SPC-830 module.

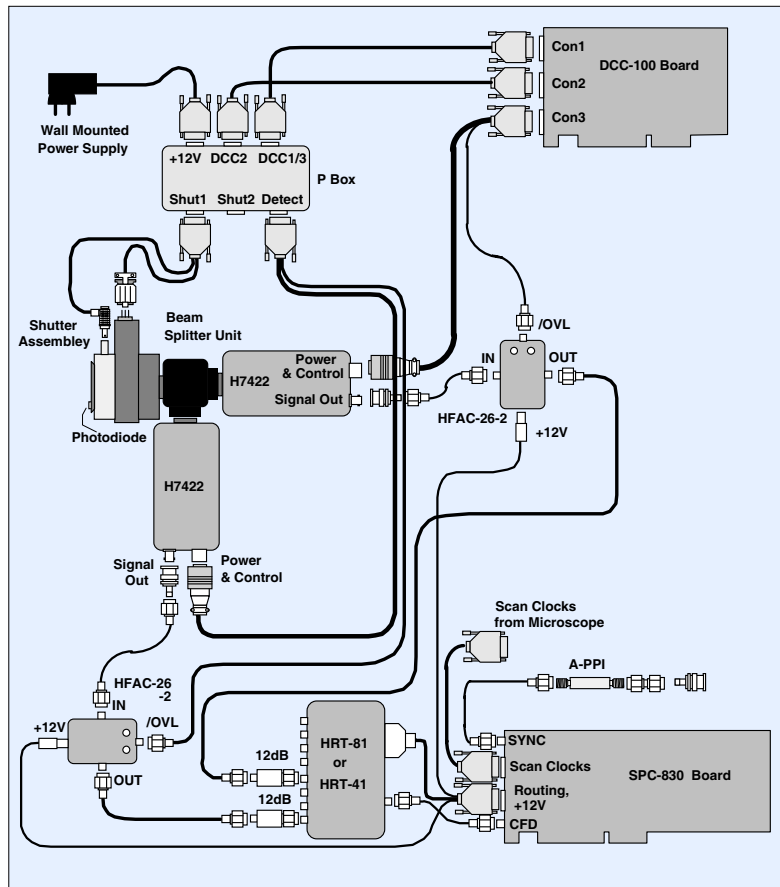


Fig. 110: Wiring diagram of a dual-detector FLIM system. One shutter, beam splitter unit, H7422 detectors, HFAC-26-2 preamplifiers, SPC-830 TCSPC module

Fig. 111 shows a dual-detector FLIM system for a Zeiss LSM 510 NLO two-photon microscope. Two R3809U MCP PMTs with individual shutters are connected to the outputs of the ‘NDD switch box’ of the LSM 510. As in the setups described above, the detectors and shutters are controlled via the DCC-100 detector controller card.

The high voltage for the R3809U detectors is provided by an FuG HCN 14-3500-A power supply. The high voltage is controlled by a signal from connector 1 of the DCC card.

The output pulses of the detectors are amplified in HFAH-26-01 preamplifiers and fed into two inputs of an HRT-41 or HRT-81 router.

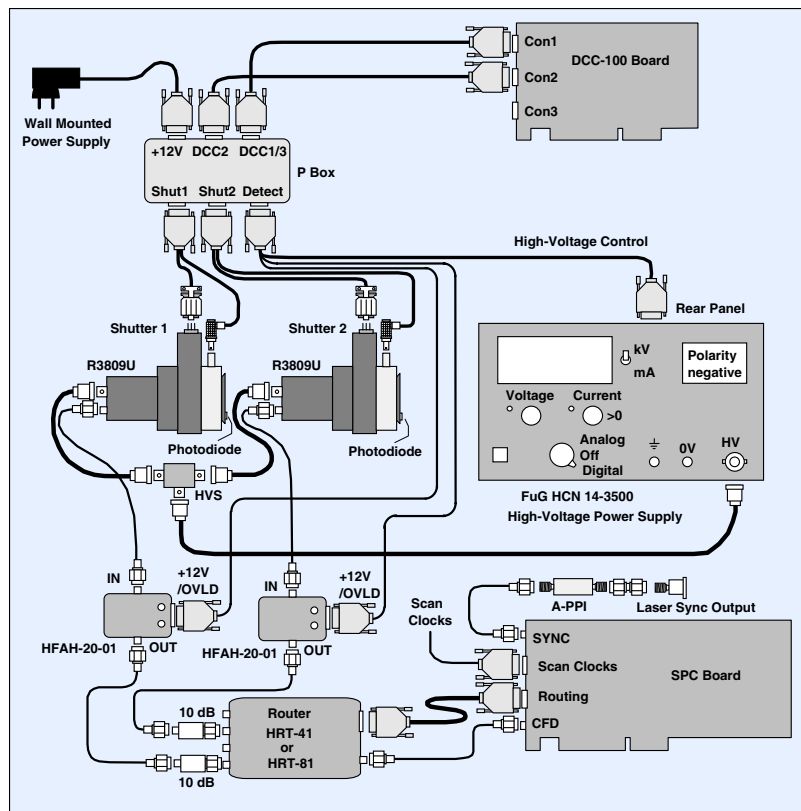


Fig. 111: Wiring diagram of a dual detector FLIM system. Two shutters, R3809U detectors, HFAH-26-01 preamplifiers, SPC-830 TCSPC module.

A wide variety of other FLIM configurations are possible, see Fig. 107 and Fig. 108. bh provides cable sets and optical adapters for a large number of microscopes and any reasonable configuration. However, to deliver the FLIM kit with the right detectors, adapters, and cables we need information about the type and the version of the laser scanning microscope, the optical outputs, the laser used, and about the planned application. Please let us also know special requirements, like space restrictions or unusual distances from the microscope components to the computer with the FLIM system.

First Light: Getting Started

Recommended System Parameters

If you have a minimum of experience with optical detectors it should be no problem for you to put an SPC setup into operation. For the first steps we recommend to use the SPC in the ‘Oscilloscope Mode’ with the parameter settings shown in Fig. 112.

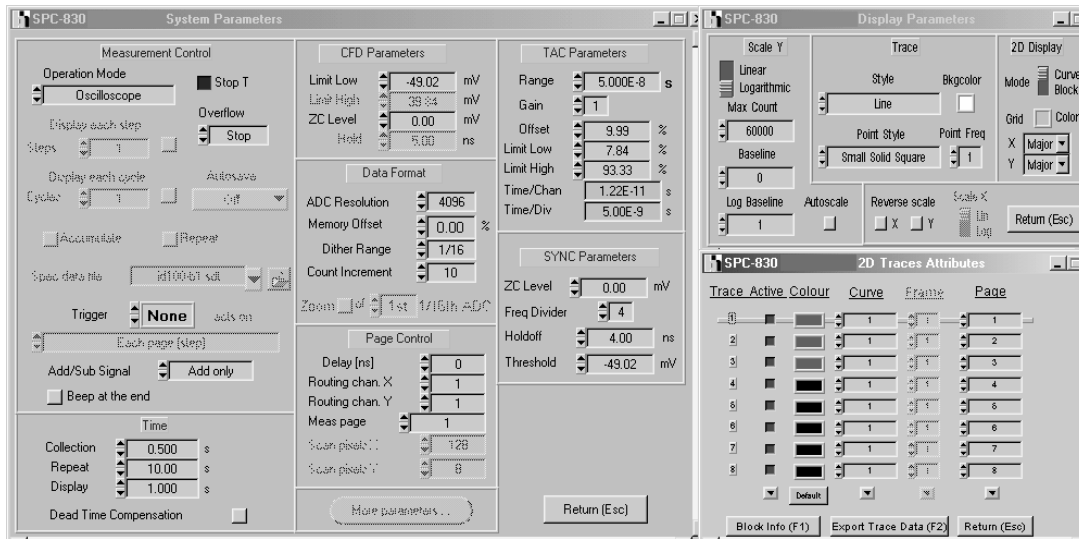


Fig. 112: Parameter settings recommended for startup: System Parameters (left), Display Parameters (upper right), Trace Parameters (lower right)

The parameters are shown for an SPC-830 module. The panels for other modules may differ slightly, but are not significantly different. When you have set the parameters, close the System Parameters panel but keep the display and trace parameter panels open. Resize and place the panels as shown in Fig. 113. Make sure that the ‘Rate’ button in the main panel is switched on.

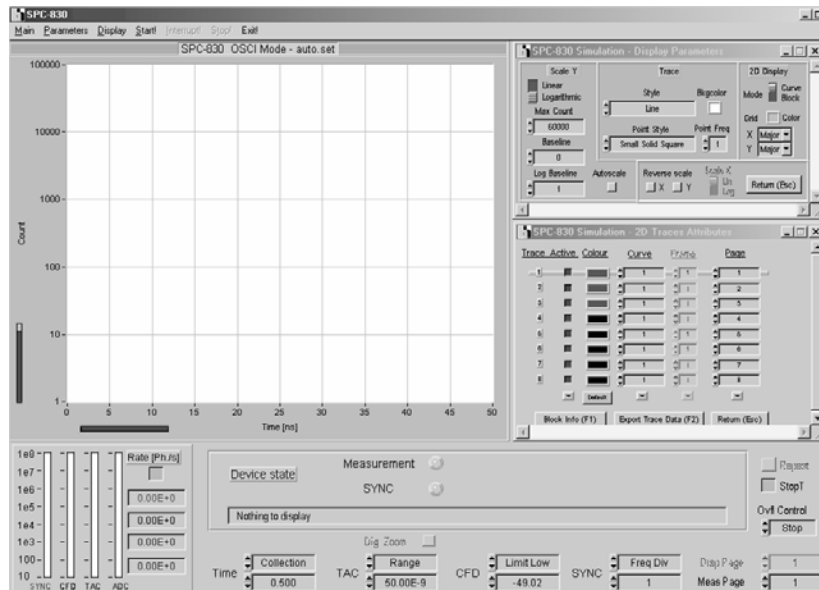


Fig. 113: Recommended configuration of the SPCM software panels for startup

If you have a DCC-100 detector controller, start the DCC software as well. The DCC panel is shown in Fig. 114. Shift down the detector gain regulators and switch on the operating voltage buttons for all three DCC connectors. If you have a cooled detector connected to the DCC, switch on the cooling and set it to ‘5V’ and ‘1A’. Then switch on the outputs by clicking on the ‘Enable Outputs’ button.

Caution: The gain sliders control the high voltage of the detectors. The DCC is used for a wide variety of detectors and high voltage power supplies. It can happen that the gain or the high voltage can be set higher than the permitted maximum of a given detector. The DCC software therefore allows the user to set limits for the Gain/HV. The limits are accessible under ‘Production & Adjust Data’, see Fig. 115. Please make sure that the limits are reasonably set for your detector and power supply. Although bh normally set correct limits in DCC modules delivered in conjunction with detectors this is not always possible if the DCC and the detectors are purchased independently.

Make sure that both the SPCM and the DCC software have recognised the modules correctly and are running in the ‘hardware mode’, see ‘Software Start’, page 84.

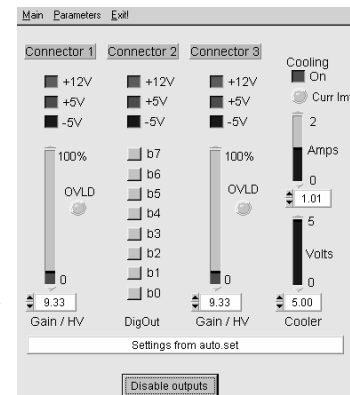


Fig. 114: DCC main panel

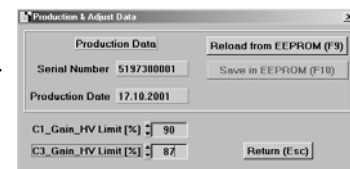


Fig. 115: Gain/High Voltage Limits of the DCC-100

Setup of Standard Fluorescence Lifetime Systems

In the majority of applications the SPC modules are used to record the waveform of a light signal that is excited by a pulsed light source, such as a Ti:Sapphire laser or a picosecond diode laser. In these cases the please follow the steps listed below:

- Turn on the light source. Make sure that the SPC modules synchronises with the laser: If the synchronisation signal arrives at the SYNC input with appropriate amplitude and polarity the SYNC rate bar should show the correct laser repetition rate.
- If you have a shutter in front of the detector, and the shutter is controlled by the DCC-100, check whether the shutter can be opened and closed. With the standard shutter cable sets, a single shutter is opened and closed by switching on and off b0 of connector 2. A second shutter is controlled via b1.
- Reduce the light intensity at the detector as far as possible. If you have a shutter, close it. If you have a monochromator, close the slit. If you regulate the intensity by variable ND filters, set them to maximum attenuation.
- If you have a simple PMH-100 detector: Connect its power supply cable now. If you connect it to a sub-D connector of the SPC modules it is active when the SPCM software is active. If you have the PMH connected to the DCC-100 you can switch it on and off via the ‘+12V’ button of the corresponding connector. If the overload LED or the beeper of the PMH-100 turns on, disconnect or switch off the detector immediately. Find the reason of the overload before you proceed.
- SPADs: Turn on the SPAD module. SPAD modules have no gain setting. Therefore, you can skip the optimisation of the detector gain described in the next steps.
- Other PMT detectors: Increase the gain or high voltage of the detector. If you control the detector via a DCC-100, use the ‘Gain/HV’ slider of the connector to which the detector is connected. Make sure that you do not exceed the maximum high voltage permitted for the detector. Keep the overload indicator LEDs of the preamplifier or of the detector in sight.

If the LEDs turn on the maximum output current of the detector is reached, i.e. there is too much light at the detector. If this should happen you have to find the reason of the overload before you further increase the gain. If you are using the DCC-100 you can be relatively relaxed. Provided the system is correctly connected the DCC-100 shuts down the detector when an overload occurs.

- When the gain comes into the region of 80 to 100% of the maximum permitted for the detector you should see the first detected photons. The CFD, TAC and ADC rate bars start to display a rate, and the first photons should show up in the curve display. (Please note that 'Count Increment' was set to 10, therefore a single photon is displayed as a vertical line of 10 counts.) Even if there is absolutely no light at the detector the SPCM software should display occasional dark pulses of the detector. If the system does not record any photons at this stage, make sure that the signal cables are connected correctly and that the power supply cable to the preamplifier is connected. If this is the case, check the detector as described under 'Quick Test of a PMT', page 141.
- After you managed to record reasonable counts from the detector, open the detection light path so that the detector gets light. If the repetition rate of your laser is higher than 20 MHz you should immediately see the waveform of your signal in the curve window. **Important:** If you are not familiar with photon counting, please be careful when increasing the intensity. Single-photon detectors are extremely sensitive. Any light intensity you can *see* exceeds the overload threshold of the detector by orders of magnitude!
- If the repetition rate of your light source is lower than 20 MHz it may happen that you record a wrong time interval of the signal period. An indication of this situation is a high CFD and TAC rate, but an extremely low ADC rate. If this happens, probably the delay in the synchronisation path is too small. Try with 2 or 3 m of additional cable length in the SYNC path. Please see 'Adjusting the SYNC and CFD Cable Length', page 124.
- The parameters suggested in Fig. 112 contain a 'Sync Frequency Divider' = 4. This means, if the signal period is shorter than 12.5 ns four signal periods are recorded and displayed. (If the period is longer not all periods may be visible.) To record only a single signal period, set 'Sync Frequency Divider' = 1. Usually it happens then that the wrong part of the signal period is recorded. The signal may be shifted left or right, and it may wrap around the recorded period. The signal period may also be considerably shorter than the TAC range and fill only a part of the TAC interval. To centre the signal correctly in the TAC interval, change the cable length in the SYNC or detector path as described under 'Adjusting the SYNC and CFD Cable Length', page 124. If this is done, stretch the signal to be recorded over the full time axis by increasing 'TAC Gain' and 'TAC Offset', see 'Adjusting the TAC Parameters', page 126.
- The TAC window in which the photons are recorded is specified by 'TAC Limit Low' and 'TAC Limit High'. It is recommended to use these parameters to exclude artefacts of the ADC error correction from being recorded.
- When you are sure that you record the correct time interval of the signal, you can start to optimise the detector and CFD parameters. The general procedure is described under 'Optimising the CFD Parameters', page 120. With decreasing CFD threshold the count rate increases. At some level the increase flattens, and, for good detectors, turns into a plateau. When you see something like a plateau (it may be not very pronounced) you have reached the correct operating point of the detector. Of course, the optimum CFD threshold depends on the detector gain, or the high voltage of the PMT. In other words, a decrease in the CFD threshold and an increase in the detector gain (or high voltage) are largely equivalent. However, the larger single-photon pulses obtained at higher gain have a better signal-to-noise ratio. Moreover, the operating voltage decreases the TTS and the SER width of the PMT. Higher gain or voltage therefore usually yields shorter IFR and better differential

nonlinearity. However, afterpulsing, possibly even instability, and early detector overload may limit the gain that can practically be used. Typical gain and high voltage values are

Detector	High voltage / Gain Control DCC
R3809U MCP	-2.9 to -3.1 kV
R7400	-800 to -950 V
PMC-100-0, -1	80 to 90%
PMC-100-20	90 to 100%
H5773, H5783	80 to 90% (0.8 to 0.9V)
H7422-40, -50	80 to 90% (0.8 to 0.9V)

Please note: No CFD adjustments have to be done for single-photon avalanche photodiode (SPAD) detectors. These detectors have their own internal discriminators and deliver a pulse of defined amplitude and duration for each photon. Once these pulses are detected by the CFD of the SPC module further adjustment has negligible influence on the efficiency and the RF shape.

- When you have found a reasonable set of CFD and TAC parameters, do not forget to save the results. The file created by the save routine not only contains the recorded photon distribution but also the complete set of system parameters, see ‘Save Panel’ page 243.

Setup of Scanning Systems

When laser scanning microscopes are upgraded with FLIM systems it is recommend to start with the same procedure as described above. Use an easy sample that contains stained tissue to be sure that there is fluorescence throughout the whole image. Bring the sample into focus and switch the light path to direct fluorescence to the FLIM detector. Start a ‘continuous’ (repetitive) scan in the microscope. When reasonable decay curves are recorded in the oscilloscope mode, and the detector, CFD, and TAC parameters are set proceed with the following steps:

- Change the operation mode to ‘Scan Sync In’. Use the system parameters and the display parameters shown in Fig. 116, but retain the CFD, SYNC, and TAC parameters found in the procedure described under ‘Setup of Standard Fluorescence Lifetime Systems’.

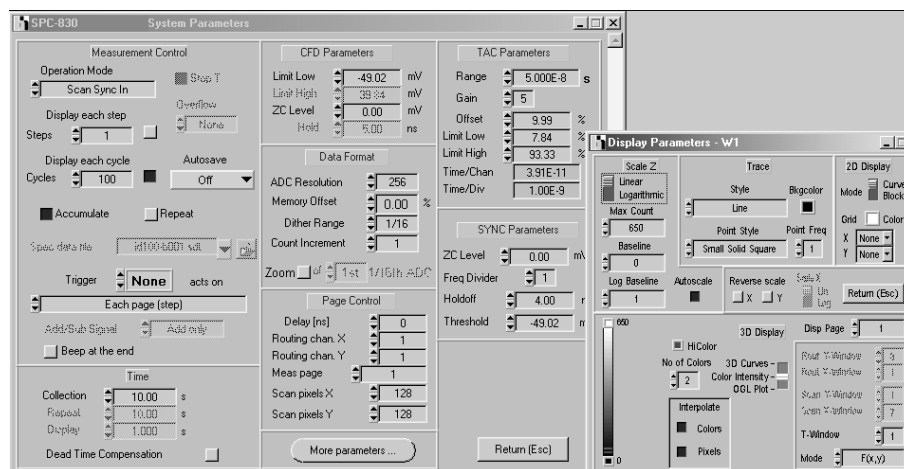


Fig. 116: Startup System and Display parameters for Scan Sync In mode. The parameters work with any of the SPC-140/144, SPC-730 and SPC-830 modules. For the SPC-830 ‘ADC Resolution’ can (but need not) be increased to 1024.

- Click into ‘System Parameters’, ‘More Parameters’. If the microscope delivers a pixel clock, use the settings shown for external pixel clock, Fig. 117, left. These settings bin the

typical 512x512 pixel scan of the microscope into the 127 x 127 pixel image defined in the system parameters. If the microscope does not deliver a pixel clock , use the settings shown for internal pixel clock, Fig. 117, right. The pixel time used is 5 us. Please note that this is only a preliminary guess. It may be not always clear what the pixel dwell time in the microscope is, and some try-and-error work may be required.

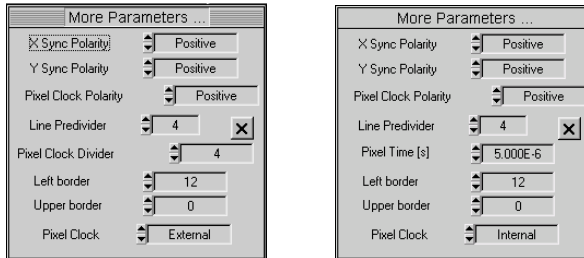


Fig. 117: ‘More Parameters’ for external (left) and internal (right) pixel clock. The parameters used bin a 512 x 512 pixel scan into a 128 x 128 pixel TCSPC image

- Define the Window Parameters as shown in Fig. 118. The ‘time windows’ define time gates in which the intensity is displayed. Window 1 covers the complete ADC range, the other windows define subsequent time gates over the ADC range.

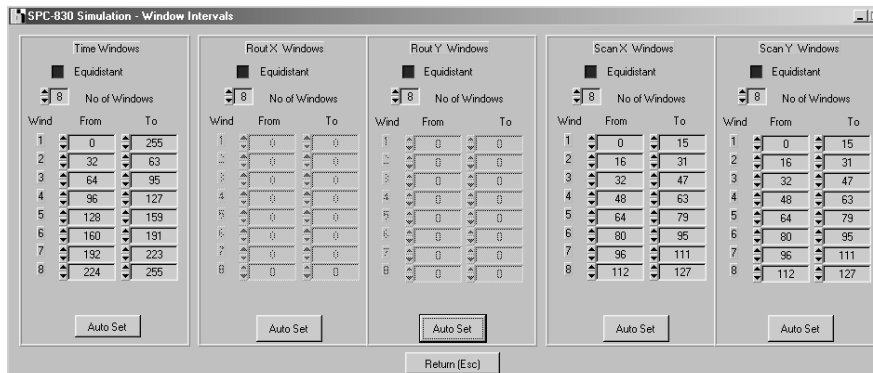


Fig. 118: Window parameters. Time window 1 covers the photons of all time channels, the other time windows define subsequent time gates in which the intensity can be displayed

- Click the System Parameters and Window Parameters off. Turn the ‘Display Parameters’ on and configure the main panel as shown in Fig. 119.

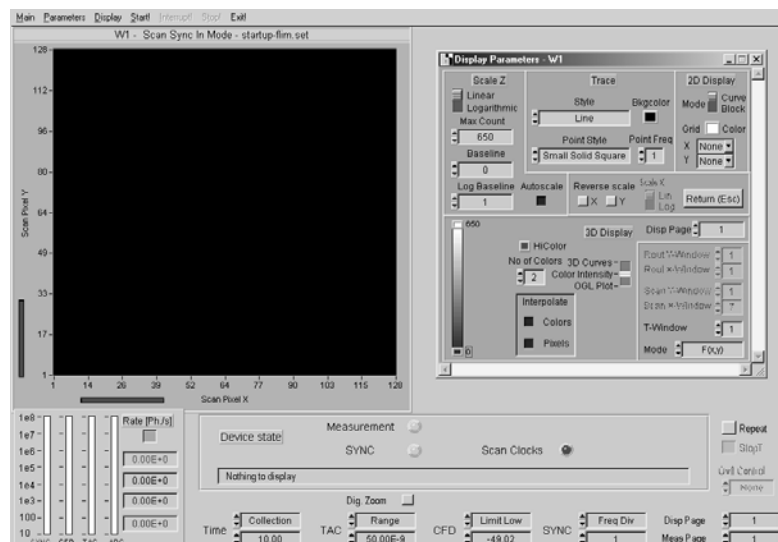
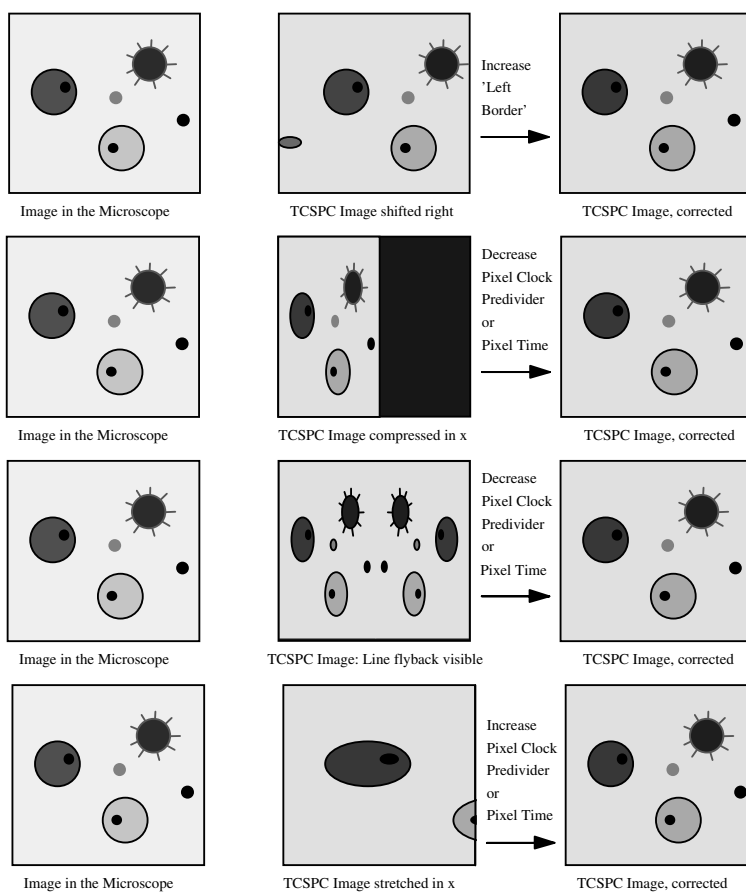


Fig. 119: Main panel configuration recommended for FLIM

- Start a continuous scan in the microscope. Check the ‘Scan Clocks’ indicator. If the scan clocks are present the indicator should turn green. It may cycle between red and green if the frame rate is slower than one frame per second. Put the mouse cursor on the indicator to see all three (or two, for internal pixel clock) scan clocks. If one or several clocks are missing, check whether you have the right scan clock cable for your microscope, and whether it is connected correctly. At the SPC-730 and -830 it has to be connected to the *upper* sub-D connector.
- If the scan clocks are there, activate the detector. Start the measurement in the SPCM software. With the system parameters shown in Fig. 116 the measurement runs for 10 seconds, stops, displays an image, and restarts. Because the autoscale function is on the accumulation over the subsequent 10 s cycles may not be apparent at first glance. The increase of image intensity is therefore not visible, only the increase in signal-to-noise ratio. The measurement continues until 100 such cycles are accumulated. You can stop the recording at any time.
- The image you get may be badly shifted, or the x or y axis may be reversed. Moreover, the image may be stretched or compressed in one or both axis. The reason of a shift may be that the active edge of the scan clocks does not correspond to the definitions in ‘More parameters’. A slight shift, especially in x direction, is normal and easily corrected by setting ‘left border’ > 0. Reversion of the x or y axis can be corrected in the Display Parameters. If the image is stretched or compressed either the line and pixel clock dividers are not set according to the ratio of the pixel numbers in the microscope scan and the SPC recording, or the pixel time of the internal pixel clock is too short or too long. The settings under ‘More Parameters’ allow for correction in all these cases. Some typical cases are shown in Fig. 120.



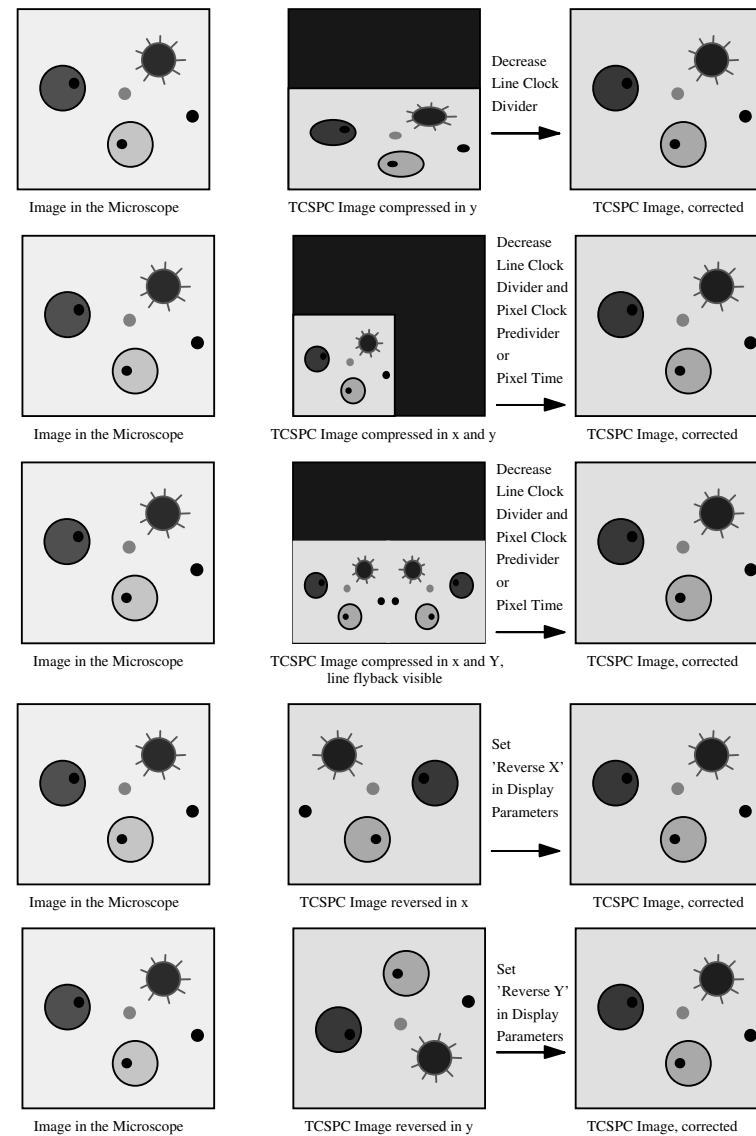


Fig. 120: Typical cases of distorted images and methods of correction

Some microscopes have an option to use a bi-directional scan. Other microscopes, e.g. the Leica SP1, deliver pixel clock pulses both at the start and at the end of each line. The result is an image as shown in Fig. 121. If you have effects like these, please check that you are using an unidirectional scan. If this does not help please contact BH. We have adapters to transform odd scan control signals into useful frame and line pulses.

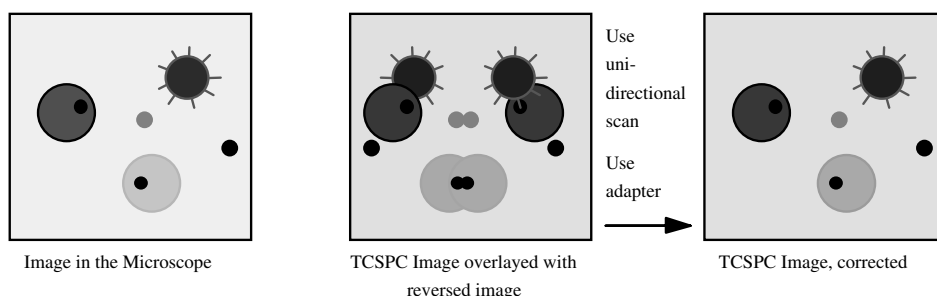


Fig. 121: Images obtained with pixel clocks at both ends of the line, or with bi-directional scan

- When you obtained the correct image, save a setup or data file, see 'Save Panel' page 243.

- We recommend to run the same procedure for a number of different image configurations, i.e. different numbers of pixels, time channels, and (in multi-detector systems) different numbers of detectors.
- It is also useful to define a setup for ‘life imaging’: Set ‘ADC Resolution’ = 1, Scan pixels X and Y = 128 or 256, a collection time roughly corresponding to the frame time. Activate ‘repeat; and switch off ‘cycles and ‘accumulate’. The setup displays a fast sequence of steady-state images.
- Save the setups and load them into the list of predefined setups, see ‘Predefined Setups’ page 245.

Multi-Detector Systems

For multi-detector systems we recommend to start with the procedures described above. The recommended settings merge the photons of all detectors into a single decay curve or a single image. In systems with several individual detectors it may therefore be indicated to keep only one detector active at a time. When the system is generally working, proceed as described below:

- Standard Lifetime Systems with several individual detectors: Activate the multi-detector operation by setting ‘Routing Channels X’ to the actual number of detector channels. Define the ‘2D Trace Parameters’ to display several ‘Curves’, see Fig. 122.

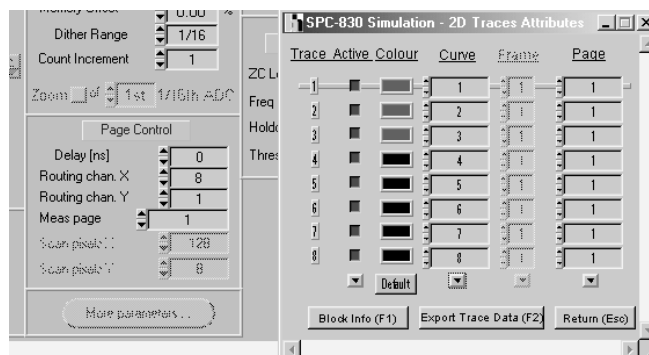


Fig. 122: Setup for up to 8 individual detectors. ‘Page Control’ section of the system parameters and 2D trace parameters

- Start a measurement in the oscilloscope mode. The signals of the detectors are displayed as individual traces. Do some experiments with different values of ‘Delay’ until you have best efficiency and minimum crosstalk of the channels. For most routers and detectors ‘Delay’ is between 0 and 30 ns.
- PML-16 detector: Generally you can proceed as described above. In the oscilloscope mode you can, however, display only 8 of the curves simultaneously recorded by the PML-16. It may therefore be better to use the ‘f(x,yt)’ mode. Default settings are shown in Fig. 123.
- Imaging Systems: Change ‘Routing Channels X’ to the number of actually used detector channels. It can happen that you have to reduce the number of pixels (Scan Pixels X and Y) or the number of time channels (ADC Resolution). To display the images of the individual detector channels you have two options. You can switch between the images by stepping through different ‘Routing X Windows’ in the display parameters. You can also display the images of several detectors simultaneously (see ‘Configuration of the SPC Main Panel’, page 233). As for standard lifetime systems, you should make some recordings for different ‘Delay’ and find the value for best channel separation and efficiency. For most routers and detectors ‘Delay’ is between 0 and 30 ns.

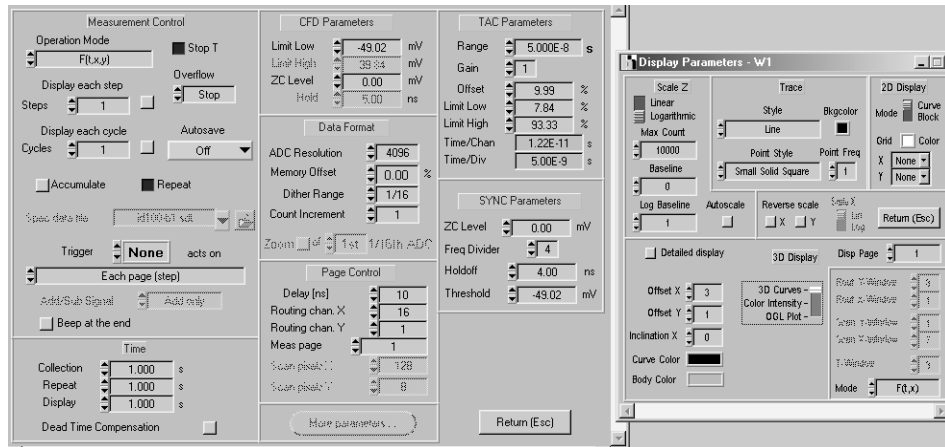


Fig. 123: Default setup for the PML-16 detector, f(x,y) mode. System Parameters and Display Parameters.

Setup Procedure for Other TCSPC Applications

There are other TCSPC applications that do not use a pulsed light source as for the startup procedure described above, see ‘Picosecond Photon Correlation’ and ‘Fluorescence Correlation Spectroscopy’. If such experiments are performed with PMTs the systems should be optimised by using a pulsed light source and general procedures described above under ‘Setup of Standard Fluorescence Lifetime Systems’. Otherwise it is difficult to find an optimum of the detector operating conditions.

Optimising a TCSPC System

General Recommendations

Optimisation of a TCSPC system is often believed a complicated process facing the user to numerous mysteries and pitfalls. This may in part be true for classic TCSPC systems built from NIM modules. For a bh SPC system the only optimisation steps that are really important are to set the operating conditions of the detector and the cable lengths in the synchronisation and detection path. The required steps are described on page 120, 122 and 124.

The optimisation of a bh TCSPC system can be done very efficiently in the 'Oscilloscope Mode'. In the Oscilloscope Mode the measurement is repeated automatically at the maximum available speed. The result is displayed at the end of each measurement cycle. Furthermore, by switching on the 'Trace Statistics' button the overall number of counts and the half-width of the measured signal can be displayed. To obtain a fast response to the adjustments made we recommend a 'Collection Time' of 0.1s to 0.5s and a 'Count Increment' of 10 to 100.

For all optimising work you should obey the general rule that reproducibility is more important than pure time resolution. The shortest instrument response function is of little value if its temporal location or shape varies with the time, the count rate or with the setting of the optical system. For system optimisation the following recommendations should be taken into consideration.

Before spending much time to optimise the instrument response function you should check the laser for pulse stability. This may be done by inspecting the pulses from the SYNC photodiode with an oscilloscope. Amplitude modulation, drift or jitter should be as small as possible. The influence of these effects on the timing will be small due to the constant fraction characteristic of the SYNC channel, but it cannot be absolutely avoided. Especially synchronously pumped dye lasers and mode locked argon lasers are prone to instability. In this case we suggest to monitor the laser action by a fast oscilloscope connected to the SYNC diode or a second photodiode. It is also recommended to switch on the count rate displays in the SPC main panel and check the sync frequency. This is recommended especially if the laser system tends to produce prepulses or afterpulses. If you use active mode locking in your laser, make sure that the mode locking frequency does not interfere with the SYNC signal. This frequency is one half the repetition rate and can seriously affect the synchronisation.

If possible do not use pulse pickers or cavity dumpers. It is not only that these devices produce very unpleasant electrical noise, they also transmit satellite pulses of considerable amplitude. This can make the synchronisation difficult. If you must work with a pulse picker for whatever reason, use an SPC-x30 module, which is able to discriminate between different pulse amplitudes at the sync input.

Make sure that your system does not pick up noise from power lines and network cables. Use a distribution box to connect the power cables of all system components to only one socket. This avoids ground loops which can induce high noise currents in signal ground connections. If the computer is connected to a network, disconnect the network cable for sensitive measurements. Another source of noise pickup is poor electrical shielding of the detectors. Noise pickup in the detector can result both in poor time resolution and high differential nonlinearity (see 'TAC Linearity', page 128). Advice for proper shielding and grounding is given in [46].

Often the optical system has a great influence on the time resolution and the stability of the instrument response (see 'Quick Test of a PMT', page 141). Critical parts are monochromators, which can introduce a considerable dependence of the IRF on the wavelength. A com-

mon source of trouble are also reflections in a optical system. Reflections show up as secondary peaks in the IRF and, consequently, as steps in the recorded fluorescence decay functions (see Fig. 152, page 144). They are often mistaken for differential nonlinearity of the TCSPC module. Reflections are especially strong if one or two highly reflective surfaces, e.g. interference filters, reflective ND filters, PMT cathodes, or the brackets of a narrow monochromator slit are involved (see ‘Avoiding Optical Reflections’, page 144). Hints for the design of optical systems are given in [46].

A common source of errors in the measured IRF are scattering solutions or cuvettes of large diameter. If the scattering coefficient is too high pulse broadening by some 100 ps can result. Moreover, the transit time in a fully illuminated 1 cm cuvette adds almost 100 ps to the IRF with. For optimising the time resolution of a detector we recommend not to used scattering. It is better to put a package of absorptive ND filters in front of the PMT and to illuminate it directly by the laser.

Configuring the CFD and SYNC Inputs

The function of the constant fraction discriminators in the detector and reference channel of the SPC modules is described under ‘Detailed Description of Building Blocks’, page 42. The CFDs in the detector and reference channels are different for the -00 and -30 SPCs. Especially the -00 reference (sync) channel has no threshold discriminator. However, all input circuits are based on a pulse shaping network that converts the unipolar detector pulse into a bipolar pulse, and on zero-cross triggering on the shaped pulse. Fig. 124 shows the pulse shaping for the -30 input circuits.

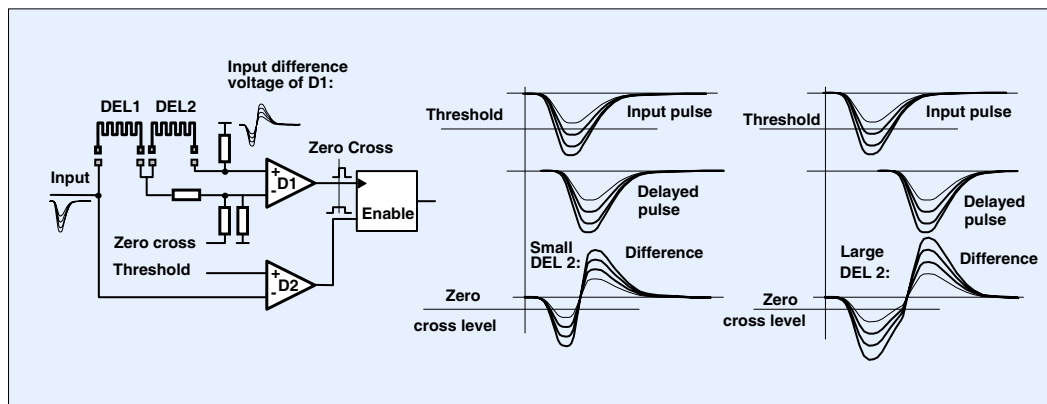


Fig. 124: Principle of constant fraction triggering

Pulse Shaping

The CFD and SYNC inputs can be configured for different detector rise times by replacing the delay lines, DEL1 and DEL2, in the zero cross shaping network. In the SPC modules the influence of the pulse shaping is much smaller than in TCSPC systems built from NIM modules. The reason is probably that the discriminators of the SPC CFDs are faster and more sensitive. In general, the influence of the delay lines on the shape of the zero transition is not entirely predictable. The bandwidth of the discriminators depends on the signal amplitude and is not exactly known. It is therefore not clear how the discriminator actually ‘sees’ the transition. A longer DEL2 may result in an unfavourable shape of the zero transition but in a higher signal amplitude. On the other hand, a short DEL2 may yield a steeper zero transition but may not improve the timing because it reduces the amplitude of the shaped signal. Therefore, the im-

portance of the pulse shaping should not be overestimated. For the majority of detectors a reasonably good IRF is obtained with the default delay lines inserted in the SPC boards.

The delay lines for the CFD and SYNC inputs are shown in Fig. 125.

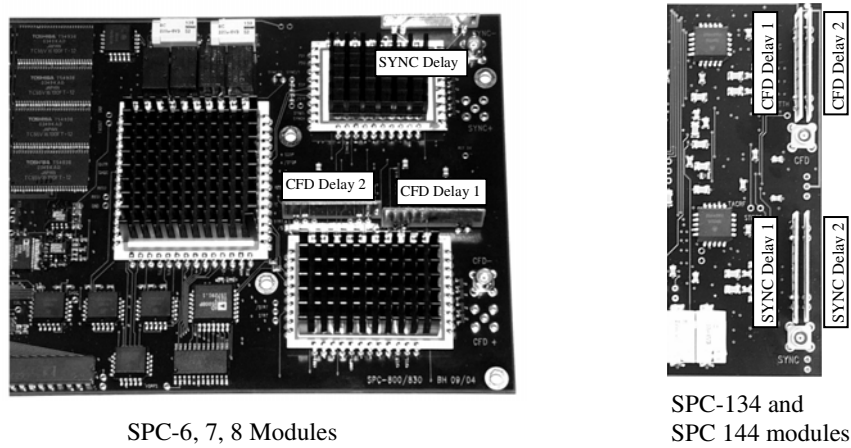


Fig. 125: Delay lines in the inputs of the SPC modules. Left: SPC-6, -7, -8 modules. Right: SPC-130/134 and SPC-144 modules

The table below gives some recommendations for the CFD configuration.

Detector for CFD Channel	SER Rise Time	-30 Modules		-00 Modules		SPC-134, 144	
		Delay 1	Delay 2	Delay 1	Delay 2	Delay 1	Delay 2
MCPs (Hamamatsu R3809)	< 0.5 ns	0 or 0.6ns	0	0	don't change	0.6ns	0.6ns
Fast PMTs (PMH-100, R7400)	0.7 ns	0 or 0.6ns	0 or 0.6ns	0 or 0.6ns	don't change	0.6ns or 1ns	0.6 or 1ns
Standard PMTs (R928)	1 .. 3 ns	0 or 0.6ns	1ns	1ns	don't change	1ns	1ns
EG&G APD-Modules	>1ns	0 or 0.6ns	0.6 or 1ns	0.6ns or 1ns	don't change	0.6ns or 1ns	0.6 or 1ns

If you do not know the shape of the SER you can measure it with a fast oscilloscope when the PMT is illuminated with a weak continuous light (please see ‘Checking the SER of PMTs’, page 140).

For the SYNC channel, the configuration usually has negligible influence on the timing performance. Unless the synchronisation amplitude is unstable or a PMT in the photon counting mode is used (e.g. for correlation experiments) the delay lines have negligible influence in the IRF. The recommended configuration is shown in the table below.

Detector for SYNC Channel	typ. Rise Time	-30 Modules		-00 Modules		SPC-134	
		Delay 2*	Delay2*	Delay 1	Delay 2	Delay 1	Delay 2
MCPs (Hamamatsu R3809)	< 0.5 ns	0 ns	0ns	0.6ns or 1ns	0.6ns	0.6ns or 1ns	0.6ns
Fast Photodiode (PHD-400)	< 0.5 ns	0 ns	0ns	0.6ns or 1ns	0.6ns	0.6ns or 1ns	0.6ns
Ultra-Fast PMTs (PMH-100)	0.7 ns	0 or 0.6 ns	0 or 0.6 ns	1ns	1ns	1ns	1ns
Standard PMTs	1 .. 3 ns	1ns	1ns	1ns	1ns	1ns	1ns
EG&G APD-Modules	1ns	0.6 ns or 1 ns	0.6 ns or 1 ns	0.6ns or 1ns	0.6ns or 1ns	0.6ns or 1ns	0.6ns or 1ns

* The discriminator modules of the SPC-6, 7, 8 modules have internal DEL1

Configuration for Positive Input (SPC-x00 only)

For the SPC-600 and -700 modules, the SYNC and CFD inputs can be configured for positive and negative input pulses. To change the configuration, connect the signal cable on the module to the appropriate connector (CFD+, CFD-, SYNC+ or SYNC-) and plug the matching resistor into the unused input. Please note that this is possible only for the -00 modules. The -30 modules and the SPC-134 work with negative pulses only. Connecting the cable of a -30 SPC to SYNC+ or CFD+ will cause no damage to the module, it just does not work.

Optimising the CFD Parameters

Adjusting the CFD Threshold

The threshold and the zero cross level of the CFD of the detector channel have a noticeable influence on the shape and the width of the IRF and on the efficiency of a TCSPC system. Both the threshold and the zero cross level should therefore be adjusted for any particular detector, or if the high voltage of a PMT or the gain control voltage of a PMT modules is changed.

Counting Efficiency

As shown in Fig. 20, page 15, the single-photon pulses of PMTs have a considerably amplitude jitter. The general shape of the pulse amplitude distribution is shown in Fig. 126, left (see also Fig. 55, page 55).

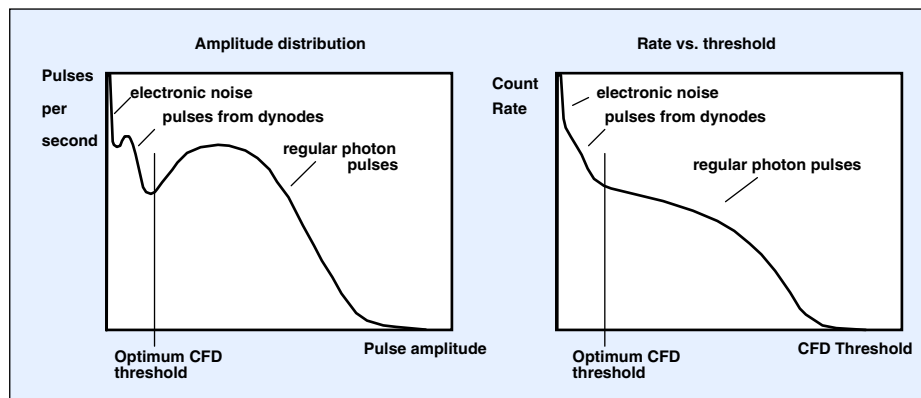


Fig. 126: Amplitude distribution of the single-photon pulses of a PMT (left) and dependence of the count rate on the discriminator threshold (right)

The pulse amplitude distribution consists of three major components. The regular single-photon pulses, i.e. the pulses originating from electron emission at the photocathode, form a wide peak at relatively high amplitudes. Thermal emission, photoelectron emission, and reflection of primary electrons at the dynodes forms a secondary peak at lower amplitudes. At very low amplitudes electronic noise, either from the preamplifier or from the environment, causes a third peak of extremely high count rate. A TCSPC system should record the regular photon pulses, but not the dynode pulses and the electronic noise background. Therefore, the optimum CFD threshold is in the valley between the regular photon pulse distribution and the peak caused by dynode emission.

The corresponding dependence of the count rate on the discriminator threshold is shown in Fig. 126, right. When the PMT is illuminated with light of low intensity and the discriminator threshold ('CFD limit Low') is decreased the count rate increases. At a sufficiently low threshold the increase of the count rate flattens, and in the ideal case forms a plateau. At very low threshold the count rate increases again because the dynode pulses or electronic noise are detected. In practice the dynode peak may be not very prominent or even be hidden in the electronic noise. Also the plateau may be not very pronounced. However, at least a flattening of the count rate increase should be found. If this is not the case probably the gain of the PMT is too low. The operating voltage of the PMT, or, in case of a PMT module, the gain control voltage must then be increased. The gain of a PMT depends steeply on the operating voltage, and the absolute width of the pulse amplitude distribution changes correspondingly (see Fig. 55, page 55).

In practice the IRF shape may degrade at low threshold settings, or prepulses may appear in the IRF. Therefore, the IRF should be checked when the threshold is optimised. If a reasonable IRF cannot be obtained by adjusting the zero cross level (see below) it may be impractical to reduce the threshold too far.

The timing jitter and the influence of electronic background noise is smaller for higher pulse amplitude. Therefore higher PMT gain and higher threshold settings in general yield shorter IRF widths. The threshold is therefore often increased above the value that yields best efficiency. This is not objectionable as long as no more than 90% of the pulses are rejected and the corresponding loss in counting efficiency is taken into account. However, it should be noted that the efficiency and the IRF is less stable than in the counting plateau. Moreover, a large fraction of the detector output current is wasted for the rejected photons. The maximum safe count rate, especially for MCP PMTs, is therefore reduced.

The SPC-x00 modules have an additional ‘Limit High’ threshold. It can be used to reject pulses of high amplitude and may partially help to suppress afterpulses, see below. Also, a narrower amplitude window in principle decreases the influence of the amplitude jitter on the timing. However, the pulse amplitude distribution drops steeply at high amplitude so that the effect of the higher threshold is not very pronounced. If too many pulses are rejected by the higher threshold it may happen that reflections of these pulses on the signal cables trigger the CFD. The result is a second IRF peak after twice the cable transit time.

Detector Background

It is sometimes attempted to reduce the dark count rate of a detector by increasing the CFD threshold. Except for cases when the background is caused by electronic noise these attempts are not promising. The amplitude distribution is almost the same for the photon pulses and the dark pulses, and the CFD threshold suppresses both likewise.

High CFD threshold and low detector gain may even result in an apparent increase of the counting background. The effect is usually accompanied by slow bumps in the IRF some 10 ns after the main peak. The reason of these effects is afterpulsing, see page 60.

Most of the afterpulses appear within a few 100 ns after a photon was detected. With a CFD threshold correctly adjusted a large fraction of the afterpulses is suppressed within the dead time caused by the previously detected photon. Only afterpulses arriving in later signal periods (when the dead time is over) are recorded. In high-repetition rate experiments they deliver a count-rate dependent background, see Fig. 149, page 139.

If the CFD threshold is increased (or the detector gain decreased) too far a large fraction of detector pulses is suppressed. Unfortunately, afterpulses have average amplitudes higher than the photon pulses. The suppression therefore acts mainly on the photon pulses. Worse, photons suppressed by the CFD threshold do not cause dead time. Afterpulses are therefore also recorded in the first 100 ns after a photon, i.e. when afterpulsing is particularly strong. The result is a dramatic increase of the relative afterpulsing background. Moreover, the uneven distribution of the afterpulsing probability results in slow bumps in the IRF some 10 ns after the main peak.

An example is shown in Fig. 127. The PMT used was in the counting threshold at a CFD threshold of -50 mV. At -100 mV the PMT still performs normal, see Fig. 127, left. However, if the CFD threshold is increased to only -300 mV (Fig. 127, right) the ratio of the IRF / background ratio becomes totally unacceptable.

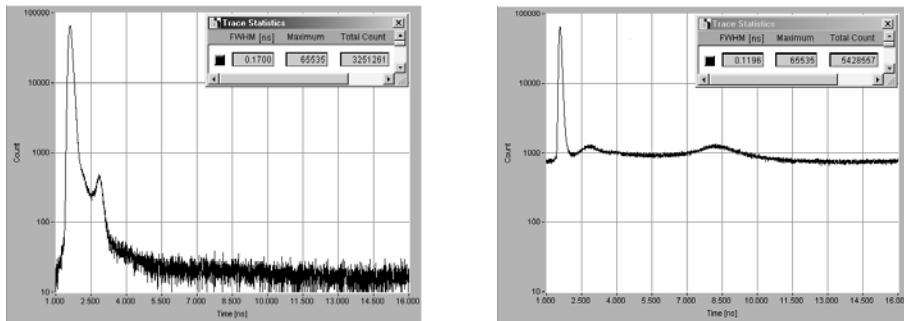


Fig. 127: Increase of afterpulsing background by setting the CFD threshold too high. Left: The PMT performs normal at a threshold of -100 mV. Right: At -300 mV mainly afterpulses are recorded.

Multi-Photon Detection

Excessively high CFD thresholds in combination with low detector gain can entirely suppress the detection of single-photon pulses. If the light intensity is increased, eventually multi-photon events are detected. Particularly at low pulse repetition rates, this may remain unnoticed because high peak intensities can be applied without getting an exceedingly high average detector current. A typical example of multi-photon detection is shown in Fig. 128.

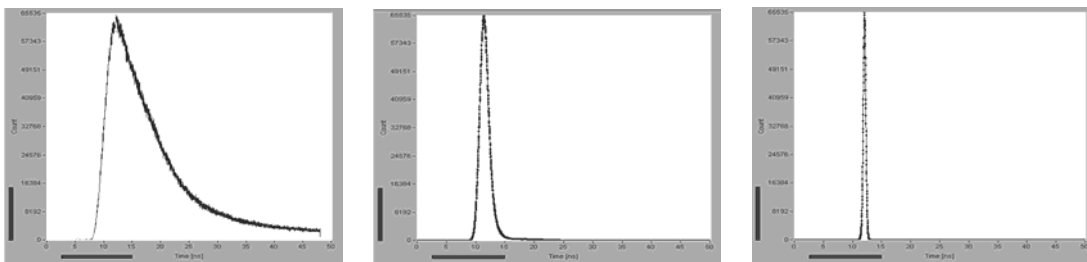


Fig. 128: Detection of multi-photon events at low detector gain. Left: Correctly recorded signal, recorded at a detector gain of 10^6 and a count rate of $3.7 \cdot 10^4 \text{ s}^{-1}$. Centre and right: The same signal recorded at a detector gain of 10^5 and 10^4 . The light intensity was increased until the PMT signal triggered the CFD.

The left curve was recorded at a detector gain of 10^6 and shows the true shape of the light pulse. The curves in the middle and right were recorded at a detector gain of 10^5 and 10^4 , respectively. At a gain this low a single photon does not trigger the CFD. However, if the light intensity is increased, the PMT signal eventually turns into a continuous signal representing the shape of the light pulse. If the amplitude of the signal reaches the CFD threshold, the CFD triggers. The count rate steeply increases from zero to the signal repetition rate, and extremely narrow pulse shapes are recorded. Operating the PMT in this multi-photon mode results in an extreme distortion of the recorded signal waveform. An extremely short ‘IRF’ of less than 20 ps duration can be obtained. This IRF is, of course, entirely useless for any waveform recording.

CFD Zero Cross Level

The zero cross level adjustment minimises the timing jitter induced by the amplitude jitter of the detector pulses. The zero cross level is therefore often called ‘walk adjust’. In early TCSPC systems the walk adjust had an enormous influence on the shape of the instrument response function (IRF). In modern systems the influence is smaller. The reason is probably that detectors with shorter single-electron response are used and the discriminators in the newer CFDs are faster. Therefore, the effective slope of the zero cross transition is steeper, with a correspondingly smaller influence on the zero cross level.

Theoretically the best IRF should be expected at a zero-cross level of exactly zero (see Fig. 124). However, in practice the zero-cross discriminator has an offset voltage of a few mV. Moreover, the intrinsic delay of the discriminator depends on the amplitude of the input signal. The corresponding contribution of the discriminator to the timing jitter can be compensated for by slightly offsetting the zero-cross level from the signal baseline. Therefore the best zero cross value can be some tens of mV above or below zero. A zero-cross level extremely close to the signal baseline can even cause problems. In that case, the zero-cross discriminator may trigger due to spurious signals from the synchronisation channel or may even oscillate. Of course, spurious triggering and oscillation stop when an input pulse arrives, but some after-ringing may still be present and modulate the trigger delay. The result is poor differential non-linearity or a double structure in the IRF.

Extremely large zero cross settings in combination with small threshold settings should be avoided. In those cases it may happen that the threshold discriminator triggers, but the zero cross discriminator does not. Consequently, there are no output pulses from the CFD, although the threshold discriminator indicates a trigger rate.

Optimising the SYNC Parameters

In most cases the constant fraction discriminator is triggered by a reference signal from the light source. The SYNC parameters have little influence on the time resolution as long as the amplitude of the reference signal is stable. If the reference signal has amplitude fluctuations, or if the SPC modules is used for start-stop experiments with a second detector the parameters of the SYNC channel are optimised as described for the detector channel.

If the synchronisation signal has reflections, ringing, or afterpulses multiple triggering can occur. The effect on the recorded signal is shown in Fig. 129. If you see effects like these, increase the ‘Sync Threshold’ (SPC-x30 only) or ‘Sync Holdoff’.

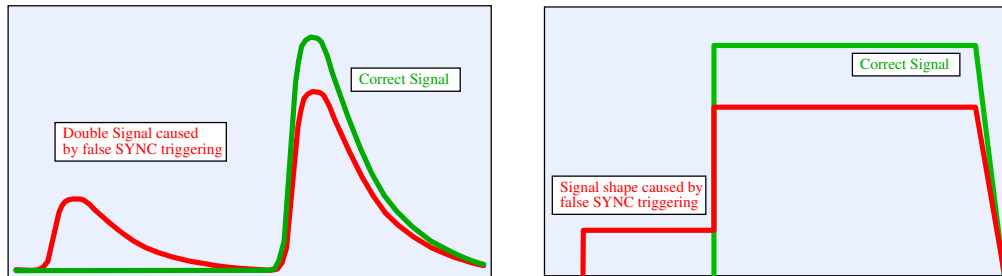


Fig. 129: Effect of false SYNC triggering on recorded signal shape. Left pulsed signal, right continuous light

The ‘Sync Frequency Divider’ setting determines the number of signal periods that are recorded, see Fig. 130. Values greater than one are convenient to find the signal in high repetition rate applications. Furthermore, they can be used to check or calibrate the time scale by comparing the displayed pulse distance with the known pulse repetition rate.

However, fluorescence data analysis programs usually expect data for only one signal period. Spreading the recorded photons over several periods and analysing only one means wasting at least 50% of the photons. Furthermore, recording several periods in multidimensional measurements may waste memory space. Moreover, the time from the photon detection to the next stop pulse adds to the effective dead time. Recording several signal periods thus increases the average dead time and the corresponding counting loss. Therefore, if counting efficiency or memory space are an issue, the ‘Sync Frequency Divider’ should be set to ‘one’.

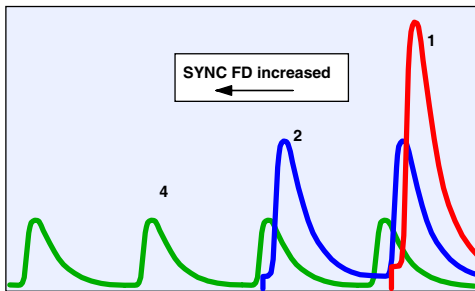


Fig. 130: High repetition rate signal recorded with different Sync Frequency Divider settings

Adjusting the SYNC and CFD Cable Length

When working with ‘Sync Frequency Divider’ = 1 and a sufficiently long TAC Range the SPC module records one signal period less a few ns required to start and stop the TAC. The location of the recording interval within the signal period depends on the optical path lengths, the cable lengths in the CFD and SYNC channels and on the delays in the PMT and SYNC detectors. Therefore, it usually happens that the SPC does not record the correct time interval of the signal. Because of the reversed start-stop operation the effects are often confusing to TCSPC users. Some typical cases and the method of correction are shown below.

The effect of the CFD and SYNC cable length is shown in Fig. 131. The original curve is (1). A longer SYNC cable or a longer SYNC light path shifts the curve left (2), a longer CFD cable or a longer detection light path shifts the curve right (3). 1 ns corresponds to 30 cm light path or 20 cm cable length.

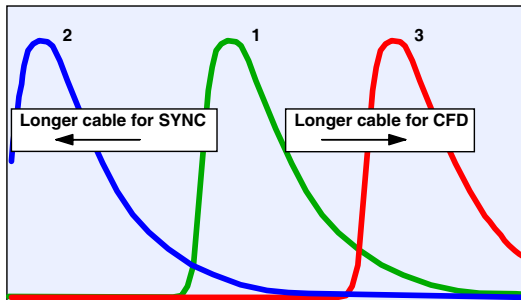


Fig. 131: Effect of the CFD and SYNC cable length

As long as the recorded time interval is shorter than the full signal period the curve can also be shifted by changing ‘TAC Offset’, see ‘Optimising the TAC Parameters’. However, if ‘TAC Offset’ is too small the beginning of the TAC characteristic comes into view (Fig. 132, left). In the first nanosecond the TAC characteristic is nonlinear. The corresponding signal interval displays as a short peak with no photons right of it, see Fig. 132, left. If the signal photons arrive too late they are recorded in the next signal period. The corresponding part of the signal either wraps around the signal period and appears on the left or is outside the conversion range and is not recorded. The method of correction is to use a shorter CFD cable or a longer SYNC cable. The peak at the start of the TAC characteristic can be shifted out of the recorded range by increasing the TAC offset.

The opposite effects happen if a part of the signal photons arrive too early. Due to the reversed start-stop, early photons cause large TAC times. Of course, with FD = 1 TAC times larger than one signal period do not exist. The recorded waveform then drops abruptly to zero left of a TAC time corresponding to one signal period. The part of the signal left of this point is either lost or wraps around the signal period and appears at the right side of the recorded

range. The method of correction is to increase the CFD cable length or decreasing the SYNC cable length.

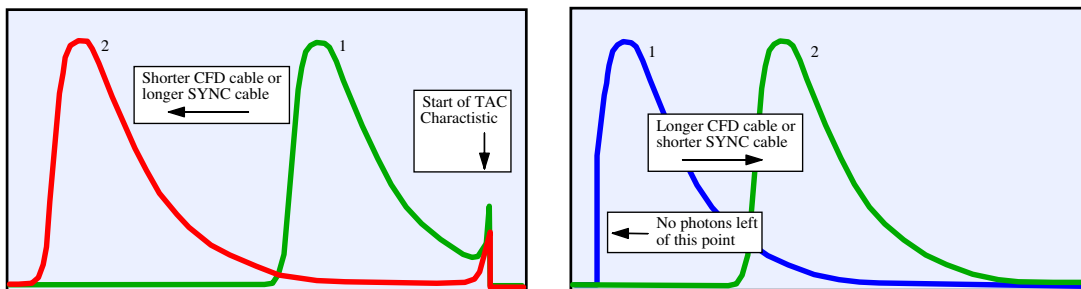


Fig. 132: Left: Photons too late and TAC offset too small, end of TAC characteristic comes into view. Right: Photons too early, no photon with TAC time larger than one signal period recorded

Reversed start-stop operation of TCSPC requires a reference pulse at the end of the signal period or at the end of the recorded time interval. If a high-repetition rate laser is used for excitation this is normally not a problem. However, it is not always clear which laser pulse actually stops the time measurement. It can happen that the stop pulse is not the same laser pulse that excited the detected photon but a pulse from a period before or after. Stopping with a pulse from a different period is no problem if the laser pulses have a constant period and no pulse-to-pulse jitter. This is certainly the case for a Ti:Sapphire laser. Diode lasers, however, may have selectable pulse periods. Moreover, the clock oscillator of a diode laser may have a pulse-to-pulse jitter of some 10 ps. If the reference pulses come from the wrong signal period the position of the recorded signal in the TAC range changes when the laser period is changed. Moreover the pulse-to-pulse jitter adds to the transit time spread of the TCSPC system.

To stop the TAC with the correct laser pulse, the reference signal must be delayed so that the reference pulse arrives after a photon pulse from the same period. The correct delay in the reference channel is the detector transit time, plus the width of the recorded time interval, plus a few ns for the TAC start delay. The relation of the detector and reference delay is shown in Fig. 133.

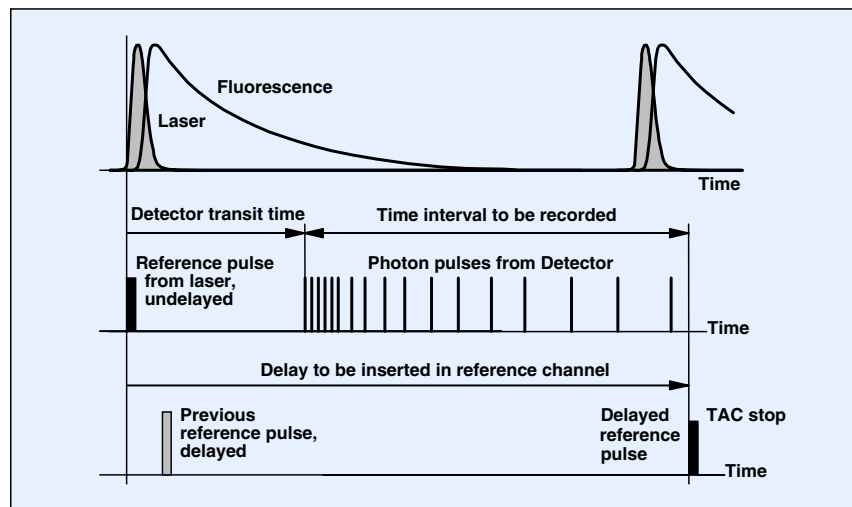


Fig. 133: Reversed start-stop should be used with a delay in the reference channel to stop the TAC with the correct laser pulse

The detector transit time is about 1 ns for an MCP, 5 to 6 ns for a TO-8 PMT or a photosensor module, and 20 to 30 ns for side-window and linear-focused PMTs (see 'Signal Transit Time',

page 56). A good reference delay to start with is 15 ns or 3 m cable for an MCP PMT and 25 ns or 5 m cable for TO-8 PMTs.

An appropriate delay in the reference path is particularly important in experiments with pulse pickers or kHz lasers. With insufficient delay in the reference path it can happen that a time interval completely outside the signal is recorded. In other cases extremely unfavourable TAC settings are used. The signal period is a few 100 ns, and the signal photons appear in the first part of the signal period. Without a delay in the Sync channel the times of the photons are measured to the next laser pulse. This results in extremely long TAC times that vary only within a small interval. This small time interval is then magnified by an extremely large TAC Gain. The situation is illustrated in Fig. 134, left.

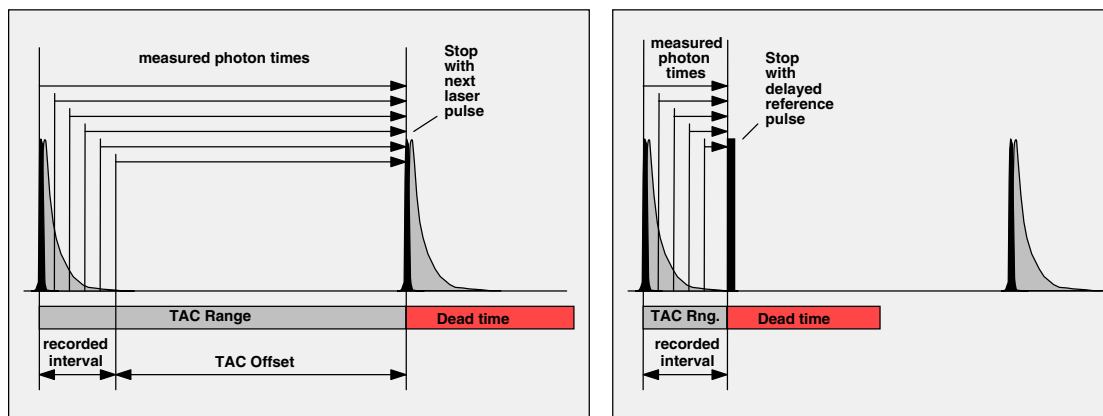


Fig. 134: Recording a short signal within a long laser pulse period. Left: Stop with the undelayed laser pulses; the TAC is stopped by the next laser pulse. Right: Stop with the delayed laser pulses.

There are several serious disadvantages of this way to operate the TAC: The electronic noise from the TAC core is unnecessarily amplified, a possible pulse-to-pulse jitter of the laser appears in the photon times, and the dead time is unnecessarily long. Moreover, the dead time extends into the next signal period. Because the photons appear only in the first part of the period the system is unable to record a photon in the next laser period. Thus, the system has an effective dead time of a full signal period.

A far better solution is to use a delay cable in the reference channel. The delay shifts the stop pulse to a time after the photons to be recorded. The photon times are shifted to smaller TAC times (Fig. 134, right). Consequently, a shorter TAC range and a smaller TAC gain can be used. The result is lower noise in the TAC signal and a correspondingly better time resolution. Because a shorter TAC range is used also the dead time is shorter (see ‘Dead Time’). For long signal periods the dead time may even be entirely hidden in the last part of the signal period where no photons are recorded (Fig. 134, right). The influence of different TAC operation on the effective dead time is discussed in [46].

Adjusting the TAC Parameters

The TAC parameters determine the time scale and the part of the signal that is recorded. The bh SPC modules work in the ‘reversed start-stop’ configuration, i.e. a photon pulse from the detector starts the TAC and the next pulse from the SYNC - or the SYNC frequency divider - stops it. The direction of the time axis is corrected by reversed readout of the photon distributions. As a result, ‘time zero’ of the TAC is right, and shifting the TAC signal down by increasing the ‘TAC Offset’ shifts the curve right, see Fig. 135.

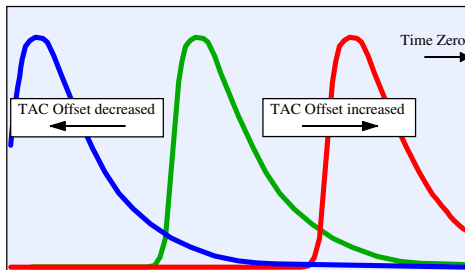


Fig. 135: Effect of TAC Offset

However, if ‘TAC Offset’ is too small the beginning of the TAC characteristic comes into view. Since the very first part of the TAC characteristic is nonlinear it displays as a short peak with no photons right of it (Fig. 136, left). TAC Offset should be high enough - usually a few % - to shift the beginning of the TAC characteristic out of the recorded time interval. If the signal is too far right so that it interferes with the beginning of the TAC characteristic, change the CFD or SYNC cable length as described above under ‘Adjusting the SYNC and CFD Cable Length’.

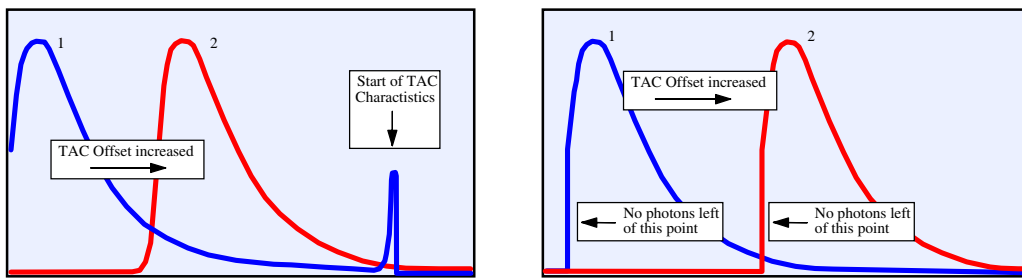


Fig. 136: Left: Increasing the TAC Offset shifts the recorded curve right, and shifts the beginning of the TAC characteristic out the recorded range. Right: No photons with times larger than the stop period are recorded.

The opposite effects happens if some of the photons arrive prior to the previous SYNC pulse. Then the recorded photon distribution drops to zero left of the time where the SYNC pulse is detected (Fig. 136, right). Although the curve can be shifted right by increasing TAC Offset, the part of the signal before the SYNC pulse cannot be detected. The method of correction is increasing the CFD cable length or decreasing the SYNC cable length while decreasing ‘TAC Offset’. (see ‘Adjusting the SYNC and CFD Cable Length’).

The parameter ‘TAC Range’ determines the time scale of the recording. The parameter works in conjunction with ‘TAC Gain’ (Fig. 137). ‘TAC Range’ sets the slope gradient of the TAC ramp, ‘TAC Gain’ the gain of the TAC output amplifier. Therefore, TAC Range determines the maximum recording interval, and ‘TAC Gain’ works as a magnifier for a part of this interval, see Fig. 137.

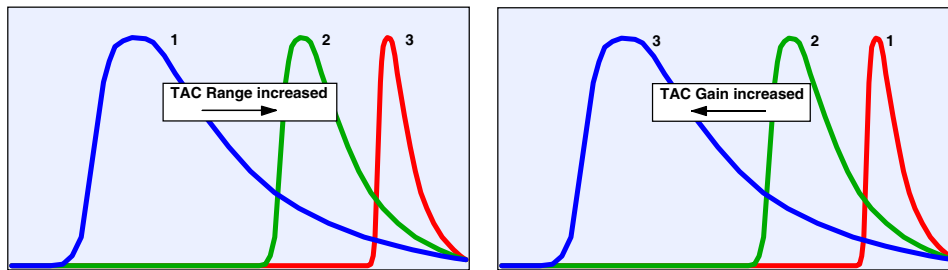


Fig. 137: Effect of TAC Range (left) and effect of TAC Gain (right)

As long as a smaller ‘TAC Range’ is available there is normally no need to use a ‘TAC Gain’ > 1 (see also ‘Dead Time’). However, to obtain maximum resolution within the minimum ‘TAC Range’ of 50 ns ‘TAC Gain’ can be increased to values up to 15.

TAC Linearity

The differential nonlinearity (DNL) of the time measurement is the most important source of errors in TCSPC measurements. Often the TAC and the ADC are considered the source of differential nonlinearity. They are, however, not the only source of the linearity errors. More important are usually parasitic coupling of start and stop pulses - synchronous noise pickup of the detector, coupling between the detector and synchronisation cables, and coupling between the CFD and the SYNC circuits. This causes a nonuniformity of the channel width and consequently a nonuniform count result in the particular channels. The errors appear as additional noise, ripple or curve distortion. Differential nonlinearity should not be confused with optical reflections. The resulting distortions in fluorescence decay curves may look very similar to differential nonlinearity, see Fig. 152, page 144.

Compared to conventional NIM systems the bh SPC modules achieve a very low differential nonlinearity even at high pulse repetition rates. Some unavoidable linearity errors are, however, detectable. The following advice may help to keep linearity errors small:

Use a reasonable value of the parameter ‘Dither Width’. The parameter controls the ADC error correction, see ‘ADC Error Correction’, page 48. Dither Width = 0 switches the error correction off and is intended for test purpose only.

Good electrical shielding of the detector is extremely important. Noise pickup from the laser or from the synchronisation channel into the detector signal is the most frequent source of poor differential nonlinearity.

Strictly avoid any coupling of the SYNC signal or other excitation-related signals into the detector signal. Separate detector and synchronisation cables spatially. Avoid very small SYNC amplitudes at high CFD amplitudes and vice versa. Avoid noise radiation by active mode lockers, cavity dumpers, laser diodes or flash lamps.

Often home-made diode lasers are a source of TAC linearity problems. To achieve short laser pulses, the diodes are driven by extremely steep and powerful current pulses. If the lasers are not shielded very carefully noise from the driver couples into the PMT signal or directly into the SPC module. If the trigger for the SPC is taken directly from a connector at a poorly shielded laser diode controller noise coupling via the trigger cable will almost surely cause problems. The only way to avoid the problem is a correct design of the laser housing.

The PMT should be operated at a gain as high as possible. Use a good photomultiplier which is specified for single photon counting. These devices have a higher gain and, consequently, a narrower narrow SER pulse amplitude distribution. Fig. 138 shows the basic mechanism of interaction of synchronous noise with the PMT pulse height spectrum.

If synchronous noise is present, the complete pulse height spectrum (shown grey in Fig. 138) is shifted up and down with the warped pulse baseline. Consequently, the probability of the photon pulses to exceed the threshold changes with the time in the signal period. The result is a modulation of the measured waveform by the spurious signal. If the detector has a narrow pulse height distribution and the threshold is adjusted correctly, the effect on the detection probability is small (Fig. 138, left). However, if the pulse height spectrum is broad or the detector is not operated in the counting plateau even a small ripple on the baseline causes serious distortions of the measured waveform (Fig. 138, right).

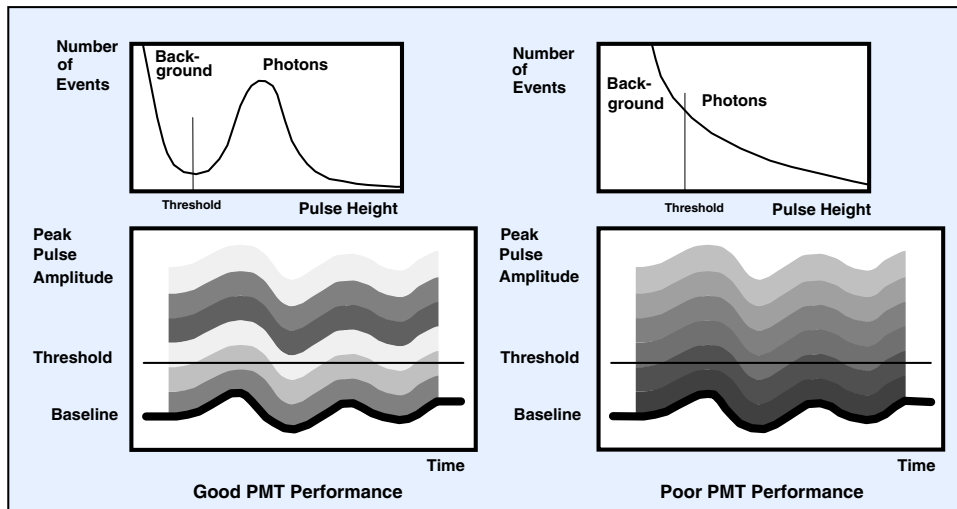


Fig. 138: Interaction of spurious signals with the PMT pulse height spectrum

Spurious signals in the PMT channel also have a direct effect on the timing because the zero cross pickoff in the CFD is influenced. Although in this case the time axis is warped the apparent result is the same as described above.

Noise signals which are not related to the excitation (e.g. radio transmitters) have no direct influence on the differential nonlinearity. They affect, however, the time resolution and cause an apparent widening of the pulse height spectrum.

For spurious signals in the SYNC channel the direct effect on the timing dominates. Some peculiar effects can appear if noise from active modelockers or cavity dumpers (with 1/2, 1/4 etc. of the SYNC frequency) is coupled into the SYNC channel. To decouple the SYNC photodiode from such sources we recommend to isolate it from the optical setup so that the only ground connection is via the signal and power supply cables from the SPC module.

The SYNC signal should have a short rise time and a clean pulse shape. The SYNC zero cross level should be adjusted for optimum trigger performance.

For measurements that require maximum accuracy we recommend to record a reference curve with a continuous light source and to divide the measurement results by this reference curve. The operation can easily be performed by the SPCM operating software of the SPC modules, see ‘2D Data Processing’, page 324. Because the reference curve has the same linearity errors as the measurement results, the division reduces the errors considerably. Introducing noise of the reference measurement into the quotient can be largely avoided by smoothing the reference curve [46].

Dead Time

Next to differential nonlinearity, system dead time is the most serious error source in TCSPC experiments. The system dead time is the time the system is ‘blind’ after the detection of a photon. Dead time does not only limit the maximum count rate that can be used in a given measurement setup, it can also introduce distortions of the signal waveform and errors in the measured intensities. The sources of the dead time, its influence of the measured photon numbers and on the recorded waveforms is discussed in the following paragraphs.

Fig. 139 shows the timing diagram of the TAC/ADC combination for a single detected photon.

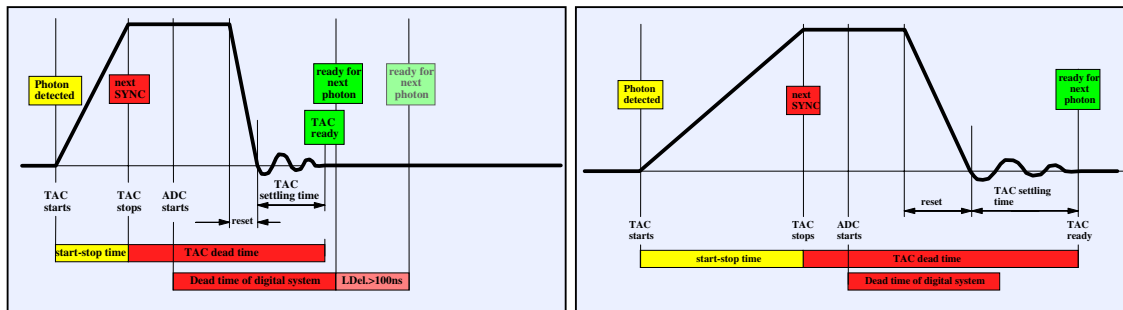


Fig. 139: Timing diagram for TAC Range < 100 ns (left) and TAC Range >100 ns (right)

When the photon is detected the TAC ramp starts until the next STOP pulse arrives at the TAC. Depending on the ‘SYNC Frequency Divider’ setting this can be the next synchronisation pulse from the light source or one of the next 2, 4, 8 or 16 pulses. Some 10 ns after the TAC has stopped the ADC is started. When the ADC is ready the TAC is reset, i.e. the TAC capacitor is discharged. After some additional recovery time needed for the TAC output amplifiers to settle the TAC is ready to convert the next photon.

With the start of the ADC, i.e. in parallel with the TAC reset the digital signal processing sequence for the current photon is initiated. The digital system sends a ‘not ready’ signal to the TAC which holds the TAC in the reset state until the next photon can be accepted.

For TAC ranges smaller than 100 ns and for a ‘Latch Delay’ smaller than 100 ns the end of the TAC dead time and the end of the digital signal processing are almost coincident. For ‘Latch Delay’ > 100 ns the digital dead time increases because the digital signal processing machine has to wait until the routing signal has been latched.

For longer TAC ranges the TAC reset and recovery time can be significantly longer because the TAC capacitor is larger. Approximate TAC dead times are given in the table below:

TAC Range	TAC Dead Time: SPC-6, -8	SPC-134, -144	SPC-7
50 ns to 99 ns	125 ns	100 ns	150 ns
100 ns to 199 ns	150 ns	140 ns	160 ns
200 ns to 499 ns	180 ns	180 ns	180 ns
500 ns to 999 ns	260 ns	260 ns	260 ns
1 us to 2 us	550 ns	550 ns	550 ns

The times depend on the time difference between start and stop, because the TAC reset time increases with the TAC output voltage. The values in the table are for 50% TAC output voltage.

The ‘Dead Time’ given in data sheets is the time from the stop pulse to the moment when the system is ready for the next photon. The effective dead time for a particular photon is this ‘Dead Time’ plus the start-stop time. The start-stop time depends on the operating conditions, particularly on the signal duration and the time from the signal to the next sync pulse. For a typical Ti:Sa laser experiment with 12 ns pulse spacing the average start-stop time is on the order of 6 ns so that the dead time is not significantly increased. However, for fluorescence decay measurements in the 100 ns range there can be a noticeable contribution of the start-stop time. Fig. 140 shows how the overall dead time depends on the start-stop time.

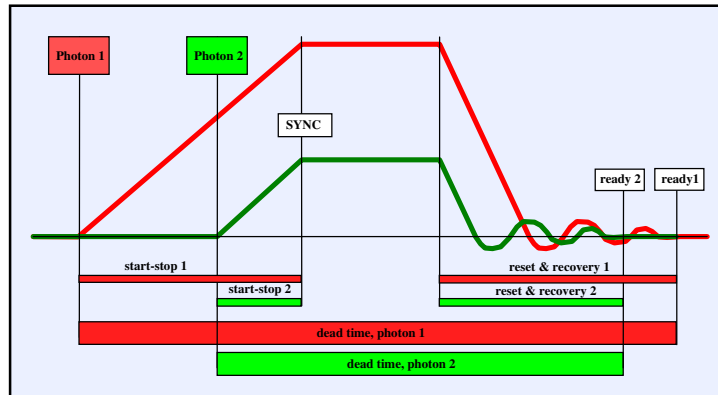


Fig. 140: Influence of the start-stop time on the overall dead time

Please note that the start-stop time not only contributes to the overall dead time, also the TAC reset time increases proportionally. To hold the effective dead time as short as possible we recommend:

- Use the smallest possible TAC range. This holds the TAC reset and recovery time short.
- Avoid unnecessarily long start-stop times. Use ‘Sync Frequency Divider’ = 1 and a ‘TAC Offset’ as small as possible. Adjust the SYNC and CFD cables to shift the signal as far as possible right.
- For measurements at low repetition rate, use a delay cable in the SYNC path. Delayed stop operation can eliminate the effect of dead time entirely, see Fig. 134.
- Set a short ‘Latch Delay’. Values above 100 ns increase the dead time and are not normally required for bh routers or multichannel detectors.

Counting Loss

When recording a light signal the single photon pulses from the detector occur at random intervals. Therefore, even if the average time interval between the pulses is much longer than the dead time of the counting system, a fraction of the pulses is lost. For the calculation of the counting loss is important whether a photon lost in the dead time causes new dead time or not. In TCSPC a lost photon clearly does not cause any noticeable dead time. Under this condition the recorded rate, r , for a input pulse rate, r_0 , is

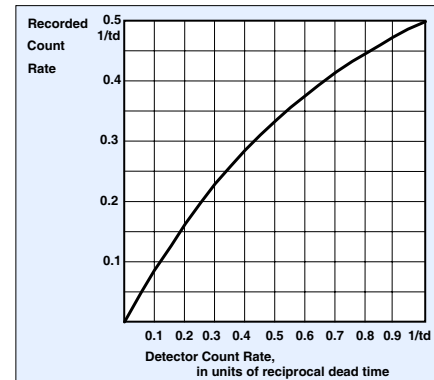
$$r = \frac{r_0}{1 + r_0 t_d}, \text{ with } t_d = \text{dead time}$$

The counting efficiency, E , is

$$E = \frac{r}{r_0} = \frac{1}{1 + r_0 t_d}$$

For an input count rate of the reciprocal dead time, $1/t_d$, the recorded count rate is 50% of the input count rate. bh defines the recorded count rate for 50% loss as the ‘maximum useful count rate’:

$$r_{mu} = 0.5 / t_d$$

Fig. 141: Recorded count rate vs. input count rate for a counter with the dead time t_d

The input (or detector) count rate, r_0 , at the maximum useful count rate, r_{mu} is the reciprocal dead time, $1/td$.

Often data sheets of photon counters specify a ‘maximum count rate’ which is simply the reciprocal dead time. Of course this count rate can be reached only for infinite input count rate. Better the term ‘saturated count rate’ should be used, see ‘Specification’, page 355.

The consideration above assumes that the detected light signal is continuous. However, signals measured by TCSPC are usually pulsed. Moreover, the photon detection and consequently the dead time is synchronised with the signal period. The equation given above applies with satisfactory accuracy to reversed start-stop measurements at high pulse repetition rate. In other cases the counting loss depends on the operating conditions. Depending on the system configuration, there may be no dead-time related counting loss at all, or the effective dead time can be a full signal period (see Fig. 134). A detailed discussion is given in [46].

Dead-Time Compensation

The bh TCSPC modules provide an optional ‘dead-time compensation’ in the device hardware. The idea behind the dead-time compensation is to increase the collection time by the sum of all dead time intervals that occurred during the measurement. The principle is shown in Fig. 142.

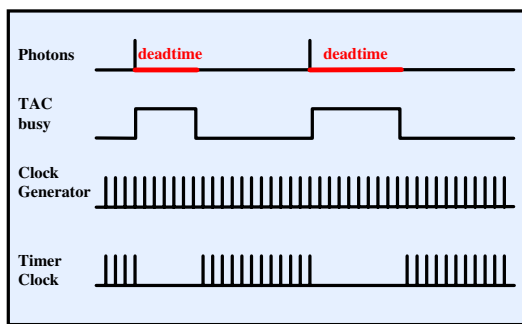


Fig. 142: Dead time compensation by gating the timer clock

The TAC delivers a ‘busy’ signal as long as it is unable to accept a new photon. A high frequency clock is gated with the ‘busy’ signal, and the gated clock is used to drive the collection timer. Thus, the collection timer is stopped in the dead-time intervals.

We recommend to use dead-time compensation for measurements that require an accurate intensity scale. However, please take into regard that the compensated collection time changes with the count rate and can be noticeably longer than the selected collection time.

The dead time compensation works with satisfactory accuracy if the photons can be considered to appear in random intervals, and in a virtually continuous stream. This is the case for reversed-start-stop measurements at high repetition rate, when the signal period is several times shorter than the dead time. The dead time compensation is not necessarily correct for measurements at low repetition rate, see Fig. 134, right. The compensation does not work for simulated detector pulses delivered by a pulse generator at a fixed frequency.

Pile-Up Effects

Pile-up effects result from the fact that a TCSPC device can detect only one photon per signal period. If the detection rate is so high that the detection of a second photon within the recorded time interval becomes likely the signal waveform is distorted.

Classic Pile-Up

The classic pile-up effect [265] is shown in the figure right. Pile-up becomes noticeable when the count rate exceeds a few percent of the pulse repetition rate. Detection and loss of a second photon is more likely to occur in the later part of the signal, therefore the recorded waveform is distorted (Fig. 143).

Classic pile-up is the principal source of signal distortion in experiments with lasers or flashlamps working at a repetition rate in the kHz range [225, 223, 224, 310, 379]. If the experiment is run at too high a count rate, extreme pile-up effects can impair the results so severely that any attempt at correction is useless. If the detector actually sees hundreds or thousands of photons per laser pulse, pile-up can even mimic signals shorter than the detector transit time spread.

Classic pile-up should not be confused with multi-photon detection. Multi-photon detection can happen if the discriminator threshold in the detection channel is set above the single-photon pulse amplitude. In this case, events are recorded only if several photons are detected within the single-electron-response width of the detector.

The distortion of the signal shape by classic pile-up is predictable and - within reasonable limits - correctable if the detector count rate and the signal repetition rate are known [85, 86, 87, 265, 379]. It is commonly believed that the pile-up becomes a problem if the count rate exceeds 0.1 to 1% of the pulse repetition rate. However, a calculation of the pile-up error in a detected fluorescence lifetime shows that much higher count rates can be used [46].

The pile-up effect adds virtual lifetime components of $\tau/2$, $\tau/3 \dots \tau/n$, to the recorded waveform. A mean lifetime, τ_{meani} , of the recorded curve can be defined as an average of the lifetimes, τ_i weighted by their integral intensities, [220]:

$$\tau_{meani} = \frac{\sum a_i \tau_i^2}{\sum a_i \tau_i}$$

with a_i = intensity coefficients of the lifetime components, τ_i .

The pile-up distorted τ_{meani} is

$$\tau_{meani} = \tau \frac{1 + \frac{1}{2} \frac{1}{2!} P + \frac{1}{3} \frac{1}{3!} P^2 + \frac{1}{4} \frac{1}{4!} P^3 + \dots}{1 + \frac{1}{2!} P + \frac{1}{3!} P^2 + \frac{1}{4!} P^3 + \dots}$$

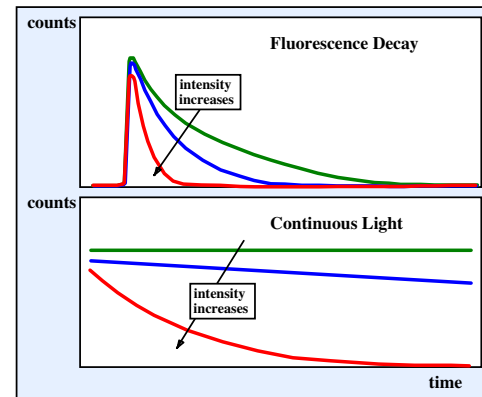


Fig. 143: Effect of classic pile-up on the waveform

with P = average number of photons per laser period [46]. For small values of P the mean lifetime is

$$\tau_{\text{mean}} \approx \tau (1 - P/4)$$

Fig. 144 shows the recorded intensity-weighted mean lifetime as a function of the number of photons per laser period, P , relative to the correct lifetime, τ .

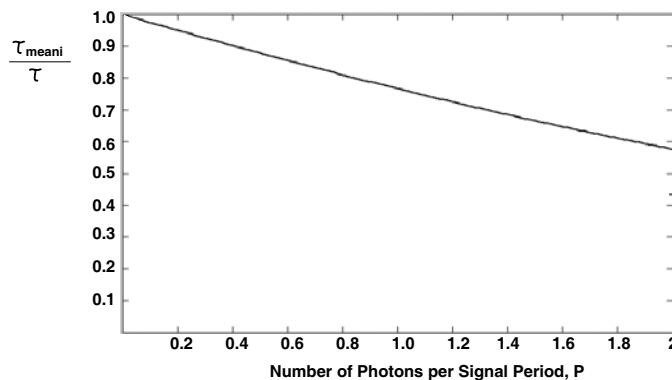


Fig. 144: Intensity-weighted lifetime as a function of the number of photons detected per signal period, P

The influence of the pile-up on the obtained lifetimes is surprisingly small. A 5% change in the intensity-weighted mean lifetime is often tolerable. The corresponding P is about 0.2, i.e. the detector count rate is 20% of the pulse repetition rate. With pile-up correction, even higher count rates appear possible. Classic pile-up is therefore not a severe problem at pulse repetition rates between 50 to 90 MHz, typical for titanium-sapphire lasers and diode lasers.

Inter-Pulse Pile-Up

Inter-pulse pile-up is a problem of high-repetition rate experiments. It is actually a counting loss effect, but it causes signal distortions as the classic pile-up does. The effect is shown in Fig. 145. After a photon was detected the system is blind for the start-stop time and the TAC/ADC dead time. The TAC/ADC dead time starts with the next SYNC pulse and ends somewhere in one of the next SYNC periods. Consequently, no photon can be detected in the first part of this period.

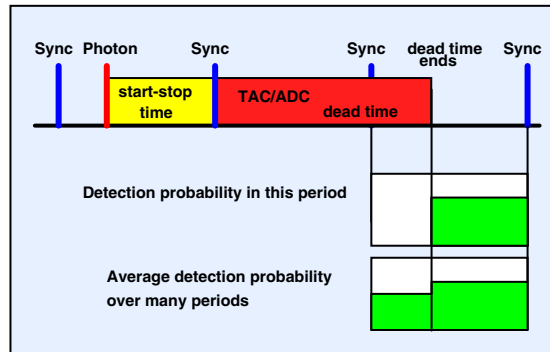


Fig. 145: Mechanism of inter-pulse pile-up

Averaged over a large number of periods, the result is a step in the recording probability. The recorded waveforms are thus distorted. The size of the distortion depends on the ratio of the count rate to the signal repetition rate and can be estimated as follows:

The probability, P , to detect a photon in a particular laser period is

$$P = r_{det} / f_{rep}$$

with r_{det} = detector count rate at the CFD input, f_{rep} = signal repetition rate. However, a photon in the early part of the period can be recorded only if no photon was detected in the signal period a dead-time interval before. The probability, p_{early} , of detecting a photon in the early part of the period is therefore

$$p_{early} = \frac{r_{det}}{f_{rep}} \left(1 - \frac{r_{det}}{f_{rep}} \right)$$

The relative size of the distortion is

$$(p_{late} - p_{early}) / p_{late} = r_{det} / f_{rep}$$

Interestingly, the size of the dead-time-related distortion does not depend on the dead time. The absolute size of the distortion is of the same order as the distortion by classic pile-up. It even counteracts the classic pile-up because it happens in the early part of the signal period. Although the size of the distortion is predictable, the actual shape of the distortion is not. If the recorded time interval is shorter than one signal period the distortion may be outside the recorded interval. It may differ from a clean step because the dead time may vary due to the TAC voltage of the detected photon, and the transition from the blind into the active state may cause some ripple in the TAC characteristic for a few ns. Moreover, in practice the dead time is determined by CMOS logic circuits and active delay lines in the control circuitry of the TCSPC module. The dead time can therefore be expected to be stable within a few ns at best. The temporal position of a possible distortion is therefore not absolutely stable. Thus, it is difficult to correct for dead-time-related distortion.

In practice the distortion can be minimised in the same way as classic pile-up, i.e. by maximising the signal repetition rate, or, more exactly, maximising the TAC stop rate. The signal repetition rate should be as high as possible, and the setup should avoid frequency division in the reference channel and pulse-by-pulse multiplexing with a common stop pulse (see below, Fig. 147).

It should be noted here that distortions by inter-pulse pile-up have exactly the same appearance as distortions by optical reflections (see Fig. 152, page 144). In fact, the vast majority of step-like distortions is caused by optical reflections, not by inter-pulse pile-up. Therefore the optical system should be checked before a TCSPC module is suspected to produce distortions by inter-pulse pile-up.

Fighting Pile-Up Effects

Low Repetition Rate Measurements

The dominating problem of low-repetition rate applications is classic pile-up. Later photons are more likely to be lost so that the recorded waveform is distorted. This limits the count rate to about 10% percent of the signal repetition rate. A number of pile-up rejection circuits were suggested in early times of TCSPC [310, 372]. The circuits detected a possible second photon in one signal period, and, when a second photon was detected, suppressed the storing of both photons in the memory. Consequently, only photons from signal periods with one photon were

used. In practice this approach has, however a significant flaw. Typical fluorescence lifetimes are of the order of a few ns, i.e. in the same range as the width of the detector pulses. Because of the broad amplitude distribution of the detector pulses it is not possible to distinguish reliably between one or two photons within the detector pulse width. If the fluorescence lifetime is significantly longer than the detector pulse width a second photon can, in principle be recognised by counting the threshold transitions in the CFD. However, detector pulses are normally not free of ringing or reflections. For the larger detector pulses ringing and reflections commonly cause multiple threshold transitions. Consequently, a large number of good detector pulses would be rejected.

It has also been attempted to record several photons per signal period, i.e. by fast multiscaler principles or by time-to-digital conversion (TDC) circuits. These solutions face the same problems as pile-up correction. Two photons detected within a fluorescence decay time of a few ns cannot be distinguished in the detector signal, and multiple triggering by ringing and reflections causes distortions in the recorded curves.

Nevertheless, there is a way to reduce the classic pile-up. If the light is spread over several detectors multi-photon events in one detector become less likely. Instead, simultaneous detection will occur in different detectors so that it can be recognised, see Fig. 146.

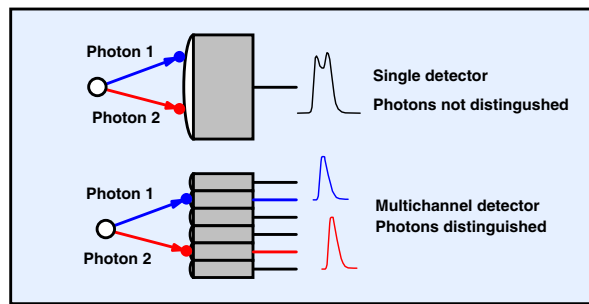


Fig. 146: Separation of photons by multi-detector setup

The light signal is spread over several detector channels. These may be individual detectors or the channels of a multi-anode PMT. If several photons appear in the same signal period they are more likely to hit different detectors channels than the same one. Photons detected at the same time in different detectors can, however, easily be separated.

The straightforward solution is to record the photons in several detector channels is to use several parallel TCSPC channels, e.g. an SPC-134, SPC-144 or SPC-154 package.

Pile-up-rejection is, however, also possible by using a single TCSPC channel with a router [336]. The router monitors the output signal of all detector channels by fast discriminators. When a detector delivers a photon pulse the corresponding discriminator triggers and an encoder generates a digital ‘detector channel’ number (see Fig. 29, page 25). If several detectors deliver pulses within the response time of the discriminator/encoder circuitry, the encoder delivers a ‘Disable Count’ signal. This signal suppresses the storing of the complete detection event, i.e. of both photons, in the memory of the TCSPC module. Thus, waveform distortion by classic pile-up is reduced. The time interval in which several photons are recognised as a multi-photon event is usually of the order of several tens of ns.

High Repetition Rate Signals

Both the classic pile-up and the inter-pulse pile-up depend on the ratio of the count rate and the pulse repetition rate, or, more exactly, the stop rate of the TAC. Counting loss depends on the ratio of the dead time and the stop rate. Consequently, both pile-up and counting loss is

minimised by keeping the effective TAC stop rate high. Moreover, counting loss is reduced by running the TCSPC module in a way that the dead time is at minimum.

Therefore, unnecessarily long start-stop times (see ‘Dead Time’ page 129) should be avoided: Use the right delay in the detector and Sync signal path. Shift the curves as far as possible right, i.e. to small TAC times. Use the shortest possible TAC range.

Use a laser repetition rate as high as possible. Even if a fluorescence does not decay completely within one laser period it is often easier to correct for incomplete decay than for pile-up effects.

Avoid anything that reduces the effective TAC stop rate. Do not use Sync frequency divider settings larger than one. Avoid multiplexing signals on a pulse-by pulse basis. Pulse-by-pulse multiplexing was originally introduced by to simultaneously record two signals in classic TCSPC setups [371]. Two ore more signals are given different optical delays. They are then detected through the same detection path and recorded in the same TAC range. Pulse-by pulse multiplexing can also be achieved by interlacing the pulses of several lasers. The reference signal is derived from only one of the lasers. Although pulse-by-pulse multiplexing looks elegant at first glance it has severe drawbacks at high count rate.

The situation is illustrated in Fig. 147. The upper part of the figure shows pulse-by-pulse multiplexing. Compared with the detection of a single signal the effective stop rate is divided by the number of multiplexed signals. The required TAC range is multiplied by the number of signals. In practice it must even be longer because enough time between the signals must be provided to avoid overlapping of the tail of one signal into the rising part of the next. The result is increased classic pile-up, increased inter-pulse pile-up, and increased counting loss.

A better way to record several signals is multiplexing via the routing signals, see lower part of Fig. 147. The lasers are multiplexed at microsecond rate, and the routing signals are used to send the photons into separate memory blocks (see also Multiplexed TCSPC, page 27). The stop rate is the full laser repetition rate, and the TAC range needs to be no longer than the signal duration. Moreover, any temporal overlap of the two signals is avoided.

If count rates exceeding $5 \cdot 10^6 \text{ s}^{-1}$ are to be recorded a single TCSPC module is unable to record the photons with a reasonably low counting loss and pulse distortion. Moreover, the detector count rate under these conditions is about 10^7 s^{-1} . The IRF of most single-photon detectors degrades at detector count rates this high. Detector overload may even preclude count rates higher than a few 10^6 s^{-1} altogether. The solution is then to use several fully parallel detector and TCSPC channels. Suitable modules exist in form of the bh SPC-134 and SPC-144 multi-module TCSPC systems.

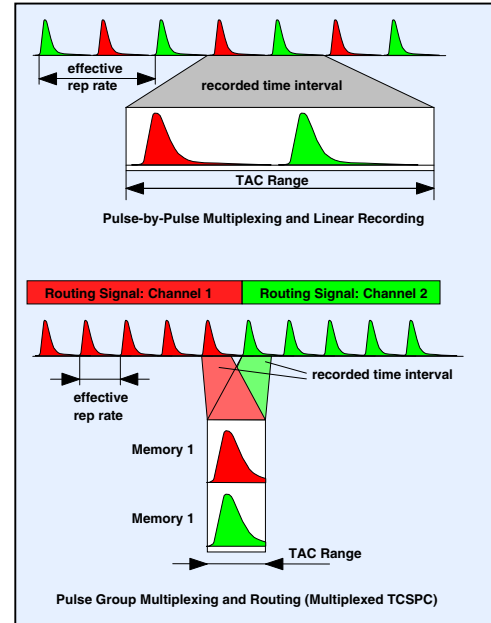


Fig. 147: Pulse group multiplexing and routing is more efficient than pulse-by pulse multiplexing and linear recording

Optimising the Photomultiplier

In older books and papers about TCSPC a numerous hints were given how to improve the time resolution of a photomultiplier [71, 192]. Optimised voltage divider chains, changed voltages at the focusing electrodes, operation at a reduced number of dynodes, or even magnetic fields in the photocathode region were reported to improve the resolution by nearly one order of magnitude. This may be true for the PMTs of that time, especially if the optimisation started with a poorly designed voltage divider.

Now, the fastest detectors are the Hamamatsu R3809U MCPs. There is nothing you could adjust at these detectors. Another fast detector, the Hamamatsu H5783 module with its 150 ps FWHM is completely sealed. Thus, there is little you can do to improve the response of these detectors. However, sometimes PMTs of conventional design must be used because of the spectral range, the dark count rate or price constraints. For such applications some hints are given below.

Voltage Divider

Conventional fast photomultipliers often have one or more focusing electrodes between the cathode and the first dynode. The voltage at these electrodes influences the transit time spread, the ‘colour shift’ (dependence of the IRF on the wavelength) and the dark count rate. The adjustment can be difficult because the trimpots are at high voltage potentials. Therefore, the photomultiplier housing should contain a light protection between the voltage divider and the tube. The adjustment then need not be done in the dark and is less dangerous.

For almost all photomultipliers the time resolution improves with increasing the voltage between the photocathode and the first dynode. Increasing this voltage also reduces the ‘colour shift’, i.e. the dependence of the system response on the wavelength. It may also be useful to increase the voltage between the first two dynodes.

The FWHM decreases reciprocally with the square root of the voltage. The effect of the voltage between the cathode and the first dynode for an R5600 PMT is shown in Fig. 148. The response functions were measured with the nominal voltage divider and with a circuit applying a 3-fold increased voltage between the cathode and the first dynode. Unfortunately for most PMTs no maximum values for this voltage are given. Consequently there is some risk to damage the photomultiplier if the voltage is increased too much.

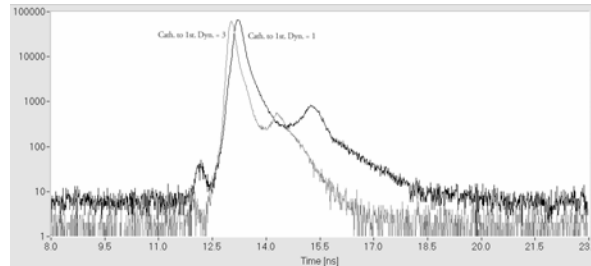


Fig. 148: Effect of the voltage between the cathode and the first dynode of an R5600 PMT

Illuminated Area

To achieve a good time resolution with a conventional photomultiplier the light has to be focused onto a small area of the photocathode. Even for a focus diameter below 1mm an effect can be detectable. Therefore, means to adjust the optical focus should be provided. Also the position of the light spot on the photocathode has an influence on the time resolution, see Fig. 66, page 65.

However, under no circumstances the light should be focused on the cathode of an MCP PMT. The lifetime of an MCP PMT is limited by degradation of the coating of the micro-

channels. This degradation is caused by sputtering under the influence of the secondary electrons. In first approximation, the degradation of a channel is proportional to the overall charge it has delivered. Spreading the light over the full cathode area extends the lifetime of the MCP by reducing the load at the individual channels. Moreover, the IRF stability at high count rate improves dramatically for larger illuminates area (see Fig. 64, page 64). Therefore MCP PMTs should always be operated with the full cathode area being illuminated.

Signal-Dependent Background

All photon counting detectors suffer more or less from afterpulsing (see ‘Afterpulsing’, page 60). Afterpulsing occurs on the time scale of a few microseconds. In high-repetition-rate TCSPC experiments, the afterpulses of many signal periods accumulate and deliver a considerable background level. The afterpulsing background can be disastrous if the detector is operated at a gain too low or a CFD threshold too high, see Fig. 127, page 122. However, even with a correctly adjusted CFD threshold a substantial afterpulsing background is detected.

An example is shown in Fig. 149. It shows recordings of a fluorescence signal (top) and of the dark counts (bottom) for a cooled H5773-20 photosensor module (left) and an R3809U-50 MCP-PMT (right). The pulse repetition rate was 50 MHz, the count rate approximately 400 kHz, the acquisition time 40 seconds.

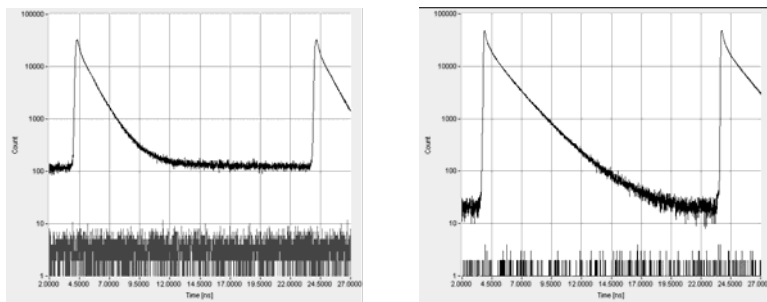


Fig. 149: Signal-dependent background. Fluorescence signals and dark counts recorded by a cooled H5773-20 PMT module (left) and a R3809U-50 MCP-PMT.

For both detectors the background of the fluorescence measurement is considerably higher than the dark count level. However, the ratio of the fluorescence counts to the background counts is more than 10 times better for the R3809U-50 than for the H5773-20. This result is in agreement with the low afterpulsing probability found for the R3809U-50 [28, 46].

For a given detector, the afterpulsing probability and thus the background can be reduced by reducing the gain. The reduced detector gain must be compensated for by a higher preamplifier gain or a reduced discriminator threshold. However, in practice the loss in time resolution and the increase in differential nonlinearity set a lower limit to the detector gain.

Another way to increase the dynamic range is to reduce the pulse repetition rate. The downside of this solution is the increase of pile-up distortion or acquisition time.

It should be noted that filter fluorescence can cause a signal-dependent background that is almost indistinguishable from the background caused by afterpulsing. Therefore, if background is a problem, the optical system should also be checked. Filter fluorescence can be distinguished from the afterpulsing background by changing the detector gain. The relative amount of afterpulsing changes with the gain, filter fluorescence does not.

However, the afterpulsing background is in the range of some % of the system response, no adjustment will remove the problem entirely. Such PMTs have either poor vacuum or have

been stressed by overload. For tubes severely plagued by afterpulsing or even instability we recommend the same treatment which Russell W. Porter (the father of amateur telescope making) suggested for warped telescope mirrors: '*Seek out a good hard, solid hydrant. Hurl the mirror (the photomultiplier) as fiercely as possible at said hydrant. Walk home.*'

Dark Count Rate

For high-sensitivity applications a low dark count rate of the PMT is important. Attempts to decrease the dark count rate by increasing the CFD threshold are not very promising. Except for very small pulses caused by thermal emission or electron scattering at the first dynodes, the pulse height distribution is the same for dark pulses and photon pulses (see Fig. 56, page 56). Thus, with increasing threshold the photon count rate decreases by almost the same ratio as the dark count rate. To achieve a low dark count rate, the following recommendations can be given:

- The most efficient way to reduce the dark count rate is to cool the detector. For PMT cathodes which are sensitive in the infrared region (Ag-O-Cs, InGaAs) cooling is absolutely required. Unfortunately most coolers for PMTs are bulky and expensive. In many cases there is a simple and inexpensive solution to the cooling problem: Put the PMT in a fridge. This is no problem if the light is coupled through an optical fibre, or if the complete experiment can be put into the fridge. A decrease in temperature of 10 degrees Celsius typically reduces the dark count rate by a factor of five to eight. (To get paid for the fridge it may be better say it is for food supply than for spectroscopy!)
- Avoid heating the detector by the voltage divider or by step motors, shutters, preamplifiers, etc. Already a few degrees increase of temperature can double the dark count rate.
- Use a PMT with the smallest possible cathode area and with a cathode type not more red sensitive than required for your application.
- Keep the PMT in the dark even if the operating voltage is switched off. After exposing the PMT to daylight the dark count rate is dramatically increased. It can take several hours or even days until the PMT reaches the original dark count rate. An example for an H5773P-01 is shown in Fig. 60, page 60.
- Do not overload the PMT. This can increase the dark count rate permanently. Extreme overload conditions are sometimes not noticed, because the count rate saturates or even decreases at high light levels.
- Keep the cathode area clear from lenses, windows and housing parts. The cathode area is at high voltage. Contact with grounded parts can cause tiny discharges or scintillation in the glass of the PMT.
- Keep the cathode area absolutely clean.
- Avoid the contact of the PMT with helium. Helium permeates through the glass and impairs the vacuum in the tube.

Checking the SER of PMTs

If you do not know the amplitude or shape of the Single Electron Response of your PMT you can measure it with a fast oscilloscope. The oscilloscope must have sufficient bandwidth to show the correct amplitude and width of the pulses. For conventional PMTs the bandwidth must be at least 400 MHz, for MCP PMTs several GHz. Connect the PMT output to the oscilloscope. Do not forget to switch the oscilloscope input to 50Ω . Set the trigger to 'internal', 'normal', 'falling edge'. Start with no light at the PMT. Switch on the high voltage and change the trigger level of the oscilloscope until it is triggered by the dark pulses. This should happen at a trigger level of -5 mV to -50 mV. When the oscilloscope triggers, give some light to the PMT until you get enough pulses to see a clear trace.

Please obey the usual safety rules for operating a PMT. In particular, do not connect or disconnect the signal cable when the high voltage is switched on. This may damage the input circuitry of the oscilloscope (see ‘Safety Recommendations for Using Detectors’, page 76).

The single photon pulses have an amplitude jitter of 1:5 or more. The amplitude jitter causes a very noisy curve at the oscilloscope display. Nevertheless, the pulse shape can be roughly estimated from the displayed curves. A typical result is shown in 141.

For checking the SER of an MCP PMT we recommend to use a HFAC-26-01 or HFAH-26-01 preamplifier. The preamplifier gives a warning if the maximum output current of the MCP PMT is exceeded. Moreover, the amplified signal has sufficient amplitude to be displayed by the oscilloscope.

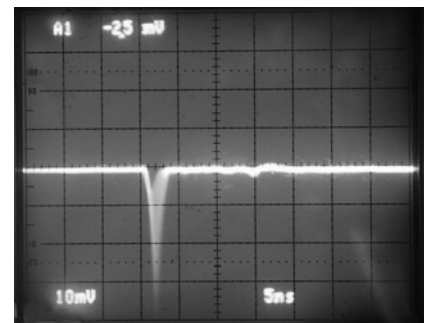


Fig. 150: SER of an R5600 PMT displayed by a 400 MHz oscilloscope

Quick Test of a PMT

In a TCSPC system it may be necessary to test whether or not a PMT is working. A simple test can be made by a general-purpose oscilloscope. To withstand a possible accident like a discharge in a damaged tube or voltage divider, the oscilloscope should have a maximum input voltage of several hundred V. Nevertheless, before you apply a high voltage to the PMT, you should make sure that the cable connections are not damaged and that there is a reliable ground return path. Do not connect to or disconnect the PMT cable from the oscilloscope when the high voltage is on, see ‘Safety Recommendations for Using Detectors’, page 76.

To run the test, switch the oscilloscope input to $1 \text{ M}\Omega$, DC, and select an input voltage range of 10 mV per division or less and a time base of 10 μs per division. Connect the PMT - without a preamplifier - to the oscilloscope input. Activate the trigger for the oscilloscope channel being used and select the ‘norm’ trigger mode and a trigger level of -5 to -10 mV. Make sure that there is *no* light on the PMT. Then start to increase the operating voltage of the PMT. For PMT modules with internal high-voltage generator, switch on the power supply and increase the gain control voltage. When the PMT operating voltage approaches 80% of the permitted maximum you should see the first dark pulses of the PMT. The pulses are negative and have a sawtooth shape, with a steep leading edge and a slow exponential trailing slope, see Fig. 151. Of course, this pulse shape is not the true shape of the single-photon pulse delivered by the PMT. It is simply the result of the RC time-constant formed by the sum of the PMT anode capacitance, the cable capacitance, and the oscilloscope input capacitance in conjunction with the total load resistance ($1 \text{ M}\Omega$ parallel with a resistor possibly connected to ground inside the PMT housing).

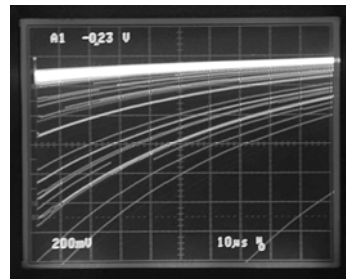


Fig. 151: Test of the general function a PMT with an oscilloscope. XP2020RU PMT, $R_{\text{load}} = 500 \text{ k}\Omega$, $V = -2.9 \text{ kV}$, 200 mV/div

Optical System

Optical systems used for TCSPC usually collect less than 10% of the photons emitted by the sample. Consequently, if the detection efficiency is to be increased, the largest potential is in the optical system, not in the detector or in the TCSPC module. Nevertheless, TCSPC users are often more willing to spend 10,000 dollars for a detector of a slightly higher quantum efficiency or 100,000 dollars for a stronger laser than a few hundred dollars for some good lenses and other high-quality optical components. However, a good optical system often not only improves the detection efficiency dramatically, but also reduces typical error sources, such as signal distortion by reflections, pulse dispersion, instability or wavelength-dependence of the IRF, and leakage of excitation light or daylight. A description of the most frequently used optical elements and their use in optical systems for TCSPC is given in [46].

Lenses

The most frequently used optical elements are lenses. A simple spherical lens suffers from spherical and chromatical aberration. Both aberrations increase steeply with the numerical aperture or the f-number of a lens. Aberrations are considerably reduced in achromatic doublets or triplets. However, achromatic lenses contain a flint glass element and therefore turn intransparent at wavelengths below 360 nm. Therefore TCSPC optics often used single element lenses made of BK7 glass or even fused silica. The unavoidable aberrations can be minimised by using lenses of the right shape, and by inserting them into the beam path with the right orientation [46].

Absorptive Colour Filters

There are a large number of long-pass colour filters with transition wavelengths from 300 to 800 nm. Because colour filters absorb the light in the stopband they do not cause noticeable reflections. However, colour filters often show fluorescence. They should therefore be inserted in a plane of the beam path that is not conjugate with the detector plane. The fluorescence lifetimes of filters can be anywhere from a few ns to several μ s [46]. Therefore, if a TCSPC system suffers from unexplained background signals, it should be checked for possible filter fluorescence.

Interference Filters

Interference filters are made by depositing a number of dielectric and metallic layers on a glass substrate. Short pass, long pass, bandpass, and notch filters are available. The transition from the stopband into the passband can be extremely steep. Good interference filters do not show any noticeable fluorescence.

Interference filters work with their specified performance only if placed in a parallel beam of light. For oblique rays the transition wavelengths shifts to shorter values. The filters should therefore be used in a collimated beam. Baffles should be provided to prevent scattered excitation light from entering the filter at oblique angles.

Light that is not transmitted by the filter is reflected back into the beam path. Because the filter is placed in a collimated beam reflected excitation light is often perfectly focused back into the sample. This can cause noticeable afterpulses in the IRF. The size of the afterpulse may depend on the scattering coefficient of the sample and therefore be different for the IRF measurement and the measurement of the sample. To avoid multiple reflections interference filters should not be stacked.

Monochromators and Polychromators

A problem of monochromators in picosecond-spectroscopy applications is colour shift and pulse dispersion. The path length from the entrance slit to the grating and from the grating to the exit slit is different for both sides of the grating. The path length difference depends on the angle of the grating. Therefore a pulse travelling through the monochromator broadens, and the amount of broadening depends on the selected wavelength. It may even shift in time if the optical axis is not perfectly aligned.

Pulse dispersion and pulse shift can be avoided by using a double monochromator of the ‘subtractive dispersion’ type. In this design the second monochromator is turned by 180 °, and the gratings are moving in opposite directions. Thus the path length differences for both sides of the gratings and for different wavelength cancel.

The grating of the monochromator disperses the light into several diffraction orders. The light of the unused orders can cause substantial straylight problems. A monochromator should therefore always be used with an additional filter than blocks the excitation wavelength.

Optical Fibres

Optical fibres are increasingly used because they are convenient to send light from one place to another. Optical fibres come in different versions.

Multi-mode fibres consist of a core with a high refractive index covered by a cladding with a lower refractive index. The light stays inside the fibre core by total internal reflection. The fibres come in diameters up to several millimeters. To further increase the cross section a large number of fibres can be combined in a fibre bundle. Multi-mode fibres accept light inside a numerical aperture as large as 0.35. However, rays entering the fibre under different angles have different path lengths and, consequently, different transit times. The pulse dispersion depends on the NA of the light cone at the input of the fibre, but not on the diameter of the fibre [229]. If the full NA of a fibre is used the pulse dispersion can easily be 100 ps per meter. By changing the focal length of the lens in front of a fibre, NA can be traded against diameter. Consequently, using a fibre of large diameter at a low NA reduces the pulse dispersion.

Light leaving a multi-mode fibre is emitted from the entire core cross section, and into a cone of large NA. It is therefore not possible to focus light from a multi-mode fibre into a diffraction limited spot.

Single-mode fibres have a core diameter of only a few μm . Only a single wave-mode can propagate through the fibre. The output of a single-mode fibre can therefore be focused into a diffraction limited spot. The problem is, however, that only light of high beam quality can be efficiently coupled into a single-mode fibre. Coupling light from laser diodes requires appropriate beam shaping. Coupling fluorescence light from a cuvette or another macroscopic sample into a single-mode fibre is a hopeless enterprise.

Baffles and Aperture Stops

A good optical system has a number of circular stops and baffles to prevent scattered light from propagating through the system. As a rule of thumb, no parts of the housing, lens holders, or the insides of optical tubes should be visible from the detector. This can be achieved by circular stops that restrict either the field of view of the detector (field stops) or the effective aperture of a beam (aperture stops). The term ‘baffle’ is often used; baffles are cylindrical or conical tubes or circular stops that keep off unwanted light from the detector [65].

Avoiding Optical Reflections

Reflections in optical systems can change the shape of the TCSPC IRF noticeably. Even worse, the distortions depend on the absorption and scattering properties of the sample, on the transmission wavelength of filters and monochromators, and on neutral density filters possibly used to control the intensity. The measured IRF is therefore not necessarily the effective IRF. A deconvolution of the measurement data from the measured IRF may deliver a poor fit or plainly wrong results.

Reflections show up as secondary peaks in the IRF and, consequently, as single or multiple steps in recorded fluorescence decay curves. The typical appearance of a single reflection in a fluorescence decay curve is shown in Fig. 152. The amplitude of the reflected pulse is about 6%, the delay about 0.5 ns.

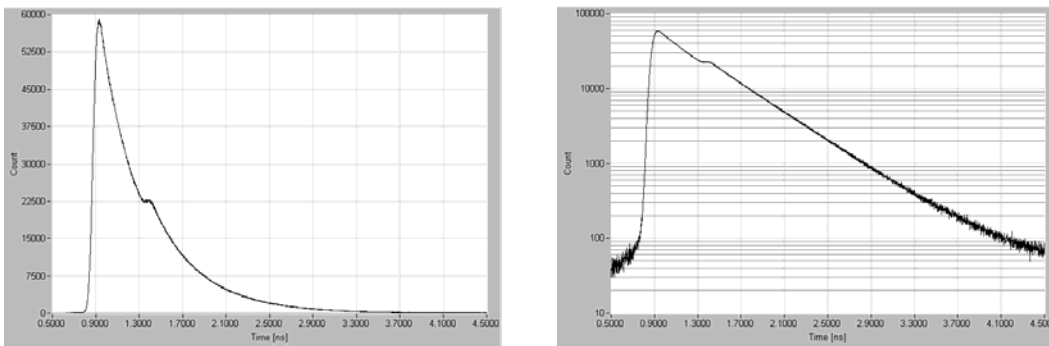


Fig. 152: Reflection in a recorded fluorescence decay curve. Time scale 400 ps per division.

Reflections are especially troublesome between two highly reflective surfaces, and between a highly reflective surface and a glass surface. Highly reflective surfaces are interference filters, reflective neutral density filters, and the cathodes of PMTs. Also the brackets of monochromator slits can reflect a large amount of light. A number of typical cases of reflections and their effect on the IRF are shown in [46]. In practice any design is a compromise between reflections, efficiency, filter performance, and filter fluorescence. Reflections can be directed out of the detection path by tilting the critical part, or by placing it in a non-parallel part of the beam. It must be decided whether the resulting change in the characteristics of a filter can be tolerated or not. Often slight changes in the beam geometry have a large effect, especially if aperture and field stops are used in the right places.

Fluorescence Depolarisation

A general problem of fluorescence lifetime measurements arises from fluorescence depolarisation [220, 379]. Consider a cuvette that is excited by a vertically polarised laser beam under an angle of 90° from the optical axis of detection. The laser preferentially excites molecules which have their dipoles oriented parallel with the polarisation of the laser. In the first moment after an excitation pulse the fluorescence is therefore partially polarised. Due to the random rotation of the molecules the anisotropy of the fluorescence decays with a typical time constant in the 100 ps range. One might presume that the anisotropy decay has no effect on the fluorescence decay curve measured with a detector that does not prefer a special direction of polarisation. This is, however, not the case. The situation is illustrated in Fig. 153.

The fluorescence is excited by a beam along the Z axis and a polarisation parallel to the Y axis. I_P and I_S are the intensities of the projections of the electrical field vectors parallel and perpendicular to the excitation, in the corresponding directions of detection. Detection in X direction delivers I_{PX} and I_{SX} , detection in Z direction delivers I_{PZ} and I_{SZ} , and detection in Y

direction delivers two I_{SY} components. Obviously, the orientational relaxation cancels if all these components are detected with the same efficiency. Because the angular distribution of the molecules is symmetrical around the Y axis, the intensity is the same for all I_p components and for all I_s components:

$$I_{Px} = I_{Pz} \quad I_{Sx} = I_{Sy} = I_{Sz}$$

The sum of all intensity components is therefore

$$I_{SUM} = 2I_p + 4I_s$$

Consequently, a signal proportional to $I = I_p + 2I_s$ must be recorded to reject the rotational relaxation from a lifetime measurement. However, for detection along X, Z or any other direction in the X-Z plane $I_p + I_s$ is detected.

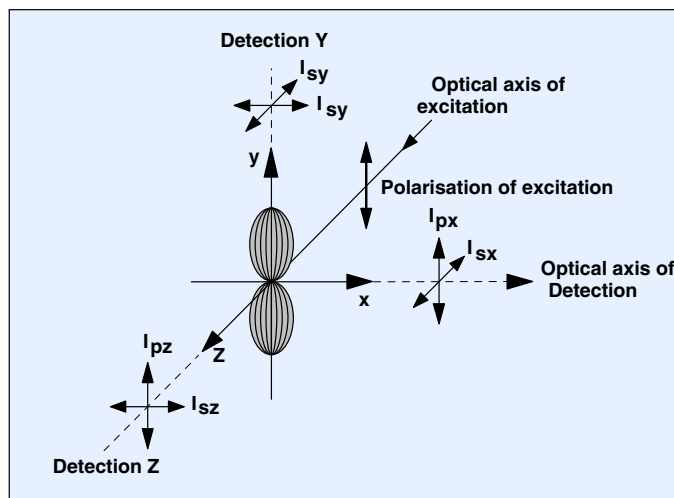


Fig. 153: Polarisation components of the signals detected along the X, Y, and Z axis

Except for a few special cases, there are similar polarisation effects for other angles between the optical axis of the excitation and the X-Z plane, different polarisation of the excitation, and even for unpolarised excitation. Methods to reject depolarisation effects from the measured decay curves in different geometric configurations are discussed in detail in [248, 265, 331]. The commonly used solution is to place a polariser in the detection path. The polariser is rotated by 54.7° from the polarisation of the excitation. The detection efficiency of I_s is then twice the efficiency of I_p , resulting in detecting a signal proportional to $I = I_p + 2I_s$.

It should be noted that the considerations above apply strictly only to excitation and detection by parallel beams of light. The situation is different for excitation and detection through lenses of large numerical aperture. For an optical axis along the Z axis high NA focusing leads to field vectors in x and z direction [8, 12, 292, 326, 327, 382]. Consequently, additional I_p is detected. For excitation and detection through an NA=1.4 oil-immersion microscope lens the sum $I = I_p + 1.0I_s$ (not $I = I_p + 2I_s$) was found free of the anisotropy decay [46].

Re-Absorption

If the absorption and fluorescence spectra of the sample overlap an appreciable part of the molecules can be excited by absorbing fluorescence photons from other molecules. The result is a change in the apparent fluorescence lifetime and in the decay profile. Re-absorption is noticeable especially in highly concentrated samples and samples of large optical thickness. Moreover, if the optical system is not well aligned or plagued by serious aberrations, it can

happen that the detector mainly sees light from molecules which are excited by re-absorption. Due to the high sensitivity of the TCSPC method such situations are sometimes not noticed. Therefore, check for possible re-absorption effects if you record suspiciously long fluorescence lifetimes and unexpected multi-exponential decay profiles.

TCSPC Applications

Measurement of Luminescence Decay Curves

Early TCSPC fluorescence lifetime spectrometers used nanosecond flashlamps for excitation [161, 379]. The pulse duration of a ns flashlamp is on the order of one nanosecond. Lifetimes shorter than 100 ps are therefore difficult to measure, especially if the decay functions are multi-exponential. The most severe drawback is the low repetition rate and the low excitation power, which result in extremely long acquisition times. Flashlamps have, however, the benefit that almost any excitation wavelength can be selected by a monochromator in the excitation path. A number of flashlamp-based systems are therefore still in use.

Modern instruments for fluorescence decay measurement use picosecond diode lasers or frequency-doubled or tripled Ti:Sapphire lasers. Also mode-locked argon lasers or frequency-multiplied Nd:YAG lasers may be used. These lasers deliver pulse repetition rates of up to 80 MHz. The count rate of a TCSPC device is then not longer limited by pile-up effects (see ‘Pile-Up Effects’, page 133). With bh TCSPC devices reasonable fluorescence decay curves can be obtain within acquisition times in the millisecond range (see Fig. 24, page 19).

Monochromator-Based Systems

The typical setup of a fluorescence lifetime spectrometer is shown in Fig. 154. The laser is usually vertically polarised and enters the cuvette under an angle of 90° from the optical axis of the detection system. Front-side illumination can be used for samples of high absorption or scattering. However, 90° illumination is usually preferred because fluorescence depolarisation effects (see ‘Fluorescence Depolarisation’, page 144) are easier to handle and possible fluorescence of the cuvette walls is not detected.

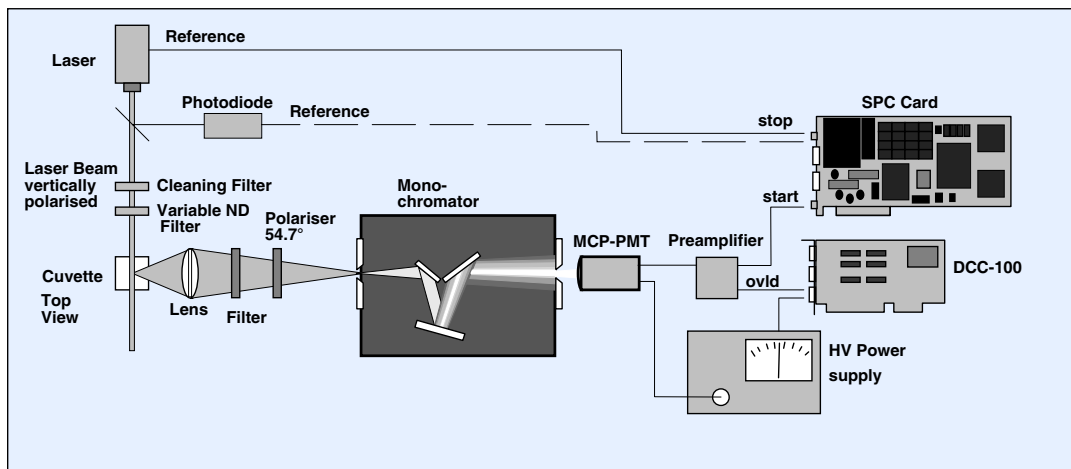


Fig. 154: Typical setup of a fluorescence lifetime spectrometer

A cleaning filter removes unwanted emission wavelengths from the laser beam. The filter is especially important for blue and ultraviolet diode lasers. These lasers emit a substantial amount of light at longer wavelengths. A neutral density filter is used to control the intensity.

The fluorescence light from the sample is collected by a lens and projected on the entrance slit of a monochromator. The effect of rotational depolarisation on the decay curves is removed by inserting a polariser under the ‘magic angle’ of 54.7 degrees (see ‘Fluorescence Depolarisa-

tion', page 144). An additional long-pass filter is recommended to block scattered excitation light.

The monochromator selects the wavelength to be detected. In many laser-based lifetime spectrometers an R3809U MCP-PMT is used for detection. Its short transit-time-spread, clean IRF function, and low afterpulsing probability makes the R3809U superior to conventional PMTs.

The single-photon pulses of the detector are amplified and used as start pulses for the TCSPC module. The stop pulses come either from a reference output of the laser or are generated by a photodiode module (see 'Generating the Reference Signal', page 89). Any of the bh SPC modules can be used for classic fluorescence decay measurements.

A lifetime spectrometer should include precautions against detector damage by overload. It is therefore recommended to use one of the HFAC or HFAH series preamplifiers and to control the high voltage of the detector by a DCC-100 detector controller. If overload occurs the preamplifier delivers an overload signal which causes the DCC-100 to shut down the high voltage of the PMT. A detailed connection scheme is shown in Fig. 96, page 95.

An example of a lifetime measurement is shown in Fig. 155.

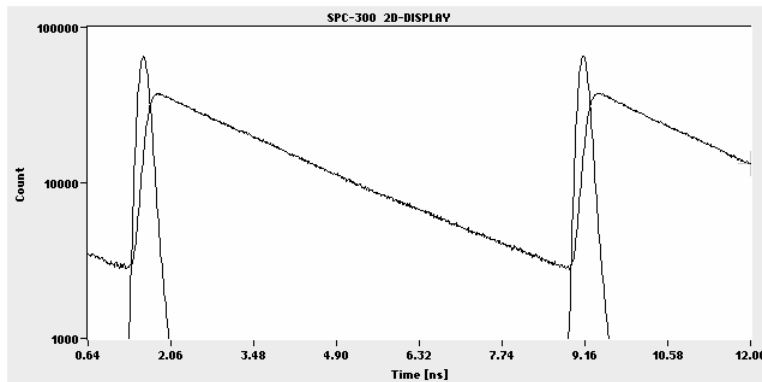


Fig. 155: Fluorescence decay curves obtained with SPC-300 module and mode-locked Ar⁺ laser

Classic fluorescence lifetime instruments are used for an extremely wide range of applications. The publications do not always make clear which TCSPC technique was used. The selection given below is therefore somewhat arbitrary:

Lifetime changes induced by solvent interaction, conformational changes and different binding state to proteins, peptides or lipids are described in [106, 193, 194, 236, 260, 269, 276]. The dependence of the lifetime on the refractive index of the environment was investigated in [114, 279, 337, 338]. Pressure effects on the lifetime are shown in [342, 343]. Electron and proton transfer are subject of [324, 325, 339, 358]. Lifetime spectroscopy on constructs relevant for photodynamic therapy is described in [152, 204, 244, 375]. Lifetimes of fluorescent proteins were measured in [88, 89, 169, 170, 171, 361]. Time-resolved FRET measurements are described in [73, 151]. Enhanced radiative decay rates and enhanced photostability of dyes conjugated to metallic nanoparticles are reported in [137, 138, 237]. For indocyanine green attached to silver colloid particles the fluorescence could be increased by a factor of 30 while the average (amplitude-weighted) lifetime decreased from 548 ps to 68 ps. Extremely short components of multi-exponential decay functions down to less than 10 ps were measured in [254, 380]. Fluorescence decay measurements at semiconductors in the microsecond range are described in [134, 135, 136].

Time-Resolved Spectra

The setup shown in Fig. 154 can be upgraded with a step motor that drives the monochromator, or a monochromator with an internal step motor drive can be used. The system can then be used to record time-resolved fluorescence spectra or complete wavelength-resolved decay profiles. The recording in the SPC module can be synchronised with the wavelength scan by using an STP-340 step motor controller, by running a time-controlled recording sequence in one of the sequential modes of the SPC module, or by using the repeat function of the SPC module in conjunction with an experiment trigger from the step motor controller.

The principle of recording time-resolved spectra is shown in Fig. 156. The wavelength is scanned, and for each wavelength a fluorescence decay curve is recorded. The counts in the time channels of the decay curve are averaged within selectable time intervals. The averaged counts are stored as functions of the wavelength. Several independent time windows can be used simultaneously; therefore several spectra in different time windows are obtained simultaneously. A suitable operation mode is implemented in all SPC modules, see ‘fi(EXT) Mode’, page 264.

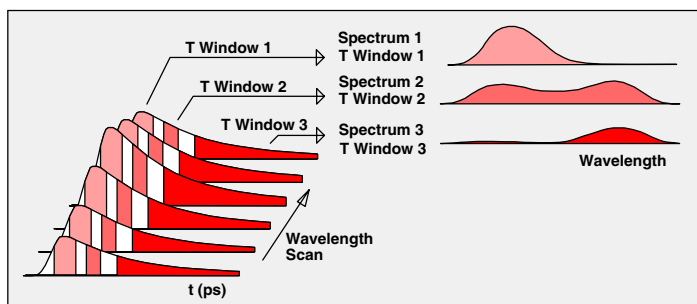


Fig. 156: Recording time-resolved spectra

Unfortunately, there are general objections against the gated spectrum recording technique. The problems are already stated in [265] and result from the obvious fact that the data are not de-convoluted from the instrument-response function. The effective time window in which a spectrum is obtained is a convolution of the averaging-time interval with the IRF. No matter how short a time interval is selected, the effective time interval cannot be shorter than the IRF.

The second objection concerns gated detection in general. Gated spectrum recording is normally used to separate the fluorescence spectra of different kinds of molecules by their fluorescence lifetimes. However, whatever gate interval is used, the integral over the interval contains fluorescence of *all* of the types of molecules. Unless the fluorescence lifetimes are *very* different, gated detection is a poor technique to separate the fluorescence signals of different species. Theoretically the separation efficiency can be improved by using several time gates, but the choice of gate intervals is limited because they are smeared by the instrument response function.

A far better way to obtain time- and wavelength-resolved fluorescence data is to record a sequence of fluorescence decay curves during the wavelength scan [30, 265]. All bh TCSPC devices have sequential recording modes or ‘page stepping’ implemented so that there is actually no argument for using gated spectral recording. The recording sequence in the TCSPC device can be controlled the same way as for gated detection, i.e. either by software or by a hardware sequencer and a trigger pulse from the monochromator drive. An example of a wavelength-resolved sequence is shown in Fig. 157.

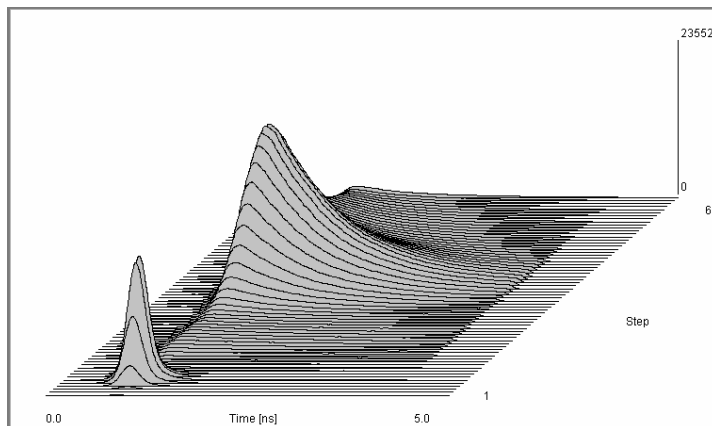


Fig. 157: Sequence of decay curves versus emission wavelength. DODCI, excited by AR⁺ laser at 514 nm

The monochromator used in the setup shown in Fig. 154 makes the system relatively expensive. Moreover, the monochromator can cause a number of unpleasant effects.

One drawback is that the monochromator makes the detection path relatively inefficient. It rejects any photons outside a narrow wavelength band. Moreover, the slit width and the numerical aperture of the monochromator limit the numerical aperture by which the light can be collected from the sample. Moreover, the slits of monochromators are normally vertical, but the illuminated volume in the cuvette is a horizontal line. It may therefore be useful to turn the monochromator by 90 degrees.

The second problem of a monochromator is colour shift and pulse dispersion. The path length from the entrance slit to the grating and from the grating to the exit slit is different for the two sides of the grating. Therefore a pulse broadens as it travels through the monochromator. The path-length difference depends on the angle of the grating, and therefore on the wavelength selected. The signal may even shift in time if the optical axis is not perfectly aligned. The problems can be avoided in a double monochromator with ‘subtractive dispersion’. The gratings of the two monochromators are moving in opposite directions, which compensates for the path length variation.

The drawbacks of monochromators can be avoided in simple filter-based systems, see paragraph below.

Filter-Based Systems

The principle of a filter-based fluorescence lifetime system is shown in Fig. 158.

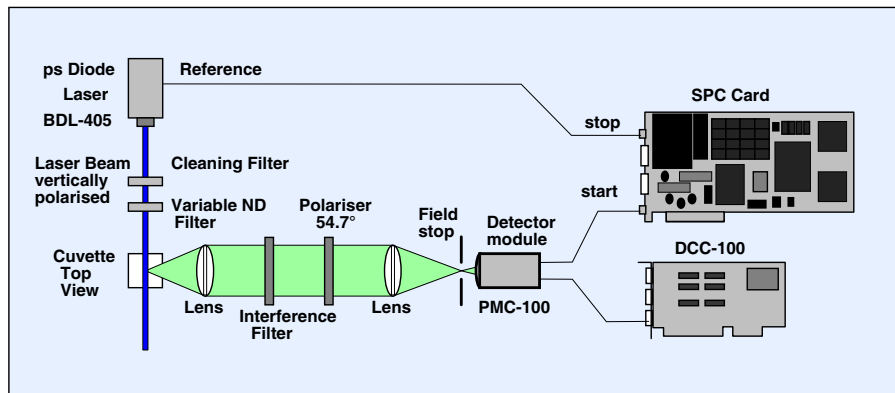


Fig. 158: Filter-based fluorescence lifetime system

A picosecond diode laser, e.g. a bh BDL-375 or -405 [26] is used for excitation. To avoid excessive anisotropy effects the polarisation of the laser has to be vertical or at an angle of about 60° from the horizontal. The fluorescence light from the sample is collimated by a lens. An interference filter is used to select the desired detection wavelength interval. The polariser removes depolarisation effects for excitation with vertical polarisation. A second lens is used to concentrate the light on the detector. It is recommended to place a field stop in front of the detector. The stop reduces the straylight sensitivity, suppresses optical reflections, and prevents possible fluorescence of the cuvette walls from being recorded. Moreover, detecting from a smaller spot in the cuvette reduces transit-time effects and thus reduces the IRF width.

An example is shown in Fig. 159. The sample was a Rhodamine 110 solution; a BDL-405 laser was used for excitation. The detector was a PMC-100-1.

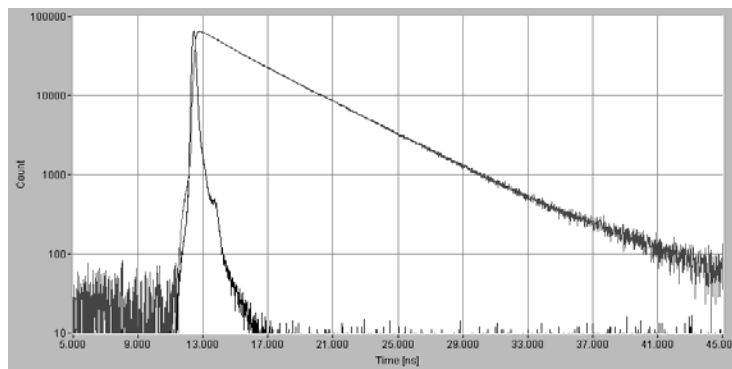


Fig. 159: Fluorescence decay of Rhodamine 110 in water, excitation at 405nm, PMC-100-1 detector, SPC-830 TCSPC module

For high-resolution measurements an MCP PMT can be used as shown in Fig. 154. Also fast SPADs, such as the id-100 of idQuantique [179] or the PDM-50 of Micro Photon Devices [247], yield high time resolution. The effective IRF width for these detectors is mainly determined by transit-time effects in the cuvette and the laser pulse width. The effective IRF width for the MCPs and the fast SPADs is therefore almost the same. Problems can, however, result from the wavelength-dependence of the IRF in SPADs, see Fig. 74, page 71.

Filter-based systems often use the PMC-100 or the PMH-100 detector modules. With these modules extremely simple systems can be built. Despite of their simplicity, the systems have an extremely high sensitivity. Thus, the systems deliver high count rates at relatively low laser power. This is a benefit in biological applications when the samples have poor photostability. Moreover, often dynamic effects of the fluorescence lifetime have to be recorded (see Fig. 170, page 159). This requires short acquisition times, high count rate, and consequently high detection efficiency.

To obtain accurate results of fluorescence lifetime measurements it is important to avoid the rotational depolarisation to distort the fluorescence decay curve, see Fig. 153. The usual way of recording fluorescence decay curves is with vertically polarised excitation and a polariser in the detection path. The polariser is turned by 54.7° from the polarisation of excitation. Unfortunately, this angle may be different if the fluorescence is detected at high numerical aperture, as it may be the case in filter-based systems. The best angle may therefore slightly differ from 54.7° . A second (sometimes easier) way to reduce the effect of rotational polarisation is to tilt the polarisation plane of the excitation laser. The exact tilt angle depends on the refractive index of the solvent, but is not very critical. An example is shown in Fig. 160. The fluorescence of Rhodamine 110 in water was excited by a BDL-405SMC diode laser (405 nm) and detected by an idQuantique id-100-50 SPAD.

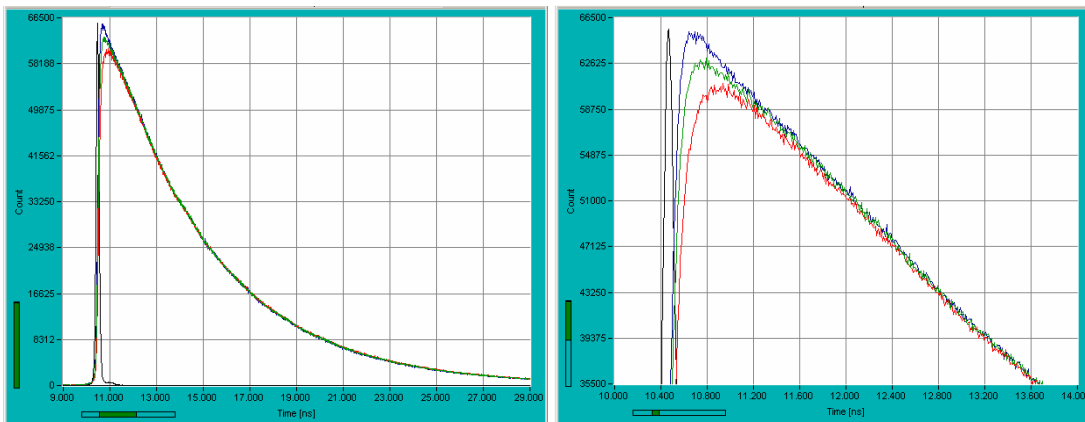


Fig. 160: Effect of the rotational depolarisation on the measured decay curve. Rhodamine 110 in water, excitation at 405 nm, polarisation of laser vertical (upper decay curve, blue), 45° (green curve, middle), and horizontal (lower curve, red). Left: full decay curve. Right: Zoom into the peak of the fluorescence decay.

The depolarisation time is about 100 ps. With the laser polarised vertically, too much of the I_p (parallel) components are detected. Consequently, the intensity is measured too high within the first 100 ps. With the laser polarised horizontally, almost exclusively I_s is recorded. The intensity is therefore measured too low. With the laser at 45° the detection efficiency of I_s and I_p is almost balanced, and the measured decay function comes close to the correct one.

Multi-Spectral Lifetime Experiments

Simultaneous multi-wavelength operation of a fluorescence lifetime instrument can be achieved by using a system of dichroic mirrors and a corresponding number of individual detectors. The general optical setup is shown in Fig. 161.

The fluorescence light is collected and collimated by lens 1. A filter blocks scattered excitation light. The fluorescence light is split spectrally by several dichroic mirrors and focused onto several detectors via lens 2 through lens 4. The numerical aperture of lens 1 can be made relatively large so that a high collection efficiency is achieved. The setup is often used for TCSPC laser scanning microscopy [39, 40] and single-molecule spectroscopy [287]. Suitable beam splitter / detector assemblies are available from bh, please see ‘Detector, Shutter and Beam Splitter Assemblies for TCSPC Microscopy’, page 12.

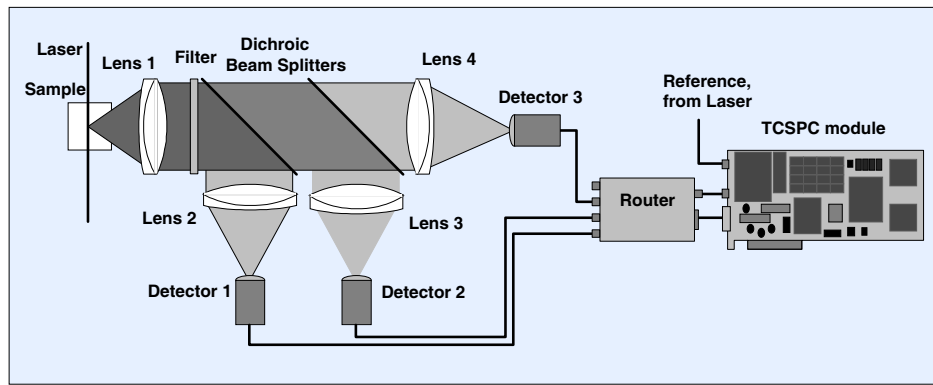


Fig. 161: Multi-wavelength detection system with dichroic beamsplitters

A more detailed fluorescence spectrum is obtained by using a polychromator (or spectrograph) and recording the spectrum with a multi-anode PMT. bh delivers a complete multi-spectral detection system based on the PML-16 16-channel detector head and a MS 125-8M polychromator (LOT) [18]. The optical principle is shown in Fig. 162.

The sample is excited in the usual way by a high-repetition rate pulsed laser. The fluorescence light from the sample is transferred by a lens to the input slit of the polychromator. The polychromator splits the light spectrally and projects a fluorescence spectrum on the cathode of a PML-16 multichannel detector [37, 42, 190, 333]. For each photon, the routing electronics generate a timing pulse and a digital data word that indicates in which channel the photon was detected. These signals are used in the TCSPC module to build up the photon distribution over the time in the fluorescence decay and the wavelength (see also Multi-Detector TCSPC, page 24). Consequently, all photons detected by the PMT are used to build up the result, and the maximum possible signal-to-noise ratio is obtained for a given number of photons emitted by the sample.

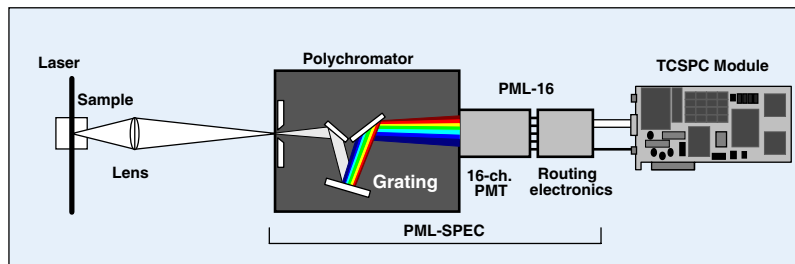


Fig. 162: Multi-wavelength fluorescence experiment

A multi-wavelength system based on a polychromator is by far more efficient than a system that scans the spectrum by a monochromator. Moreover, because the photons of all wavelength channels are recorded simultaneously, the system can be used for the recording of transient lifetime effects.

Fig. 163 shows decay curves of a mixture of rhodamine 6G and fluorescein, both at a concentration of $5 \cdot 10^{-4}$ mol/l, recorded by a bh PML-Spec system. High concentration caused some re-absorption of the Rhodamin 6G fluorescence, resulting in a clearly visible change in the shape of the decay curves and an increased lifetime.

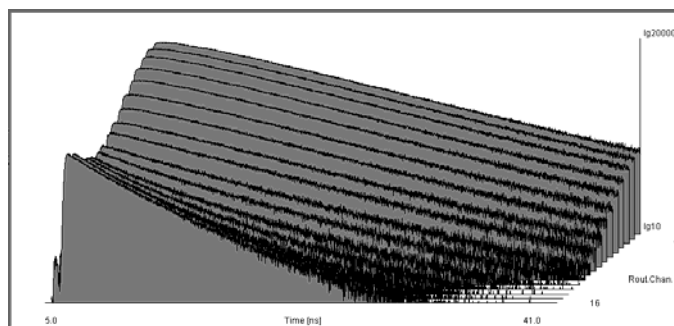


Fig. 163: Fluorescence of a mixture of Rhodamin 6G and fluorescein, simultaneously recorded over time and wavelength

The PML-Spec system is also available with a fibre probe at the polychromator input and with a fibre bundle that connects to non-descanned detection ports of multiphoton laser scanning microscopes [18, 20, 21, 22]. Please see ‘FLIM Systems for Laser Scanning Microscopes’, page 101 and ‘Multi-Wavelength FLIM’, page 169.

Measurement of Time-Resolved Fluorescence Anisotropy

If the fluorescence of a sample is excited by linearly polarised light the fluorescence is partially polarised, see ‘Fluorescence Depolarisation’, page 144. The fluorescence anisotropy, r , is defined as

$$r(t) = \frac{I_p(t) - I_s(t)}{I(t)}$$

with I_p = fluorescence intensity parallel to excitation, I_s = fluorescence intensity perpendicular to excitation, I = total intensity.

The fluorescence anisotropy decays with the rotational relaxation time, τ_{rot} . The relaxation time is an indicator of the size of the dissolved molecules, dye-solvent interactions, aggregation states, and the binding state to proteins [84, 220, 379]. Typical rotational relaxation times of free fluorophores in water are in the range from 50 to a few 100 ps.

Time-resolved measurements of the anisotropy are difficult because $I_p(t) - I_s(t)$ is small compared to the fluorescence components $I_p(t)$ and $I_s(t)$ themselves. Moreover, $I_p(t)$ and $I_s(t)$ are detected with different efficiency, especially if a monochromator is used. The effect depends on the angle of the grating, i.e. on the wavelength, and on the slit width and the beam geometry. If a monochromator is not really required a filter-based setup is often a better solution. However, anisotropy measurements in any case require calibration of the efficiency of the $I_p(t)$ and $I_s(t)$ detection channels. The relative efficiency, E_p/E_s , of the I_p and I_s detection channels is the ‘G factor’:

$$G = \frac{E_p}{E_s}$$

There are two ways to determine the G factor [220, 265]. The first way is to run a measurement with horizontal polarisation of the excitation beam. For an angle of 90° between the optical axis of excitation and emission, the excited-state distribution is oriented towards the axis of observation, see Fig. 153, page 145. Consequently equal perpendicular polarisation components are emitted into both measurement channels. The ratio of the measured intensities represents the G factor.

The second way to obtain G is ‘tail matching’. A sample with a depolarisation time substantially shorter than the fluorescence lifetime is measured. The G factor is obtained from the intensities in the later parts of the decay curves. The advantage of tail matching is that it can be used also for optical systems with excitation and detection along the same optical axis.

To separate the rotational relaxation from the fluorescence decay it is essential that the correct total intensity, $I(t)$ be taken for the denominator of $r(t)$. It is normally assumed that both the excitation and emission light cones have negligible numerical aperture, and that the excitation is polarised perpendicularly to the plane defined by both optical axes. The total intensity is then $I(t) = I_p(t) + 2 I_s(t)$. The factor of 2 results from the geometrical fact that light polarised longitudinally to the optical axis of observation is not detected [220, 379], see Fig. 153, page 145. The factor can be smaller than 2 for excitation and detection through an optical system of high-NA, e.g. a microscope lens [8, 46].

In the simplest case, i.e. for similar molecules rotating freely in a solvent, the terms $I_p(t) - I_s(t)$ and $I_p(t) + 2I_s(t)$ are single exponential, and so is the anisotropy $r(t)$. Deconvolution of a single exponential decay is possible with a much high accuracy and requires much less photons then the deconvolution of multi-exponential decays. However, single exponential decay analysis of the terms $I_p(t) - I_s(t)$ and $I_p(t) + 2I_s(t)$ requires that the IRFs for I_p and I_s be identical

and that differences in the recording efficiency for I_P and I_S are calibrated before the deconvolution starts. If an identical IRF for both channels cannot be achieved a multi-exponential deconvolution can be used both for $I_P(t)$ and $I_S(t)$ so that the anisotropy decay can be calculated from the fitted decay curves. However, a better solution is to use the right models for the rotational relaxation and the fluorescence decay and to fit them to the measured data with the two different IRFs.

A wide variety of anisotropy measurement setups are used. The simplest possibility is to use a standard fluorescence setup with a polariser in the detection path, see Fig. 164. The components $I_P(t)$ and $I_S(t)$ are measured one after another with the polariser in 0° and 90° orientation. The advantage of this setup is that the instrument response function is the same for both measurements. The drawback is that two measurements are required, and drifts in the detector efficiency, photobleaching or temperature changes in the sample can impair the results. Moreover, about 50% of the photons remain unused. This can be a drawback if the photostability of the sample is an issue. Moreover, the fact that $I_P(t)$ and $I_S(t)$ are measured consecutively makes it impossible to record dynamic affects in the anisotropy and fluorescence decay times.

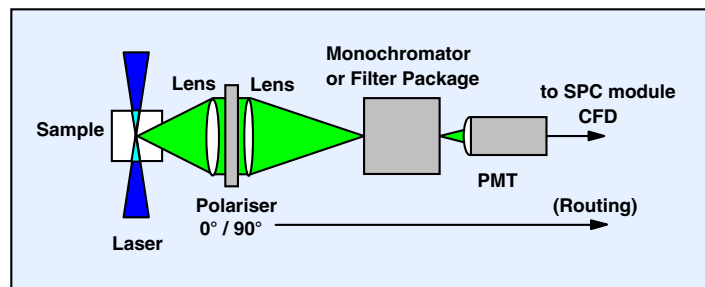


Fig. 164: Single-detector anisotropy setup

The flipping of the polariser between 0° and 90° can be combined with controlling the destination of the photons in the SPC memory via one of the routing bits. The fluorescence decay curves for I_P and I_S are then automatically stored in separate memory blocks. An instrument with periodical switching was used in [105] and [106].

Another commonly used setup for anisotropy measurements is the ‘T geometry’, see Fig. 165. The sample (usually a cuvette) is measured from both sides under different polarisation angles. Two detectors and a router are used to detect I_P and I_S simultaneously. The T geometry has the benefit of increased efficiency. However, the instrument response functions of the two detectors are different, which makes the data analysis more difficult than for the single detector setup. The timing problem can be relaxed if extremely fast detectors, i.e. R3809U MCPs, are used and the optical and electrical path length of both channels are carefully balanced.

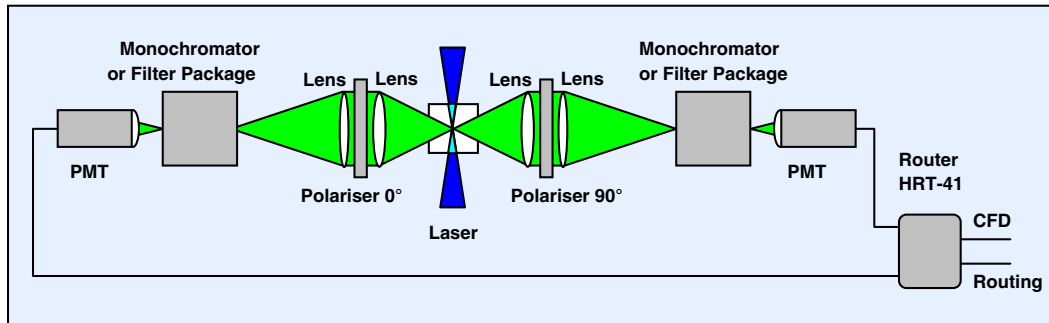


Fig. 165: ‘T geometry’ anisotropy setup

In cases where the light cannot be collected from both sides of the sample, i.e. in a confocal microscope setup, a 1:1 beamsplitter and two polarisers or a polarising beamsplitter can be used to separate I_p and I_s .

Multiplexed TCSPC can be used to measure I_p and I_s quasi-simultaneously. The components are separated by a beamsplitter and two polarisers (or a polarising beamsplitter) and optically multiplexed into one detector, see Fig. 166. The photons for I_p and I_s are routed into different memory blocks.

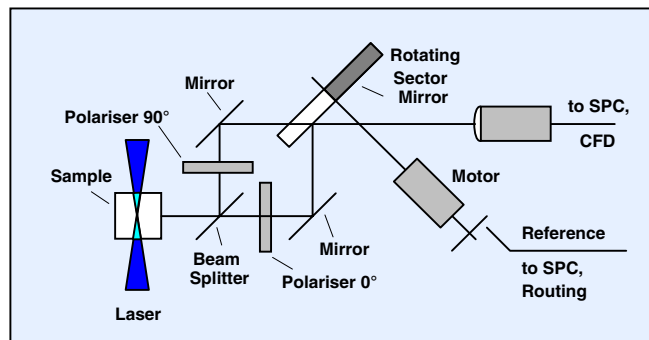


Fig. 166: Alternating measurement of I_p and I_s . Lenses and filters not shown

The benefit of the setup is that changes in the sample and changes of the detector efficiency influence I_p and I_s likewise. The drawback is that the optical system is complicated. A sector mirror is not commonly available, and it must be well aligned on the rotation axis to avoid that the reflected beam wobbles. Although the same detector is used for both light paths it is not simple to obtain exactly the same IRF in both channels. An optical system of the design shown above is described in [30].

In principle, a fluorescence anisotropy system can be built with a rotating polariser. A possible setup is shown in Fig. 167.

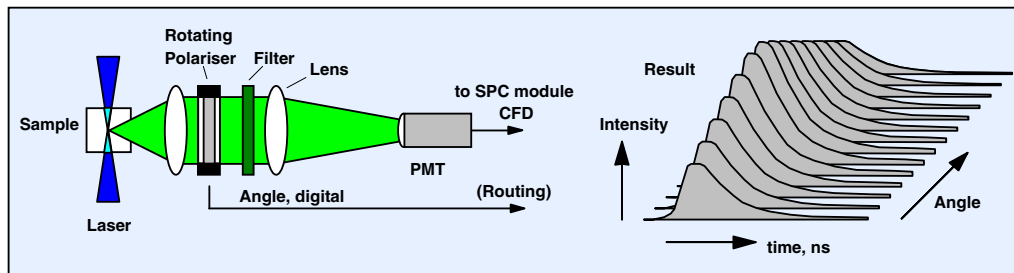


Fig. 167: Anisotropy measurement by a rotating polariser

The polariser is rotated during the measurement. The photons are recorded into a large number of curves in the SPC memory. The recording is synchronised with the rotation, so that the recorded decay curves correspond to different rotation angles. Synchronisation can be achieved by using a digital angle signal from the rotator as a routing signal or by using pulses from the rotator as synchronisation for the 'Scan Sync In' mode of an SPC-730 or -830 module. The setup shown above can be used for samples that have an intrinsic optical activity. Although a system with a rotating polariser is relatively simple no such instrument has yet been described.

Anisotropy measurements are not only used for macroscopic samples, such as solutions in cuvettes, but also for single molecules [210, 287, 307] and in conjunction with lifetime imaging in cells.

A fluorometer for anisotropy measurements by two-photon excitation is described in [360]. The quadratic characteristic of two-photon excitation results in a higher initial anisotropy than for one-photon excitation.

Lock-in TCSPC

Every detector generates a background signal which is caused by thermal emission of electrons. This background signal limits the sensitivity and degrades the accuracy of the numerical data analysis. It is possible to reduce the background by cooling, but this often causes unpleasant problems like frost on optical windows or water in the PMT voltage divider chain.

The SPC modules provide a digital lock-in technique that eliminates the background from the results. The principle is shown in Fig. 168.

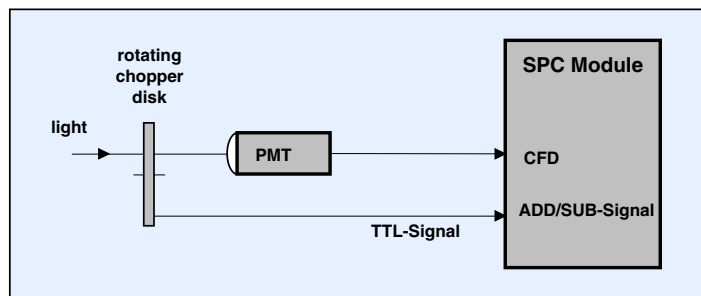


Fig. 168: Multiplexed TCSPC

The light chopper interrupts the light with an on/off ratio of 1:1. At the same time the chopper disk controls the /SUB signal which is connected to the /SUB input of the SPC module. This signal acts in a way that the photons in the bright phase are added and in the dark phase are subtracted in the memory. Because both phases have the same duration the background (but not the background noise) is eliminated from the result.

For luminescence measurements the chopper disk may be conveniently placed in the excitation light path in front of the sample cell. Similar arrangements are possible to measure two different objects (for instance the sample cell and a reference cell with the solvent) quasi-simultaneously. The excitation and luminescence light beams are handled by rotating sector mirrors or by light choppers and 50% mirrors. For early TCSPC devices Lock-in TCSPC was an elegant way to increase the sensitivity of a lifetime measurement beyond the limit set by Raman scattering or solvent fluorescence [30]. With advanced TCSPC modules lock-in TCSPC is not often used. These modules have enough on-board memory to use multiplexed detection. The fluorescence and the background are then recorded into different memory blocks. The background is eliminated by subtracting the background measurement from the fluorescence measurement. The advantage of multiplexed measurement is that possible differences in the sensitivity or in the duration of the two multiplexing intervals can be compensated for.

Transient Fluorescence Phenomena

Many biological systems show dynamic changes in their fluorescence, absorption, and scattering behaviour. The fluorescence transients in living plants are caused by light-induced changes in the efficiency of the photosynthesis. In experiments of diffuse optical tomography (DOT, see Diffuse Optical Tomography, page 187) changes are driven by the heart beat and by the haemodynamic response to brain stimulation. Protein folding and other biochemical reactions can be traced by continuous flow or stopped flow mixing techniques. Other examples are electro-physiological stimulation of cells and experiments of photodynamic therapy. Some typical applications of TCSPC to transient phenomena are described in the paragraphs below.

Chlorophyll Transients

A typical example of dynamic fluorescence lifetime changes are the chlorophyll transients found 1931 by Kautsky and Hirsch [188]. The effects have been termed fluorescence induction, fluorescence transients, or Kautsky effect [142, 143, 240]. When a dark-adapted leaf is exposed to light the intensity of the chlorophyll fluorescence starts to increase. After a steep rise the intensity falls again and finally reaches a steady-state level. The rise time is of the order of a few milliseconds to a second, the fall time can be from several seconds to minutes.

The initial rise of the fluorescence intensity is attributed to the progressive closing of reaction centres in the photosynthesis pathway. Therefore the quenching of the fluorescence by the photosynthesis decreases with the time of illumination, with a corresponding increase of the fluorescence intensity. The fluorescence quenching by the photosynthesis pathway is termed ‘photochemical quenching’. The slow decrease of the fluorescence intensity at later times is termed ‘non-photochemical quenching’. It is believed that it is a mechanism the plant uses to protect itself from photodamage.

Measurements of non-photochemical quenching by TCSPC is very simple. In most cases it is sufficient to record a sequence of fluorescence decay curves at a rate of about one curve per second. Sequences this slow can be obtained by software-controlled sequencing, i.e. in the $f(t,T)$ mode or simply by activating the ‘page stepping’ function of a bh SPC module. The principle of a simple experiment is shown in Fig. 169.

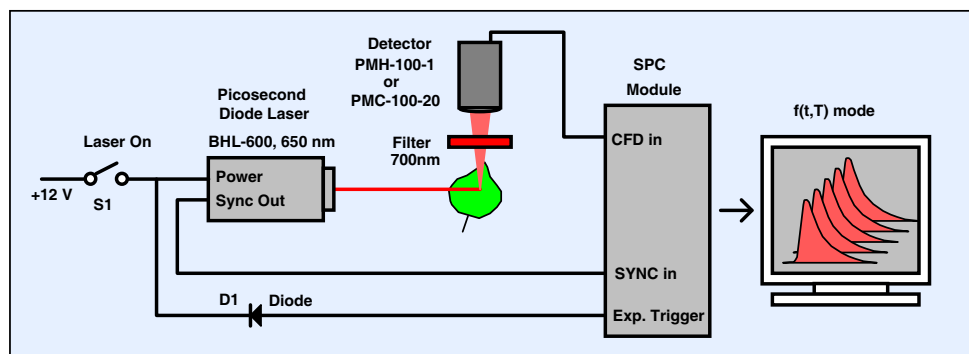


Fig. 169: Recording non-photochemical fluorescence quenching in a living plant

The fluorescence of chlorophyll in a leaf is excited by a picosecond diode laser. The fluorescence is separated from the scattered excitation light by a bandpass filter that transmits a wavelength range around 700 nm. The fluorescence light is detected by a PMH-100-1 or a PMC-100-20 detector. The single-photon pulses are connected into the ‘CFD’ input of the SPC module; the reference pulses come from the laser.

After the leaf has been kept a few minutes in the dark, the laser is switched on by closing the switch, S1. The operating voltage of the laser is connected to the ‘experiment trigger’ input of the SPC module via a small-signal diode, D1. In conjunction with the pull-up resistor of the experiment trigger input this generates a positive trigger edge. This edge triggers the start of a sequence of measurements in the SPC module.

Typical results are shown in Fig. 170. A bh BHL-600 laser module was used, with a wavelength of 650 nm, 80 ps pulse duration, and 50 MHz repetition rate. The incident power density at the surface of the leaf was approximately 1 mW/mm². The detection wavelength was selected by a 700 ± 15 nm bandpass filter. A sequence of fluorescence decay curves was recorded at a rate of one curve in 2 seconds. The count rate was approximately $2 \cdot 10^6$ s⁻¹. Dead time compensation was used to avoid the influence of counting loss on the recorded intensity.

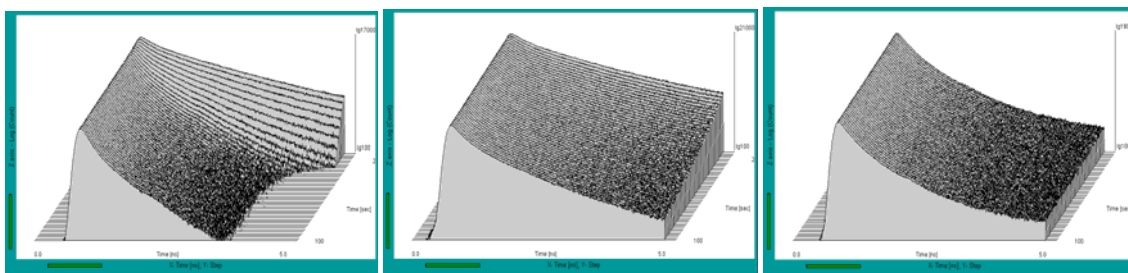


Fig. 170: Sequences of fluorescence decay curves measured at a leaf after start of illumination. Left to right: Fresh leaf, faded leaf, dried leaf. Time per curve 2 seconds, logarithmic intensity scale. The sequence starts from the back.

A result obtained from a fresh dandelion leaf is shown left. The fluorescence lifetime decreases considerably within the first 10 seconds of illumination. The peak intensity remains almost constant. This shows that the change in the fluorescence behaviour is mainly a change in the fluorescence quenching rate, not a change in the number of fluorescing molecules. In a faded leaf the lifetime change is slower and less pronounced. A dry leaf does not show any noticeable lifetime change.

Sequential recording of photochemical quenching transients requires a time resolution of about 100 μ s per step. A sequence this fast cannot be recorded by software-controlled sequencing. Moreover, it is impossible to obtain enough photons in a single-shot experiment. Therefore a hardware-controlled sequencing mode, e.g. the continuous flow mode or the scan sync out mode, must be used. The recording of the sequence is repeated and the counts accumulated until enough photons have been collected. A suitable experiment setup is shown in Fig. 171.

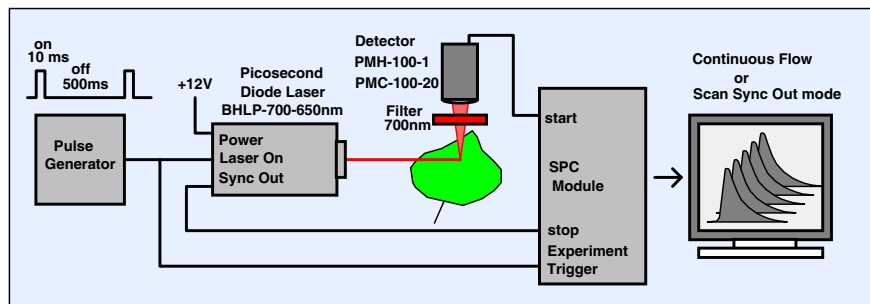


Fig. 171: Measurement of photochemical quenching transients

The setup uses a picosecond diode laser with fast on/off capability. For the results shown below a bh BHL-700 laser with a wavelength of 650 nm was used. The laser is controlled by a

pulse generator that turns the light periodically on and off. The ‘on’ duration is 10 ms, the ‘off’ duration 500 ms. Within the ‘on’ phases, the laser delivers picosecond pulses at a pulse period of 20 ns. The leaf is excited by this pulse sequence. The fluorescence photons are detected by a PMC-100-20 PMT module and recorded in an SPC-630 TCSPC module. The SPC-630 module is operated in the continuous flow mode. It runs a hardware-controlled sequence of recordings, with a time per curve of 100 us and an overall number of 128 curves. The start of the sequence is triggered with the rising edge of the ‘laser on’ signal, and a large number of such cycles is accumulated.

Each ‘laser on’ period initiates a normal transient of the chlorophyll fluorescence. Photochemical quenching decreases with its typical time constant within the 10 ms ‘on’ period. In the subsequent ‘off’ period, photochemical quenching recovers to its initial state. Due to the low duty cycle of the ‘laser on’ signal, the average excitation intensity is low and does not cause much non-photochemical quenching. Therefore, the change of photochemical quenching can be recorded independently, if only the duty cycle of the laser on/off control signal is kept low enough. A result is shown in Fig. 172. 10,000 on/off cycles were accumulated. The sequence starts at the front.

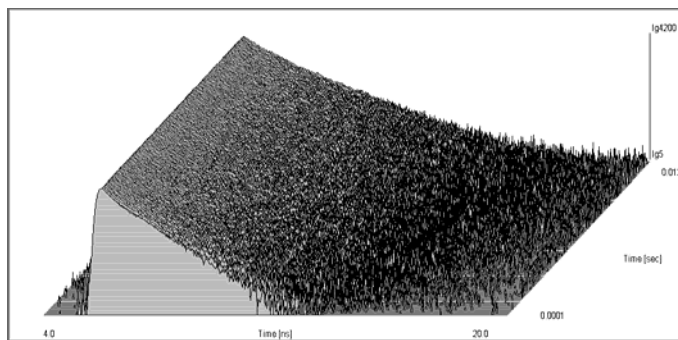


Fig. 172: Photochemical quenching transient measured in a dandelion leaf. The sequence starts at the front. Time per curve 100 us, 10,000 on/off cycles were accumulated.

Green leaves show the typical chlorophyll fluorescence around 700 nm, and a blue-green fluorescence which originates from flavinoids. Due to the Kautski effect, the fluorescence intensity and lifetimes are different for different excitation wavelength and different excitation intensity. It is therefore difficult to obtain comparable results for different excitation conditions. An experiment that avoids this problem is shown in Fig. 173.

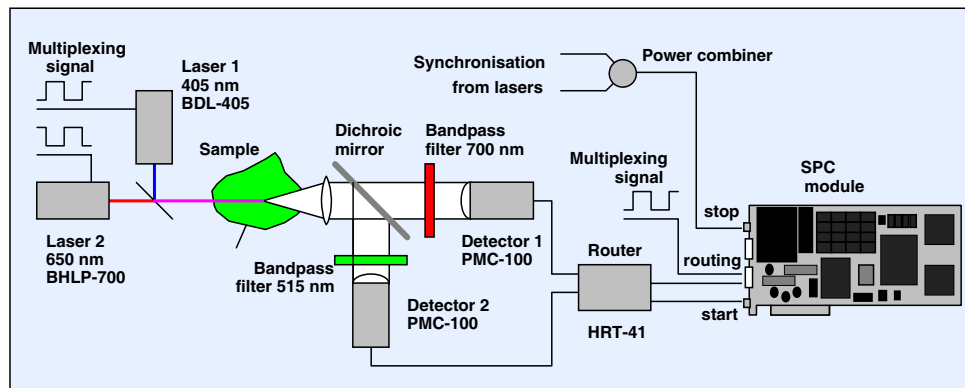


Fig. 173: Simultaneous measurement at two excitation and two emission wavelengths

The sample is excited by two lasers at 405 nm and at 650 nm. The lasers are multiplexed by a TTL signal from a pulse generator. The light from the sample is split into a 515-nm and a 700-nm component by a dichroic mirror and two bandpass filters. The fluorescence compo-

nents are detected by two PMT modules. The PMTs are connected to the TCSPC module via a HRT-41 router. Thus, both fluorescence components are recorded simultaneously. One routing bit is required to separate the photons of both detectors. A second routing bit is used to separate the photons excited by the two lasers. The stop signal for the TCSPC module comes from the synchronisation outputs of the lasers. Because only one laser is active at a time, the pulses can be combined by a simple power combiner. A typical result is shown in [46].

Stopped Flow Techniques

Stopped flow techniques are based on the mixing of two reagents in a flow cell. The flow of the reagents is periodically stopped, and the reaction is observed by recording the transient changes in absorption, fluorescence intensity, or fluorescence lifetime. An overview about the technique is given in [305]. The principle of a TCSPC-based detection system for stopped flow is shown in Fig. 174.

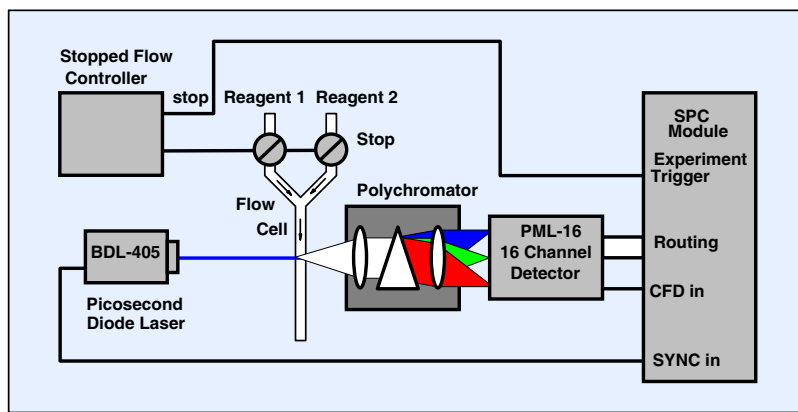


Fig. 174: Stopped Flow Experiment with TCSPC and multi-spectral detection

A laser is focused at the flow channel of the mixing cell shortly behind the mixing region, and the fluorescence from this spot is detected. The flow of the reagents through the cell is periodically stopped by two valves. Commercial instruments stop the flow within approximately one millisecond. For each stop of the flow, the TCSPC device records a sequence of fluorescence decay curves. Because the number of 'stop' events is limited by the amount of reagents available good exploitation of the fluorescence photons is important. It is therefore advisable to combine stopped flow experiments with multi-detector operation. Several PMTs can be used to detect under 0° and 90° of polarisation, or to detect in different wavelength intervals. Another possibility is multi-spectral detection, e.g. with the bh PML-16 detector or the bh PML-Spec system, as shown in Fig. 174.

Results obtained in an SPC-630 based single-detector system are shown in [46]. An instrument with two detectors, a router and a bh SPC-630 modules is described in [305]. Both instruments used sequential recording in the continuous flow mode.

Continuous Flow Mixing Techniques

The time-resolution of stopped-flow mixing techniques is limited by the speed of the valves which stop the flow. The resolution is about 1 ms. Higher resolution is obtained by continuous flow mixing techniques. Two reagents are fed under high pressure into separate inputs of a flow cell. They are combined in a mixing region and then flow through the observation channel. The observation channel is illuminated by a laser, and the absorption or the fluorescence along the channel is recorded. Because the velocity in the observation channel is known, the

distance along the channel represents the time scale of the reaction. With micro-machined channels, a resolution down to a 25 μ s is achieved [53].

Continuous flow mixing can be combined with TCSPC by scanning the position along the flow channel and recording a fluorescence decay curve for each position, see Fig. 175. Any bh TCSPC modules can be used. An SPC-630 based instrument and its use for investigating protein-folding reactions is described in [53].

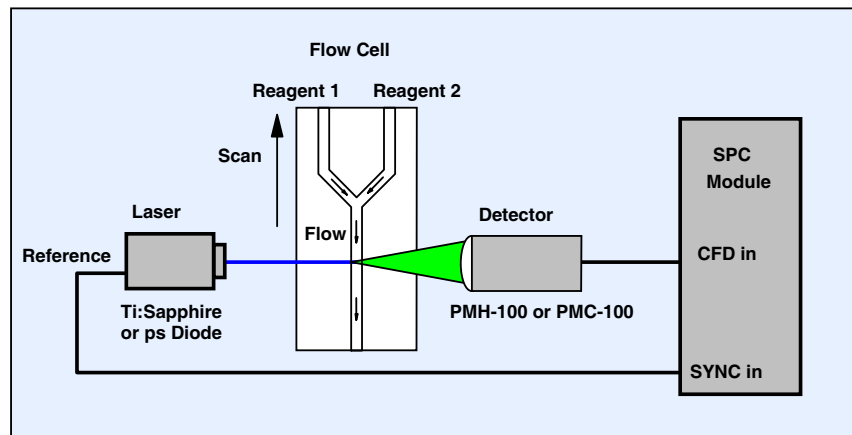


Fig. 175: Continuous flow mixing with fluorescence lifetime detection

The benefit of scanning the position is that the instrument can easily be combined with several detectors, e.g. for fluorescence anisotropy decay measurement or detection in several spectral intervals. By using the bh PML-Spec system multi-spectral detection can be achieved.

The drawback of the scanning principle is that the instrument consumes large amounts of reagents. Reagent economy can be largely improved by using multichannel detection along the flow channel. The flow channel is illuminated along its full length, and the fluorescence decay curves along the channel are detected simultaneously by a PML-16 multi-anode detector head. However, it is difficult to obtain constant excitation intensity and sensitivity along the channel. Illumination by a laser tends to produce speckles, and the sensitivity of the PML-16 channels is not uniform. Both effects are not necessarily stable over longer periods of time, so that calibration may be difficult.

Simultaneous Measurement of Fluorescence and Phosphorescence Decay

Simultaneous measurement of fluorescence and phosphorescence decay functions is difficult because the time scales and the intensities differ by three, often six orders of magnitude. If the excitation pulses are made short enough to measure the fluorescence decay either the fluorescence in the first few ns saturates the detector or the phosphorescence is so weak that it is lost in the detector background. Reasonable phosphorescence decay functions can only be obtained with excitation pulses of long duration, which, however, make the detection of the fluorescence decay impossible.

The problem can be solved by using the triggered sequential recording capability of multidimensional TCSPC in combination with a picosecond diode laser with fast on/off capability. The excitation of fluorescence and phosphorescence is illustrated in Fig. 176.

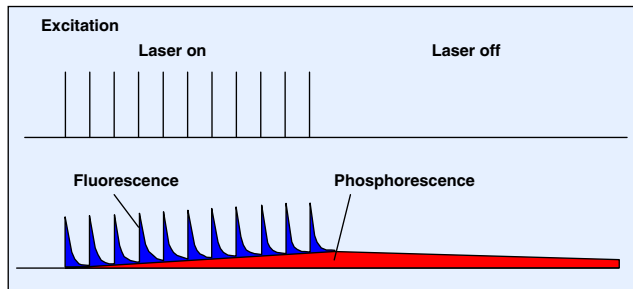


Fig. 176: Excitation of fluorescence and phosphorescence by laser on/off switching

The diode laser delivers excitation pulses at a repetition rate of 40 to 80 MHz. The laser is switched on and off at a period in the microsecond or millisecond range. In the ‘laser on’ phases normal fluorescence decay can be observed. A single excitation pulse does not cause any detectable triplet population and thus no detectable phosphorescence. However, during the complete ‘laser on’ phase a noticeable triplet population is accumulated. The phosphorescence is then observed in the ‘laser off’ period.

To record the signals a TCSPC device is operated in a triggered sequential mode. The start of the sequence is triggered with the ‘laser on’ signal. The length of the sequence is slightly shorter than the complete on-off period of the laser. A large number of on/off periods are accumulated. A result is shown in Fig. 177.

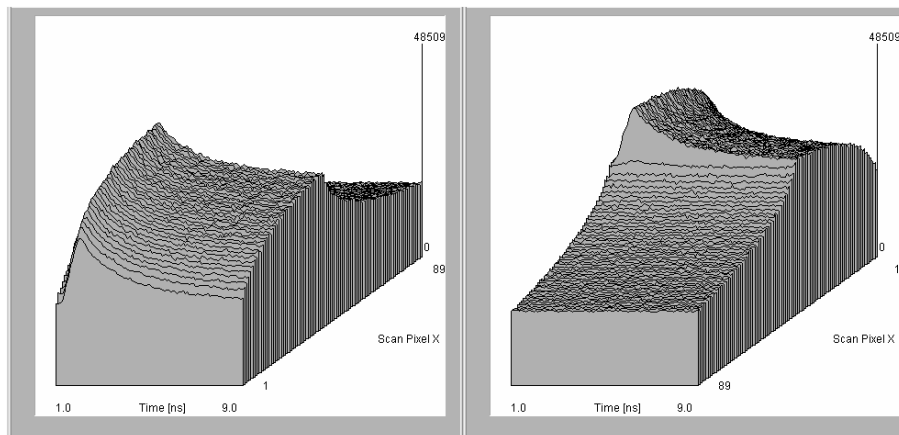


Fig. 177: Detection of fluorescence and phosphorescence by laser on/off switching and triggered sequential recording. The sequence begins with the start of the ‘laser on’ period. Left: Sequence shown from the beginning, ‘laser on’ period at the front. Right: Sequence shown from the end, ‘laser on’ period at the back

The laser on/off period was 90 ms, the duty cycle 50%. The laser repetition rate was 50 MHz. Thus, $2.25 \cdot 10^6$ laser pulses were sent into the sample during the 45 ms of the ‘laser on’ period. These pulses build up a substantial amount of phosphorescence. The build-up of the phosphorescence can be seen at the bottom of the sequence of fluorescence decay functions (Fig. 177, left). During the ‘laser off’ phases no fluorescence is excited, and the pure phosphorescence is detected (Fig. 177, right).

Fig. 177 gives an impressive demonstration of the double-kinetic recording capability of multidimensional TCSPC. It should, however, be noted that the phosphorescence of the sample was extremely strong. A strong phosphorescence was used to demonstrate both the build-up and the decay of the phosphorescence. In practice the ‘laser on’ period is usually entirely dominated by the fluorescence, and the build-up of the phosphorescence is not observable. However, the decay of the phosphorescence in the ‘laser off’ period is not disturbed by fluorescence and observable even if the phosphorescence is weak.

Time-Resolved Laser Scanning Microscopy

Confocal [253] and two-photon [103] laser scanning microscopes have initiated a breakthrough in biomedical imaging. The high image quality obtained by these instruments results mainly from the fact that out-of-focus light is strongly suppressed or, in the case of two-photon excitation, even not excited. As a result, images of high contrast are obtained, and 3D imaging becomes feasible. Moreover, the scanning technique can be combined with detection in several wavelength channels and multi-spectral detection [111]. In recent years more features have been added, including excitation wavelength scanning, polarisation imaging, and second-harmonic imaging. These multi-dimensional features make laser scanning microscopes an almost ideal choice for steady-state fluorescence imaging of biological samples [110, 197, 273, 275, 374].

Due to the scanning process used a laser scanning microscope can be combined with multi-dimensional TCSPC (see TCSPC Scanning Techniques, page 30). A TCSPC laser scanning microscope can be used for a number of applications which are difficult or impossible with steady-state detection techniques.

In the simplest case, the fluorescence lifetime can be used as an additional parameter to separate or identify the emission of different fluorophores. The application of the lifetime as a separation parameter is particularly useful to distinguish the autofluorescence components in tissues. These components often have poorly defined fluorescence spectra but can be distinguished by their fluorescence lifetime [201, 217]. Moreover, the fluorescence lifetime of endogenous fluorophores often varies with the binding to proteins or lipids [219, 272]. FLIM has also been used to verify the laser-based transfection of cells with GFP [348].

Unlike the fluorescence intensity, the fluorescence lifetime (within reasonable concentration limits) does not depend on the concentration of the fluorophore. It does, however, depend on local environment parameters. It can therefore be used to probe cell parameters such as ion concentrations or oxygen saturation. Fluorophores may also exist in a protonated and a deprotonated form; the equilibrium between them is pH-dependent. If the protonated and the deprotonated fluorophore have different lifetimes, the average lifetime is an indicator of the local pH [4, 160, 304]. Moreover, the lifetime of many fluorophores changes when they bind to proteins, lipids, or DNA [194, 219, 272, 359]. There are a large number of other fluorophores and labelling procedures [163], most of which have not yet been investigated for target-induced lifetime changes. Lifetime variations have also been used as an indicator of the local refractive index changes [354].

The distance between two different fluorophore molecules can be probed by fluorescence resonance energy transfer (FRET) [128, 220]. FRET occurs if the emission band of one fluorophore, the donor, overlaps the absorption band of a second one, the acceptor. The energy transfer rate from the donor to the acceptor depends on the sixth power of the distance. FRET becomes noticeable at distances on the order of a few nm and therefore occurs only if the donor and acceptor are physically linked. By labelling different proteins with different fluorophores, acting as donor and acceptor for FRET, interactions between these proteins can be investigated. Although a number of steady-state FRET techniques are available these are either destructive or require complicated calibration procedures, including measurements of cells containing only the donor and only the acceptor. With TCSPC FLIM techniques, FRET results are obtained from a single lifetime image of the donor [9, 34, 40, 58, 60, 67, 70, 77, 115, 277, 278].

It is sometimes believed that FLIM in cells does not require a particularly high time resolution. It is certainly correct that the fluorescence lifetimes of typical fluorophores used in cell

imaging are on the order of a few ns. However, the lifetime of autofluorescence components and of the quenched donor fraction in FRET experiments can be as short as 100 ps. Lifetimes of dye aggregates in cells have been found as short as 50 ps [189]. The lifetime of fluorophores bound to metallic nano-particles [237, 137, 138] can be 100 ps and shorter.

The fluorophore populations in biological specimens are normally not homogeneous. Several fluorophores may be present in the same pixel, or one fluorophore may exist in different binding or protonation states. The fluorescence decay functions are therefore usually multi-exponential. Resolving multi-exponential decay functions requires a large number of photons. Therefore photobleaching [270, 113] and photodamage [176, 196, 199] become a problem in precision FLIM experiments. FLIM data must therefore be recorded at low excitation intensity. Consequently, recording efficiency is another key parameter of a FLIM technique.

Due to its high time resolution, its capability to resolve complex decay profiles, its multi-wavelength capability, and its high efficiency TCSPC has early been used in combination with scanning microscopes [69]. However, the classic TCSPC technique was limited not only to relatively low count rates but also to slow scanning [68]. The situation changed with the introduction of the multi-dimensional TCSPC technique of bh. The first devices with scanning interfaces were the bh SPC-535 modules. Although these modules were already designed for fast scanning they were mainly used in combination with piezo-driven scan stages [181, 309]. The breakthrough came in 1999 with the combination of the bh SPC-730 modules with the laser scanning microscopes of Zeiss, Leica and Biorad. Since then multi-dimensional TCSPC has become a standard lifetime imaging technique for laser scanning microscopes.

Implementing TCSPC in Laser Scanning Microscopes

The TCSPC Laser Scanning Microscope

The general optical principle of a laser scanning microscope is shown in Fig. 178. A number of different optical principles are used which will be discussed below.

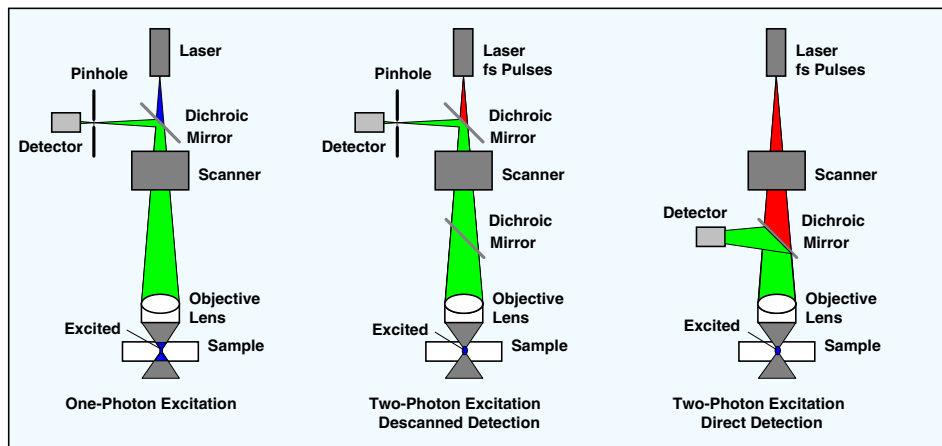


Fig. 178: Principle of a laser scanning microscope. Left: One-photon excitation and descanned detection. Middle: Two-photon excitation and direct detection. Right: Two-photon excitation and direct detection. Microscope light path simplified.

One-Photon Excitation with Confocal Detection

The laser is fed into the optical path via a dichroic mirror and focused into the sample by the microscope objective lens (Fig. 178, left). Scanning is achieved by deflecting the beam by two galvanometer-driven mirrors. The excitation light excites fluorescence within a double cone throughout the whole depth of the sample. The fluorescence light from the sample goes back

through the objective lens, and through the scanner. After travelling back though the scanner the beam of fluorescence light is stationary or ‘descanned’. The light is focused into a confocal pinhole in an image plane conjugate with the image plane in the sample. Light from outside the focal plane is not focused into the pinhole and therefore substantially suppressed [110, 253, 273]. Out-of-focus suppression is the basis of the superior image quality and the optical sectioning capability of scanning systems. For FLIM out-of-focus suppression is even more important. Any mixing of the (possibly different) fluorescence lifetimes of different focal planes adds additional lifetime components to the apparent decay functions. However, the difficulties of unmixing lifetime components increase dramatically with the number of components. Out-of-focus suppression is therefore mandatory to obtain good FLIM results.

One-photon confocal microscopes are normally equipped with several excitation lasers. These lasers are, of course, CW lasers and thus unable to deliver picosecond pulses for FLIM excitation. Normal ‘confocals’ must therefore be upgraded with a picosecond laser before they can be used for FLIM. In most cases an input fibre for a picosecond diode laser is available or can be installed, see [20, 22].

Two-Photon Excitation with Descanned Detection

With a fs or ps Ti:Sa laser the sample can be excited by two-photon absorption [103, 104, 140, 153]. The efficiency of two-photon excitation increases with the square of the excitation power density. Noticeable excitation is therefore obtained only in the focus. Thus, two-photon excitation is a second way to obtain depth resolution and suppression of out-of-focus fluorescence, see Fig. 178, middle and right. Different from one-photon excitation and confocal detection, which avoids out-of-focus *detection*, two-photon excitation avoids out-of-focus *excitation*. Therefore, detection through a confocal pinhole is not required to obtain a good image quality. Nevertheless, feeding the fluorescence light back through the scanner and the pinhole often has benefits. The accuracy of FLIM can be seriously impaired by detection of background light and by optical reflections in the beam path. A pinhole, even if wide enough to transmit virtually all fluorescence light from a thin sample, yields substantial suppression of daylight and of optical reflections.

Two-Photon Excitation With Direct Detection

Since the scattering and the absorption coefficients at the wavelength of the two-photon excitation are small the laser beam penetrates relatively thick tissue. Two-photon excitation can therefore be used to excite fluorescence in tissue layers as deep as 1 mm [103, 110, 197, 198, 273, 275, 329, 344]. The problem of deep-tissue imaging is, however, that the fluorescence photons are strongly scattered on their way out of the sample and emerge from a relatively large area of the sample surface. Moreover, the surface is not in the focus of the objective lens. No matter which optical system is used, it is impossible to focus this light into a pinhole.

The solution to deep-tissue imaging is ‘direct’ or ‘non-descanned’ detection. The fluorescence light is diverted by a dichroic mirror directly behind the microscope lens and transferred into a detector, see Fig. 178, right. Thus, photons leaving the sample from a large area are collected and fed into the detector.

Unfortunately the large detection area of a direct-detection system has also a drawback: It increases the detection efficiency for scattered photons and for photons of background light likewise. Any direct detection system with TCSPC has therefore to be operated in *absolute darkness*.

The absence of a pinhole in a two-photon microscope with non-descanned detection makes the optical path relatively easy to align. Two-photon microscopes can therefore be built by upgrading a one-photon system with a Ti:Sapphire laser or by attaching the laser and an optical scanner to a conventional microscope [108, 109].

TCSPC in Descanned (Confocal) Detection Systems

The descanned detectors of most laser scanning microscopes are included in the scan head. Although the detectors yield reasonable single-photon performance they are usually not fast enough for reasonable FLIM operation. Unfortunately, replacing these detectors with faster ones is normally not possible. Upgrading a confocal laser scanning microscope with TCSPC therefore requires one or several fast detectors to be attached to a suitable optical output from the scan head.

Fibre-Coupled Confocal Detectors

A relatively simple way to build a lifetime microscope with descanned detection is to use a fibre output from the scanning head [38]. Fibre outputs are available for the Bio-Rad Radiance 2100, the Olympus Fluo View FV1000, and for the Zeiss LSM 510, LSM 510 NLO and LSM 510 Meta systems. The general setup is shown in Fig. 179.

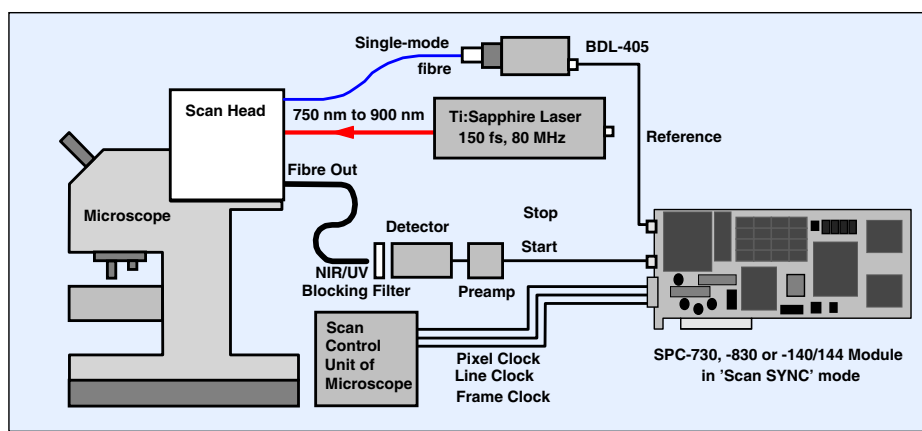


Fig. 179: TCSPC FLIM system with a fibre output from the scan head of the microscope

The fluorescence light from the sample is collected by the microscope lens, descanned, and delivered to the detector via the fibre output from the scan head. Often the fibre outputs do not contain any filters. Therefore an excitation blocking filter or a bandpass filter may be required in front of the detector. For details, please see [20, 22]. Applications of a Zeiss LSM 510 NLO two-photon microscope with fibre output and a Becker & Hickl SPC-730 TCSPC module to FRET and autofluorescence are described in [34, 35, 38].

Direct-Coupled Confocal Detectors

Unfortunately, fibre outputs are often relatively inefficient compared to the internal detection light paths of the scan head or to non-descanned detection [115]. The Leica SP 2 and SP 5 microscopes have therefore direct-coupled descanned outputs at their scan heads which are used to connect the bh FLIM systems [21]. The bh FLIM systems for the Olympus Fluo View FV1000 bh include a direct-coupled FLIM adapter [22]. The adapter can be used to attach a PMC-100 PMT module, an R3809U MCP PMT, or an H7422P-40.

Coupling of Diode Lasers into Confocal Microscopes

A FLIM system with descanned detection can be used both with two-photon excitation and one-photon excitation. Two-photon excitation is obtained from a Ti:Sapphire laser. One-photon excitation for FLIM can be obtained by frequency-doubling the Ti:Sapphire laser or by attaching a picosecond diode laser to the microscope. The microscopes usually have several fibre inputs for visible lasers, one of which can be used for the diode laser. The fibres are single-mode fibres, and a diode laser with a suitable fibre coupler must be used, see Fig. 10, page 9. Please note that inside the scan head the lasers are coupled into the beam path via dichroic

mirrors, see Fig. 178, left. The right mirrors must therefore be installed, and not all laser wavelengths may be applicable.

One-photon FLIM systems based on the bh technique are available for the Zeiss LSM 510 [20], the Leica SP2 and SP5 microscopes [21], and the Olympus Fluo View FV1000 [22]. Although TCSPC FLIM with picosecond diode laser excitation has been demonstrated earlier [300, 301] the Leica D-FLIM system was the first commercially available TCSPC FLIM system with fast scanning and pulsed diode laser excitation.

Diode-laser based one-photon FLIM is inferior to multiphoton FLIM when deep tissue layers are to be imaged. Moreover, time resolution is limited by the width of the diode-laser pulses. With the BDL-SMC lasers and the R3809U MCP PMT an IRF width of 60 to 90 ps is obtained, compared to 30 ps for multiphoton systems. On the other hand, one-photon excitation probably causes less photobleaching within the scanned image plane. Therefore high photon numbers per pixel can be obtained, which in part compensates for a possibly wider IRF. Fig. 189, page 176, gives an example of the accuracy that can be reached for bright samples of high photostability. An application of a diode-laser FLIM system to FRET is shown [22].

TCSPC in Non-Descanned (Direct) Detection Systems

Multiphoton FLIM with non-descanned detection requires a fast detector to be attached to a suitable optical port of a two-photon microscope. In the Zeiss LSM 510 NLO the standard detectors can be replaced with bh detector/shutter assemblies by loosening a single screw [20]. Other microscopes have unused optical ports to which the light can be directed. Often these ports are C-mount compatible. In these cases C-mount compatible versions of the bh detector assemblies can directly be used. In other cases attaching a FLIM detector requires purchasing or machining a suitable adapter. Normally a field lens is required to transfer the light efficiently to the available detector area and to avoid vignetting the image. The lens projects an image of the microscope lens into the plane of the detector [46]. The bh detector assemblies include a lens that is designed for ports with approximately parallel beam paths. For other beam geometry it may be required to replace the lens with one of different focal length. The general system configuration is shown in Fig. 180.

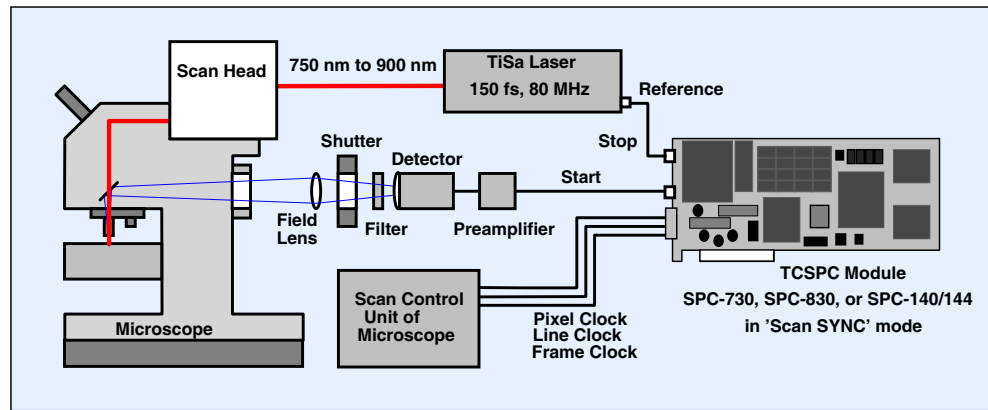


Fig. 180: TCSPC laser scanning microscope with non-descanned (direct) detection

Compared to descanned detection through a confocal pinhole, non-descanned detection collects the light from a much larger area. The large detection area yields high efficiency for highly scattering samples. It does, however, also make non-descanned detection extremely sensitive to daylight. A high background count level can, however, severely impair the lifetime accuracy. Therefore, TCSPC FLIM systems with non-descanned detection have to be operated in absolute darkness.

Due to the large light collection area non-descanned detectors can be severely overloaded by daylight leaking into the detection path. Moreover, the halogen or mercury lamp of the microscope is a potential source of detector damage. Therefore, an NDD FLIM system must protect the detectors against overload, see (see ‘Preamplifiers and Detector Control’, page 73 and [19]).

Another potential source of trouble is insufficient blocking of the laser light. A large amount of excitation light is scattered in the acousto-optical modulator used to control the laser intensity, at the dichroic mirror, and at the edge of the microscope objective lens. This light is not focused. In a descanned (confocal) detection system it is substantially suppressed by the pin-hole. In a non-descanned system there is no such suppression. A good blocking filter is therefore important [46].

Two-photon NDD FLIM systems with bh SPC modules have been built for the Biorad MRC 600 [124], MRC 1024 [2, 3, 257] and Radiance 2000 [9, 10, 62, 77], the Zeiss LSM 410 [34, 35, 300, 301] and LSM 510 [39, 41, 60, 115], the Leica TCS-SP1 and TCS-SP2 [298, 354] the Olympus FV 300, the Nikon PCM 2000 and a number of specialised or home-made two-photon scanning microscope systems [144, 201, 355].

Leica delivers complete multiphoton FLIM systems based on the bh SPC-830 and DCC-100 modules and the PMH-100 detector [21]. The systems normally use descanned detection. However, non-descanned detection systems, different detector versions, and dual-wavelength detection are available on demand.

A non-descanned (‘direct’) FLIM detection module with two wavelength channels for Radiance 2000 microscope has been developed in cooperation of Biorad and bh. The detector module contains computer-controlled dichroic beamsplitters and filters, preamplifiers, and overload shutdown of the detectors. The preamplifiers simultaneously deliver photon pulses to a Becker & Hickl SPC-830 TCSPC module and intensity signals to the standard steady-state recording electronics. Unfortunately all Biorad scanning microscopes were discontinued in 2004.

FLIM upgrade kits for the Zeiss LSM 510 NLO are available from bh. Versions for one-photon or multiphoton excitation, with one or two detectors and a large number of detector versions, including the R3809U, the H7422P-40, the PMC-100, and the PML-Spec multi-wavelength detection system are available [20]. The essential components of a single-detector system for the LSM 510 multiphoton microscopes are shown in Fig. 181.



Fig. 181: Single-detector FLIM upgrade kit for the Zeiss LSM 510 NLO. Left to right: Detector/shutter assembly with Hamamatsu R3809U MCP, DCC-100 detector controller card for shutter and detector control, SPC-830 TCSPC module.

An overview about the bh FLIM systems is given under ‘FLIM Systems for Laser Scanning Microscopes’, page 101.

Multi-Wavelength FLIM

By using the multi-detector capability of the SPC module several FLIM detection channels can be operated simultaneously in different wavelength intervals, or under different angle of polarisation. For the LSM 510 NLO dual-wavelength FLIM is a standard option [20]. It uses

the two outputs of the ‘NDD Switch Box’ of the LSM 510. A bh detector/shutter assembly is connected to each of the outputs. Applications are described in [39, 40, 46, 58, 60, 115].

Multi-wavelength TCSPC-FLIM in 16 wavelength channels has first been demonstrated in [37]. The system described used the fibre output from an LSM 510 NLO microscope, a polychromator, a bh PML-16 detector and an SPC-730 module. The application of the system to FRET measurements was demonstrated in [61]. A similar system attached to a Zeiss LSM 410 microscope was used for tracking the metabolites of 5-ALA (5-aminolevulinic acid, an approved sensitiser for photodynamic therapy) in living cells [302, 303].

A multi-spectral FLIM system for two-photon microscopes with non-descanned detection was described in [56]. An image of the aperture of the microscope objective lens was projected on the input of a 1-mm multi-mode fibre. The fibre delivered the fluorescence light to a polychromator. The spectrum was recorded by a bh PML-16 detector, and the 16 wavelength channels were recorded simultaneously by a bh SPC-830 module.

The MW-FLIM system available from bh uses a fibre bundle to transfer the light from a non-descanned port to the polychromator [18]. The principle is shown in Fig. 182, the essential parts in Fig. 183.

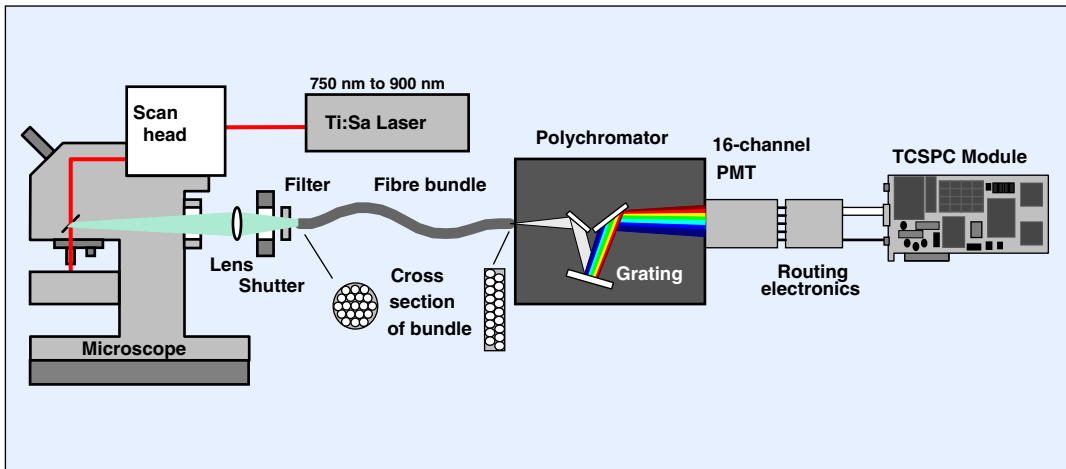


Fig. 182: Multi-spectral two-photon FLIM system with non-descanned detection

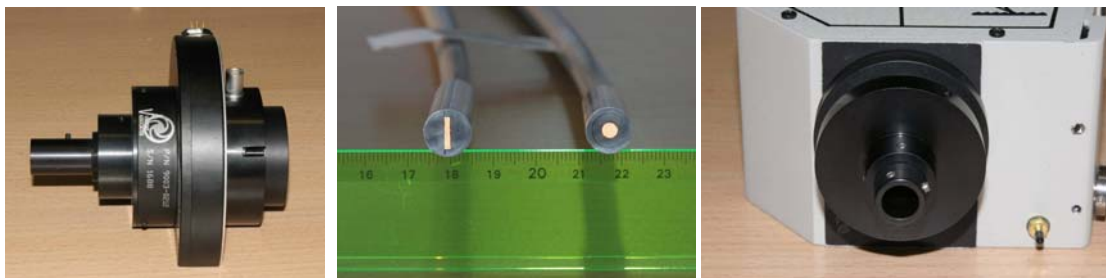


Fig. 183: Parts of the NDD MW-FLIM system. Left: Shutter assembly with integrated field lens, fibre bundle adapter and adapter to Zeiss LSM-510 NDD switch box. Middle: Fibre bundle. Right: Input side of polychromator with adapter for fibre bundle.

A field lens projects an image of the effective aperture of the microscope lens on the input of a fibre bundle. The fibre bundle has a circular cross section at the input, and a rectangular cross section at the output. Thus, the input matches the image of the microscope lens aperture. The output, in turn, matches the input slit of the monochromator. The system features high efficiency even for highly scattering samples. Compared to the single-fibre system described in

[56] the fibre bundle is used at a relatively moderate numerical aperture so that pulse dispersion is kept at a noticeably lower level.

A multi-spectral lifetime image of a stained wood sample obtained by this system is shown in Fig. 184. The sample delivered a count rate of a few MHz without noticeable photobleaching. The image shown was therefore obtained within an acquisition time of only 20 seconds.

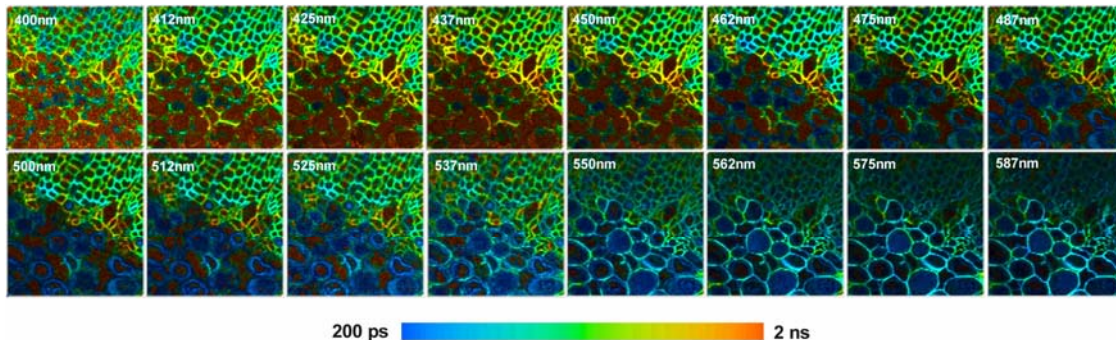


Fig. 184: Multi-wavelength lifetime image of a stained wood sample. Wavelength channels from 400 nm to 587 nm. bh MW-FLIM system with SPC-830 TCSPC module. Acquisition time 20 seconds.

It should, however, be noted that the sample used for Fig. 184 is not typical for FLIM. Most samples have much lower fluorophore concentration and lower photostability. The excitation power must then be reduced; the count rates decreases and the acquisition time becomes longer. A multi-spectral autofluorescence image is shown in Fig. 198, page 184.

Multi-Module FLIM Systems

A single bh TCSPC module has a saturated count rate of $8 \text{ to } 10 \cdot 10^5 \text{ s}^{-1}$ and a ‘maximum useful count rate of $4 \text{ to } 5 \cdot 10^5 \text{ s}^{-1}$. In general, the count rates obtained for FRET and autofluorescence experiments in living cells and tissue are rarely higher than a few 10^5 s^{-1} . Consequently, the typical count rates are well within the reach of a single TCSPC module. Nevertheless, higher count rates may be obtained from fixed samples stained with high concentrations of fluorophores of high quantum efficiency. To exploit count rates in excess of $5 \cdot 10^6 \text{ s}^{-1}$, the bh SPC-144 or SPC-154 four-channel TCSPC packages (see page 6) can be used.

The light from the sample is split into several detection channels and fed into separate PMTs. A detector/beamsplitter unit with four PMH-100 detectors is shown in Fig. 185, left. Each PMT was connected to one channel of the SPC-144 package. The SPC-144 channels have a dead time of 100 ns. The maximum useful (recorded) count rate of each individual channel is $5 \cdot 10^6 \text{ s}^{-1}$. The system can be used at a total recorded count rate up to $20 \cdot 10^6 \text{ s}^{-1}$, or a total detector count rate of $40 \cdot 10^6 \text{ s}^{-1}$.

Fig. 185, middle and right shows images of a mouse-kidney section (Molecular Probes, F-24630) stained with Alexa Fluor 488 WGA, Alexa Fluor 568 phalloidin, and DAPI. Two photon excitation at 860 nm was used. The laser power was about 400 mW at the input of the LSM 510 microscope. The objective lens was a 100x, NA=1.3. The count rate was $14 \cdot 10^6 \text{ s}^{-1}$, the acquisition time 10 s. A double-exponential fit was used to analyse the data. The colour of Fig. 185, middle, represents a single-exponential approximation of the lifetime obtained by weighting both lifetime components with their relative intensities. Fig. 185, right, shows an image of the relative amplitude of the fast lifetime component. The colour range from blue to red corresponds to a relative amplitude of 10 to 90%.

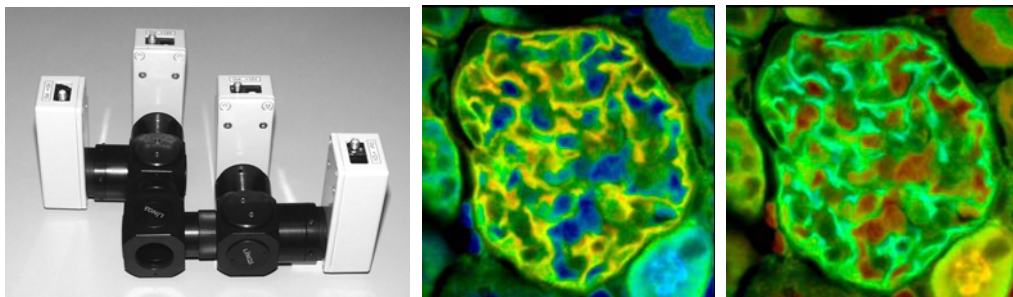


Fig. 185: Left: Four-channel detector unit for an SPC-144 four-module TCSPC package. Middle: Single-exponential lifetime image; the colour represents the amplitude-weighted mean lifetime, blue to red = 0.7 to 1.7 ns. Right: Fraction of the fast lifetime component of double-exponential decay. The colour represents the amplitude of the fast lifetime component, blue to red = 0.1 to 0.9. From [41]

The setup records single-exponential lifetime images in less than 1 s and double-exponential lifetime images in less than 10 s. However, the high excitation power can cause substantial photobleaching and, consequently, changes in the observed lifetimes. Details are described in [41, 46].

Acquisition Time of TCSPC FLIM

Due to its near-ideal counting efficiency TCSPC imaging gives the shortest possible acquisition time for a given count rate obtained from the sample and for a given lifetime accuracy. Unfortunately that does not necessarily mean that the acquisition times are short.

Samples investigated by FLIM usually have their fluorophores in highly specific sub-units of the cells. Moreover, over-labelling or over-expression of fluorescent proteins must be avoided. This implies that the average fluorophore concentrations are low. Simultaneously, photo-bleaching must be kept low to avoid photo-induced lifetime changes. Consequently, the count rates typically obtained in TCSPC FLIM experiments are low compared to steady-state imaging. The CFP-YFP FRET images shown in Fig. 193 and Fig. 195 were recorded at $50 \cdot 10^3 \text{ s}^{-1}$. An acquisition time of 20 minutes (!) was used to obtain data for accurate double-exponential FRET analysis. CFP-YFP FRET in *Caenorhabditis Elegans* [67] was recorded at $< 10^5 \text{ s}^{-1}$. Two-photon autofluorescence of skin delivers about $60 \cdot 10^3 \text{ s}^{-1}$; typical acquisition time are from 30 seconds to 5 minutes. The count rates used in these experiments were by factor of 40 to 100 lower than the maximum useful count rate of the bh TCSPC devices used.

It should be expected that much higher count rates are obtained from stained tissue. However, imaging of the pH in skin tissue by BCECF was performed at an average rate of only $2 \cdot 10^6 \text{ s}^{-1}$ [160], although the frequency-domain technique used was capable of processing much higher rates.

A count rate of $14 \cdot 10^6 \text{ s}^{-1}$ was used to record the image shown Fig. 185. This count rate comes close to the rates used in steady-state imaging. However, it caused noticeable photobleaching and lifetime changes [41, 46]. Thus, it appears that the count rates of typical FLIM applications are rather limited by the sample than by the SPC modules.

Given a maximum count rate permitted by the stability of the sample the acquisition time of TCSPC FLIM depends mainly on the required lifetime accuracy and the number of pixels in the image. From a single-exponential fluorescence decay recorded under ideal conditions the fluorescence lifetime can theoretically be obtained with a relative standard deviation or ‘coefficient of variation’, CV_τ , of

$$CV_\tau = \frac{\sigma_\tau}{\tau} = \frac{1}{\sqrt{N}}$$

with N = number of recorded photons [13, 139, 195].

The equation results from the simple fact that the lifetime of a single-exponential decay is the difference of the first moments of the decay data and the IRF [242, 265].

In other words, the fluorescence lifetime can be obtained with the same accuracy as the intensity. Measurement under ideal condition means the decay function is recorded

- with an instrument response function of negligible width
- into a large number of time channels
- within a time interval considerably longer than the decay time
- with negligible background of environment light, detector dark counts or detector after-pulsing

The equation given above can be used to estimate the number of photons and the acquisition time needed to record a single-exponential fluorescence lifetime image. The relative lifetime accuracy for a given number of photons per pixel is shown in Fig. 186, left. The diagram shows that the standard deviation improves only slowly with the number of photons. A lifetime accuracy of 10 % can ideally be obtained from only 100 photons. However, 10,000 photons are required to obtain a lifetime accuracy of 1 %.

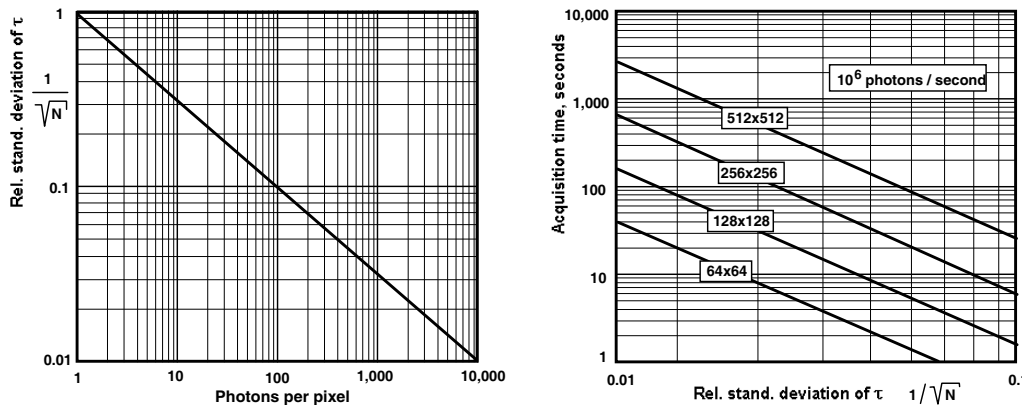


Fig. 186: Left: Relative standard deviation of the fluorescence lifetime, τ , versus the average number of photon per pixel. Right: Acquisition time as a function of the desired lifetime accuracy for different image sizes. Count rate 10^6 s^{-1} .

The acquisition time as a function of the desired standard deviation for a count rate of 10^6 s^{-1} is shown in Fig. 186, right. Even for an image of 512 x 512 pixels a relative lifetime accuracy of 0.1 (or 10%) is obtained within less than 30 seconds. A 256 x 256 pixel image of the same accuracy would be recorded within 5 seconds. However, an acquisition time of almost 1 hour would be required to record a lifetime image of 512 x 512 pixels with a lifetime accuracy of 1 %.

The accuracy obtained in practice may be lower than the values shown in Fig. 186. In particular, the background count rate in FLIM experiments is often not negligible, and the fluorescence may not decay entirely within the laser pulse period.

A considerable reduction in acquisition time for a given accuracy (or increase in accuracy for a given acquisition time) can often be achieved by binning the lifetime data in the decay analysis. Microscopy images are often spatially oversampled. The overlapping binning algorithm used in the bh SPCImage data analysis then does not noticeably impair the spatial resolution of the lifetime data [20, 21, 22]. Moreover, because only the lifetime data are binned (not the intensity data) no loss in contrast or spatial resolution is seen even in undersampled images.

Fig. 187 shows images of a mouse kidney sample stained with Alexa Fluor 488 wheat germ agglutinin, Alexa Fluor 568 phalloidin and DAPI. The excitation wavelength was 473 nm, therefore only the Alexa 488 and the Alexa 568 were excited. From top to bottom, the acquisition time was 1 second, 4 seconds, and 16 seconds. The average detector count rate was $4 \cdot 10^5$ s⁻¹. The images were analysed with different binning. From left to right, the binning was 1x1, 3x3, and 5x5 pixels.

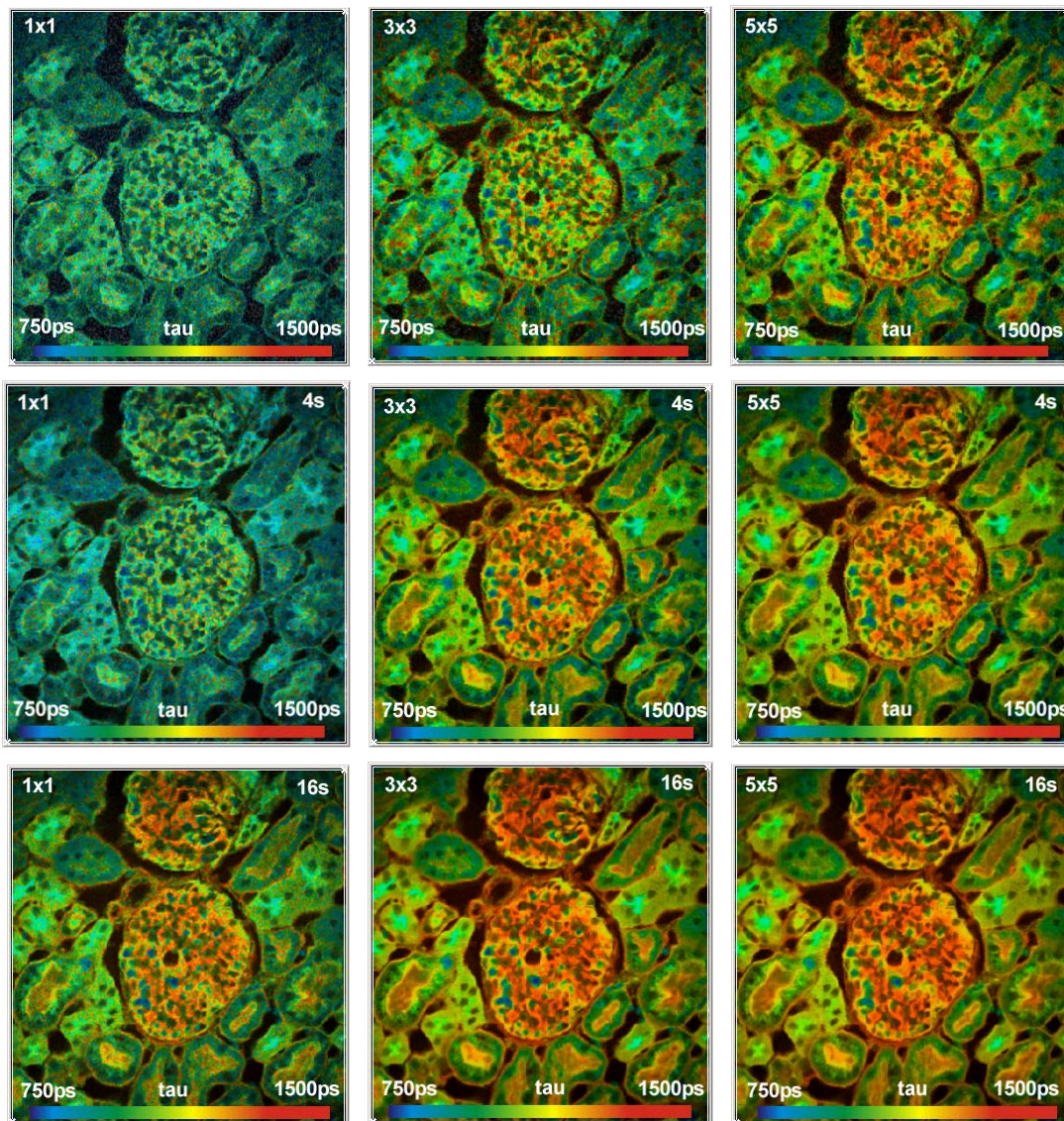


Fig. 187: Images of a stained mouse kidney sample obtained with different acquisition times and binning factors. Top to bottom: Acquisition time 1 s, 4 s, and 16 s. Left to right: Binning 1x1, 3x3, and 5x5 pixels. Data analysis: Single-exponential Levenberg-Marquardt fit.

Fig. 187 shows that FLIM results from bright samples can be obtained within short acquisition times. It does, however, also show a problem of the frequently used Levenberg-Marquardt fit: If the number of photons is low the fit fails to deliver a reasonable decay time. The source of the problem are time channels that do not contain any photons so that no reasonable weight in the χ^2 calculation is obtained.

For low photon numbers other algorithms are therefore more efficient. The best numerical stability is obtained by the first-moment technique. The first moment of a fluorescence decay curve is identical with the average arrival time of the photons. The fluorescence lifetime is the

difference of the first moments of the IRF and the decay data [242, 265]. Lifetime analysis via the first moments is merely a calculation, not a fitting process. It thus avoids any numerical instabilities. Lifetime images analysed by the first-moment technique are shown in Fig. 188.

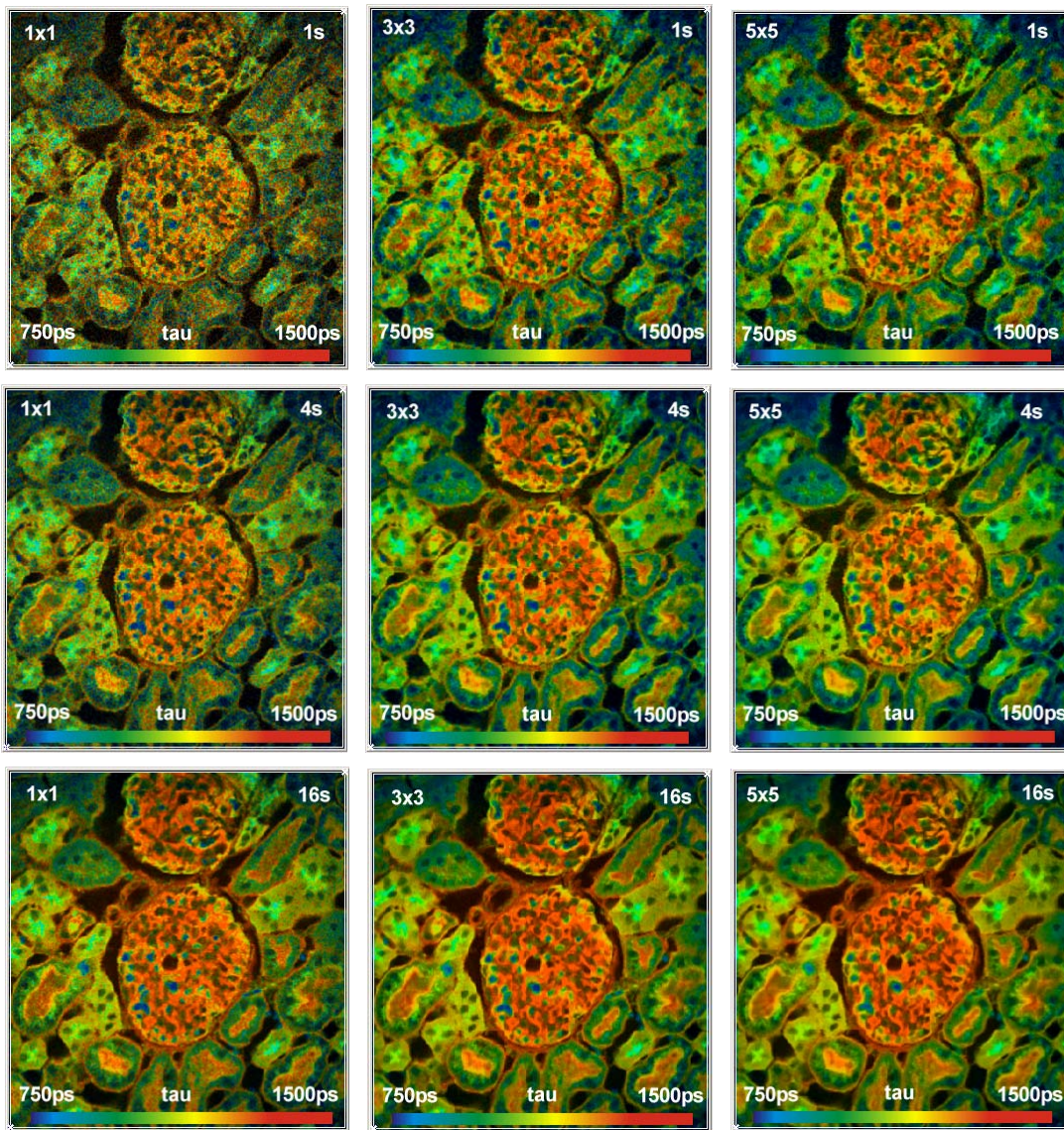


Fig. 188: Images of a stained mouse kidney sample obtained with different acquisition times and binning factors. Top to bottom: Acquisition time 1 s, 4 s, and 16 s. Left to right: Binning 1x1, 3x3, and 5x5 pixels. Data analysis: First moments

Fig. 188 shows that the long acquisition times often reported for TCSPC FLIM are *not* a feature of FLIM in general or TCSPC FLIM in particular. As shown above, the lifetime accuracy is comparable to the accuracy of intensity images. The difference is that typical FLIM samples deliver low count rates and that typical TCSPC FLIM applications are aiming at effects not or not fully accessible by steady-state imaging. The lifetime changes caused by these effects are naturally small. Consequently, the accuracy requirements (and the expectations) to FLIM results are higher than to steady-state images.

Multi-Exponential Decay Functions

The required number of photons increases if double-exponential decay functions are to be resolved. In [195] the number of photons required to resolve a double-exponential decay was

estimated to be $N = 400,000$. A number of photon per pixel this high is, of course, entirely beyond the limits set by the photostability of a biological sample. [195] is therefore often used as an argument that double-exponential lifetime imaging is impossible.

Fortunately, the prospects of separating two lifetime components improve dramatically with the ratio of the two lifetimes and with the amplitude factor of the short lifetime component. The lifetime components assumed in [195] were 10 % of 2 ns and 90 % of 4 ns. This is an extremely unfavourable situation which indeed requires an extremely high number of photons. Fortunately, the decay profiles found in FRET and autofluorescence measurements have a much more favourable composition. Usually the lifetime components are separated by a factor of 4 to 10, and the amplitude of the fast component is 50 to 90%, see Fig. 194 and Fig. 196. Under such conditions double exponential analysis is feasible on no more than a few 1000 photons per pixel, and very satisfactory results are obtained from 10,000 photon per pixel, see Fig. 195 and Fig. 197.

For bright samples with favourably spaced lifetime components even triple-exponential analysis can be feasible. Fig. 189 shows an example. The sample was measured for 250 seconds at an average count rate of about $1 \cdot 10^6 \text{ s}^{-1}$, the image size was 256×256 pixels. The upper row shows images of the lifetimes of the fast, medium, and slow decay component, the lower row images of the corresponding amplitudes.

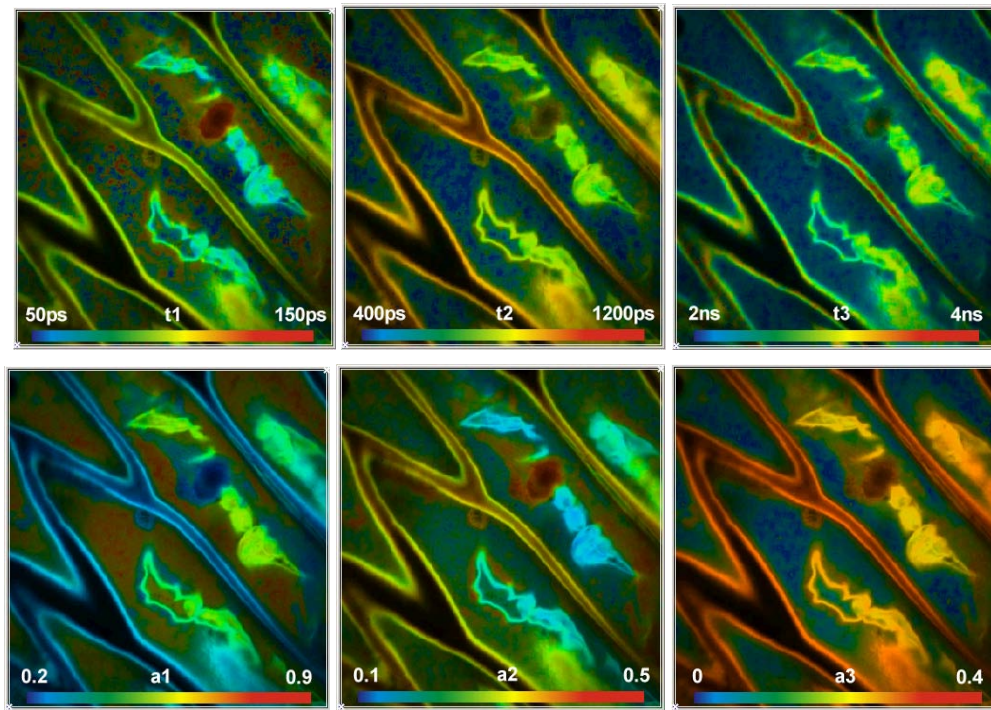


Fig. 189: Triple-exponential decay analysis. Upper row: Lifetimes of the fast, medium, and slow decay component. Lower row: Amplitudes of the decay components

IRF Recording

Recording the IRF in a TCSPC scanning microscope may appear simple at first glance. The sample would be replaced with a scattering medium or a mirror, and a TCSPC image or a single waveform would be recorded at the wavelength of the excitation laser.

In practice recording an accurate IRF in a microscope can be very difficult. The excitation wavelength is usually blocked by a filter that cannot easily be removed. Moreover, the laser is

scattered and reflected at many surfaces in the microscope itself. A recording taken at the laser wavelength therefore usually contains a number secondary peaks, or, in extreme cases, does not show any scattering image of the sample at all. The recorded pulse profile therefore does not represent the true excitation profile of the sample. Reflecting the laser light back by a mirror requires the mirror to be placed accurately in the focus of the microscope lens and perpendicular to the optical axis. Therefore, some scepticism is also recommended if an IRF is recorded this way.

For a two-photon microscope the situation is even more complicated. Even if the NIR blocking filter is removed, a detector with a bialkali or GaAsP cathode is insensitive at the laser wavelength. Of course, by increasing the laser power something is detected in any PMT. However, in the NIR a photocathode for the visible is almost transparent, and a large fraction of the photoelectrons may be emitted not from the cathode but from the first dynode. The detector response recorded in the NIR is therefore not necessarily identical with the response at the normal detection wavelength.

The logical way to record an IRF in a two-photon microscope is to use second-harmonic generation (SHG). SHG in a single crystal is not very useful because the light is emitted in the direction of the laser radiation. Returning it into the microscope lens with the right NA is difficult. A useful way to record an IRF in a microscope is SHG by Hyper-Rayleigh scattering in a suspension of gold nanoparticles [150]. Also urea micro-crystals and sputtered gold on a object carrier are said to produce enough SHG for IRF measurement.

If the IRF cannot be recorded, it is often derived from the data themselves. The IRF is approximated by a gaussian function, and the width is adjusted to give the best fit to the rising edge of the decay functions. The method yields acceptable results for lifetimes down to the FWHM of the IRF. It does, however, not take into account the tails and low-amplitude bumps present in the IRF of many PMTs. In multi-exponential decay analysis the simplification of the IRF can result in false lifetime components of low amplitude.

Biological FLIM Applications

Measurement of Local Environment Parameters

Microscopic pH imaging can be achieved by staining the skin with a pH-sensitive fluorescent probe. These probes usually have a protonated and a deprotonated form. There is an equilibrium between both forms that depends on the pH of the local environment. If both forms have different fluorescence lifetimes the average lifetime is a direct indicator of the pH [220]. A typical representative of the pH-sensitive dyes is 2',7'-bis-(2-carboxyethyl)-5-(and-6)-carboxyfluorescein (BCECF) [163]. In aqueous solution the lifetimes of the protonated form and the deprotonated form have been found 2.75 ns and 3.90 ns, respectively [160]. In the pH range from 4.5 to 8.5 both forms exist, and the fluorescence decay function is a mixture of both decay components. Thus, the lifetime of a single-exponential fit can be used as an indicator of the pH. An example of pH imaging of skin tissue is shown in Fig. 190. A single-exponential lifetime image is shown left.

Decay curves from different areas of the image are shown right. In areas of low pH fluorescence components of both protonated and deprotonated BCECF are found. The decay profile is therefore double-exponential. In areas of high pH essentially deprotonated BCECF is found, and the decay profile is single-exponential. It should be noted that the lifetimes of free BCECF differ from the lifetimes of BCECF bound in the tissue. The lifetime-pH relation must therefore be calibrated for bound BCECF.

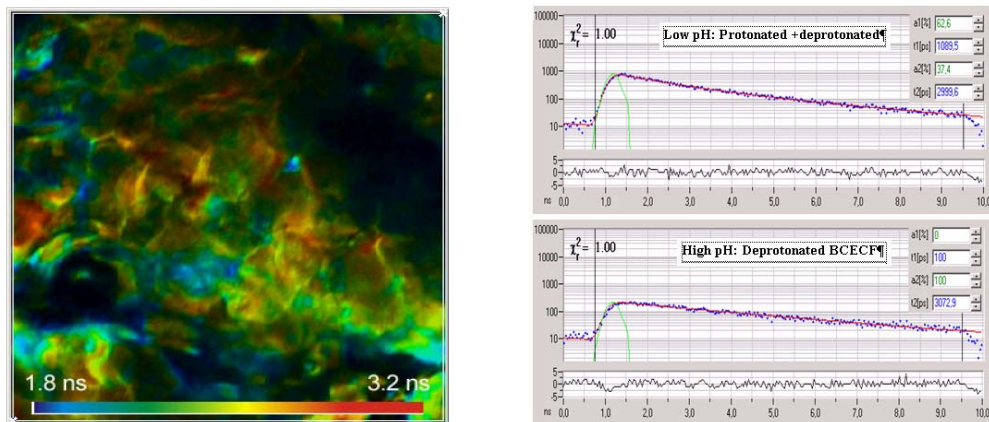


Fig. 190: Left: Lifetime image of skin tissue stained with BCECF. The lifetime is an indicator of the pH. Right: Fluorescence decay curves in an area of low pH (top) and high pH (bottom)

The measurement of the concentration of intracellular Cl^- in neurones by TCSPC FLIM was described in [183]. MQAE was used as fluorescent probe. MQAE is quenched by Cl^- , and the concentration can be calculated from the lifetime change via the Stern-Volmer relation. A bh SPC-720 module was used in conjunction with 2-photon excitation. Because 2-photon excitation does not cause photobleaching and photodamage outside the focal plane the authors were able to obtain z-stacks of the Cl^- concentration in dendrites over depth intervals up to 150 μm .

Fluorescence Resonance Energy Transfer (FRET)

FRET is an interaction of two fluorophore molecules with the emission band of one dye overlapping the absorption band of the other, see Fig. 191. In this case the energy from the first dye, the donor, can be transferred immediately to the second one, the acceptor. The energy transfer itself does not involve any light emission and absorption [128, 220]. Förster resonance energy transfer, or resonance energy transfer (RET), are synonyms of the same effect. FRET results in an extremely efficient quenching of the donor fluorescence and, consequently, decrease of the donor lifetime.

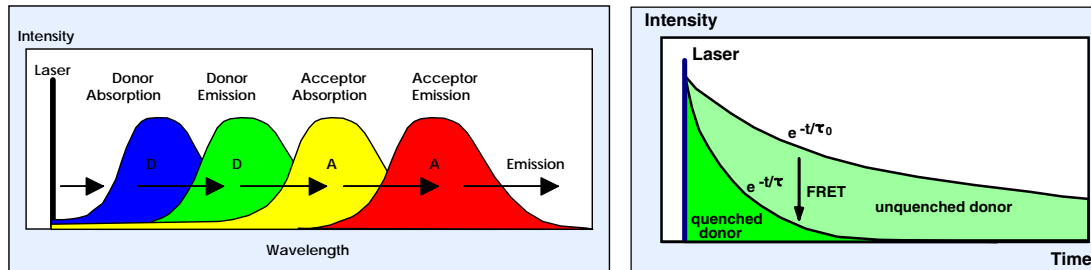


Fig. 191: Fluorescence Resonance Energy Transfer (FRET)

The energy transfer rate from the donor to the acceptor decreases with the sixth power of the distance. Therefore, it is noticeable only at distances shorter than 10 nm [220].

FRET has become an important tool of cell biology. Different proteins are labelled with the donor and the acceptor. FRET is used to verify whether labelled proteins are physically linked, and to determine distances on the nm scale.

The obvious difficulty of steady-state FRET measurements in cells is that the concentrations of the donor and acceptor are variable and unknown. Moreover, the emission band of the donor extends into the emission band of the acceptor, and the absorption band of the acceptor extends into the absorption band of the donor. A further complication is that usually only a fraction of the donor molecules are linked to an acceptor molecule. These effects are hard to distinguish in steady-state FRET measurements. Nevertheless, a number of FRET techniques

based on steady-state imaging have been developed [275]. The techniques use calibration based on different cells, each containing only the acceptor and the donor, and several measurements at the donor and acceptor emission wavelength. FRET can also be measured by the acceptor-photobleaching technique. A donor image is recorded, then the acceptor is destroyed by photobleaching, and another donor image is recorded. The FRET efficiency is obtained from the relative increase of the donor fluorescence intensity. The drawback of the technique is that it is destructive. It is therefore impossible to run successive FRET measurements in the same cell. It is also difficult to use in living cells because the acceptor recovers by diffusion effects.

FLIM-based FRET techniques have the benefit that the results are obtained from a single lifetime image of the donor [9, 34, 40, 115]. They do not need calibration by different cells, and are non-destructive.

A general problem of FRET experiments in cells is that not all donor molecules interact with an acceptor molecule. The most obvious reason is that the orientation of the dipoles of the donor and acceptor molecules is random. The corresponding variation of the interaction efficiency results in a distribution of the lifetimes. The effect on FRET results is predictable and correctable [220].

A more severe problem is that some of the donor molecules may not be linked to their targets, and not all of the acceptor targets may be labelled with an acceptor. This can happen especially in specimens with conventional antibody labelling. Surprisingly, the problem of incomplete labelling [218] is rarely mentioned in the FRET literature and is normally not taken into account.

In cells expressing fusion proteins of the target proteins and variants of the green fluorescent protein (GFP), however, the labelling can be expected to be complete. The resulting donor decay functions can be approximated by a double exponential model, with a slow lifetime component from non-interacting (unquenched) and a fast component from the interacting (quenched) donor molecules [40]. Because the labelling is complete these decay components directly represent the fractions of interacting and non-interacting proteins. The composition of the donor decay function is illustrated in Fig. 192.

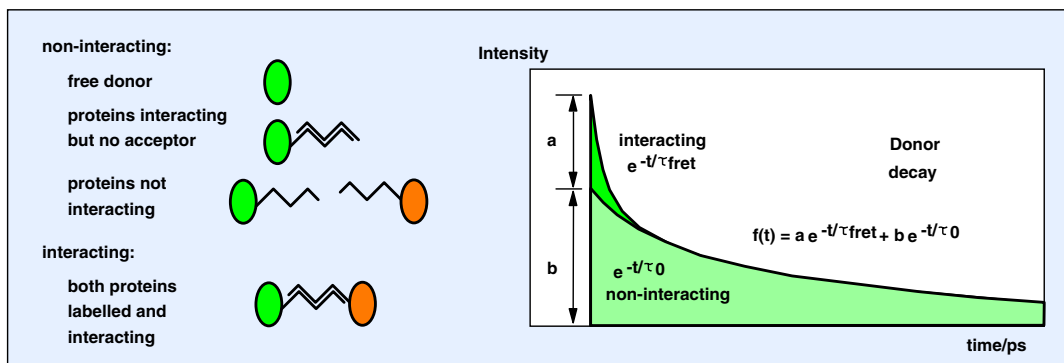


Fig. 192: Fluorescence decay components in FRET systems

Quantitative FRET measurements therefore require double exponential decay analysis that delivers the lifetimes, τ_0 and τ_{FRET} , and the intensity factors, a and b , of the two decay components. From these parameters can be derived the FRET efficiency, E_{fret} , the ratio of the distance and the Förster radius, r/r_0 , and the ratio of the number of interacting and non-interacting donor molecules, N_{fret}/N_0 :

$$E_{fret} = 1 - \tau_{fret} / \tau_0$$

$$(r/r_0)^6 = \tau_{fret} / (\tau_0 - \tau_{fret}) \quad \text{or} \quad (r/r_0)^6 = \frac{1}{E_{fret}} - 1$$

$$N_{fret} / N_0 = a/b$$

Fig. 193 to Fig. 195 show FRET results obtained for a cultured HEK (human embryonic kidney) cell expressing two interacting proteins labelled with CFP and YFP. The microscope was a Zeiss LSM 510 NLO. Two R3809U MCP PMTs were used to detect the fluorescence of the CFP and the YFP simultaneously. The signals were recorded in an SPC-730 TCSPC module.

Lifetime images of the donor (CFP) and the acceptor (YFP) are shown in Fig. 193. Both images show the lifetime obtained by fitting the decay curves with a single-exponential model.

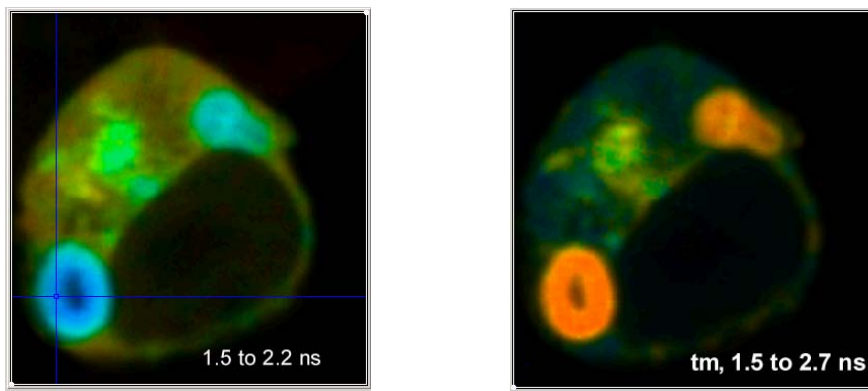


Fig. 193: HEK cells expressing two interaction proteins labelled with CFP and YFP. Left: Donor (CFP) image. Right: Acceptor (YFP) image. Two-photon excitation at 860 nm. Single-exponential lifetime images, colour represents lifetime, blue to red = indicated lifetime range

The single-exponential donor lifetime varies from about 1.5 ns in the region of strong FRET to about 1.9 ns in regions with weak FRET. The YFP intensity is highest in the regions where the CFP lifetime is shortest. This is a strong indication that FRET does indeed occur between CFP and YFP. The decay in the acceptor channel is a mixture of the FRET-excited acceptor fluorescence, a small amount of directly excited acceptor fluorescence, and about 50% bleedthrough from the donor fluorescence. Because YFP has a longer lifetime than CFP, regions of strong FRET show an increased lifetime.

Fig. 194 shows the fluorescence decay curves in a selected spot (array of 4 adjacent pixels) of the donor image (see blue cursor lines in Fig. 193).

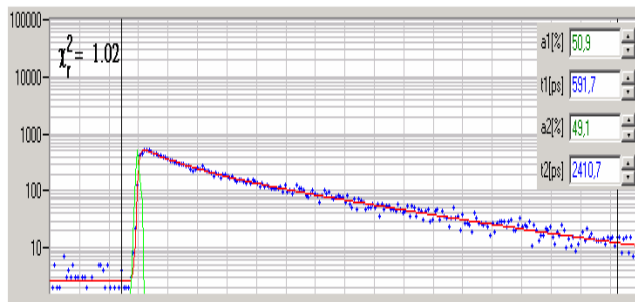


Fig. 194: Fluorescence decay curve in a selected spot of Fig. 193. The decay profile is clearly double-exponential.

The fluorescence decay is clearly double-exponential, with a fast lifetime component, τ_{fret} , of about 590 ps, and a slow lifetime component, τ_0 , of about 2.41 ns.

Fig. 195 shows the result of a double-exponential analysis of the data. The left image shows the ratio of the lifetimes of the non-interacting and interacting donor fractions, $\tau_0/\tau_{\text{fret}}$. The distribution of $\tau_0/\tau_{\text{fret}}$ in different regions is shown far left. The locations of the maxima differ by only 10%, corresponding to a distance variation of about 2%. However, the variation in the intensity coefficients, a/b , is about 10:1.

The results show clearly that the variation in the single-exponential lifetime (see Fig. 193) is almost entirely caused by a variation in the fraction of interacting proteins, *not* by a change in distance. In other words, interpreting variations in the single-exponential lifetime as distance variations leads to wrong results.

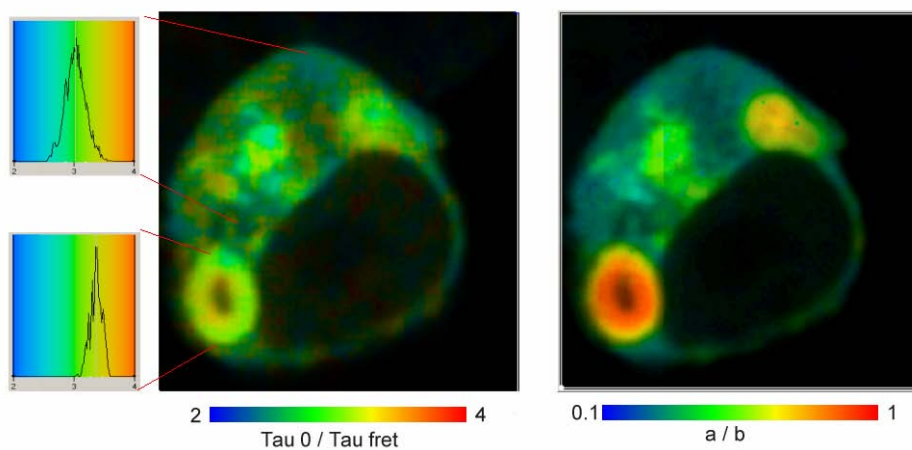


Fig. 195: Left: Ratio of the lifetimes of the non-interacting and interacting donor fractions, $\tau_0/\tau_{\text{fret}}$, with distribution in selected regions of the cell. Right: Ratio of the intensity coefficients of the interacting and non-interacting fractions, a/b

Similar double exponential decay behaviour is commonly found in FRET experiments based on multi-dimensional TCSPC [9, 34, 39, 40, 60, 70, 115, 274, 277]. Double-exponential decay profiles have also been confirmed by streak-camera measurements [58, 59].

It is sometimes suggested to improve the double-exponential analysis of the lifetime data of FRET systems by global analysis. Because the fast decay component originates from the interacting, the slow decay component from the non-interacting donor at least the lifetime of the slow component could be considered constant for all pixels of the image. Even the lifetime of the fast component would be constant if the distance between donor and acceptor does not vary significantly. A global fit with the same lifetime for all pixels would then increase the accuracy of the fraction of interacting and non-interacting donor significantly [274]. Accurate measurements in cells containing only-donor labelled proteins have, however, shown that there are lifetime variations on the order of 100 to 200 ps [45]. If the slow lifetime is used as a global parameter such variations induce large systematic errors in the values obtained for non-global parameters. It should therefore carefully be checked whether or not a parameter can be fitted globally.

It has been attempted to obtain additional FRET information from the donor emission measured simultaneously with the donor emission in a dual-detector TCSPC system [178]. An a/b image of the acceptor decay should display the ratio of the acceptor emission excited via FRET and directly. The integral intensity of FRET-excited acceptor emission could then be used as a second way to obtain the net energy transfer rate. Unfortunately, in the CFP-YFP

system, the acceptor decay cannot be observed directly because of the strong overlap of the donor fluorescence into the acceptor fluorescence spectrum. An attempt was made in [41] to subtract the donor bleedthrough from the acceptor decay and to build up an *a/b* image. In any case, using the acceptor fluorescence requires simultaneous detection of both the donor and acceptor images to reject photobleaching artefacts from the results. A promising way to use the acceptor fluorescence may be multi-spectral FLIM [61].

An enormous amount of FRET papers related to the bh FLIM technique has been published in the recent years. A detailed description of a TCSPC-FLIM-FRET system is given in [115]. The system was used for FRET between ECFP-EYFP and FM1-43 - FM4-64 in cultured neurones. A general characterisation of TCSPC-FLIM FRET for monitoring protein interactions is given in [60, 77, 78, 277, 328].

A comparison of the accuracy of FRET measurements by different techniques is given by Pellet et al. [274]. The authors compared FLIM, spectral imaging, and two-channel intensity imaging with calibration of excitation and emission crosstalk. For the individual measurements they used identical optical paths, comparable data acquisition times and comparable fluorescence intensities. It turned out that the FRET results obtained from the FLIM data had a three-times smaller standard deviation than those obtained from the dual-channel and spectral measurements.

Applications of FLIM_FRET to protein interaction related to Alzheimer's disease are described in [9, 10, 48, 49, 50]. Enzymatic activity in neuronal microcompartments were detected in [381]. Interactions between the PCK and NKKB signalling pathways have been investigated in [257]. [335] investigated the association of protein kinase C alpha (PKCa) with caveolin. FRET between GFP and RFP and FRET cascades from GFP via Cy3 into Cy5 are demonstrated in [278] and [2]. The agglutination of red blood cells by monoclonal antibodies was studied using FRET between Alexa 488 and DiI [298]. Interaction of the neuronal PDZ protein PSD-95 with the potassium channels and SHP-1-target interaction were studied in [58, 60]. It has also been shown that FRET can be used to monitor conformational changes of proteins in cells by FLIM-FRET [70, 233].

FRET between ECFP and EYFP in plant cells was demonstrated in [62]. FRET measurements in plant cells are difficult because of the strong autofluorescence of the plant tissue. The authors show that two-photon excitation can be used to keep the autofluorescence signal at a tolerable level. Protein interactions upon intrusion of fungal pathogens into plant cells were investigated in [52].

All these applications used bh FLIM systems based on the SPC-830 or SPC-730 modules. A wide range of microscopes were used, including the Zeiss LSM 510 NLO, the Biorad 1024 and Radiance 2000, the Leica SP2, and a number of specialised 2-photon microscopes.

Autofluorescence Microscopy of Tissue

Biological tissue contains a wide variety of endogenous fluorophores [201, 217, 315]. However, the fluorescence spectra of endogenous chromophores are often broad, variable, and poorly defined. Moreover, the absorbers present in the tissue may change the apparent fluorescence spectra. It is therefore difficult to disentangle the fluorescence components by their emission spectra alone. Autofluorescence lifetime detection not only adds an additional separation parameter but also yields direct information about the metabolic state and the microenvironment of the fluorophores [219, 220, 272]. Lifetime detection can also be used to obtain SHG images simultaneously with lifetime images [217]. Moreover, autofluorescence imaging has benefits in cases when the reaction of tissue to optical radiation is to be investigated, such as tumor induction by UV irradiation [203]. Such experiments forbid the use of exogenous fluorophores because energy or electron transfer from the fluorophores to the proteins could induce additional photodamage.

The samples used for tissue imaging are considerably thicker than samples containing single cells. Often tissue imaging is even performed on living animals. Therefore optical sectioning and a large penetration depth is required. The method of choice is therefore two-photon excitation with non-descanned detection.

The fluorescence decay profiles of tissue autofluorescence are multi-exponential, with decay components from about 100 ps to several ns. The deviations from single-exponential decay are substantial, see Fig. 196. Extracting meaningful decay parameters from the data therefore requires at least double-exponential analysis.

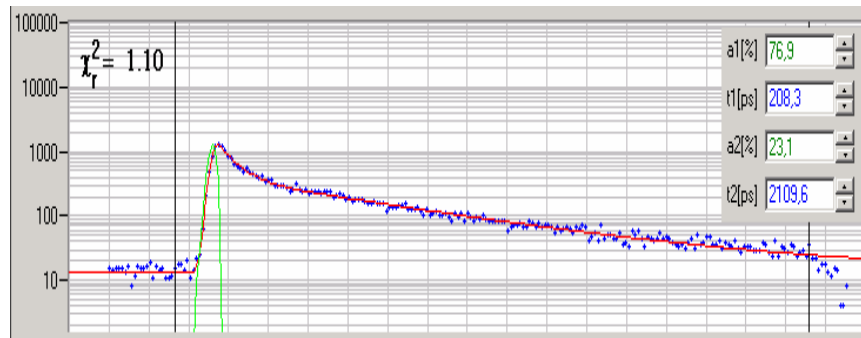


Fig. 196: Typical decay curve of tissue autofluorescence. Stratum corneum of human skin, two-photon excitation at 800 nm. Selected spot of the sample shown in Fig. 197.

Autofluorescence images of human skin are shown in Fig. 197. The upper row shows the stratum corneum (upper row, 5 μm deep), the lower row the stratum spinosum (lower row, 50 μm deep). Double-exponential decay analysis was applied to the data. The colour represents the fast lifetime component, τ_1 , the slow lifetime component, τ_2 , the ratio of lifetime components, τ_1 / τ_2 , and the ratio of the amplitudes of the components, a_1 / a_2 . The brightness of the pixels represents the intensity. The decay parameters show considerable variations throughout the image. The biological meaning of the decay variations still remains subject of investigation [201, 202, 203, 217, 376].

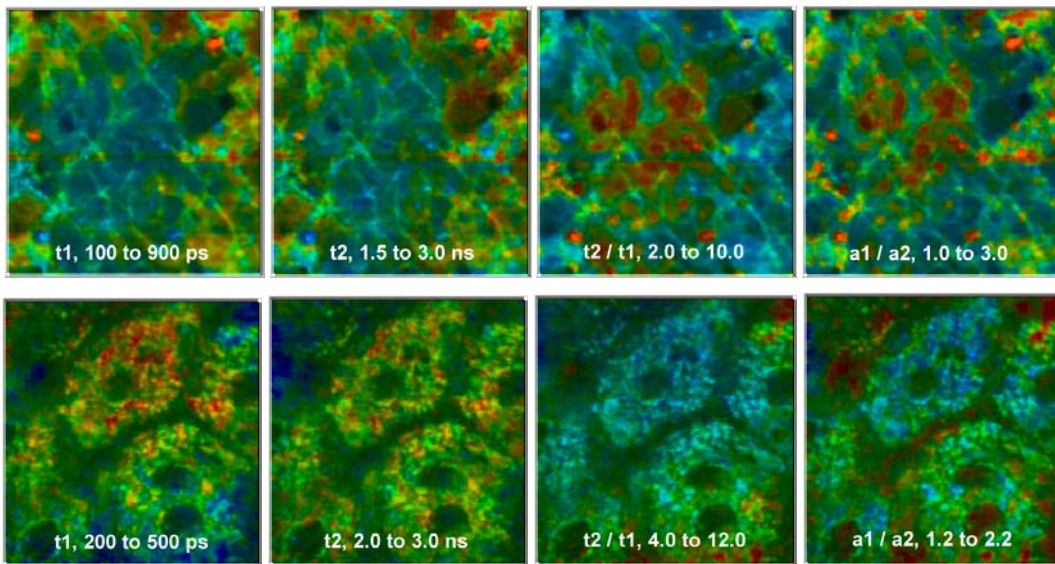


Fig. 197: Time-resolved in-vivo autofluorescence images of human stratum corneum (upper row, 5 μm deep), and stratum spinosum (lower row, 50 μm deep). Double-exponential analysis, left to right: fast lifetime component, τ_1 , slow lifetime component, τ_2 , ratio of the lifetime components, τ_1 / τ_2 , and ratio of amplitudes, a_1 / a_2 . The indicated parameter range corresponds to a colour range from blue to red.

Even more information can be expected from multi-wavelength autofluorescence lifetime images. Fig. 198 shows images of a mouse kidney section recorded by a bh MW-FLIM system (see Fig. 182). The microscope was a Zeiss LSM 5210 NLO. Two-photon excitation at a wavelength of 750 nm was used. The colour of the images represents the lifetime obtained by a single-exponential fit.

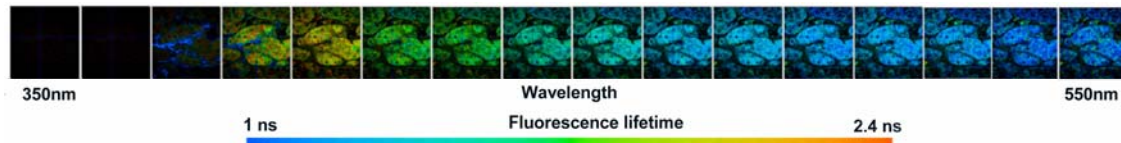


Fig. 198: Multi-wavelength autofluorescence FLIM images of mouse kidney tissue

Due to the different fluorophores present in the tissue, the lifetimes in the individual wavelength intervals are different. The image of the 375 nm channel contains also light generated by SHG (second harmonic generation). SHG reveals itself as an infinitely short lifetime component, see the blue features in the image.

From the multi-wavelength TCSPC data images in any wavelength interval within the recorded range can be calculated. An example is given in Fig. 199. Each of the four images shown is a combination of four adjacent detector channels. The wavelength intervals are 335 to 380 nm, 380 to 430 nm, 430 to 480 nm, and 480 to 530 nm (left to right).

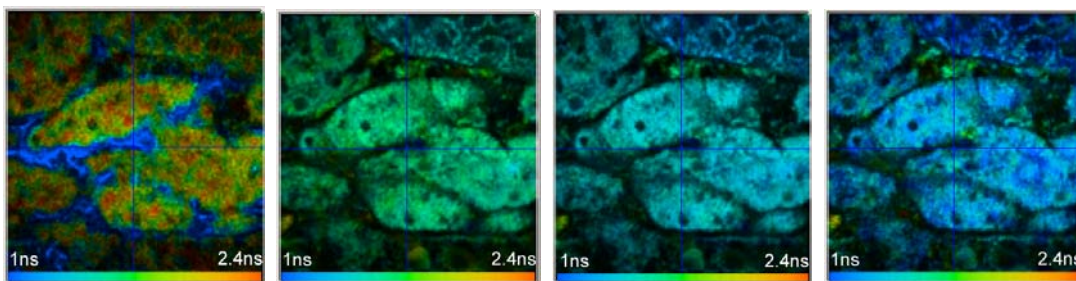


Fig. 199: Multi-wavelength fluorescence lifetime images of a mouse kidney section. Two-photon excitation at 750 nm. Left to right: 335 to 380 nm, 380 to 430 nm, 430 to 480 nm, 480 to 530 nm.

The photon numbers in the wavelength intervals of Fig. 199 are sufficient for double-exponential decay analysis. Fig. 200 shows the fast lifetime component, the slow lifetime component, and the amplitude ratio of both for the 430 to 480 nm interval. The fluorescence in this interval is dominated by NADH. The lifetime of NADH is known to depend on the binding to proteins [219, 220, 272]. The images can therefore be expected to represent different binding states of NADH.

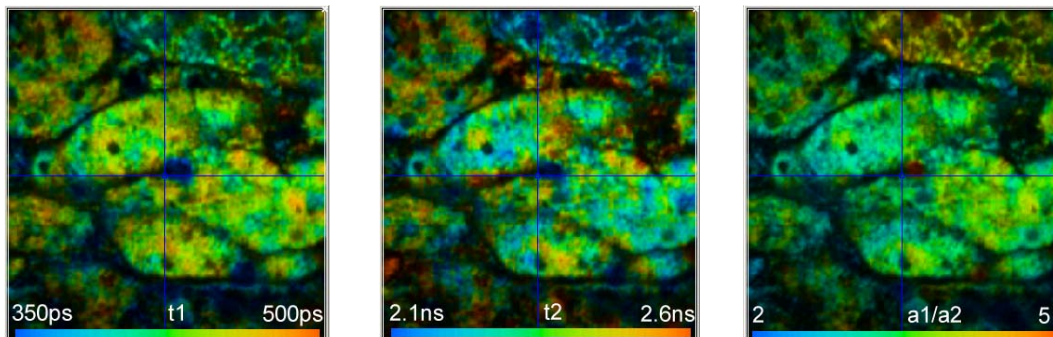


Fig. 200: Images of the lifetime components and amplitude ratio of a double exponential fit, 430 to 480 nm interval

Full exploitation of multi-wavelength FLIM data requires a global fit with a suitable model that includes the effective spectra of the expected fluorophores. Although the numerical algorithms do exist, no such analysis has been described yet.

Internalisation and Conversion of Photosensitisers for Photodynamic Therapy

Cells incubated with photosensitisers used in photodynamic therapy (PDT) show significant changes of the fluorescence lifetime with the incubation time and the exposure time. The effects can be used to reveal the binding of the photosensitiser to different protein structures and to track the formation of photoproducts. An SPC-730 module in combination with a bh PML-Spec system attached to a Zeiss LSM 410 microscope was used for tracking the metabolites of 5-ALA (5-aminolevulinic acid, an approved sensitisier for photodynamic therapy) in living cells [302, 303]. In the cells 5-ALA converts into protoporphyrin-9, which causes clearly detectable changes in the fluorescence lifetime.

Lifetime imaging has also been used to investigate the internalisation of aggregated photosensitisers by tumor cells and the monomerisation of the aggregates inside the cells [189].

Time-Resolved Optical Near-Field Microscopy (SNOM)

The optical near-field microscope (SNOM or NSOM) combines the principles of the atomic force microscope and the laser scanning microscope [116]. A sharp tip is scanned over the sample and kept in a distance comparable to the diameter of a single molecule. The tip can be the end of a tapered fibre through which the laser is fed to the sample, see Fig. 201, left. Or, the tip is illuminated by focusing the laser through the microscope objective on it. The evanescent field at the tip is used to probe the sample structure (Fig. 201, right). In both cases the fluorescence photons are collected through the microscope objective.

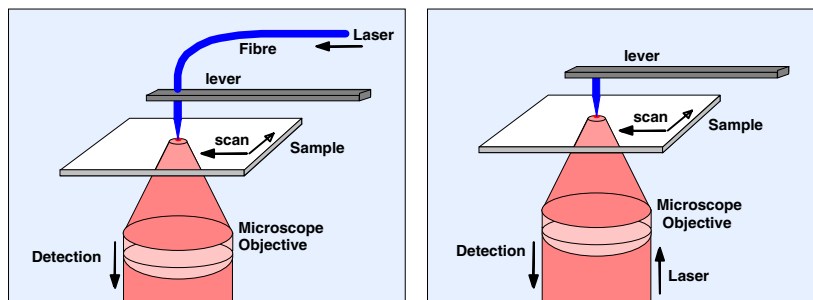


Fig. 201: Optical near-field microscope

The optical near-field microscope reaches a resolution of a few 10 nm, i.e. about 10 times better than the laser scanning microscope. Imaging of cells with this technique is difficult and possibly restricted to special cases. The realm of the optical near-field microscope are certainly applications where fluorescing molecules or nano-particles are fixed on a flat substrate.

Generally, the SNOM principle can be combined with fluorescence lifetime imaging in the same way as the normal laser scanning microscope, i.e. via pixel, line, and frame clock pulses. Only a few combinations of a SNOM with TCSPC have been published yet. All published applications used TCSPC techniques in combination with SPAD detectors. In [177, 246] an SPC-730 module was used; [214] used a classic TCSPC setup based on NIM modules. However, NSOM lifetime images presented so far have been not very impressive. It is not clear whether the reason is lack of photons, detector background, or inefficient data analysis and image-reconstruction software. Moreover, it is not clear in detail how the lifetime information of NSOM measurements can be used. The proximity of the tip changes the radiative and non-radiative decay rates. Therefore the obtained lifetimes do not necessarily represent the lifetimes of the undisturbed sample.

Diffuse Optical Tomography

Diffuse optical tomography, or DOT, aims to resolve the spatial distribution of optical properties in highly scattering media. Biomedical applications of DOT are based on illumination of thick tissue by NIR light, detection of diffusely transmitted or reflected light, or the fluorescence of endogenous or exogenous fluorophores [79, 271, 373]. Typical applications of DOT techniques are optical mammography, brain imaging, and non-invasive investigations of drug effects in small animals.

The scattering in tissue is not isotropic. A considerably larger amount of light is scattered forward rather than in reverse [255, 373]. For describing the penetration of light into thick tissue it is, however, sufficient to assume isotropic scattering with a reduced scattering coefficient. The reduced scattering coefficient, μ'_s , is

$$\mu'_s = \mu_s (1 - g)$$

with g being the average cosine of the scattering angle. For biological tissue g is typically in the range from 0.7 to 0.9 [99]. Reduced scattering coefficients for various types of tissue are given in [255].

Typical values of μ'_s are around 10 cm^{-1} . Consequently, there are practically no unscattered or ‘ballistic’ photons for tissue thicker than 1 cm. Instead, the photons must be considered to diffuse through the tissue. Consequently, the spatial resolution of DOT images is extremely poor and cannot compete with positron emission, X ray and MRI techniques.

The NIR absorption in tissue is dominated by oxy-haemoglobin, deoxy-haemoglobin, lipids, and water [99]. There is an absorption minimum from approximately 650 to 900 nm. Therefore, NIR light can be transmitted and detected through tissue layers as thick as 10 cm. Absorption coefficients for various types of tissue are given in [255].

In spite of the poor spatial resolution, DOT in the NIR has the benefit that the measured absorption coefficients are related to the biochemical constitution of the tissue, such as haemoglobin concentration and blood oxygenation [99, 241]. If exogenous markers are used, the absorption or fluorescence delivers additional information about blood flow, blood leakage, ion concentrations, or protein binding state.

In images obtained by continuous illumination and detection it is difficult to distinguish between the effects of scattering and absorption. The situation is much better if pulsed or modulated light is used to transilluminate the tissue and the pulse shape or the amplitude and phase of the transmitted light are recorded. The general effect of variations in the scattering and absorption on the shape of the transmitted pulses is shown in Fig. 202.

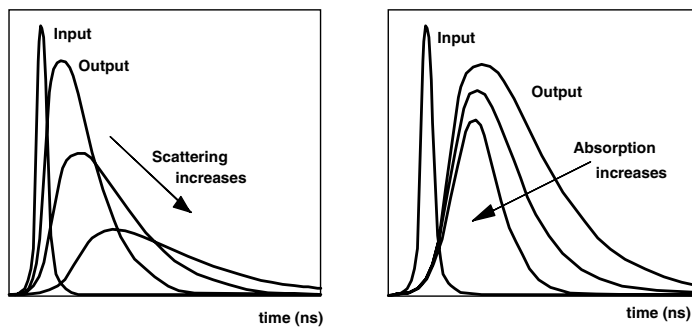


Fig. 202: Effect of scattering and absorption on the shape of a pulse transmitted through thick tissue

Both increased scattering and absorption decrease the integral output intensity. However, increased scattering increases the pulse width, while stronger absorption tends to decrease it. Therefore, the shape of the ‘time-of-flight distribution’ of the photons can be used to distinguish between scattering and absorption.

Moreover, in diffuse reflection experiments (i.e. with the source and the detectors at the same side of the tissue) the depth of scattering and absorption changes in the tissue can be derived from time-resolved data much better than from pure intensity data [164, 334]. The computation of the absorption and scattering coefficients can be considerably simplified by using the first and second moments, i.e. the mean time of flight and the variance of the time of flight [228, 231]. It has been shown that variations of the absorption and scattering coefficients calculated from the moments are obtained from considerably larger depth than such calculated from the intensity. The situation is shown qualitatively in Fig. 203.

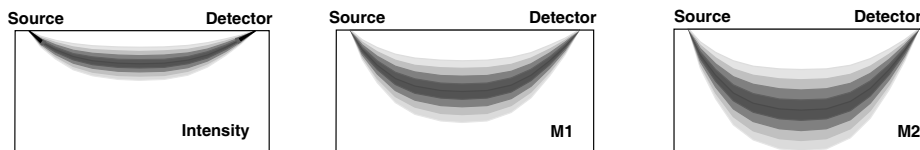


Fig. 203: Diffuse reflection experiment, depth in the tissue from which changes in the absorption and scattering coefficients are obtained. Left calculation from intensity data, middle calculation from M1 (mean time of flight), right calculation from M2 (variance of time of flight)

The banana-shaped pattern shows the depth from which absorption and scattering changes are obtained. (Please note that it does *not* represent anything like the mean path of the photons!)

The complete reconstruction of tissue structures and optical properties from time resolved data is extremely demanding and not entirely solved yet. A number of different approaches are used to solve the ‘inverse problem’ of DOT [5, 6, 81, 126, 133, 264, 282, 352, 362]. All approaches use a large number of time-resolved detection channels for different wavelengths, varying source-detector distances, or varying transillumination angles. The time-channel width required to quantify absorption and reduced scattering coefficient is of the order of 10 ps [264]. Moreover, low noise data are required to reconstruct the tissue properties from the relatively small intensity and pulse shape changes. This requires to record a large number of photons. Because the illumination intensity and the measurement time for in vivo measurements are limited a high detection efficiency is essential. Detection efficiency becomes even more important if fluorescence is to be detected in combination with normal DOT. Therefore, simultaneous detection in many time-resolved channels is an absolute requirement. Two typical setups used in DOT are shown in Fig. 204.

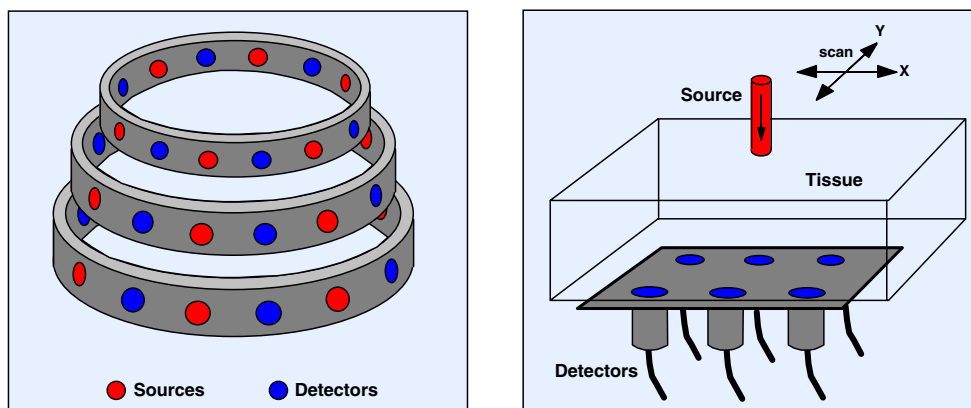


Fig. 204: Source-detector setups for optical tomography. Left: Circular arrangement of sources and detectors. Right: Scanning setup with one source and several detectors. Source and detectors are scanned simultaneously across the sample.

The traditional tomography setup is shown left. A large number of sources and detectors are arranged around the sample. The light sources are switched on one after another. For each source, time-of-flight distributions are recorded by all detectors [7, 165, 262, 308]. The setup is used for breast imaging and infant brain imaging. Because the setup is compact, mechanically simple, and can be built from purely non-metallic materials it is also used for optical tomography in conjunction with MRI imaging [261, 263]. When the setup is used for adult brain imaging, the detectors opposite to the source do not detect reasonable signals. Therefore detectors and sources are arranged at only side of the head. The configuration can be considered a sub-set of the arrangement shown in Fig. 204, left.

The right setup uses a scanning technique. Several lasers of different wavelength are multiplexed into a single optical source. The light source and the detector or a number of detectors are scanned simultaneously across the sample. The scanning technique is successfully used for optical mammography [102, 145, 146, 148, 283, 340, 341, 351, 352]. A scanning setup for small-animal imaging is described in [131]. The benefit of scanning is that it obtains a high spatial density of data points. Therefore the Nyquist condition is fulfilled for both spatial dimensions. However, problems can arise from edge effects. Not only can the detectors be damaged if the scan runs over the edge of the sample, but also the reconstruction of the sample properties has to cope with different photon migration near the edge. The problem can be solved by immersing the sample into a matching fluid [363].

In both setups different wavelengths are multiplexed into the optical source channels. The wavelengths can be multiplexed on a pulse-by pulse basis and recorded in the same TAC interval or in longer intervals and recorded in different memory blocks by using the multiplexing capability of the SPC modules. The benefit of the second technique is that there is no crosstalk between the wavelength channels and reduced signal distortion due to pile-up effects (see Fig. 147, page 137).

Optical tomography techniques for human medicine are currently at the stage of clinical tests. Frequency domain instruments using modulation techniques are competing with time-domain instruments using TCSPC.

An overview of TCSPC-based DOT techniques is given in [46], an overview of frequency-domain DOT techniques in [74]. It is now commonly believed that TCSPC instruments are more complex, but superior in terms of efficiency and sensitivity. The excellent results obtained with TCSPC-based instruments under clinical conditions clearly confirm the applicability of TCSPC to DOT [148, 149, 232, 340, 341].

Many TCSPC-based DOT instruments still use single lasers or several multiplexed lasers and record in a single SPC-330 or SPC-630 channel [97, 146, 148, 149, 147, 228, 284, 351]. Multi-detector operation of up to eight detectors connected to a single SPC-330 or SPC-630 channel was used in [98, 101, 102, 262, 263, 353]. A system with 32 fully parallel TCSPC channels based on conventional NIM modules was described in [308] and used for breast and brain imaging [165, 166, 168]. Recent TCSPC-based instruments use the bh SPC-134 packages of four parallel TCSPC devices [36, 231, 232, 283, 285, 340, 341, 352, 363, 364].

Optical mammographs and brain imagers are complex instruments with their own control, data acquisition and data processing software. Nevertheless, TCSPC-based instruments have a number of technical features in common. The general technical approaches and some typical results are described below.

Scanning Mammography

The principle of a typical TCSPC-based scanning mammograph is shown in Fig. 205.

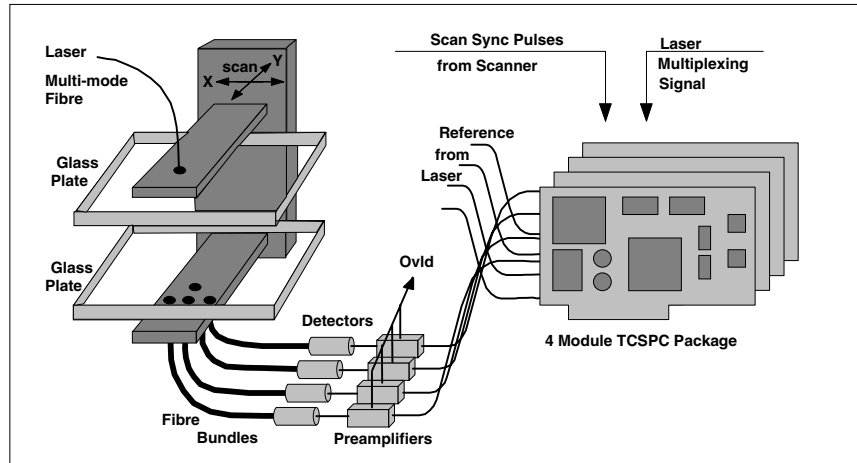


Fig. 205: General principle of a TCSPC scanning mammograph

The breast is slightly compressed between two glass plates. Due to the high sensitivity of TCSPC compression to about 6 cm is sufficient to obtain enough signal at the detectors.

The laser light is delivered via a multi-mode fibre. The transmitted light is collected by four fibre bundles and fed into four detectors. Fibres and fibre bundles are certainly not a favourable solution in terms of pulse dispersion, timing stability and detection efficiency. However, they decouple the electrical part of the system from the patient. The fibres are therefore an important part of the system to satisfy safety regulations for medical instruments.

Both the source fibre and the detection fibre bundles are assembled on a scanning stage. One scan typically contains 1000 to 5000 pixels, enough to avoid artefacts due to spatial undersampling. The scan amplitudes and the shape of the scanning area are different for different patients. To ensure that the detectors are not damaged by overload, the scanner must be prevented from running beyond the edge of the breast. This is achieved by using preamplifiers with overload detection (see ‘Preamplifiers and Detector Control’, page 73). When the detector currents exceed a reasonable limit the scan direction is reversed.

The four detector signals are connected into individual channels of a four-module TCSPC system. In practice, variable neutral-density filters and long-pass filters are placed in front of the detectors to compensate for different intensity at different breast thickness and to reduce the daylight sensitivity.

Usually several laser wavelengths are multiplexed into a single source fibre. The wavelengths can be multiplexed on a pulse-by pulse basis and recorded in the same TAC interval [148, 283, 340, 341, 351, 352] or in intervals of 50 to 200 μ s (2500 to 10.000 pulses) and recorded in different memory blocks by using the routing capability of the SPC modules (see Fig. 147, page 137). The benefit of the second technique is that there is no crosstalk between the wavelength channels, and signal distortion due to pile-up effects is reduced.

The number of wavelength channels can be increased by generating a super-continuum in a photonic crystal fibre and TCSPC multi-wavelength detection [333]. The technique delivers superior spectral data, but is probably too expensive for routine application.

The recording in the TCSPC channels can be synchronised with the scanning by software. In this case the time-of-flight distributions are read out from the TCSPC modules for each individual pixel. The bh SPC-630 and SPC-130/134 modules can avoid devoting time to readout

during the scan by using sequential recording in the Continuous Flow mode (see ‘Sequential Recording’ page 28). Another convenient mode is hardware-controlled scanning (see ‘TCSPC Scanning Techniques’, page 30) by an SPC-144 package. In this mode the TCSPC modules hold the time-of-flight distributions of all pixels of a scan in their memories. The data are read out when the scan is completed.

In both cases the data acquisition in the TCSPC channels is synchronised with the scanning by clock pulses from the scan controller. It must, however, be taken into account that the length of the lines of the scan varies since the return points of the scan are controlled by the detector overload signals. Therefore, the scan software must store the positions of the return points and the number of pixels between. These positions are used later to adjust the lines horizontally.

If fluorescence is to be detected in combination with DOT, detection efficiency may become a crucial point. The detection efficiency increases with the total detection area and, therefore, with the number of detectors. It can therefore be advantageous to use more than the four detectors shown in Fig. 205. In that case, several detectors are connected to one TCSPC channels via a router.

Fig. 206, left, shows the time-of-flight distributions for four detectors detecting at different projection angles at a single pixel of a breast scan. The acquisition time was 100 ms per pixel. The source-detector geometry is shown at right. The time offsets between the curves are due to different delays in the fibre bundles, detectors, and TCSPC channels. Mammograms were calculated from the photons in the 8th of 10 equidistant time windows spread over the time-of-flight distribution. The result [36] is shown in Fig. 207.

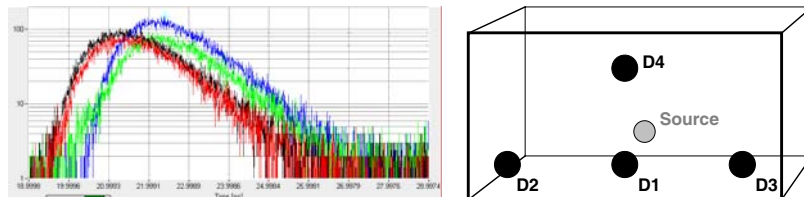


Fig. 206: Left: Time-of-flight distributions in one pixel of a breast scan. Different projection angels, acquisition time 100 ms per pixel. Right: Detector and source configuration. D1 is the direct detector, D2, D3 and D4 are offset by 2 cm.

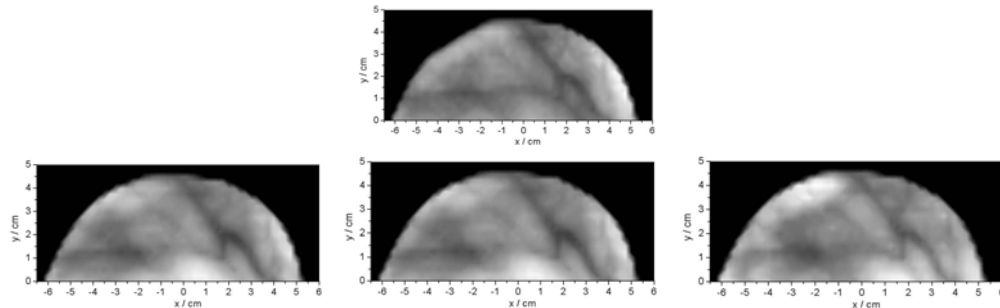


Fig. 207: Mammograms of a healthy volunteer recorded simultaneously at four projection angles. The images were generated from photon counts in a late time window. The arrangement of the mammograms corresponds to that of the detectors D1-D4 in Fig. 206. From [36]

Images in early and late time windows show qualitatively the scattering and the absorption in the tissue [96]. They can therefore be used to distinguish tumours in breast tissue. Most tumours have increased absorption due to increased haemoglobin content and blood leakage. These tumours are therefore prominent in the late time window. Cysts have decreased scatter-

ing and are visible in early time windows [340]. An additional benefit of the late time window is that the images are almost free of edge effects [146].

Quantitative data of the absorption and reduced scattering coefficients require the application of an appropriate analytical model [81, 80, 362]. The modelled distribution is convoluted with the IRF and fitted to the measured time-of-flight distributions in the individual pixels at several wavelengths [146, 148, 332, 352]. A comparison of the accuracy of scattering and absorption coefficients obtained by the time-window technique and by fitting a homogeneous diffusion model to the data is given in [96].

Static Brain Imaging

Structural tomography data of the brain are acquired in the traditional tomography setup, see Fig. 204, left. For each source position time-of-flight distributions are recorded for all laser wavelengths in all detector channels. Switching between the source positions is performed by fibre switches. Consequently, there is enough time to read out the time-of-flight distributions for each source position. The number of waveform memory blocks in the TCSPC modules is the number of detector positions multiplied by the number of laser wavelengths. Typically, the TCSPC system needs a total of 128 waveform memory blocks, or 32 blocks per TCSPC channel. The connection of a 32-channel tomography setup to an SPC-134 system with four HRT-81 routers is shown in Fig. 208.

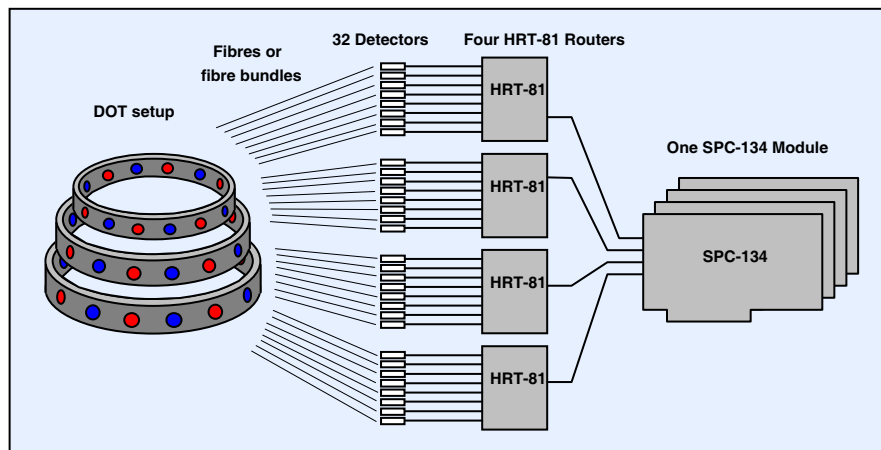


Fig. 208: Connecting a 32-channel tomography setup to an SPC-134 for-channel TCSPC package

The count rates in the individual detector channels may differ over a wide range depending on the distance from the source. For channels directly adjacent to the current source position, the count rate can be as high as several MHz. The PMTs can even be driven into overload. On the other hand, channels opposite to the source position may not collect any reasonable number of photons at all. In a TCSPC system with routers, the overloaded detector may block the router to which it is connected and thus prevent other signals from being recorded. Therefore, if the count rate of a detector becomes too high, either this detector must be switched off or an automatic intensity regulator of some kind must be placed in front of the detectors.

Typical time-of-flight distributions are shown in Fig. 209. The curves were recorded with a bh BHLP-700 diode laser of 2.5 mW power, 785 nm wavelength, and 50 MHz repetition rate. The detector was a bh PMC-100-20. The curves show the time-of-flight distribution for two different locations at the forehead together with the instrument response function. The source-detector distance was 6 cm. The acquisition time was 20 s, the count rates were between 800 kHz and 1 MHz.

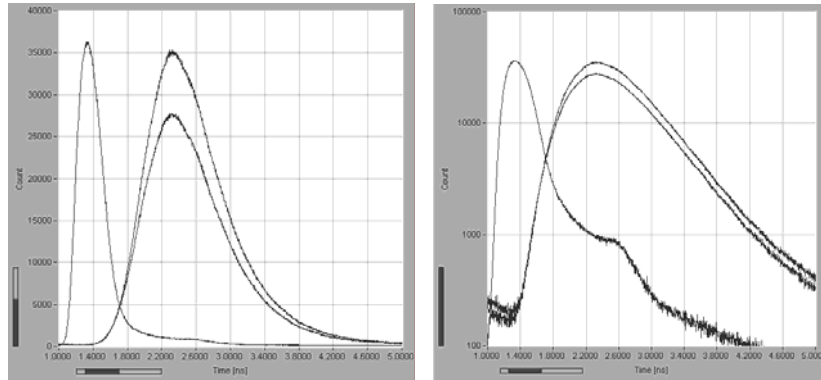


Fig. 209: Time-of-flight curves for two different source and detector positions at the forehead, and instrument response functions. Left linear scale, right logarithmic scale. Source-detector distance 6 cm, Laser 2.5 mW, 785 nm, 50 MHz. Acquisition time 20 s, ADC resolution 4096 channels.

The obtained count rates drop dramatically with increasing source-detector distance. With a laser power of a few mW, meaningful signals can be recorded diametrically through an infant head. For an adult head this is impossible. However, weak signals can be detected from temple to temple, as shown in Fig. 210. With a BHLF-700, 2.5 mW, 785 nm laser and a PMC-100-20 detector a total number of photons of 29,000 and 107,000 was acquired within an acquisition time of 60 s.

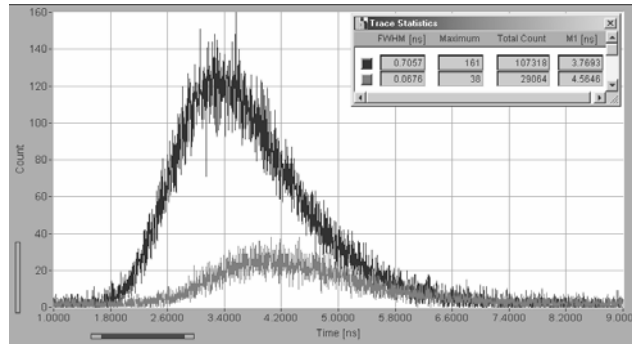


Fig. 210: Time-of-flight curves detected from temple to temple through an adult head. Slightly different source and detector positions. Laser power 2.5 mW, wavelength 785 nm, PMC-100-20 detector, acquisition time 60 s, ADC resolution 4096 channels.

Dynamic Brain Imaging

Dynamic changes in the time-of-flight distributions are caused by the heart beat, variable oxy- and deoxyhemoglobin concentration induced by brain activity, and effects of associated physiological regulation. The haemodynamic response to brain stimulation is on the time scale of a few seconds [117, 129, 130, 349, 350].

Recently Liebert et al. have demonstrated that advanced TCSPC is able to record effects of brain activity with 50 ms time resolution, clear separation of scattering and absorption, and probably better depth resolution than CW or frequency-domain techniques [227, 230, 231, 232]. A bh SPC-134 four-channel TCSPC system with four individual detectors and several multiplexed laser diode lasers was used. A fast sequence of time-of-flight distributions was recorded in consecutive time intervals of 50 to 100 ms. Variations of the optical properties in the brain are derived from the intensity and the first and second moments of the time-of-flight distributions [228].

Quaresima et al. used a single SPC-630 channel and a multi-anode PMT to record sequences of time-of-flight curves in eight parallel channels [289]. The acquisition time per step of the sequence was 166 ms. The data of five steps were averaged. Values of μ_s' and μ_a were calculated from the averaged data by using a standard model of diffusion theory.

Fig. 211 shows 20 time-of-flight curves selected from a continuous-flow sequence recorded by an SPC-134 and a H5773-20 detector. The acquisition time is 100 ms per curve, the ADC resolution 1024 channels. The left sequence was detected at a source-detector distance of 5 cm, the right sequence at a distance of 8 cm. The count rates were $1.8 \cdot 10^5 \text{ s}^{-1}$ and $4.5 \cdot 10^6 \text{ s}^{-1}$, respectively.

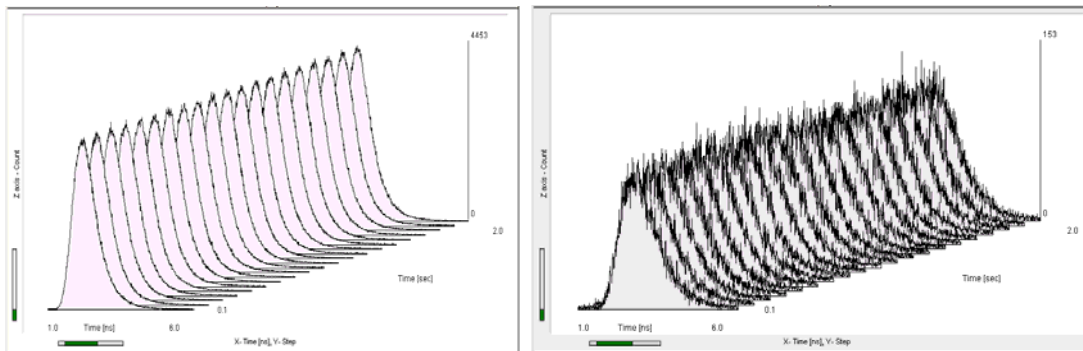


Fig. 211: 20 steps of a TOF sequence recorded in the Continuous Flow mode of an SPC-134. Acquisition time 100 ms per curve, ADC resolution 1024 channels. Left: Source-detector distance 5 cm, count rate $4.5 \cdot 10^6 \text{ s}^{-1}$. Right: source-detector distance 8 cm count rate $1.8 \cdot 10^5 \text{ s}^{-1}$

It should be noted that a count rate of $4.5 \cdot 10^6 \text{ s}^{-1}$ is at the very limit of currently available TCSPC devices. Intensity measurements at rates this high require a correction for counting loss (see ‘Counting Loss’, page 131). The moments of the time-of-flight distributions are not noticeably influenced by counting loss. This is another benefit of the moments technique developed by Liebert et. al.

The standard deviation of the photon numbers and the first moments of the data in Fig. 211, left, is about 0.15 % and 800 fs, respectively. These values are substantially lower than the typical changes caused by the haemodynamic response. In principle, useful response curves could therefore be obtained by recording only a moderate number of stimulation events. However, in practice there is a strong variation in the data due to heart beat and respiration. The haemodynamic brain response can only be separated from these effects by recording a TOF sequence over a large number of stimulation events. Therefore, all the experiments mentioned above used the ‘continuous flow’ mode of the SPC-134 or SPC-630.

Typical results of haemodynamic response measurements [227] are shown in Fig. 212. Visual stimulation was used. An annular black and white checkerboard alternating at 8Hz on a computer screen was shown to the patient. During the rest period a dark grey screen was presented while fixation was maintained. The stimulation periods lasting 30s were repeated 20 times separated by 30s of rest. Signals from 20 stimulation periods were averaged. Three multiplexed laser wavelengths were used. The photons were detected by four R7400 PMTs at different source-detector positions. The TOF curves were recorded by an SPC-134 system in the continuous-flow mode. Fig. 212, left to right, shows the intensity change, the change in the mean time of flight, and the change in the variance of the time of flight over the stimulation period. Depth-resolved intra- and extra-cerebral changes of the oxy- and deoxyhemoglobin concentrations calculated from the data of the four detectors at the three wavelengths are shown in Fig. 213.

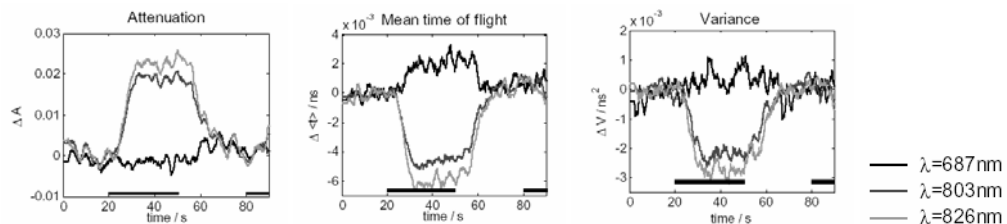


Fig. 212, Left to right: Intensity change, change in the mean time of flight, and change in the variance of the time of flight over the stimulation period. The horizontal bars indicate the periods of stimulation. From [227], Liebert et. al., Proc. SPIE 5138.

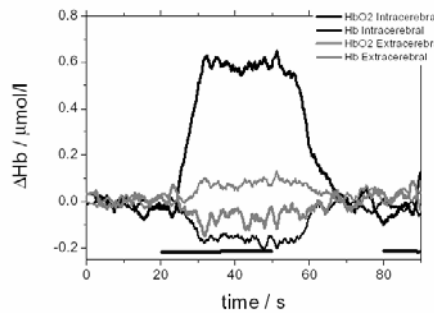


Fig. 213: Intra- and extra-cerebral changes of oxy- and deoxyhemoglobin concentrations during visual stimulation obtained from DTOFs measured at 3 wavelengths and four source-detector separations. The horizontal bars indicate the stimulation period. From [227], Liebert et. al., Proc. SPIE 5138.

Other DOT Experiments

Muscle and Bone Studies

Time-resolved DOT is sometimes used for optical biopsy of bone tissue, and to track haemodynamics and oxygen kinetics in muscle tissue. Compared with instruments used for structural brain imaging the number of source and detection channels is normally considerably reduced.

Instruments described in [98, 101, 353] used two lasers multiplexed pulse-by-pulse and eight detection channels routed into a single SPC-630 channel. An instrument described in [16] used super-continuum generation in a photonic crystal fibre and a multi-wavelength TCSPC system based on a PML-16 and an SPC-630. Absorption and scattering coefficients were obtained at 16 wavelengths simultaneously.

An instrument for optical biopsy of bones based on a diode laser and a single SPC-330 TCSPC channel was described in [118, 119]. Other instruments use a tuneable synchronously pumped dye laser and a Ti:Sapphire laser [284]. The lasers are switched into a single source fibre by a fibre switch. A single SPC-630 channel records the diffusely reflected light and a reference signal split off from the source fibre.

Exogenous Absorbers

Exogenous chromophores can be used by detecting either their absorption or their fluorescence. The only endogenous chromophore currently approved for use at human patients is indocyanine green (ICG) [256]. It absorbs strongly between 650 and 850 nm and therefore clearly shows up in the time-of-flight distributions of DOT.

ICG can be used to detect blood-flow dynamics. In the brain the absorption change after an ICG bolus shows differences in superficial and deeper blood vessels [230, 231, 232], and may be useful to indicate occlusion of vessels and areas of increased stroke risk. ICG dynamics

have also been used for breast tumor identification. Tumors usually have increased blood content, an increased number of blood vessels, and increased leakage of dye from the vessels into the tissue. Even with ICG injection, however, the contrast between tumour tissue and healthy tissue remains low. Moreover, the dwell time of ICG in the tissue is only about 10 minutes so that short acquisition times are required.

Fluorescence in DOT

For a given number of recorded photons, fluorescence detection in general yields a better intrinsic SNR than an absorption measurement. However, compared to the diffusely transmitted or reflected intensity the fluorescence intensity is much lower. The SNR actually obtained depends on the efficiency of the optics and the detection system, the tissue thickness, the fluorophore concentration and quantum yield, and the acceptable acquisition time.

Fluorescence applications in DOT are based either on the accumulation of a fluorophore in the blood or on intensity and lifetime changes induced by the local environment parameters or the binding state to proteins or lipids.

Fluorescence DOT as a diagnostic tool of human medicine is in an early stage, mainly because currently only indocyanine green (ICG) is approved for application in human patients. ICG in water has a fluorescence quantum yield of about 4% [107]. The fluorescence lifetime of ICG bound to human serum albumin (HSA) in water was determined to be double exponential, with contributions of 84% of 615 ps and 16% of 190 ps [137, 237]. The lifetime is clearly dependent on the solvent; in ethanol 600 to 650 ps are obtained. Lifetimes this short are difficult to separate from the time-of-flight distribution in thick, inhomogeneous tissue. It is therefore difficult to exploit possible lifetime changes of ICG for tissue characterisation.

The extraction of pH-induced fluorescence lifetime variations from time-of-flight curves recorded by TCSPC was studied in [132]. The fluorescence of beads stained with IRD38 (Li-Cor, Inc.) embedded in agarose phantoms was recorded by TCSPC. A femtosecond titanium-sapphire laser was used for excitation, and a H7422-50 PMT module for detection. The decay curves were recorded by an SPC-730 TCSPC module. The authors show that the fluorescence decay can be separated from the instrument response function and the time-of-flight distribution of the bulk medium.

Small-Animal Imaging

Small-animal imaging is not limited by the strict constraints placed on DOT in human patients. In particular, many exogenous chromophores are available [322]. Moreover, the typical tissue thickness is only a few millimeters, so that the excitation wavelength is not restricted to the NIR only. Visible and NUV excitation can be used to excite not only exogenous, but also a large number of endogenous fluorophores, including GFP and its mutants in transgenic organisms. The non-invasive character of DOT allows one to track the growth of a tumor, angiogenesis, invasion and metastasis, the progress of photodynamic therapy, or the action of drugs [100, 322].

A complete time-resolved small-animal imager is available from ART Advanced Research Technologies Inc., Montreal, Canada. The animal (a mouse or a rat) is placed on a platform mounted on a translation stage. Scanning in the X direction is accomplished by moving the translation stage. In the Y direction the laser beam is scanned by a galvanometer mirror. The fluorescence light is collected by a lens, descanned by a second galvanometer mirror, and detected by a PMT. The signal is recorded by an SPC-130 TCSPC module. First results were presented in [131]. Detection of a tumor in a mouse was demonstrated in [57]. A dye-labelled hexapeptide was used as a tumor marker. The marker accumulated in the tumor and the major

excretion organs. In the tumor a fluorescence lifetime of 1.03 ns was found, compared to 800 ps in other tissue.

Technical Aspects of DOT

Optical Fibres

Almost all devices for diffuse optical tomography are using fibres or fibre bundles to transmit the light from the lasers to the patient and to feed the diffusely transmitted or reflected light from the patient into the detectors. The fibres do not only simplify the optical setup but also decouple the patient electrically from the recording electronics. Unfortunately the temporal dispersion in the fibres noticeably impairs the time resolution. Moreover, the effective instrument response function (IRF) depends on the numerical aperture of the light cone coupled into the fibres. The effective aperture can be different for the recording of the IRF and the time-of-flight distribution at the patient, and severe errors in the determined optical properties can result [229]. A solution to the dispersion problem is to use a thin diffuser for IRF recording. The diffuser is placed in front of the detector fibres and illuminates the fibre with the same aperture as the sample. Because a thin diffuser does not broaden the IRF noticeably the recorded IRF shape has been found very close to the correct one [229].

Any other optical elements that can change the effective numerical aperture at the entrance or exit if a fibre or fibre bundle have to be strictly avoided. Under no circumstances an iris should be used for intensity regulation. However, also absorptive and reflective neutral density filters yield different attenuation for rays of different obliquity.

Changes of the effective NA can be particularly strong if a narrow-band interference filter is placed in the light cone in front of the fibre. The transmission wavelength of an interference filter shifts to shorter wavelength for oblique rays. With a narrow-band filter in a divergent or convergent beam, the outer part of the useful NA of the fibre can be entirely blocked by the filter. The correct solution is to put the filters into a collimated part of the beam.

Collimation of the filter beam path is important also for fluorescence detection in a DOT setup. To separate the fluorescence from the much stronger excitation light, an extremely steep long-pass interference filter has to be used. If this filter is not used in a parallel beam, the filter transition broadens towards shorter wavelengths, with disastrous effect on the blocking of the excitation light.

Detectors

The typical width of the time-of-flight distributions recorded in DOT is on the order of a few ns. Therefore a detector IRF width of 150 to 300 ps is normally sufficient. Even longer detector IRFs are sometimes tolerated, especially if the pulse dispersion in long fibre bundles dominates the IRF width. It can, however, be expected that the stability of a curve fitting procedure and the standard deviation of the first and second moments of the recorded signal shape decrease dramatically when the IRF width reaches or exceeds the true width of the time-of-flight distribution.

More important than the IRF width is the IRF stability. To reveal effects of brain activity, variations corresponding to changes in the first moment (M_1) of a few ps must be reliably recorded. Maintaining a timing stability of a few ps over a wide range of count rates is anything but simple. The most critical parts of the system are the PMT and its voltage divider.

Extremely good timing stability has been obtained with the H5773, H5783 photosensor modules and, consequently, with the bh PMC-100 detectors that are based on these modules (see Fig. 67, page 66). Also the H7422 modules yields good timing stability [46].

TCSPC-based DOT requires PMTs with a high efficiency in the NIR. Although the commonly used multi-alkali cathode works up to 820 nm, the efficiency above 750 nm is not satisfactory. Extended-red multi-alkali cathodes work well up to 850 nm. The most efficient cathodes in the wavelength range of DOT are GaAs cathodes. Although the cathode efficiency of different devices may differ considerably, a factor of 10 can be gained at 800 nm compared to a multi-alkali cathode. Currently the most frequently used GaAs PMT module is the H7422-50 [158]. Recently, Hamamatsu has developed a ‘high efficiency extended red’ cathode, the NIR efficiency of which comes close to that of the GaAs cathode. The new cathode is available in the H5773-20 and H5783-20 photosensor modules. The high timing stability, the short IRF, and the relatively low price of these modules make them the most useful single channel DOT detectors currently available. However, reasonably low dark count rates can be obtained from these detectors only when they are cooled. Therefore, the bh PMH-100-20 detector module contains a thermoelectric cooler attached to an H5773-20 photosensor module.

An ideal solution to many tomography detection problems could be large-area multi-anode PMTs. Unfortunately the most interesting ones, such as the Hamamatsu H8500 with 8 x 8 channels and 5 x 5 cm overall area, are available with bialkali cathodes only. Detectors like the H8500, but with NIR-sensitive cathodes, could give TCSPC-based optical tomography techniques a new push.

Currently available single-photon avalanche photodiodes (SPADs) are not well applicable to optical tomography. Although the efficiency in the NIR can be up to 80% [280], the detector area is only of the order of 0.01 mm². Diffusely emitted light cannot be concentrated on such small an area. SPADs manufactured in epitaxial processes are even smaller and have quantum efficiencies of less than 10% at 800 nm [179, 247]. A simple calculation shows that SPADs cannot compete with PMTs in terms of efficiency unless their active area is increased considerably. The detectors may, however, be a solution to diffuse-reflection setups with small source-detector distance.

Autofluorescence of Tissue

Biological tissue contains a wide variety of endogenous fluorophores [297]. The fluorescence spectra of endogenous chromophores are often broad and poorly defined. It is therefore difficult to separate the fluorescence components by their emission spectra alone. A considerable improvement can be achieved by simultaneous detection of the fluorescence spectrum and the fluorescence lifetime. Fluorescence lifetime detection not only adds an additional separation parameter but also yields direct information about the metabolic state and the microenvironment of the fluorophores [219, 220, 272, 376].

Most endogenous fluorophores are excited efficiently only in the UV, in the range from 280 nm to 400 nm. Traditionally, nitrogen lasers and nitrogen-laser pumped dye lasers are used for time-resolved autofluorescence measurements. These lasers work at pulse repetition rates on the order of 10 to 100 Hz. Any attempt to use TCSPC at a repetition rate this low is hopeless. This may be a reason that, in spite of its obvious benefits, TCSPC is still rarely used in autofluorescence spectroscopy of biological tissue.

However, multi-spectral TCSPC in combination with high-repetition rate NUV diode lasers, frequency-doubled or tripled Ti:Sapphire lasers or two-photon excitation have delivered excellent autofluorescence data. A few selected applications are described below.

Single-Point Multi-Wavelength Measurement

A suitable optical setup for single-point measurements of tissue autofluorescence is shown in Fig. 214, left. The setup is based on the bh ‘PML-Spec’ multi-wavelength detection system. It consists of a 405 nm picosecond diode laser, a fibre probe, a polychromator, a 16-anode PMT with routing electronics, and a TCSPC module. Multi-spectral fluorescence decay data of human skin obtained this way are shown right. The count rate was about $2 \cdot 10^6$ s⁻¹, at an excitation power of about 60 μ W.

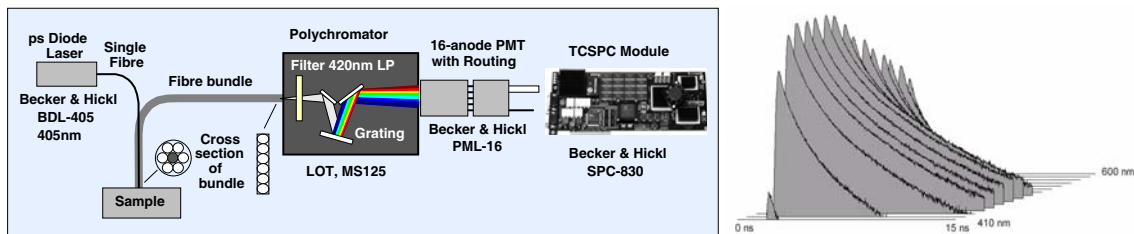


Fig. 214: Left: Optical setup for single-point autofluorescence measurement. Right: Multi-spectral fluorescence decay data of human skin. Time scale 0 to 15 ns, wavelength scale 410 to 600 nm, intensity scale logarithmic from 500 to 30,000 counts per channel

High lateral and longitudinal resolution can be obtained by using a microscope and confocal detection. Further discrimination of fluorophores is achieved by using different excitation wavelengths, e.g. several multiplexed diode lasers or the SHG of a Ti:Sapphire laser. A system with Ti:Sapphire-laser excitation has been used to identify the fluorescence components of bound and unbound NADH and FAD, and of Collagen and Keratin in different layers of epithelial layers [376].

Autofluorescence Lifetime Imaging

The same detection system (without the excitation fibre) can be connected to a laser scanning microscope and used to record multi-wavelength fluorescence lifetime images, see Fig. 182,

page 170, and Fig. 199, page 184. Macroscopic samples can, in principle, be scanned by using the same optical principles. Suggestions for the optical system are given in [46].

If the area to be imaged is no larger than a few millimeters the laser can be focused onto the tissue by a microscope lens of high numerical aperture. With a femtosecond Ti:Sapphire laser the fluorescence can be excited by two-photon excitation. The benefit of two-photon excitation is that noticeable excitation occurs only in the focal plane. An instrument with 2-photon excitation can therefore be used to record spatially 3-dimensional data. Moreover, the NIR light penetrates deeper into the tissue than NUV radiation. Therefore clear images down to a depth of several 100 μm can be obtained [200, 201, 202, 293]. Autofluorescence lifetime images of human skin recorded in a commercial two-photon laser scanning microscope are shown in Fig. 197, page 184.

Of course, a normal laser scanning microscope is inconvenient to use at a human patient. A commercial instrument for skin inspection has therefore been designed by Jenlab, Jena, Germany. The ‘Dermainspect’ is based on a Ti:Sapphire laser, a fast optical scanner, and a bh SPC-830 TCSPC module. The instrument is shown in Fig. 215. Applications are described in [201, 202, 203].



Fig. 215: ‘Dermainspect’ system of Jenlab GmbH, Jena, Germany

Ophthalmic Imaging

Reflection and fluorescence imaging of the ocular fundus is an established tool of diagnosing eye diseases [330, 299]. As usual, the fluorescence signals contain components of several fluorophores which cannot be clearly separated in intensity images. Moreover, intensity variations by oxygen quenching or different binding states cannot be distinguished from concentration variations. Fluorescence lifetime imaging is therefore considered a potential technique of diagnosing eye diseases.

A severe problem of measurements in the eye is the limitation of the excitation power. Moreover, the transmission of the eye lens drops dramatically at wavelengths below 450 nm. Wavelengths longer than 450 nm are not particularly efficient in exciting autofluorescence. The main constituents of the fundus fluorescence are components of Lipofuscin and FAD, with weak contributions from advanced glycation end products (AGE), and collagen and elastin in the connective tissue [316]. The photon flux returned from the retina is therefore low. Due to its near-ideal counting efficiency and its multi-wavelength capability, TCSPC imaging is clearly the best signal recording technique for fluorescence lifetime imaging of the retina [311, 313, 315, 316].

Ophthalmic imagers normally use a scanning technique with the pupil of the eye placed in the exit pupil of the scanning system [323]. This reduces image distortion and blurring due to the poor optical quality of the lens of the eye. Moreover, confocal detection can be used to sup-

press reflection, scattering, and fluorescence signals from the lens of the eye. Due to the scanning principle used, ophthalmic imaging can relatively easily be combined with TCSPC imaging. The general principle of an ophthalmic FLIM instrument used in [44, 313, 315, 316] is shown in Fig. 216.

The instrument uses one or two SPC-830 TCSPC modules in combination with a modified cLSO scanning ophthalmoscope (Zeiss Jena). The scanner has optical fibres both for the input of the excitation light and the output of the light returned from the fundus. Thus, it can relatively easily be combined with different light sources and detectors.

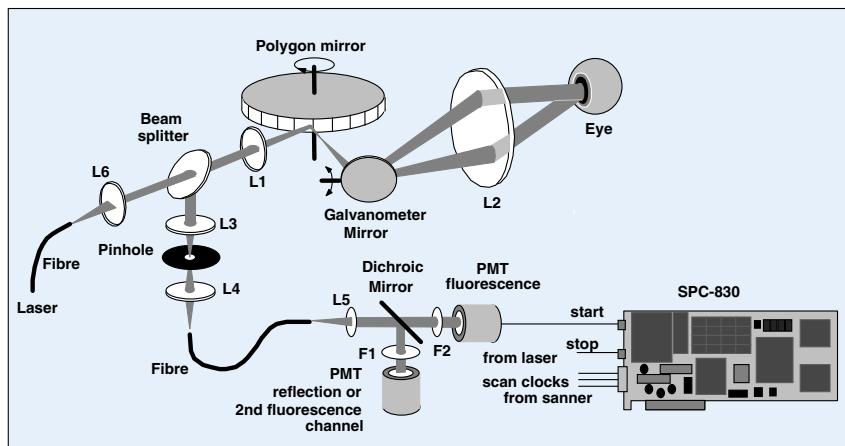


Fig. 216: Principle of the instrument used in [44, 315]

A 440 nm or 473 nm picosecond diode laser is used for fluorescence excitation. The laser beam is deflected by an ultra-fast scanner. The scanner consist of a fast-rotating polygon mirror for x deflection and a galvanometer mirror for y deflection. A lens, L1, forms a focus approximately in the middle of the polygon mirror and the galvanometer mirror. A second lens, L2, sends a parallel beam of light into the eye. The beam wobbles with the scanning, with a virtual pivot point in the pupil of the eye. The lens of the eye focuses this beam on the retina. The light emitted by the retina leaves the eye via the same beam path, travels back via the scan mirrors, and is separated from the laser light by a beam splitter. It is focused into a pinhole by a third lens, L3, and transferred to the detectors by an optical fibre.

Different detector assemblies can be used. Normally a dichroic beamsplitter and two detectors are used to detect the reflected light and the fluorescence. In this case the reflected light is detected by a low-cost side-window PMT. For fluorescence detection a fast R3809U MCP PMT is used. The wavelength intervals are selected by the dichroic mirror and two bandpass filters, F1 and F2.

However, the detection channels can also be used to detect fluorescence simultaneously in two wavelength channels [44]. In this case fast detectors have to be used on both channels. The setup described in [44] uses two R3809U MCP PMTs. The detection wavelength intervals were 500 to 550 nm and 550 to 620 nm, according to the emission maxima of flavinadenindinucleotide (FAD) and lipofuscin [220, 316]. Due to the low count rates two fluorescence detectors can be connected to one TCSPC module via a router. However, if one of the detectors is used both for fluorescence and reflected light detection it is better to connect the detectors to separate TCSPC modules [44].

The typical count rates are on the order of 1000 to 10,000 s⁻¹. Therefore acquisition times of about 10 s and 100 to 200 seconds are required for single-exponential and double-exponential analysis, respectively.

A problem associated with ophthalmologic imaging in general is that it is almost impossible for a patient to keep his eye fixed to a target point for longer than a few seconds. The vision periodically wanders off from the fixed point and jumps back. Due to the limitation of the excitation power it is impossible to collect enough photons for lifetime imaging in a time this short. The problem can be solved by acquiring a sequence of images in the Scan Sync In mode of the SPC-830 with page stepping. The images are inspected later, blurred images are discarded, and the good images are centred one over another and accumulated. The resulting data set contains enough photons in the time bins of the individual pixels to run a fit procedure of the fluorescence decay. A result is shown Fig. 217.

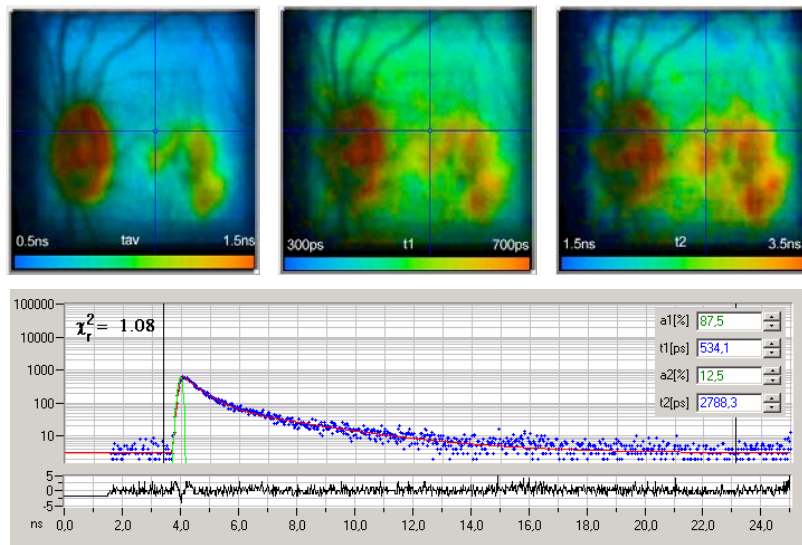


Fig. 217: TCSPC lifetime images of the human ocular fundus Upper left: Average lifetime. Upper middle: Fast lifetime component. Upper right: Slow lifetime component. Lower part: Decay curve in the selected spot and fit results. [46] and courtesy of Dietrich Schweitzer, Friedrich Schiller University Jena, Germany

The figure shows lifetime images of the amplitude-weighted average lifetime, τ_{av} , of the fast lifetime component, τ_1 , and of the slow lifetime component, τ_2 . The fluorescence decay and the result of the fit for the pixel at the cursor position are shown in the lower part of the figure.

The lifetimes are clearly dependent on the oxygen saturation, as has been proved by oxygen breathing experiments. Moreover, significant differences in the fast and slow lifetime components have been found for healthy volunteers and patients with age-related macular degeneration (AMD) [315].

Picosecond Photon Correlation

Classic light sources emit photons randomly, independent of each other. Typical examples are thermal sources or fluorescence from a large number of molecules. The distribution of the time intervals between successive photons drops exponentially for increasing time intervals.

For light generated by nonlinear optical effects and fluorescence of single molecules [15], single quantum dots [245, 346, 384, 387] or other semiconductor nano-structures this is not necessarily the case. A molecule cannot perform a new absorption-emission cycle before the previous one is completed. Similar effects are observed in semiconductor nanostructures. Thus the fluorescence photons are no longer independent of each other - the distribution of the photons drops at times shorter than the lifetime of the excited state. The opposite can happen by nonlinear optical effects in crystals. An example is parametric downconversion. Such effects can literally split one photon of the pump radiation into two, which are then highly correlated [249, 250, 251]. Investigation of all these effects requires the detection and correlation of photons on the ps and ns scale.

Picosecond photon correlation experiments have some similarities to fluorescence correlation spectroscopy (FCS). FCS investigates the fluctuations of the fluorescence intensity of a small number of molecules confined in a small sample volume (see 'Fluorescence Correlation Spectroscopy', page 206). The intensity fluctuations are correlated on a time scale from microseconds to milliseconds. Therefore, FCS differs from typical picosecond correlation experiments in the way the photons are correlated. Moreover, FCS effects are driven by diffusion, intersystem crossing, conformational changes, or other sample-internal effects, while typical picosecond correlation effects are driven by the absorption of the photons of the excitation light.

Optically driven photon correlation experiments normally require confining the detection or the excitation to a sample volume on the order of femtoliters. This is achieved either by confocal detection or two-photon excitation in a microscope. The optical principles are the same as in confocal and two-photon laser scanning microscopes, see Fig. 178, page 165. However, most correlation experiments do not require fast scanning and can be performed in relatively simple microscopes.

The classic photon correlation experiment records a histogram of the time intervals between the photons of the investigated signal [15, 159]. Unfortunately, the detector dead time makes it impossible to detect the photons in a single detector and to measure the times between the photons on the ps time scale. Moreover, ringing in the detector, reflections in the detector signal, and afterpulsing preclude a reasonable correlation of the pulses from a single detector on a time scale below 100 ns. The problem of the detector dead time is avoided by the Hanbury-Brown-Twiss setup [159]. This setup is the basis of almost all TCSPC photon correlation experiments.

The principle is shown in Fig. 218. The investigated light signal is split by a 1:1 beam splitter, and the two light signals are fed into separate detectors. One detector delivers the start pulses, the other the stop pulses of a TCSPC device. The stop pulses are delayed by a few ns to place the coincidence point in the centre of the recorded time interval. The setup delivers a histogram of the time differences between the photons at both detectors. Because separate detectors are used for start and stop, there is no problem with the detector dead time.

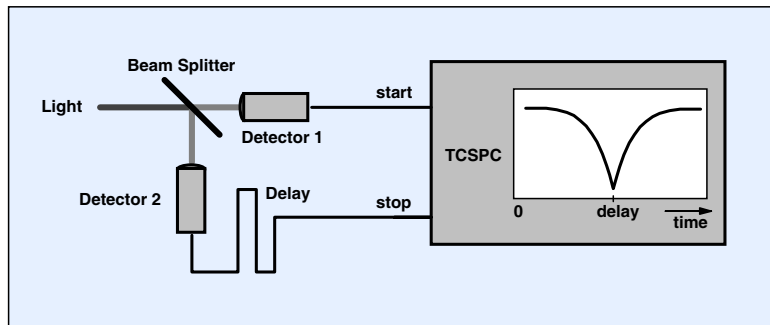


Fig. 218: Dual-detector (Hanbury-Brown Twiss) photon correlation setup

Antibunching

In fluorescence experiments the Hanbury-Brown-Twiss setup can be used with continuous excitation or with excitation by picosecond pulses. Continuous excitation of a small number of fluorescent molecules delivers the typical ‘antibunching’ curve [15]. An example is shown in Fig. 219. The curve was recorded with two H7422-40 PMT modules (Hamamatsu) connected to one channel of a bh SPC-134 TCSPC package.

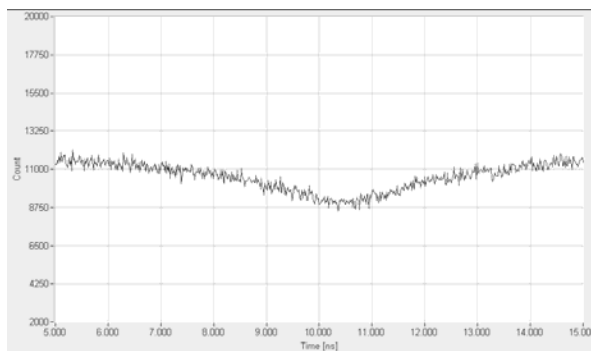


Fig. 219: Antibunching curve for Rhodamine 110, CW excitation, one SPC-134 channel, H7422-40 detectors, 1 ns/div

Similar TCSPC-based antibunching experiments have been used to investigate single photon emission from optically [346, 387] and electrically [384] driven quantum dots.

The setup shown in Fig. 218 is also used for experiments based on parametric downconversion. A nonlinear crystal produces photon pairs the energy of which is equal to the energy of the pump photons. The measurement then delivers a correlation peak on a baseline of randomly detected background photons. The effect can be used for tests of quantum mechanics and a number of metrological applications [64]. The measurement of absolute detector quantum efficiencies by using photon pairs generated by parametric downconversion [215, 249, 250, 251, 290, 369] is shown in Fig. 248, page 230.

Antibunching experiments with pulsed excitation are described in [127] and [370]. The measurement delivers a number of correlation peaks spaced by the laser pulse interval. If the laser pulse width is much shorter than the fluorescence lifetime there is almost no chance that a single molecule is excited several times within one laser pulse. Consequently, the emission of a photon pair from a single molecule becomes extremely unlikely. The ratio of the height of the central coincidence peak to the adjacent peaks is therefore an indicator of the number of the molecules in the excited volume, see Fig. 220.

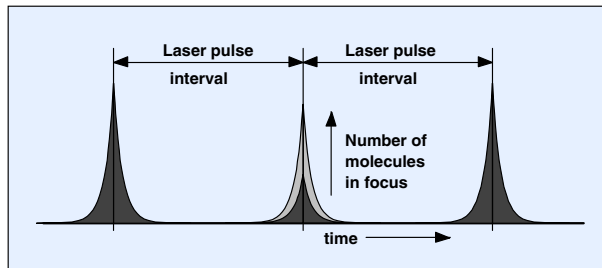


Fig. 220: Anti-bunching with pulsed excitation. The result is a train of correlation peaks spaced by the laser pulse period. The height of the central correlation peak depends on the number of molecules in the focus.

Technical Aspects

Because the correlation experiments described above are simple start-stop experiments they can be performed with any bh TCSPC module. For experiments with PMTs the SPC-x30 modules should be preferred because these allow the user to define a discriminator threshold both in the start and the stop channel (see ‘CFD in the Synchronisation (Stop) Channel’, page 44).

The coincidence rate (the rate of complete start-stop events) of the Hanbury-Brown-Twiss experiment is normally very low. At the light intensity obtained from typical samples, it is relatively unlikely that two photons appear within a time interval of a few nanoseconds. Consequently the coincidence rate depends on the square of both efficiency of the optical system and the detector efficiency. The design of the optical system and the selection of the detectors are therefore crucial points of photon correlation experiments.

Most photon correlation experiments use single photon avalanche photodiodes (SPADs), especially the SPCM-AQR detectors of Perkin Elmer [280]. However, these detectors often experience timing shift and transit time jitter dependent on the wavelength and the count rate. Although the timing drift of both detectors of a Hanbury-Brown-Twiss experiment may partially compensate, it is difficult to obtain a time resolution better than 0.5 ns or to investigate changes in the correlation function versus intensity.

A troublesome effect of SPADs is light emission from the APD. When an avalanche is triggered in the APD, a small amount of light is emitted. The effect and its implications for photon correlation experiments and quantum key distribution are described in detail in [356] and [213]. If the detectors are not carefully optically decoupled, false coincidence peaks appear. The effect on TCSPC correlation measurements and the way to avoid artefacts are discussed in [46].

Timing instability and optical crosstalk can be avoided by using PMTs with high-efficiency GaAsP photocathodes, such as the Hamamatsu H7422-40 module [158]. The IRF of these has a width of 200 to 350 ps. The IRF is almost independent of the wavelength and remains stable up to count rates in the MHz range. The quantum efficiency reaches 40% around 500 nm, see Fig. 58, page 59.

Fluorescence Correlation Spectroscopy

Principle

Fluorescence correlation spectroscopy (FCS) is based on exciting a small number of molecules in a femtoliter volume and correlating the fluctuations of the fluorescence intensity. The fluctuations are caused by diffusion, rotation, intersystem crossing, conformational changes, or other random effects. The technique dates back to a work of Magde, Elson and Webb published in 1972 [235]. Theory and applications of FCS are described in [51, 294, 295, 296, 318, 319].

The required femtoliter volume can be obtained one-photon excitation and confocal detection or by two-photon excitation. The principle is the same as in a laser scanning microscope, see Fig. 178, page 165. A continuous or high-repetition rate laser beam is focused into the sample through the microscope objective lens. The fluorescence light from the sample is collected by the same lens, separated from the laser by a dichroic mirror, and fed through a pinhole in the upper image plane of the microscope lens. In a confocal microscope the fluorescence light from above or below the focal plane is not focused into the pinhole and therefore is substantially suppressed. With a high-aperture objective lens the effective sample volume is of the order of a femtoliter, with a depth of about 1.5 μm and a width of about 400 nm. A similarly small sample volume can be obtained by two-photon excitation. Typical FCS devices use one detector or two detectors working in different wavelength intervals. More detectors can be added to correlate photons in more than two wavelength intervals, or photons of different polarisation.

FCS and fluorescence lifetime experiments are often used in combination to explore the fluorescence dynamics of dye-protein complexes. The traditional approach is to acquire FSC and lifetime data in separate experiments [169, 320]. However, almost all bh TCPCS devices are able to record lifetime data and FCS data simultaneously [43, 46]. The advantage compared to the traditional approach is that FCS and lifetime data originate from the same sample, from the same spot of a sample, or even from the same molecules. TCSPC data can therefore be used to distinguish between different types of molecules, different quenching states, or different binding or conformation states of dye-protein complexes. It is also possible to calculate higher-order correlation or to include lifetime variations in the correlation [252, 378, 345, 383]. Moreover, the same raw data can be used to for FIDA (fluorescence intensity distribution), FILDA (fluorescence intensity and lifetime distribution), and BIFL (burst-integrated fluorescence lifetime) analysis. The principle of TCSPC-based FCS is shown in Fig. 221.

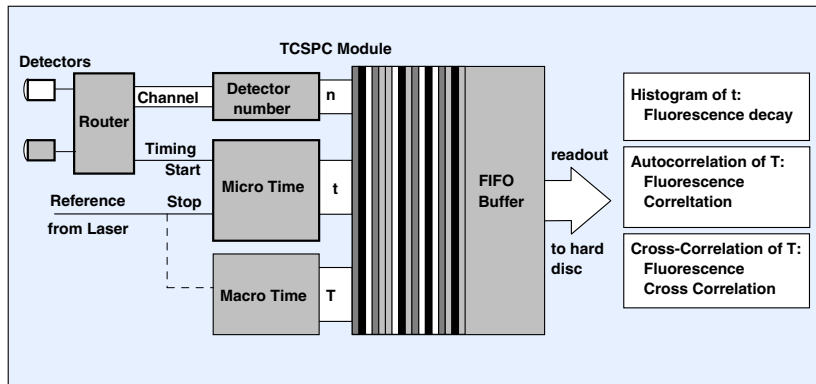


Fig. 221: Combined FCS and fluorescence lifetime recording by TCSPC

The single-photon pulses of the detectors are fed into a router. For each photon detected in any of the detectors, the router delivers a single-photon pulse and the number of the detector that detected the photon. The TCSPC module is operated in the ‘FIFO’ mode. It determines the time of the photon in the laser pulse sequence (the ‘micro time’) and the time from the start of the experiment (‘macro time’). The detector number, the micro time, and the macro time are written into a first-in-first-out (FIFO) buffer (see also ‘Time-Tag Recording’, page 31). The output of the FIFO is continuously read by the computer, and the photon data are written in the main memory of the computer or on the hard disc. By analysing the photon data fluorescence decay curves and FCS curves are obtained. The decay curves of the individual detectors are obtained by building up the histograms of the micro times, fluorescence correlation curves by correlating the macro times of the photons. Cross-correlation curves are obtained by correlating the macro time of the photons of different detectors.

For photon counts, N , in successive, discrete time channels the autocorrelation function, $G(\tau)$, is

$$G(t) = \sum N(t) \cdot N(t + \tau)$$

In typical FIFO mode data, the clock period of the macro time, T , is shorter than the dead time of the TCSPC device. Therefore only one photon can be recorded at a particular macro time. Consequently, $N(t)$ and $N(t + \tau)$ can only be 0 or 1. The multiplication in the autocorrelation function becomes a simple compare (or an exclusive-or) operation, and the integral of the autocorrelation becomes a shift, compare, and histogramming procedure. The calculation of FCS from TCSPC data is illustrated in Fig. 222.

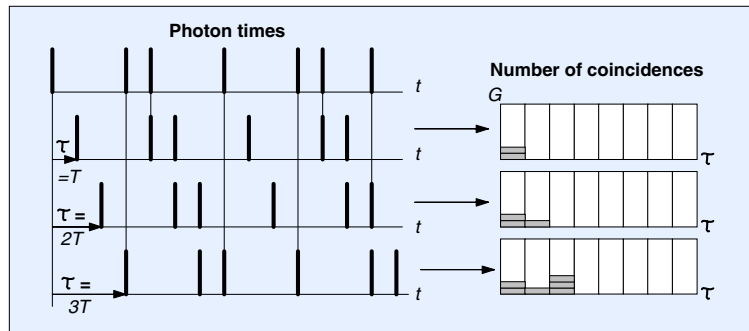


Fig. 222: Calculation of the autocorrelation function from TCSPC time-tag data

The times of the individual photons are subsequently shifted by one macro time clock period, T , and compared with the original detection times. The coincidences found between the shifted and the unshifted data are transferred into a histogram of the number of coincidences, G , versus the shift time, τ . The obtained $G(\tau)$ is the autocorrelation function.

The cross-correlation function between two signals is obtained by a similar procedure. However, the photon times of different signals are compared.

The result obtained by the shift-and-compare procedure is not normalised. Normalisation can be interpreted as the ratio of the number of coincidences found in the recorded signal to the number of coincidences expected for an uncorrelated signal of the same count rate. The normalised autocorrelation and cross-correlation functions are

$$G_n(\tau) = G(\tau) \frac{n_T}{N_P^2}$$

with n_T = total number of macro time intervals, Np = total number of photons, and

$$G_{ncross}(\tau) = G_{cross}(\tau) \frac{n_t}{N_{P1}N_{P2}}$$

with N_{P1} = total number of photons in signal 1, N_{P2} = total number of photons in signal 2.

The described procedure yields $G(\tau)$ in equidistant τ channels equal to the macro-time clock period, T . There is no distortion of the correlation function or of the photon statistics by binning. This is an advantage if a model has to be fit to the obtained function. The downside is that the number of τ channels is extremely high, especially if $G(\tau)$ is calculated up to large values of τ , and that the noise in the individual τ channels does not decrease with increasing τ . The curves therefore have a different appearance than the results of the multi- τ algorithm commonly used in ‘hardware’ correlators. One way to obtain a similar result as the multi- τ algorithm is to apply progressive binning to the calculated $G(\tau)$ data. Another way is to periodically apply binning steps to the photon data during the $G(\tau)$ calculation. The SPCM operating software of the bh TCSPC modules has both algorithms implemented (see ‘FIFO Mode Run-Time Display’, page 282).

A typical result of TCSPC FCS is shown in Fig. 223 and Fig. 224. A GFP solution was excited by a femtosecond Ti:Sapphire laser. The detector was an SPCM-AQR module from Perkin Elmer, the TCSPC module an SPC-830. The count rate integrated in 1 s intervals fluctuated between 5 and 7 kHz. The total acquisition time was 980 seconds.

Fig. 223 shows the fluctuations of the photon flux integrated in 1 ms intervals over an interval of one second. Fig. 224 shows the fluorescence decay function over several laser periods and the FCS function.

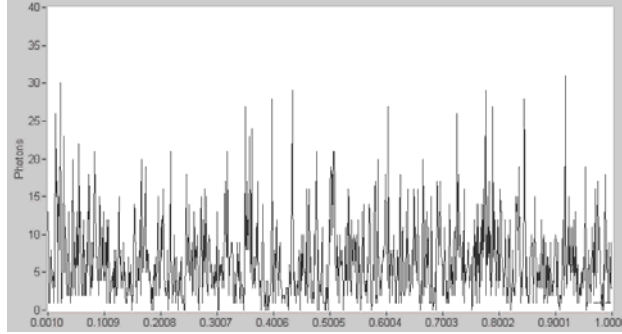


Fig. 223: GFP solution excited by Ti:Sapphire laser. Fluctuation of the photon counts in 1 ms intervals over a 1 s interval of the data stream [43, 46]

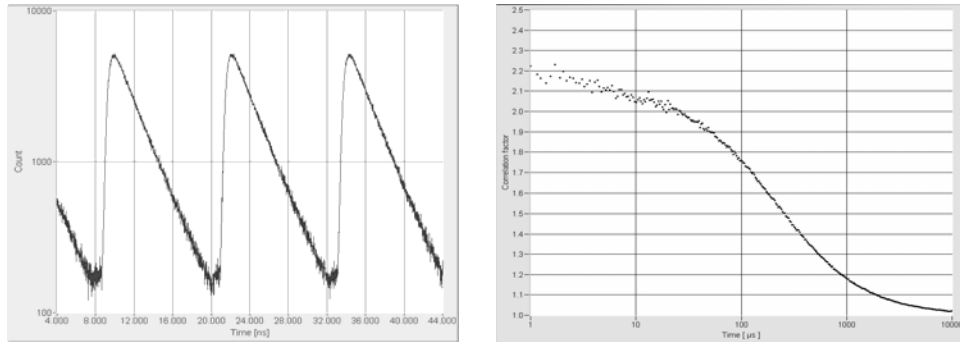


Fig. 224: Fluorescence decay curve (left) and FCS curve (right) of a GFP solution. Count rate 5 to 7 kHz, acquisition time 980 s. From [43, 46].

FCS in Live Cells

A laser scanning microscope with TCSPC-FLIM by multi-dimensional TCSPC can, in principle, be used for FCS as well. The TCSPC technique has the benefit that high-quality lifetime images, fluorescence correlation and cross-correlation data, and precision single-point lifetime data can be recorded in a single instrument and from the same sample [43, 45]. The general requirements are a TCSPC module that can be operated in the ‘Scan Sync In’ and in the ‘FIFO’ mode, and a scanning microscope with a beam parking function of high spatial stability. In practice the stability of the beam position can be a problem. Even if beam jitter is not noticeable in normal imaging operation, it can make the recorded data useless for correlation. Therefore not all laser scanning microscopes are suitable for FCS experiments. Moreover, the detectors in TCSPC FLIM microscopes are usually selected for high time resolution, not for highest efficiency and low afterpulsing. FCS recording can therefore require a relatively long acquisition time. Currently the best detector for combined FLIM and FCS operation is the H7422-40 module.

It should also be noted that FCS measurements in cells are more difficult than in solution. Especially in transfected cells the fluorophore concentration cannot be accurately controlled. It is usually much higher than required for FCS. The number of molecules in the focus can easily be on the order of 100, resulting in an extremely small amplitude of the correlation function. Moreover, there is usually motion in living cells that shows up in the FCS curves at a time scale above 100 ms. Nevertheless, useful FCS data can be obtained.

Fig. 225 shows an FSC recording obtained in a two-photon laser scanning microscope [43, 45]. The FLIM image was obtained in the Scan Sync In mode and is shown at left. After the FLIM recording a single-point FIFO measurement was performed in the marked spot. The acquisition time of this measurement was 130 s, at an average count rate of $15 \cdot 10^3 \text{ s}^{-1}$. A fluorescence decay curve and an FCS curve in a selected spot are shown in the middle and at right. Please note the small amplitude of the FCS curve. The maximum of the correlation coefficient is only 1.016, compared to 2.2 for the GFP solution (Fig. 224).

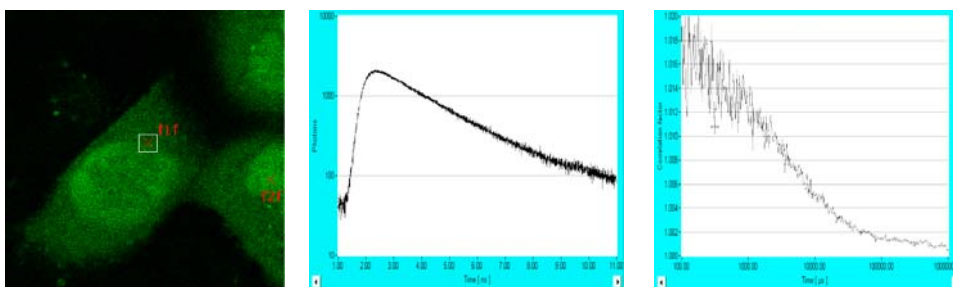


Fig. 225: FLIM image (left), decay curve (middle) and FCS curve (right) recorded in a selected spot (1). Home-made laser scanning microscope, two-photon excitation, SPCM-AQR detector, SPC-830 TCSPC module. [43] and courtesy of Zdenek Petrasek and Petra Schwille, Biotec TU Dresden.

Scanning FCS

A frequently asked question is whether or not FCS data recording and scanning a sample can be combined. It is, of course, generally impossible to scan a sample at a scan rate on the order of the photon times to be correlated. The frame time must either be faster than the shortest correlation time, which is practically impossible, or the pixel time must be longer than the correlation time interval. It should, therefore, be possible to obtain FCS images of moderate pixel numbers by scanning a sample at a pixel dwell time much longer than the longest time to be correlated.

Scanning is either performed by the scanner of a laser scanning microscope, or a scan stage is used to scan the sample in one or two directions. The scan controller delivers three control signals - a ‘pixel’ signal that changes its state at the transition to the next pixel, and a ‘line’ signal that changes its state at the transition to the next line.

The easiest way to record FCS scanning data is to use an SPC-140/144 or SPC-150/154 module in the ‘FIFO Imaging’ mode, see page 285. The FIFO imaging mode records a FIFO data file that contains markers at the beginning the transition from one frame to the next, one line to the next, and one pixel to the next. Simultaneously, an image is calculated from the photon data and displayed on-line. The data format of the FIFO file is described under ‘FIFO Files’, page 335. The data can easily be used to calculate FCS in the individual pixels. The basic setup is shown in Fig. 226, left. Instead of the scan stage, the confocal scanner of a laser scanning microscope can be used. The system configuration is identical with that of a FLIM system, see Fig. 179 and Fig. 180, page 167.

A solution for SPC modules which do not have the FIFO imaging mode is shown in Fig. 226, right. The scan control pulses of the microscope (line clock and pixel clock) are divided by two, which can be easily accomplished by a single SN 74 HCT74 CMOS device.

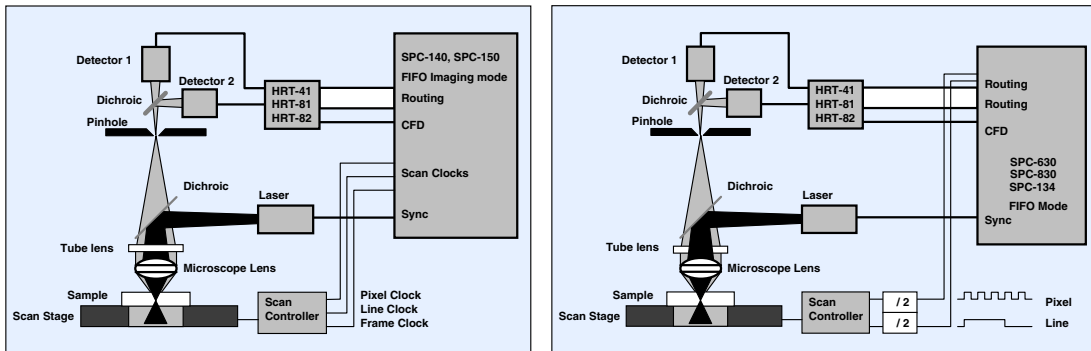


Fig. 226: Combination of FCS with scanning. Left: For SPC-140/144 and SPC-150/154. Right: For SPC-630, SPC-830, and SPC-130/134

The scan signals are fed into two of the unused routing input bits of the TCSPC module. The scan rate is made slow enough to get a full FCS recording in each pixel. This requires a time of several seconds. In this time a large number of photons is recorded so that all transitions of the ‘pixel’ and ‘line’ signals appear in the data stream. Therefore, the scanning action can be tracked by analysing the state of the pixel and line signals in the data file, and separate FCS functions for the individual pixels can be calculated.

However, the acquisition time of an FCS scan must be expected extremely long. Even for samples that deliver near-perfect correlation, e.g. single molecules spread over a solid substrate, at least a few seconds acquisition per pixel are required. For living cells with hundreds of molecules per pixel and correspondingly small correlation coefficients the acquisition times must be considerably longer. It is therefore unlikely that FCS images with the same pixel numbers as in laser scanning microscopy can be obtained.

Correlation of Delayed Detector Signals

A single TCSPC module detecting via several detectors and a router (see Fig. 221) is unable to record several photons within the dead time of the TCSPC module. The signals of the detectors therefore cannot be correlated at a time scale shorter than the dead time. The problem can be solved by routing of delayed detector signals [370]. The principle is shown in Fig. 227.

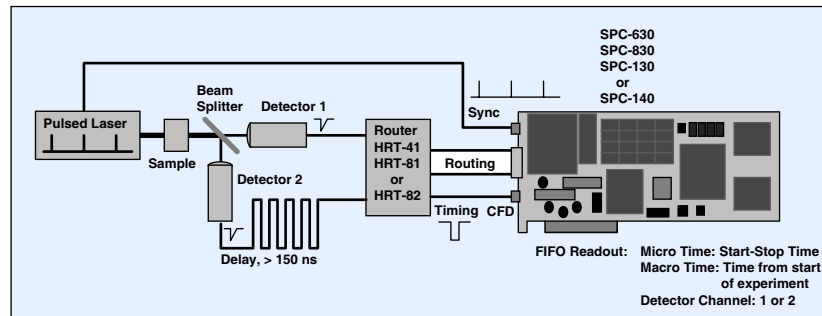


Fig. 227: Routing of delayed detector signals

Several detectors are connected via a router to the same TCSPC module. The photon pulses from the second detector are delayed by more than the dead time of the TCSPC module. More than two detectors can be used if their delay lines are different by more than the module dead time. The stop pulses for the TCSPC module come from the pulsed laser, or, if a CW laser is used, from an external clock generator. Due to the different delay of the detector signals, photons detected simultaneously do not arrive simultaneously at the router inputs. Therefore, photons detected in the same laser pulse period are recorded at different times and stored in the FIFO data file with a macro time offset. The differences in the macro times caused by the delay line in front of the router are known and can be corrected for when the photons are correlated.

The setup shown in Fig. 227 was used to track the intensity fluctuations, the lifetime, and the number of molecules in the laser focus simultaneously [370]. An application to single-molecule FRET is described in [175].

Fluorescence Correlation down to Picoseconds

A single TCSPC channel is able to deliver FCS data down to a correlation time of the module dead time, i.e. about 100 to 125 ns. Correlation on a time-scale shorter than the dead time is obtained by using a system of two or more synchronised TCSPC channels. The system configuration is shown in Fig. 228.

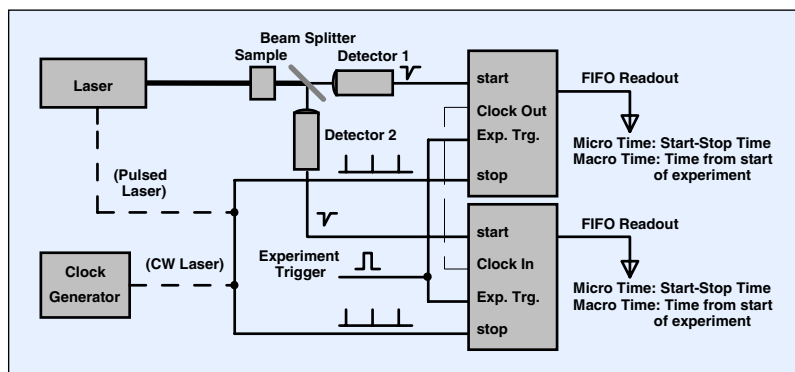


Fig. 228: Correlation setup with two synchronised TCSPC modules

The start pulses for the TCSPC modules come from the detectors, the stop pulses from the laser, or, if a CW laser is used, from an external clock source. To make the detection times in both modules comparable, the internal macro time clocks of the modules must be synchronised. This is achieved either by a clock interconnection, i.e. by using the internal macro time clock of one module for both, or by using the stop signals (i.e. the reference pulses from the laser) as macro time clocks (please note that the SPC-130/134, SPC-140/144, SPC-150/154

and SPC-830 modules have this option). Of course, the recording must be started simultaneously in all modules by an external experiment trigger. The setup can be used to cross-correlate the signals from both detectors down to the minimum macro-time period accepted by the TCSPC modules, i.e. about 10 ns.

Correlation down to the picosecond time scale is possible by including the micro times of both modules in the calculation of the correlation function. The problem with this approach is that the micro time scales of the modules may be slightly different, and the macro time transitions may be shifted due to different transit times in the detectors, cables and TCSPC modules. Correcting all these effects is extremely difficult, yet not impossible. Suitable calibration and correlation algorithms were developed by S. Felekyan et al. [127]. The authors demonstrate the technique for a Rhodamine 110 solution. A typical correlation curve is shown in Fig. 229.

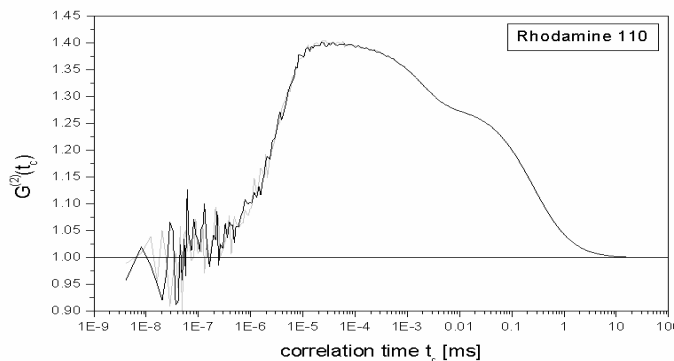


Fig. 229: Correlation curve covering a continuous range from 10 ps to 100 ms obtained by correlating two synchronised SPC-130 modules. Correlation of detector A vs. detector B (grey) and detector B vs. detector A (black). Courtesy of S. Felekyan, R. Kühnemuth, V. Kudryavtsev, C. Sandhagen, and C.A.M. Seidel

By fitting a suitable model to the data the diffusion time, the antibunching time, the triplet lifetime, and the mean triplet population was obtained. In principle, the technique is able to reveal also conformational changes of dye-protein complexes, FRET effects, and rotational depolarisation.

Practical Tips

TCSPC-FCS with CW Excitation

The TCSPC-FCS technique can also be used in conjunction with a continuous laser. Of course, a single TCSPC module in this case does not deliver a meaningful micro time, and no lifetime data are obtained. However, the macro times of the recorded photons can be used to calculate FCS curves. Because the TCSPC module needs a synchronisation pulse to finish the time measurement for a recorded photon, an artificial stop pulse must be provided. This can be the delayed detector pulse itself or a signal from a pulse generator; see Fig. 230.

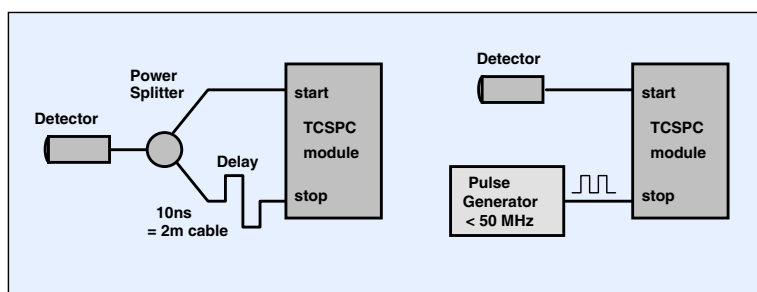


Fig. 230: Stop pulse generation for TCSPC-FCS with a continuous laser

The additional cable length in the SYNC path should be about 2 m, corresponding to about 10 ns start-stop time. If a pulse generator is used the pulse period should be shorter than 20 ns. Unnecessarily long delay cables or long pulse periods cause unnecessarily long start-stop times and, consequently, increase the dead time and the counting loss. In any case, the cable delay and the signal period of the pulse generator must be shorter than the recorded TAC time interval (TAC Range / TAC Gain).

Interference of the Laser Period with the Recording Clock

If FCS experiments are excited by a pulsed laser the laser pulse repetition frequency can interfere with the macro time clock frequency. The result is a periodical variation of the number of laser pulses per macro-time period. The same period shows up in the correlated intensity. Periodicity can appear on any time scale, depending on the difference of the laser and macro-time clock frequencies or their harmonics. The problem is most pronounced if both frequencies are almost identical. In the bh SPC-830, SPC-130/134, SPC-140/144 and SPC-150/154 modules the problem is anticipated by providing an optional clock path from the timing reference (Sync) input to the macro time clock, see ‘FIFO Mode’, page 281. The macro time clock is then synchronised with the laser pulse repetition rate, which removes the problem entirely. Moreover, using the Sync signal as a macro time clock is a simple way to synchronise several TCSPC channels of a multi-module system, see Fig. 228. Of course, using the Sync input as a clock source for FCS requires that the Sync signal is free of glitches.

Detectors

Compared to fluorescence decay measurements, the efficiency of FCS measurements is relatively low. For a given number of photons, N, the SNR of a fluorescence decay measurement is proportional to $N^{1/2}$, whereas the SNR of FCS is proportional to N itself. This somewhat surprising behaviour results from by the fact that two photons are needed to obtain one macro-time coincidence in the correlation histogram. The strong dependence of the SNR on the count rate makes detection efficiency an important issue in FCS.

Most FCS setups therefore use single photon avalanche photodiodes [226, 291], usually SPCM-AQR detectors from Perkin Elmer [280]. The SPCM-AQRs have a quantum efficiency that reaches almost 80% at 800 nm. However, the SPCM-AQRs often have a timing delay dependent on wavelength and count rate. The changes can be of the order of 1 ns, see Fig. 71, page 69. Recording a fluorescence decay curve with a detector this unstable delivers questionable results.

Better timing stability can be achieved with SPADs manufactured in epitaxial processes, such as the id 100-20 of id Quantique [179] and the PDM 50 CT of Micro Photon Devices [247]. The quantum efficiency up to 550 nm is comparable, above 650 nm lower than for the SPCM-AQR.

Timing problems can be entirely avoided by using PMTs with high-efficiency GaAsP photocathodes, such as the Hamamatsu H7422-40 module [158]. The modules have a stable and almost wavelength-independent transit time spread of about 300 ps duration. The quantum efficiency reaches 40% at 550 nm, see Fig. 58, page 59.

Afterpulsing

All photon counting detectors show a more or less pronounced afterpulsing (see ‘Afterpulsing’, page 60). Afterpulsing causes a steep rise of the autocorrelation function towards short times in the range below one microsecond.

The absolute amount of afterpulsing in PMTs increases with the gain. Reducing the operating voltage of a PMT while increasing the preamplifier gain therefore helps, but does not remove

the problem entirely. Moreover, the height of the afterpulsing peak in the autocorrelation function is proportional to the reciprocal count rate. The reason is that the probability of detecting an afterpulse of a previously detected photon is constant, whereas the probability of detecting another photon increases with the count rate. The effect of the count rate on the afterpulsing peak in the correlation function is shown in Fig. 231.

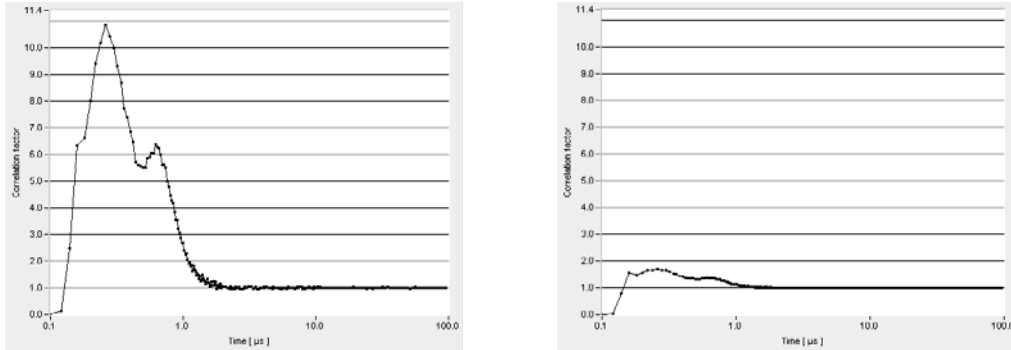


Fig. 231: Effect of the count rate on the height of the afterpulsing peak. H74222-40 detector, count rate 10 kHz (left) and 100 kHz (right)

Afterpulsing can be almost entirely rejected from FCS results by cross-correlation. The light is split into two equal beams that are detected by individual detectors. Afterpulses in one detector are not correlated with any counts in a second detector and therefore do not noticeably change the cross-correlation function. An example for two H7422-40 detectors is shown in Fig. 232. Curves a and b are the autocorrelation curves of the individual detectors. Curves c and d are cross-correlation curves of the signals of detector 1 against detector 2 and vice versa. The afterpulsing is almost entirely removed in the cross-correlation.

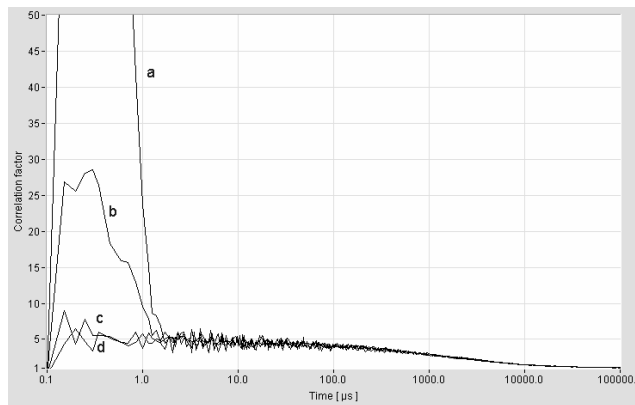


Fig. 232: Rejection of detector afterpulsing by cross correlation. GFP solution, two H7422-40 detectors, 2-photon excitation, LSM 510 NLO microscope in beam-stop mode. Curves a and b: Autocorrelation of the signals of the two detectors. Curves c and d: Cross-correlation detector 1 against detector 2 and vice versa.

Background Signals

Background signals are a frequent source of failure in attempts to record FCS curves. Background signals may result from detector background, leakage of daylight, leakage of excitation light, emission of LEDs within the microscope, spurious laser emission at different wavelengths, or fluorescence of filters. The background reduces the apparent correlation coefficient or even makes the fluorescence correlation entirely undetectable.

It is often difficult to identify the sources of the background. In pulsed excitation systems, the amount of background can easily be estimated from the recorded fluorescence decay: Any

intensity that remains after the fluorescence has decayed is caused by background effects. Leakage from room lights has a strong correlation at the line frequency. The light can therefore be identified by checking the autocorrelation function in the 20-ms range. Other sources of background light can often be removed by bandpass filters in the excitation and detection beam path. In two-photon systems background light can often be reduced by using a pinhole in a conjugate focal plane. Although the pinhole is not required for two-photon FCS it suppresses background signals which do not come from the excited sample volume.

Beam Jitter

Instability of the beam position results in a distortion of the FCS curves or, in most cases, in a de-correlation of the fluorescence signal. Complete de-correlation occurs if the beam jitters faster than the average photon count rate. Subsequent photons then come from different molecules and are not longer correlated.

Sample Volume

Fluorescence correlation functions can, of course, only be obtained if the focal volume is small enough. For two-photon excitation through a good microscope lens this is achieved (almost) automatically. For one-photon excitation a pinhole must be placed in a plane conjugate with the focus in the sample. The diameter of the pinhole depends on the magnification on the way from the sample to the pinhole. High-end microscopes have objective lenses corrected for infinite conjugate ratio, i.e. the fluorescence light leaves the back aperture of the lens in a parallel beam. The light is focused into the eyepiece plane by a tube lens. A pinhole placed in this plane should have a diameter that is approximately the airy disc diameter multiplied by the power of the objective lens. Often an additional lens is placed in front of the pinhole. In this case, the magnification is approximately the ratio of the focal lengths of the microscope lens and the lens in front of the pinhole. The required pinhole diameter is therefore considerably smaller than without the lens.

Optical Aberrations

FCS measurements in solution are often done in the setup shown in Fig. 233, left. A cover slip is placed directly on top of the microscope lens of an inverted microscope. A droplet of a diluted dye solution is placed on the cover slip. The same setup is often used for testing the FCS capability of laser scanning microscopes.

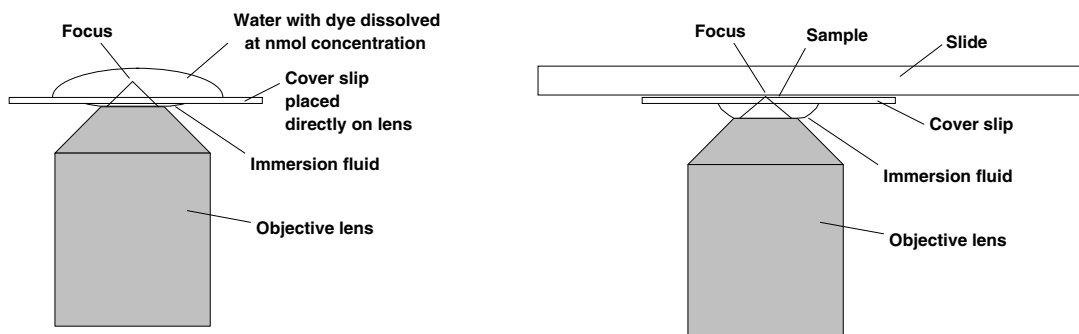


Fig. 233: FCS measurement of a dye solution. Left: Cover slip placed directly on microscope lens, sample solution placed on cover slip. A large part of the beam path is in the sample. Right: Correct optical configuration, the beam path is in the immersion fluid.

The setup is simple and easy to use. It does, however, pose a serious pitfall to inexperienced users. The microscope lens is corrected for a beam path that has a defined spacing (the ‘working distance’) between the lens and the cover slip, see Fig. 233, right. This gap is filled with the immersion fluid. In the commonly used setup of Fig. 233, left, however, the working dis-

tance is above the cover slip, i.e. in the dye solution. The dye is normally dissolved in water, or a solvent of similar index of refraction. The setup of Fig. 233, left, therefore works only for a water immersion lens. For an oil immersion lens the mismatch of the refractive index is so severe that a reasonably small focal volume is not obtained. Consequently, a TCSPC FIFO measurement shows a fluorescence decay curve, but no fluorescence correlation.

If you want to run an FCS test measurement with an oil immersion lens you may use the setup shown in Fig. 233, right. However, because of the low fluorescence intensity of a highly diluted dye solution it is difficult to find the right focal plane. Moreover, fluorescence of the glass of the slide may be a problem. It is therefore easier to use the setup shown in Fig. 233, left, and fill the working distance with one or two cover slips of appropriate thickness (use immersion oil between them). This reduces the index mismatch and will allow you to record at least some correlation function. Or you may use immersion oil as a test solution. Low fluorescence grade immersion oil usually contains enough fluorescent contamination the fluorescence decay and FCS functions of which can be recorded.

FCS with Commercial Laser Scanning Microscopes

The confocal and non-descanned detection paths of laser scanning microscopes are not necessarily designed (and specified) for FCS detection. It is therefore not guaranteed that the beam stability in the beam park mode, the efficiency, the confocal detection volume and the background suppression will meet the requirements of FCS. Nevertheless, many confocal and multiphoton laser scanning microscopes can be used for FCS. When the microscopes are upgraded with a bh FLIM system they can therefore often be used not only for FLIM but also for FCS.

TCSPC System parameters suggested for combined decay and FCS measurement in a single detector channel are shown in Fig. 234. The recommended main panel configuration is shown in Fig. 235 (see also ‘Configuration of the SPC Main Panel’, page 233).

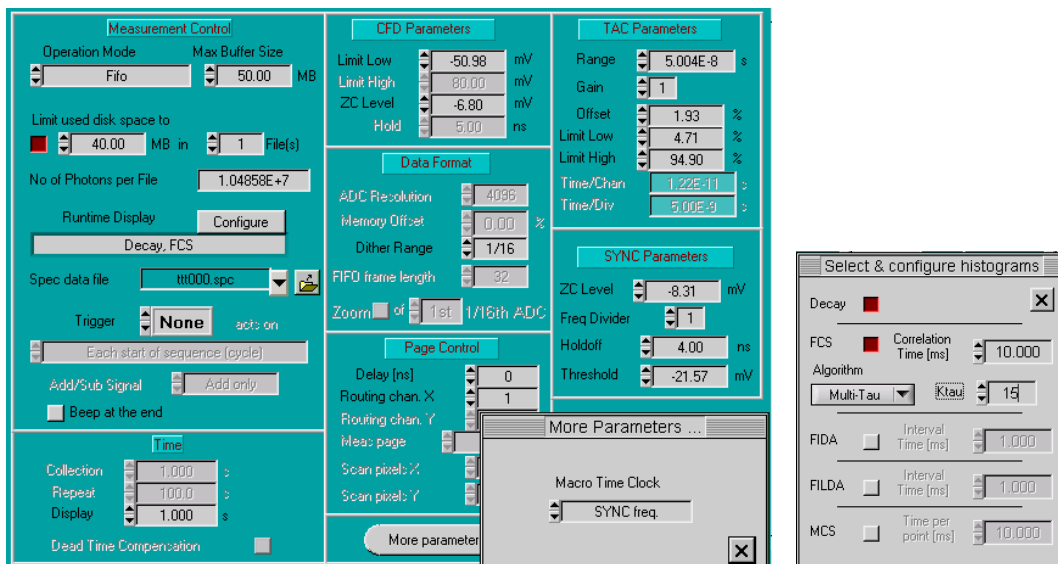


Fig. 234: System parameters for combined decay and FCS measurement

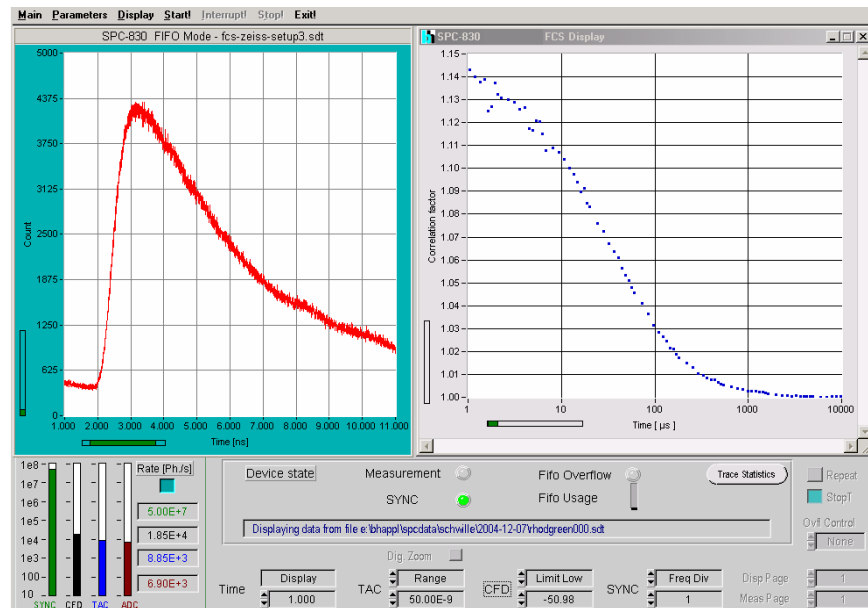


Fig. 235: Main panel configuration for combined decay and FCS measurement

For FCS measurements it is important that the beam be parked in the spot of interest and that the detection volume is confined to less than a few femtoliters. The pinhole of a confocal system must therefore be set to a diameter of approximately 1 airy unit. Also the alignment of the pinhole is important. If your microscope allows you to optimise the lateral and longitudinal position of the pinhole it is recommended to do so. Two photon systems with the detectors in the non-descanned detection path are sometimes plagued by large background signals. Operation in absolute darkness and correct spectral filtering is important for these systems. Both in one-photon and in multiphoton microscope it is important that refractive-index mismatch of the microscope lens is avoided. Therefore, either use a water immersion lens or follow the hints given under ‘Optical Aberrations’.

Fig. 236 shows FCS curves obtained in an LSM 510 NLO multiphoton microscope. H7422-P40 detectors were used at the two outputs of the NDD module. The sample was a diluted solution of protein-GFP constructs. Two-photon excitation at 860 nm was used.

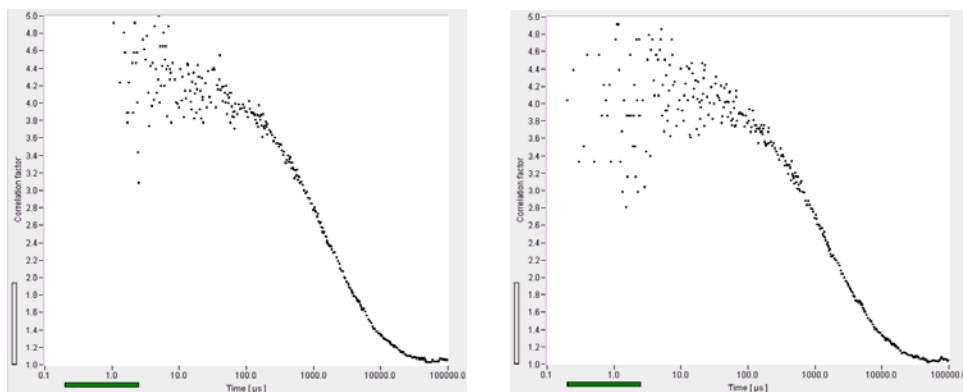


Fig. 236: FCS functions measured in an LSM 510 NLO multiphoton microscope. SPC-830 FLIM module, two H7422P-40 detectors attached to the NDD module. Left: Autocorrelation of one detector. Right: Cross-correlation between both detectors.

Fig. 236, left, shows the autocorrelation function of one detector channel, Fig. 236, right the cross-correlation between both detector channels. Because both detectors were used at the same wavelength the results are identical down to a correlation time of 1 μs. Below 1 μs the

autocorrelation function is impaired by detector afterpulsing. Afterpulsing does not appear in the cross-correlation. Therefore the right curve shows correlation data down to 125 ns, i.e. the dead time of the SPC-830.

Suppression of Raman Scattering and Detector Background

Raman scattering in the solvent can be a serious problem in FCS measurements. Raman lines can often be suppressed by filters. However, if the lines are within the fluorescence band of the molecules to be measured filtering becomes difficult. TCSPC in combination with pulsed excitation offers a second way to suppress the Raman signal. Because Raman scattering is a ‘prompt’ process the Raman signal forms a sharp peak at the beginning of the fluorescence decay function, see Fig. 237, left. The Raman signal can therefore be suppressed by time-gating [221]. Time gating can be achieved in the data analysis, i.e. by correlating only photons with micro times longer than the temporal location of the Raman peak. Another way is to use the TAC limit parameters to exclude the peak from being correlated. This is especially efficient in the SPC-130, -140 and -150 modules, where the TAC limits cause a sharp cutoff in the recorded data. In the SPC-630 and -830 satisfactory gating can be obtained by using a ‘dither width’ of 1/32.

Fig. 237, left shows a recording without gating. The fluorescence decay is shown left, the FCS curve right. Fig. 237, right shows a recording from the same sample with time gating. A comparison of the decay curves shows that the amplitude of the FCS curve (and consequently the signal-to-noise ratio) is increased by the gating.

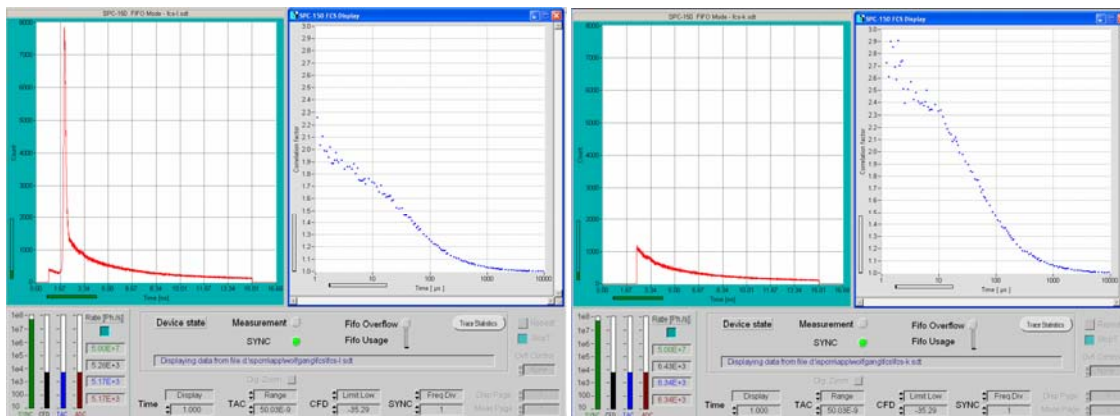


Fig. 237: Left: Ungated FCS recording. The sharp peak in the decay curve is caused by Raman scattering. Right: Gated FCS recording. The Raman peak is suppressed, with a corresponding increase of the correlation coefficient.

The same technique can be used to partially suppress short-lifetime fluorescence of contaminants. A partial suppression of continuous background signals, e.g. dark counts or slow luminescence of optical components, can be achieved by gating off late photons.

Important: If you use your own software to calculate FCS functions from FIFO data please remember that photons outside the TAC window are recorded but marked as ‘invalid’, see ‘FIFO Files’, page 335. TAC gating therefore requires these photons to be excluded from the correlation procedure.

Time-Resolved Single-Molecule Spectroscopy

The techniques described under ‘Picosecond Photon Correlation’ and ‘Fluorescence Correlation Spectroscopy’ exploit the correlation between the photons emitted by single molecules or by a small number of molecules. Picosecond photon correlation techniques investigate effects driven by the absorption of a single photon of the excitation light. The effects investigated by FCS are driven by Brownian motion, rotation, diffusion effects, intersystem crossing, or conformational changes. Because of these random and essentially sample-internal stimulation mechanisms, correlation techniques do not necessarily depend on a pulsed laser.

A second way to obtain information about single molecules is time-resolved spectroscopy with pulsed excitation at high repetition rate. The borderline between correlation techniques and time-resolved single-molecule spectroscopy is flowing and somewhat artificial. In general, time-resolved single-molecule spectroscopy delivers spectroscopic information about *individual* molecules by recording the fluorescence in a short period of time. Photon correlation techniques normally derive average molecular properties from the observation of *different* molecules over a longer period of time.

The optical systems used for both techniques are essentially the same. A small sample volume is obtained by confocal detection or two-photon excitation in a microscope. Several detectors are used to detect the fluorescence in different spectral ranges or under different angles of polarisation. Therefore correlation techniques can be combined with fluorescence lifetime detection, and the typical time-resolved single-molecule techniques may use correlation of the photon data. This paragraph focuses on single-molecule experiments that not only use, but are primarily based on pulsed excitation and time-resolved detection. An overview of time-resolved single-molecule spectroscopy is given in [46].

Burst-Integrated Fluorescence Lifetime (BIFL) Techniques

Molecules diffusing in a solution or travelling through a capillary are in the focus of a microscope lens for a time of a few hundred microseconds to a few milliseconds. Immobilised molecules under high excitation power cycle between the S₀/S₁ (singlet) states and the non-fluorescent triplet state. The fluorescence signal therefore consists of random bursts corresponding to the transit of individual molecules through the focus or to the dwell time in the singlet state. Under typical conditions, from a highly fluorescent molecule a few hundred photons are detected within a single burst. The idea behind burst-integrated fluorescence lifetime detection, or BIFL, is to identify the bursts of the molecules, obtain spectroscopic information within the bursts, and thus characterise the individual molecules.

BIFL by Sequential Recording

Lifetime detection within individual bursts was accomplished even with early PC-based TCSPC modules, such as the SPC-300 and SPC-330 [259, 385]. Software-controlled sequencing or an external counter connected to the routing inputs was used to record a sequence of fluorescence decay curves. The time per curve was typically 10 ms, the number of curves per sequence 128. Of course, a resolution of 10 ms per curve did not yield reliable information about the burst duration and the burst size. Therefore, often intensity tracing and FCS recording were performed in parallel by a multi-channel scaler (MCS) and a correlator [386]. The technique was applied to single-molecule identification in a capillary [386] and to the identification of antigen molecules in human serum [306].

Far better burst resolution was obtained by bh TCSPC modules with an internal sequencer. In particular, sequencing in combination with memory swapping (the ‘continuous flow’ mode) was used to record a virtually infinite sequence of decay curves in time intervals of 100 µs and shorter [33, 347]. A part of a sequence recorded this way is shown in Fig. 238.

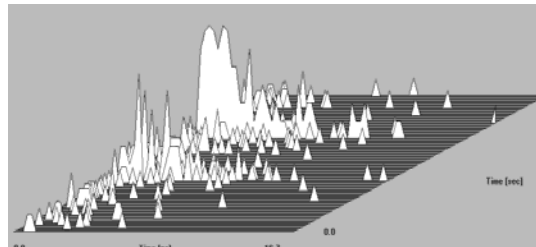


Fig. 238: Bursts of single molecules. Part of a longer sequence recorded by sequencer-controlled memory swapping. 1 ms per step of the sequence, 64 ADC channels.

A burst is identified by detecting more than a defined number of photons in several successive steps of the sequence. For fluorescence-lifetime calculation, the photon distributions of all time-steps within the burst are accumulated and the lifetime is obtained by a maximum-likelihood algorithm [88, 194, 195, 307]. A histogram of the lifetimes obtained in a large number of bursts yields information about the homogeneity of the molecules and their local environment. Information about the quantum efficiency or ‘molecular brightness’ is obtained by building up a histogram of the burst size. For freely diffusing molecules the diffusion time constant can be estimated from a histogram of the burst duration. In a capillary the histogram of the burst duration is an indicator of the speed of the molecules.

Burst-recording in the continuous-flow mode can be combined with multi-detector operation. The detectors can be used to record the fluorescence in different wavelength intervals or under different angles of polarisation. This ‘multi-parameter’ detection technique delivers the lifetime, the angle of polarisation, the fluorescence anisotropy, and the emission wavelength within the individual bursts [307, 347].

For a burst resolution around 1 ms, detection by the continuous flow mode is relatively efficient in terms of data size. The drawback of the continuous flow mode is that the burst resolution is limited by the increase of the data size and, and consequently, by the available data readout rate [46].

BIFL by Time-Tag Recording

BIFL results with a burst resolution down to the laser pulse period can be obtained by recording the photons in the ‘FIFO’ or ‘time-tag’ mode of TCSPC, see ‘Time-Tag Recording’, page 31. Because the full information about all photons is recorded time-tag data are extremely flexible. Conformational dynamics, rotational relaxation, and intersystem crossing can be investigated at almost any time scale [120, 121, 210, 347].

An impressive practical demonstration of the technique was given in [287]. A frequency-doubled mode-locked Nd-YAG laser delivers pulses of 532 nm wavelength, 150 fs pulse width, and 64 MHz repetition rate. The laser is coupled into the beam path of a microscope and focused into the sample. The sample is mounted on a piezo-driven sample stage. The fluorescence light from the sample is collected by the microscope lens and separated from the excitation light by a dichroic mirror and a notch filter. The light is split into its 0° and a 90° components. The 0° component is further split into a short-wavelength and a long-wavelength component. The signals are detected by SPAD modules and recorded by a single bh SPC-431 TCSPC module via a router. The TCSPC module records the photons in the FIFO mode.

The molecules to be investigated are embedded in polymethylmethacrylate (PMMA). An image of the sample is obtained by scanning and assigning the photons to the individual pixels by their macro time. Based on this image, appropriate molecules are selected for further investigation.

These molecules are then brought into the focus and time-tag data are acquired. By analysing these data a surprisingly large number of spectroscopic parameters can be determined. The intersystem crossing yield is obtained from a histogram of the number of photons in the bright periods. The histogram of the dark periods reflects the triplet decay and delivers the triplet lifetime. The fluorescence lifetime is obtained by building up the fluorescence decay functions from the micro times.

The polarisation of the fluorescence is obtained by comparing the counts in the SPAD detecting under 0° polarisation with the counts in both SPADs detecting the 90°. The anisotropy decay can be calculated from the micro times of the photons in these detector channels. The authors show that there is some rotational relaxation, in spite of the solid matrix in which the molecules are embedded. They derive the initial and final anisotropy, the angle of the cone of wobbling, and the rotational correlation time.

The authors managed even to observe the spectral relaxation of single molecules. They placed a dichroic mirror between two SPADs, with a transition in the centre of the fluorescence band of the molecule being investigated. The spectral relaxation is obtained from the ratio of the counts of these detectors in the individual time channels. For the spectral relaxation of an Alexa 546 molecule conjugated to a single protein a spectral shift of 4 nm and a spectral relaxation time of 0.3 ns was found [287].

The same instrument was used to monitor conformational changes in the citrate carrier CitS [184]. A version of the instrument uses an annular aperture stop in the beam path of the microscope. With this stop, different Airy disks are obtained for different orientation of the dipoles of the molecules [326, 327]. Comparing the observed intensity patterns of the molecules with calculated diffraction patterns makes it possible to derive the 3D orientation of the molecules. In [208] the lifetime of DiI molecules in a 20 nm polymer film at a glass surface is investigated by this technique. The lifetime varied between 4.7 ± 0.7 ns and 2.11 ± 0.1 ns, depending on the orientation of the molecules to the surface.

Correlation of Lifetime Fluctuations

Spontaneous conformational fluctuations of biomolecules are closely related to fluctuations in the enzymatic rate constant and have therefore become subject of a large number of single-molecule experiments. The fluctuations occur in a wide range of time scales from microseconds to hundreds of seconds. Conformational changes can be investigated by single-molecule FRET techniques or by optically induced electron transfer between an electron donor and an electron acceptor within the same biomolecule. The corresponding changes in the fluorescence can be investigated by BIFL techniques, FCS, or by recording photon counting histograms within different sampling time intervals. Direct information about the rate of the fluctuations can be obtained by correlating fluorescence lifetimes obtained from single molecules within millisecond sampling time intervals. The technique was demonstrated by Yang et al. [383]. The lifetime changes were attributed to electron transfer between FAD and nearby residues, such as Trp and Tyr. For every 100 photons a fluorescence lifetime was obtained by a maximum likelihood estimation. The lifetimes were converted into electron transfer rates and

distances, which were correlated subsequently. A similar experiment with electron transfer in a fluorescein-tyrosine pair within a single protein complex was described in [252].

Identification of Single Molecules

Identification of single molecules has relevance for spectroscopic DNA sequencing and drug screening. Molecules can be identified by using the fluorescence lifetime, the fluorescence anisotropy, the lifetime in conjunction with the emission wavelength, and the burst size and duration.

Identification purely based on the fluorescence lifetime is described in [125]. The true shape of the signal, i.e. the convolution of the IRF with the expected decay function, is pre-calculated for different molecules. The photon distributions in the individual bursts are then compared with these pre-calculated functions. The rhodamine derivatives JF9, JA67, and JA53 were identified with an error rate between 0.1 and 0.01.

The problem of pure lifetime identification is that the lifetime differences are often relatively small. Moreover, there may be some variation in the lifetime of a single type of molecule due to different local environments. It is therefore useful to add more parameters to the identification algorithm. By using the fluorescence anisotropy, rhodamine 133 and EYFP were identified with only 1% misclassification [307].

Prummer et al. used the lifetime and the emission wavelength for on-line classification of molecules [286]. A dichroic mirror splitted the fluorescence into two wavelength intervals, which were detected by two SPAD modules (SPQ141, EG&G). The pulses of the APDs were connected into a bh SPC-402 module via an HRT-82 router. Classification was performed online in the incoming FIFO data stream. The procedure uses a lookup table that returns the probability that a photon originates from a particular type of molecule as a function of the micro time and the wavelength channel. The identification procedure starts when the time lag between 50 consecutive counts is below 2 ms. The probabilities are accumulated for successive photons until the molecule is identified or the time lag between 50 consecutive counts exceeds 2 ms. The technique was demonstrated for the dyes rhodamine 6G (R6G), sulforhodamine B (SRB), dibenzanthranthene (DBATT), and 1,1'-dioctadecyl-3,3,3',3'-tetramethyl-indocarbocyanine perchlorate (DiI). Identification required less than 300 photons per molecule.

Photon Counting Histograms

The photon counting histogram (PCH) of an optical signal is obtained by recording the photons within successive sampling-time intervals and building up the distribution of the frequency of the measured counts versus the count numbers. For a light signal of constant intensity the PCH is a Poisson distribution. If the light fluctuates, e.g. by fluctuations of the number of fluorescent molecules in the focus of a laser, the PCH is broader than the Poisson distribution. A characterisation of the PCH was given in 1990 by Qian and Elson [288]. The technique is also called fluorescence intensity distribution analysis, or FIDA. The principle is explained in Fig. 239.

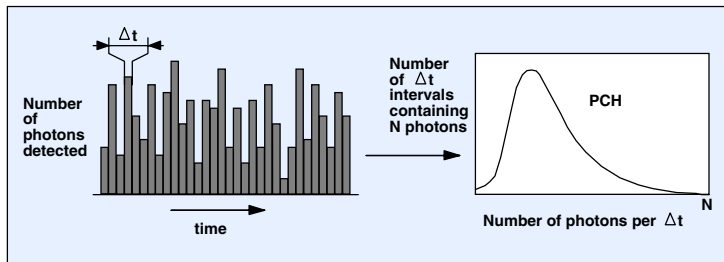


Fig. 239: Photon counting histogram. Left: Photons counted in successive sampling time intervals. Right: Histogram of the number of time intervals containing N photons

The optical setup for PCH experiments is the same as for BIFL or one-photon or two-photon FCS. The sample is excited by a laser through a microscope objective lens. The effective sample volume is confined to a few femtoliters by two-photon excitation or by confocal detection. PCH recording requires a high-efficiency detector and a multichannel scaler that records either the photon counts in successive time bins or the time-tag data for the photons.

The optimum sampling time interval depends on the time-scale of the fluctuations and is usually in the 10 μs to 1 ms range. Recording directly into fixed time bins yields relatively compact data sets. Time-tag recording yields more flexibility and is usually preferred. Time-tag data can be used to calculate several PCHs in different sampling time intervals, and to calculate FCS curves and PCHs from the same data. A photon counting device for PCH measurement is described in [122].

The PCH delivers the average number of molecules in the focus and their molecular brightness. Several molecules of different brightness can be distinguished by fitting a model containing the relative brightness and the concentration ratio of the molecules to the measured PCH. The technique is also called ‘fluorescence intensity distribution analysis’, or FIDA. The theoretical background is described in [75, 76, 185, 187, 258, 267, 268, 288].

The PCH/FIDA technique can be extended for two-dimensional histograms of the intensity recorded by two detectors in different wavelength intervals or under different polarisation. 2D FIDA delivers a substantially improved resolution of different fluorophores [186, 187]. Further improvement is achieved by using pulsed excitation and using the fluorescence lifetime as an additional dimension of the histogram. The techniques is termed ‘Fluorescence Intensity and Lifetime Distribution Analysis’ or FILDA [187, 267]. Of course, accurate lifetimes cannot be obtained from the small number of photons within the individual sampling time intervals. However, useful lifetime information may be obtained from the photon arrival times in the laser period averaged over the sampling time interval. The average arrival time is directly related to the first moment of the decay function and therefore to the fluorescence lifetime.

FIDA, 2D-FIDA and FILDA do not directly deliver information about the diffusion times of the fluorescent species. Diffusion times can, however, be obtained by calculating the PCHs in different sampling time intervals and fitting the result with a model that contains both the molecular brightness and the diffusion time [187].

In principle, FIDA, 2D-FIDA, and FILDA are possible by using any bh TCSPC module that has the FIFO mode implemented. The data recorded in the FIFO mode contain the individual arrival time of each photon in the laser pulse sequence, the time from the start of the experiment, and the number of the detector that detected the photon. Thus, both decay curves, FCS curves and PCHs can be calculated from these data. The PCHs can obtained for each individual detector and for virtually any sampling-time interval. Data measured at a solution of Rhodamin 6G molecules attached to a protein are shown in Fig. 240.

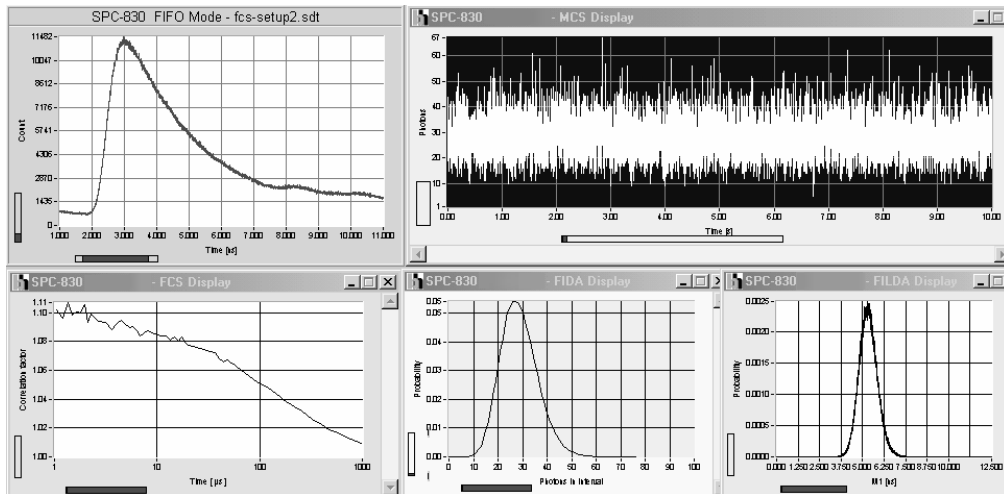


Fig. 240: Decay curve, intensity (MCS) trace, FCS curve, photon counting histogram and lifetime histogram for a Rhodamine 6G solution. Sampling times for photon counting and lifetime histograms 1 ms, time per channel of MCS trace 1 ms. Two-photon excitation, SPC-830 TCSPC module with SPCM software, acquisition time 490 s, count rate $28 \cdot 10^3 \text{ s}^{-1}$.

Fig. 241 shows distributions of the average photon arrival time for different sampling time intervals. The average arrival time is identical with the first moment of the photon distribution and, except for a constant offset, represents the fluorescence decay time. The width of the distribution contains both the statistical variance of the arrival time and the real inhomogeneity of the lifetimes of the molecules. If the sampling time is reduced, the number of photons per time interval decreases, and distribution of the arrival time becomes wider. For very small sampling time intervals most of the time intervals contain either no photon or one photon. The distribution of the arrival time then converges into the fluorescence decay curve. Multi-exponential analysis of the decay curve is, in principle, a second way to reveal inhomogeneity of the lifetimes.

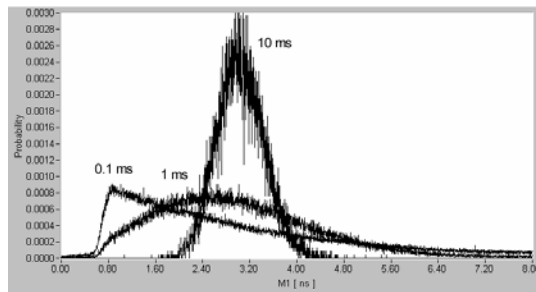


Fig. 241: Distribution of the first moment, $M1$, of the photon arrival times, calculated from TCSPC time-tag data. Sampling time interval 100 μs , 1 ms, and 10 ms. SPC-830 TCSPC module, count rate 3000 photons per second.

Although TCSPC is used successfully for BIFL experiments, little has been published about applications for FIDA. The reason is probably that the dead time of TCSPC is considered a drawback. However, a simple consideration shows that the detectable burst rate is not substantially reduced by the dead time of the TCSPC device. The commonly used detectors lose 50% of the photons at an input rate of about $16 \cdot 10^6 \text{ s}^{-1}$ [280], fast TCSPC modules (SPC-140/144) at $10 \cdot 10^6 \text{ s}^{-1}$. This means the dead time of the TCSPC module is only slightly shorter than the dead time of the detector. The use of TCSPC for PCH experiments therefore does not result in a considerable increase of dead-time-related errors. Moreover, BIFL applications have shown that the burst count rates are well within the counting capability of TCSPC.

Two-Photon Excitation by Picosecond Diode Lasers

Two-photon excitation has become a standard technique in laser-scanning microscopy and fluorescence correlation spectroscopy. The excitation wavelength is twice the absorption wavelength of the molecules to be excited. Because two photons of the excitation light must be absorbed simultaneously, the excitation efficiency increases with the square of the excitation power density. The technique requires pulsed excitation with high peak power, i.e. femtosecond pulses, and focusing into a diffraction limited volume within the sample. In most cases Ti:Sapphire lasers are used for two-photon excitation [103, 360, 361].

Two-photon fluorescence excitation with a picosecond diode laser cannot be expected to work with the same efficiency. The average intensity is only a few mW. Moreover, the pulse duration is of the order of 100 ps, so that the peak power is many orders of magnitude lower than for a femtosecond Ti:Sapphire laser. The question whether two-photon excitation at a noticeable level can be obtained by a picosecond diode laser may therefore appear a bit academic. However, two-photon excitation by a diode laser may be reasonable, e.g. for fluorescence excitation deeply within a highly absorbent sample.

It can indeed be demonstrated that two-photon excitation by a picosecond diode laser delivers fluorescence signals that can easily be detected by TCSPC [46]. A result is shown in Fig. 242.

A bh BHL700 laser was used for excitation. The laser emits at a wavelength of 785 nm. The average power of the laser was adjusted to approximately 10 mW. The pulse width at this power was about 300 ps FWHM. The laser beam was focused into a 1-mm sample cuvette by a microscope objective (NA = 0.4). The relatively low NA was used to obtain a convenient working distance to the sample cuvette. The fluorescence light was detected from the back of the cuvette. 6 mm of Schott BG39 filter glass was used to block the laser light from the detector. The fluorescence light was detected by a Hamamatsu H7422P-40 photomultiplier module connected to a bh SPC-730 TCSPC module.

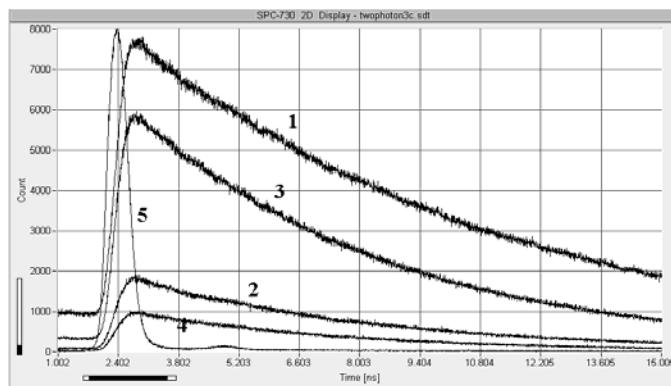


Fig. 242: Fluorescence decay curves obtained by two-photon excitation. 1) Rhodamin 6G, 10^{-3} mol/l in ethanol, 2) Rhodamin 6G 10^{-4} mol/l in ethanol, 3) Fluorescein Na 10^{-3} mol/l in pH 7.4 buffer, 4) Fluorescein Na 10^{-4} mol/l in pH 7.4 buffer, 5) Laser pulse

Curves 1, 2, 3 and 4 are the recorded decay functions of Rhodamin 6G, 10^{-3} mol/l, Rhodamin 6G 10^{-4} mol/l, Fluorescein 10^{-3} mol/l and Fluorescein 10^{-4} mol/l. Curve 5 is the laser pulse, detected through ND filters without the NIR blocking filters. The count rates were 4500 s^{-1} , 900 s^{-1} , 3000 s^{-1} and 400 s^{-1} , respectively. The overall acquisition time was 3000 s each. The fluorescence lifetimes are 5.4 ns and 7.9 ns for the 10^{-4} mol/l and 10^{-3} mol/l Rhodamin 6G solutions, and 4.7 ns and 5.6 ns for the 10^{-4} mol/l and 10^{-3} mol/l Fluorescein solutions. The increase of the lifetime with the concentration can be explained by re-absorption.

Re-absorption is more critical for two-photon than for one-photon excitation, because locations much deeper in the sample can be excited.

The efficiency can certainly be improved by using a lens of higher NA, by using a low-pass filter with a steeper transition than the BG 39, and by matching of the laser wavelength and the absorption maximum of the fluorophores. All in all, an improvement in the detected count rate by a factor of 10^2 to 10^3 appears feasible. If this is correct, two-photon diode-laser-excited fluorescence can be detected from a large number of marker dyes in biologically relevant concentrations.

Barrier Discharges

The study of barrier discharges (also referred to as dielectric barrier discharges or silent discharges) is important for understanding mechanisms of degradation and breakdown of insulators as well as the reactions in the gas of the discharge. A barrier discharge consists of a large number of micro-discharges of nanosecond duration. The micro-discharges appear at random times and random locations over the surface of an insulator.

The general principle of a barrier-discharge experiment [63, 205, 206, 207, 365, 366, 367] is shown in Fig. 243. The barrier discharge occurs between two glass-coated electrodes. The electrical field between the electrodes is driven by a high-voltage transformer. The input signal of the transformer is generated by a digital waveform generator, in this case a bh PPG-100.

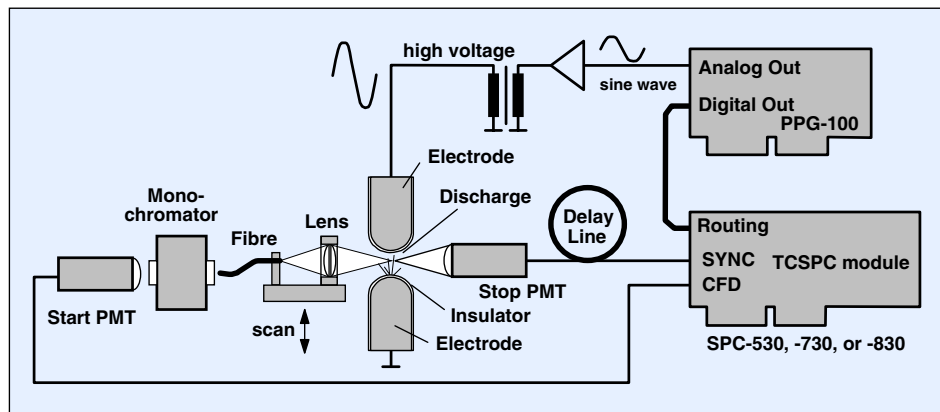


Fig. 243: Detection barrier discharges. The pulse shape is recorded as a function of the voltage across the discharge gap, the wavelength, and the location in the discharge gap

Because the discharges occur at random times the stop signal for the TCSPC module is generated from the light pulses themselves. The stop detector is a bh PMH-100 module operated at a gain below the single-photon detection level. It delivers a timing reference signal of relatively low jitter (see ‘Generating the Reference Signal’, page 89). The pulses of the stop PMT are delayed and fed into the SYNC (stop) input of the TCSPC module.

The light from the other side of the discharge gap is focused on the input of an optical fibre and fed into a monochromator. The light of the selected wavelength is detected by the start PMT. Due to the low numerical aperture and narrow wavelength interval transmitted by the monochromator, the light intensity at the detector is much lower than at the stop detector. Therefore the start PMT detects single photons at a rate considerably lower than the average rate of the discharge pulses. The single-photon pulses are used as start pulses of the TCSPC module and processed in the ordinary way.

The waveform generator feeds a digital equivalent of the sine-wave voltage into the routing input of the TCSPC module. When a photon is detected, it is written into a memory block corresponding to the momentary voltage and into a time channel corresponding to its time referred to the stop pulse. Therefore the TCSPC module records the photon distribution over the voltage across the discharge gap and the time within the discharge duration. A large number of such distributions are obtained sequentially by scanning the monochromator wavelength or the fibre position along the discharge gap.

Theory and various results are described in [63, 205, 206, 207, 365, 366, 367]. An overview of typical results is given in [46].

Positron Lifetime Measurements

Positron lifetime measurements can be used to investigate the type and the density of lattice defects in crystals [209]. In solid materials positrons have a typical lifetime of 300 to 500 ps until they annihilate with an electron. When positrons diffuse through a crystal they may be trapped in crystal imperfections. Since the electron density in these locations is different from the density in a defect-free crystal the positron lifetime depends on the type and the density of the crystal defects.

The positrons for the lifetime measurement are conveniently obtained from the β^+ decay of ^{22}Na . In ^{22}Na a 1.27 MeV γ quantum appears simultaneously with the positrons. This 1.27 MeV quantum is used as a timing reference for the positron lifetime measurement.

When a positron annihilates with an electron two γ quanta of 511 keV are emitted. The γ quanta can easily be detected by a PMT and a scintillator. The general experimental setup is shown in Fig. 244.

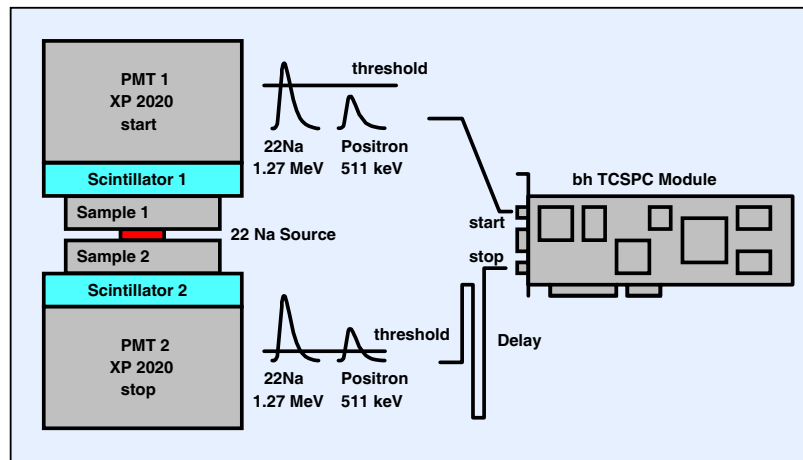


Fig. 244: Positron lifetime experiment

The ^{22}Na source is placed between two identical samples. Two XP 2020 photomultipliers equipped with scintillators are attached directly to the two samples. The pulses from the photomultipliers are used as start and stop pulses for the bh TCSPC module. The pulses from PMT 2 are delayed by a few ns so that a stop pulse arrives after the corresponding start pulse. The TCSPC module can be any SPC-x30, i.e. a module with a discriminator threshold in the SYNC channel. The amplitudes of the photomultiplier pulses are proportional to the energy of the particle that caused the scintillation. The discriminator thresholds for start and stop are adjusted in a way that the stop channel detects all, the start channel only the larger ^{22}Na

pulses. The rate of the ^{22}Na events is on the order of a few kHz or below. Therefore it is unlikely that a time measurement is started and stopped by two subsequent ^{22}Na events. The by far most likely event is the detection of a ^{22}Na decay in the start PMT followed by the detection of a positron in the stop PMT. The distribution of these events gives the desired positron lifetime distribution. A typical result is shown in Fig. 245.

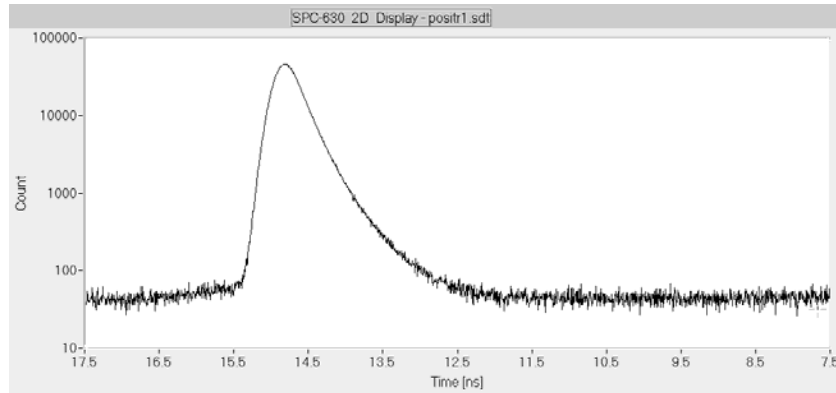


Fig. 245: Result of a positron lifetime measurement. TCSPC Module SPC-630, PMTs XP2020. Acquisition time 20 minutes

Ranging Systems

The high time resolution of the bh SPC modules in conjunction with fast detectors can be used to build up high-resolution ranging or three-dimensional imaging systems. The system described in [238, 239, 368] uses a 20 ps diode laser, an actively quenched avalanche photodiode [94] and a bh SPC-300 TCSPC module. The photons reflected from the target and a reference pulse are recorded within the same TAC range. A slow scanning procedure is employed, i.e. the photons for one pixel of the image are collected, the time-of-flight distribution is read out from the SPC module, and the next pixel is scanned.

The system achieves a distance repeatability of 10 μm and 30 μm for a 1 m and 25 m stand-off, respectively. The distance accuracy corresponds to a time accuracy of 33 fs to 100 fs. The authors use a fitting algorithm [357] which gives a better timing accuracy than the usual centroid estimation. The surprisingly high resolution can be explained by the fact that the average timing jitter of a large number of detected photons decreases with the square root of the photon number. Of course, an accuracy this good can only be achieved with short laser pulses, a detector of low transit time spread, efficient cancellation of system drifts, and with a TCSPC time-channel width short enough to sample the IRF adequately.

Advanced SPC modules, such as the SPC-630, SPC-730 or SPC-830 can be used to readout the module during the measurement or to acquire the complete image at a fast scan rate.

Remote Sensing

With a suitable optical system TCSPC is able to record fluorescence decay or diffusely reflected laser signals over remarkable distances. The setup shown in Fig. 246 records the fluorescence of chlorophyll in plants over a distance of several 100 meters.

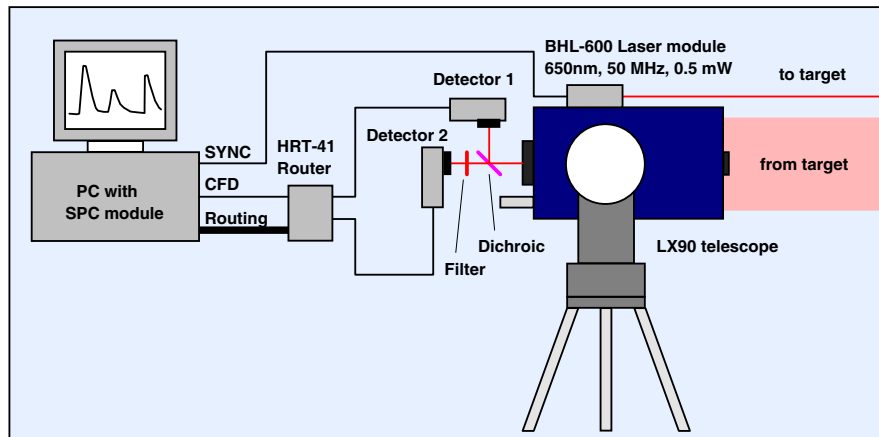


Fig. 246: Fluorescence measurement over large distance

A bh BHL-600 laser sends a beam of ps pulses to the target. The repetition rate of the laser pulses is 50 MHz, the average power 0.5 mW. An 8-inch telescope (Meade LX90 EMC) is used to collect the photons from the target. The fluorescence and the reflected light are separated by a dichroic mirror and a 700 ± 15 nm bandpass filter and detected simultaneously by two PMH-100 detectors. Consequently, detector 1 detects the diffusely reflected laser, detector 2 the fluorescence of the leaves. Despite of the low laser power chlorophyll fluorescence is detected over a distance of several 100 meters, with count rates on the order of 1000 photons per second. At a count rate this low the background signal is an important issue, which implies that reasonable results can only be obtained at night. A typical result is shown in Fig. 247.

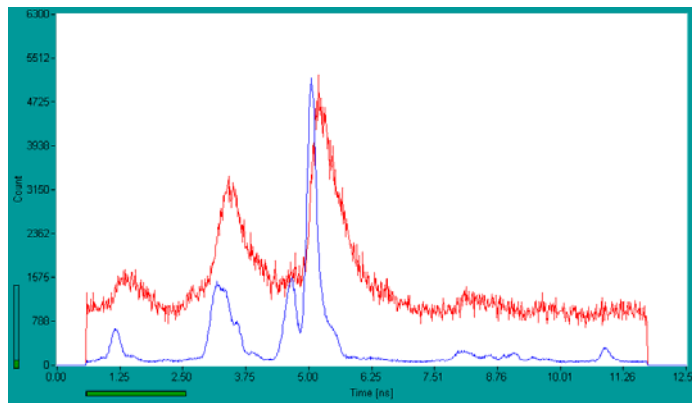


Fig. 247: Fluorescence and reflectance of leaves in a forest 300 meter away

The telescope and the laser were pointed into a forest approximately 300 m away. The red curve is the detected fluorescence, the blue curve the reflected laser. It is almost impossible to hit only one leaf over a distance this long. Therefore the signals from several leaves in different distances are detected. Moreover, the signal intensity fluctuates considerably at the scale of seconds, due to the motion of the leaves in the wind. However, because the reflectance and the fluorescence signals are detected simultaneously, the reflectance can be used as an approximation of the instrument response function to analyse the fluorescence data. This approach is not absolutely correct because the reflected photons can come from non-fluorescent target components too. It does, however, deliver fluorescence decay times of reasonable accuracy [46].

Measurement of Absolute Detector Quantum Efficiency

A technique for measuring the quantum efficiency of a photon counting detector without a calibrated reference detector was described in [215, 249, 250, 251, 290, 369]. The technique is based on the generation of photon pairs by parametric downconversion. The principle is shown in Fig. 248.

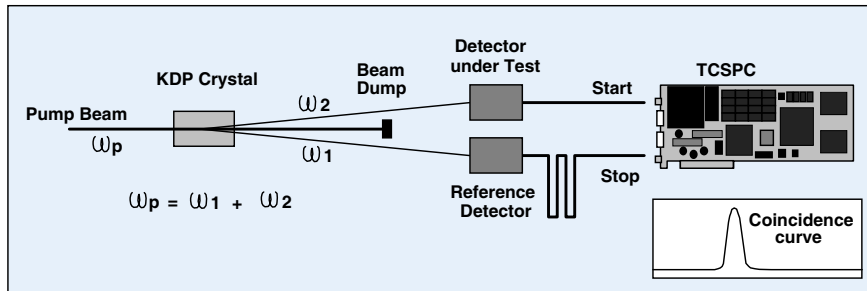


Fig. 248: Absolute measurement of the detector quantum efficiency by parametric down-conversion

A NUV laser pumps a KDP (potassium dihydrogen phosphate) crystal. Down-conversion in the crystal generates photon pairs with a total energy equal to the energy of the pump photons. The photons of a pair leave the crystal in slightly different directions and can therefore be separated spatially. One photon is sent to the detector being tested, the other photon to a timing reference detector. A photon pulse from the reference detector indicates that a photon pair has been produced. The quantum efficiency of the detector being tested is the probability that it detects the other photon of the pair. The result does not depend on the efficiency of the reference detector.

Scattered pump light is blocked by interference filters in front of the detectors. These filters are the only parts of the system that need calibration. Because the transmission is in the 10 to 90% range, a highly accurate calibration is possible. Errors due to detector background and possible filter leakage are avoided by using the pulses of the detectors as the start and stop of a TCSPC device. The result is a coincidence curve that can be clearly separated from uncorrelated background signals.

Optical Oscilloscope

At a count rate of 10^5 to 10^6 photons per second a reasonably accurate waveform is recorded within less than 100 ms. All bh TCSPC modules can therefore be used as optical oscilloscopes. A repetitive measurement cycle is performed in short intervals and the recorded photon distribution versus time is displayed. Even with a low-cost PMT module, e.g. the Hamamatsu H5783, an IRF width of about 150 ps is achieved; SPADs yield an IRF width of about 40 ps. These IRF widths correspond to signal bandwidths of more about 2 GHz and 9 GHz, respectively. The time channel width can be made as short as a picosecond, which results in an equivalent sample rate of 1000 GS/s.

Fig. 249 shows an example of a TCSPC oscilloscope measurement. The fluorescence of chlorophyll in a leaf was recorded at a count rate of $4 \cdot 10^6$ photons per second and an acquisition time of 100 ms. Two successive traces were overlaid to reproduce the visual impression.

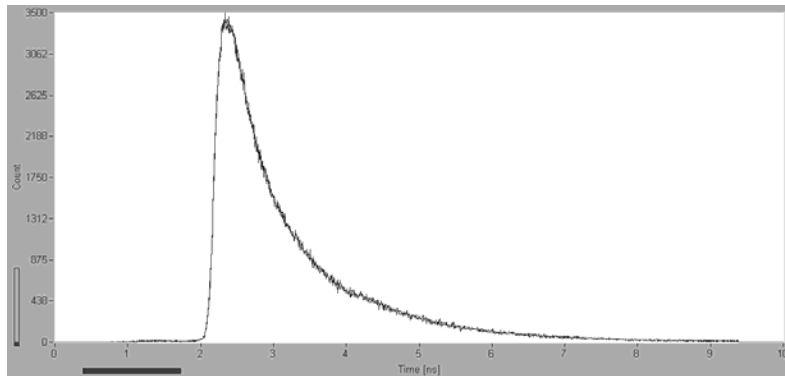


Fig. 249: Fluorescence signal recorded in the oscilloscope mode. SPC-140 module in a ‘Simple-Tau’ system, detector count rate 6 MHz, recorded count rate 4 MHz, 1024 time bins per curve, acquisition time and screen update rate 100 ms. To reproduce the visual impression, two successive traces were overlaid.

Convenient detectors for oscilloscope application are the Hamamatsu H5783 or H5773 modules, or the bh PMC-100 detector heads based on these modules. The modules have a built-in high-voltage generator so that any handling of high voltage is avoided. This is an important feature for practical use.

Recently fast and relatively inexpensive SPAD modules have become available, such as the id 100-20 of id Quantique [179], the PDM 50 CT of Micro Photon Devices [247]. The detectors have an active area of 20 to 100 μm diameter and are overload-proof. The IRF width is about 40 ps, resulting in an equivalent signal bandwidth of about 9 GHz. Although the small active area can cause some alignment problems, these detectors are excellently suitable for TCSPC oscilloscopes.

The oscilloscope mode has become an indispensable tool for a large number of technical jobs. Alignment and optimisation of optical systems often requires not only maximising the efficiency but also localising and removing optical reflections, leakage of excitation light, or pulse dispersion. The oscilloscope mode is also used to optimise the operation conditions of detectors and the driving conditions of picosecond diode lasers. Furthermore, the oscilloscope mode is a convenient way to optimise TCSPC system parameters, such as signal delay, CFD zero cross and threshold, and TAC parameters.

Agents: Boston Electronics, (800)347-5445, TCSPC@boselec.com

Agents: Boston Electronics, (800)347-5445, TCSPC@boselec.com

SPCM Software

All bh TCSPC modules come with the ‘Multi SPC Software’, a comfortable software package that allows to operate up to four SPC-600/630, four SPC-700/730, four SPC-830 or one SPC-134, 144 or 154 package. It includes measurement parameter setting, measurement control, step motor control, loading and saving of measurement and setup data, and data display and evaluation in 2-dimensional and 3-dimensional modes. For data processing with other software packages conversion programs to ASCII and Edinburgh Instruments formats is included. The SPCM software runs under Windows 2000, NT, and XP. For installation of the SPCM software, please see ‘Software Installation’, page 79.

The SPCM software can be started with or without an SPC module being installed in the computer. When the software is started the initialisation window shown in Fig. 250 appears. Without an SPC module the software starts in the ‘simulation mode’, see ‘Starting the SPC Software without an SPC Module’, page 86. After selecting the desired type of the SPC module the SPCM software can be started and used to display or process SPC data.

If one or several SPC modules are found the software starts in the hardware mode. The installed modules are marked as ‘In use’, see Fig. 250. The modules are shown with their serial number, PCI address and slot number.

The software runs a simple hardware test when it initialises the modules. If an error is found, a message ‘Hardware Errors Found’ is given and the corresponding module is marked red. In case of non-fatal hardware errors you can start the main panel by selecting ‘Hardware Mode’ in the ‘Change Mode’ panel. Please note, however, that this feature is intended for trouble shooting and repair rather than for normal use.

When the initialisation window appears, click on ‘OK’. This opens the main panel of the SPCM Software, see Fig. 251. The upper part of main panel contains one or several windows that display data, e.g. decay curves, images, FCS curves or photon counting histograms. The lower part displays information about the count rates and the status of the measurement, and allows the user easy access to the most frequently used system and measurement control parameters. Functions like load and save, conversion of file formats, definition of the TCSPC system parameters and operation modes, display configuration and display routines are accessible via a menu bar at the top of the main panel.

Configuration of the SPC Main Panel

General Configuration

The main panel is configurable by the user. A number of typical configurations are shown in Fig. 251. The upper row shows configurations typically used for traditional fluorescence decay measurements. For a single-detector setup often a display window is used that fills the upper part of the main window entirely (upper row, left). The curves displayed are the instrument response function and one or several fluorescence measurements. The displayed traces are defined in the ‘Trace Parameters’ which are accessible via the menu bar.

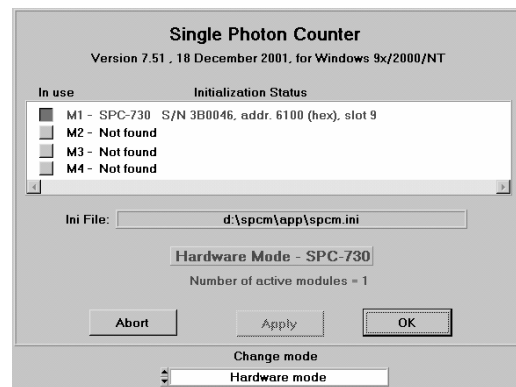


Fig. 250: Initialisation panel

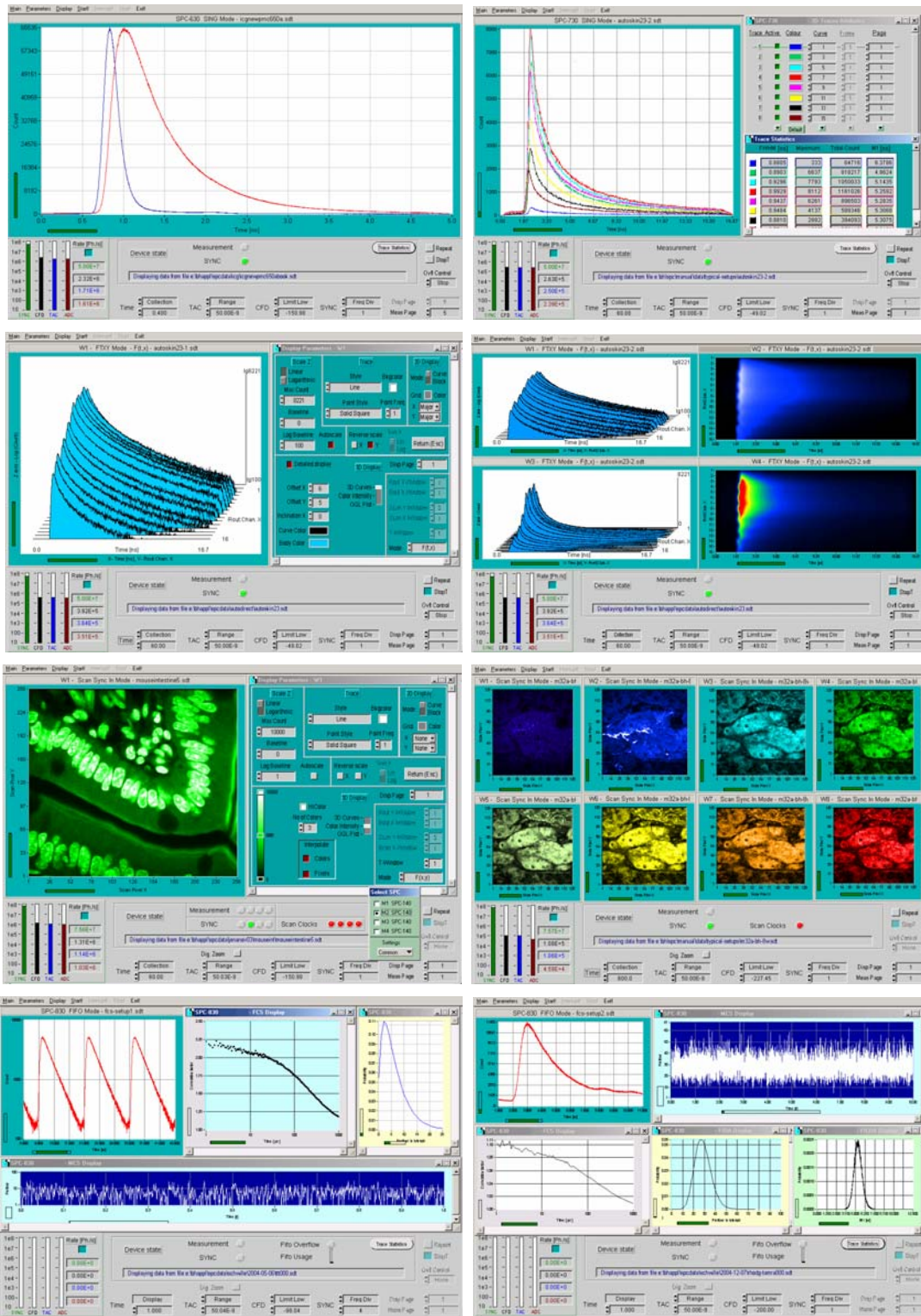


Fig. 251: Main panel of the SPCM software, examples of different configurations. Upper row measurement of single and multi-wavelength decay curves; Second row multi-detector or sequential measurements, three dimensional display, third row Fluorescence lifetime imaging, lower row single molecule spectroscopy, with decay curves, FCS curves, photon counting histograms and intensity (MCS) traces.

However, often several measurements are performed one after another in subsequent memory pages, or a number of decay curves are recorded simultaneously by using the multi-detector capability of the SPC modules. It may then be convenient to have the trace definitions directly available (upper row, right). The display window is therefore reduced in size, and the ‘Trace

'Parameter' panel is kept open and placed right of the display window. The FWHM, the maximum and total counts, and the first moments of the curves are displayed by keeping the 'Trace Statistics' open.

The second row shows typical configurations for multi-wavelength measurements. The left panel shows a three-dimensional graph of the decay curves in the subsequent wavelength channels. The graph is controlled by the 'Display Parameters' which are kept open in the right part of the main panel. Other options are shown in the main panel configuration on the right. Four display windows are defined. The same data set is shown in linear and logarithmic scale, and as a three-dimensional curve and a colour-intensity plot. Similar panel configurations can be used for sequential measurements.

The configurations shown in the third row are typical of FLIM measurements. The configuration shown left uses one display window. To change between images in different time windows or different detector channels, the 'Display Parameter' panel is kept open; different TCSPC channels of a multi-module system can be selected by the 'Select SPC' panel. The main panel configuration shown right is used for multi-wavelength FLIM. Eight display windows are used to display images in subsequent wavelength intervals. The same configuration can be used to display subsequent images of page-stepping sequence.

The last row show configurations for single-molecule spectroscopy. The left panel displays the decay function, the FCS curve, a photon counting histogram and a curve of the recorded intensity over a selected time interval of the measurement. Photon counting lifetime histograms can be displayed as well, see lower row right, lower right curve.

Display and Trace Parameters

The main panel is configured by the 'Display Parameters' the '2D Trace Parameters', and the '3D Trace Parameters'. The corresponding panels are shown in Fig. 252.

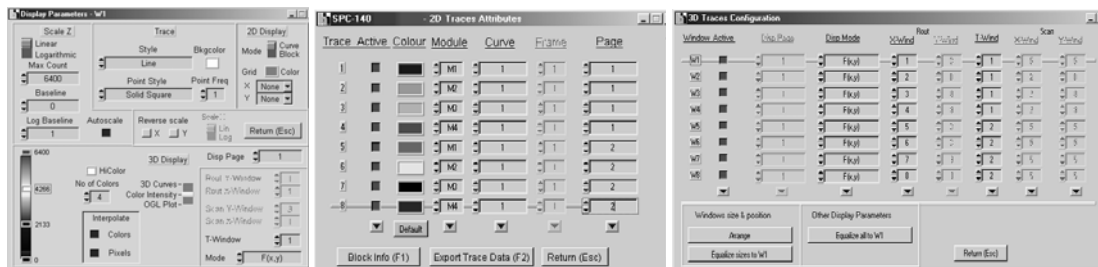


Fig. 252: Left to right: Display parameters, 2D Trace parameters, and 3D Trace Parameters

The *Display Parameters* (shown left) allow you to define how your results will be displayed. The range of the count numbers to be displayed can be defined upper left. The style of the curves displayed can be defined under 'Trace' and '2D display'. The lower part of the Display Parameters applies mainly to multi-dimensional data sets as they are obtained in the imaging and sequencing modes. A 3D curve mode, a colour-intensity mode, and an OGL plot are available. Sub-sets of multi-dimensional data sets can be selected in the lower right part of the panel. For details, please see 'Display Parameters', page 301.

As shown in Fig. 251, the main panel may have several display windows open. The windows have separate Display and 2D Trace Parameters. To select the right set of display parameters, click into the top bar of the particular display window.

The *2D Trace Parameters* define the curves displayed 2-dimensional display modes. Curves from different modules of a multi-module TCSPC system ('Module'), individual curves from a multi-detector measurement ('Curve'), and from different measurements or steps of a meas-

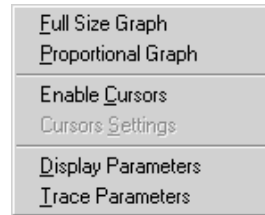
urement sequence ('Frame' or 'Page') can be selected. A curve may also contain accumulated data of several detector channels or measurement steps. Please see '2D Trace Parameters', page 307.

The *3D Display Parameters* define up to eight display windows for multi-dimensional measurements. For each window, the display mode can be defined individually. Thus, images in defined time windows, sequences of curves in defined windows of an image, or a defined windows of the detector number can be defined. Each window has separate display parameters. Thus, windows showing results in the curve and colour intensity mode and in different display scale can be created. For details, please see '3D Trace Parameters', page 311.

Resizing the Display Windows

All display windows are resizable. To resize a window, grab the edge of the widow with the mouse cursor and drag the panel to the desired size.

Clicking into a display window area by the right mouse key opens the panel shown in the figure right. 'Proportional Graph' sets the display proportions according to the 'Scan Pixels X' and 'Scan Pixels Y' of a Scan measurement. 'Full Size Graph' spreads the display window over the maximum available area.



Cursors in the Display Windows

Cursors in any of the display windows are enabled by clicking into the window with the right mouse key. This opens a small panel (shown right) in which the cursors functions can be enabled or disabled. 'Cursor Settings' opens a cursor panel that can be placed anywhere in the screen area. The cursor panel is shown in Fig. 253.

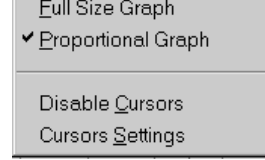
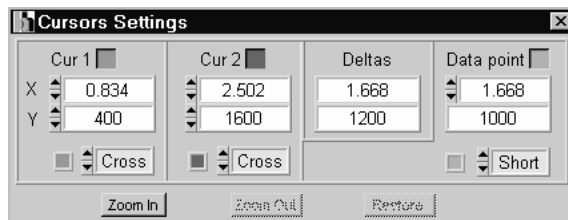
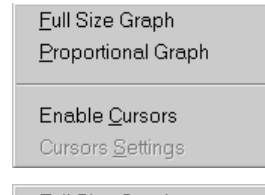


Fig. 253: Cursor panel. The panel opens by clicking into a display window with the right mouse key and selecting 'Cursor settings'

The cursor panel displays the cursor positions and the position of an additional 'Data Point'. Furthermore, the style and the colour of the cursors can be changed and a zoom function is available. The function is the same as for the cursors in the 2D Display, see 'Display Routines', page 323.

Trace Statistics

By clicking on the 'Trace Statistics' button a window is opened in which the FWHM values, the peak counts, the overall counts and the first moment of the photon distribution are displayed for all active traces. The window can be placed anywhere in the screen area. The trace statistics display is an efficient tool to adjust the system for maximum resolution, counting efficiency, and IRF stability.

FWHM [ns]	Maximum	Total Count	M1 [ns]
0.2995	65535	17952820	1.8165
0.2941	65535	17772130	1.8200
0.2954	65535	17930495	1.8246
0.2986	65535	18086180	1.8226

Fig. 254: Trace statistics panel

On-Line Display

In all photon-distribution modes results can be displayed at the end of the measurement, in intervals of ‘Display Time’. In the sequential modes, such as f(t,T) or Continuous Flow, the result after each individual measurement step can be displayed by switching on the ‘display each step’ or ‘display each cycle’ functions in the system parameters. In the imaging modes, intermediate images can be displayed by activating ‘accumulate’ and ‘display each cycle’.

When the SPC-630, SPC-830, SPC-134, and SPC-144 modules are operated in the FIFO mode they do not build up photon distributions but store the information about the photons individually. To display results on-line, the SPC software analyses the incoming photon data and calculates decay functions, FSC functions, photon counting histograms and intensity traces in intervals defined by the parameter ‘Display Time’. Please see ‘FIFO Mode Run-Time Display’, page 282.

The on-line display functions are an efficient way to observe the progress of a measurement. However, on-line calculation and display consumes an appreciable part of the computing power. Therefore it may be not feasible for FCS calculation with long correlation time and extremely high count rates, sequential recording at high step rates, or other applications requiring maximum data throughput.

System Parameter Settings

The complete system parameter set is accessible under ‘System Parameters’, page 253. The system parameter panel is shown in Fig. 255.

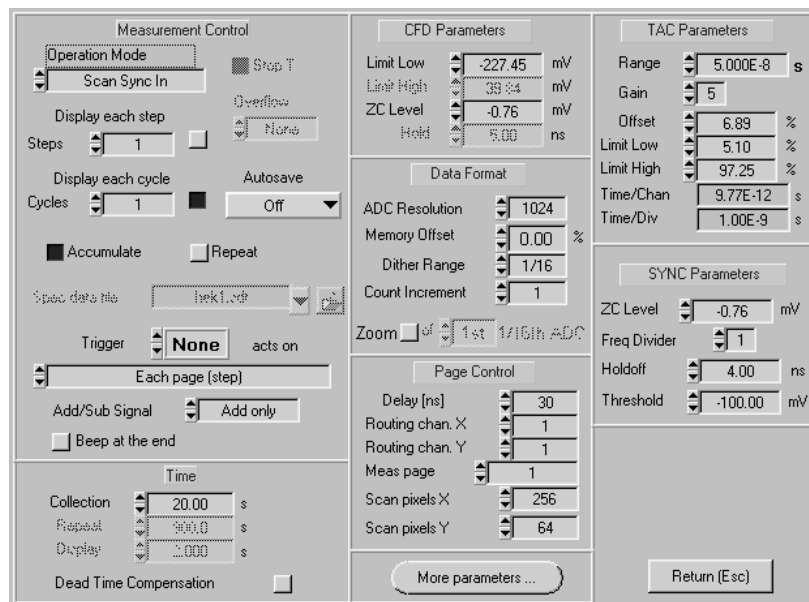


Fig. 255: System parameter panel

The system parameter panel contains the operation mode, the measurement control parameters, and all hardware parameters of the particular SPC module. For detailed description please see ‘System Parameters’, page 253.

To facilitate on-line adjustments the essential hardware and measurement control parameters are also accessible directly from the main panel, see Fig. 256.



Fig. 256: Access to system and control parameters from main panel

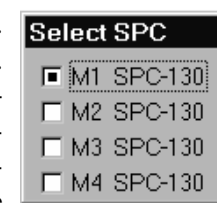
The parameters directly accessible are:

- Time: Collection Time, Display Time, Repeat Time
- TAC: Range, Gain, Offset, Limit Low, Limit High
- CFD: ZC Level, Hold, Limit Low, Limit High (SPC-x00 only)
- SYNC: Freq Divider, ZC Level, Holdoff, Threshold (SPC-x30 only)
- Ovfl Control: None, Stop on Overflow, Correct Overflow
- Page: Memory area (destination) for measurement data
- Repeat: Repeat measurement
- Stop T: Stop after Collection Time

If the system contains a step motor controller the CFD and SYNC part can be replaced with a window for stepping motor control. Please note that not all parameters are available in all operation modes or in all module types. Please see 'System Parameters', page 253.

Module Select (Multi-SPC Systems)

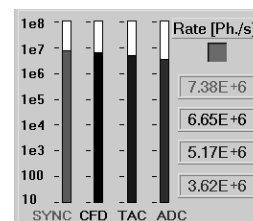
The Multi SPC Software is able to control up to four TCSPC channels, i.e. up to four SPC-6, -7 or -8 modules or one SPC-134 or SPC-144 package. Many (though not all) system parameters can be set differently in the individual modules. The parameters shown in the 'Main Panel' and in the 'System Parameters' panel belong to the only one of the modules that is selected in the 'Select SPC' panel, see figure right. This small panel can be placed anywhere in the screen area.



Status Information

Count Rate Display

The rate display informs about the count rates the CFD, the TAC the ADC and (in the -30 SPC versions) the SYNC rate. The CFD rate represents all pulses with an amplitude greater than 'CFD Limit Low'. The TAC rate is the working rate of the TAC. It can be slightly smaller than the CFD rate because the TAC is not started by pulses exceeding 'CFD Limit High' (-00 SPCs only) and by pulses detected within the dead time of a previously detected photon. 'ADC Rate' is the conversion rate of the ADC. It represents all events inside the selected TAC window. The count rate display is active also when the measurement is running. The count rate display can be switched off to increase the display update rate.



Count Rate Display, SPC-x30

Device State

'Device state' informs about the status of the device, see Fig. 257.

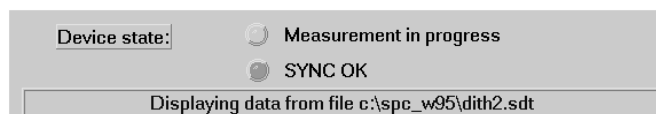


Fig. 257: Device status information

The most important status messages are

Collecting Data:	Measurement running
Displaying Data:	Measurement finished, final result is displayed
Displaying data from file:	Displaying data loaded from an SPC data file
No SYNC:	No synchronisation signal detected
SYNC OK:	Synchronisation signal present
SYNC Overload:	Synchronisation amplitude too high
FIFO Overflow:	The FIFO has run full, not all photons could be recorded
Waiting for Trigger:	Measurement started, waiting for experiment trigger
Waiting for Scan Signals:	Scan measurement started. Waiting for next frame clock to start or to stop the measurement

Status of the Scan Control Signals

When the SPC-730, SPC-830, or SPC-140/144 modules are operated in the ‘Scan Sync In’ mode the status of the scan control signals - frame clock, line clock and pixel clock - is displayed, see Fig. 258.



Fig. 258: Status of the scan clocks

The ‘Scan Clocks’ lamp turns on when all used scan control pulses - i.e. Frame and Line Clock for internal pixel clock and Frame, Line and Pixel Clock for external pixel clock - are present. To display the state of the individual clocks, move the mouse cursor on the ‘Scan Clocks’ lamp. This opens a window with indicators for the individual clocks.

Important: The lamps indicate only whether the signals are pulsing or not. They don’t indicate that the frequency of the clocks is correct. Furthermore, the state is read one time per second. Therefore the ‘Scan Clock’ and the ‘Frame’ pulse indicator may flash if the frame clock is slower than one pulse per second.

The Scan clock indicator exists for SPC-700/730 modules with serial numbers higher than 3B0062 and for all SPC-830, SPC-140/144 and SPC150/154 modules.

Agents: Boston Electronics, (800)347-5445, TCSPC@boselec.com

Agents: Boston Electronics, (800)347-5445, TCSPC@boselec.com

Main

The functions for loading, saving and converting data and the print functions are available under ‘Main’.

Load Panel

The ‘Load’ menu is shown in Fig. 259. It contains fields to select different file types, to specify a file, to display information about the file selected, and to select different load options.

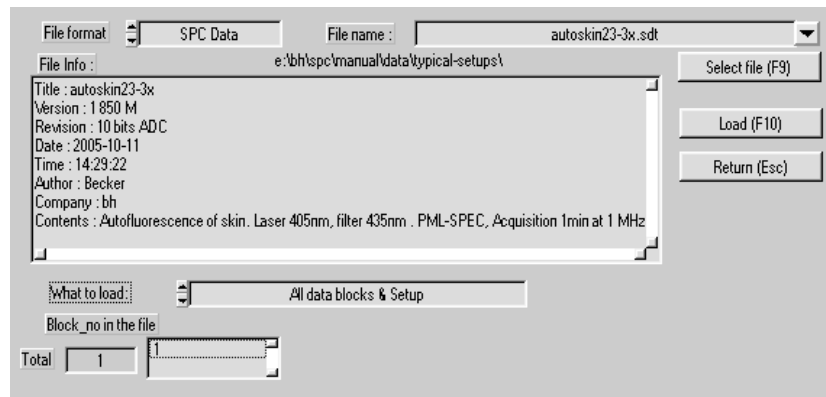


Fig. 259: Load panel

File Format

You can chose between ‘SPC Data’ and ‘SPC Setup’. The selection refers to different file types. With ‘SPC Data’, .sdt files are loaded. These files contain both measurement data and system parameters. Thus the load operation restores the complete system state as it was in the moment when the file was saved.

If you chose ‘SPC Setup’, .set files are loaded. These files contain the system parameters only. The load operation sets the system parameters, but the actual measurement data are not influenced.

Note: Measurements in the ‘FIFO’ (time tag) mode deliver an .spc file that contains the micro time, the macro time, and the detector channel for each individual photon. These files are loaded by using the ‘Convert’ routines, see ‘Converting FIFO Files’, page 248.

File Name / Select File

The file to be loaded can is selected in ‘File Name’ field. ‘Select File’ opens a dialog box that displays the available files. These are ‘.sdt’ files or ‘.set’ files depending on the selected file format. A history of previously loaded files is available by clicking on the button.

File Info

The file info window displays information about the file selected. The first three lines of the file info are inserted automatically when a file is saved. The last three items can be typed in by the operator, see ‘Save Panel’.

Block Info

Activating a data block in the ‘Block Number in File’ field enables a ‘Block Info Button’. Clicking on this button opens a list that contains the device number of the SPC modules by which the data were recorded, the time and data of the recording, and all system parameters, see Fig. 260. At the end of the block information the minimum and maximum count rates of

the corresponding measurement are shown (see Fig. 260, right). The block info often helps to recover the exact recording conditions of an older measurement.

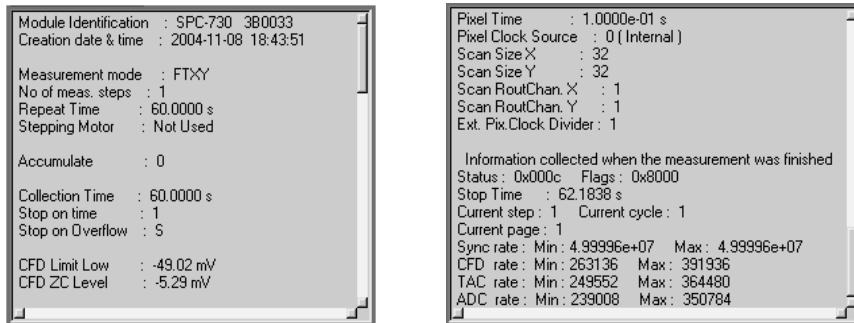


Fig. 260: Block info window of the load panel

Load Options

Under ‘What to Load’ the options ‘All data blocks & setup’, ‘Selected data blocks without setup’ or ‘Setup only’ are available. The default setting is ‘All data blocks & setup’, which loads the complete information from a previously saved data file. *Except for special cases (see below) we recommend to use the ‘All data blocks & setup’ option.*

Loading selected Parts of a Data File

‘Setup only’ loads the setup data only, the measurement data in the SPC memory remains unchanged.

With ‘Selected data blocks without setup’ a number of selected curves or data sets out of a larger .sdt file can be loaded. A data set is a number of curves measured with identical hardware parameters, e.g. a decay curve stored on one ‘page’ of a ‘Single Mode’ measurement, or the decay curves of all pixels of a ‘Scan’ mode measurement.

For ‘Selected data blocks without setup’ the lower part of the ‘Load’ menu changes as shown in Fig. 261.

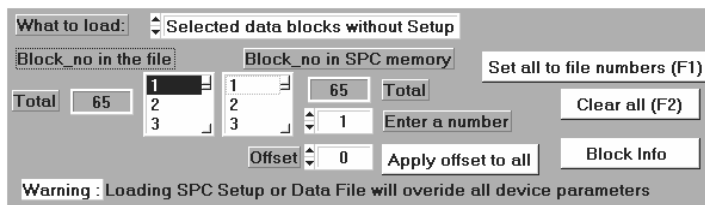


Fig. 261: Selecting data blocks to be loaded from a larger data set

The list ‘Block no in the file’ shows the curves (or data sets) available in the file. Under ‘Block no in the memory’ the destination of the data blocks (curves or sets of curves) in the memory is shown. With ‘Set all to file numbers’ the destination in the memory can be set to the same block numbers as in the file. To set the destination of the data to locations different from the block numbers in the file, click on the a block number in the ‘Block no in the memory’ list and change the number in the ‘Enter Number’ field. ‘Clear all’ clears the ‘Block no in the memory’ list.

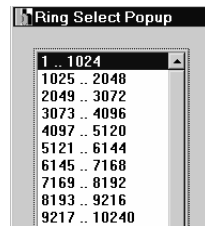
For the SPC-134, SPC-144, or other multi-SPC systems operated by the Multi-SPC Software, the block designator contains the module number and a curve number (module_curve).

‘Apply offset to all’ loads data with a constant offset referred to the file block numbers. It can be used to conveniently load large data blocks to a memory location different from the location in the file.

A sequence of blocks can be selected by pressing the ‘Shift’ key and clicking on the start and stop number.

Creating the ‘Block No’ list can take some time, especially on slow computers. Therefore, for high number of blocks the list is created on demand by clicking on the ‘Detail’ button. When the list is switched on, a menu can be opened from which the location in the block number list can be selected in groups of 1024 blocks.

‘Block Info’ opens a new window which gives information about the data in a selected data block. An example for the block information window is given in the section ‘Trace Parameters’.



Loading Files from older Software Versions

Older software versions may contain less system parameters than newer ones. Therefore, loading older files into a newer software (or vice versa) can cause warnings of missing or unknown parameters. To load the file, click on the ‘Continue’ button until the file is loaded. Unknown parameters are ignored, and missing parameters are replaced with default values. To avoid further problems with such a file, we recommend to save it in the current software version (Use option ‘All used data blocks’, see ‘Save Panel’).

Save Panel

The ‘Save’ menu is shown in Fig. 262. It contains fields to select different file types, to select or specify a file, to display information about existing file, and to select between different save options.

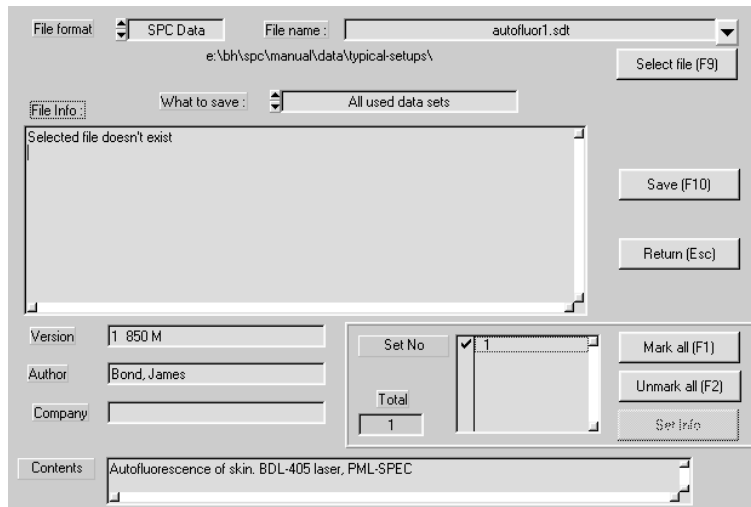


Fig. 262: Save panel

File Format

You can chose between ‘SPC Data’ and ‘SPC Setup’. The selection refers to different file types. With ‘SPC Data’ files are created which contain both measurement data and system parameters. When this file is loaded not only the measurement data are restored but also the complete system setup. With ‘SPC Setup’ files are created that contain the system parameters only. When such files are loaded the system setup is restored, but no data are loaded. Files created by ‘SPC Data’ have the extension ‘.sdt’, files created by ‘SPC Setup’ have the extension ‘.set’.

File Name / Select File

A file name can be written into the ‘File Name’ field. ‘Select File’ opens a dialog box that allows you to change or create directories. Moreover, it shows the names of existing files. These are ‘.sdt’ files or ‘.set’ files, depending on the selected file format. If you want to overwrite an existing file you can select it in the ‘File Name’ field. A history of previously saved files is available by clicking on the  button.

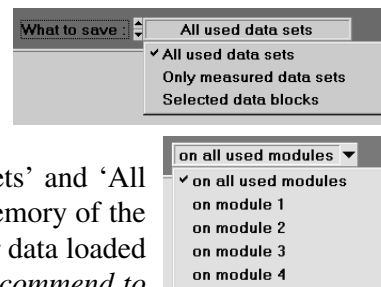
File Info

After selecting the file text can be written into the ‘Author’, ‘Company’ and ‘Contents’ fields. Both for ‘SPC data’ and ‘SPC setup’ the file information is saved in the file. The file information helps considerably to later identify a particular measurement among a large number of data files. We therefore strongly recommend to spend a few seconds on typing in a reasonable file information.

If you have selected an existing file the file information contained in it is displayed in the ‘File info window’. If you want to overwrite this file you can edit the existing file information.

Selecting the data to be saved

Under ‘What to Save’ the options ‘All used data sets’, ‘Only measured data sets’ or ‘Selected data blocks’ are available. Furthermore, for the SPC-134 or other systems operated by the Multi-SPC software a module can be selected the data of which is to be saved. The default setting is ‘All used data sets’ and ‘All used Modules’, which saves all valid data available in the memory of the SPC modules. These can be measured data, calculated data or data loaded from another file. *Except for special cases (see below) we recommend to use the ‘All used data sets’ and ‘All used Modules’ option.*



‘All used data sets’ and ‘Only measured data sets’

A ‘Data Set’ is the result of a single measurement, e.g.

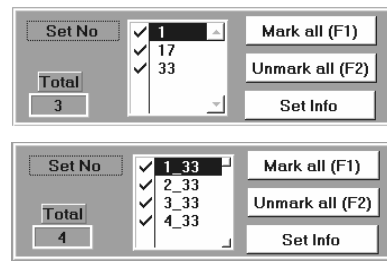
- a decay curve measured by a single detector in the ‘Single’ mode
- the decay curves measured in a multi-detector configuration in the ‘Single’ or $f(t,x,y)$ mode
- a sequence of decay curves measured in the $f(t,T)$ or $f(t,\text{ext})$ mode
- the time-resolved spectra obtained for the 8 time windows of the $f_i(T)$ or $f_i(\text{ext})$ mode
- the decay curves for the pixels of an image recorded in the ‘Scan’ modes

‘All used data sets’ saves all data obtained in the current session, data loaded from a file, and results of the 2D and 3D data operations.

‘Only measured data sets’ saves only the data which was obtained by *measurements* in the current session. Data loaded from files or results of data operations are *not* saved.

Data Set Info

The save routine saves device number of the SPC modules by which the data were recorded, the time and date of the recording, and the system parameters for individual data sets. The start curve numbers of the available data sets are shown in the lower part of the ‘Save’ panel, see figure right. For the SPC-134 or other multi-SPC systems operated by the Multi-SPC Software, the data set designator contains the module number and the start curve of the data set.



Activating a data set enables the ‘Set Info’ button. Clicking on this button opens a list that contains the device number of the SPC modules by which the data were recorded, the time and data of the recording, and all system parameters, see Fig. 260. At the end of the block information the minimum and maximum count rates of the corresponding measurement are shown (see Fig. 260, right).

Saving Selected Data Blocks

With ‘Selected data blocks’ a single curve or number of selected curves can be saved. This option is used to create files of selected curves from larger data sets, e.g. to save selected curves of a ‘Scan’ measurement for processing by an external data analysis program.

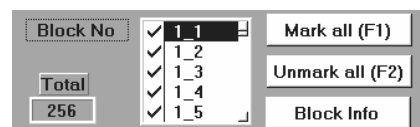
The list ‘Block No’ shows the individual curves which are available in the memory. The desired curves are selected (or deselected) from this list by a mouse click into the marked area. ‘Mark all’ selects all curves, ‘Unmark all’ deselects all curves.

For the SPC-134 or other multi-SPC systems the block designator contains the module number and a curve number. A sequence of blocks can be selected by pressing the ‘Shift’ key and clicking on the start and stop number.

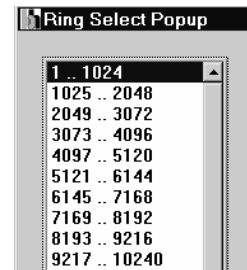
Creating the ‘Block No’ list can take some time, especially for modules with large memories in slow computers. Therefore, for high number of blocks the list is created by clicking on the ‘Detail’ button. When the list is switched on, a menu can be opened from which the location in the block number list can be selected in groups of 1024 blocks.



Selecting Data Blocks, SPC-6 through -8



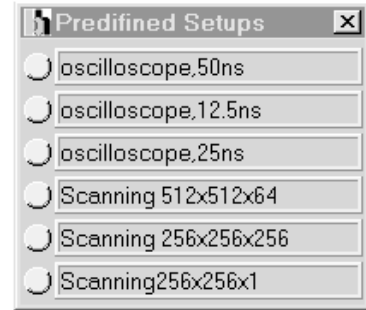
Selecting Data Blocks, SPC-134 or SPC-144



Predefined Setups

Setups of frequently used system configurations can be added to a list of ‘predefined setups’. Changing between these setups then requires only a mouse click.

To use the predefined setup option, click on ‘Main’, ‘Load Predefined Setups’. This opens the panel shown right. A setup is loaded by clicking on the button left of the name of the setup.



To add or delete setups to or from the list, or to change the names of the setups, click into one of the name fields with the right mouse key. This opens the panel shown in Fig. 263.

To add a setup, click on the disc symbol right of the ‘File Name’ field and select a ‘.set’ file. Default setups coming with the SPCM software are in the ‘default_setups’ folder of the working directory defined during the software installation. Please note that there may be sub-directories for different classes of applications. Select the files you want to put into the list of predefined setups, and click on the ‘Add’ button. Every setup has a user-defined ‘nickname’. The default nickname is the file name of the .set file. To change the nickname, click into the nickname field and edit the name. Then click on ‘Replace’.

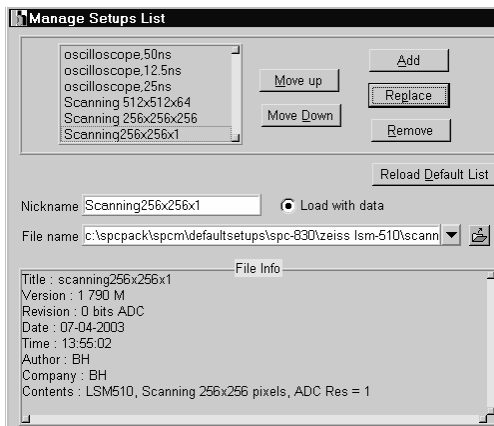


Fig. 263: Editing the list of predefined setups

To create your own predefined setups, first save a setup file of the system configuration you want to add the list. Use the ‘Save’ panel, option ‘setup’ as described under ‘Save’. Then add the file to the setup list as described above.

You can also add an ‘.sdt’ file to the setup list. The .sdt file contains not only the system setting but also measurement data. You can define whether the file is loaded with or without the data by clicking on the ‘load with data’ marker. Please note that loading files with data can take a longer time than without, especially for data recorded in the scan modes of the SPC-730 or SPC-830.

Multi-File View

Measurements with page stepping or autosave, and measurements in the continuous flow mode can produce a large number of subsequent data files. Loading these data one after another by the ‘Load’ procedure and comparing them by the standard display routine may be too time-consuming. Moreover, it may be desirable to see the results of a sequential measurement in form of a time-sequence, i.e. as the data were recorded. Therefore SPCM provides a ‘Multi-File View’ function. The multi-file view panel is shown in Fig. 264.

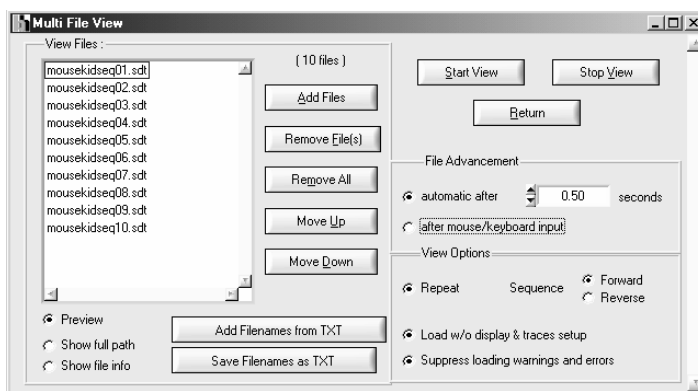


Fig. 264: Control panel of the Multi-File View function

The names of the files to be displayed are specified in a window on the left. Use the ‘Add File’ or ‘Remove File’ buttons to add or remove files. The cursor in the list can be moved up and down by the ‘Move UP’ and ‘Move Down’ buttons, or by a mouse click on a file name. A list of file names can be imported from a .txt file, or exported to a .txt file.

The display of data in the subsequent files can be advanced by an operator command or automatically in defined intervals. The shortest available interval is 0.1 seconds. For large files,

e.g. data of the TCSPC imaging modes loading may take longer than 0.1 s; the view may then advance slower than specified.

The file show can be run only once, or be repeated in a loop ('Repeat' on). It may happen that the subsequent files have different trace or display parameters. In this case activate the 'Load w/o display & traces setup' button. It may also be indicated to switch off possible load warnings, i.e. when data from older software versions are loaded, or the data were measured in a different SPC module.

Convert

The 'Convert' functions are used to convert the .sdt data files of the Multi SPC Software into ASCII files or into the files for the Edinburgh Instruments data analysis software. Furthermore, the FIFO files of the SPC-6 and SPC-134 FIFO mode can be converted into 'Continuous Flow' mode files.

Converting .sdt Files

The 'Convert' for the .sdt files of the menu is shown in Fig. 265. The source file name is selected in a field on top of the Convert panel. After selecting the source file, the corresponding file information text is displayed. The first part of this text was created automatically by the 'Save' function; the last part was written by the operator when the file was saved.

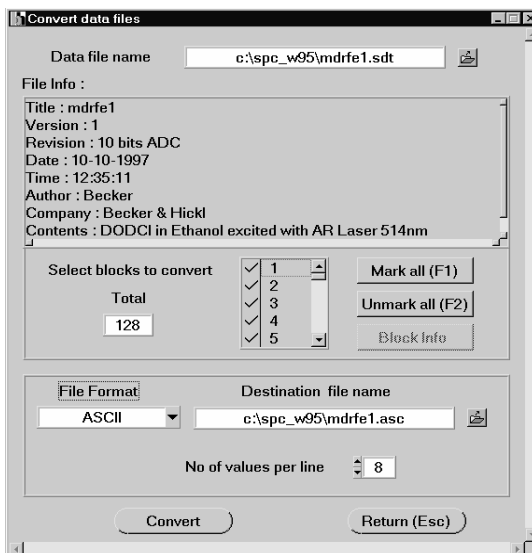


Fig. 265: Conversion of .sdt data into ASCII data

By 'Select blocks to convert' specified blocks (curves) from the source file can be selected for conversion. At the beginning all curves of the source file are marked. Thus, no selection is required if all blocks of the source file are to be converted.

The output file format can be 'ASCII', 'ASCII with Setup' or 'EI'. 'ASCII' converts the measurement data only. 'ASCII with Setup' converts the SPC system parameters and the measurement data. For the measurement data part the number of data values per line can be specified. 'EI' converts into the format of the Edinburgh Instruments data analysis software.

The entering of the destination file name is optional. If no destination file name is entered the source file name is used with the extension '.asc'.

Converting FIFO Files

Measurements in the ‘FIFO’ (time tag) mode deliver an .spc file that contains the micro time, the macro time, and the detector channel for each individual photon. During a FIFO measurement normally decay curves, FCS curves, or photon counting histograms are calculated online. These data are saved in normal .sdt files. However, it may happen that not all of the desired functions were calculated during the measurement, or that the calculation was not done with the optimal binning parameters or sampling time intervals. Moreover, on-line data analysis may have not been used altogether to increase the data throughput rate. In these cases, the ‘Convert FIFO File’ function allows you to read the data from the FIFO (.spc) file created during the measurement and calculate the desired correlation functions or histograms. The Convert FIFO panel is shown in Fig. 266.

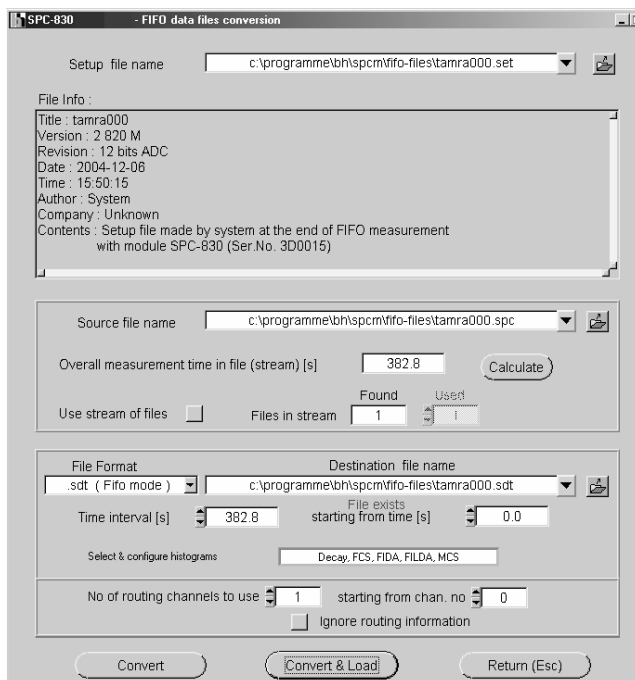


Fig. 266: Conversion of FIFO data into .sdt data

Each FIFO mode measurement creates a setup (.set) file which has the same name as the .spc file (or the last .spc file if several are recorded sequentially). The name of this setup file must be specified under ‘Setup File name’. As in the load and save panels, the file is specified in file name field. Clicking on the disc symbol opens a dialog box that displays the available files. A history of previously used setup files is available by clicking on the button. The ‘File Info’ displays information about the corresponding measurement.

The FIFO (.spc) file is specified under ‘Source File Name’. A FIFO measurement may produce several .spc files. The data of all these files are combined by activating the ‘Use Stream of Files’ button. ‘Overall Measurement Time’ informs about the total time over which the measurement has been run.

The lower part specifies the .sdt file to be created. The file name is specified under ‘Destination file name’. The conversion routine suggests a file with the same name as the .spc file.

The ‘Convert FIFO’ routine allows you to convert .spc files into different destination file types. The destination file type is specified in the ‘File Format’ field in the lower part of the Convert panel. The most frequently used conversion is into .sdt files of the FIFO mode, see Fig. 267.

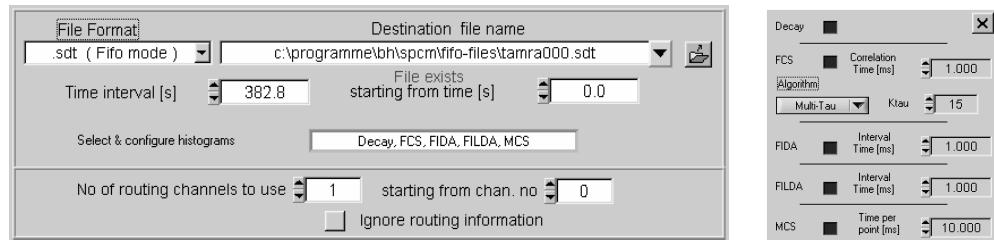


Fig. 267: Conversion of .spc files into .sdt files of the FIFO mode. Left: Configuration of destination data. Right: Selection of the functions to be calculated and calculation parameters.

The functions to be calculated are defined in the ‘Select & configre histograms’ field. A click into this field opens the panel shown in Fig. 267, right. It is the same panel used to configure the online display of the FIFO mode, see page 281. You can specify the calculation of decay curves, FCS functions, photon counting histograms (FIDA), photon counting lifetime histograms (FILDA), and FCS traces.

A FIFO measurement may have been run over a long acquisition time and contain data from several routing channels (detectors). Therefore, parameters are provided to control the structure of the calculated data. With ‘Time Interval’ and ‘Starting from Time’ a time interval within the ‘Overall measurement time’ of the FIFO measurement can be selected. Moreover, if the .spc data were recorded in several detector channels the full routing information may be used, only a specified range of channels may be converted, or the routing information may be ignored altogether, i.e. all detector channels merged.

The results to be calculated from the .spc data are specified under ‘Select & configre histograms’, see Fig. 267, right. The panel opens by clicking into the ‘Select & configre histograms’ field. The options are the same as in the ‘Configure’ menu of the System Parameter panel in the FIFO mode: Decay curves, FCS curves, photon counting histograms and MCS traces can be calculated.

FIFO data can also be converted into data of the Continuous Flow mode, see Fig. 268.

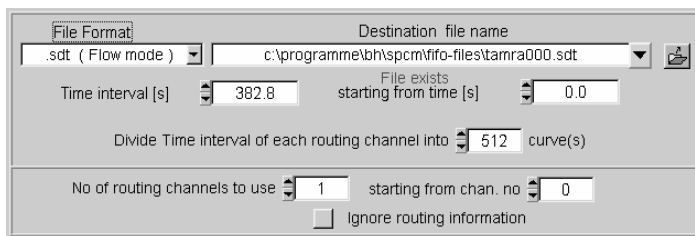


Fig. 268: Conversion of .spc files into .sdt files of the continuous flow mode

With ‘Time Interval’ and ‘Starting from Time’ a time interval within the ‘Overall measurement time’ of the FIFO measurement can be selected. This time interval can be divided into a number of subsequent curves by ‘Divide Time Interval of each Routing Channel into ... Curves’. If only one routing channel (one detector) was used this gives a data file which can be displayed in the ‘Continuous Flow’ or f(t,T) mode of the SPC Standard Software. As for conversion into FIFO mode data, the routing information can be used, ignored, or a specified range of detector channel ranges can be converted.

Fig. 269 shows how .sdt data are converted into ASCII data. Several options are available. The macro time in the destination file may be absolute, or the macro-time differences between subsequent photons may be generated. The micro times, the routing channels, and the ‘invalid’ and ‘overrun’ flags may or not be included in the destination file.

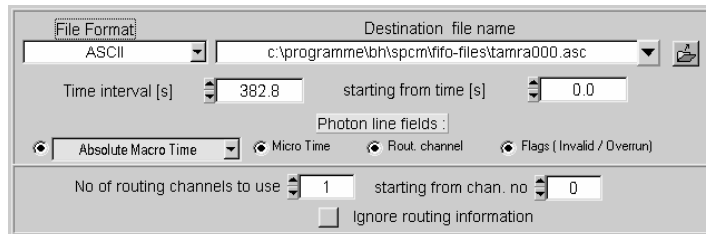


Fig. 269: Conversion of .spc files into ASCII data

Send Data to SPCImage

The function is a link to the SPCImage data analysis routines of fluorescence lifetime imaging [23]. It sends the data of the active display window to the SPCImage software. Please see [20, 21, 22] for details.

Print

The ‘Print’ function sends the current screen pattern to a printer. You can print either the whole panel or the visible part only. ‘Portrait’ or ‘Landscape’ selects the orientation on the sheet. The dimensions are set by ‘Autoscale’, ‘Full Size’ or ‘Size X’ and ‘Size Y’.

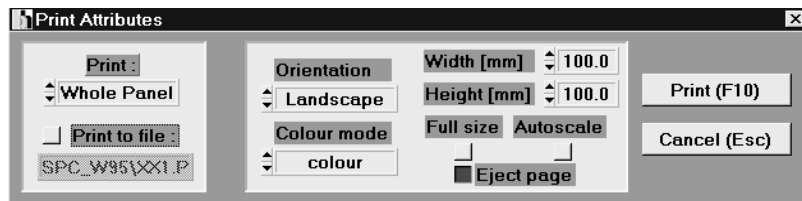


Fig. 270: Print panel

If you want to create a printer file of a screen pattern you can use the ‘Print to File’ option. If you select a postscript-compatible printer the result is a postscript file which can be loaded into many text and image processing programs.

However, another (often more convenient) option to save a screen pattern is the ‘print screen’ key. When this key is pressed, Windows stores the screen pattern to the clipboard from where it can be loaded into an image processing program (Photo Paint, PhotoShop etc.).

Sleep policy

Windows is a multi-task operating systems. However, different applications are not really running simultaneously; the operating system cycles between different applications. The amount of attention the SPCM software gets from the operating system can be changed by setting the ‘sleep policy’, see Fig. 271.

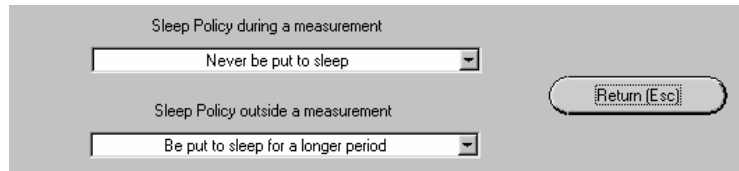


Fig. 271: Sleep policy

The highest level is ‘Never be put to sleep’. On this level the SPCM software claims almost the full power of the CPU. The advantage is short reaction time to any request from the SPC module. The downside is that other applications may be extremely slowed down.

The lowest level is ‘Be put to sleep for a longer period’. It means that the SPCM software claims only a minimum of attention from the CPU. The result are long reaction times. The SPCM software allows you to set different sleep policy during a running measurement and outside a measurement. We recommend to use the settings shown in Fig. 271. The best settings may, however, depend on your operating system and on other applications possibly running in parallel with the SPCM software.

It should be noted here that the data acquisition in the photon distribution (histogram) modes of the bh SPC modules is performed by pure hardware functions. Software activities are only required to read out the data, to initiate the next step of a page stepping sequence, to display status messages, and for operator interactions. Long reaction times of the SPCM software in the ‘Put to sleep’ configurations are therefore rarely a problem.

Agents: Boston Electronics, (800)347-5445, TCSPC@boselec.com

Agents: Boston Electronics, (800)347-5445, TCSPC@boselec.com

System Parameters

The ‘System Parameters’ contain all parameters defining the internal functions of the SPC module hardware and the data transfer between the hardware and the software. The system parameter define the operation mode, including the control of sequential measurements, page stepping, repeat, accumulation and autosave functions. Furthermore, the system parameters control the settings of the CFD, SYNC, TAC and ADC parameters as well as the routing and scanning parameters. Because not all parameters may be applicable to all operation modes and SPC modules some details of the system parameter panel change with the operation mode and module type. The typical system parameter panel of the Multi SPC Software is shown Fig. 272.

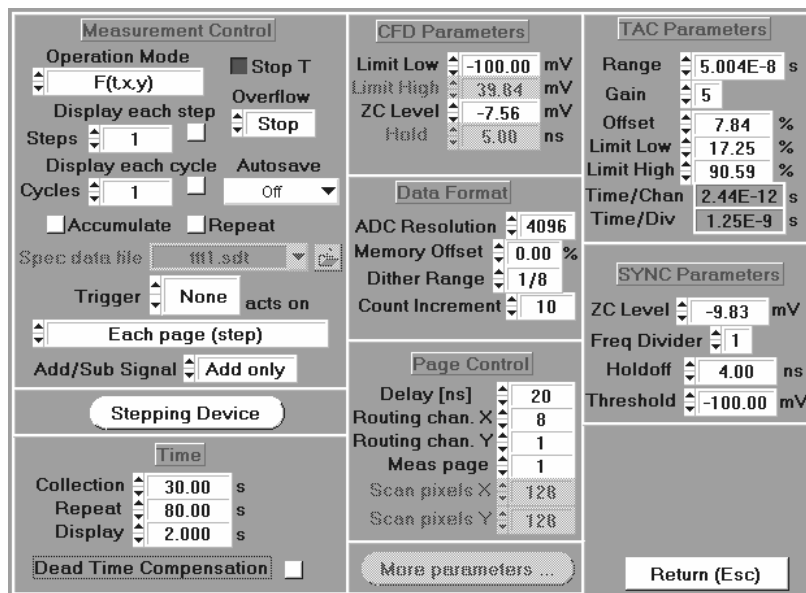


Fig. 272: System parameter panel

The panel contains a measurement control part that allows you to set the operation mode, to configure the measurement procedure by defining page stepping, cycle, accumulate and auto-save functions, and to define the action of the experiment trigger. Due to different hardware in different SPC modules the measurement control part of the panel changes with the module type and with the operation mode selected.

The collection time, repeat time, and display time are defined in the ‘Time’ section below the measurement control parameters.

Under ‘data Format’ and ‘Page Control’ the ADC resolution and the ADC error correction parameter, the number of detector channels, the number of the pixels of a scan, and the memory page in which a measurement is started are defined. The CFD, SYNC, and TAC parameters are arranged in upper right.

‘More Parameters’ opens an additional panel that contains hardware parameters which are specific for the particular operation mode.

Operation Modes

When the bh SPC modules are operated via the SPCM software a wide variety of operation modes is available, see Fig. 273.

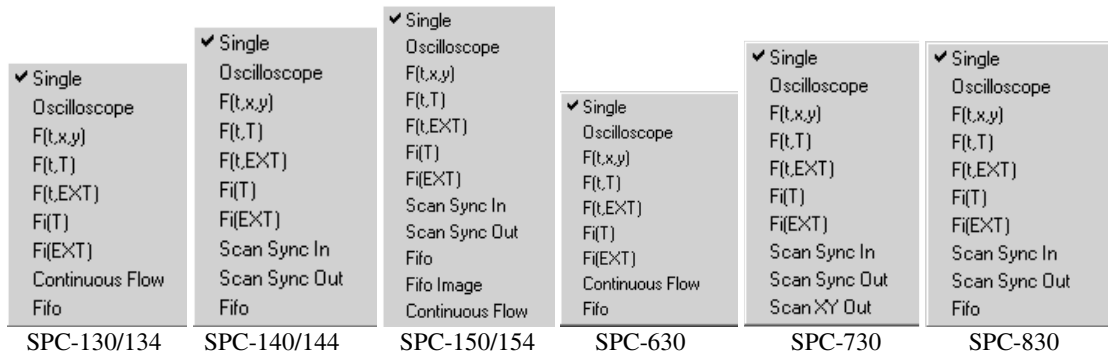


Fig. 273: Operation modes available in different SPC modules

An overview of the operation modes is given in the table below.

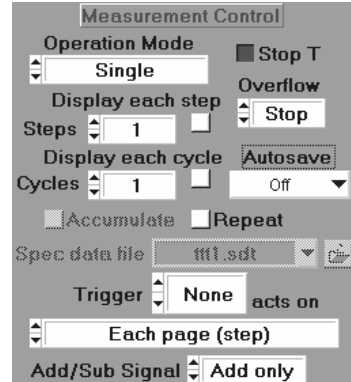
Mode available for SPC	134	144	154	630	730	830	Typical Application
Single	x	x	x	x	x	x	Classic fluorescence lifetime
Oscilloscope	x	x	x	x	x	x	System adjustment and optimisation
f(t,x,y)	x	x	x	x	x	x	Detector arrays, multi-parameter experiments
f(t,T)	x	x	x	x	x	x	Software-controlled sequential recording
f(t,EXT)x	x	x	x	x	x	x	Fluorescence lifetime with λ scanning, slow scanning
f(T)	x	x	x	x	x	x	Time-gated intensity curves
f(EXT)	x	x	x	x	x	x	Time-gated fluorescence spectra, λ scanning
Continuous Flow	x		x	x			Fast sequential recording, optical tomography
Scan Sync In		x	x		x	x	Imaging, laser scanning microscopy
Scan Sync In / Cont. Flow				x			Fast imaging sequences
Scan Sync Out		x	x		x	x	Imaging, fast sequential recording
Scan XY Out					x		Imaging with piezo stages
FIFO	x	x	x	x		x	Single molecules, FCS, FIDA, BIFL
FIFO Imaging		(x)	x				Imaging, Single molecules, FCS, FIDA, BIFL

'Single' Mode

The measurement control parameters for the 'Single' mode are shown right. With the settings shown a single measurement cycle is performed. Several curves can be measured simultaneously if several detectors and a router are used. Up to eight curves can be displayed simultaneously. The displayed curves are selected in the '2D Trace Parameters', see page 307.

The photon collection is controlled by the parameters 'Stop T', 'Repeat' and the options under 'Overflow'. The measurement stops

- at the end of 'Collection Time' if 'Stop T' is set
- at the first overflow if 'Stop Ovfl' is set



If both stop conditions are set the measurement stops in both cases. Without any stop condition the measurement runs until it is stopped by the operator. If the results run out of the data range (65535 counts per time channel) the overflowing parts are clipped.

To collect more than 65535 photons per time channel a 'Correct Overflow' function is provided. With 'Correct Overflow', the measurement data are transferred to the PC memory at each overflow and accumulated. The measurement data memory is cleared after each overflow and the measurement is restarted. When the collection time is over the result is divided by the number of overflows and written back to the measurement memory. The result has 16 bit resolution and a maximum count number of 65535. However, because several recordings were

averaged the standard deviation is reduced by the square root of the number of overflows. The ‘Correct Overflow’ function is available in the ‘Single’ mode only.

During the measurement intermediate results are shown on the screen in intervals of ‘Display Time’. Up to eight curves can be displayed. The curves are specified in the ‘Trace Parameters’, see page 307.

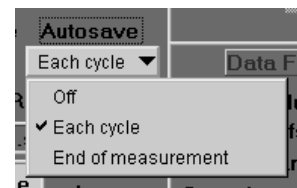
Stepping through Pages

A ‘Single’ measurement can be repeated in intervals of ‘Repeat Time’ and the results be written into subsequent ‘Pages’ of the memory. The number of subsequent measurements is defined by ‘Steps’. The measurement starts in the ‘Measured Page’ defined in the main panel. The stepping function can be combined with routing, i.e. several detector channels can be measured in each step.

Cycles and Autosave

A stepping sequence (or, if ‘Steps’ = 1, one ‘Single’ measurement) can be repeated for a defined number of ‘Cycles’.

The results of subsequent cycles can be written to the hard disk by using the ‘Autosave’ function. To activate ‘Autosave’ for each cycle, click on ‘Autosave’, ‘Each Cycle’.



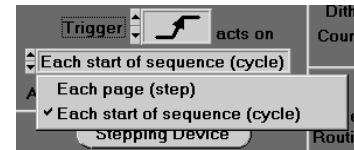
‘Autosave’ can also be initiated at the end of the measurement, i.e. after the last cycle only.

Repeat

After pushing the ‘Repeat’ button the complete measurement cycle repeats until the measurement is stopped by the operator.

Trigger

Either the ‘Steps’ or the ‘Cycles’ of a page-stepping sequence can be triggered. To activate the trigger, select ‘rising edge’ or ‘falling edge’ as ‘Trigger Condition’, see figure right.



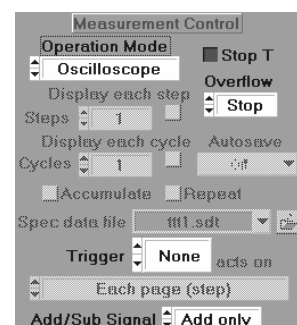
Multidetector Operation

Several curves can be measured simultaneously if a multi-channel detector module or several detectors and a router are used. The number of detector channels are defined under ‘Page Control’, ‘Routing Channels X’ or ‘Routing Channels Y’, see page 298. Up to eight curves can be displayed simultaneously during a Single-Mode measurement. The displayed curves are selected in the ‘Trace Parameters’.

Oscilloscope Mode

In the ‘Oscilloscope Mode’ the measurement is repeated automatically at the maximum available speed. The photon collection is controlled by the parameters ‘Collection Time’, ‘Stop T’, and the stop condition defined under ‘Overflow’. The measurement cycles are finished

- at the end of ‘Collection Time’ if ‘Stop T’ is set
- at the first overflow if ‘Stop Ovfl’ is set

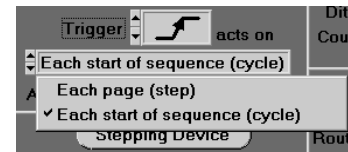


The result is displayed on the screen at the end of each measurement cycle. Please note that at least one stop condition must be set to

complete the measurement cycle and to display the data.

Experiment Trigger

The cycles of an ‘Oscilloscope’ measurement can be triggered. To activate the trigger, select ‘rising edge’ or ‘falling edge’ as ‘Trigger Condition’, see figure right.



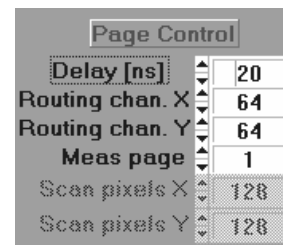
Multi-detector Oscilloscope Operation

Several curves can be measured simultaneously if a multi-channel detector module or several detectors and a router are used. The number of detector channels are defined under ‘Page Control’, ‘Routing Channels X’ or ‘Routing Channels Y’, see page 298. Up to eight curves can be displayed simultaneously during an Oscilloscope-Mode measurement. The displayed curves are selected in the ‘Trace Parameters’.

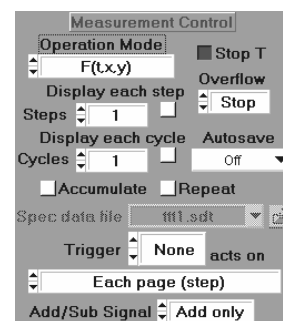
f(txY) Mode

The f(txY) mode is used for measurements with a multichannel detector module, such as the PML-16, with a large number of individual detectors, and for other applications that control the destination of the photons in the memory via the routing signal inputs. These may be multi-parameter measurements (page 226), imaging applications (page 99), or applications that multiplex a large of light sources (page 192). In terms of signal acquisition the f(txY) mode is identical with the ‘Single’ mode. The only difference is that the f(txY) mode interprets the data as a one-dimensional or two-dimensional array of waveform recordings. These are displayed in the 3-D display modes of the SPCM software.

The number of detector channels is defined under ‘Page Control’ (figure right, see also ‘Page Control’, page 298). The measurement simultaneously records an array of decay curves defined by ‘Routing Channels X’ and ‘Routing Channels Y’. The maximum number of curves depends on the module type and on the ADC resolution.



The photon collection is controlled by the parameters under ‘Measurement Control’.



The measurement stops

- at the end of ‘Collection Time’ if ‘Stop T’ is set
- at the first overflow if ‘Stop Ovfl’ is set as overflow option.

If both stop conditions are set the measurement stops in either case. Without any stop condition the measurement runs until it is stopped by the operator. If the results run out of the data range (65535 counts per time channel) the overflowing parts are clipped.

Stepping through Pages

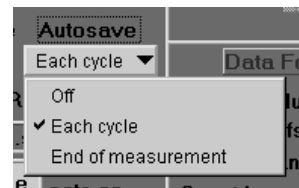
A ‘f(txY)’ measurement can be repeated in intervals of ‘Repeat Time’ and the results be written into subsequent ‘Pages’ of the memory. The number of subsequent measurements is defined by ‘Steps’. The available number of steps depends on the memory size, i.e. on the module type, on ‘Routing Channels X’ and ‘Routing Channels Y’, and on the ADC resolution.

Due to the available memory size, there is a cross-dependence of ‘Routing Channels X’, ‘Routing Channels Y’, ‘Steps’ through subsequent pages, and ‘ADC Resolution’. If one of these parameters is changed beyond the limit set by memory size the software automatically limits it to the maximum possible value.

Cycles and Autosave

A stepping sequence (or, if ‘Steps’ = 1, a single f(tx,y) measurement) can be repeated for a defined number of ‘Cycles’.

To write the results of subsequent cycles to the hard disk the ‘Autosave’ function is used. To activate Autosave for each cycle, click on ‘Autosave’, ‘Each Cycle’.



‘Autosave’ can also be initiated at the end of the measurement, i.e. after the last cycle only. This is reasonable if the cycling function is used in conjunction with ‘Accumulate’.

Accumulate

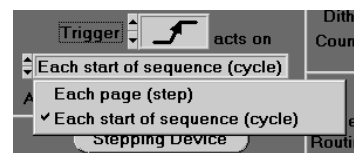
The ‘Accumulate’ function accumulates the results of several ‘Cycles’. It is often used to display intermediate results of a multi-dimensional measurement. After each cycle of the measurement is stopped, and the results are read from the SPC memory and displayed. Then the measurement is continued. The results of all cycles are accumulated. If you want to save the results automatically at the end of the accumulation, use ‘Autosave’, ‘End of Measurement’.

Repeat

After pushing the ‘Repeat’ button the complete measurement sequence repeats until the measurement is stopped by the operator.

Trigger

Either the ‘Steps’ or the ‘Cycles’ of the measurement sequence can be triggered. To activate the trigger, select ‘rising edge’ or ‘falling edge’ as ‘Trigger Condition’.



f(tx,y) Display

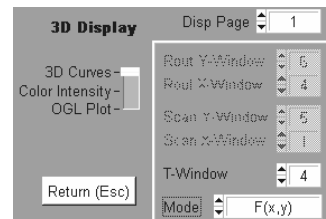
The results of an f(tx,y) measurement are displayed as a three-dimensional figure. The display style (multiple curve plot, colour intensity plot or OGL plot) is defined in the ‘Display Parameters’. Up to eight display windows can be defined to display the data of different detector or multiplexing channels, data in different time channels, or different sub-sections of a multi-dimensional data set. Please see ‘Display Parameters’, page 301, ‘3D Trace Parameters’, page 311, and ‘Window Intervals’, page 313.

During the individual measurement steps intermediate results are displayed in intervals of ‘Display Time’. Furthermore, the result can be displayed after each step and after each cycle by switching on ‘Display after each Step’ and ‘Display after each Cycle’. However, displaying intermediate results requires some time. The ‘Display Time’ and ‘Display after each Step’ options and should be used for collection times longer than a few seconds only.

If both ‘Routing Channels X’ and ‘Routing Channels Y’ are greater than one, or if page stepping is used the results are three- or four-dimensional data arrays. Therefore different 3D display modes are possible, e.g.

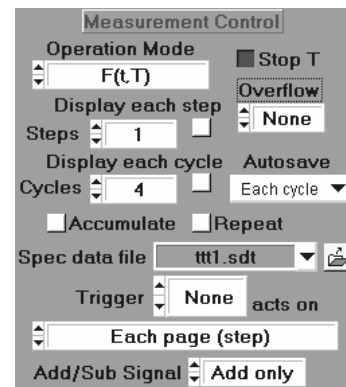
- an f(t,x) display within a selectable ‘Routing y Window’
- an f(t,y) display within a selectable ‘Routing x Window’
- an f(x,y) display within a selectable ‘Time Window’

Furthermore, a ‘Display Page’ can be defined to display a particular step of a stepping sequence. The 3D display plane and the ‘Display Page’ are selected in the ‘Display parameters’, see figure right. For details, please see ‘Display Parameters’, page 301.



f(t,T) Mode

In the f(t,T) mode the measurement of a single curve is repeated in intervals of 'Repeat Time', and the results are written into subsequent pages of the memory. The number of subsequent measurements is defined by 'Steps'. The measurement starts in the 'Measured Page' defined in main panel. The stepping function can be combined with routing, i.e. several detector channels can be simultaneously measured in each step. The measurement sequence is similar to a 'Single' measurement with stepping through a number of pages. However, the data are interpreted as a sequence of data blocks and displayed by the 3D display routines of the SPCM software.



Steps

The number of subsequent measurements is defined by 'Steps'. The measurement starts in the 'Measured Page' defined in the main panel.

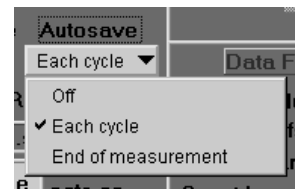
The photon collection for each step is controlled by 'Stop T' and the options under 'Overflow'. The measurement of each particular step stops

- at the end of 'Collection Time' if 'Stop T' is set
- at the first overflow if 'Stop Ovfl' is set

If both stop conditions are set the measurement stops in both cases. If the results run out of the data range 0...65535 the overflowing parts are clipped. Please note that at least one stop condition - usually Stop T - must be set to achieve reasonable operation.

Cycles and Autosave

A stepping sequence can be repeated for a defined number of 'Cycles'. To write the results of subsequent cycles to the hard disk the 'Autosave' function can be used. To activate 'Autosave' for each cycle, click on 'Autosave', 'Each Cycle'.



'Autosave' can also be initiated at the end of the measurement, i.e. after the last cycle only. 'End of Measurement' is normally used in conjunction with 'Accumulate'.

Accumulate

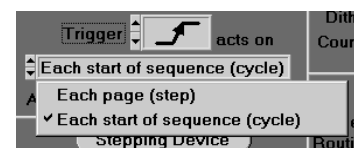
The 'Accumulate' function accumulates the results of several 'Cycles', i.e. several f(t,T) sequences. If you want to save the results automatically at the end of the accumulation, activate 'Autosave', 'End of Measurement'.

Repeat

By pushing the 'Repeat' button the complete measurement sequence can be repeated until the measurement is stopped by the operator.

Trigger

Either the 'Steps' or the 'Cycles' of the measurement sequence can be triggered. To activate the trigger, select 'rising edge' or 'falling edge' as 'Trigger Condition'.



f(t,T) Multidetector Operation

The f(t,T) mode can be combined with multi-detector operation or multiplexing. In this case separate curve sequences are obtained for the individual detector or multiplexing channels, see Fig. 274

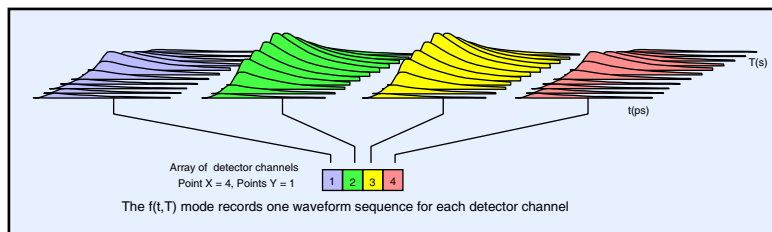


Fig. 274: f(t,T) mode, multi-detector operation

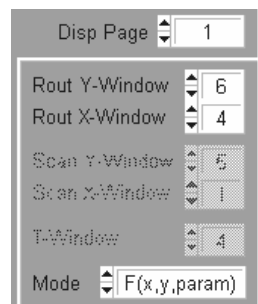
The number of detector channels is defined under ‘Page Control’, ‘Routing Channels X’ or ‘Routing Channels Y’, see page 298.

Due to the available memory size, there is a cross dependence of ‘Routing Channels X’, ‘Routing Channels Y’, ‘Steps’ through subsequent pages, and ‘ADC Resolution’. If one of these parameters is changed beyond the limit set by memory size the software automatically limits it to the maximum possible value. Some combinations are given in the table below.

Module Type	ADC Resol.	Routing Channels	Steps	Module Type	ADC Resol.	Routing Channels	Steps	Module Type	ADC Resol.	Routing Channels	Steps	Module Type	ADC Resol.	Routing Channels	Steps
SPC-8	4096	1	4096	SPC-7	4096	1	1024	SPC-6	4096	1	64	SPC-134	4096	1	32
	4096	8	512	SPC-144	4096	8	128		4096	8	8		4096	8	4
	256	1	65536		256	1	16384		256	1	1024		256	1	512
	256	8	8192		256	8	2048		256	8	128		256	8	64
	64	1	262144		64	1	65636		64	1	4096		64	1	2048
	64	8	32768		64	8	8192		64	8	512		64	8	256

f(t,T) Display

The results of an f(t,T) measurement are displayed as a three-dimensional figure. The display style (multiple-curve plot, colour intensity plot or OGL plot) is defined in the ‘Display Parameters’, see figure right. Up to eight display windows can be defined to display the data of different detector or multiplexing channels. Please see ‘Display Parameters’, page 301, ‘3D Trace Parameters’, page 311, and ‘Window Intervals’, page 313.

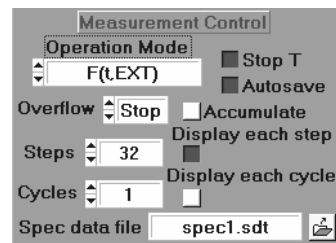


An f(t,T) measurement can contain a large number of subsequent curves. If the display is in the ‘3D Curve’ mode the finite screen resolution limits the number of curves to 128 curves. To see later parts of a longer sequence, change ‘Display Page’ in the Display Parameters or in the main panel.

During the individual measurement steps intermediate results can be displayed in intervals of ‘Display Time’. Furthermore, the result can be displayed after each step and after each cycle. However, displaying intermediate results requires some time. The ‘Display Time’ and ‘Display after each Step’ options and should be used for collection times longer than a several seconds per step only.

f(t,EXT) Mode

The measurement of a single curve is repeated in intervals of ‘Repeat Time’. The results are written into subsequent pages of the memory. Simultaneously with the page stepping an external parameter in the measurement setup is varied. The external parameter can be the wavelength of a monochromator or the position of the detector. To control the external parameter the stepping motor controller STP-340 can be used (see data sheet or www.becker-hickl.com). The STP-340 is an additional PC module which is controlled directly by the SPC software. The device is configured by the file STP.CFG which includes minimum and maximum values for the position, step width, motor speed, the unit of the controlled parameter etc. (see STP-340 description). The f(t,ext) mode can also be used to record a sequence of IRF functions for different values of the CFD threshold or the CFD zero cross level.



Steps

The number of subsequent measurements is defined by ‘Steps’. The measurement starts in the ‘Measured Page’ defined in the main panel. The stepping function can be combined with routing, i.e. several detector channels can be measured in each step.

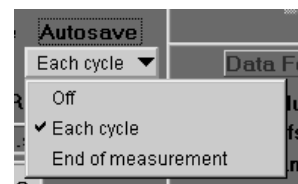
The photon collection for each step is controlled by ‘Stop T’ and the options under ‘Overflow’. The measurement of each step stops

- at the end of ‘Collection Time’ if ‘Stop T’ is set
- at the first overflow if ‘Stop Ovfl’ is set

If both stop conditions are set the measurement stops in both cases. If the results run out of the data range 0...65535 the overflowing parts are clipped. Please note that at least one stop condition - usually Stop T - must be set for reasonable operation.

Cycles and Autosave

The stepping sequence can be repeated for a defined number of ‘Cycles’.



To write the results of subsequent cycles to the hard disk the ‘Autosave’ function is provided. To activate Autosave for each cycle, click on ‘Autosave’, ‘Each Cycle’. ‘Autosave’ can also be initiated at the end of the measurement, i.e. after the last cycle only. ‘End of Measurement’ is normally used in conjunction with ‘Accumulate’.

Accumulate

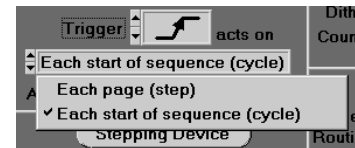
The ‘Accumulate’ function accumulates the results of several ‘Cycles’, i.e. several f(t,ext) sequences. It is often used for triggered sequences to acquire more photons than in a single shot. If you want to save the results automatically at the end of the accumulation, use ‘Autosave’, ‘End of Measurement’.

Repeat

By pushing the ‘Repeat’ button the complete measurement sequence can be repeated until the measurement is stopped by the operator.

Trigger

Either the ‘Steps’ or the ‘Cycles’ of the measurement sequence can be triggered. To activate the trigger, select ‘rising edge’ or ‘falling edge’ as ‘Trigger Condition’.



f(t,EXT) Multidetector Operation

As in the f(t,T) mode, multi-detector operation or multiplexing can be used to record several signals in each step of the f(t,EXT), see Fig. 275.

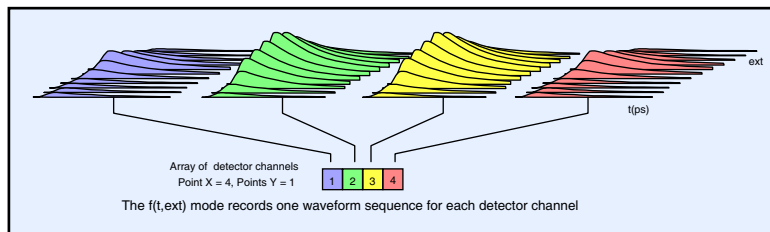


Fig. 275: f(t,EXT) mode, multi-detector operation

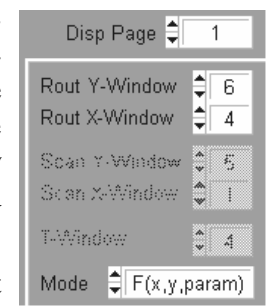
The number of detector channels are defined under ‘Page Control’, ‘Routing Channels X’ or ‘Routing Channels Y’, see page 298.

Due to the available memory size, there is a cross dependence of ‘Routing Channels X’, ‘Routing Channels Y’, ‘Steps’ through subsequent pages, and ‘ADC Resolution’. If one of these parameters is changed beyond the limit set by memory size the software automatically limits it to the maximum possible value. Some combinations are given in the table below.

Module Type	ADC Resol.	Routing Channels	Steps	Module Type	ADC Resol.	Routing Channels	Steps	Module Type	ADC Resol.	Routing Channels	Steps	Module Type	ADC Resol.	Routing Channels	Steps
SPC-8	4096	1	4096	SPC-7	4096	1	1024	SPC-6	4096	1	64	SPC-134	4096	1	32
	4096	8	512	SPC-144	4096	8	128		4096	8	8		4096	8	4
	256	1	65536		256	1	16384		256	1	1024		256	1	512
	256	8	8192		256	8	2048		256	8	128		256	8	64
	64	1	262144		64	1	65636		64	1	4096		64	1	2048
	64	8	32768		64	8	8192		64	8	512		64	8	256

f(t,EXT) Display

The results of an f(t,ext) measurement are displayed as a three-dimensional figure. The display style (multiple curve plot, colour intensity plot or OGL plot) is defined in the ‘Display Parameters’, see figure right. Up to eight display windows can be defined to display the data of different detector or multiplexing channels. Please see ‘Display Parameters’, page 301, ‘3D Trace Parameters’, page 311, and ‘Window Intervals’, page 313.



An f(t,EXT) measurement can contain a large number of subsequent curves. If the display is in the ‘3D Curve’ mode the finite screen resolution limits the number of curves to 128 curves. To see later parts of a longer sequence, change ‘Display Page’ in the Display Parameters or in the main panel.

During the individual measurement steps intermediate results can be displayed in intervals of ‘Display Time’. Furthermore, the result can be displayed ‘after each step’ and ‘after each cycle’. Please note that displaying intermediate results requires some time. The ‘Display Time’ and ‘Display after each Step’ options and should be used for collection times longer than a several seconds per step only.

fi(T) Mode

The ‘fi’ modes are intended for recording time resolved spectra. A waveform measurement is repeated in intervals of ‘Repeat Time’. The counts in the channels of each curve are averaged within selectable time intervals (see ‘Window Intervals’, page 313). The results of this averaging procedure represent the intensities in the selected time windows. The fi(T) mode records a time-controlled sequence of these intensity values, see Fig. 276. Up to eight spectra in different time windows are obtained for each detector channel.

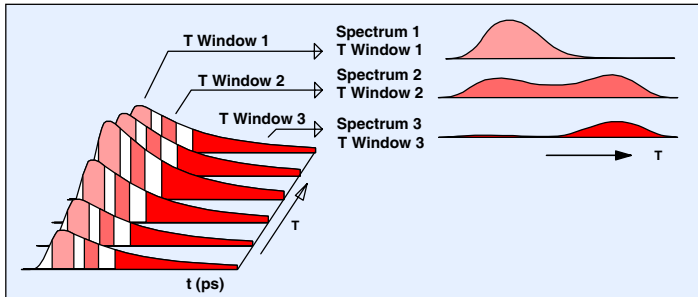


Fig. 276: fi(T) mode. Intensities within selectable time windows are calculated and displayed as functions of the time from the start of the experiment

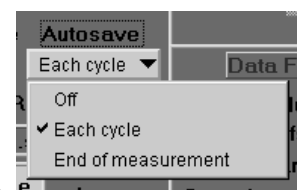
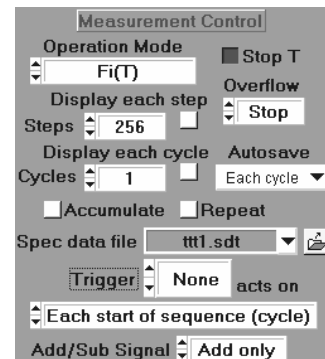
Steps

The number of subsequent intensity values is defined by ‘Steps’. The stepping function can be combined with routing, i.e. several detector channels can be measured in each step.

The photon collection for each step is controlled by the parameters ‘Stop T’ and the options under ‘Overflow’. The measurement of each step stops

- at the end of ‘Collection Time’ if ‘Stop T’ is set
- at the first overflow if ‘Stop Ovfl’ is set

If both stop conditions are set the measurement stops in both cases. If the results run out of the data range 0...65535 the overflowing parts are clipped. Please note that ‘Stop T’ must be set for reasonable operation of the fi(T) mode.



Cycles and Autosave

The sequence described above can be repeated for a defined number of ‘Cycles’.

The ‘Autosave’ function can be used to write the results of subsequent cycles to the hard disk. To activate Autosave for each cycle, click on ‘Autosave’, ‘Each Cycle’. ‘Autosave’ can also be initiated at the end of the measurement, i.e. after the last cycle only. ‘End of Measurement’ is normally used only in conjunction with ‘Accumulate’.

Accumulate

The ‘Accumulate’ function accumulates the results of several ‘Cycles’, i.e. several intensity sequences. If you want to save the accumulated results automatically at the end of the measurement, use ‘Autosave’, ‘End of Measurement’.

Trigger

Either the ‘Steps’ or the ‘Cycles’ of the measurement sequence can be triggered. To activate the trigger, select ‘rising edge’ or ‘falling edge’ as ‘Trigger Condition’.

Repeat

By pushing the ‘Repeat’ button the complete measurement sequence can be repeated until the measurement is stopped by the operator.

fi(T) Multidetector Operation

The fi(T) mode can be used in combination with multi-detector operation or multiplexing. In these cases individual spectra are obtained for the individual detector or multiplexing channels, see Fig. 277.

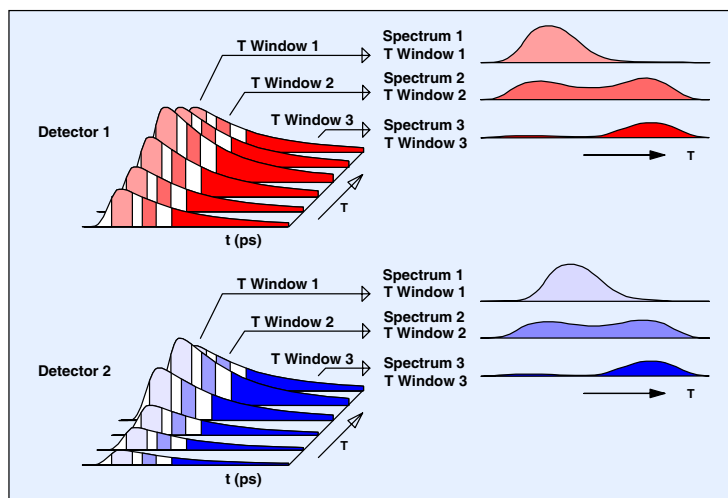


Fig. 277: fi(T) mode, multi-detector operation

The number of detector channels is defined under ‘Page Control’, ‘Routing Channels X’ or ‘Routing Channels Y’, see page 298. The maximum number of detector channels for an fi(T) measurement depends on the module type, the ADC Resolution, the number of Time Windows and the number of routing channels used.

fi(T) Display

The display of the results is controlled by the ‘Trace Parameters’, see page 307. You can define traces for spectra in different time windows and recorded by different detectors. Two typical settings are shown in Fig. 278.

Trace	Active	Colour	Curve	Frame	Page	T-Wind	Trace	Active	Colour	Curve	Frame	Page	T-Wind
1	■	■	■	1	1	1	1	■	■	■	1	1	1
2	■	■	■	1	1	2	2	■	■	■	1	1	1
3	■	■	■	1	1	3	3	■	■	■	1	1	1
4	■	■	■	1	1	4	4	■	■	■	1	1	1
5	■	■	■	1	1	5	5	■	■	■	1	1	1
6	■	■	■	1	1	6	6	■	■	■	1	1	1
7	■	■	■	1	1	7	7	■	■	■	1	1	1
8	■	■	■	1	1	8	8	■	■	■	1	1	1

Fig. 278: Trace parameters for the fi modes. Left: Spectra of detector 1 in subsequent time windows. Right: Spectra in time window 1 for different detectors

Intermediate results can be displayed after each step and after each cycle by switching on ‘Display after each Step’ and ‘Display after each Cycle’. However, displaying intermediate results requires some time. The ‘Display after each Step’ option should only be used for collection times longer than a few seconds.

fi(EXT) Mode

The measurement of a single waveform is repeated in intervals of ‘Repeat Time’ and for different settings of an externally variable parameter, typically for variable wavelength. The counts in the channels of each curve are averaged within selectable time intervals (see ‘Window Intervals’, page 313). The results of the averaging procedure represent the intensities in the selected time windows. The fi(EXT) mode records of these intensity values versus the external parameter, see Fig. 279. Up to eight time intervals can be defined. Consequently, up to eight spectra are obtained for each detector channel.

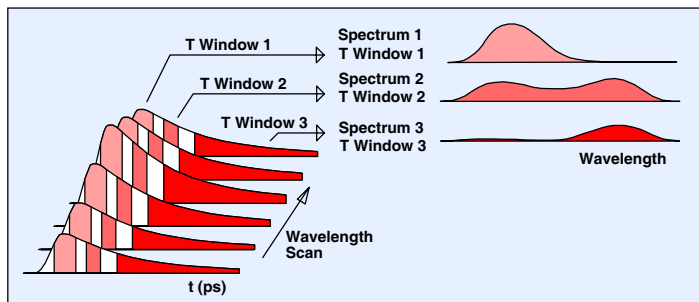


Fig. 279: fi(EXT) mode. Intensities within selectable time windows are calculated and displayed as functions of an external parameter

To control the external parameter the stepping motor controller STP-340 is used (see data sheet or www.becker-hickl.de). The STP-340 is an additional PC module which is controlled directly by the SPC software. The device is configured by the file STP.CFG which includes limiting values for the position, step width, motor speed, the unit of the controlled parameter etc. (see STP-240 description).

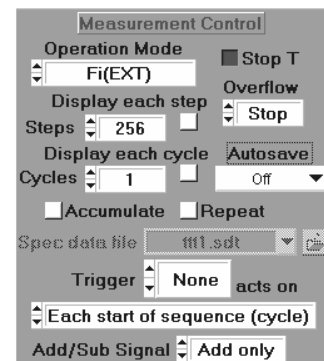
Steps

The number of subsequent intensity values is defined by ‘Steps’. The stepping function can be combined with routing, i.e. several detector channels can be measured in each step.

The photon collection for each step is controlled by the parameters ‘Stop T’ and the options under ‘Overflow’. The measurement of each step stops

- at the end of ‘Collection Time’ if ‘Stop T’ is set
- at the first overflow if ‘Stop Ovfl’ is set

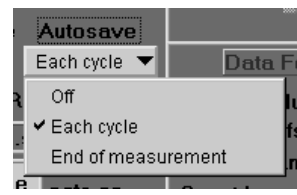
If both stop conditions are set the measurement stops in both cases. If the results run out of the data range 0...65535 the overflowing parts are clipped. Please note that ‘Stop T’ must be set for reasonable operation of the fi(ext) mode.



Cycles and Autosave

The sequence described above can be repeated for a defined number of 'Cycles'.

The 'Autosave' function can be used to write the results of subsequent cycles to the hard disc. To activate Autosave for each cycle, click on 'Autosave', 'Each Cycle'. 'Autosave' can also be used at the end of the measurement, i.e. after the last cycle only. The 'End of Measurement' option is normally used in conjunction with 'Accumulate'.

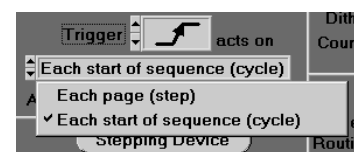


Accumulate

The 'Accumulate' function accumulates the results of several 'Cycles', i.e. several intensity sequences. If you want to save the results automatically at the end of the accumulation, use 'Autosave', 'End of Measurement'.

Trigger

Either the 'Steps' or the 'Cycles' of the measurement sequence can be triggered. To activate the trigger, select 'rising edge' or 'falling edge' as 'Trigger Condition'.



Repeat

By pushing the 'Repeat' button the complete measurement sequence can be repeated until the measurement is stopped by the operator.

fi(EXT) Multidetector Operation

The fi(T) mode can be used in combination with multi-detector operation or multiplexing. In these cases individual spectra are obtained for the individual detector or multiplexing channels, see Fig. 280.

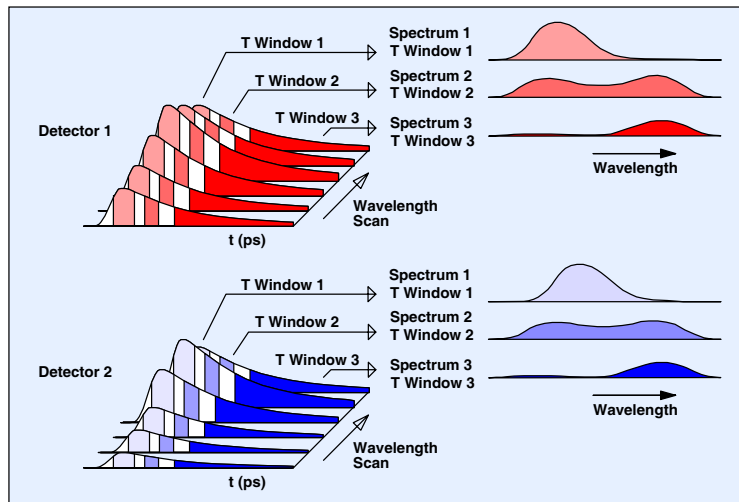


Fig. 280: fi(EXT mode, multi-detector operation

The number of detector channels is defined under 'Page Control', 'Routing Channels X' or 'Routing Channels Y', see page 298. The maximum number of detector channels for an fi(EXT) measurement depends on the module type, the ADC Resolution, the number of Time Windows and the number of Routing Channels used.

fi(EXT) Display

The display of the results is controlled by the ‘Trace Parameters’. You can select spectra obtained in different time windows and recorded by different detectors of a multi-detector arrangement. Two typical settings are shown in Fig. 281.

Trace	Active	Colour	Curve	Frame	Page	T-Wind
1				1	1	1
2				1	1	2
3				1	1	3
4				1	1	4
5				1	1	5
6				1	1	6
7				1	1	7
8				1	1	8

Trace	Active	Colour	Curve	Frame	Page	T-Wind
1				1	1	1
2				2	1	1
3				3	1	1
4				4	1	1
5				5	1	1
6				6	1	1
7				7	1	1
8				8	1	1

Fig. 281: Trace parameters for the fi modes. Left: Spectra of detector 1 in subsequent time windows. Right: Spectra in time window 1 for different detectors

Intermediate results can be displayed after each step and after each cycle by switching on ‘Display after each Step’ and ‘Display after each Cycle’. However, displaying intermediate results requires some time. The ‘Display after each Step’ option and should be used for collection times longer than a one second only.

Continuous Flow Mode

The Continuous Flow mode records a sequence of decay curves or other waveforms. Unlike f(t,T), the ‘Continuous Flow’ mode is strictly hardware-controlled and thus provides an extremely accurate recording sequence. Moreover, sequential recording can be combined with memory swapping so that virtually unlimited sequences can be recorded, see ‘Sequential Recording’, page 28. The Continuous Flow mode can also be used to accumulate fast, triggered sequences with stepping times down to a few microseconds. ‘Continuous Flow’ operation requires that the TCSPC module has two independent memory banks. Thus, the mode is available for the SPC-630, SPC-130/134, and SPC-150/154 modules only.

The principle of the mode is shown in Fig. 33, page 29. Decay curves are measured in time intervals of ‘Collection Time’. The measurement is repeated while the measurement system switches through all memory pages of both memory banks of the TCSPC module. While the measurement is running in one memory bank, the results of the other bank are read and stored on the hard disk. Thus, a virtually unlimited number of decay curves (or other photon distributions) can be recorded without any time gaps between subsequent recordings. In the SPC-150/154 modules continuous flow can even be combined with imaging, see . The measurement control parameters are shown in Fig. 282.

Banks and Steps

‘Banks’ defines the number of memory banks to be recorded. The number recording steps - or curves - in each memory bank depends on the selected ADC resolution, on the number of detector channels used, and on the module type. Some typical combinations are given in the table below.

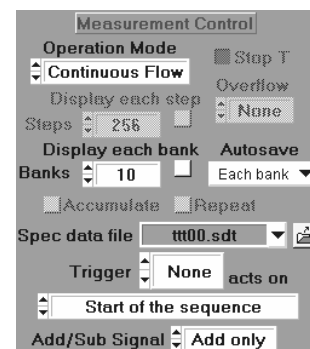


Fig. 282: Measurement control parameters of the continuous flow mode

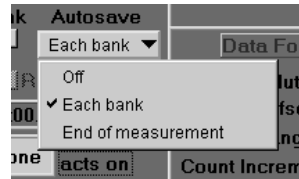
SPC-630			SPC-130/134			SPC-150/154		
ADC Resolution	Routing Channels	Steps per Bank	ADC Resolution	Routing Channels	Steps per Bank	ADC Resolution	Routing Channels	Steps per Bank
4096	1	64	4096	1	32	4096	1	512
4096	8	8	4096	8	4	4096	8	128
1024	1	256	1024	1	128	1024	1	2048
1024	8	32	1024	8	16	1024	8	512
256	1	1024	256	1	512	256	1	16384
256	8	128	256	8	64	256	8	2048
64	1	4096	64	1	2048	64	1	65536
64	8	512	64	8	256	64	8	8192

Collection Time

The photon collection for each step is controlled by ‘Collection Time’. ‘Repeat Time’ and ‘Stop Condition’ are not used in the Continuous Flow mode. ‘Display after each Step’, ‘Accumulate’ and ‘Repeat’ are not available.

Autosave

Normally the ‘Continuous Flow’ mode is used with ‘Autosave’, ‘Each Bank’. That means, while the measurement is running in one memory bank, the results of the other bank are read and saved into an individual data file. The file name is specified under ‘Spec data file’. The software extends the file name with a number that counts up for the subsequent banks. A list of previously used data file names is available by clicking on the symbol. *Important:* Before starting a new measurement define a new file name for the continuous flow data. If you don’t do so you are in danger to overwrite the data of an earlier measurement.



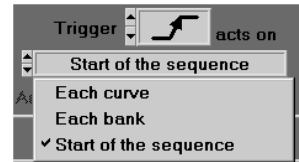
‘Autosave’ in combination with ‘End of Measurement’ is normally used for automatic saving of accumulated sequences, see below.

Accumulate

The ‘Accumulate’ function accumulates the results of repetitive sweeps through one ‘Bank’. It is normally used for fast triggered sequences. If the time per curve is less than a few milliseconds not enough photons are acquired to obtain a reasonable photon distribution in a single sweep. Thus, the stimulation of the experiment is repeated, the start of the sequencer sweep is triggered with the stimulation, and a large number of sweeps are accumulated. For accumulating fast triggered sequences set the trigger to ‘Start of Sequence’, activate the ‘Accumulate’ button, and set ‘Steps’ to a number smaller than the number of curves per memory bank. If you want to save the results automatically at the end of the accumulation, activate ‘Autosave’, ‘End of Measurement’.

Trigger

Either ‘Each Curve’, ‘Each Bank’ or the ‘Start of the Sequence’ can be triggered in the Continuous Flow mode. To activate the trigger, select ‘rising edge’ or ‘falling edge’ as trigger condition.



The trigger functions in the Continuous Flow mode can be used to create extremely powerful measurement procedures. As described above, triggering the ‘start of the sequence’ in combination with ‘accumulate’ can be used to record extremely fast sequences of decay curves, see ‘Transient Fluorescence Phenomena’, page 158.

Fast transient effects can also be recorded by triggering ‘Each bank’. In this case, the recording runs through the current memory bank, and stops. Recording in the next bank is

started with the next trigger. Thus the individual sequences are recorded in subsequent banks and stored in subsequent data files. ‘Each bank’ can also be used to synchronise the recording with a two-dimensional scanner. A new bank is triggered at the beginning of each line. The subsequent banks then represent the lines of the scan, the curves within each bank the pixels within the line.

‘Each curve’ triggering can be used to synchronise the recording with the steps of a one-dimensional scan.

Continuous Flow Multidetector Operation

The Continuous Flow mode can be used with multi-detector operation or multiplexing, see Fig. 283.

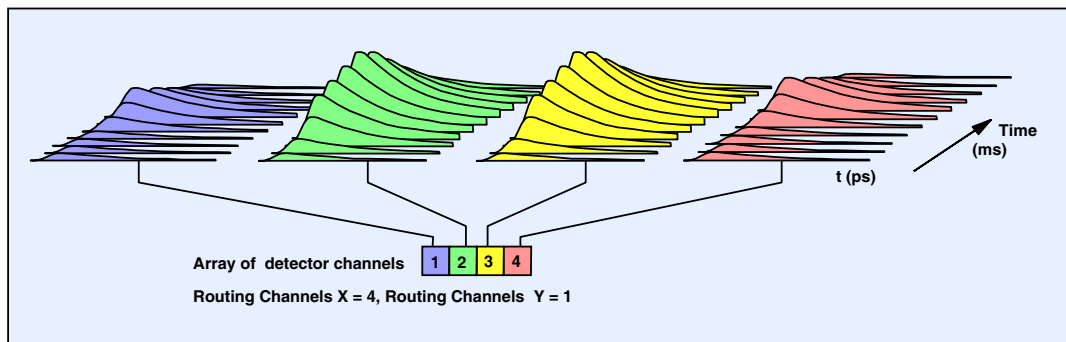


Fig. 283: Continuous Flow mode, multi-detector operation

The number of detector channels is defined under ‘Page Control’, ‘Routing Channels X’ or ‘Routing Channels Y’, see page 298. Due to the available memory size, there is a cross dependence of ‘Routing Channels X’, ‘Routing Channels Y’, ‘ADC Resolution’ and ‘Steps’ in one memory page. If one of these parameters is changed beyond the limit set by the memory size the software automatically limits it to the maximum possible value. With increasing number of detector channels the number of subsequent recordings per memory bank and consequently the maximum gap-free stepping speed decreases.

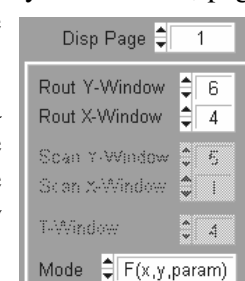
Continuous Flow Display

A Continuous Flow measurement is usually run through a large number of memory banks, and the results are saved in subsequent files. Only the last memory bank is displayed at the end of the measurement. To display the subsequent files produced by a continuous flow measurement, use the ‘Multi-File View’ function, see page 246.

The results of a Continuous Flow measurement are displayed as three-dimensional figures. The display style (multiple curve plot, colour intensity plot or OGL plot) is defined in the ‘Display Parameters’, see figure right. Up to eight display windows can be defined to display the data of different detector or multiplexing channels. Please see ‘Display Parameters’, page 301, ‘3D Trace Parameters’, page 311, and ‘Window Intervals’, page 313.

On bank (or one file) of a Continuous Flow measurement can contain a large number of subsequent curves. If the display is in the ‘3D Curve Mode’ a maximum of 128 curves can be displayed due to the finite screen resolution. To see later parts of the sequence, change ‘Display Page’ in the Display parameters or in the Main Panel.

Intermediate results can be displayed after each bank. Displaying intermediate results requires some time and should not be used for time-



Display Parameters

critical recordings. If the display is not ready to read the data before the recording in this bank is started a gap in the recording sequence appears.

Scan Sync Out Mode

The ‘Scan Sync Out’ mode is used to record time resolved images by sending synchronisation pulses to an external scanner. The mode is implemented in the SPC-830, SPC-700/730, and the SPC-140/144 modules. The principle is shown in Fig. 284.

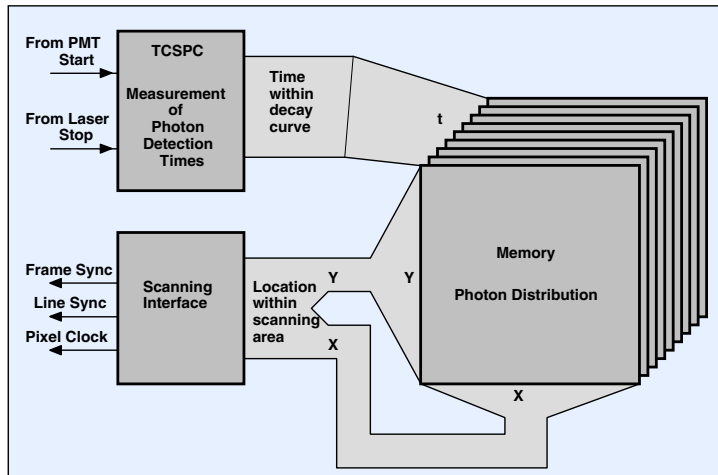


Fig. 284: Scan Sync Out mode (routing not shown)

In the ‘Scan Sync Out’ mode the SPC module controls the destination curve number and delivers synchronisation pulses to an external scanning device. For each pixel of the scanned image a complete waveform is recorded. The ‘Scan Sync Out’ mode can be combined with routing, i.e. the photons in several detector channels can be recorded simultaneously. The dwell time for each pixel is ‘Collection Time’. The maximum number of pixels depends on the ADC resolution selected:

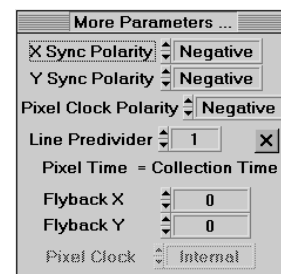
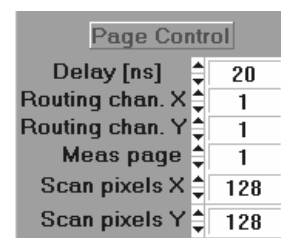
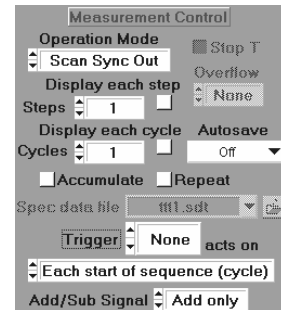
ADC Resolution	1	4	16	64	256	1024	4096
No of Pixels (SPC-7)	n.a.	n.a.	n.a.	65536	16384	4096	1024
No. of Pixels (SPC-8)	16 M	4 M	1 M	262144	65536	16385	4096
No of Pixels (SPC-144)*	4 M	1 M	262144	65536	16384	4096	1024
No of Pixels (SPC-154)*	4 M	1 M	262144	65536	16384	4096	1024

* per module

The scan can be either one-dimensional or two-dimensional. The number of steps in X- and Y-direction is specified by the parameters ‘Scan Pixels X’ and ‘Scan Pixels Y’ in the ‘Page Control’ Part of the System Parameters, see figure right.

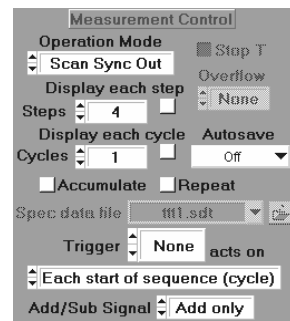
The scanning parameters are defined under ‘More Parameters’. The meaning of the scanning parameters is listed below:

- X Sync Polarity: Polarity of X Sync Pulses, (H/L or L/H)
- Y Sync Polarity: Polarity of Y Sync Pulses, (H/L or L/H)
- Pixel Clock Polarity: Polarity of Pixel Clock Pulses, (H/L or L/H)
- Line Predivider: Values >1 combine several lines of the scanner into 1 line of the result
- Flyback X: Flyback time of the scanner for the X axis, in multiples of ‘Collection Time’.
- Flyback Y: Flyback time of the scanner for the Y axis, in multiples of ‘Collection Time’.



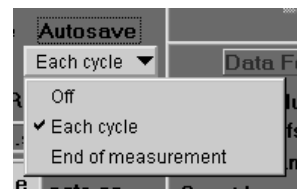
Stepping through Pages

A ‘Scan Sync Out’ measurement can be repeated after a scan is completed and the results written into subsequent ‘Pages’ of the memory. The number of subsequent measurements is defined by ‘Steps’. The stepping function can be combined with routing, i.e. several detector channels can be simultaneously measured in each step. The available number of steps depends on the memory size, i.e. on the module type, on ‘Routing Channels X’ and ‘Routing Channels Y’, and on the ADC resolution.



Cycles and Autosave

A stepping sequence (or, if ‘Steps’ = 1, a single ‘Scan Sync Out’ measurement) can be repeated for a defined number of ‘Cycles’.

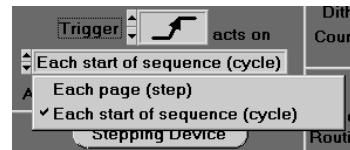


To write the results of subsequent cycles to the hard disk the ‘Autosave’ function is used. To activate ‘Autosave’ for each cycle, click on ‘Autosave’, ‘Each Cycle’.

‘Autosave’ can also be initiated at the end of the measurement, i.e. after the last cycle only. This is reasonable if the cycling function is used in conjunction with accumulate.

Accumulate

The ‘Accumulate’ function accumulates the results of several ‘Cycles’. It is used to accumulate subsequent scans or to accumulate the results of a triggered stepping sequence. If you want to save the results automatically at the end of the accumulation, use ‘Autosave’, ‘End of Measurement’.



Trigger

Either the ‘Steps’ or the ‘Cycles’ of the measurement sequence can be triggered. To activate the trigger, select ‘rising edge’ or ‘falling edge’ as ‘Trigger Condition’.

Repeat

By pushing the ‘Repeat’ button the complete measurement sequence can be repeated until the measurement is stopped by the operator.

Multidetector Operation

Multi-detector operation and multiplexing is also available in the Scan Sync Out mode. The principles is shown in Fig. 285. For each PMT pulse, i.e. for each photon, the SPC module determines the time of the photon in the laser pulse sequence, t, and the beam location in the scanning area, X and Y. Furthermore, the detector channel number, n, for the current photon is read into the detector channel register. The obtained values of t, x, y and n are used to address the histogram memory. Thus, in the memory the distribution of the photons over the time, the image coordinates and the detector number builds up. For each detector channel a stack of images for subsequent time channels in the fluorescence decay curve exists.

It should be pointed out that ‘Scan Sync Out’ Multidetector Operation does not involve any time gating or wavelength scanning. Therefore, the method yields a near-perfect counting efficiency and a maximum signal to noise ratio for a given acquisition time.

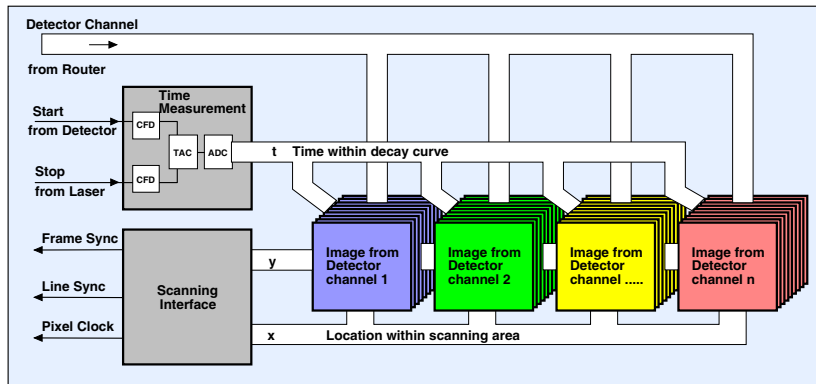


Fig. 285: Scan Sync Out mode, multidetector operation

The number of detector channels are defined under ‘Page Control’, ‘Routing Channels X’ or ‘Routing Channels Y’, see figure right.

Due to the available memory size, there is a cross dependence of Routing Channels X, Routing Channels Y, Steps through subsequent pages, Scan Pixels X, Scan Pixels Y and ADC Resolution. If one of these parameters is changed beyond the limit set by memory size the software automatically limits it to the maximum possible value. Without stepping through pages the maximum number of pixels is:

Page Control	
Delay [ns]	20
Routing chan. X	16
Routing chan. Y	1
Meas page	1
Scan pixels X	64
Scan pixels Y	64

ADC Resolution, Channels	1	4	16	64	256	1024	4096
No of Pixels SPC-7, 1 detector	n.a.	n.a.	n.a.	65536	16384	4096	1024
SPC-7, 4 detectors	n.a.	n.a.	n.a.	16384	4096	1024	256
SPC-7, 16 detectors	n.a.	n.a.	n.a.	4096	1024	256	64
No. of Pixels SPC-8, 1 detector	16 M	4 M	1 M	262144	65536	16385	4096
SPC-8, 4 detectors	4 M	1 M	262144	65536	16385	4096	1024
SPC-8, 16 detectors	1M	262144	65536	16385	4096	1024	256

Sequential Recording in the Scan Sync Out mode

Scanning in the Scan Sync Out is fully hardware-controlled. The SPC module uses a sequencer that steps through the memory blocks of the subsequent pixels in accurately defined time intervals. Therefore the Scan Sync Out mode can also be used for sequential recording. The stepping time can be as short as 100 ns, the start of the sequence can be triggered, and an extremely large number of waveform blocks is available. Thus, the Scan Sync Out mode can be used both for recording single sequences and fast triggered accumulation of sequences.

To record a sequence in the Scan Sync Out mode define an ‘image’ of one line, with a number of ‘Scan pixels’ corresponding to the desired number of steps. The Page-Control parameters shown right give an example of a sequence of 1024 steps and four detector channels. An SPC-830 allows you to use no less than 4096 time channels under these conditions.

Page Control	
Delay [ns]	10
Routing chan. X	4
Routing chan. Y	1
Meas page	1
Scan pixels X	1024
Scan pixels Y	1

The time per step of the sequence is ‘Collection Time’. To record a fast triggered sequence, set a trigger condition different from ‘none’, ‘Accumulate’, and the desired number of ‘Cycles’.

Scan Sync In Mode

The ‘Scan Sync In’ mode is designed to record images by scanners which deliver synchronisation pulses to the SPC module. ‘Scan Sync In’ is the most powerful scan mode of the bh SPC modules and normally used for fluorescence lifetime imaging with laser scanning microscopes. It can also be used with ultrafast ophthalmic scanners. The mode is available in the SPC-700/730, SPC-830, SPC-140/144 and SPC-150/154 modules. The principle of the ‘Scan Sync In’ mode is shown in Fig. 286.

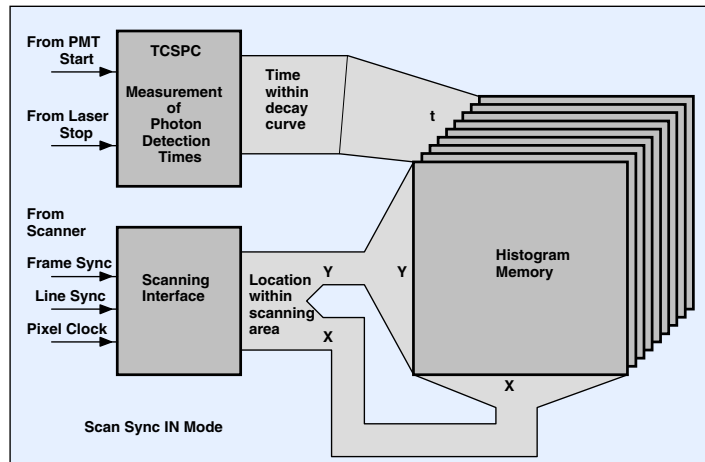


Fig. 286: Module configuration in the Scan Sync In mode

In the ‘Scan Sync In’ mode the SPC module receives synchronisation pulses from the scanner to control its internal destination curve number. For each PMT pulse, i.e. for each photon, the SPC module determines the time of the photon in the laser pulse sequence and the beam location in the scanning area. These values are used to address the histogram memory in which the events are accumulated. Thus, in the memory the distribution of the photon density over X, Y, and the time within the fluorescence decay function builds up.

The data acquisition works at any scanning rate of a laser scanning microscope. The acquisition can be run over as many frame scans as necessary to collect enough photons. Due to the synchronisation via the scan synchronisation pulses, the zoom functions of a scanning microscope automatically act also on the TCSPC recording and can be used in the normal way.

The parameter ‘Collection Time’ defines the overall image recording time. When the measurement is started the recording starts with the next Frame Sync pulse, i.e. at the beginning of the next frame. When the collection time is over the measurement stops with the next Frame Sync pulse, i.e. when the current frame is completed.

The number of pixels in X- and Y-direction is specified by the parameters ‘Scan Pixels X’ and ‘Scan Pixels Y’ in the ‘Page Control’ Part of the system parameters, see figure right.

The maximum number of pixels depends on the used ADC resolution. For a single detector measurement without stepping the maximum number of pixels per image is:

Page Control	
Delay [ns]	20
Routing chan. X	1
Routing chan. Y	1
Meas page	1
Scan pixels X	256
Scan pixels Y	256

ADC Resolution	1	4	16	64	256	1024	4096
No of Pixels (SPC-7)	n.a.	n.a.	n.a.	65536	16384	4096	1024
No of Pixels (SPC-140)	4 M	1 M	262144	65536	16384	4096	1024
No of Pixels (SPC-150)	4 M	1 M	262144	65536	16384	4096	1024
No. of Pixels (SPC-8)	16 M	4 M	1 M	262144	65536	16385	4096

The synchronisation of the recording process in the SPC module with the operation of the scanner requires a number of hardware parameters to be defined. To define these parameters, click on ‘More Parameters’. This opens the panel shown in Fig. 287. The configuration of the panel changes with the definition of the pixel clock source, compare Fig. 287 left and right.

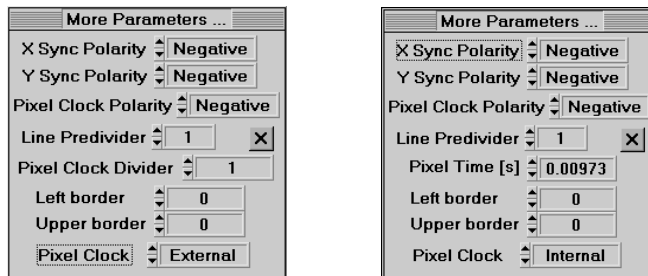


Fig. 287: Scanning parameters of the Scan Sync In mode. Left: External pixel clock. Right: Internal pixel clock.

The meaning of the scanning parameters is listed below:

X Sync Polarity:	Polarity of X Sync Pulses, (H/L or L/H)
YSync Polarity:	Polarity of Y Sync Pulses, (H/L or L/H)
Pixel Clock Polarity:	Polarity of Pixel Clock Pulses, (H/L or L/H)
Line Predivider:	Predivider for X Sync. Values >1 merge several lines of the scanner into one line of the result.
Pixel Clock Divider:	Divider for ‘Pixel Clock External’, values >1 merge several pixels of the scanner into 1 pixel of the result.
Pixel Time:	For ‘Pixel Clock Internal’ only. Dwell Time per pixel for ‘Pixel Clock Internal’ Within one line, the pixel number is counted up in fixed time intervals set by ‘Pixel Time’.
Pixel Clock Predivider:	For ‘Pixel Clock External’ only. For Predivider > 1 several subsequent pixels of the scanner are combined into one result pixel.
Upper Border:	Number of lines which are not recorded at the start of each frame. Used to zoom into the image without changing the scanner operation.
Left Border:	Number of pixels which are not recorded at the start of each line. Used to zoom into the image without changing the scanner operation.
Pixel Clock:	The source of the pixel clock can be external (from the scanner) or internal. The internal pixel clock is derived from the system clock of the SPC board. Internal pixel clock required that the Xsync frequency from the scanner be constant and stable.

For scanners that deliver a pixel clock the setup of the scan parameters is straightforward. Set the line and pixel clock dividers according to the ratios of the pixel numbers of the scanner and the pixel numbers of the TCSPC image (Scan pixels X and Scan Pixels Y). For correcting possible image shifts or distortions, please see Fig. 120, page 114.

If the internal pixel clock has to be used the pixel time must be defined correctly. This may be difficult if the speed of the scanner is not known. We suggest to start with an approximate pixel time and then correct the setting by try and error, see Fig. 120, page 114. For video-compatible scanning (64us per line) the number of recorded pixels per line is

Pixel Time ns	400	800	1600	3200
Pixels / Line	160	80	40	20

The number of lines in the recorded image is:

Line Predivider	1	2	4	8
Lines / Frame	256	128	64	32

Stepping through Pages

A ‘Scan Sync In’ measurement can be repeated after a scan is completed and the results be written into subsequent ‘Pages’ of the memory. The number of subsequent measurements is defined by ‘Steps’. The stepping function can be combined with routing, i.e. several detector channels can be measured in each step. The available number of steps depends on the memory size, i.e. on the module type, on ‘Routing Channels X’ and ‘Routing Channels Y’, and on the ADC resolution.

Cycles and Autosave

A stepping sequence (or, if ‘Steps’ = 1, a single ‘Scan Sync In’ measurement) can be repeated for a defined number of ‘Cycles’.

To write the results of subsequent cycles to the hard disk the ‘Autosave’ function is provided. To activate ‘Autosave’ for each cycle, click on ‘Autosave’, ‘Each Cycle’.

‘Autosave’ can also be initiated at the end of the measurement, i.e. after the last cycle only. This is reasonable if the cycling function is used in conjunction with accumulate.

Accumulate

The ‘Accumulate’ function accumulates the results of several ‘Cycles’. It is used to accumulate subsequent scans or to accumulate the results of a triggered stepping sequence. If you want to save the results automatically at the end of the accumulation, use ‘Autosave’, ‘End of Measurement’.

‘Accumulate’ can be used to obtain on-line display during the image acquisition: Define a ‘Collection Time’ of about 10 seconds. Specify a large number of ‘Cycles’. Switch on ‘Accumulate’ and ‘Display each Cycle’. The SPC module will run subsequent acquisition cycles with the specified collection time, accumulate the photons of the cycles, and display the accumulated image.

Trigger

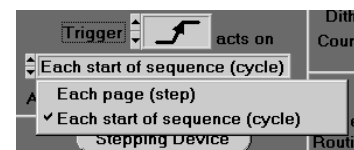
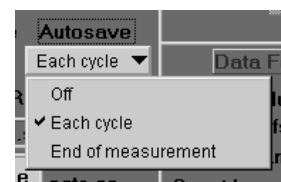
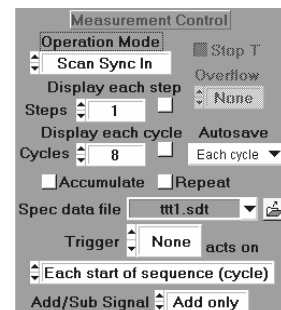
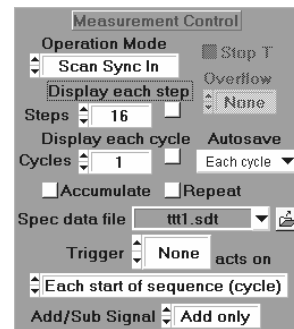
Either the ‘Steps’ or the ‘Cycles’ of the measurement sequence can be triggered. To activate the trigger, select ‘rising edge’ or ‘falling edge’ as ‘Trigger Condition’.

Repeat

By pushing the ‘Repeat’ button the complete measurement sequence can be repeated until the measurement is stopped by the operator.

Multidetector Operation

The Scan Sync In mode can be used in combination with multi-detector operation or multiplexing. The principle is shown in Fig. 288. For each PMT pulse, i.e. for each photon, the SPC module determines the time of the photon in the laser pulse sequence, t, and the beam location in the scanning area, X and Y. Furthermore, the detector channel number, n, for the current photon is read into the detector channel register. The obtained values of t, x, y and n are used to address the histogram memory. Thus, in the memory the distribution of the photons over the time, the image coordinates and the detector number builds up. The result can be



interpreted as a number of data sets for the individual detectors. Each data set contains a large number of images for consecutive times in the fluorescence decay.

It should be pointed out that Scan Sync In multidetector operation does not involve any time gating or wavelength scanning. Therefore, the method yields a near-perfect counting efficiency and a maximum signal to noise ratio for a given acquisition time.

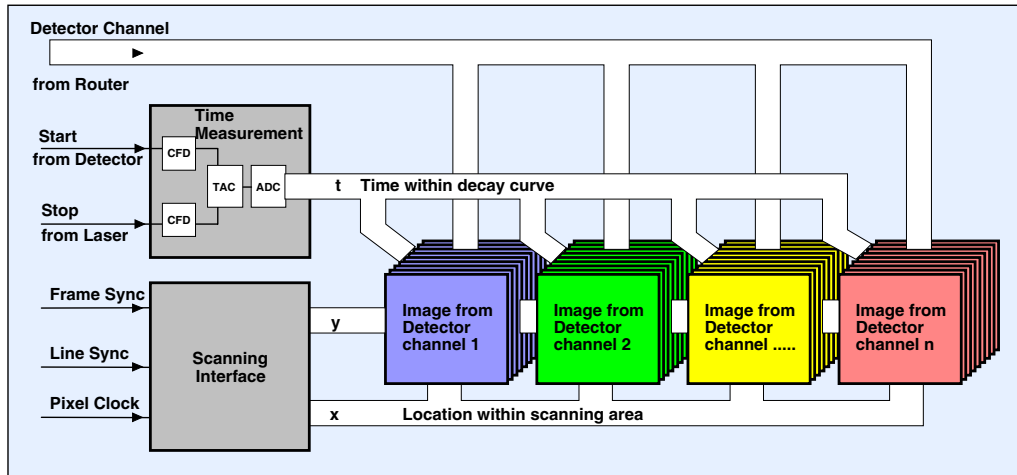


Fig. 288: Scan Sync In mode, multidetector operation

The number of detector channels are defined under ‘Page Control’, ‘Routing Channels X’ or ‘Routing Channels Y’, see figure right.

Due to the available memory size, there is a cross dependence of Routing Channels X, Routing Channels Y, steps through subsequent pages, Scan Pixels X, Scan Pixels Y, and ADC Resolution. If one of these parameters is changed beyond the limit set by memory size the software automatically limits it to the maximum possible value. Without stepping through pages the maximum number of pixels is:

Page Control	
Delay [ns]	20
Routing chan. X	16
Routing chan. Y	1
Meas page	1
Scan pixels X	64
Scan pixels Y	64

Module, no. of detectors	ADC Resolution, Channels						
	1	4	16	64	256	1024	4096
SPC-730							
1 detector	n.a.	n.a.	n.a.	65536	16384	4096	1024
4 detectors	n.a.	n.a.	n.a.	16384	4096	1024	256
16 detectors	n.a.	n.a.	n.a.	4096	1024	256	64
SPC-830							
1 detector	16 M	4 M	1 M	262144	65536	16385	4096
4 detectors	4 M	1 M	262144	65536	16385	4096	1024
16 detectors	1M	262144	65536	16385	4096	1024	256
SPC-140							
1 detector/channel	4 M	1 M	262144	65536	16384	4096	1024
4 detectors/channel	1 M	262144	65536	16384	4096	1024	256
16 detectors/channel	262144	65536	16384	4096	1024	256	64
SPC-144							
4 detectors	4M	1 M	262144	65536	16385	4096	1024
SPC-150							
1 detector/channel	4 M	1 M	262144	65536	16384	4096	1024
4 detectors/channel	1 M	262144	65536	16384	4096	1024	256
16 detectors/channel	262144	65536	16384	4096	1024	256	64
SPC-154							
4 detectors	4M	1 M	262144	65536	16385	4096	1024

Scan Sync In, Continuous Flow Imaging

In the SPC-150/154 modules imaging in the Scan Sync In mode can be combined with ‘continuous flow’ operation. The device memory is split into two memory banks. The banks are used by turns. While the measurement is running in one bank the data of the other bank are read, and vice versa. Thus, an infinite sequence of images is recorded, without gaps between the recordings. The procedure is similar to the ‘continuous flow mode’ for sequences of curves, see page 266. The measurement and page control parameters are shown in Fig. 289.

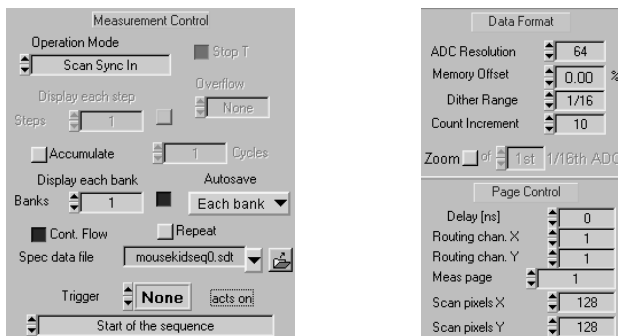


Fig. 289: Control parameters for continuous flow imaging. Left: Measurement control parameters. Right: ADC and page control parameters

Continuous flow operation of Scan Sync In is activated by clicking on the ‘Cont. Flow’ button in the measurement control parameters.

‘Banks’ defines the number of memory banks to be recorded. The recording in each bank starts with the next frame clock pulse, and continues until the first frame clock pulse after the end of the ‘collection time’. The data of each bank are saved into a separate data file. The name of the files is specified under ‘Spec data file’. The software extends the file name with a number that counts up for the subsequent banks. A list of previously used data file names is available by clicking on the symbol. *Important:* Before starting a new measurement define a new file name for the continuous flow data. If you don’t do so you are in danger to overwrite the data of an earlier measurement.

To see the results of the individual measurement steps you may activate the ‘Display each bank’ button. However, please remember that the build-up of the images takes time and computing power. It may therefore reduce the speed at which the image sequence can be recorded.

Continuous-flow operation can be used in combination with the experiment trigger. Either the start of the sequence or the starts of the measurements in the individual memory banks can be triggered.

The ADC and page control parameters are shown in Fig. 289, right. The numbers of time channels, detectors, and pixels are defined as in the standard Scan-Sync-In mode. Because the device memory of the TCSPC module is split in two banks the maximum images size or the ADC resolution is only 50% of the size in the Scan Sync In mode without continuous flow. This may be considered a drawback. However, continuous-flow operation aims at very fast recording sequences on the order of one second and below. The low photon numbers accumulated within a collection time this short by itself requires a reduction of the pixel number. (For collection times longer than a few seconds you may use the standard Scan-Sync-In mode with autosave.)

To display the subsequent files produced by a continuous flow measurement, use the ‘Multi-File View’ function, see page 246.

Scan XY Out Mode (SPC-700/730 only)

The SPC-700/730 modules have a ‘Scan XY Out’ mode that sends digital X-Y signals to an external scanner. The principle is shown in Fig. 290.

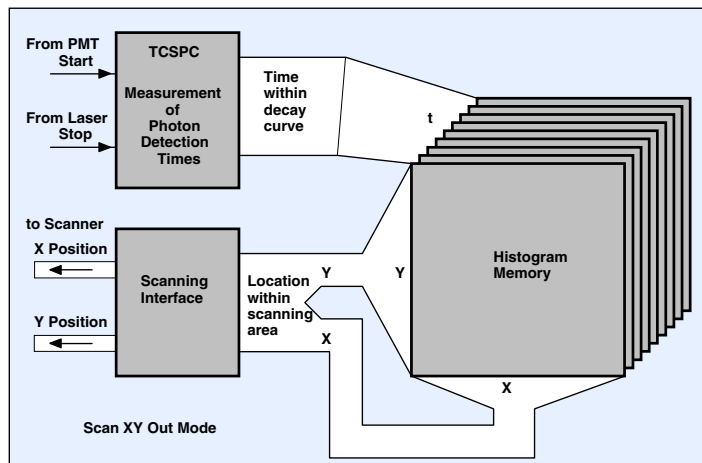


Fig. 290: Module configuration in the Scan XY Out mode

In the ‘Scan XY Out’ mode the SPC-700 and -730 modules control the destination curve number internally and deliver digital X and Y position signals to an external scanning device.

The XY position is available at the routing connector of the module. Thus, the maximum number of XY bits is 14, and the maximum number of pixels is 16384. Since the routing lines of the SPC modules are used for XY output the ‘Scan XY Out’ mode cannot be used with routing.

For each pixel of the image a complete waveform is recorded. The dwell time for each pixel is ‘Collection Time’. The maximum number of pixels depends on the selected ADC resolution:

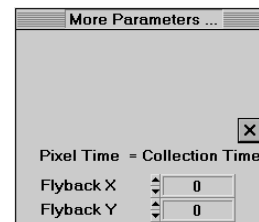
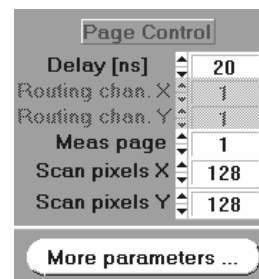
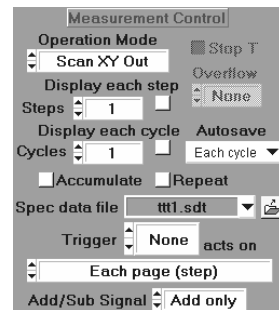
ADC Resolution	64	256	1024	4096
No of Pixels	16384	16384	4096	1024

The scan can be either one-dimensional or two-dimensional. The number of steps in X- and Y-direction is specified by the parameters ‘Scan Pixels X’ and ‘Scan Pixels Y’ in the ‘Page Control’ Part of the System Parameters.

The scanning parameters are defined under ‘More Parameters’. The meaning of the scanning parameters is listed below:

Flyback X: Flyback time of the scanner for the X axis, defined as multiples of ‘Collection Time’. After the X position signal has switched back to the ‘0’ position the operation is suspended for the ‘Flyback X’ time to give the scanner mirror time to settle.

Flyback Y: Flyback time of the scanner for the Y axis, defined as multiples of ‘Collection Time’. After the Y position signal has switched back to the ‘0’ position the operation is suspended for the ‘Flyback Y’ time to give the scanner mirror time to settle.



Stepping through Pages

A ‘Scan XY Out’ measurement can be repeated after a scan is completed and the results be written into subsequent ‘Pages’ of the memory. The number of subsequent measurements is defined by ‘Steps’. The available number of steps depends on the memory size, i.e. on the module type, on ‘Routing Channels X’ and ‘Routing Channels Y’, and on the ADC resolution.

Cycles and Autosave

A stepping sequence (or, if ‘Steps’ = 1, a single ‘Scan XY Out’ measurement) can be repeated for a defined number of ‘Cycles’.

To write the results of subsequent cycles to the hard disk the ‘Autosave’ function is used. To activate ‘Autosave’ for each cycle, click on ‘Autosave’, ‘Each Cycle’.

‘Autosave’ can also be initiated at the end of the measurement, i.e. after the last cycle only. This is reasonable if the cycling function is used in conjunction with accumulate.

Accumulate

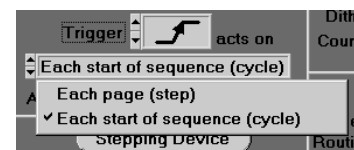
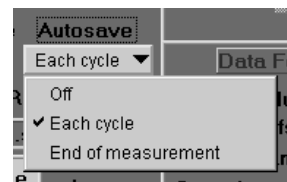
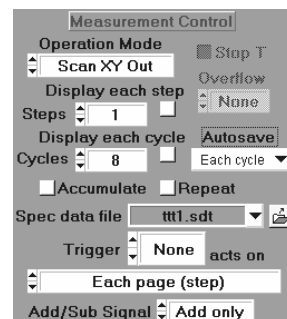
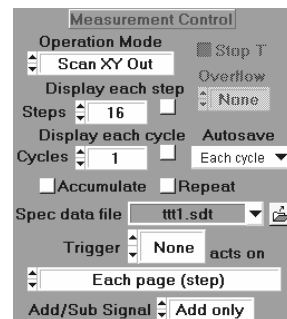
The ‘Accumulate’ function accumulates the results of several ‘Cycles’. It is used to accumulate subsequent scans or to accumulate the results of a triggered stepping sequence. If you want to save the results automatically at the end of the accumulation, use ‘Autosave’, ‘End of Measurement’.

Trigger

Either the ‘Steps’ or the ‘Cycles’ of the measurement sequence can be triggered. To activate the trigger, select ‘rising edge’ or ‘falling edge’ as ‘Trigger Condition’.

Repeat

By pushing the ‘Repeat’ button the complete measurement sequence can be repeated until the measurement is stopped by the operator.



Scan Mode Display

The results of a Scan mode measurement are multi-dimensional data arrays. The dimensions are the two coordinates of the scanning area, X and Y, the time in the fluorescence decay, t, and possibly the detector channel number and the step number.

This section gives a general introduction of how the data obtained in the Scan modes can be displayed. A detailed description of the display modes of the Multi SPC Software is given under ‘Display Parameters’. Typical ‘Display Parameter’ settings for the Scan modes are shown in Fig. 291.

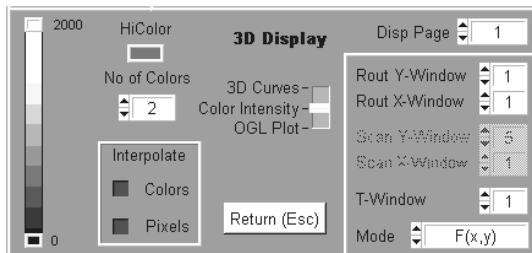


Fig. 291: 3D section of the display parameter panel

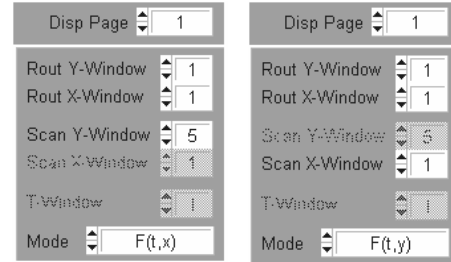
The recommended display mode is the ‘Colour Intensity’ mode in conjunction with the $F(x,y)$ option. This mode displays an image over the scan coordinates showing the total number of photons over the time channels of a specified time window. The time window is defined in the ‘Window Intervals’ and selected under ‘T Window’ in the ‘Display Parameters’. By stepping through subsequent ‘T Windows’ images in subsequent time windows can be displayed.

If the measurement is performed in a multidetector setup, i.e. ‘Routing Channels X’ or ‘Routing Channels Y’ in the System Parameters are greater than one, several ‘Routing Windows’ are available. The Routing Windows are defined in the ‘Window Intervals’ panel. Images in different Routing Windows can be selected in the Display Parameters, see Fig. 291.

Furthermore, if stepping through subsequent pages was used, a particular step of a page stepping sequence can be selected via the ‘Display Page’ of the display parameters, see Fig. 291.

The intensity scale is defined by the vertical bar in the left part of the 3D section of the ‘Display Parameters’. Please note that the photons of a ‘Scan’ mode measurement are spread over a large number of time channels, pixels, detector channels and possibly measurement steps. To obtain a reasonable display scale we recommend to activate the ‘Autoscale’ button of the display parameters.

In addition to the X, Y image described above t, X images and t, Y images can be displayed. These options are shown in the figure right. The t, X image is displayed in a selectable Scan Y window, the t, Y image in a selectable Scan X window. The Scan X and Scan Y windows are defined in the ‘Window Parameters’ and represent vertical or horizontal stripes of the image.



The ‘3D Trace Parameters’ allow you to define up to eight display windows in the main panel. An example is given in Fig. 251, page 234. Thus, you can display images in specified time windows or wavelength windows, or decay curves along a vertical or horizontal stripe of the image for different detectors.

During the individual measurement steps intermediate results can be displayed ‘after each step’ and ‘after each cycle’. The corresponding buttons are in the measurement control section of the System Parameters. Displaying the results of a ‘Scan’ measurement can take some seconds. Therefore, the ‘Display Time’ and ‘Display after each Step’ options and should be handled with care and used only for collection times no shorter than 10 seconds.

FIFO Mode

The 'FIFO' mode differs from the other modes in that it does not build up any histogram of the photon detection times. Instead, the detection time of each individual photon in the laser pulse sequence is stored together with the time from the start of the experiment and the detector channel number. The memory is configured as a FIFO (First In First Out) buffer. It receives the photon data at the input and is continuously read at the output. Therefore, the FIFO mode produces a continuous stream of photon data which is stored in the main memory of the computer or on the hard disk (see also 'Time-Tag Recording' page 31).

The 'FIFO' mode is available in the SPC-600/630, SPC-830, SPC-130/134, SPC-140/144 and SPC-150/154 modules.

FIFO data can be used for a wide variety of fluorescence analysis techniques (see 'Fluorescence Correlation Spectroscopy', page 206, and 'Time-Resolved Single-Molecule Spectroscopy', page 219).

By calculating a histogram of the 'Micro Times', i.e. the times of the photons in the laser pulse sequence, the fluorescence decay functions for the individual detectors are obtained. FCS curves are obtained by calculating the autocorrelation functions of the 'Macro Times', i.e. the times from the start of the experiment. Cross correlation curves of different detector channels are obtained by calculating the cross-correlation functions. The data can also be used to calculate photon counting histograms, lifetime histograms, and intensity traces. The SPCM software calculates these functions either on-line from the stream of photon data and off-line from the generated FIFO data files.

FIFO Measurement Control

The measurement control section of the System Parameters for the FIFO mode is shown right. The name of the FIFO data file is specified in the 'Spec Data File' field. To change the file name, click on the disc symbol right of the name field. A list of previously used data file names is available by clicking on the symbol. **Important:** Before starting a new measurement define a new file name for the FIFO data. If you don't do so you are in danger to overwrite the FIFO data of an earlier measurement.

Data recorded in the FIFO mode can easily reach sizes of tens or hundreds of megabytes. The maximum used disk space can be limited by activating the 'Limit Disk Space' button and specifying the maximum file size. The measurement stops when the specified disk space has been filled.

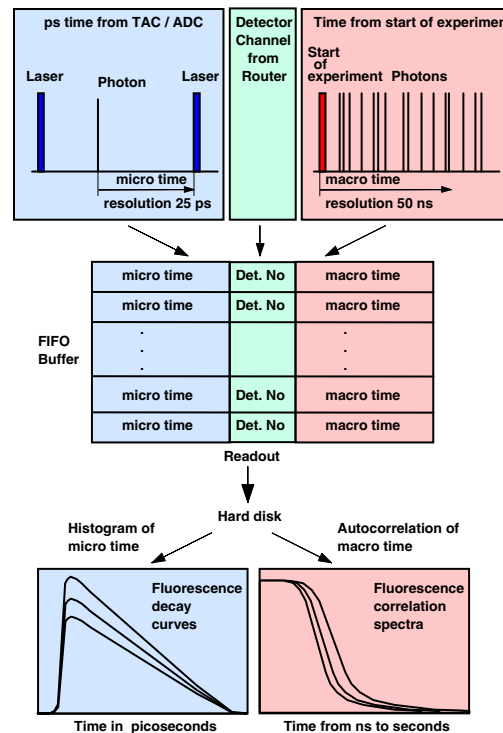
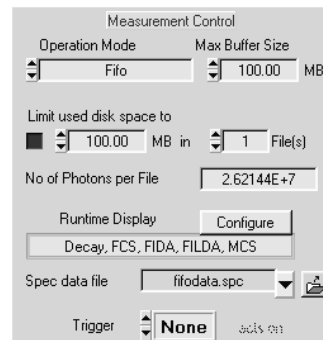


Fig. 292: Recording in the FIFO Mode



The measurement data can be divided into several subsequent data files. The file names are then automatically extended with a 3-digit number that is automatically incremented for each subsequent file. 'No of Photons per File' is calculated automatically.

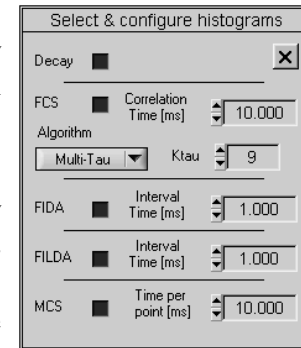
By 'Maximum Buffer Size' a buffer is defined in the computer memory. The buffer stores the data before they are saved to the hard disk. If possible, the buffer should be large enough to buffer the FIFO data of the complete measurement. Usually, the buffer size can be as large as 100 or 200 Mb for a computer with 512 Mb RAM. Under no circumstances a buffer size larger than the available memory space of the computer should be used. Windows may then attempt to provide virtual memory, i.e. to swap memory space with the hard disc. This makes the computer extremely slow and almost certainly causes problems with the data transfer from the SPC module.

If a sufficiently large buffer is not available use a buffer smaller than the value specified under 'limit disk space'. Of course, the SPCM software writes to the hard disk when the buffer is full. Although this may slow down the data transfer from the SPC module the loss is by far smaller than for memory swapping.

FIFO Mode Run-Time Display

The functions that are calculated on-line are shown in the field under 'Run Time Display'. The run time display can be configured by clicking on the 'Configure' button. This opens the panel shown right. The available on-line functions are

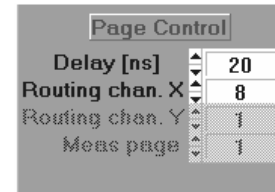
- Calculation of decay curves for the individual detectors
- FCS by a linear- τ algorithm with subsequent binning or FCS by a multi- τ algorithm. The maximum time up to which the correlation is calculated is defined by 'Correlation Time'.
- Fluorescence cross correlation between different detectors. (Use the 2D Trace parameters to define the detector channels)
- Calculation of photon counting histograms for the individual detectors ('FIDA'). The sampling time interval is specified on the right.
- Calculation of lifetime histograms (FILDA) for all detectors. The sampling time interval is specified on the right.
- Intensity traces (MCS) for the individual detectors.



For all functions individual display windows are provided in the main panel, see Fig. 251, page 234.

To display the results of several detector channels, set 'Routing Channels X' to the actual number of detectors (figure right).

For definition of correlation and cross correlation, configure the 'Trace Parameters' to display the appropriate 'Curves' as shown in Fig. 293. 'Curve' defines the detector numbers of decay functions to be displayed. 'Cross-FCS Curve' defines the detector number to correlate with. If 'Curve' and 'Cross-FCS Curve' are the same the autocorrelation is calculated. For different numbers the cross-correlation of the corresponding detectors is calculated. The configuration shown in Fig. 293 calculates the decay functions (histograms) of detector 1 and 2, the autocorrelation of detector 1 and 2, and the cross-correlation of detector 1 and 2.



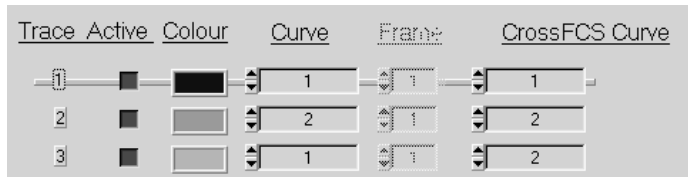


Fig. 293: Trace Parameters for the FCS display of FIFO mode

On-line calculation of correlation functions requires a considerable amount of computing power. This can slow down the display sequence below the specified ‘Display Time’ period. Moreover, the run-time calculations may dramatically reduce the readout rate from the SPC module. This is not really a problem for the modules with large FIFO size and fast bus interface, such as the SPC-830 and SPC-150/154. However, for the SPC-630 and the SPC-134 the on-line display can limit the count rates to 30 to 50 kHz. Therefore, make sure that the FIFO does not overflow when you use the on-line display.

For reasons of computation speed, the software is only able to calculate one correlation function per detector channel. If the Trace Parameters define several correlation functions for one channel, e.g. an autocorrelation and a cross-correlation with another channel, only the first correlation is calculated during the measurement. The other ones are calculated and displayed after the measurement is completed.

Device State

During a FIFO measurement the device state panel of the main window shows the number of collected photons and the amount of used FIFO buffer space, see Fig. 294.



Fig. 294: Device state during the FIFO mode

Make sure that the FIFO does not overflow. If you see that the FIFO runs full check whether you can do without some of the functions of the online display.

When you stop a FIFO measurement (by clicking on the ‘Stop’ button of the main panel) there may still be photon data in the FIFO buffer of the SPC module. You have the option to discard these photons or to continue the readout and the on-line calculation until all photons have been stored and processed. Please note that this can take some time (the SPC 830 can buffer 8 million photons!).

Calculating Correlation Functions After the Measurement

If additional correlation functions are specified immediately after a measurement, i.e. before closing the SPCM application, they are calculated when the corresponding traces are activated. If the SPCM application has been closed in the meantime, the FIFO file has to be re-loaded by using the ‘Convert’ function, see ‘Converting FIFO Files’, page 248.

Trigger

As in all operation modes, the start of a FIFO measurement can be triggered by a TTL or CMOS signal. To activate the trigger, set the trigger condition to ‘rising edge’ or ‘falling edge’. Triggering is important for parallel FIFO measurements in several SPC-134, SPC-144 or SPC-154 channels with synchronised macro time clocks. To obtain comparable macro times all channels *must* be started simultaneously by the trigger.

Source of Macro Time Clock

If FCS experiments are excited by a pulsed laser the laser pulse repetition frequency can interfere with the macro time clock frequency. The result is a periodical variation of the number of laser pulses per macro-time period. Periodicity can appear on any time scale, depending on the difference of the laser and macro-time clock frequencies or their harmonics. The problem is most pronounced if both frequencies are almost identical. The bh SPC-830, SPC-130/134, SPC-140/144 and SPC-150/154 provide an optional clock path from the SYNC input to the macro time clock. Synchronising the macro time clock with the SYNC (stop) signal removes the problem entirely.

The source of the macro time clock is selected via the ‘More Parameters’ button. Clicking on this button opens the panel shown in Fig. 295.

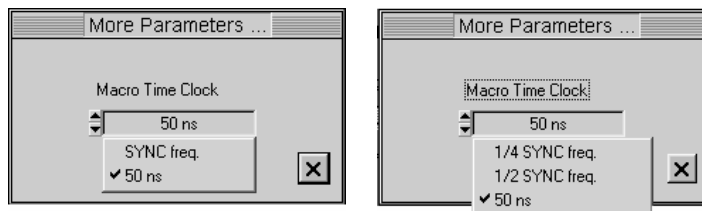


Fig. 295: Selection of the macro time clock source. Left: SPC-830. Right: SPC-130/134, -140/144 and -150/154

For the SPC-830, -140/144 and -150/154 you can select between the internal 50-ns¹ macro-time clock period and the external SYNC frequency. The SPC-130/134, SPC-140/144 and SPC-150/154 have a frequency divider in the SYNC path. The macro time clock frequency can be 1/2 or 1/4 of the sync frequency.

FIFO Data Format

For the SPC-600/630 two different data formats are available, see figure right, ‘FIFO frame length’. You can chose between 4096 time channels plus 256 detector channels or 256 time channels plus 8 detector channels. Due to the smaller number of bytes per photon the maximum continuous count rate is slightly higher for the second format. For the SPC-134 the data format is fixed to 4096 time channels and 8 detector channels. The formats are shown in the table below.

	FIFO Frame Length byte	Bytes/Photon	ADC Resolution channels	Macro Time Resol. bit	Routing channels
SPC-6	48	6	4096	24	256
SPC-6	32	4	256	16	8
SPC-830	32	4	4096	12	16
SPC-134**	32*	4	4096	12	8**
SPC-144	32*	4	4096	12	16
SPC-154	32*	4	4096	12	16

Data Format	
ADC Resolution	4096
Memory Offset	0.00 %
Dither Range	1/32
FIFO frame length	48
Page Control	
Delay [ns]	0
Routing chan. X	8
Routing chan. Y	1
Page	1

* Each of the four TCSPC channels delivers its own data file

** Routing requires 8m cable between router and CFD input

A detailed description of the FIFO file format is given under ‘FIFO Files’, page 335.

¹ 25 ns for SPC-150/154 modules and SPC-140/144 modules later than Sep. 2006

FIFO Imaging Mode

The SPC-150/154 and SPC-140/144² have a ‘FIFO Imaging’ mode implemented. The mode is intended to facilitate scanning FCS and to record fluorescence lifetime images with pixel numbers or time-channel numbers beyond the limit set by the memory of the SPC module. The FIFO Imaging is similar to the standard FIFO mode, i.e. stores the data of the individual photons. However, the FIFO imaging mode stores also synchronisation pulses from a scanner. The location of the photons in a scanning area can therefore be recovered by analysing the FIFO file. The general FIFO file format is the same as for the FIFO mode. However, one bit in the FIFO data word is used to identify the scan clock entries, see ‘FIFO Files’, page 335. The data analysis software uses this bit to interpret an entry either as a photon or as a clock pulse.

Measurement Control

The general measurement control parameters of the FIFO Imaging mode are the same as for the FIFO mode. The measurement-control area of the system parameter panel is shown in Fig. 296, left.

The name of the FIFO data file is specified in the ‘Spec Data File’ field. To change the file name, click on the disc symbol right of the name field. A list of previously used data file names is available by clicking on the symbol. *Important:* Before starting a new measurement define a new file name for the FIFO data. If you don’t do so you are in danger to overwrite the FIFO data of an earlier measurement.

You can limit the amount of data recorded by ‘Limit used disk space’. The measurement stops when the specified data size is reached.

Before the data are written to the hard disk they are buffered in the main memory of the computer. The buffer size is defined by ‘Max Buffer Size’. The SPCM software checks whether enough memory is available; buffers sizes too large are rejected.

Only when the buffer is filled the data are stored on the hard disc. If possible, the buffer size should therefore be large enough to buffer the full measurement. If not enough buffer is available the computer has to periodically transfer the buffered data to the hard disc. The hard-disk actions may slow down the readout from the FIFO memory of the TCSPC module. It may then happen that the FIFO memory of the TCSPC module overflows. If this happens it may be better to reduce ‘Max Buffer Size’ to a few Megabyte. The data are then written in smaller portions, and within time intervals that are buffered by the FIFO. The better solution is, however, to upgrade your computer with more memory.

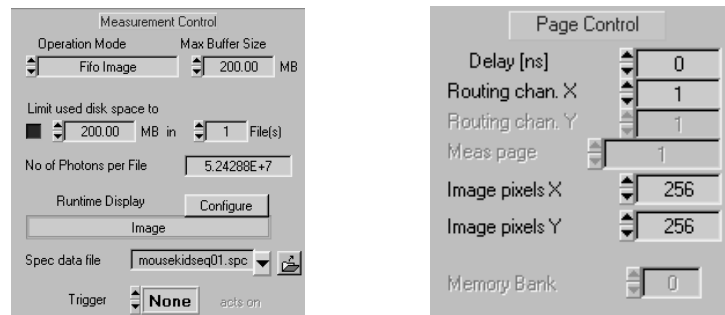


Fig. 296: FIFO Imaging Mode. Left: measurement control parameters. Right: Page control parameters

² The FIFO imaging mode is implemented in SPC-140/144 modules manufactured later than September 2006

Under ‘Runtime Display’ can be defined whether or not images are calculated from the incoming FIFO data stream. Several images for different detector channels, ranges of detector channels or images within specified time windows can be displayed simultaneously. Please see ‘Display Parameters’, ‘3D Trace Parameters’ and ‘Window Intervals’.

Image Format

The number of detector channels and the pixel numbers are defined under ‘Page Control’, in the lower middle of the system parameters, see Fig. 296, right.

In the FIFO imaging mode the image is built up in the computer memory. Therefore there is no limitation of the image size and time-channel number by the memory of the TCSPC module. However, also the memory size of the computer is finite. The available image size therefore depends on the computer. Typical image sizes are

Detector Channels	Pixels	Time Channels
1	256x256	1024
1	1024x1024	256
2	256x256	256
2	1024x1024	64

By using the standard ‘Save’ procedure you can store the images as .sdt files (see page 243). Please note, however, that the file size may become very large. The file size for the image formats given in the table above is 134 Mb.

Please note also that the large image size of the FIFO imaging mode may be obtained on the expense of the maximum count rate. The average (‘sustained’) count rate is limited by the bus transfer rate. Although the transfer rate is theoretically on the order of $5 \cdot 10^6$ photons per second it may be lower when background activities and hard disk actions are involved.

Scan Synchronisation Parameters

The hardware parameters controlling the synchronisation with the scanner are defined under ‘More Parameters’. The setup panel is shown in Fig. 297.

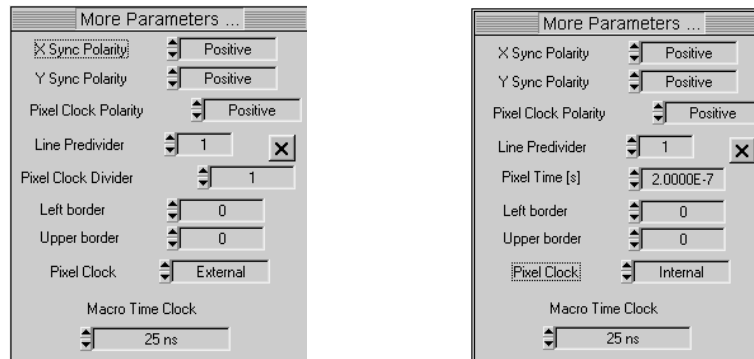


Fig. 297: Scan synchronisation parameters of the FIFO Imaging mode. Left: Synchronisation via frame, line and pixel clock. Middle: Synchronisation via frame and line clock.

The parameters are essentially the same as for the Scan Sync In mode, see page 273.

The easiest way to synchronise the SPC module with the scanner is via Frame Clock (Y Sync), Line Clock (X Sync) and Pixel Clock pulses. The corresponding scan-parameter setup is shown in Fig. 297, left. The panel allows you to define the polarity (active edge) of the synchronisation pulses and predividers (binning factors) for the lines and pixels. For details, please see page 273. For correction of possible image shift and distortion, see Fig. 120, page 114.

Using all three clocks (frame, line and pixel) is the easiest and most reliable way of synchronising the recording with the scanner. However, the FIFO imaging mode writes an entry for each synchronisation pulse into the FIFO. For fast scanners the number of pixel clock entries can therefore exceed to number of entries for the detected photons. It may also happen that the scanner does not deliver a pixel clock altogether. The pixel clock definition can be changed to ‘internal’, see Fig. 297, left. For internal pixel clock the SPCM software calculates the position of the current photon within a line from the macro time difference of the photon and the previous line clock. The procedure is the same as for the ‘Scan Sync In’ mode with internal pixel clock, except for the fact that the build-up of the image is done by software.

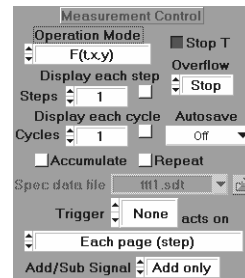
Source of the Macro Time Clock

If FCS experiments are excited by a pulsed laser the laser pulse repetition frequency can interfere with the macro-time clock frequency. The result is a periodical variation of the number of laser pulses per macro-time period. Although this variation is rarely a problem for fluorescence lifetime imaging it can be a problem in FCS applications. Periodicity can appear on any time scale, depending on the difference of the laser and macro-time clock frequencies or their harmonics. The problem is most pronounced if both frequencies are almost identical. The SPC-140/144 and SPC-150/154 modules provide an optional clock path from the SYNC input to the macro time clock. Synchronising the macro time clock with the SYNC (stop) signal removes the problem entirely. The clock source is selected by clicking into ‘Macro Time Clock’ in the ‘More Parameters’ panel. You can select between an internal 25 ns clock, or 1/2 or 1/4 of the Sync frequency.

Control Parameters (Photon Distribution Modes)

The measurement control parameter section of the system parameter panel is shown in the figure on the right. The effect and availability of the measurement control parameters depend on the module type and the operation mode selected. Therefore the control parameters are described in conjunction with the operation modes in the previous section. The description given should be considered an overview. For details, please see 'Operation Modes'.

The FIFO (time-tag) mode has entirely different control parameters. Please see FIFO Mode, page 281.



Stop Condition and Overflow Handling

Stop T

With 'Stop T' the measurement (or the current measurement step) is stopped at the end of 'Collection Time'. 'Stop T' can be used together with 'Stop Overflow' to stop the measurement either after a defined collection time or at the first overflow.

Stop Ovfl

With 'Stop Ovfl' a 'Single', 'Oscilloscope' or 'f(tx,y)' measurement stops at the first overflow in the measurement system. Overflow means the count number in one of the time channels exceeds 65635. Please note that the count number is not necessarily the number of photons. There is a parameter 'Count Increment' in the 'Data Format' section of the system parameters. This parameter allows you to add any number from 1 to 255 at the detection of one photon. You can use this parameter to get a 'stop on overflow' for photon numbers as low as 257. With the measurement being stopped on overflow different recordings are normalised to their peak count numbers.

If page stepping is active or one of the $f(t,T)$, $f(t,EXT)$, $f_i(T)$ or $f_i(EXT)$ is used a 'stop on overflow' stops the acquisition for the current step of the sequence. The sequence itself continues as specified by the measurement control parameters.

For multidetector operation an overflow in any of the detector channels stops the acquisition for all detectors.

'Stop Overflow' and 'Stop T' can be combined to stop the measurement either after a defined collection time or at the first overflow.

Corr Ovfl

The 'Correct Overflow' function is used in the 'Single' mode to record data with more than 65535 photons per channel. The measurement is stopped when an overflow occurs, and the data are transferred into the main memory of the computer. Then the memory of the SPC module is cleared and the measurement is restarted. The data of many such cycles are accumulated in the computer memory. When the collection time is over the result is divided by the number of overflows and written back into the measurement memory. Although the result has 16 bits again, the standard deviation of the data is reduced by the square root of the number of overflows. The 'Correct Overflow' function is available in the 'Single' mode only. It acts only on the active traces.

Steps

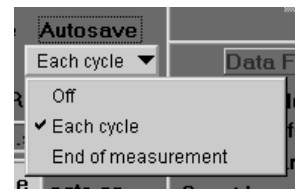
In most of the operation modes the measurement can be repeated and the results written into subsequent ‘Pages’ of the memory. The number of subsequent measurements is defined by ‘Steps’. The available number of steps depends on the operation mode, on ‘Routing Channels X’ and ‘Routing Channels Y’, the ADC resolution and the module type.

In the $f(t,T)$, $f(t,\text{Ext})$ modes ‘Steps’ is the number of subsequently measured curves. In the $f_i(T)$ and $f_i(\text{Ext})$ modes ‘Steps’ is the number of intensity values. Please refer to paragraph ‘Operation Modes’.

Cycles and Autosave

A stepping sequence (or, if ‘Steps’ = 1, a single measurement in the selected operation mode) can be repeated for a defined number of ‘Cycles’.

To write the results of subsequent cycles to the hard disk an ‘Autosave’ function is provided. In most cases ‘Autosave’ is used for ‘Each cycle’ of a measurement. However, ‘Autosave’ can also be initiated at the ‘End of the measurement’, i.e. after the last cycle only. This option is used in combination with ‘Accumulate’.



Accumulate

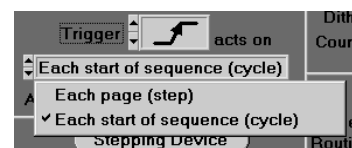
The ‘Accumulate’ function accumulates the results of several ‘Cycles’. If you want to save the results automatically at the end of the accumulation, use ‘Autosave’, ‘End of Measurement’.

Repeat

After pushing the ‘Repeat’ button the complete measurement cycle repeats until the measurement is stopped by the operator. The repeat function is often used to run subsequent measurements and display the results in short intervals. The repeat function is an efficient way to obtain online display in multi-dimensional modes, like $f(x,y,t)$ or Scan Sync In. For the single-curve recording online display can be obtained more efficiently in the ‘Oscilloscope’ mode. In all cases ‘Repeat’ can be used in conjunction with ‘Autosave’.

Trigger

Any single measurement, or the ‘Steps’ or ‘Cycles’ of a measurement sequence can be triggered by the experiment trigger input (see ‘Using the Experiment Trigger’, page 98). The function of the trigger for the particular mode is described under ‘Operation Modes’. The trigger condition can be set to ‘Rising Edge’, ‘Falling Edge’ or ‘None’. ‘None’ means the measurement is started immediately, without waiting for any trigger signal. The trigger input shared the same line with the ‘Add/Sub’ line used for lock-in-SPC, see ‘Routing and Control Signals’, page 348. Therefore, the trigger is not available when the Add/Sub signal is used and vice versa.



Display after each step and each cycle

During the individual measurement steps intermediate results can be displayed ‘after each step’ and ‘after each cycle’. Displaying the results of large multi-dimensional measurement results can take some seconds. Therefore, these online display options and not used for fast sequential recording or other high-throughput applications.

In some operation modes intermediate results can also be displayed in intervals of a specified ‘Display Time’, see ‘Timing Control Parameters’.

Add / Sub Signal

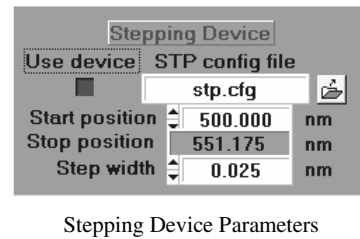
The ‘Add / Sub’ signal is used for Lock-in SPC, i.e. to externally control whether a photon is added or subtracted. The Add / Sub signal shares one pin of the control signal connector with the ‘Measurement Trigger’ signal, see ‘Routing and Control Signals’, page 348. Therefore, the Add/Sub signal is not available when the trigger is used and vice versa. Add / Sub should be set to ‘Add Only’ when it is not used.

Stepping Device

Under 'Stepping Device' the parameters of the (optional) step motor controller are accessible.

Use Stepping Device

This button switches the software part for the stepping device on and off. If no stepping device is present in the system, the button must be in the 'off' state.



Stepping Device Parameters

STP Config file

The step motor control is configured by the specific file. By default the file 'STP.CFG' is used. To vary the drive parameters several configuration files may be created and selected by 'STP config file'.

Start Position

This parameter specifies the start position of the drive. It can be set within the limits set by the configuration file. The unit for the start position is also taken from this file.

End Position

The end position is calculated from the selected start position and step width.

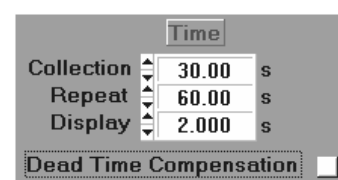
Step width

The step width of the drive is selected with 'Step width'. It can be set within the limits set by the configuration file. The unit for the step width is also taken from this file.

Timing Control Parameters

Collection Time

In most operation modes 'Collection Time' is the acquisition time of a measurement, a step of a page stepping sequence, or a ‘cycle’ of a repetitive measurement. The Collection Time can be ‘dead-time compensated’. With dead-time compensation the collection time automatically increases by the time the system is



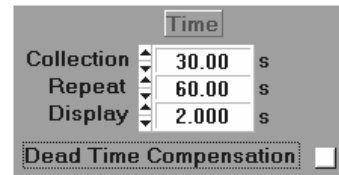
'blind' due to the processing of the detected photons, see 'Dead-Time Compensation', page 132. The dead time compensation can be switched on and off. Dead-time compensation is available in the Single, Oscilloscope, f(x,y), f(t,T), f(t,EXT), fi(T) and fi(EXT) modes. If sequential modes are used with dead time compensation, or if page stepping or cycling is used, please use a 'Repeat' time longer than 'Collection Time' to provide some margin for the SPC hardware to extend the effective collection time interval.

In the Scan Sync Out and Scan XY Out modes 'Collection Time' is the time to acquire one pixel of the image, in the Scan Sync In mode the total acquisition time of an image.

Repeat Time

The 'Repeat Time' controls the repetition of a measurement in the 'Single', f(tx,y), f(t,T), f(t,EXT), fi(T) and fi(EXT) modes.

The measurement is repeated in intervals of 'Repeat Time'. If page stepping or cycling is active, or if a sequential mode is used the complete sequence is repeated.

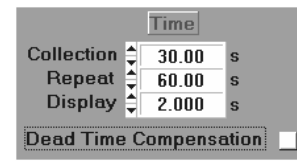


Values smaller than 'Collection time' are rejected by the software to avoid conflicts of the acquisition time with the repeat time. However, if 'dead time compensation' is used the effective acquisition time may be longer than the specified 'collection time'. If the current measurement step or cycle is not finished when 'Repeat Time' is over the next measurement step starts when the current step is complete. If an exact stepping time is important, please use a 'Repeat' time longer than 'Collection Time' to provide some margin for the SPC hardware to extend the effective collection time interval.

Display Time

Photon Distribution Modes

In the 'Single', f(t,x,y)', f(t,T), f(t,EXT), fi(T) and fi(EXT) modes intermediate results are displayed in intervals of 'Display Time'. The measurement is stopped, the memory of the SPC module is read, the measurement is continued, and the results are displayed.



Readout and display takes time, especially for multi-dimensional data and 3D display modes. This may slow down the measurement or the time intervals of a page stepping sequence. Therefore unnecessarily short display times should be avoided.

FIFO Mode

In the FIFO mode intermediate results can be calculated and displayed on-line. The software analyses the photon data when it transfers the FIFO data into the computer memory, continuously builds up histograms and correlation functions, and displays the results (see 'FIFO Mode', page 281). Online calculation may consume a substantial amount of computation power, especially for FCS functions of long correlation time. Thus, the actual display rate may be lower than defined by the display time. More important, on-line calculation may slow down the data transfer from the SPC module into the computer. Therefore, please check the FIFO filling status during the measurement if you use the online display features.

On-line results are calculated only if 'Display Time' is set > 1 s. Thus, you can switch off the online display by defining a display time smaller than 1 second.

Dead Time Compensation

The ‘Dead Time Compensation’ function increases the collection time intervals by the sum of the dead time caused by the processing of all recorded photons. Thus, a linear intensity scale is achieved up to extremely high count rates. Please note that dead time compensation results in an effective acquisition time longer than the specified ‘collection time’. The ‘Dead Time Compensation’ is not available in the FIFO mode, the Continuous Flow mode, and in the Scan modes.

CFD Parameters

The bh SPC modules use constant-fraction discriminators (CFDs) both in the detector and at the reference (Sync) input. A CFD triggers at a constant fraction of the pulse amplitude, thus avoiding pulse-height-induced timing jitter. In practice constant-fraction triggering is achieved by triggering on the zero cross point of the sum of the input pulse and the delayed and inverted input pulse, see Fig. 38, page 35. Furthermore, the CFD contains a discriminator that enables the zero-cross trigger only for input pulses larger than a defined discriminator threshold. The CFD threshold is adjusted to reject noise from the environment, noise from preamplifiers or small background pulses from the detector, see ‘Configuring the CFD and SYNC Inputs’, page 118. There are two versions of SPC modules, see ‘CFD in the Detector (Start) Channel’, page 42. The -00 versions have internal amplifiers and a lower and an upper threshold. The -30 versions have faster discriminators, no amplifiers and no upper threshold.

Limit Low

'Limit Low' is the lower discriminator threshold, the ‘CFD threshold’. Pulses with amplitudes smaller than 'Limit Low' are not counted. The parameter range for 'Limit Low' is 5 mV to 80 mV for SPC-x00 modules and 0 to -500 mV for SPC-x30 modules.

CFD Parameters			
Limit Low	-100.00	mV	
Limit High	39.84	mV	
ZC Level	-7.56	mV	
Hold	5.00	ns	

SPC-x30 CFD Parameters

Limit High (SPC-x00 only)

'Limit High' is the upper discriminator threshold of the -00 SPC versions. Pulses with amplitudes greater than 'Limit High' are not counted. They do, however contribute to the displayed CFD count rate due to the structure of the CFD (see 'Constant Fraction Discriminator'). The range for 'Limit High' is 5 mV to 80 mV.

CFD Parameters			
Limit Low	-100.00	mV	
Limit High	39.84	mV	
ZC Level	-7.56	mV	
Hold	5.00	ns	

SPC-x00 CFD Parameters

ZC Level

'ZC Level' is the reference level of the zero cross trigger in the CFD. The value has a range of -10 mV to +10 mV for the SPC-x00 modules and -100 mV to +100 mV for the SPC-x30 modules.

Hold (SPC-x00 only)

When the CFD has detected a pulse within the window 'Limit Low' to 'Limit High' this information is valid for the selected 'Hold' time only. The parameter is normally set to 5ns. Longer values may be useful for detectors with rise times greater than 5ns. 'Hold' is available for the SPC-x00 modules only.

SYNC Parameters

The bh SPC modules use constant-fraction discriminators (CFDs) both in the detector and at the reference (Sync) input. A CFD triggers at a constant fraction of the pulse amplitude, thus avoiding pulse-height-induced timing jitter. In practice constant-fraction triggering is achieved

by triggering on the zero cross point of the sum of the input pulse and the delayed and inverted input pulse, see Fig. 38, page 35. There are two versions of SPC modules, see ‘CFD in the Synchronisation (Stop) Channel’, page 44. The -00 versions have internal amplifiers but no discriminator to reject small-amplitude pulses. The -30 versions have no amplifiers. They are faster and have a discriminator to reject pulses smaller than a defined threshold.

ZC Level

‘ZC Level’ is the reference level of the zero cross trigger in the SYNC channel. The value has a range of -10 mV to +10 mV for the SPC-x00 modules and -100 mV to +100 mV for the SPC-x30 modules.

Holdoff

When the SYNC has triggered the detection of a new trigger pulse is rejected for the ‘Holdoff’ time. ‘Holdoff’ is used to avoid multiple triggering by pulse ringing or reflections. The ‘Holdoff’ range is from 4 ns to 16 ns. Please make sure that you don’t set ‘Holdoff’ longer than the period of your SYNC signal. This can produce non-equidistant internal synchronisation signals with correspondingly wrong measurement results.

Threshold (SPC-x30 only)

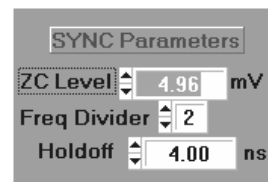
Input pulses with amplitudes smaller than the selected ‘Threshold’ are rejected by the SPC-x30 SYNC circuits. The range is from -20 mV to -500 mV. The parameter is available for SPC-x30 modules only.

Freq Div

‘Freq Div’ is the frequency divider ratio in the SYNC channel. The setting determines the number of signal periods recorded, see ‘Optimising the SYNC Parameters’, page 123. Important: ‘Freq Div’ must be set to 1 for measurements at low repetition rates and for non-reversed start-stop measurements.



SPC-x30 SYNC Parameters



SPC-x00 SYNC Parameters

TAC Parameters

The TAC measures the times of the photons from the moment of the detection to the next synchronisation pulse. The core of the TAC is a linear ramp generator. The ramp is started when a photon pulse triggers the CFD of the detector channel and stopped when the next pulse in the reference (SYNC) channel is detected. The output voltage of the ramp generator is amplified by a biased amplifier. The amplifier is used to select a time interval within the range of the ramp generator and stretch it over the full output voltage range. Moreover, the TACs of the SPC-6, -7 and -8 modules have discriminators to reject photons outside a selectable amplitude window of the TAC output signal. The SPC-1 modules have no such discriminators but achieve a similar effect by digital comparators in the ADC data path. The details of the TAC are described under ‘Time-to-Amplitude Converter’, page 46. The optimisation of the TAC parameters is described under ‘Adjusting the TAC Parameters’, page 126.

Range

'Range' is the maximum start-stop time of the linear-ramp generator, i.e. the total time interval in which photons can be measured. TAC ranges from 50 ns to 2 us are available. Internally the setting is accomplished in five steps, in conjunction with a 12-bit fine adjustment within the steps. Therefore virtually any TAC range between 50 ns and 2 us is available.

TAC Parameters	
Range	5.004E-8 s
Gain	15
Offset	7.45 %
Limit Low	7.84 %
Limit High	91.76 %
Time/Chan	8.15E-13 s
Time/Div	4.17E-10 s

TAC Parameters

Gain

'Gain' is the gain of the biased amplifier of the TAC. 'Gain' stretches the time scale of the TAC, see 'Adjusting the TAC Parameters', page 126. Values from 1 to 15 are available.

Offset

With 'Offset' the displayed time range is shifted on the TAC characteristic, see 'Adjusting the TAC Parameters', page 126. The result is shifted in X direction on the screen. 'Offset' can be set to 0...100 % of the overall TAC range. However, the remaining part of the TAC characteristic (from 'Offset' to 100%) should be long enough to fill the display window for the selected TAC Gain. The resolution of 'TAC Offset' is 12 bit for the SPC-6, -7, and -8 modules, and 8 bit for the SPC-1 modules.

Limit Low

The TAC contains a window discriminator to suppress events outside a selected time interval. 'Limit Low' sets the lower limit of this interval. 'Limit Low' can be set from 0% to 100% of the display window, but not higher than 'Limit High'. Typical Limit Low values are from 3 to 10%.

Limit High

The TAC contains a window discriminator to suppress events outside a selected time interval. 'Limit High' sets the upper limit of this interval. 'Limit High' can be selected from 0% to 100% of the display window, but not lower than 'Limit Low'. Typical values are 90 to 97%.

Time/Channel

'Time/Channel' is the width of one time channel in the recorded photon distribution. It is

$$\text{Time / Channel} = \frac{\text{Range}}{\text{Gain} \cdot \text{ADCresolution}}$$

'Time/Channel' is calculated from the given values of TAC Range, TAC Gain and ADC Resolution (in channels) and displayed for information only. The minimum 'Time/Channel' is 815 femtoseconds.

Time/div

This value is the time per division. It is displayed for information only. It is calculated from the settings of TAC Range, TAC Gain, ADC Resolution and, for the SPC-830, ADC Zoom.

Data Format

ADC Resolution and ADC Zoom (Photon Distribution Modes)

'ADC Resolution' defines the number of time channels per curve of a waveform recording. For the SPC-6 and -7 modules and the SPC-134 an ADC Resolution of 64, 256, 1024 or 4096 time channels can be selected, see Fig. 298.

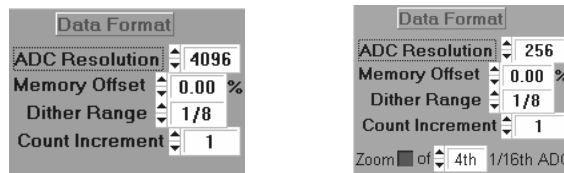


Fig. 298: Data Format panel for the SPC-6, -7, -130/134 (left) and the SPC-830 and SPC-140/144(right)

For SPC-830 and the SPC-140/144 an ADC resolution of 1, 4, 16, 64, 256, 1024 or 4096 time channels is available. Moreover, the SPC-830 and the SPC-140/144 have an ‘ADC Zoom’ function to stretch a part of the ADC range over the full display scale. Only the stretched part of the data is recorded. The ADC Zoom function is mainly used to record large images or other multi-curve data simultaneously with a high number of pixels or curves and high time resolution. Please see also ‘ADC Zoom’, page 50. Fig. 299 explains the ADC Zoom feature for an ADC resolution of 256 channels.

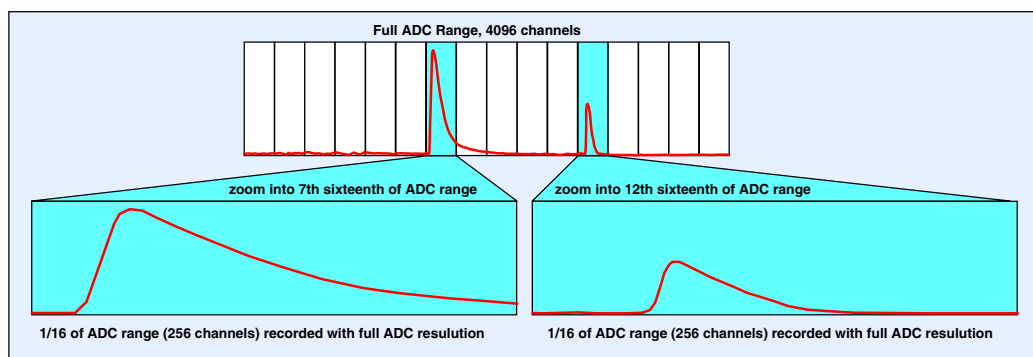


Fig. 299: ADC Zoom function of the SPC-830 and SPC-140/144

Originally the ADC converts the complete TAC interval (TAC Range / TAC Gain) into 4096 time channels. The zoom function selects 1/16th of the ADC range, i.e. 256 channels. Any 16th part of the ADC range can be selected, and only the selected part is displayed and recorded. The ADC zoom is a powerful function to record ultra-fast signals in high pixel resolution imaging applications.

For single-curve measurements normally an ADC resolution of 4096 or 1024 time channels per curve is used. For sequential measurements, stepping through pages, ‘Continuous Flow’ measurements and scanning often a tradeoff between ADC resolution and number of curves and pages or pixel number must be made. The maximum number of curves for a single detector setup is given below.

SPC-134	64	256	1024	4096
ADC Resolution				
No of Curves	8192	2048	256	64
No of curves addressed by external routing signal	128	128	128	64
min. time channel width	52ps	3.26ps	3.26ps	815fs
SPC-144, SPC-154				
ADC Resolution	1	4	16	64
No of Curves (f(t,T, Scan Sync IN/Out)	16 M	4 M	1 M	65536
No of curves addressed by external routing signal	128	128	128	128
min. time channel width	3.34ns	834ps	209ps	52ps
min. time channel width, with ADC zoom		52ps	13ps	3.26ps
ADC zoom factor		16	16	16
SPC-600/630				
ADC Resolution	64	256	1024	4096
No of Curves	8192	2048	256	64
No of curves addressed by external routing signal	128	128	128	64
min. time channel width	52ps	3.26ps	3.26ps	815fs

SPC-700/730

ADC Resolution	64	256	1024	4096
No of Curves (f(t,T, Scan Sync IN/Out)	65536	16384	4096	1024
No of curves addressed by external routing signal	16384	16384	4096	1024
min. time channel width	52ps	3.26ps	3.26ps	815fs

SPC-830

ADC Resolution	1	4	16	64	256	1024	4096
No of Curves (f(t,T, Scan Sync IN/Out)	16 M	4 M	1 M	262144	65536	16384	4096
No of curves addressed by ext. routing signal	16384	16384	16384	16384	16384	16384	4096
min. time channel width, without ADC zoom	3.34ns	834ps	209ps	52ps	13ps	3.26ps	815fs
min. time channel width, with ADC zoom		52ps	13ps	3.26ps	815fs	815fs	
ADC zoom factor		16	16	16	16	16	4

For multi-detector experiments or measurements with page stepping the memory is shared between the individual detection channels and pages so that the available number of curves is reduced. Please see ‘Operation Modes’, page 253.

ADC Resolution (FIFO Modes)

The ‘Data Format’ section of the system parameters for the FIFO mode is shown in Fig. 300.

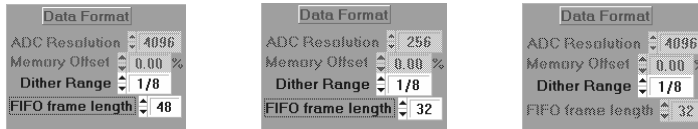


Fig. 300: ADC Resolution in the FIFO mode for the SPC-630 for ‘Frame Length’ 48 and 32 and for the SPC-134, SPC-830 and SPC-140/144 (right)

For the SPC-600/630 modules the ADC resolution depends on the ‘Frame Length’, i.e. on the number of bits per photon saved in the FIFO data file. For the SPC-830, the SPC-130/134 and the SPC-140/144 the frame length and consequently the ADC Resolution are fixed to 32 and 4096, respectively.

Memory Offset

When the Lock-in capability of the bh SPC modules is used the light is modulated by a chopper. The photons in the ‘On’ phases are added and the photons in the ‘Off’ phases subtracted. Consequently, negative photon numbers can occur in the memory. By using a ‘Memory Offset’ greater than zero the baseline of the recording can be shifted to positive values.

Dither Range

‘Dither Range’ controls the ADC error correction of the bh TCSPC modules. The principle of the error correction is described under ADC Error Correction, page 48. The technique is based on adding an auxiliary signal to the ADC input voltage. The digital equivalent of the signal is subtracted from the ADC output words. Thus, the TAC output voltage is periodically shifted up and down the ADC characteristic. The result is that the non-uniformity of the ADC channels is averaged out. ‘Dither Range’ controls the amplitude of the shift signal. It is defined as a fraction of the total ADC input range.

Larger values of ‘Dither Range’ improve the differential nonlinearity. However, the sum of the TAC signal and the shift signal is limited to the available ADC input voltage range. Therefore the first and last parts of the ADC characteristic cannot be used for conversion. The effect of ‘Dither Range’ on a recorded curve is shown in Fig. 301, left.

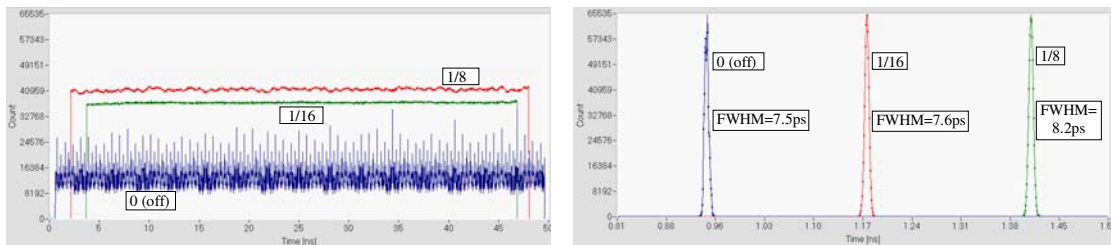


Fig. 301: ADC error correction. Left: Unmodulated light recorded without error correction, and with ‘Dither Width’ 1/16 and 1/8. right: Corresponding instrument response function for an electrical test signal. SPC-134

It should be pointed out that large values of ‘Dither Range’ do *not* impair the time resolution, see Fig. 301, right. Therefore, use a ‘Dither Range’ as large as possible. Under normal conditions 1/8 or 1/16 is adequate. Dither Range = 0 switches the error correction off. It is intended for test purposes, not for measurement application.

Count Increment

‘Count Increment’ is the value which is added in the memory at the detection of each photon. The parameter may look unusual at first glance, especially if you are familiar with conventional NIM TCSPC systems. Of course, a ‘Count Increment’ greater than one does not yield any improvement in accuracy for a given number of photons. It is, however, a convenient means to make the measurement control more flexible.

In ‘Single’ and ‘Oscilloscope’ measurements a Count Increment greater than 1 can be used to reduce the time required to reach the overflow level for a given count rate. If ‘Stop Overflow’ is set instead of ‘Stop T’, a measurement is stopped when the maximum of the curve reaches 65535. Thus, the measured curves are normalised to the same height independently of the pulse shape and the count rate. This normalisation helps to compare different curves in terms of pulse shape or width.

If you run a fitting procedure on SPC data recorded with a Count Increment greater than one, please don’t be surprised by the large value of χ^2 . To get the true χ^2 you have to divide the value by the Count Increment.

In earlier SPCM versions a Count Increment greater than one had to be used to avoid rounding effects in the display of images. In later versions the pixel intensities are calculated by floating point arithmetics. An increased count increment is therefore not longer needed.

FIFO Frame Length (FIFO Mode)

This parameter sets the data format for the SPC-600/630 in the FIFO Mode. For the SPC-830, SPC-134, and SPC-144 the FIFO Frame Length is fixed.

FIFO Frame Length	Bytes/Photon	ADC Resolution	Macro Time Resol.	Routing
byte		channels	bit	channels
SPC-6	48	6	4096	256
SPC-6	32	4	256	8
SPC-134	32*	4	4096	8**
SPC-144	32*	4	4096	16
SPC-154	32*	4	4096	16
SPC-830	32	4	4096	16

* Each of the four TCSPC channels delivers its own data file

** Routing with the SPC-134 requires 8 m cable between the router and the CFD input

For the SPC-600/630 the ‘FIFO Frame Length’ determines also the ADC resolution. Please see ‘ADC Resolution (FIFO Modes)’.

Page Control

The Page Control section of the system parameters defines the number and the arrangement of the detector channels, the number of pixels in the Scan modes, and the memory page in which a measurement starts.

The Page Control parameters are used to define the number and the spatial arrangement of the detector channels or the number and arrangement of the pixels of an image in the SPC-7, SPC-8, and SPC-140/144 Scan modes. If the number of curves per measurement is less than 50% of the module memory size the memory can hold the results of several measurements. A ‘Page’ is a memory segment that holds the curves (photon distributions) for all detectors and - in the ‘Scan’ modes of the SPC-7 and SPC-8 modules - pixels of one measurement or measurement step.

The number of available ‘Pages’ depends on the used ‘ADC Resolution’, ‘Routing Channels X’, ‘Routing Channels Y’ and, in the ‘Scan’ modes, on ‘Scan Pixels X’ and ‘Scan Pixels Y’. If one of these parameters is changed beyond the limit set by memory size the software automatically limits it to the maximum possible value.

Delay (Not for SPC-134)

‘Delay’ determines the moment when the routing and control signals for multidetector measurements are read. The delay is referred to the pulse at the CFD input. For the bh routers and the bh PML-16 multichannel detector the optimum ‘Delay’ is 0 to 30 ns.

For other applications a ‘Delay’ in the range from 0 to 255ns can be used. Please note that an internal delay of the data latch of 5 to 10 ns and the cable transit times must be taken into account. Values larger than 100ns reduce the maximum count rate of the SPC module and should therefore be avoided.

The ‘Delay’ parameter is not available for the SPC-130/134. If you want to use an SPC-134 with a bh router, please connect 7 to 8 m cable between the router and the CFD input of the SPC module. The cable delays the photon pulse. Thus, the routing signal is valid when the photon pulse arrives at the CFD input, and the correct detector number is written into the channel register.

Routing Channels X, Routing Channels Y

‘Routing Channels X’ and ‘Routing Channels Y’ are the number of rows and columns of a two-dimensional array of detector channels. Some examples are in Fig. 302.

Page Control	
Delay [ns]	20
Routing chan. X	1
Routing chan. Y	1
Meas page	1

Single detector measurement

Page Control	
Delay [ns]	20
Routing chan. X	8
Routing chan. Y	1
Meas page	1

Multidetector measurement
8 Detectors, linear arrangement

Page Control	
Delay [ns]	20
Routing chan. X	4
Routing chan. Y	4
Meas page	1

Multidetector measurement
16 detectors, 4x4 arrangement

Fig. 302: Definition of the number of routing channels

Measured Page

A ‘Page’ is a memory segment that holds the curves (waveforms) for all detectors. If the number of curves per measurement is less than 50% of capacity of the module memory several pages can be defined. Each page holds the data of a complete measurement or step of a page stepping sequence. In the ‘Scan’ modes a page contains the waveforms of all pixels of the image.

For a single-step measurement, 'Measured Page' is the memory page in which the result of the measurement is stored. For a measurement with page stepping the measurement starts in 'Measured Page' and steps through subsequent pages.

Scan Pixels X, Scan Pixels Y

These parameters are used for the 'Scan' modes of the SPC-830, SPC-700/730 and SPC-140/144 modules. 'Scan Pixels X' and 'Scan Pixels Y' are the number pixels per line and the number of lines per frame in the recorded image.

The 'Scan' modes can be used in conjunction with multidetector operation. Therefore a configuration with 'Scan Pixels X' and 'Scan Pixels Y' greater than one can be used with 'Routing Channels X' and 'Routing Channels Y' greater than one. Some examples are shown below.

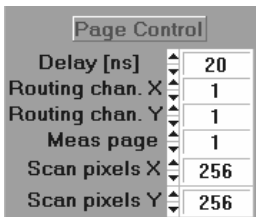


Image of 256 x 256 pixels
Single detector measurement
1 page available for ADC Res = 64

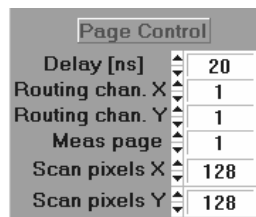


Image of 128 x 128 pixels
Single detector measurement
4 pages available for ADC Res = 64
1 page available for ADC Res = 256

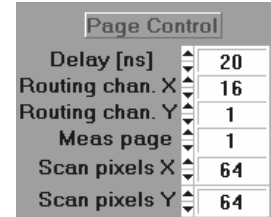
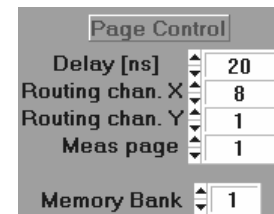


Image of 64 x 64 pixels
16 detector channels
1 page available for ADC Res = 64

Memory Bank (SPC-600/630 and SPC-134)

The SPC-600/630 and the SPC-134 have a dual memory, i.e. two memory banks of the same size and configuration. Normally the banks are used for unlimited sequential recording in the 'Continuous Flow' mode. You can, however, use the banks to hold the results of two measurements in the SPC memory. 'Memory Bank' = 0 or 1 switches between the two memory banks.



More Parameters

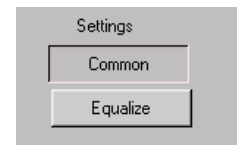
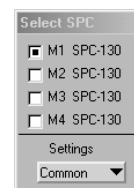
Depending on the module type and the operation mode special parameters (e.g. to control a scanner) are available. These parameters are described under the 'Operation Modes' for these modules.

Parameter Management for Multi-Module SPC systems

In multi-module SPC systems each module has its own system parameters, and the currently displayed System Parameter panel refers to one of the modules only. To specify the module to which the parameters refer a small 'Select SPC' panel is displayed, see figure right. It can be conveniently placed anywhere in the screen area.

Furthermore, you can decide whether parameter changes apply to all modules or to the specified module only. Use the Common/Separate button in the lower right part of the system parameter panel.

If a parameter has different values in different modules it is highlighted by a different colour in the system parameter panel. If you want to set the equal system parameters for all modules, click on the 'Equalise' button.



The parameters for the current module are then transferred into the system parameters of all other modules.

Display Parameters

The measurement modes of the SPC-6, SPC-7, SPC-8, SPC-134, and SPC-144 modules deliver single decay curves, FCS functions, photon counting histograms, sets of curves for different detector channels or steps of a sequential measurement, two-dimensional arrays of decay curves and multi-dimensional data arrays versus the time, the coordinates of a scanning area, and the detector number. The display of these data is controlled by the 'Display Parameters' in conjunction with the 2D and 3D Trace parameters.

The 'Display Parameters' are used to configure the style, colour, and ranges of the display, to select the display mode and to define the display plane through a multi-dimensional data array.

Depending on the main-panel configuration several sets of display parameters may exist (see Configuration of the SPC Main Panel, page 233). For example, a FIFO mode measurement may deliver fluorescence decay curves, fluorescence correlation curves and photon counting histograms simultaneously. The results of a scan measurement may be displayed in different time windows or for different detector channels. The results of sequential recording may be displayed in the curve mode or in the colour-intensity mode, or for different detectors. Each of the display windows has its own set of Display Parameters.

The display parameter panel is shown in Fig. 303. The panel is different for display windows in 2D and 3D display modes.

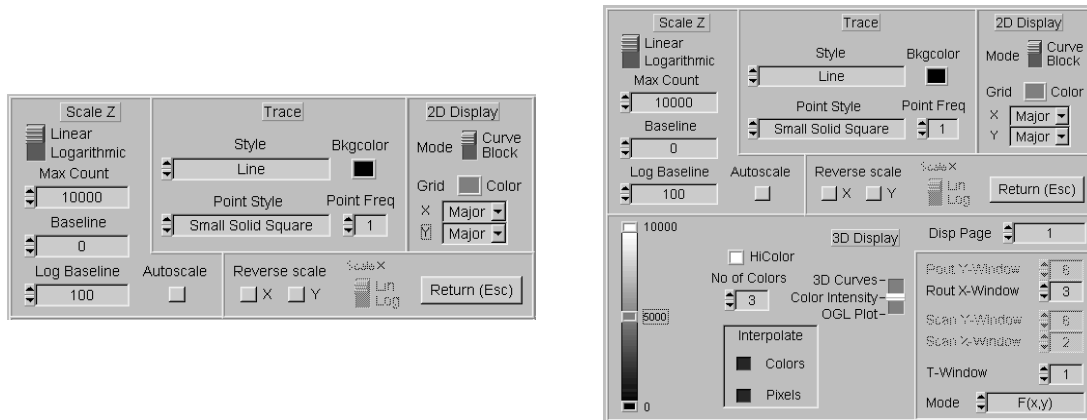


Fig. 303: Display parameter panel. Left: 2D display modes. Right: 3D display modes

General Display Parameters

Scale Y

Under 'Scale Y' you can switch between a linear or a logarithmic scale and set the display range of the photon count number.

Linear / Logarithmic: Linear or logarithmic Y-scale

Max Count: Upper limit of the display range for linear and logarithmic scale

Baseline: Lower limit of the display range for linear scale

Log Baseline: Lower limit of the display range for logarithmic scale

Trace

Bkgcolor: Background colour of the display window to which the display parameters apply.

Style: Display style of the curves. The styles 'Line', 'Points Only' and 'Connected Points' are available.

Point Freq: At values >1 each nth point is displayed only. 'Point Freq' has no influence if 'Line' is selected.

Autoscale: Normalises the display range to the maximum count number found in the displayed data. Autoscale works both for 2D display modes (curves) and 3D display modes (images or sequences of curves).

Reverse: Reversing one or both axis of the display can be achieved by the two buttons 'X scale' and 'Y scale'. It is often used in the 'Scan' modes to swap an image into the right orientation. 'Reverse' works in all display modes. It acts on the display only, not on the data in the memory.

2D Display Parameters

Grid Color: Grid colour, only if a grid is defined.

Grid X, Grid Y: Different grid sizes can be defined by using 'major' or 'minor'. 'None' switches the grid off.

Curve Mode: Each curve (trace) on the screen is related to one curve in the memory which is set by the 'Trace Parameters'.

Block Mode: Each curve (trace) on the screen is the average of several curves in the memory. The relation is set by the 'Trace Parameters' and the 'Window Intervals'. The block mode of the display is used to display multichannel measurements in the 2D display mode.

The parameters 'Curve Mode' and 'Block Mode' are not available in the FIFO Mode.

3D Display Parameters

To display results obtained in the f(t,x,y), f(t,ext), f(t,T) or Scan modes three different three-dimensional display modes are provided. Examples of the three display modes are given in Fig. 304.

The '3D Curves' mode (shown left) displays the results as a set of curves. The Z axis represents the number of photons, the X and Y axis two of the parameters x, y, t or EXT.

The 'Colour Intensity' mode (Fig. 304, middle) transforms the light intensity into a grey scale or colour scale. The X and Y axis represents two of the parameters x, y, t or EXT.

The 'OGL Plot' mode (Fig. 304, right) shows the results as a curved and coloured surface with the number of photons as Z axis and two of the parameters x, y, t or EXT as X and Y axis. If the OGL plot is used only one display window is available.

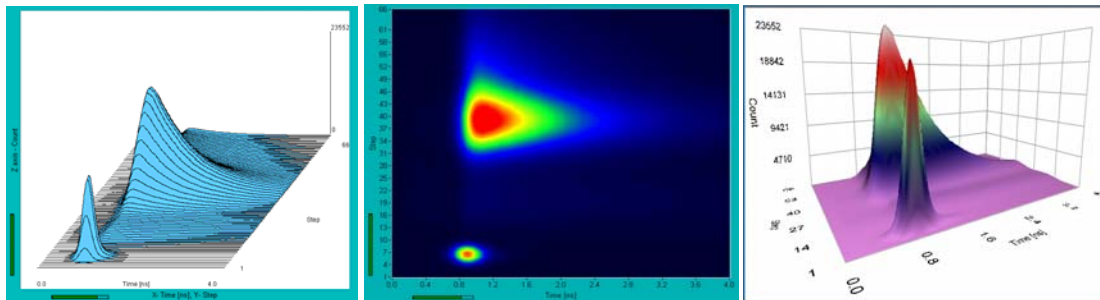


Fig. 304: 3D display modes. Left to right: Curve mode, Colour intensity mode, OGL plot

3D Curve Mode Parameters

The ‘3D Display’ part of the display parameter menu changes with the display mode selected. When the 3 D display is switched to ‘3D Curves’ the display parameters are as shown in Fig. 305.

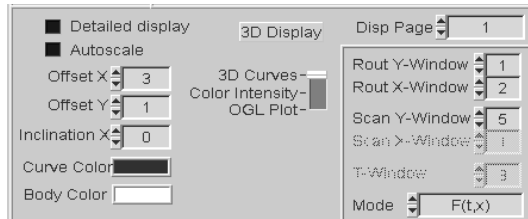


Fig. 305: 3D display parameters for the ‘Curve Mode’

Offset X, Offset Y, Inclination X, Curve Color, and Body Color define the layout of the displayed curve sequence. The effect of these parameters is shown in Fig. 306.

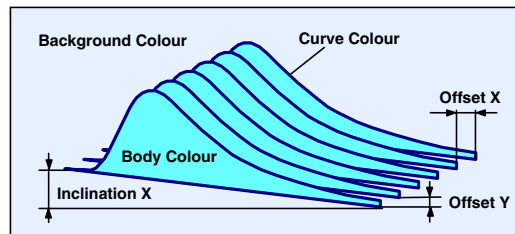


Fig. 306: Parameters controlling the layout of the 3D curve display

In the ‘Detailed Display’ mode all points of the result curves are displayed. For a high number of curves and high ADC resolution this can be time-consuming. Moreover, for signals containing a large amount of noise the result may be not satisfactory. Therefore, a compressed display style is available by switching off the ‘Detailed Display’ function.

The ‘Autoscale’ function automatically changes ‘max count’ to fit the data into the display range.

To display subsets of multi-dimensional data arrays different modes, ‘Routing Windows’, ‘Scan Windows’ and a ‘t Window’ can be selected. Please see ‘Displaying Subsets of Multi-dimensional Data’, page 304, and ‘Window Intervals’, page 313.

3D Colour-Intensity and OGL Mode Parameters

In the colour-intensity mode and the OGL plot mode the photon counts are represented by a colour scale. The corresponding display parameters are shown in Fig. 307, left.

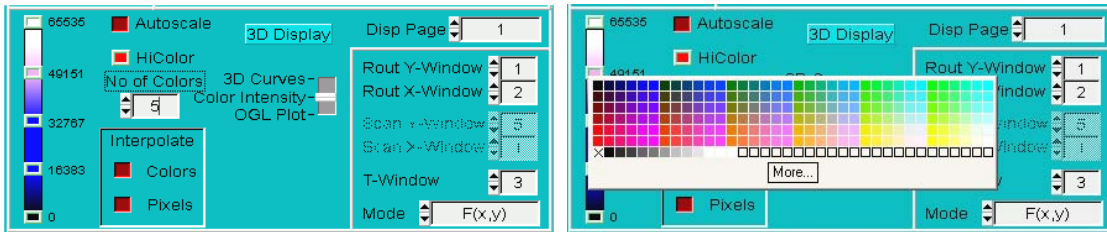


Fig. 307: Left: Display parameters in the colour-intensity and OGL display mode. Right: Selecting the colours for the colour-intensity and OGL display mode

The colours are selected by clicking on the exaggerated fields in the colour bar. This opens a colour table from which the colours can be selected, see Fig. 307, right.

For image areas with photon numbers exceeding the range defined by ‘Max Count’ ‘HiColor’ is used. The colour can be defined by clicking on the ‘HiColor’ button.

The ‘Interpolate’ function is used to deliver intermediate colours (‘Interpolate Color’ button) and to interpolate the images between the pixels (‘Interpolate Pixels’ button).

To display subsets of multi-dimensional different display plane within the data ($f(x,y)$, $f(x,t)$, etc, and different ‘Routing Windows’, ‘Scan Windows’ and ‘T Windows’ can be defined. Please see below, ‘Displaying Subsets of Multidimensional Data’ and ‘Window Intervals’ page 313.

Special OGL Plot Parameters

More OGL Plot parameters are available via the ‘Properties’ in the display window of the OGL plot.

Displaying Subsets of Multidimensional Data

The sequential modes, the $f(txy)$ mode and the scan modes deliver multi-dimensional data arrays versus time, the coordinates of a scanning area, and the detector number. To display these results subsets of the data in selectable ‘Routing Windows’, ‘Scan Windows’ and ‘t Windows’ can be defined. The windows are selected in the right part of the 3D display parameter section and defined in the ‘Window Intervals’ panel. (Please see ‘Window Intervals’ page 313)

Mode Selection

The photon density can be displayed versus different coordinates. The corresponding part of the display parameters and the effect on the display are shown in

Fig. 308.

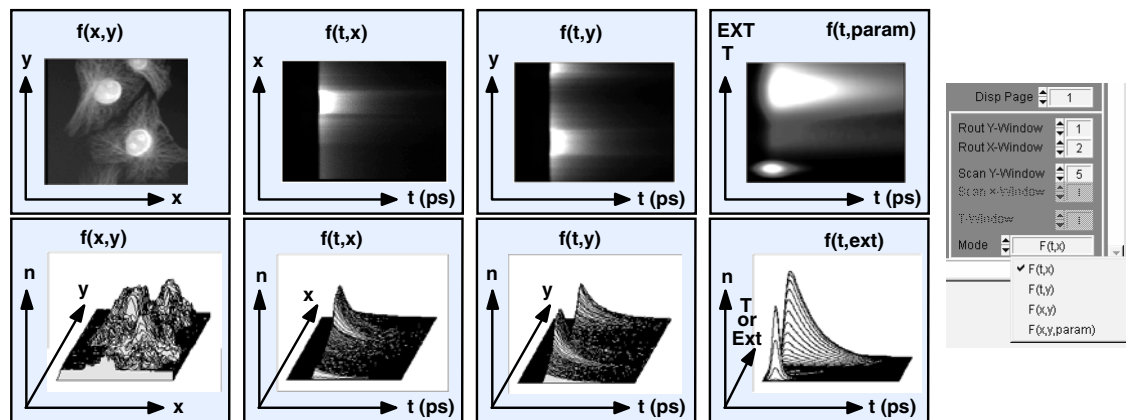


Fig. 308: Display versus different coordinates of multi-dimensional data. Upper row colour-intensity display, lower row multi-curve display. Left to right: Intensity versus image coordinates, intensity versus time and x coordinate, intensity versus time and y coordinate, Intensity versus time in decay curve and time from start of experiment or external parameter. Far right: Display parameters selecting the display coordinates.

The $f(x,y)$ mode displays the intensity versus the image coordinates, x and y . The intensity is calculated within a window of routing channels, time channels and possibly different memory pages. The result for a FLIM data set is shown in the left column of

Fig. 308.

The same data can be displayed versus the time in the fluorescence decay. Two such displays exist. The intensity can be displayed versus the time, t , and the x coordinate, x , within a ‘Scan Y window’ $f(t,x)$ or versus the time, t , and the y coordinate, y , within a ‘Scan X window’

$f(t,y)$. If several detector channels were used also a window of routing channels can be defined.

The right column shows data measured in a sequential recording mode. The data are displayed versus the time in the fluorescence decay and a second parameter. This may be the time from the start of the experiment or an externally varied parameter, such as the wavelength of a monochromator. Also here several such patterns may exist for different windows of routing channels.

Selection of Routing, Scan, and Time Windows

Depending on the used mode option, ‘Routing Windows’, ‘Scan Windows’ and a ‘t Window’ can be selected. The count numbers displayed are calculated within these windows. Furthermore, different ‘Display Pages’ of a multistep measurement can be selected. Depending on the operation mode, the spatial arrangement of the detector channels, possible sequencing or page stepping actions, or scanning multi-dimensional data versus different coordinates are obtained. The effect of the windows for $f(t,x,y)$ mode data is shown in Fig. 309.

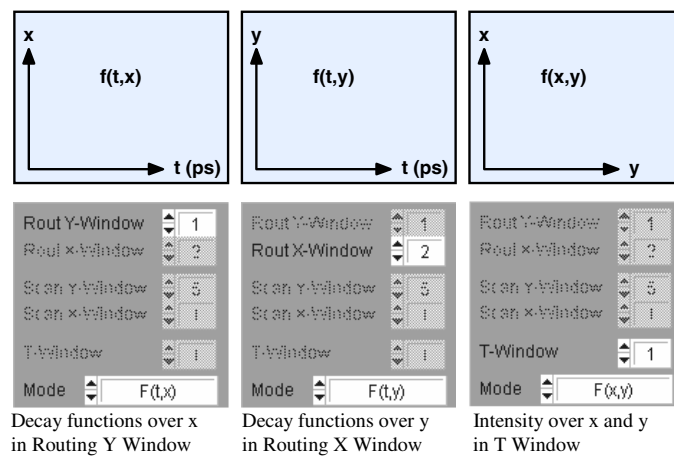


Fig. 309: 3D Display options for $f(t,x,y)$ mode data

For the ‘Scan’ modes not only ‘Routing Windows’ but also windows over the scan coordinates exist. The options are shown in Fig. 310.

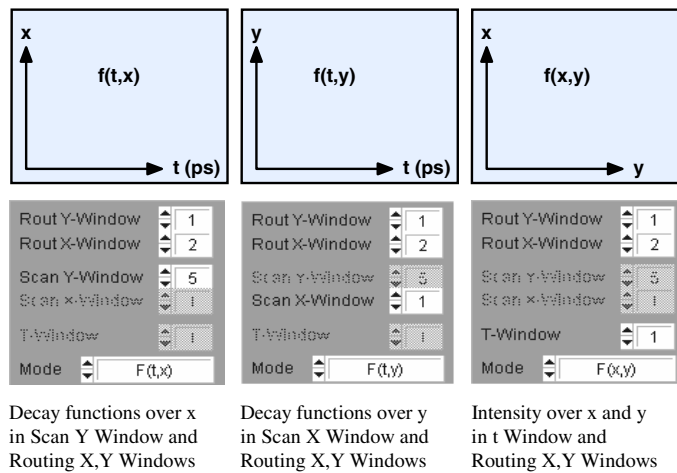


Fig. 310: 3D Display options for ‘Scan’ mode data

Display Parameters for Different Display Windows

Several display windows can be defined in the main panel of the SPCM software (see ‘Configuration of the SPC Main Panel’, page 233). The display windows have separate display parameters. Thus, the windows can be used to display different detector channels, different steps of a page stepping measurements, or different subsets of multi-dimensional data. Moreover, the results can be displayed in the curve mode, the colour-intensity mode, or in linear or logarithmic scale. An example is given in Fig. 311. The display parameters of the individual display windows are reached by placing the mouse cursor in the display window and clicking on the right mouse key. If a display parameter panel is already open, click into the display window by the left mouse key to get the corresponding parameters displayed.

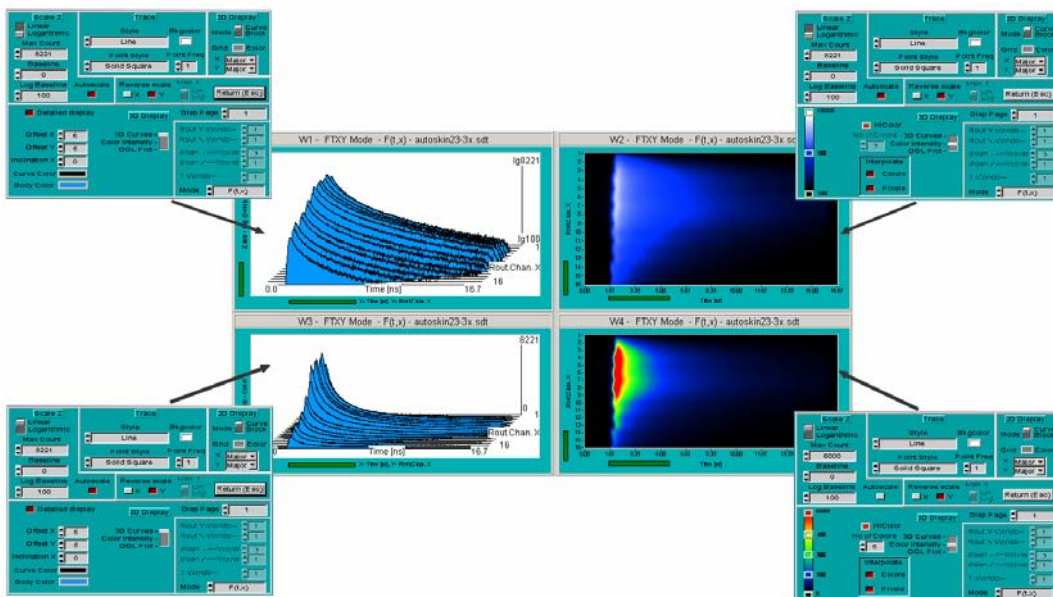


Fig. 311: The display windows of the main panel have separate display parameters

2D Trace Parameters

The 2D display can show up to eight curves simultaneously. In the ‘Curve Mode’ of the 2D display these curves are waveforms, or time resolved spectra measured in the ‘fi’ modes. In the ‘Block Mode’ of the 2D display the displayed curves are accumulated data from several detector channels of a multidetector measurement, or from several pixels of a ‘Scan’ measurement. Please see ‘Display Parameters’, page 301, and ‘Window Intervals’, page 313. The curves on the screen are referred to as ‘Traces’. The ‘Trace Parameters’ define which information the traces contain and in which style and colour they are displayed.

Trace Parameters for 2D Curve Mode

The Trace Parameter panel depends on the number of active SPC modules, on the module type, on the operation mode, and on the 2D display mode set in the ‘Display Parameters’. Fig. 312 shows the trace parameters of a single SPC module (left) and of a multi-module SPC system (right).

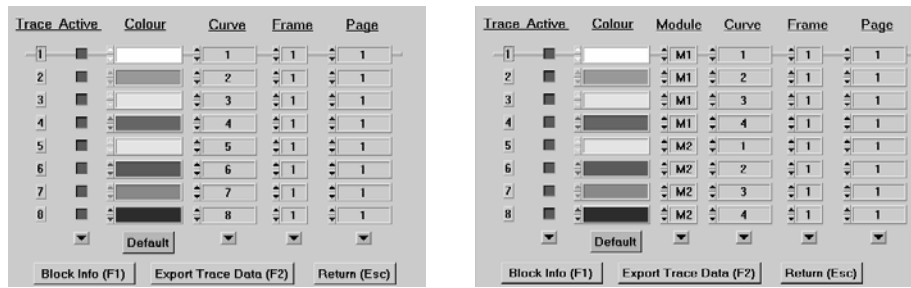


Fig. 312: Left: Trace parameters for a single SPC module. Right: Trace parameters for a multi-modules system.

The panel contains the definitions of eight traces. For each trace the display can be switched on and off by the ‘Active’ button, and different colours can be defined.

‘Curve’ is used to select a single decay curve from a larger data set. For a ‘Single’, $f(x,y,t)$, $f(t,T)$, $f(t,EXT)$, $fi(T)$ or $fi(Ext)$ and ‘Continuous Flow’ measurements ‘Curve’ is the number of the detector channel in a multidetector setup. In a ‘Scan’ measurement, ‘Curve’ is the number of the decay curve in the image, i.e. the number of the pixel in the scan.

‘Frame’ is used to select decay curves from the ‘Scan mode’ recorded in a multidetector setup. In this case each pixel of the image contains decay curves from several detectors, i.e. the data array is a stack of images for the individual detectors. ‘Frame’ selects the data from one of the detectors.

‘Page’ defines a step of a page stepping sequence, a step of sequence recorded in one of the sequencer modes, or one of several measurements that were performed in different memory pages.

For the ‘fi’ spectrum scan modes the trace parameters also contain a ‘Time Window’. The ‘Time Window’ is used to select the spectra (i.e. a sequence of intensity values) obtained in different time windows of the decay curve. (Please see also ‘Window Intervals’).

If a curve is activated that has not been used before it may contain random data. The curve is cleared when a measurement is started in the corresponding memory page. The memory can also be cleared by clicking into ‘Main’, ‘Clear TCSPC Memory’. This does, however, clear the entire memory of the SPC module.

'Module' selects an SPC module from a multi-SPC setup, see Fig. 312, right. For each of the modules individual frames, pages or time windows may exist.

Some typical examples of the application of the trace parameters are given in Fig. 313 to Fig. 316.

The settings shown in Fig. 313 are normally used for single-detector measurements. The eight pages contain the results of eight individual measurements or eight steps of a page stepping measurement. More pages may exist depending on the module type and the used ADC resolution.

Fig. 314 shows trace parameters normally used for multi-detector measurements in the 'Single' or 'Oscilloscope' mode. The 2D Display shows the first eight detector channels of the first memory page. Other curve numbers can be used within the number of existing detector channels. Different measurements or steps of a page stepping measurement can be displayed by selecting another 'Page'.

The Trace Parameters are also used to display time-resolved spectra recorded by the 'Spectrum' modes $f_i(T)$ and $f_i(\text{ext})$. These modes record spectra in the 8 'T Windows' of each detector channel, see 'Operation Modes', page 253 and 'Window Intervals', page 313. With the setting shown in Fig. 315, the spectra recorded in the T Windows 1 to 8 are displayed for the detector channel defined by 'Curve'. Different pages containing different measurements or steps of a page stepping measurement can be selected by selecting another 'Page'. Different detector channels of a multidetector setup are selected by 'Curve'.

During a FIFO measurement accumulated fluorescence decay, FCS, cross-FCS curves and photon counting histograms can be displayed in intervals of 'Display Time'. Which of these functions are calculated is defined in the System Parameters, see 'FIFO Mode Run-Time Display', page 282. Each of the functions is displayed in a separate display window, with separate trace parameters.

The trace parameters for the FCS display window of the FIFO mode are shown in Fig. 316. 'Curve' defines a detector number. 'Cross-FCS Curve' defines the number of the detector to which the photons of the first one are to be correlated. If the detector numbers of 'Curve' and 'Cross-FCS Curve' are identical an autocorrelation function is calculated. If the numbers are different the results is a cross-correlation function. The configuration shown right calculates the autocorrelation functions of detector 1 and 2, and the cross correlation function of

Trace Active	Colour	Module	Curve	Frame	Page
1		MI	1	1	1
2		MI	1	1	2
3		MI	1	1	3
4		MI	1	1	4
5		MI	1	1	5
6		MI	1	1	6
7		MI	1	1	7
8		MI	1	1	8

Fig. 313: Trace Parameters for a single-detector measurement

Trace Active	Colour	Module	Curve	Frame	Page
1		MI	1	1	1
2		MI	2	1	1
3		MI	3	1	1
4		MI	4	1	1
5		MI	5	1	1
6		MI	6	1	1
7		MI	7	1	1
8		MI	8	1	1

Fig. 314: Trace parameters for a multidetector measurement

Trace Active	Colour	Module	Curve	Frame	Page	T-Wind
1		MI	1	1	1	1
2		MI	1	1	1	2
3		MI	1	1	1	3
4		MI	1	1	1	4
5		MI	1	1	1	5
6		MI	1	1	1	6
7		MI	1	1	1	7
8		MI	1	1	1	8

Fig. 315: Trace Parameters for an $f_i(T)$ or $f_i(\text{EXT})$ measurement

Trace Active	Colour	Curve	Frame	CrossFCS Curve
1		1	1	1
2		2	1	2
3		1	1	2
4		2	1	1
5		1	1	1
6		1	1	1
7		1	1	1
8		1	1	1

Fig. 316: Trace Parameters for the FCS display window of a FIFO mode measurement

detector 1 and 2.

For reasons of computation speed, the SPCM software calculates only one correlation function per detector channel on-line. If the Trace Parameters define several correlation functions for one channel, e.g. an autocorrelation and a cross-correlation with another channel, only the first correlation is calculated during the measurement. All other correlation functions are calculated when the measurement is finished.

Trace Parameters for 2D Block Mode

In the ‘Block Mode’ of the 2D display the displayed curves are averaged data from several detector channels of a multidetector measurement or from several pixels of a ‘Scan’ measurement. The Trace Parameter panel in the ‘Block Mode’ of the 2D Display is shown in Fig. 317.

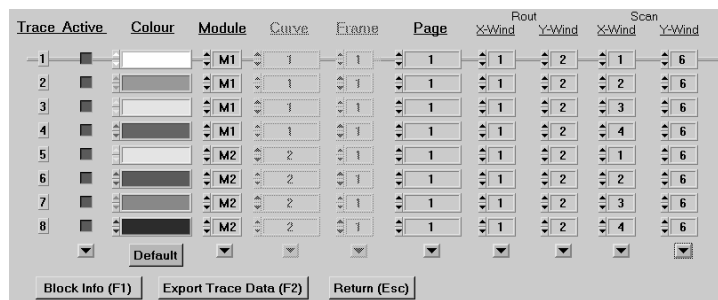


Fig. 317: Trace Parameters for a system of two SPC-730 modules, Block Mode of the 2D display

The left part of the panel is the same as for the 2D curve mode. ‘Module’ selects an SPC channel from a multi-module system. If ‘Stepping through Pages’ was used ‘Page’ selects a particular measurement step. If individual measurements were performed in different memory pages ‘Page’ selects the data set of one of these measurements.

The right part of the panel contains the windows in which accumulated waveforms are calculated. The ‘Routing X Windows’ and ‘Routing Y Windows’ are used to define detector channel areas in ‘ $f(t,x,y)$ ’ mode results. Furthermore, they are used to select a group of detector channels from $f(t,T)$, $f(t,\text{ext})$, $f_i(T)$, $f_i(\text{ext})$ or Continuous Flow data. For ‘Scan’ mode data the ‘Routing Windows’ select images (i.e. arrays of decay curves) from different detector channels. The data from the decay curves of the defined area are averaged within the ‘Scan X’ and Scan Y’ windows and assigned to the selected trace. Please see also ‘Window Intervals’, page 313.

Some examples of trace parameters in the ‘Block Mode’ of the 2D display are shown in Fig. 318.

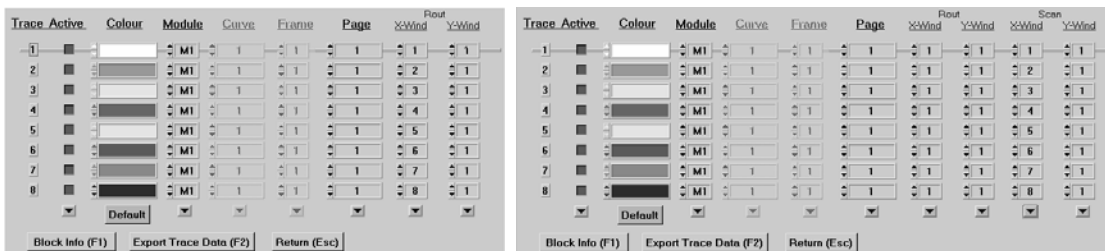


Fig. 318: Left: Trace Parameters for the ‘Single’, ‘Oscilloscope’, or $f(x,y,t)$ mode. Different detector channels are selected.. Right: Trace Parameters for the ‘Scan’ mode. Different image areas are selected.

Fig. 318, left, shows the selection of a range of detector channels in a f(xyt) measurement or a ‘Single’ or ‘Oscilloscope’ measurement with a large number of detector channels. The channels are selected by the ‘Routing X’ and the ‘Routing Y’ window. For the setting shown right averaged decay curves in the first eight Routing X windows and the first Routing Y Window are displayed. Other combinations of Routing X and Y windows can be used depending on the number of existing detector channels and ‘Routing’ windows defined in the Window Intervals.

Fig. 318, right, shows the selection of a region of pixels from a ‘Scan’ measurement. The pixels are selected by the ‘Scan X’ and the ‘Scan Y’ window. For the setting shown right averaged decay curves in the first eight Scan X windows and the first Scan Y Window are displayed. Other combinations of Scan X and Y windows can be used depending on the number of existing pixels and the ‘Scan’ windows defined in the Window Intervals.

Block Info

The ‘Block Info’ button opens a window containing detailed information about a selected data block. The information includes the type and the number of the modules used to measure these data and the corresponding system parameters. The Block Info window is shown in Fig. 319. The block info in the trace parameters is identical with the block info in the load panel, see Fig. 260, page 242.

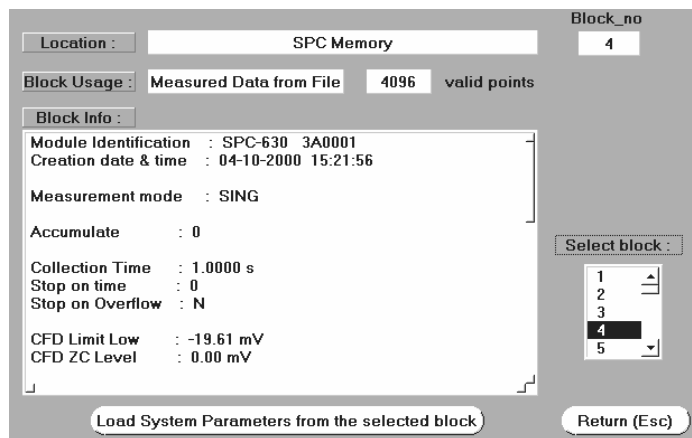


Fig. 319: Block information panel of the trace parameters

Export of Trace Data

The measurement data contained in a selected trace can be exported into an ASCII file. A click on the ‘Export Trace Data’ button opens dialog box. In this box you can choose a file name and start the conversion.

Exporting trace data is also possible in the ‘Block Mode’ of the display. In this case the trace data are calculated by averaging the set of curves selected for this trace.

Exporting trace data is convenient if selected parts of a ‘Scan’ or ‘Multichannel’ measurement are to be processed by an external data analysis program. For exporting larger data sets, please see ‘Convert’.

3D Trace Parameters

The SPCM main panel can be configured to display multi-dimensional TCSPC data in up to eight independent display windows, see Fig. 251. The windows are configured by the ‘3D Trace Parameters’ in combination with the ‘Display Parameters’, see page 301. Thus, data of different detector channels, different steps of a page-stepping sequence, data in different time windows, or data in different areas of a scan can be displayed. The data can be shown in different display modes (curve or colour-intensity mode), in different intensity scale, and in different colour. The 3D trace parameter panel is shown in Fig. 320.

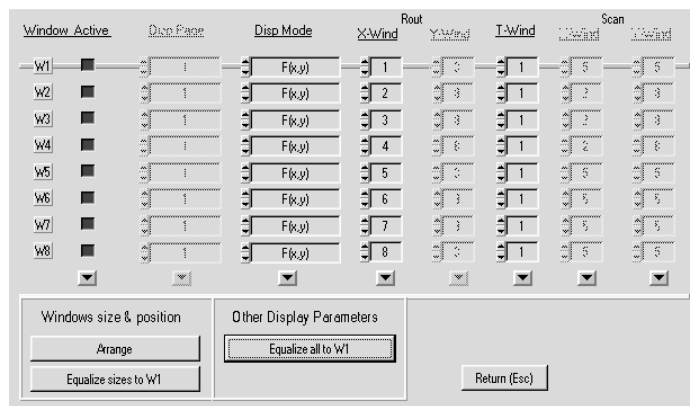
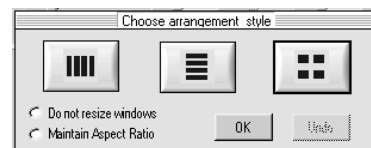


Fig. 320: 3D Trace parameter panel

The panel allows you to define up to eight display windows, W1 through W8. The windows are activated by the ‘Active’ buttons. The fields right of the buttons provide a shortcut to the display parameters. Each window may display data in a specified page (‘Display page’), a specified routing window (‘Rout W Wind’ and ‘Y Wind’), a specified time window (‘T Wind’) or specified scan windows (‘Scan X Wind’ and ‘Y Wind’). For the definition of the windows, please see ‘Window Intervals’, page 313. ‘Disp Mode’ defines different subsets of multidimensional data to be displayed. These may be intensities in specified time windows, the decay function in specified areas of a scan, or decay functions for different time after the start of the experiment. Please see ‘Display Parameters’, ‘Displaying Subsets of Multidimensional Data’, page 304.

The buttons in the lower part of the 3D trace parameter panel simplify the configuration of the display windows in the main panel. ‘Arrange’ opens the panel shown right. It helps you to arrange to display windows in the main panel. You can also select one of the windows by clicking on the W1 to W8 buttons. You can then equalise the sizes of all other windows to the size of the selected one. Display parameters not shown in the 3D trace parameter panel (such as display scales) can be made equal by clicking on ‘Other Display Parameters’, ‘Equalize to W..’.



Some examples of 3D trace parameter settings and the resulting display windows are shown in Fig. 321. Multi-detector scan mode data are displayed with different 3D trace and display parameters. The upper row shows images in subsequent routing (spectral) windows and the corresponding 3D trace parameters. Images in subsequent time windows within the fluorescence decay are displayed in the middle row. The lower row shows decay curves over the x coordinate for subsequent horizontal stripes of the image.

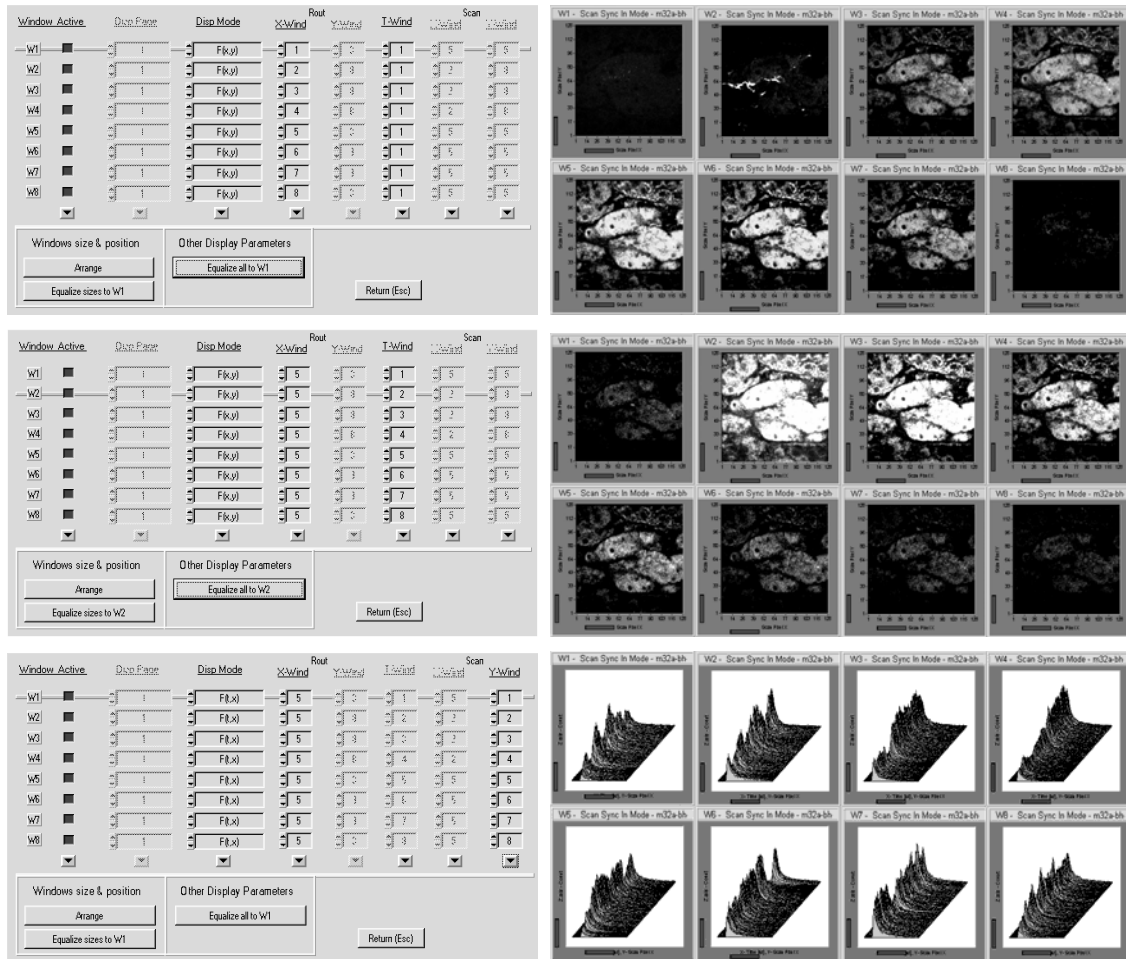


Fig. 321: The same data set displayed with different 3D trace and display parameters. Top: Images in subsequent routing (spectral) windows. Middle: Images in subsequent time windows within the fluorescence decay. Bottom: Decay curves over the x coordinate for subsequent horizontal stripes of the image

Window Intervals

The display routines of the SPCM software display subsets of multi-dimensional data arrays. These can be images within specified time windows or ranges of detector channels, decay curves along one coordinate within a spatial interval of the other coordinate, time-controlled sequences of waveforms within a range of detector channels, or intensity values along a one-dimensional scan within specified time windows.

The required window definitions are provided by the ‘Window Intervals’. The Window Interval panel for the SPC-600/630 and for the SPC-134 modules is shown in Fig. 322. It contains Time Windows, Routing X Windows and Routing Y Windows. The windows are used for the 3D display modes, for the 2D display in the ‘Block Mode’, and for the fi(T) and fi(EXT) spectrum modes.

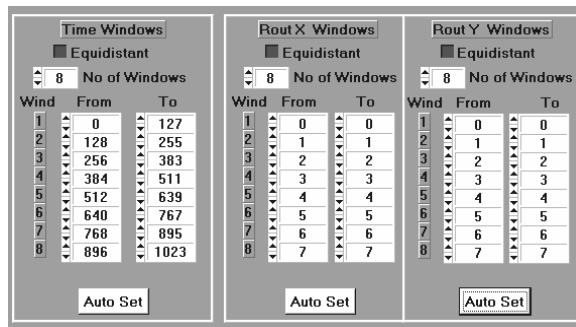


Fig. 322: Window Interval panel of the SPC-600/630 and SPC-134 modules

For the SPC-700/730, SPC-830, and SPC-140/144 the ‘Window Interval’ panel contains also a ‘Scan X’ and a ‘Scan Y’ window, see Fig. 323.

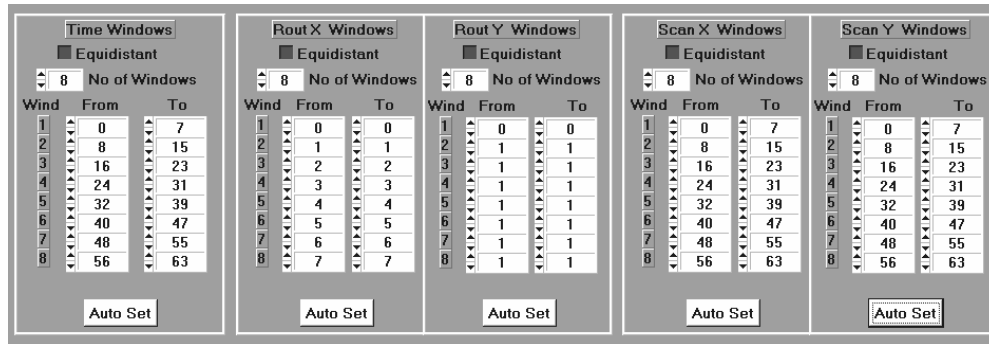


Fig. 323: Window Interval panel of the SPC-700/730, -830, and SPC-140/144 modules

Time Windows

The ‘Time Windows’ are used for calculating integral photon numbers in selected time intervals of decay curves or other waveforms. The time windows are used by the 3D display modes and by the spectrum modes fi(ext) and fi(t).

f(xyt) Mode Data

The f(txty) mode delivers a data array for a one- or two-dimensional array of detector channels. For each detector an individual decay curve is obtained. The results are three-dimensional data cubes of photon numbers over the coordinates x, y, and t. To display these data, one of the variables x, y, t is fixed and data are displayed as a function of the other two variables. For the f(x,y) mode of the 3 D display, the ‘Time Windows’ define intervals in which integral photon

numbers are calculated and displayed as a function of x and y. Fig. 324 shows how a 4x8 pixel intensity pattern is derived from the array 4x8 waveforms.

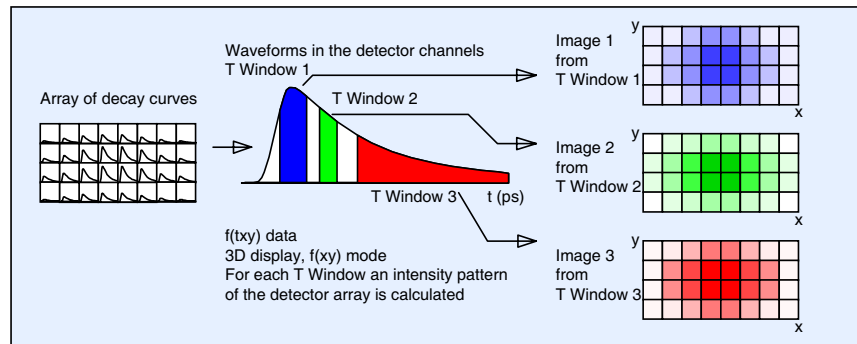


Fig. 324: Calculating integral photon numbers within time windows of an $f(tx)$ measurement

Scan Mode Data

Images obtained in the 'Scan' modes of the SPC-700/730 can be five-dimensional data arrays. The coordinates are the time t in the decay curve, the image coordinates X and Y, and the routing channels of a two-dimensional detector array, e.g. an 8 by 2 array for wavelength and polarisation. The images are usually displayed by the $f(xy)$ option of the 'Colour Intensity' display mode. The t windows are used to calculate integral photon numbers in selectable time intervals for the individual pixels of the image. The method is the same as for the $f(xyt)$ mode above except that x and y are the coordinates of the pixels in the image.

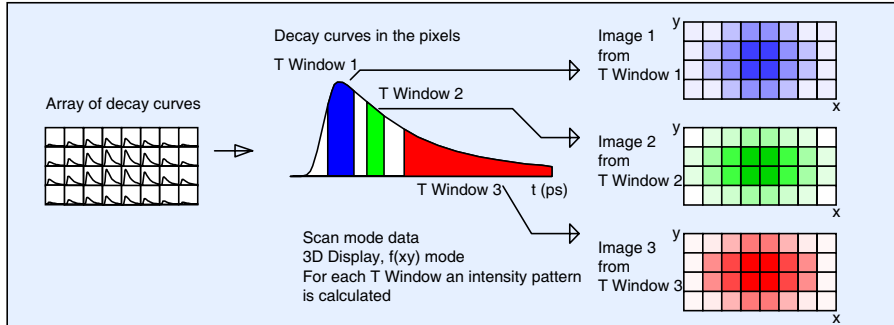


Fig. 325: Calculating integral photon numbers within time intervals of a scan mode measurement

fi Mode Data

In the 'fi' (spectrum) modes the measurement of a single waveform is repeated in intervals of 'Repeat Time' for different settings of an external parameter. From the waveform of each measurement step integral photon numbers are calculated within the 'T Windows'. The results (i.e. the intensities) are displayed as functions of the time from the start of the measurement or as a function of an external parameter (e.g. wavelength). Up to eight time intervals can be defined. Thus, up to eight spectra can be generated up for each detector channel. The principle is shown in Fig. 326.

The spectrum modes can be used with routing. In this case individual sets of spectra with different T Windows are calculated for the individual channels or selected ranges of detector channels. Please see also 'fi(T) Mode', page 262.

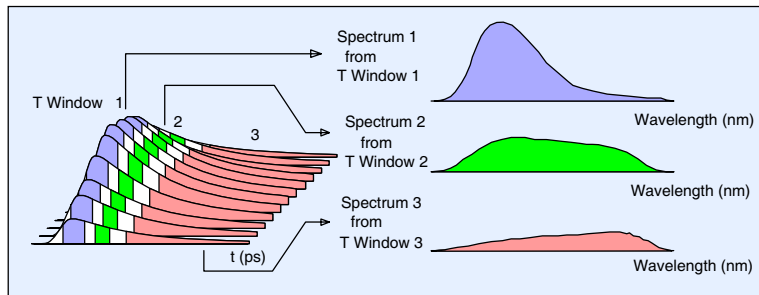


Fig. 326: A sequence of decay curve is recorded during a wavelength scan. For each decay curve integral photon numbers are calculated within defined time windows and displayed as functions of the wavelength

Routing X and Y Windows

The 'Routing X Windows' and 'Routing Y Windows' are used to define detector channels or ranges of detector channels in which integral decay curves are calculated and displayed. Some examples are described below.

f(tx,y) mode Data

In Fig. 327 horizontal stripes of detector channels are selected from a 8x8 pixel array of an ' $f(t,x,y)$ ' mode measurement. The stripes are defined by the 'Routing Y Windows'. The waveforms are displayed as functions of t and x in the $f(t,x)$ display mode. Depending on the 'Routing Y Window' settings up to 8 of these waveform patterns can exist.

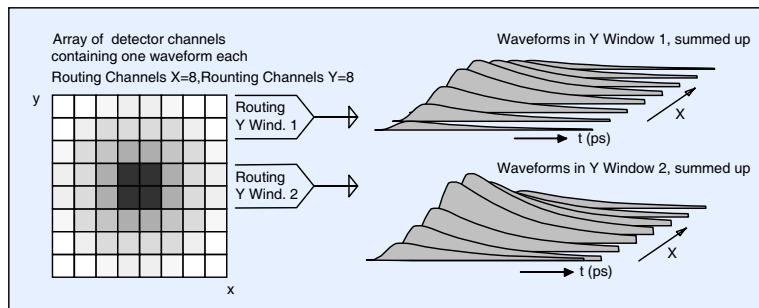


Fig. 327: Selection of horizontal stripes of detector channels from a two-dimensional array, calculation of integral decay curves over the width of the stripe, and display of decay curves as a function of x

In Fig. 328 two vertical stripes are selected from the same 8x8 pixel array. The waveforms are displayed as functions of t and y . The stripes are defined by the 'Routing X Windows'.

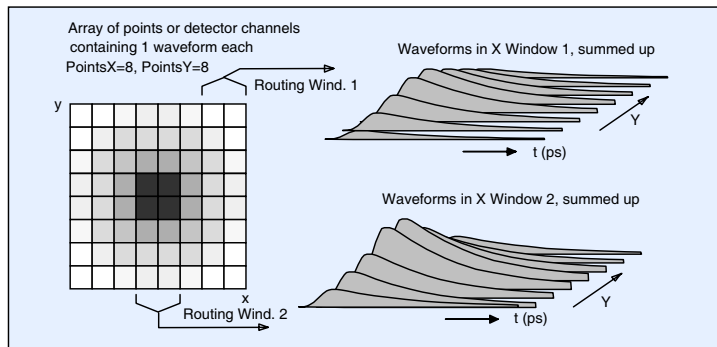


Fig. 328: Selection of vertical stripes of detector channels from a two-dimensional array, calculation of integral decay curves over the width of the stripe, and display of decay curves as a function of y

Scan Mode data

In ‘Scan’ mode data the ‘Routing Windows’ select different detector channels or ranges of detector channels of a multidetector setup. If the routing window is a single detector channel it defines an image that contains a decay curve of this detector in each pixel. If the window covers several detector channels it defines an image that contains decay curves accumulated for all these detectors.

In most scanning applications the detector channel array is one-dimensional, e.g. for multi-wavelength systems. In these cases only ‘Routing X windows’ exist. However, also two-dimensional arrays are possible, e.g. 8 wavelength channels for both directions of polarisation. An example for the $f(xy)$ option of the Colour Intensity display mode is in Fig. 329.

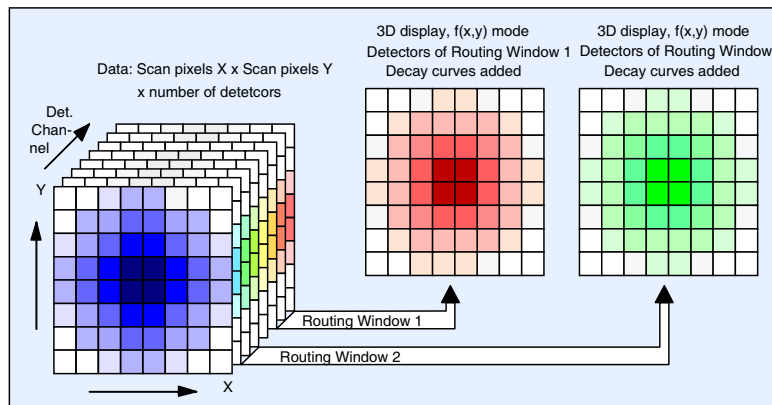


Fig. 329: Selection of detector channels or ranges of detector channels from multi-detector scan mode data

Data recorded by Sequential Modes

In data recorded in the sequential modes and spectrum modes the Routing Windows select different detector channels or ranges of detector channels. If the routing window is a single detector channel it defines a sequence that contains a decay curve of this detector in each step. If the routing window covers several detector channels it defines a sequence that contains curves that are sums of the decay curves of all these detectors.

In most sequencing applications the detector channel array is one-dimensional, e.g. for multi-wavelength systems. In these cases only ‘Routing X windows’ exist. The selection of a data subset from a sequential measurement with a linear array of 8 detectors is shown in Fig. 330.

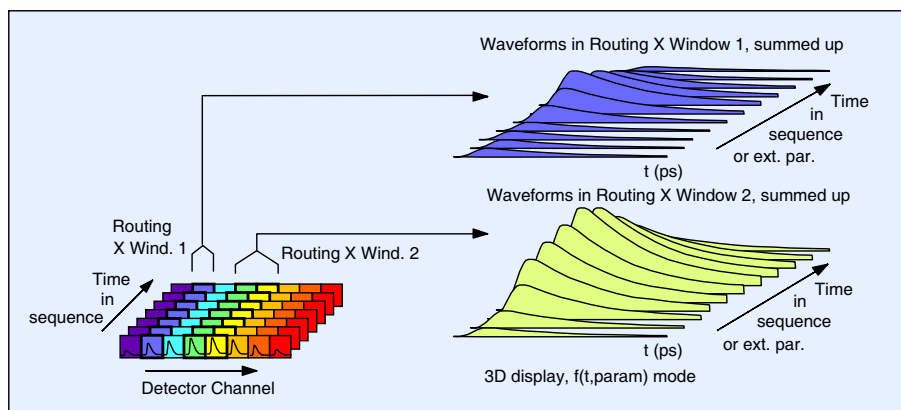


Fig. 330: Selection of routing channels from sequential multi-detector data, one-dimensional detector array

For a 2-dimensional detector array, a data subset is displayed for the detector channels which are both inside the X Window and the Y Window, see Fig. 331.

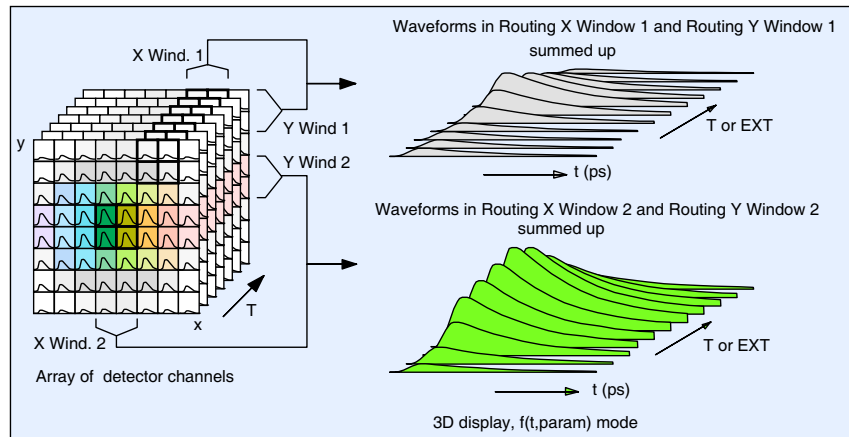


Fig. 331: Selection of routing channels from sequential multi-detector data, two-dimensional detector array

fi Mode Data

The function of the Routing Windows in the fi (spectrum scan) modes are similar as for the sequential modes. However, instead of integral decay curves integral photon numbers within time windows are calculated. The influence of the X and Y Windows on an $f_i(T)$ or $f_i(ext)$ measurement is shown in Fig. 332. The routing windows define either single detector channels or ranges of detector channels. For each routing window and time window a separate spectrum is calculated.

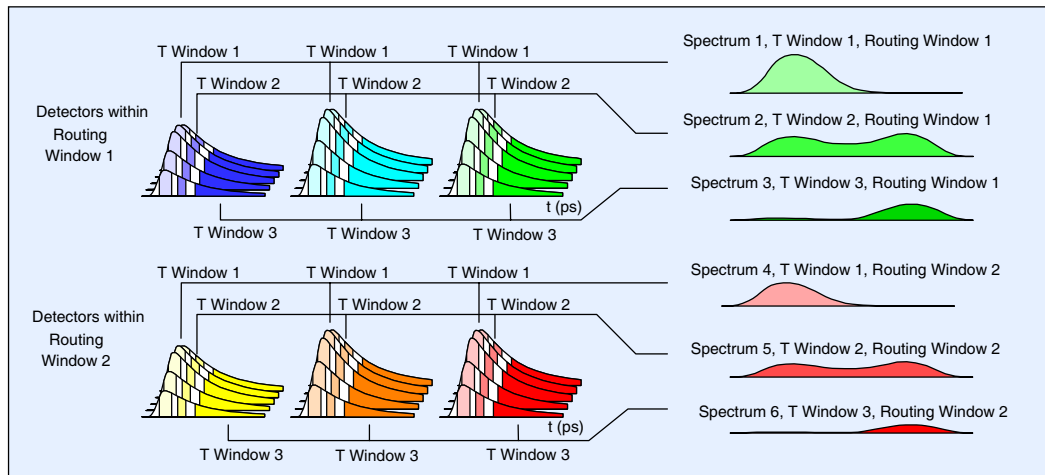


Fig. 332: Routing Windows in the fi modes. For each routing window and time window a separate spectrum is calculated

2D block mode display

The 2D display of the SPCM software is used to display decay curves in selected ranges of detector channels. Up to eight independent areas can be defined by the Routing X and Routing Y windows. The decay curves in the detector channels of the selected range are summed up and displayed as a trace in the 2D display, see ‘Trace Parameters for 2D Block Mode’, page 309. The principle is shown in Fig. 333. In scan images the Routing X and Y windows work in conjunction with the Scan X and Scan Y windows, see Fig. 336.

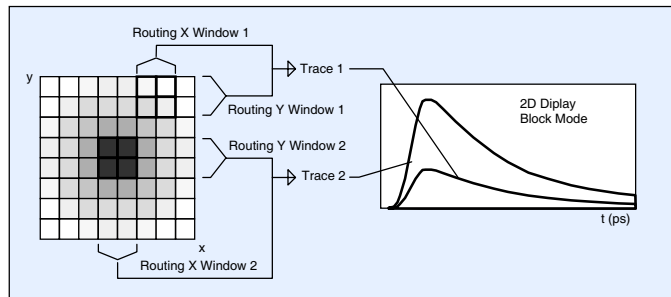


Fig. 333: Selection of a range of detector channels for the block mode of the 2D display. The decay curves of the detector channels within the selected range are summed up and displayed as a single trace.

Scan X and Y Windows

3D display of scan mode results

The 'Scan X Windows' and 'Scan Y Windows' are used to define spatial (x,y) areas in 'Scan' mode results. The effect is very similar as for the Routing X and Y windows in the $f(x,y)$ mode. The 'Scan X Windows' and 'Scan Y Windows' are used for the $f(t,x)$ and $f(t,y)$ options of the 3D display and for the 2D display block mode. Fig. 334 shows how different horizontal stripes are defined in a two-dimensional scan. The results are displayed as a sequence of decay curves versus X.

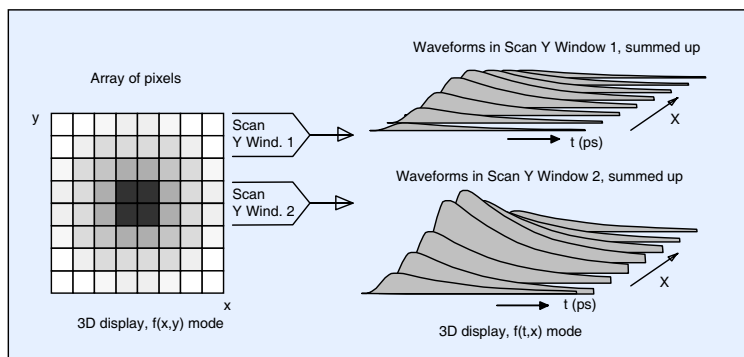


Fig. 334: Selection of horizontal stripes of pixels from a two-dimensional scan, calculation of integral decay curves over the width of the stripe, and display of decay curves as a function of x

In Fig. 328 two vertical stripes are selected from the same pixel array. The stripes are defined by the 'Scan X Windows'; the waveforms are displayed as functions of t and y.

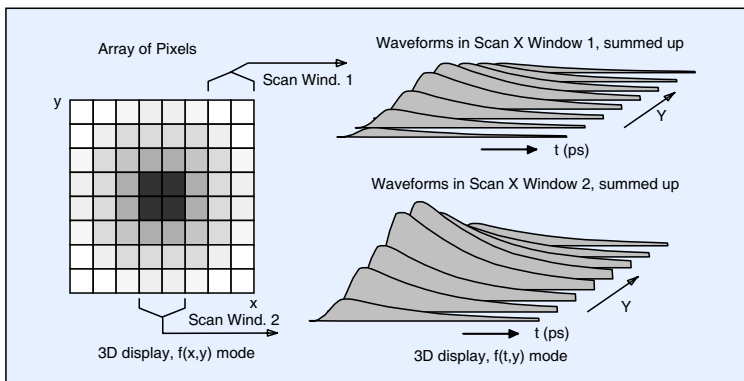


Fig. 335: Selection of vertical stripes of pixels from a two-dimensional scan, calculation of integral decay curves over the width of the stripe, and display of decay curves as a function of y

2D block mode display

The 2D display of the SPCM software can be used to display decay curves in selected areas of a scan. Up to eight independent areas can be defined by the Scan X and Scan Y windows. The decay curves in the pixels of the selected area are summed up and displayed as a trace in the 2D display, see ‘Trace Parameters for 2D Block Mode’, page 309. The principle is shown in Fig. 336. The Scan X and Scan Y windows work in conjunction with the Routing X and Y windows, see Fig. 333.

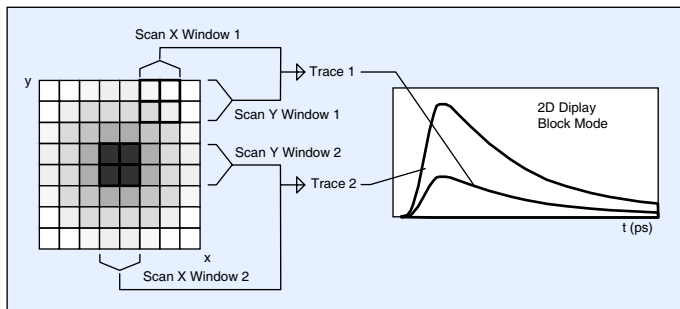


Fig. 336: Selection of an area within a scan for the block mode of the 2D display. The decay curves of the pixels within the selected area are summed up and displayed as a single trace.

Auto Set Functions

For all window parameters up to eight independent intervals can be defined. The intervals can be defined manually or set automatically by the 'Auto Set' function. To control 'Auto Set' the following options are provided.

Equidistant: The available window range is divided into eight equal intervals.
If the number of points cannot be divided by 8 (this can happen for X and Y) the last window can be wider than the windows 1 to 7.

Non Equidistant: The start values of the intervals are set by the operator. The end values are set by the autoset function in a way that the intervals fit closely together.

No of Windows: Number of windows to be set by the autoset function.

After a change in the ADC resolution, the number of detector channels, or the number of pixels of a scan the window intervals are re-calculated automatically.

Agents: Boston Electronics, (800)347-5445, TCSPC@boselec.com

Agents: Boston Electronics, (800)347-5445, TCSPC@boselec.com

Adjust Parameters

Most of the required hardware adjustments in the SPC modules are done via the SPCM software. The adjust values are stored in an EEPROM on the SPC module. The SPCM software reads the EEPROM, corrects the setup parameters according to the adjust values, and sends the corrected setup data to the SPC module.

The adjust values are accessible via the adjust parameters menu. To change the adjust parameters a certain knowledge about the SPC hardware is required. Wrong inputs may seriously de-adjust the module. Therefore you can change the adjust parameters, but not save them to the EEPROM. The changed adjust values are used by the device, but they will be replaced with the original values after restarting the SPC software.

The Adjust Parameters for the SPC-630, 730, -830 and the SPC-130/134 and -140/144 modules are shown in Fig. 337.

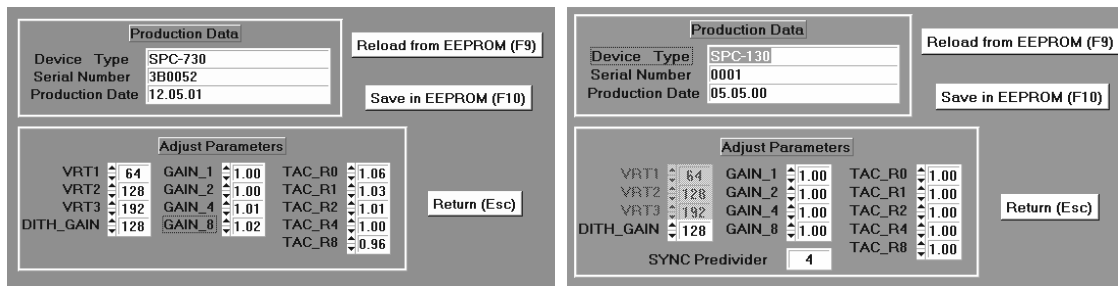


Fig. 337: Adjust parameters for SPC-6, -7, -8 modules (left) and for SPC-134 and -144 modules (right)

Production Data

This area contains manufacturing information about the particular module: The module type, the serial number, and the manufacturing data. The information is used by the software to recognise different module versions. Please do not change these parameters.

Adjust Values

VRT1...VRT3 (Voltage of Resistor Tap, SPC-6, -7, -8)

These parameters adjust the large-scale linearity of the ADC. Imagine the ADC characteristic as a rubber band that is fixed at the zero point and the full scale point. At 1/4, 1/2 and 3/4 of this band other bands are fixed which pull the ADC characteristic up or down. The default values are VRT1=64, VRT2=128 and VRT3=192.

Dither Gain

'Dither Gain' changes the gain of the DAC in the error correction part of the ADC (see 'ADC Error Correction', page 48). To adjust the parameter, a short pulse is measured in a slow TAC range with the maximum value of 'Dither Width'. 'Dither Gain' is adjusted to get a minimum pulse width. The range of the parameter is from 0 to 255, the default setting is 128.

Gain1, Gain2, Gain4, Gain8

These parameters correct the time scale of the TAC for different values of 'TAC Gain'. The correction is done by slightly changing the effective TAC range, see below.

Internally the 'TAC Gain' is set by a combination of four binary graded resistors. Therefore, only four parameters are required to set all 15 gain steps. 'Gain1' corrects for errors in the

value of TAC Gain = 1, 'Gain2' corrects for errors of TAC Gain = 2, and so on. If the gain is correct for 1, 2, 4, and 8 also the other values are correct (dynamic errors neglected). The default values are 1, greater values increase the effective TAC Gain, smaller values decrease it.

TAC_R0 toTAC_R8

These adjust values correct the 'TAC Range' parameter. The adjust parameters act on the following TAC Ranges:

TAC_R0	TAC Range = 50ns to <100ns
TAC_R1	TAC Range = 1000ns to <2000ns
TAC_R2	TAC Range = 500ns to <1000ns
TAC_R4	TAC Range = 200ns to <500ns
TAC_R8	TAC Range = 100ns to <200ns

The default setting is 1. Values >1 increase TAC Range, i.e. decrease the width of a signal recorded, values <1 decrease TAC Range, i.e. increase the width of a signal. Values from 0.9 to 1.1 are accepted.

SYNC Predivider (SPC-134 and SPC-144 only)

In the SPC-134 and SPC-144 modules the internal SYNC frequency is divided by 2 or by 4 before it is fed into the SYNC-Rate Counter. The divider ratio is set by a jumper on the board, see Fig. 338. To obtain correct SYNC-rate display 'SYNC Predivider' must correspond to the jumper setting.

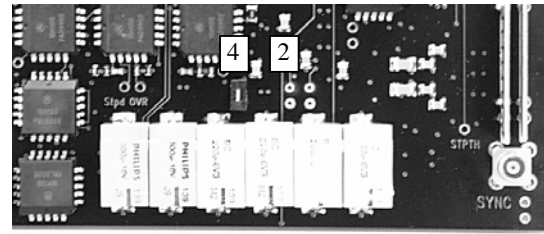


Fig. 338: SPC-130/-140: Jumpers for SYNC- predi-
vider ratio

Display Routines

2D Display

The 2D display of the SPCM software is used to display waveforms, spectra, or other two-dimensional data. These may be single decay curves, multiple decay curves of a multi-detector measurement, decay curves in selected areas of a scan, or results of the $f_i(T)$ or $f_i(\text{ext})$ spectrum scan modes. The 2D display can display up to eight different curves simultaneously. The 2D display is shown in Fig. 339, left. The curves on the screen are referred to as 'Traces'. The traces are defined in the 'Trace Parameters', see Fig. 339, right. For details of the trace definitions, please see '2D Trace Parameters', page 307.

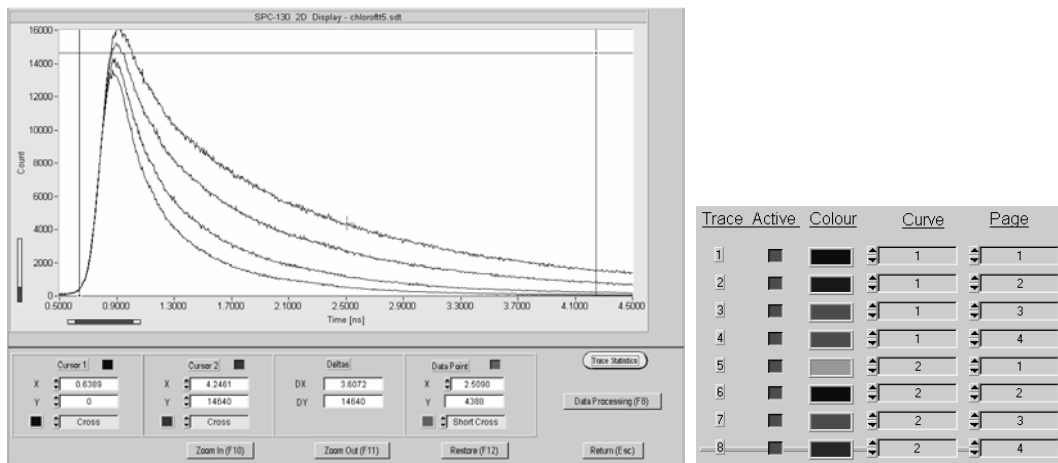


Fig. 339: 2D display panel (left) and trace parameter panel (right)

The 2D display can be operated in the 'Curve Mode' or in the 'Block Mode', see '2D Trace Parameters', page 307.

In the 'Curve Mode' of the 2D display the traces are decay curves or time-resolved spectra of a single detector channel, as single step of a page stepping sequence, or a single pixel of a scan.

In the 'Block Mode' of the 2D display the traces are sums of decay curves in defined ranges of detector channels or areas of a scan. The waveforms of the selected detector channels or pixels are summed up and displayed as a single trace.

Cursors

Two cursors are available to select curve points and to display the data values numerically. The cursors can be switched on and off by clicking on the buttons right of 'Cursor 1' and 'Cursor 2'. The cursors positions are displayed in the lower part of the 2D display panel ('X' and 'Y'). The style of the cursors can be changed by clicking into the field below the cursor position. The options are 'Cross' (crossed lines) and 'Vertical Line' and 'Horizontal Line'. The colour can be changed by clicking on the colour button left of the style field.

The cursors can be moved with the mouse or with the keyboard. When the keyboard is used, the cursor is selected with 'page up' and 'page down' and shifted with the cursor keys. By pressing the cursor keys together with the 'shift' key a fine stepping is achieved. Moreover, a cursor can be set to an exact position by typing the coordinates into the position fields.

Data Point

In addition to the cursors, the 'Data Point' can be used to measure data values. The data point is a small cross that can be shifted across the screen by the mouse. By releasing the mouse key the data point drops to the next data point of the nearest trace. At the same time X and Y values are displayed.

Zoom Function

The display scale can be changed in both axis by zooming the area defined by the cursor lines. 'Zoom In' zooms into the area selected by the two cursors. If the cursors are vertical lines the zoom works only horizontally; if the cursors are horizontal lines the zoom works only vertically. For crossed-line cursors zooming works in both directions. 'Zoom Out' restores the state from before the last zoom action. This includes not only the zoom state but also the other display parameters such as 'linear' or 'logarithmic'. 'Restore' restores the zoom state as it was before the 'Zoom' function was entered.

2D Data Processing

The 2D display contains a range of data processing operations. The data processing panel opens by clicking on the 'Data Processing' button of the 2D display panel, or by clicking into the menu bar, 'Display' and '2D Data Processing'. The data processing window is shown in Fig. 340.

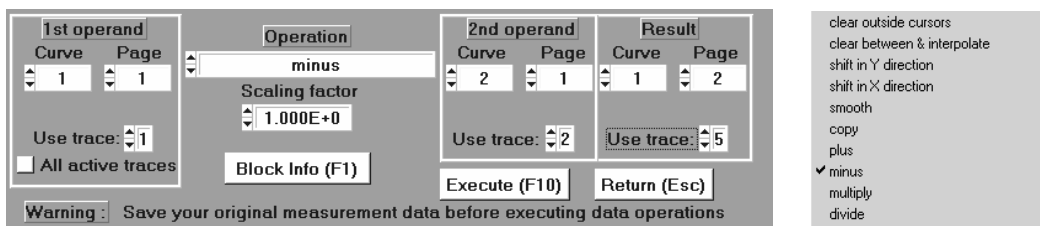


Fig. 340: 2D data processing panel (left) and available operations (right)

The panel allows you to select the arithmetic operation, the curves to which the operation is to be applied, a scaling factor, and the destination of the result.

1st operand

Under '1st operand' the curve and page number of the first operand is specified. Alternatively, you can select an active trace by clicking into the 'Use trace' field. In this case 'Curve' and 'Page' are set according to trace definition in the trace parameters. We recommend to keep the Trace Parameters open for selecting the operands. 'Curve' and 'Page' are displayed in the colour of the selected trace. If 'all active traces' is selected the specified operation is applied to all active traces.

Operation

'Operation' selects the operation to be applied to the operands, see Fig. 340, right. To keep the result inside the data range of the measurement memory (0...65535) the result is multiplied by a 'Scaling Factor'. This factor can be set to any floating point number.

2nd operand

Under '2nd operand' the curve and page number of the second operand are specified. Alternatively, you can select an active trace by clicking into the 'Use trace' field. In this case 'Curve' and 'Page' are set according to trace definition in the trace parameters. We recommend to

keep the Trace Parameters open for selecting the operands. ‘Curve’ and ‘Page’ are displayed in the colour of the selected trace.

Result

Under ‘Result’ the curve and page number of the result are specified. If the definitions are identical with one of the operands the operand is overwritten. Therefore, make sure that you have saved the results before you start any data processing operation.

An example of a data processing operation is shown in Fig. 341. The decay curve, A, shown left, is badly distorted by an optical reflection. The amplitude of the reflection is about 5.2%, the delay 0.467 ns. An approximate waveform of the reflected part of the signal can be obtained by shifting the curve by 0.467 ns, and multiplying it with 0.052 (use ‘add’ with the original curve for both operands, and a scaling factor of 0.026). The result is curve B. Curve B is then subtracted from curve A. The result is curve C, which is almost free of the reflection.

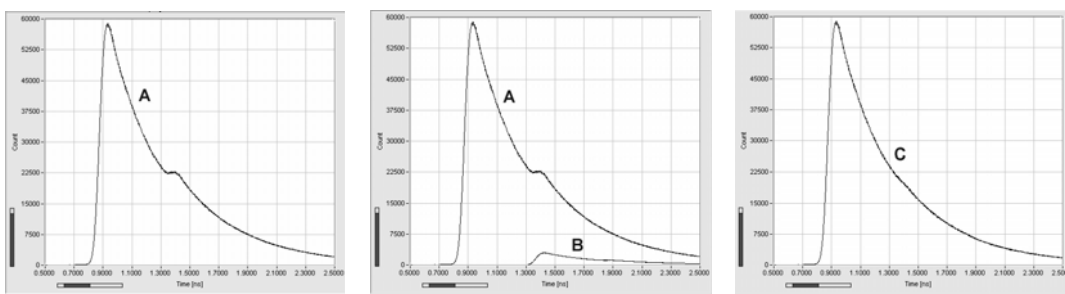


Fig. 341: Using 2D data processing to remove an optical reflection from a decay curve

3D Display

Display of Multi-Dimensional Data

‘Curve Display 3D’ is used to display multi-dimensional TCSPC data. The data may be results of results a sequential measurement, a multi-detector measurement, a scan measurement, or combinations of these. The corresponding photon distributions may be built up versus several parameters, such as the time in a fluorescence decay, the time in a sequence of decay curves, the wavelength, or the coordinates of a scan area. To display these data the SPCM software provides different three-dimensional display modes, see Fig. 342.

The ‘3D Curve’ mode displays the results as a set of curves. The Z axis represents the number of photons, the X and Y axis two of the parameters x, y, t or EXT. The ‘Colour Intensity’ mode transforms the photon density into a grey scale or colour scale. The X and Y axis represents two of the parameters x, y, t or EXT. The ‘OGL Plot’ mode shows the results as a curved and coloured surface with the number of photons as Z axis and two of the parameters x, y, t or EXT as X and Y axis. Examples of the three display modes are shown in Fig. 342.

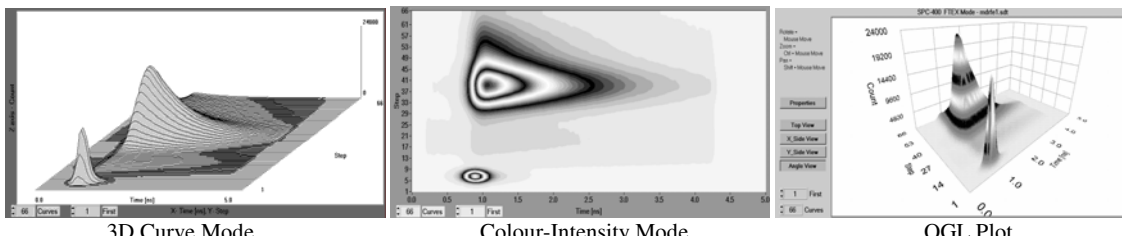


Fig. 342: Display modes of the 3D display

The display mode is selected by the ‘3D Display Parameters’. The corresponding part of the 3D parameter panel is shown in Fig. 343. The same panel is used to define other parameters of the 3D display, such as display colours and sub-sets of multi-dimensional data. For details please see ‘3D Display Parameters’, page 302.

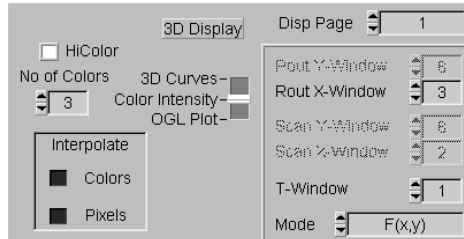


Fig. 343: 3D display parameters. Definition of the general display mode (in the centre, 3D Curves, Colour Intensity, OGL Plot) and definition of sub-sets of multi-dimensional data (at right)

A multi-dimensional TCSPC measurement may built up a photon distribution over more than two parameters. The result of a two-dimensional scan is built up over three coordinates - the image coordinates and the time in the fluorescence decay. A multi-wavelength scan has two spatial, one temporal, and one spectral coordinate. Thus, even a three-dimensional pattern is often insufficient to display the entire photon distribution. Therefore the 3D display routines provide options to display sub-sets of such data, such as images in selectable time windows, decay curves versus one coordinate of an image, or sequences of decay curves for selectable ranges of detector channels. The options are selected in the 3D display parameter panel, see Fig. 343. (For details please see ‘3D Display Parameters’, page 302). Data can be displayed versus selectable coordinates and in selectable ‘Routing Windows’, ‘Scan Windows’ and ‘t Windows’. For definition of these windows please see Window Intervals, page 313. Different display options for multidimensional data are shown in Fig. 344.

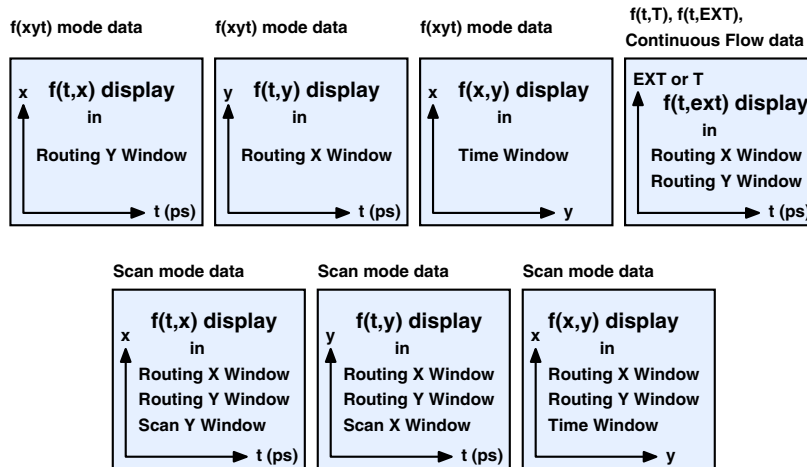


Fig. 344: Options to display multidimensional data in the 3D display

Cursor and Zoom Functions

The 3D display panel contains cursor and zoom functions, and a range of 3D data operations is provided. The 3D display panel is shown in Fig. 345.

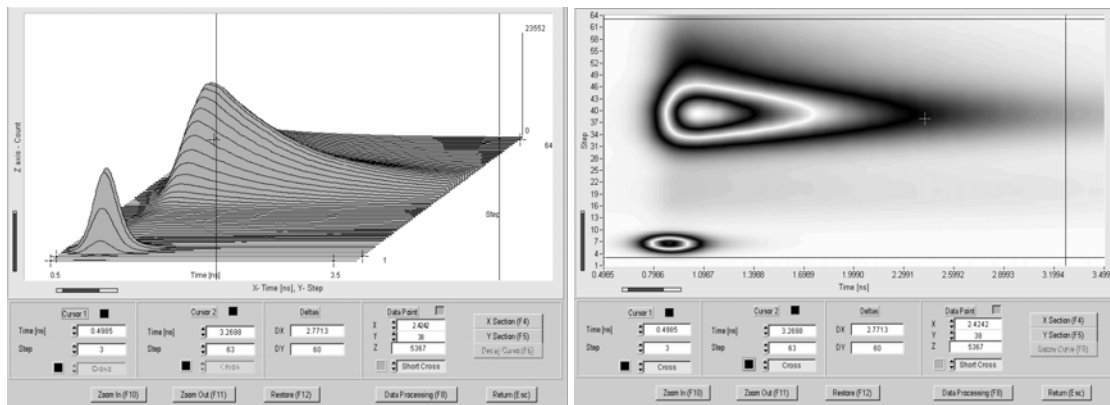


Fig. 345: 3D Display. Left: 3D Curve mode. Right: Colour-intensity mode

Cursors

The cursors can be switched on and off by clicking on the buttons right of 'Cursor 1' and 'Cursor 2'. The cursor positions are displayed in the lower part of the 2D display panel ('X' and 'Y'). The style of the cursors can be changed by clicking into the field below the cursor position. The options are 'Cross' (crossed lines) and 'Vertical Line' and 'Horizontal Line'. The colour can be changed by clicking on the colour button left of the style field.

The cursors can be moved with the mouse or with the keyboard. When the keyboard is used, the cursor is selected by the 'page up' and 'page down' keys and shifted with the cursor keys of the keyboard. By pressing the cursor keys together with the 'shift' key a fine stepping is achieved. Moreover, a cursor can be set to an exact position by typing in the coordinates in the position fields.

Setting the cursors in the 3D curve mode requires some experience. It may therefore be useful to switch to the colour intensity mode to set the cursors. The cursor settings are the same for both modes and do not change when the mode is switched.

Data Point

The 'Data Point' is an additional tool to display single data points of a three-dimensional data set. The cross-shaped marker is moved over the data by the mouse or by the cursor keys of the keyboard.

If controlled by the mouse, a horizontal movement shifts the data point across the actual curve. A vertical movement causes the data point to change to the next curve. Controlling the data point by the mouse requires some experience. Therefore the data point can also be moved by the cursor keys of the keyboard. 'Left' and 'right' shift the data point on the current curve, 'up' and 'down' cause it to jump to the next curve.

When the display is in the '3D Curve Mode' the data point can be set to invisible curve parts. To avoid confusion the data should be displayed in a way that the interesting parts are clearly visible (see 'Display Parameters', '3D Display').

Zoom

'Zoom in' magnifies the area inside the cursors to the entire width of the display window. 'Zoom Out' restores the state before the last 'Zoom in' action. This includes not only the zoom state but also the other display parameters such as 'linear' or 'logarithmic'. 'Restore' will reset the display scale to the state in the moment when the 'Zoom' function was entered.

3D Data Processing

The ‘3D Data Processing’ panel is opened by clicking on the ‘Data processing’ button or by clicking into ‘Display’ in the menu bar and selecting ‘3D Data Processing’. The 3D data processing panel is shown in Fig. 346.

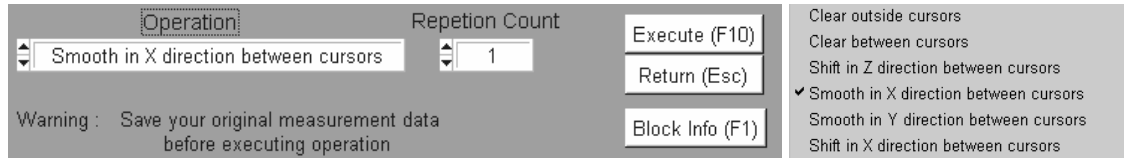


Fig. 346: 3D Data Processing Panel (left) and available operations (right)

All operations refer to the range defined by the cursors. During the operation the original data is replaced with the result. Therefore, we recommend to store the original data to a file before starting a data processing operation.

For fluorescence decay analysis of TCSPC Imaging data an individual software package is available. This ‘SPCIImage’ software is designed for single and double exponential decay analysis in the individual pixels of the image and for FRET imaging based on fluorescence decay data. Please see www.becker-hickl.com.

Starting and Stopping a Measurement

Start

The 'Start' button in the menu bar starts the measurement in the selected operation mode. Please note that the measurement may not start immediately. If a trigger condition different from 'none' is defined the SPC module waits for an active trigger edge to start the measurement. In the Scan Sync In mode the module waits until a frame clock indicates the beginning of the next frame.

If the autosave function is active or a mode with automatic writing to the hard disk is used (e.g. FIFO or Continuous Flow) the SPCM software may ask for permission to overwrite the data file specified in the system parameters. Please make sure that this file does not contain valid data of a previous measurement.

During the measurement the main menu remains active and the results are shown in the display window. The rate display gives information about the count rates in the CFD, the TAC and the ADC. The CFD rate represents all pulses with an amplitude greater than 'CFD Limit Low'. The TAC rate is the working rate of the TAC. It is slightly smaller than the CFD rate because the TAC is not started by pulses exceeding the 'CFD Limit High'. 'ADC Rate' is the conversion rate of the ADC. It represents all events inside the selected TAC window.

When a measurement is run in the FIFO mode one or more data files are written which contain the data of the subsequently recorded photons. These measurement data files have the extension '.spc'. At the end of the measurement, a setup data file is generated which contains the hardware and software parameter used. The setup data file has the same name as the last measurement data file and has the extension '.set'.

Most (though not all) system and display parameters can be changed during the measurement. The effect becomes visible with the display of the next result.

Interrupt

'Interrupt' interrupts a running measurement so that the measurement sequence goes into a 'hold' state. 'Interrupt' can be used when the system parameters or an external set-up require re-adjustment. When the measurement is in the 'hold' state it can be restarted from the current state by clicking on the 'Start' button. Of course, 'interrupt' cannot be used within a sequential measurement, a FIFO measurement or any other recording procedure that requires accurate timing.

Stop

'Stop' aborts a running measurement. After stopping the results are displayed as they were in the moment of stopping. Please note that a sequential measurement or a page stepping sequence may be incomplete. Please note also that the measurement cannot be re-started from the current state after a 'Stop' command.

In some operation modes the measurement may not stop immediately with the stop command. In the Scan Sync In mode the recording continues until the current frame is complete. When a FIFO mode measurement is stopped the FIFO may still contain valid photon data. The SPCM software then asks you whether these photons are to be processed by the online-calculation and saved in the current data file. Please note also that a FIFO measurement writes a setup file at the end of the measurement. This file contains the hardware and software parameter used.

The setup data file has the same name as the FIFO data file but the extension ‘.set’. Please do not delete this file. It is needed for possible off-line analysis of the FIFO data.

Exit

The SPC software is left by 'Exit'. When the program is left, the system and configuration parameters are saved in a setup file 'auto.set'. This file is automatically loaded at the next program start. Thus, at the next start the SPCM software system will come up with the same hardware and software parameters. If you do not want to save the last settings you can reject the writing of a new auto.set file by switching off the 'Save data on exit' button, see Fig. 347.

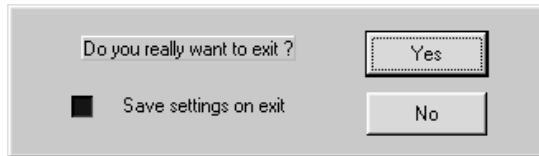


Fig. 347: Exit panel

Data file structure

Data of the Photon Distribution Modes

The ‘Save’ functions of the SPCM software generate both setup and data files. Setup files have the extension .set and contain the system and software setup parameters. Data files have the extension .sdt and contain the parameters and the measurement data. Both file types have the same general structure. They only differ in that the SET-files do not contain any measurement data.

Files generated by the ‘Autosave’ functions of the measurement routines are .sdt files. The structure is identical with that of the .sdt files generated by the ‘save’ routine.

Photon files generated by the FIFO modes have a different file format. For these files, please see ‘FIFO Files’, page 335.

With the introduction of the SPC-134 and the combined scanning and routing in the SPC-700/730 a modification of the file structure became necessary. The changes were required to identify the individual modules of a multi-SPC system and to save more than 65565 curves of a scan measurement. Older files of the SPC Standard Software for Windows, versions 2.0 to 6.9, are generally compatible with the new structure. However, loading files of version 7.0 or later into old software versions can (but need not) cause problems.

The data files consist of

- a *file header* containing structural data which are used to find the other parts of the file
- the *file information* which was typed in when the file was saved
- the *system setup* data for hardware and software
- one or more *measurement description blocks* which contain the system parameters corresponding to the particular data blocks
- *data blocks* containing sets of curves generated by one measurement.

File Header

Data recorded by the bh SPC modules may contain a large number of data blocks for different measurement steps, pixels of a scan, and detector channels. A SPCM data file may even contain several measurements, with possibly different system parameters. Therefore the SPCM data files start with a binary file header which contains general information about the location of the setup and measurement data within the file. An example of a file header is given below.

short	revision	software revision number (lower 4 bits = 11(decimal))
long	info_offset	offset of the info part which contains general information (Title, date, time, contents etc.)
short	info_length	length of the info part
long	setup_offs	offset of the setup data (system parameters, display parameters, trace parameters etc.)
short	setup_length	length of the setup data
long	data_block_offset	offset of the first data block
short	no_of_data_blocks	no_of_data_blocks valid only when in 0 .. 0x7ffe range, if equal to 0xffff the field ‘reserved1’ contains valid no_of_data_blocks
long	data_block_length	length of the longest data block in the file
long	meas_desc_block_offset	offset to 1st. measurement description block (system parameters connected to data blocks)
short	no_of_meas_desc_blocks	number of measurement description blocks
short	meas_desc_block_length	length of the measurement description blocks
unsigned short	header_valid	valid: 0x5555, not valid: 0x1111
unsigned long	reserved1	reserved1 now contains no_of_data_blocks
unsigned short	reserved2	
unsigned short	checksum	checksum of file header

The exact definition of the header is available from the file ‘spc_data_file_structure.h’. The installation procedure writes an spc_data_file_structure.h file into the same directory as the SPCM application.

File Information

The File Information part contains the general information written into the file info field during the ‘Save’ procedure (see ‘Save Panel’, page 243). The info part is stored in ASCII format. An example is given below.

```
*IDENTIFICATION
ID          : _SPC Setup & Data File_
Title       : startup
Version     : 007
Revision    : 1
Date        : 10-10-2004
Time        : 12:29:01
Author      : Bond, James
Company     : Unknown
Contents    : Tissue sample from Dr. No, 2p excitation at 750 nm
*END
```

Setup

The setup block contains all system parameters, display parameters, trace parameters, etc. It is used to set the SPC system (hardware and software) into the state in which it was when the data file was stored. All parameter values are stored together with an identifier. This method allows to maintain compatibility between different SPC versions. If a parameter is missing in the setup part, i.e. if a file from an older software version is loaded, a default value is used when the file is loaded. A typical setup part is shown in Fig. 348. The list is for information only; new parameters may be added in future software versions. For Multi-SPC Systems the system parameters section contains separate subsections for module parameters of the individual modules.

```
SYS_PARA_BEGIN:
#SP [SP_STOPT,B,I]           #DI [DI_YWIN,I,J]           #MP1 [MP_TAC_OFF,9.8039217]
#SP [PR_PDEV,I,0]             #DI [DI_XWIN,I,J]           SYS PARA_END:
#PR [PR_PPORT,I,2]           #DI [DI_TWBN,I,J]           TRACE PARA BEGIN:
#PR [PR_PWHAT,I,0]           #DI [DI_PSTYLED,I,J]         #TR,#0 [I,15,I,4,1,I]
#PR [PR_PFB,B,I]             #DI [DI_PPFBQ,I,J]         #TR,#1 [0,9,I,2,I,2,I]
#PR [PR_PFNAMES,IMAGE.PRT]   #SP [SP_EXTST,B,I]         #TR,#2 [0,10,I,3,I,3,I]
#PR [PR_PORIEN,I,I]          #SP [SP_STEPS,I,32]         #TR,#3 [0,14,I,4,I,4,I]
#PR [PR_PJECT,B,I]           #SP [SP_OFSETT,F,0]         #TR,#4 [0,14,I,5,I,1,I]
#PR [PR_PWIDTH,F,100]         #SP [SP_YWIN_N,I,8]         #TR,#5 [0,12,I,6,I,1,I]
#PR [PR_PHEIGH,F,100]         #SP [SP_XWIN_N,I,8]         #TR,#6 [0,13,I,7,I,1,I]
#PR [PR_PFULLB,B,I]          #SP [SP_TWBN_N,I,8]         #TR,#7 [0,11,I,8,I,1,I]
#PR [PR_PAUTO,B,I]           #SP [SP_X_EQUB,B,I]         TRACE PARA END:
#PR [PR_STP_FN,S,STP.CFG]    #SP [SP_Y_EQUB,B,I]         #DI [DI_ZDC25,I,0]
#PR [PR_SAVE_T,I,2]           #SP [SP_T_EQUB,B,I]         #DI [DI_ZDC25,I,0]
#SP [SP_MODE],0               #SP [SP_DITH,L,64]          WIND PARA BEGIN:
#SP [SP_CFD_LL,F,-20]         #SP [SP_EN_INT,B,0]          #WI #0 "NO *0 [0,0]
#SP [SP_CFD_LH,F,80]          #SP [SP_INCR,I,64]          #WI #0 "NO *1 [0,0]
#SP [SP_CFD_ZC,F,0]          #SP [SP_DAES,B,1]           #WI #0 "NO *2 [0,0]
#SP [SP_CFD_HF,F,5]           #SP [SP_SPE_FN,S,SPEC1.SDT] #WI #0 "NO *3 [0,0]
#SP [SP_SYN_ZCF,9.8267717]   #SP [SP_CYCLE,U,I]          #WI #0 "NO *4 [0,0]
#SP [SP_SYN_FD,I,4]           #SP [SP_DAEC,B,0]           #WI #0 "NO *5 [0,0]
#SP [SP_SYN_FOF,-20]          #SP [SP_MEM_BANK,I,0]         #WI #0 "NO *6 [0,0]
#SP [SP_SYN_HF,F,4]           #SP [SP_ITCOOMP,B,1]         #WI #0 "NO *7 [0,0]
#SP [SP_TAC_R,F,5.0000001e-08] #DI [DI_SCALE,I,0]           #WI #0 "NO *8 [0,0]
#SP [SP_TAC_G,I,1]             #DI [DI_MAXCNT,L,65535]      #WI #0 "NO *9 [0,0]
#SP [SP_TAC_OF,F,9.4993896]   #DI [DI_LBLINE,L,100]        #WI #0 "NO *A [0,0]
#SP [SP_TAC_LL,F,14.90196]    #DI [DI_BLINE,L,0]           #WI #0 "NO *B [0,0]
#SP [SP_TAC_LH,F,84.703879]   #DI [DI_GRIB,B,0]            #WI #0 "NO *C [0,0]
#SP [SP_TAC_TCF,4.8228126e-11] #DI [DI_GOOL,F,8]           #WI #0 "NO *D [0,0]
#SP [SP_TAC_TDF,6.2500001e-09] #DI [DI_GOOL_B,I,0]          #WI #0 "NO *E [0,0]
#SP [SP_ADC_REL,1024]          #DI [DI_TRACE,I,0]           #WI #1 "NO *F [0,0]
#SP [SP_EAL_DEJ,30]            #DI [DI_BOD,C,I,3]           #WI #1 "NO *G [0,0]
#SP [SP_NCX,I,1]              #DI [DI_2DDIS,I,0]           #WI #1 "NO *H [0,0]
#SP [SP_NCY,I,1]              #DI [DI_2DTRNO,I,1]          #WI #1 "NO *I [0,0]
#SP [SP_PAGE,L,1]              #DI [DI_3DOFFX,I,4]          #WI #1 "NO *J [0,0]
#SP [SP_COL,T,F,100.01]        #DI [DI_3DOFFY,I,4]          #WI #1 "NO *K [0,0]
#SP [SP REP,T,F,100.01]        #DI [DI_3DINCX,I,0]          #WI #1 "NO *L [0,0]
#SP [SP_DIS,T,F,0.9999995]    #DI [DI_3DCOLL,I,5]          #WI #1 "NO *M [0,0]
#SP [SP_REPEAT,B,0]            #DI [DI_3DMODE,I,0]          #WI #1 "NO *N [0,0]
#DI [DI_MP_TRIGGER,I,0]        #MP1 [MP_CFD_LL,F,0]         #WI #2 "NO *1 [12,255]
#DI [DI_MP_TRIGGER,I,0]        #MP1 [MP_CFD_ZC,F,7.8431373] #WI #2 "NO *2 [26,383]
#DI [DI_MP_TRIGGER,I,0]        #MP1 [MP_CFD_HF,F,4]         #WI #2 "NO *3 [34,511]
#DI [DI_MP_TRIGGER,I,0]        #MP1 [MP_SYN_FD,I,1]          #WI #2 "NO *4 [512,639]
#DI [DI_MP_TRIGGER,I,0]        #MP1 [MP_SYN_PQ,F,19.807843] #WI #2 "NO *5 [640,767]
#DI [DI_MP_TRIGGER,I,0]        #MP1 [MP_SYN_HF,F,4]          #WI #2 "NO *6 [768,895]
#DI [DI_MP_TRIGGER,I,0]        #MP1 [MP_TAC_LL,F,7.8431373] #WI #2 "NO *7 [896,1023]
#DI [DI_MP_TRIGGER,I,0]        #MP1 [MP_TAC_LH,F,9.8039217] #WI #2 "NO *8 [1024,1151]
#DI [DI_MP_TRIGGER,I,0]        #MP1 [MP_WIND,W,1]           WIND PARA END:
```

Fig. 348: Setup parameters

Measurement Description Blocks

The SPCM software allows you to run several measurements in different memory pages and to store the results in a single data file. These measurements may be done with different system parameters. Therefore, each data block can (but need not) have its own set of system parameters. These parameters may differ from the general setup parameters.

The system parameters of the individual measurements are stored in the measurement description blocks. The number of measurement description blocks can vary from one (if all stored data blocks have the same system parameters) to the overall number of saved data blocks (if all blocks were measured with different hardware parameters).

In the block header of each data block a corresponding measurement description block is specified. The number of measurement description blocks, and the length and the location of the measurement description blocks are stored in the file header at the beginning of the .sdt file.

The information in the measurement description blocks is used for the ‘Block Info’ or ‘Set Info’ function of the Load, Save and Trace Parameter panels. If the button ‘Use System Parameters from the Selected Block’ is pressed, the system parameters are replaced with the data in the measurement description block.

The measurement description blocks are stored in a binary format. The structure is shown in Fig. 349. Fig. 349 should be considered an example; more parameters may be added for new software versions or new TCSPC modules. For details of the current structure definitions, please see SPC_data_file_structure.h file of the DLL library.

```

cchar time[9];      /* time of creation */
char date[11];      /* date of creation */
char mod_ser_no[16]; /* serial number */
short meas_mode;
float cfd_ll;
float cfd_lh;
float cfd_zc;
float cfd_hf;
float syn_zc;
short syn_fd;
float syn_hf;
float tac_r;
short tac_g;
float tac_of;
float tac_ll;
float tac_lh;
short adc_re;
short eal_de;
short ncx;
short ncy;

unsigned short page;
float col_t;
float rep_t;
short stopt;
char overfl;
short use_motor;
short steps;
float offset;
short dither;
short incr;
short mem_bank;
char mod_type[16]; /* module type */
float syn_th;
short dead_time_comp;
short polarity_l;
short polarity_f;
short polarity_p;
short linediv;
short accumulate;
int flbck_y;

int flbck_x;
int bord_u;
int bord_l;
float pix_time;
short pix_clk;
short trigger;
int scan_x;
int scan_y;
int scan_rx;
int scan_ry;
short fifo_typ;
int epx_div;
int mod_type_code;
float overflow_corr_factor;
int adc_zoom;
int cycles; //cycles (accumulation cycles in
            //FLOW mode)
MeasStopInfo StopInfo;

```

Fig. 349: Measurement description block

Data Blocks

Each data block starts with a data block header which describes the length of the data block, the type of the data, and the measurement description block related to the data block.

With the software version 7.0 the data block header was changed to make a higher number of data blocks and a variable block size possible. Each data block can now contain a ‘Data Set’ i.e. the data of several curves which were obtained in one measurement. The structure of the block header is shown in Fig. 350.

short	block_no	number of the block in the file, valid only when in 0 .. 0x7ffe range, if equal to 0x7fff block_no (old software version - reserved1) field contains valid number of the block in the file
long	data_offs	offset of the data block from the beginning of the file
long	next_block_offs	offset to the data block header of the next data block
unsigned short	block_type	0: unused 1: measured block 2: flow data 3: data block from file 4: calculated data block 5: simulated data block, 11(hex): measured data set 13(hex): data set from file 14(hex): calculated data set 15(hex): simulated data set,
short	meas_desc_block_no	Number of the measurement description block corresponding to this data block
unsigned long	lblock_no	reserved1 now contains number of the block in the file*
unsigned long	block_length	reserved2 now contains block(set) length in bytes

* The field 'lblock_no' contains the data block / data set number in the bits 0 to 23 and the module number (0 to 3) in the bits 24 to 25.

Fig. 350: Structure of the data block header

The data of the set specified by the block header are stored as shown below. It follows directly after the data block header:

unsigned short	curvepoint[0][0]
unsigned short	curvepoint[0][1]
.	curvepoint[0] [adc_re -1]
unsigned short	curvepoint[1][0]
unsigned short	curvepoint[1][1]
.	curvepoint[1] [adc_re -1]
unsigned short	curvepoint[n][0]
unsigned short	curvepoint[n][1]
.	curvepoint[n] [adc_re -1]

The photon numbers in each curve point are unsigned short integers, i.e. values from 0 to 65,535. The number of curves in the data set depends on the measurement parameters, e.g. measurement mode, no of routing bits etc. The number of curves in the block is equal to 'block_length' (from the block header) divided by adc_resolution (from the corresponding measurement description block).

FIFO Files

Measurements in the FIFO mode generate one or several photon data file files containing the micro times, the macro times, and the detector channel numbers of the individual photons. Moreover, a FIFO measurement generates a setup file that contains the hardware and software setup parameters used.

The file structure is described in the paragraphs below. Please note that new features may be added in new software versions and new SPC modules. Therefore, please see also ‘spc_data_file_structure.h’. The installation procedure writes this definition file into the same directory as the SPCM application.

Setup Files

The setup files consist of

- the file header which contains structural data used to find the other parts of the file
- the file information which was typed in when the file was saved
- the system setup data for hardware and software

The structure of the setup file is the same as for the .set files of the photon distribution modes, see above.

FIFO Data Files (SPC-600/630, 4096 Channel Mode)

The information about the subsequent photons is stored one after another in the measurement data file. For each photon 6 bytes are used. The structure of these data is shown in the table below.

	Bit 7	Bit 6	Bit 5	Bit 4	Bit 3	Bit 2	Bit 1	Bit 0
Byte 0	ADC[7]	ADC[6]	ADC[5]	ADC[4]	ADC[3]	ADC[2]	ADC[1]	ADC[0]
Byte 1	0	GAP	MTOV	INVALID	ADC[11]	ADC[10]	ADC[9]	ADC[8]
Byte 2	MT[23]	MT[22]	MT[21]	MT[20]	MT[19]	MT[18]	MT[17]	MT[16]
Byte 3	R[7]	R[6]	R[5]	R[4]	R[3]	R[2]	R[1]	R[0]
Byte 4	MT[7]	MT[6]	MT[5]	MT[4]	MT[3]	MT[2]	MT[1]	MT[0]
Byte 5	MT[15]	MT[14]	MT[13]	MT[12]	MT[11]	MT[10]	MT[9]	MT[8]

ADC[11:0] ADC Data. The micro time is

$$MiroTime = \frac{(4095 - ADC) \cdot TACRange}{TACGain \cdot 4096}$$

R [7:0]	Routing Signals (inverted)
MT[23:0]	Macro Time [in 50ns intervals]
GAP	1 = Possible recording gap due to FIFO Full. There may be (and most likely is) a gap in the recording preceding this photon.
MTOV	1 = Macro Timer Overflow. Since the capacity of the macro timer is limited to 24 bit it will overflow every $2^{24} \cdot 50$ ns. The software which processes the data file has to add these $2^{24} \cdot 50$ ns to its internal macro time value on each MTOV =1.
INVALID	1 = Data Invalid. All data for this photon except the MTOV bit are invalid. The INVALID bit is used to mark photons for which no correct detector channel number, micro time, or macro time could be determined. This happens if several detectors in a multi-detector system detected photons within the response time of the routing electronics, the sum of the TAC output and the dither signal was outside the conversion range of the ADC, or in the (very unlikely) case that a photon appears within the generation of a macro time overflow entry.

The first 6 bytes in the .spc file are added by the software and contain information about the Macro Time clock and the number of routing channels used during the measurement:

byte 1 : bit 4 = 1 (Invalid photon), bits 3-0 = number of routing bits
 byte 2 and 3 = macro time clock in 0.1 ns units (for 50ns value 500 is set)

FIFO Data Files (SPC-600/630 256 Channel Mode)

Photon Data

The information about the subsequent photons is stored one after another in the measurement data file. For each photon 4 bytes are used. The structure of these data is shown in the table below.

	Bit 7	Bit 6	Bit 5	Bit 4	Bit 3	Bit 2	Bit 1	Bit 0
Byte 0	ADC[7]	ADC[6]	ADC[5]	ADC[4]	ADC[3]	ADC[2]	ADC[1]	ADC[0]
Byte 1	MT[7]	MT[6]	MT[5]	MT[4]	MT[3]	MT[2]	MT[1]	MT[0]
Byte 2	MT[15]	MT[14]	MT[13]	MT[12]	MT[11]	MT[10]	MT[9]	MT[8]
Byte 3	INVALID	MTOV	GAP	0	R[2]	R[1]	R[0]	MT[16]
ADC[7:0]	ADC Data. The micro time is							
	$MiroTime = \frac{(255 - ADC) \cdot TACRange}{TACGain \cdot 256}$							
R [2:0]	Routing Signals (inverted)							
MT[16:0]	Macro Time [in 50 ns intervals]							
GAP	1 = Possible recording gap due to FIFO Full. There may be (and most likely is) a gap in the recording preceding this photon.							
MTOV	1 = Macro Timer Overflow. A single macro timer overflow has occurred between this photon and the last recorded one. Since the capacity of the macro timer is limited to 17 bit it will overflow each $2^{17} \cdot 50$ ns. The software which processes the data file has to add these $2^{17} \cdot 50$ ns to its internal macro time value on each MTOV =1.							
INVALID	1 = Data Invalid. All data for this photon except for the MTOV bit are invalid. The INVALID bit is used to mark photons for which no correct detector channel number, micro time, or macro time could be determined. This happens if several detectors in a multi-detector system detected photons within the response time of the routing electronics, the sum of the TAC output and the dither signal was outside the conversion range of the ADC, or in the (very unlikely) case that a photon appears within the generation of a macro time overflow entry (see below).							

The first 4 bytes in the .spc file are added by the software and contain information about the Macro Time clock and the number of routing channels used during the measurement:

Bytes 0, 1, 2: macro time clock in 0.1 ns units ('500' for 50 ns macro time clock)
 Byte 3 : bits 0-2 reserved, bits 3 to 6 = number of routing bits, bit 7 = 1 ('Data invalid')

Macro Time Overflows

Due to the high macro time resolution and the limited number of macro time bits a macro time overflow occurs every 6.5536 ms. In most cases a photon will be recorded within this time. The occurrence of a single macro time overflow is then marked by the 'MTOV' bit of the next valid photon. However, for low count rates it may happen that several macro time overflows occur between subsequent photons. In this case an entry in the FIFO file is generated that contains the number of overflows since the last photon was recorded. This entry is marked by 'MTOV = 1' and 'INVALID = 1'. The structure of this entry is shown below.

	Bit 7	Bit 6	Bit 5	Bit 4	Bit 3	Bit 2	Bit 1	Bit 0
Byte 0	CNT[7]	CNT[6]	CNT[5]	CNT[4]	CNT[3]	CNT[2]	CNT[1]	CNT[0]
Byte 1	CNT[15]	CNT[14]	CNT[13]	CNT[12]	CNT[11]	CNT[10]	CNT[9]	CNT[8]
Byte 2	CNT[23]	CNT[22]	CNT[21]	CNT[20]	CNT[19]	CNT[18]	CNT[17]	CNT[16]
Byte 3	INVALID(1)	MTOV(1)	--	0	CNT[27]	CNT[26]	CNT[25]	CNT[24]

CNT[27:0] Number of macro time overflows which occurred without recording photons

FIFO Data Files (SPC-134, SPC-144, SPC-154, SPC-830)

Photon data

The information about the photons is stored one after another in the measurement data file. For each photon 2 words (4 bytes) are used. The structure of these data is shown in the table below.

	Bit 7	Bit 6	Bit 5	Bit 4	Bit 3	Bit 2	Bit 1	Bit 0
Byte 0	MT[7]	MT[6]	MT[5]	MT[4]	MT[3]	MT[2]	MT[1]	MT[0]
Byte 1	ROUT[3]*	ROUT[2]	ROUT[1]	ROUT[0]	MT[11]	MT[10]	MT[9]	MT[8]
Byte 2	ADC[7]	ADC[6]	ADC[5]	ADC[4]	ADC[3]	ADC[2]	ADC[1]	ADC[0]
Byte 3	INVALID	MTOV	GAP	MARK	ADC[11]	ADC[10]	ADC[9]	ADC[8]

ADC[11:0] ADC Data. The micro time is

$$MiroTime = \frac{(4095 - ADC) \cdot TACRange}{TACGain \cdot 4096}$$

ROUT[3:0]	Routing signals (inverted). Bit 3 is not available for early SPC-130/134 modules
MT[11:0]	Macro Time (50 ns intervals for internal Macro time oscillator. For Sync clock see below)]
MARK	SPC-150/154 and SPC-140/144 only. If MARK = 1 the event is an edge transition of a scan clock pulse, or some kind of other marker pulse connected to the scan clock lines. ROUT[0], ROUT[1] and ROUT[2] are ‘Pixel’, ‘Line’, and ‘Frame’, respectively. ROUT[3] = 0. ADC[0] ADC[11] are invalid.
GAP	1 = Possible recording gap due to ‘FIFO Full’. There may be (and most likely is) a gap in the recording preceding this photon.
MTOV	1 = Macro Timer Overflow. Since the capacity of the macro timer is limited to 12 bit it will overflow at each 2^{12} -th macro time period. For the internal macro time clock of 50 ns overflows occur every 204.8 μ s. For synchronisation of the macro-time clock with the SYNC signal this interval may even be shorter. Therefore there may even be multiple overflows without any photons detected (see below). The software which processes the data file has to add the times between overflows to its internal macro time value on each MTOV =1.
INVALID	1 = Data Invalid. The INVALID bit is used to mark photons for which no correct detector channel number, micro time, or macro time could be determined. This happens if several detectors in a multi-detector system detected photons within the response time of the routing electronics, the sum of the TAC output and the dither signal was outside the conversion range of the ADC, or in the (very unlikely) case that a photon appears within the generation of a macro time overflow entry (see below).

The first 4 bytes in the .spc file are added by the software and contain information about the Macro Time clock and the number of routing channels used during the measurement:

Bytes 0, 1, 2: macro time clock in 0.1 ns units ('500' for 50 ns macro time clock)
 Byte 3 : bits 0-2 reserved, bits 3 to 6 = number of routing bits, bit 7 = 1 ('Data invalid')

Macro Time Overflows

Since the capacity of the macro timer is limited to 12 bit it will overflow at each 2^{12} -th macro time period. In most cases the overflow is marked by the ‘MTOV’ bit of the next valid photon. However, the internal macro time clock of 50 ns overflows occur every 204.8 μ s. For synchronisation of the macro-time clock with the SYNC signal this interval may even be shorter. Therefore, it can happen that no valid photon is recorded between two subsequent macro time overflows. To enable the processing software to maintain a correct macro time for the rest of the measurement an entry in the measurement data file is written if several overflows occurred between two subsequent photons. This entry is marked by ‘MTOV = 1’ and ‘INVALID = 1’ and contains the number of macro time overflows which occurred since the last photon was recorded. The structure of this entry is shown below.

	Bit 7	Bit 6	Bit 5	Bit 4	Bit 3	Bit 2	Bit 1	Bit 0
Byte 0	CNT[7]	CNT[6]	CNT[5]	CNT[4]	CNT[3]	CNT[2]	CNT[1]	CNT[0]
Byte 1	CNT[15]	CNT[14]	CNT[13]	CNT[12]	CNT[11]	CNT[10]	CNT[9]	CNT[8]
Byte 2	CNT[23]	CNT[22]	CNT[21]	CNT[20]	CNT[19]	CNT[18]	CNT[17]	CNT[16]
Byte 3	INVALID(1)	MTOV(1)	-	0	CNT[27]	CNT[26]	CNT[25]	CNT[24]
CNT[27:0]	Number of macro time overflows which occurred without recording photons							

Trouble Shooting

Although we believe that our SPC modules work reliably tests can be recommended after an accident such as overvoltage, mechanical stress or another extreme situation. Furthermore, if a measurement setup does not work as expected a test of the SPC module can help to find out the reason. However, the best strategy before a test is required, is: *Avoid damage to the module!*

How to Avoid Damage

The best way to avoid any trouble is to avoid conditions that can cause damage to the SPC module. The most dangerous situations are described below.

Electrostatic Discharge

Electrostatic discharge can damage the module when it is inserted or removed from a computer or when it is touched for other reasons. It happens when your body is electrically charged and you touch a sensitive part of the SPC module. To avoid damage by electrostatic discharge we recommend to obey the rules given below:

When you take the SPC module out of the packaging box touch it at the front panel.

Before inserting an SPC module into a computer, touch the computer at a metallic (grounded) part to drain a possible charge off your body.

Before bringing the module into contact with the computer touch both the module at the front panel and a metallic part of the computer.

When taking a module from a computer, touch a metallic part of the computer before touching the SPC module.

There are extreme situations when sparks are crackling when touching anything. Handling any electronic equipment in such an environment should be avoided altogether. Or, if this is not possible, it is not ridiculous to take off shoes and socks when handling sensitive electronic devices.

Overvoltage at the signal inputs

The CFD, SYNC, and routing inputs of the SPC modules are protected against overvoltage. Therefore, DC overvoltage levels of a few V and pulse amplitudes of some 10 V normally do not pose any danger. However, damage cannot reliably be excluded for input pulses with amplitudes in the 100 V range, especially if these pulses have sub-ns risetime. Such pulses can be delivered by PMTs, especially by large linear-focused ones. It is therefore recommended to connect PMTs to the SPC modules only via preamplifiers or routers. Damaging these devices is less expensive than damaging the CFD input of an SPC module.

Dangerous overvoltage pulses can also originate from connecting charged cables to the input of the modules, see ‘Safety Recommendations for Using Detectors’, page 76. You should therefore obey the following safety rules:

- Don not connect a photomultiplier to the SPC module when the high voltage is switched on.
- Do not connect a photomultiplier to the SPC module if the high voltage was switched on before with the PMT output left open.
- Do not use any switches, or switchable attenuators between the PMT and the SPC module.
- Do not use cables and connectors with bad contacts.

- Obey the same rules for PIN photodiodes or APDs operated at supply voltages higher than 20V.

Furthermore, please pay attention to the usual safety rules when handling the high voltage of the PMT. Make sure that there is a reliable ground connection between the HV supply unit and the PMT. Broken cables, lose connectors and other bad contacts must be replaced immediately. Please see ‘Safety Recommendations for Using Detectors’, page 76.

Please be careful when working with low repetition rate lasers. Some of these lasers deliver pulse energies so high that a PIN or avalanche photodiode can be driven into a breakthrough state. It may then deliver an extremely high current for some tens of ns. Also PMTs can deliver pulses of more than 1 A peak current if they are hit by a single laser pulses of full power. Please use preamplifiers when you are working with such lasers.

Testing the Module by the SPC Test Program

If you suppose any problems with the bus interface, the timing and control circuits or the memory of an SPC module, run the ‘SPC Test’ program delivered with the SPCM Software. The main panel of this program is in Fig. 351.

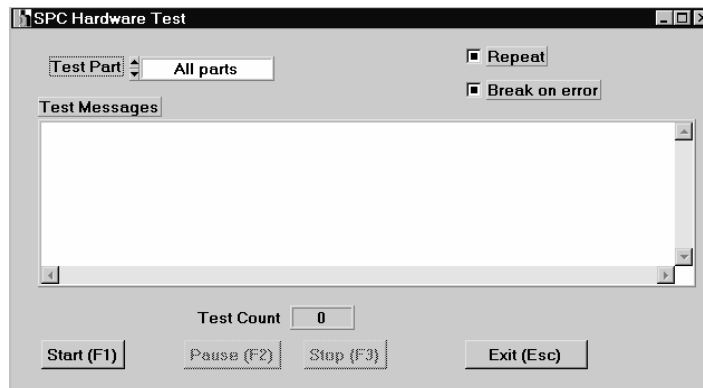


Fig. 351: Panel of the SPC test software

Switch on ‘All Parts’, ‘Repeat’ and ‘Break on Error’ and start the test. If the program performs several test loops (indicated by ‘Test Count’) without indicating an error you may be sure that the bus interface, the timing and control circuits and the memory of the module work correctly. Depending on the type of the SPC module and the speed of the computer, it can take some minutes to run one test loop.

If an error is displayed, check that the module is inserted correctly and that there is no address conflict (See ‘Frequently Encountered Problems’, page 341).

Test for General Function and for Differential Nonlinearity

This test requires two pulse generators with a pulse width of 1 to 4 ns and a repetition rate of 16 MHz and 1 MHz respectively. Do not use a diode laser controller as a test signal source unless you are absolutely sure that it does not radiate noise. The test setup is shown in Fig. 352.

It is important that the two pulse generators be really independent. Therefore, keep the generators and the cables well apart. Ideally (without any differential nonlinearity) the result is a horizontal line, with a signal to noise ratio given by the square root of the photon number per channel. Differential nonlinearity shows up as systematic ripple in the curve.

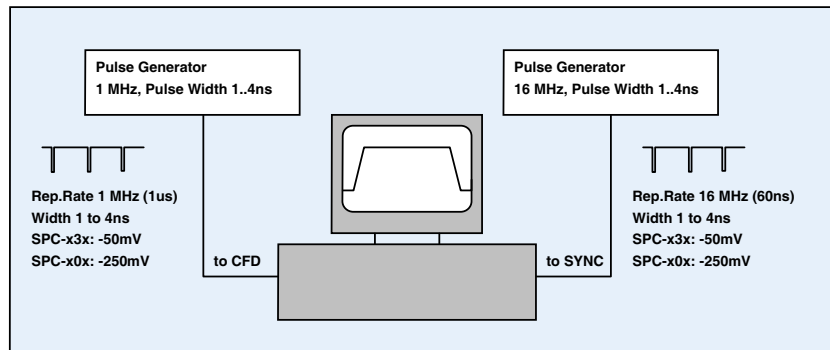


Fig. 352: Test for general function and test of DNL

Test for Time Resolution

The time resolution of the SPC modules is tested in the setup shown in Fig. 353.

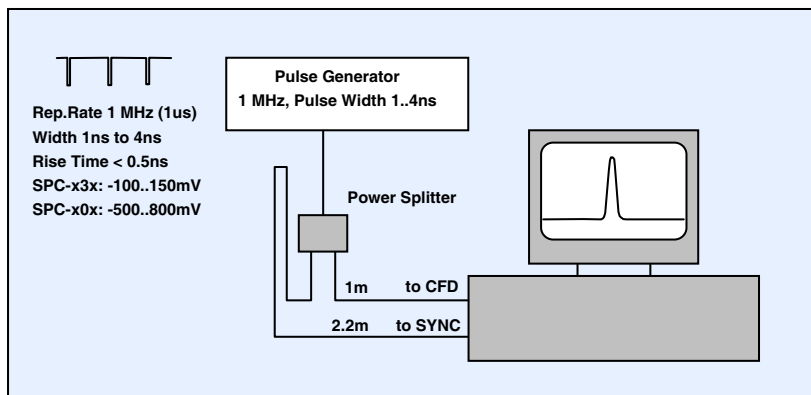


Fig. 353: Test of electronic time resolution

A pulse generator delivers pulses of about 1 MHz repetition rate. The width of the pulses should be in the range of 1 to 4 ns, the rise time shorter than 500 ps. The signal is split into a SYNC and a CFD signal by a passive power splitter. The pulses in the SYNC path are delayed by about 1.2 m of additional cable length. Thus, the SPC module receives start and stop pulses spaced by the delay in the SYNC path. A measurement in the ‘Single’ or ‘Oscilloscope’ mode displays a sharp peak. The peak represents the instrument response function of the SPC module. With a TAC range of 50 ns, a TAC gain of 15, and an ADC resolution of 4096 the width of the peak is shorter than 10 ps.

Frequently Encountered Problems

The module is not found by the SPC software

Check that the module is correctly inserted. When the computer is moved the module can work loose. Furthermore, the connectors have some longitudinal play which can cause problems in the PCI connectors. Make sure that the bus connector is clean. If necessary, clean with ethanol, isopropanol or acetone. Check also that the hardware driver is installed correctly. If other measurement hardware was installed after the SPC installation, please re-install the SPC driver. The SPC modules use commercial bus interface chips. These are used for a number of other devices too. If the drivers of these devices are not properly designed they may kill the SPC drivers.

No SYNC Rate or 'No Sync'

Check the SYNC signal. Is the polarity of the pulses correct? Is the baseline of the pulses correct? Check the signal with an oscilloscope (300 MHz or more). Don't forget to switch the oscilloscope to 50Ω , DC.

For SPC-x30 modules the polarity of the pulses must be negative. For SPC-x00 modules, make sure that the SYNC input is configured for the right polarity.

Check that the delay lines for shaping the zero cross are inserted (see Fig. 125, page 119).

Check the SYNC parameters. For -00 modules set 'SYNC ZC' to -10mV. For -30 modules, set 'SYNC Threshold' to -20mV and change 'SYNC ZC' between -100mV and +100mV.

SPC-134 and SPC-144: Is the Sync Rate Jumper inserted? (see Fig. 338, page 322)

SPC-134, -144 or other multi-SPC systems: 'No Sync' in some of the modules may indicate a power supply problem. Check the voltage at pin 1 of the sub-D connector. It should be 4.85V to 5V. If the voltage is lower the DC-DC converter for the -5V supply may shut down, and the module does not work. You can check the -5V at pin 6 of the sub-D connector. If the supply voltage is too low the reason is often the cable from the power supply to the motherboard has insufficient cross section. Make the cable shorter or use a computer with a stronger power supply. Newer SPC-134 and SPC-144 modules have an auxiliary power connector at the fan assembly board. Plug a free disk-drive power cable into this connector.

Wrong SYNC Rate

SYNC Rate too high: This problem is usually caused by reflections and ringing at the SYNC line. Check the shape of the Sync signal. Optimise the SYNC threshold. For -00 modules set 'SYNC ZC' to -10mV. For -30 modules, increase 'SYNC Threshold'. Also increasing 'SYNC Holdoff' may help.

SYNC Rate too low: Check the SYNC signal for amplitude fluctuations. Check the stability of the mode-locking of the laser. Check the SYNC parameters. For -00 modules set 'SYNC ZC' to -10mV. For -30 modules, set 'SYNC Threshold' to -20mV and change 'SYNC ZC' between -100mV and +100mV.

SPC-134: Check whether the Sync rate jumper setting corresponds to the Adjust Parameters (see Fig. 338, page 322).

No CFD Rate

Check the detector and the preamplifier. For -00 modules, make sure that the pulse polarity is correct and that the pulse amplitude is between 20 mV and 80 mV. For -00 modules, make sure that the pulses are negative. Check the CFD parameters.

Check that the delay lines for shaping the zero cross are inserted (see Fig. 125, page 119).

No TAC Rate or TAC rate much lower than CFD Rate

Check that the delay lines for shaping the zero cross are inserted (see Fig. 125, page 119).

Check the CFD parameters. Change 'CFD ZC'. For a wrong zero cross setting it can happen that the leading edge discriminator in the CFD responds, but the zero cross discriminator does not find a zero cross. In this case a CFD rate is displayed, but there are no CFD output pulses to trigger the TAC.

SPC-x00: CFD input amplitude too high or 'CFD Limit High' too low. The majority of the input pulses are above the upper CFD Threshold.

No ADC Rate

If the ADC rate is zero or extremely low the reason is almost certainly a SYNC problem.

For SPC-00 modules:

Set SYNC ZC to -10 mV. Check the SYNC signal. Is there a baseline offset? For offset signals it can happen that the baseline is above the 'SYNC OK' level, but there is no part of the signal that crosses the 'SYNC ZC' level. The module then indicates 'SYNC OK', but the internal SYNC Rate is zero. Check that the delay lines for shaping the zero cross are inserted (see Fig. 125, page 119).

For SPC-30 modules:

Check the SYNC signal. Is there a baseline offset? Check the SYNC parameters. Change 'SYNC ZC'. For a wrong zero cross setting it can happen that the leading edge discriminator in the SYNC responds, but the zero cross discriminator does not find a zero cross. In this case a SYNC rate is displayed, but there are no SYNC output pulses to stop the TAC.

For SYNC repetition rates lower than 20 MHz:

Make sure that the SYNC pulses arrive *after* the detector pulses and within a time interval not greater than the selected 'TAC Range'. Otherwise the TAC is not stopped, detects an 'Out-range' condition and resets itself without starting the ADC. What you see in this case are only some background events, not the signal photons.

Check the TAC Parameters Limit High, Limit Low and TAC Offset.

ADC Rate, but no TAC Rate

During FIFO measurement: Normal effect if no photons are detected. The ADC rate comes from the conversions which are forced by macro time overflows.

All rates present, but no curves on the screen

Check the Trace Parameters. Are you displaying the curve(s) which you are measuring? 'Page' must have the same setting as in the main window. Is the measured curve switched 'active'? Is the colour of the curve different from the background colour?

Check the Display Parameters. 'Reverse Y scale' should be off, 'Baseline' should be 0. 'Bkgcolor' must be different from the colour of the measured curve.

Check the System Parameters. For a simple test measurement, the operation mode should be 'Oscilloscope' or 'Single'. For the Oscilloscope mode 'Stop T' and a reasonable 'Collection Time' must be set. For the 'Single' mode, a display time of less than 1 second should be set. 'Routing Channels X' and 'Routing Channels Y' should be 1. 'Memory Offset' should be 0.

If you do not apply a measurement trigger to the module, the trigger condition must be 'none' ('More Parameters').

If you work with a measurement trigger, check that the trigger pulses are present and that they have appropriate levels. Low > 0.5V, High > 2.5V.

If a router is used: Make sure that the detector signal is connected to the router. Make sure that the timing cable from the router is connected to the SPC and the router is connected via the Sub-D cable. The detector signal must be connected via the router as long as the router is connected via the Sub-D cable. Connecting the detector directly to the SPC does not work as long as the router is connected via the Sub-D cable.

Curve on the screen does not change when measured

You display another curve than you are measuring. Check the trace parameters as described above.

Random data on the screen

You display a curve that has not been used before. Start a measurement in this curve to clear the memory.

Noise in the measured curves is bigger than expected, Chi Square too high

Check the ‘Count Increment’ parameter in the System Parameters. Set ‘Count Increment’ = 1 for precision measurements.

Scan Sync in Mode: Measurement does not start

Check the scan clock signals. One of the signals is missing, or the signals are mixed up. Check for correct TTL amplitudes.

Check whether your scanner delivers a pixel clock. If it does not, you have to define an internal pixel clock in the scan control parameters, see ‘Scan Sync In Mode’, page 273.

Check the scan control parameters see ‘Scan Sync In Mode’, page 273. Make sure that the ‘Left Boarder’ and ‘Upper Boarder’ is reached with your clock signals.

Scan Sync in Mode: Measurement does not finish

Check the scan clock signals. One of the signals is missing, or signals are mixed up. Check for correct amplitudes.

Scan Sync In mode: Measurement starts after collection time, then stops immediately

The scan clock signals are mixed up.

Poor Time Resolution

Check whether the SYNC and CFD inputs are configured correctly (see Fig. 125, page 119).

Check your setup for ground loops. Grounding different system components (computer, PMT, HV power supply, monochromator, etc.) at different ground systems can induce considerable noise currents in the ground lines. The resulting noise is transformed into the signal lines and can seriously impair the timing performance.

Disconnect network cables. Long network cables work as antennas and introduce noise into the system.

Check the SYNC signal with an oscilloscope for risetime and amplitude jitter.

Check the detector signal for background noise. With the HV of the PMT switched off, there should be no CFD count rate for a CFD limit low above 10..20 mV.

Is the pulse amplitude sufficient? For the SPC-x00 versions the amplitude of the majority of pulses should be above 40mV, for the SPC-0x30 versions above 100 mV to get optimum resolution. Check by changing the ‘CFD limit low’ parameter.

Be careful when checking the resolution with a scattering solution. Multiple scattering can broaden the pulses by several 100 ps. The solution should look clear under normal daylight, but show a distinct scattering effect in the laser beam. On the other hand, don’t use the Raman scattering of pure water. Although clearly detectable, this is too weak to exclude errors by the fluorescence of contamination. Surprisingly, scattering the laser at a piece of paper often gives good results. However, the best way to test the resolution is to send the laser beam through a set of filters directly to the detector.

Check for transit time effects in the optical system. A 1-cm cuvette can contribute with 80 ps to the transit time spread. Multi-mode fibres operated at full numerical aperture can cause a transit time spread of 100 ps per meter of fibre length.

High background count rate

Room light on the detector.

Light from NIR LEDs reaches the detector. LEDs are often used in optical devices to control scanners, filter carousels, shutters, etc. Insert an NIR blocking filter in front of the detector.

CFD threshold too low or noise at the detector signal. Please see ‘Adjusting the CFD Threshold’, page 120.

Temperature of detector too high. Check for possible heat sources in the experiment setup.

Operating voltage of PMT too high. Check whether the voltage is within the permitted range.

Detector damaged by overload.

High background count rate, only if signal is present

Signal-dependent background is caused by afterpulsing. CFD threshold too high. Check operating conditions of detector, see ‘Adjusting the CFD Threshold’, page 120.

Detector is operated in instability region. Reduce detector gain.

Bad Shape of System Response, Double Pulses

Check the optical system for scattered light and multiple reflections.

SPC-00: The amplitude of the majority of the detector pulses must be less than ‘CFD limit High’. Otherwise it can happen that you detect a reflection of the detector pulses rather than the pulses themselves.

Try with slightly different ‘CFD Zero Cross’.

Try with higher SYNC threshold to suppress possible reflections on the SYNC input line.

With active modelockers: Make sure that there is no pickup from the modelocker frequency. This can cause non-equidistant SYNC pulses.

CFD threshold too high. The pulses recorded are mainly afterpulses of the detector. Check operating conditions of detector, see ‘Adjusting the CFD Threshold’, page 120.

Ripple or bumps in the decay curves

Check the ‘Dither Range’ parameter in the System Parameters. It should be 1/8, 1/16, or 1/32. ‘0’ switches the error correction of the ADC off and is for test only. Please see ‘Dither Range’, page 296.

Make sure that there are no reflections in the optical path.

Peak at the right end of the recorded curve: Increase TAC offset, see ‘Adjusting the TAC Parameters’, page 126.

Check your SYNC signal. Is the amplitude correct? Is the risetime short enough to maintain clean triggering?

Keep the cables to the SYNC and the CFD input well separated.

Try with slightly different ‘CFD Zero Cross’ and ‘SYNC Zero Cross’. If the zero cross level is too close to the true signal baseline the zero cross triggers respond to spurious signals which can impair the timing accuracy.

Make sure that there is no electrical noise from your laser. Especially picosecond diode lasers sometimes are radio transmitters rather than light sources.

Recorded decay curves are shifted left or right

Change the Sync cable length and the TAC Offset. Please see ‘Adjusting the SYNC and CFD Cable Length’, page 124 and ‘Adjusting the TAC Parameters’, page 126.

Recorded decay curves shift with signal repetition rate

Change the Sync cable length. Please see ‘Adjusting the SYNC and CFD Cable Length’, page 124.

Signal is present at the detector, but only dark counts are recorded

This can happen at low signal repetition rate if a wrong time interval is recorded. Change the Sync cable length. Please see ‘Adjusting the SYNC and CFD Cable Length’, page 124.

Fan of the SPC board does not work

Older SPC-6 and SPC-7 Modules: If the fan doesn’t work you have most likely shorted the +12V at the sub-D connector and burned the connection on the SPC board. Although there is no immediate danger of overheating under normal temperature conditions, the module should be repaired as soon as possible. Remember that a photodiode or a detector supplied by the 12V from the sub-D connector may also not work correctly.

Assistance through bh

Software updates, new manual versions and application notes about new applications are available from the bh web site, www.becker-hickl.de. Furthermore, we are pleased to support you in all problems concerning the measurement of fast electrical or optical signals. This includes discussions of new applications, the installation of the SPC modules, their application to your measurement problem, the technical environment and physical problems related to short time measurement techniques. Simply call us or send us an email.

Should there be a problem with your SPC module, please contact us. To fix the problem we ask you to send us a data file (.sdt) of the questionable measurement or (if a measurement is not possible) a setup file (.set) with your system settings. Furthermore, please add the following information:

Description of the Problem

SPC Module Type and Serial Number

Software Version

Detector type, Operating voltage of the detector, PMT Cathode type

Preamplifier type, Gain, Bandwidth etc.

Laser System: Type, Repetition Rate, Wavelength, Power

SYNC Signal Generation: Photodiode, Amplitude, Rise Time

Optical System: Basic Setup, Sample, Monochromator

System Connections: Cable Lengths, Ground Connections. Add a drawing if necessary.

Environment: Possible Noise Sources

Your personal data: E-mail, Telephone Number, Postal Address

The fastest way is to send us an email with the data file(s) attached. We will check your system settings and – if necessary – reproduce your problem in our lab. We will send you an answer within one or two days.

Becker & Hickl GmbH

Nahmitzer Damm 30

12277 Berlin

Tel. +49 / 30 / 787 56 32

FAX +49 / 30 / 787 57 34

<http://www.becker-hickl.de>

email: info@becker-hickl.de

or becker@becker-hickl.de

Routing and Control Signals

All SPC modules have one or two 15 pin Sub-D connectors to connect routing and control signals of multi-detector experiments, trigger signals, or scan control signals. Moreover, the connectors provide power supply to external amplifiers, routers, PMT heads and photodiodes.

The routing and control signals are the key to the multi-dimensional TCSPC features implemented in the bh SPC modules, see ‘Multi-Dimensional TCSPC’, page 23. The functions can be used for complex experiments that require to synchronise a measurement with an externally varied parameter, such as sample position, wavelength, temperature or pressure, to record a sequence of measurements for different orientation of a polariser, or to multiplex different light sources or source intensities.

It should be noted here that experiment control functions can also be accomplished by using the SPC DLL or the SPC LabView drivers, i.e. by writing a special windows application. There is certainly no objection against designing special software for complex instruments dedicated to special applications. However, in many (if not in most) cases software control is only used because the multi-dimensional features of the modules are not understood. In other words, the SPC module is used as a software-controlled classic TCSPC device. Software control then not only causes unnecessary development effort but also results in slow and often inefficient data acquisition. Moreover, problems can arise from undefined processing times due to interrupts, hard disk actions, or other applications running on the same computer. Therefore, please check whether you can solve your control problem by using the multi-dimensional features of the SPC modules. Do not hesitate to contact bh for advice.

The paragraphs below describe the control signals of the individual SPC modules. Examples of using of the signals are given under ‘TCSPC Applications’ page 147.

Please be careful not to connect a device to the routing connectors which is not intended for this purpose. This could damage the connected device or the SPC board.

SPC-600/630

1	+5V (Load max. 100mA, Rout = 1Ω)
2	Routing Signal, /R 0
3	Routing Signal, /R 1
4	Routing Signal, /R 2
5	Ground
6	-5V (Load max. 100mA, Rout = 1Ω)
7	Routing Signal, /R 3
8	Routing Signal, /R 4
9	Routing Signal, /R 5
10	+12V (Load max. 60mA)
11	-12V (Load max. 60mA)
12	Routing Signal, /R 6
13	ADD or TRIGGER ¹ or /R7 ²
14	CNTE
15	Ground

1. If ‘Trigger Condition’ other than ‘none’
2. In the FIFO Mode only

/R0 .. /R13: Routing Inputs. Polarity is ‘active low’, i.e. /R0 ... /R13 = ‘high’ will address curve 0. The open input represents a ‘high’ value.

ADD: The ADD signal is used for the lock-in SPC method. At ADD = 1 the events are added, at ADD = 0 the events are subtracted in the memory. Open inputs represent a logical ‘1’ value. The ADD input is shared with the TRIGGER input. The ADD function is activated if the trigger condition is set to ‘none’ (please see

‘System Parameters’, ‘More Parameters’). Thus, the trigger cannot be used when the ADD/SUB function is used.

TRIGGER: If a trigger condition is set (see ‘System Parameters’, ‘More Parameters’) the measurement starts when a L/H or H/L transition at the TRIGGER Input is detected. The TRIGGER input is shared with the ADD input. The TRIGGER function is activated if a trigger condition is set to ‘rising edge’ or ‘falling edge’ (please see ‘System Parameters’, ‘More Parameters’). Therefore, the ADD/SUB function cannot be used when the trigger is used.

CNTE: CNTE=L suppresses the storing of the current photon in the SPC memory. In conjunction with a router, the signal is used to reject misrouted events. The open input represents a logical ‘1’ value.

All signals (except the trigger) are read with a selectable ‘Latch Delay’ after a valid photon pulse at the CFD input has been detected (see ‘System Parameters’, ‘Latch Delay’).

SPC-700/730 and SPC-830

Connector 1 (lower connector)

- 1 +5V (max. 100mA)
- 2 Routing Signal, /R 0
- 3 Routing Signal, /R 1
- 4 Routing Signal, /R 2
- 5 Ground
- 6 -5V (max. 100mA)
- 7 Routing Signal, /R 3
- 8 Routing Signal, /R 4
- 9 Routing Signal, /R 5
- 10 +12V (max. 60mA)
- 11 -12V (max. 60mA)
- 12 Routing Signal, /R 6
- 13 ADD
- 14 CNTE1 (CNTE=CNTE1&CNTE2)
- 15 Ground

Connector 2 (upper connector)

- 1 +5V (max. 100mA)
- 2 Routing Signal, /R 7 or ARMED²
- 3 Routing Signal, /R 8 or TRGD²
- 4 Routing Signal, /R 9 or MEASURE²
- 5 Ground
- 6 -5V (max. 100mA)
- 7 Routing Signal, /R 10 or ‘Do not Connect’²
- 8 Routing Signal, /R 11 or YSYNC¹ or FBY²
- 9 Routing Signal, /R 12 or XSYNC¹ or FBX²
- 10 +12V (max. 60mA)
- 11 -12V (max. 60mA)
- 12 Routing Signal, /R 13 or PxIClk^{1,2}
- 13 TRIGGER³
- 14 CNTE2 (CNTE=CNTE1&CNTE2)
- 15 Ground

1. ‘Scan Sync In’ Mode

2. ‘Scan Sync Out’ Mode

3. Used if ‘Trigger Condition’ other than ‘none’ only

The function of the control bits depend on the operation mode:

Single, Oscilloscope, F(t,x,y), F(t,T), F(t,ext), Fi(T), Fi(ext)

/R0 .. /R13: Routing Inputs. Polarity is ‘active low’, i.e. /R0 ... /R13 = 1 (or open) will address curve 0.

ADD: The ADD signal is used for the lock-in SPC method. At ADD = 1 the events are added, at ADD = 0 the events are subtracted in the memory. Open inputs represent a logical ‘1’ value.

TRIGGER: If a trigger condition is set (see ‘System Parameters’, ‘More Parameters’) the measurement starts when a L/H or H/L transition at the TRIGGER Input is detected.

CNTE1, 2: CNTE=L suppresses the storing of the current photon in the SPC memory. Both CNTE signals are AND connected, i.e. a photon is suppressed when one or both CNTEs are L. In conjunction with a router, the signal is used to reject misrouted events.

All signals (except the trigger) are read with a selectable ‘Latch Delay’ after a valid photon pulse at the CFD input has been detected (see ‘System Parameters’, ‘Latch Delay’).

Scan Sync In

The ‘Scan Sync In’ mode is used for image recording. The recording procedure is controlled by the scanning device via the ‘XSync’, ‘YSync’ and ‘Pixel Clock’ pulses. The control signals for the ‘Scan Sync In’ mode are listed below.

- /R0 .. /R10: Routing Inputs. Polarity is ‘active low’, i.e. /R0 ... /R6 = 1 (or open) will address curve 0. The count enable signals CNTE1 and CNTE2 must be both ‘1’ to enable the storing of the currently detected photon. In conjunction with a router, the signal is used to reject misrouted events.
- XSync (Input): X synchronisation pulse. XSync forces the start of the next line.
- YSync (Input): Y synchronisation Pulse. YSync forces the start of the next frame.
- PxlClk (Input): External Pixel Clock. If the source of the pixel clock is set to ‘external’ the signal starts the measurement of the next Pixel.
- CNTE1, CNTE2: CNTE=L suppresses the storing of the current photon in the SPC memory. Both CNTE signals are AND connected, i.e. a photon is suppressed when one or both CNTEs are L.
- ADD: The ADD signal is used for lock-in SPC measurements. At ADD=1 the events are added, at ADD=0 the events are subtracted in the memory. Open inputs represent a logical 1 (add) value.
- TRIGGER: If a trigger condition is set (see ‘System Parameters’, ‘More Parameters’) the measurement starts when a L/H or H/L transition at the TRIGGER input is detected. Once triggered, the measurement runs until it is stopped by the collection timer, by an overflow or by the user. After a stop command the measurement stops after the next Ysync pulse. If the ‘Repeat’ of ‘Accumulate’ functions are used, a trigger pulse is required to start each repetition or accumulation cycle.

Scan Sync Out

The ‘Scan Sync Out’ mode is used for image recording. The recording procedure is controlled by the SPC module via the ‘Flyback X’, ‘Flyback Y’ and ‘Pixel Clock’ pulses. The control signals for the ‘Scan Sync Out’ mode are listed below.

- /R0 .. /R6: Routing Inputs. Polarity is ‘active low’, i.e. /R0 ... /R6 = 1 (or open) will address curve 0. The count enable signals CNTE1 and CNTE2 must be both ‘1’ to enable the storing of the currently detected photon. In conjunction with a router, the signal is used to reject misrouted events.
- PxlClk (Output): ‘Pixel Clock’, indicates the start of the measurement of the next pixel. PIXEL is a 50 ns TTT H pulse. The duration of the measurement of each pixel is set by ‘Collection Time’, the number of points in X and Y direction by ‘Scan Pixels X’ and ‘Scan Pixels Y’ (see SPC system parameters).
- FBX (Output): ‘Flyback X’, controls the X flyback phase of the scanner. For polarity and duration please see ‘System Parameters’
- FBY (Output): ‘Flyback Y’, controls the Y flyback phase of the scanner. For polarity and duration please see ‘System Parameters’
- CNTE1, 2: CNTE=L suppresses the storing of the current photon in the SPC memory. Both CNTE signals are AND connected, i.e. a photon is suppressed when one or both CNTEs are L.

- ADD:** The ADD signal is used for lock-in SPC measurements. At ADD=1 the events are added, at ADD=0 the events are subtracted in the memory. Open inputs represent a logical 1 (add) value.
- TRIGGER:** If a trigger condition is set (see ‘System Parameters’, ‘More Parameters’) the measurement starts when a L/H or H/L transition at the TRIGGER input is detected. Once triggered, the measurement runs until it is stopped by the collection timer, by an overflow or by the user. After a command the measurement stops after the next Ysync pulse. If the ‘Repeat’ of ‘Accumulate’ functions are used, a trigger pulse is required to start each repetition or accumulation cycle.

The function of the PxIClk, FBX and FBY signals for a simple 8x4 matrix is shown in Fig. 354.

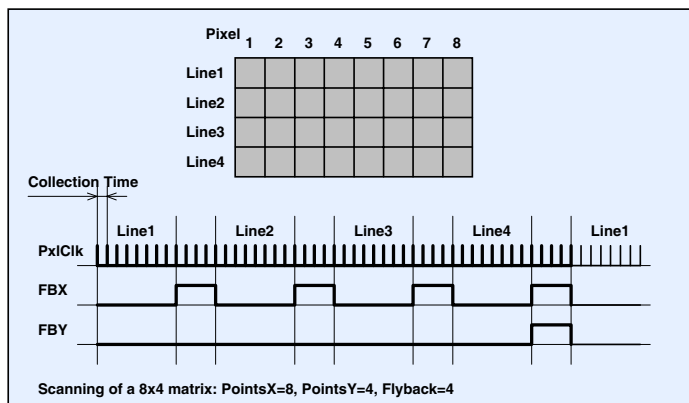


Fig. 354: Scan clock signals in the Scan Sync Out mode

Scan XY Out (SPC-700/730 only)

The ‘Scan XY Out’ mode is used for image recording. The recording procedure is controlled by the SPC module via the position signals /R0 through /R13. /R0 through /R13 are outputs and indicate the actual scan position.

/R0 .. /R13: Scan Position Outputs. Polarity is ‘active low’, i.e. /R0 ... /R13 = 1 sets the scanner position to X=Y=0 and addresses curve 0 in the SPC memory.

ADD: The ADD signal is used for the lock-in SPC method. At ADD = 1 the events are added, at ADD = 0 the events are subtracted in the memory. Open inputs represent a logical ‘1’ value. All signals are read with a selectable ‘Latch Delay’ after a valid photon pulse at the CFD input has been detected (see ‘System Parameters’, ‘Latch Delay’).

TRIGGER: If a trigger condition is set (see ‘System Parameters’, ‘More Parameters’) the measurement starts when a L/H or H/L transition at the TRIGGER Input is detected. It stops when the scan of the frame is complete. If the ‘Repeat’ or ‘Accumulate’ functions are used, a trigger pulse is required to start each repetition or accumulation cycle.

CNTE1, 2: CNTE=L suppresses the storing of the current photon in the SPC memory. Both CNTE signals are AND connected, i.e. a photon is suppressed when one or both CNTEs are L. In conjunction with a router, the signal is used to reject misrouted events.

SPC-134

1	+5V (Load max. 100mA, Rout = 1Ω)
2	Routing Signal, /R 0
3	Routing Signal, /R 1
4	Routing Signal, /R 2
5	Ground
6	-5V (Load max. 100mA, Rout = 1Ω)
7	Not used, do not connect
8	Not used, do not connect
9	Not used, do not connect
10	+12V (Load max. 60mA)
11	-12V (Load max. 60mA)
12	Not used, do not connect
13	ADD or TRIGGER
14	CNTE
15	Ground

/R0 .. /R2: Routing Inputs. Polarity is ‘active low’, i.e. /R0 ... /R13 = ‘high’ will address curve 0. The open input represents a ‘high’ value.

ADD: The ADD signal is used for the lock-in SPC method. At ADD = 1 the events are added, at ADD = 0 the events are subtracted in the memory. Open inputs represent a logical ‘1’ value. The ADD input is shared with the TRIGGER input. The ADD function is activated if the trigger condition is set to ‘none’ (please see ‘System Parameters’, ‘More Parameters’). Thus, the trigger cannot be used when the ADD/SUB function is used and vice versa.

TRIGGER: If a trigger condition is set (see ‘System Parameters’, ‘More Parameters’) the measurement starts when a L/H or H/L transition at the TRIGGER Input is detected. The TRIGGER input is shared with the ADD input. The TRIGGER function is activated if a trigger condition is set to ‘rising edge’ or ‘falling edge’ (please see ‘System Parameters’, ‘More Parameters’). Therefore, the ADD/SUB function cannot be used when the trigger is used.

CNTE: CNTE=L suppresses the storing of the current photon in the SPC memory. In conjunction with a router, the signal is used to reject misrouted events. The open input represents a logical ‘1’ value.

The /R0, /R1, /R2, ADD and CNTE signals are read approximately 10ns after a valid photon pulse at the CFD input has been detected. There is no ‘Latch Delay’ as in the other SPC modules. If the SPC-134 has to be used for multidetector operation 6 to 9 m 50 Ω cable has to be inserted from the timing output of the HRT-41, -81, and -82 router to the corresponding CFD input.

SPC-144

1	+5V (max. 100mA)
2	Routing Signal, /R 0
3	Routing Signal, /R 1
4	Routing Signal, /R 2
5	Ground
6	-5V (max. 100mA)
7	Routing Signal, /R 3
8	YSYNC ¹⁾ or FBY ²⁾ , or routing signal /R 4
9	XSYNC ¹⁾ or FBX ²⁾ , or routing signal /R 5
10	+12V (max. 60mA)
11	ADD
12	PxlClk ¹⁾ , or routing signal,/R 6
13	TRIGGER ³⁾ , or routing signal,/R 7
14	CNTE
15	Ground

- 1. 'Scan Sync In' Mode
- 2. 'Scan Sync Out' Mode
- 3. If 'Trigger Condition' other than 'none'

The function of the control bits depend on the operation mode:

Single, Oscilloscope, F(t,x,y), F(t,T), F(t,ext), Fi(T), Fi(ext)

/R0 .. /R7: Routing Inputs. Polarity is 'active low', i.e. /R0 ... /7 = 1 (or open) addresses curve 0.

ADD: The ADD signal is used for the lock-in SPC method. At ADD = 1 the events are added, at ADD = 0 the events are subtracted in the memory. Open inputs represent a logical '1' value.

TRIGGER: If a trigger condition is set (see 'System Parameters', 'More Parameters') the measurement starts when a L/H or H/L transition at the TRIGGER Input is detected.

CNTE: CNTE=L suppresses the storing of the current photon in the SPC memory. In conjunction with a router, the signal is used to reject multi-photon events.

All signals (except the trigger) are read with a selectable 'Latch Delay' after a valid photon pulse at the CFD input has been detected (see 'System Parameters', 'Latch Delay').

Scan Sync In

The 'Scan Sync In' mode is used for image recording. The recording procedure is controlled by the scanning device via the 'XSync', 'YSync' and 'Pixel Clock' pulses. The control signals for the 'Scan Sync In' mode are listed below.

/R0 .. /R3: Routing Inputs. Polarity is 'active low', i.e. /R0 ... /R3 = 1 (or open) addresses curve 0. The count enable signal CNTE must be '1' to enable the storing of the currently detected photon. In conjunction with a router, the signal is used to reject multi-photon events.

XSync (Input): X synchronisation pulse. XSync forces the start of the next line.

YSync (Input): Y synchronisation Pulse. YSync forces the start of the next frame.

PxlClk (Input): External Pixel Clock. If the source of the pixel clock is set to 'external' the signal starts the measurement of the next Pixel.

CNTE: CNTE=L suppresses the storing of the current photon in the SPC memory.

ADD: The ADD signal is used for lock-in SPC measurements. At ADD=1 the events are added, at ADD=0 the events are subtracted in the memory. Open inputs represent a logical 1 (add) value.

TRIGGER: If a trigger condition is set (see ‘System Parameters’, ‘More Parameters’) the measurement starts when a L/H or H/L transition at the TRIGGER input is detected. Once triggered, the measurement runs until it is stopped by the collection timer, by an overflow or by the user. After a stop command in the Scan Sync In mode, the measurement stops after the next Ysync pulse. If the ‘Repeat’ of ‘Accumulate’ functions are used, a trigger pulse is required to start each repetition or accumulation cycle.

Scan Sync Out

The ‘Scan Sync Out’ mode is used for image recording. The recording procedure is controlled by the SPC module via the ‘Flyback X’, ‘Flyback X’ and ‘Pixel Clock’ pulses. The control signals for the ‘Scan Sync Out’ mode are listed below.

/R0 .. /R3: Routing Inputs. Polarity is ‘active low’, i.e. /R0 ... /R6 = 1 (or open) will address curve 0. The count enable signal CNTE must be ‘1’ to enable the storing of the currently detected photon. In conjunction with a router, the signal is used to reject multi-photon events.

PxlClk (Output): ‘Pixel Clock’, indicates the start of the measurement of the next pixel. PIXEL is a 50 ns TTT H pulse. The duration of the measurement of each pixel is set by ‘Collection Time’, the number of points in X and Y direction by ‘Scan Pixels X’ and ‘Scan Pixels Y’ (see SPC system parameters).

FBX (Output): ‘Flyback X’, controls the X flyback phase of the scanner. For polarity and duration please see ‘System Parameters’

FBY (Output): ‘Flyback Y’, controls the Y flyback phase of the scanner. For polarity and duration please see ‘System Parameters’

CNTE: CNTE=L suppresses the storing of the current photon in the SPC memory.

ADD: The ADD signal is used for lock-in SPC measurements. At ADD=1 the events are added, at ADD=0 the events are subtracted in the memory. Open inputs represent a logical 1 (add) value.

TRIGGER: If a trigger condition is set (see ‘System Parameters’, ‘More Parameters’) the measurement starts when a L/H or H/L transition at the TRIGGER input is detected. Once triggered, the measurement runs until it is stopped by the collection timer, by an overflow, or by the user. After a stop command in the Scan Sync Out mode, the measurement stops after the next Ysync pulse. If the ‘Repeat’ of ‘Accumulate’ functions are used, a trigger pulse is required to start each repetition or accumulation cycle.

Specifications

SPC-600/630

Photon Channel

Principle
Time Resolution (FWHM / RMS, electr.)
Recommended Input Voltage Range
Lower Threshold
Upper Threshold
Zero Cross Adjust

SPC-600	SPC-630
Constant Fraction Discriminator	
13 ps / 7 ps	8 ps / 5 ps
$\pm 10 \text{ mV}$ to $\pm 80 \text{ mV}$	-50 mV to -1 V
5 mV to 80 mV	-20 mV to -500 mV
5 mV to 80 mV	-
-10 mV to +10 mV	-100 mV to +100 mV

Synchronisation Channel

Principle
Recommended Input Voltage Range
Threshold
Frequency Range
Frequency Divider
Zero Cross Adjust

SPC-600	SPC-630
Constant Fraction Discriminator	
$\pm 10 \text{ mV}$ to $\pm 50 \text{ mV}$	-50 mV to -1 V
-	-20 mV to -500 mV
0 to 200 MHz	
1-2-4-8-16	
-10 mV to +10 mV	-100 mV to +100 mV

Time-to-Amplitude Converter / ADC

Principle
TAC Range
Biased Amplifier Gain
Biased Amplifier Offset
Time Range incl. Biased Amplifier
min. Time / Channel
TAC Window Discriminator
ADC Principle
Diff. Nonlinearity

all SPC-6 modules
Ramp Generator / Biased Amplifier
50 ns to 2 us
1 to 15
0 to 100% of TAC Range
3.3 ns to 2 us
813 fs
Any Window inside TAC Range
50 ns Flash ADC with Error Correction
< 2% rms

Data Acquisition (Histogram Mode)

Method
Dead Time
Saturated Count Rate / Useful Count Rate
Number of Time Channels / Curve
max. Number of Curves in Memory
max. Number of Detector Channels
max. Counts / Channel
Counts / Channel ('Single' mode, repeat and acquire)
Overflow Control
Collection Time
Display Interval Time
Repeat Time
Curve Control (Internal Sequencing)
Curve Control (Multidetector Operation)
Add/Sub (Lock-in) Control
Count Enable Control
Control Signal Latch Delay

all SPC-6 modules			
on-board histogramming process over t and detector channel number			
125ns, independent of computer speed	8 MHz / 4 MHz		
64	256	1024	4096
4096	1024	256	64
128	128	128	32
	$2^{16}-1$		
	$2^{32}-1$		
none / stop / repeat and correct			
0.1 ms to 10000 s			
10ms to 1000 s			
0.1 ms to 1000 s			
up to 4096 curves			
up to 128 detector channels			
1 bit TTL			
1 bit TTL			
0 to 255 ns			

Data Acquisition (FIFO / BIFL Mode)

Method
ADC Resolution
Dead Time
Output Data Format (ADC / Macrotime / Routing)
FIFO buffer Capacity (photons)
Macro Timer Resolution
Curve Control (external Routing)
Count Enable Control
Routing Signal Latch Delay

all SPC-6 modules		
Time-tagging of individual photons and continuous writing to disk		
12 bit	8 bit	
150 ns	125 ns	
12 / 24 / 8	8 / 17 / 3	
128 k	256 k	
50 us, 24 bit	50ns, 17 bit	
8 bit TTL	3 bit TTL	
	1 bit TTL	
	0 to 255 ns	

Multi Module Systems

Number of modules operable parallel

4

Operation Environment

Computer System
Bus Connector
Power Consumption
Dimensions

PC Pentium or 486

PCI

approx. 20 W at +5V, 0.7 W at +12V

312 mm x 122 mm x 28 mm

SPC-700/730**Photon Channel**

Principle	Constant Fraction Discriminator
Time Resolution (FWHM / RMS, electr.)	13 ps / 7 ps
Recommended Input Voltage Range	$\pm 10 \text{ mV}$ to $\pm 80 \text{ mV}$
Lower Threshold	5 mV to 80 mV
Upper Threshold	5 mV to 80 mV
Zero Cross Adjust	-10 mV to + 10 mV

SPC-700

$\pm 10 \text{ mV}$ to $\pm 80 \text{ mV}$	7 ps / 4 ps
5 mV to 80 mV	- 50 mV to - 1 V
5 mV to 80 mV	- 20 mV to - 500 mV
-10 mV to + 10 mV	- 100 mV to + 100 mV

SPC-730

$\pm 10 \text{ mV}$ to $\pm 50 \text{ mV}$	7 ps / 4 ps
-	- 50 mV to - 1 V
-	- 20 mV to - 500 mV
0 to 200 MHz	0 to 200 MHz
1-2-4-8-16	1-2-4-8-16
-10 mV to + 10 mV	-100 mV to + 100 mV

Synchronisation Channel

Principle	Constant Fraction Discriminator
Recommended Input Voltage Range	$\pm 10 \text{ mV}$ to $\pm 50 \text{ mV}$
Threshold	-
Frequency Range	0 to 200 MHz
Frequency Divider	1-2-4-8-16
Zero Cross Adjust	-100 mV to + 100 mV

SPC-700

$\pm 10 \text{ mV}$ to $\pm 50 \text{ mV}$	7 ps / 4 ps
-	- 50 mV to - 1 V
-	- 20 mV to - 500 mV
0 to 200 MHz	0 to 200 MHz
1-2-4-8-16	1-2-4-8-16
-10 mV to + 10 mV	-100 mV to + 100 mV

SPC-730

Time-to-Amplitude Converter / ADC
Principle
TAC Range
Biased Amplifier Gain
Biased Amplifier Offset
Time Range incl. Biased Amplifier
min. Time / Channel
TAC Window Discriminator
ADC Principle
Diff. Nonlinearity

all SPC-7 modules

Ramp Generator / Biased Amplifier
50 ns to 2 us
1 to 15
0 to 100% of TAC Range
3.3 ns to 2 us
813 fs
Any Window inside TAC Range
50 ns Flash ADC with Error Correction
< 2% rms for 90% of TAC Range

Data Acquisition

Method	on-board 4-dimensional histogramming process over t, x, y, and detector channel number
Dead Time	180ns, independent of computer speed
Saturated Count Rate / Useful Count Rate	5.5 MHz / 2.25 MHz
Dead Time (stop to next photon)	180ns
Number of Time Channels / Curve	64
max. Number of Curves in Memory, ext. Routing	16384
max. Number of Curves in Memory, int. Routing	65536
max. Scanning Area, int. Routing	256 x 256
max. Number of Detector Channels	16384
Counts / Channel	2 ¹⁶ , 1
Counts / Channel ('Single' mode, repeat and acquire)	2 ³² , 1
Overflow Control	none / stop / repeat and acquire
Collection Time	0.1 ms to 1000 s
Display Interval Time	10ms to 1000 s
Repeat Time	0.1 ms to 1000 s
Curve Control (Multidetector Operation)	up to 16384 Curves / Detector Channels
Curve Control (Scan Sync In)	up to 65636 Curves, SYNC Pulses from Scanner to SPC
Curve Control (Scan Sync Out)	up to 65636 Curves, SYNC Pulses from SPC to Scanner
Curve Control (Scan XY Out)	up to 16384 Curves, 14 bit TTL XY from SPC to Scanner
Count Enable Control	1 bit TTL
Control Signal Latch Delay	0 to 255 ns

4

Multi Module Systems

Number of modules operable parallel

Operation Environment

Computer System	PC Pentium or 486
Bus Connector	PCI
Power Consumption	approx. 20 W at +5V, 0.7 W at +12V
Dimensions	312 mm x 122 mm x 28 mm

SPC-830

Photon Channel

Principle	Constant Fraction Discriminator
Time Resolution (FWHM / RMS, electr.)	7 ps / 4 ps
Opt. Input Voltage Range	- 50 mV to - 1 V
Min. Input Pulse Width	400 ps
Lower Threshold	- 20 mV to - 500 mV
Zero Cross Adjust	- 100 mV to + 100 mV

Synchronisation Channel

Principle	Constant Fraction Discriminator
Opt. Input Voltage Range	- 50 mV to - 1 V
Min. Input Pulse Width	400 ps
Threshold	- 20 mV to - 500 mV
Frequency Range	0 to 200 MHz
Frequency Divider	1-2-4-8-16
Zero Cross Adjust	-100 mV to + 100 mV

Time-to-Amplitude Converter / ADC

Principle	Ramp Generator / Biased Amplifier
TAC Range	50 ns to 2 us
Biased Amplifier Gain	1 to 15
Biased Amplifier Offset	0 to 100% of TAC Range
Time Range incl. Biased Amplifier	3.3 ns to 2 us
min. Time / Channel	813 fs
TAC Window Discriminator	Any Window inside TAC Range
ADC Principle	50 ns 12 bit Flash ADC with Error Correction
Diff. Nonlinearity (dither width 1/8, 90% of TAC range)	< 0.5% rms, typically <1% peak-peak

Data Acquisition, Histogram Modes

Method	on-board 4-dimensional histogramming process over t, x, y, and detector channel number
Dead Time	125ns, independent of computer speed
Saturated Count Rate / Useful Count Rate	8 MHz / 4 MHz
Number of Time Channels / Pixel	1 4 16 64 256 1024 4096
Image Size (pixels), 1 Detector Channel	4096 x 4096 2048 x 2048 1024 x 1024 512 x 512 256 x 256 128 x 128 64 x 64
Image Size (pixels), 4 Detector Channels	2048 x 2048 1024 x 1024 512 x 512 256 x 256 128 x 128 64 x 64 32 x 32
Image Size (pixels), 16 Detector Channels	1024 x 1024 512 x 512 256 x 256 128 x 128 64 x 64 32 x 32 16 x 16
Counts / Time Channel	2^{16-1}
Counts / Time Channel ('Single' mode, repeat and acquire)	2^{32-1}
Overflow Control	none / stop / repeat and acquire
Collection Time (per curve or per pixel)	100 ns to 1000 s
Display Interval Time	10ms to 1000 s
Repeat Time	0.1 ms to 1000 s
Curve Control (Internal Routing / Scan Sync In Mode)	up to 262,144 decay curves
Routing Control / Detector Channels	14 bit TTL / 16384
Count Enable Control	1 bit TTL
Control Signal Latch Delay	0 to 255 ns
Experiment Trigger	TTL

Data Acquisition, FIFO Mode

Method	Time-tagging of individual photons and continuous writing to disk
Macro Timer Resolution, internal clock	50ns, 12 bit
Macro Timer Resolution, clock from SYNC input	10ns to 100ns, 12 bit
ADC Resolution / No. of Time Channels	12 bit / 4096
Dead Time	125 ns
Output Data Format (ADC / Macrotime / Routing)	12 / 12 / 4
FIFO buffer Capacity (photons)	8 million photons

Multi Module Systems

Number of modules operable parallel	4
-------------------------------------	---

Operation Environment

Computer System	PC Pentium
Bus Connector	PCI
Power Consumption	approx. 20 W at +5V, 0.7 W at +12V
Dimensions	312 mm x 122 mm x 28 mm

SPC-130/134

Photon Channels

Principle	Constant Fraction Discriminator (CFD)
Time Resolution (FWHM / RMS, electr.)	8 ps / 5 ps
Recommended Input Voltage Range	- 50 mV to - 1 V
Lower Threshold	- 20 mV to - 500 mV
Upper Threshold	-
Zero Cross Adjust	- 100 mV to + 100 mV

Synchronisation Channels

Principle	Constant Fraction Discriminator (CFD)
Recommended Input Voltage Range	- 50 mV to - 1 V
Threshold	- 20 mV to -500 mV
Frequency Range	0 to 200 MHz
Frequency Divider	1-2-4
Zero Cross Adjust	-100 mV to + 100 mV

Time-to-Amplitude Converters / ADCs

Principle	Ramp Generator / Biased Amplifier
TAC Range	50 ns to 2 us
Biased Amplifier Gain	1 to 15
Biased Amplifier Offset	0 to 100% of TAC Range
Time Range incl. Biased Amplifier	3.3 ns to 2 us
min. Time / Channel	813 fs
ADC Principle	50 ns Flash ADC with Error Correction
Diff. Nonlinearity	< 2% rms

Data Acquisition

Method	on-board histogramming process over t and detector channel number
Dead Time	100 ns, independent of computer speed
Saturated Count Rate / Useful Count Rate (SPC-130)	10 MHz / 5 MHz
Saturated Count Rate / Useful Count Rate (SPC-134, total)	40 MHz / 20 MHz
Number of Time Channels / Curve	64
max. Number of Curves in Memory (per TCSPC Channel)	2048
max. Number of Detector Channels (per TCSPC Channel)	8
max. Counts / Channel	2 ¹⁶ -1
max. Counts / Channel ('Single' mode, repeat and acquire)	2 ³² -1
Overflow Control	none / stop / repeat and acquire
Collection Time	0.1 ms to 10000 s
Display Interval Time	10ms to 1000 s
Repeat Time	0.1 ms to 1000 s
Curve Control (internal sequencing, per TCSPC Channel)	up to 2048 curves
Curve Control (external routing)	3 bit TTL/CMOS
Count Enable Control	1 bit TTL/CMOS
Measurement Trigger	TTL/CMOS

Data Acquisition (FIFO Mode)

Method	Time-tagging of individual photons and continuous writing to disk
ADC Resolution	12 bit
Dead Time	150 ns
Output Data Format (ADC / Macrotime / Routing)	12 / 12 / 3
FIFO buffer Capacity (photons, per TCSPC Channel)	128 k
Macro Timer Resolution, internal clock	50ns, 12 bit
Macro Timer Resolution, clock from SYNC input	10ns to 100ns, 12 bit
Curve Control (external Routing)	4 bit TTL
Count Enable Control	1 bit TTL
Routing Signal Latch Delay	0 to 255 ns

Parallel Operation of TCSPC Channels

Number of parallel TCSPC channels (SPC-134)	4
CFD Inputs	independent
SYNC Inputs	independent
Routing and Control Inputs	independent

Operation Environment

Computer System	PC Pentium
Bus Connectors	PCI
Occupied PCI Slots (SPC-134 / SPC-130)	4 / 1
Power Consumption per Module	approx. 18 W at +5V, 2 W at +12V
Dimensions	225 mm x 125 mm x 85 mm

SPC-140/144

Photon Channels

Principle	Constant Fraction Discriminator (CFD)
Time Resolution (FWHM / RMS, electr.)	8 ps / 5 ps
Opt. Input Voltage Range	- 50 mV to - 1 V
Min. Input Pulse Width	400 ps
Lower Threshold	- 20 mV to - 500 mV
Upper Threshold	-
Zero Cross Adjust	- 100 mV to + 100 mV

Synchronisation Channels

Principle	Constant Fraction Discriminator (CFD)
Opt. Input Voltage Range	- 50 mV to - 1 V
Min. Input Pulse Width	400 ps
Threshold	- 20 mV to -500 mV
Frequency Range	0 to 200 MHz
Frequency Divider	1-2-4
Zero Cross Adjust	-100 mV to + 100 mV

Time-to-Amplitude Converters / ADCs

Principle	Ramp Generator / Biased Amplifier
TAC Range	50 ns to 2 us
Biased Amplifier Gain	1 to 15
Biased Amplifier Offset	0 to 100% of TAC Range
Time Range incl. Biased Amplifier	3.3 ns to 2 us
min. Time / Channel	813 fs
ADC Principle	50 ns Flash ADC with Error Correction
Diff. Nonlinearity	< 0.5% rms, typ. <1% peak-peak

Data Acquisition (Histogram Mode)

Method	on-board multi-dimensional histogramming process
Dead Time	100ns, independent of computer speed
Saturated Count Rate, per TCSPC channel / total	10 MHz / 40 MHz
Useful count rate, per TCSPC channel / total	5 MHz / 20 MHz
Channels / Curve per TCSPC channel	4096 1024 256 64 16 4 1
max. Scanning Area per TCSPC channel	16x16 64x64 128 x 128 256x256 512x512 1024x1024 2048x2048
max. Counts / Time Channel	$2^{16}-1$
Overflow Control	none / stop / repeat and correct
Collection Time	0.1 us to 10000 s
Display Interval Time	10ms to 1000 s
Repeat Time	0.1 us to 1000 s
Sequential recording	Programmable Hardware Sequencer
Synchronisation with scanning	pixel, line and frame clocks from scanning microscope
Count Enable Control	1 bit TTL
Experiment Trigger	TTL

Data Acquisition (FIFO / Time-Tag Mode)

Method	Time-tagging of individual photons and continuous writing to disk
Dead Time	100 ns
Output Data Format (ADC / Macrotime / Routing)	12 / 12 / 3
FIFO buffer Capacity (photons)	2 M
Macro Timer Resolution, internal clock	50ns, 12 bit
Macro Timer Resolution, clock from SYNC input	10ns to 100ns, 12 bit
Curve Control (external Routing)	3 bit TTL
Count Enable Control	1 bit TTL

Operation Environment

Computer System	PC Pentium
Bus Connectors	PCI
Used PCI Slots	4
Power Consumption per TCSPC channel	approx. 60 W from +5V, 2.1 W from +12V
Power Consumption, total, all 4 TCSPC channels	approx. 15 W from +5V, 0.7 W from +12V
Dimensions	225 mm x 125 mm x 85 mm

SPC-150/154

Photon Channels

Principle	Constant Fraction Discriminator (CFD)
Time Resolution (FWHM / RMS, electr.)	8 ps / 5 ps
Opt. Input Voltage Range	- 50 mV to - 1 V
Min. Input Pulse Width	400 ps
Lower Threshold	- 20 mV to - 500 mV
Upper Threshold	-
Zero Cross Adjust	- 100 mV to + 100 mV

Synchronisation Channels

Principle	Constant Fraction Discriminator (CFD)
Opt. Input Voltage Range	- 50 mV to - 1 V
Min. Input Pulse Width	400 ps
Threshold	- 20 mV to -500 mV
Frequency Range	0 to 200 MHz
Frequency Divider	1-2-4
Zero Cross Adjust	-100 mV to + 100 mV

Time-to-Amplitude Converters / ADCs

Principle	Ramp Generator / Biased Amplifier
TAC Range	50 ns to 2 us
Biased Amplifier Gain	1 to 15
Biased Amplifier Offset	0 to 100% of TAC Range
Time Range incl. Biased Amplifier	3.3 ns to 2 us
min. Time / Channel	813 fs
ADC Principle	50 ns Flash ADC with Error Correction
Diff. Nonlinearity	< 0.5% rms, typ. <1% peak-peak

Data Acquisition (Histogram Mode)

Method	on-board multi-dimensional histogramming process
Dead Time	100ns, independent of computer speed
Saturated Count Rate, per TCSPC channel / total	10 MHz / 40 MHz
Useful count rate, per TCSPC channel / total	5 MHz / 20 MHz
Channels / Curve per TCSPC channel	4096 1024 256 64 16 4 1
max. Scanning Area per TCSPC channel	16x16 64x64 128 x 128 256x256 512x512 1024x1024 2048x2048
max. Counts / Time Channel	2^{16-1}
Overflow Control	none / stop / repeat and correct
Collection Time	0.1 us to 10000 s
Display Interval Time	10ms to 1000 s
Repeat Time	0.1 us to 1000 s
Sequential Recording	Programmable Hardware Sequencer
Synchronisation with Scanning	Unlimited recording by memory swapping, in curve mode and scan mode
Count Enable Control	pixel, line and frame clocks from scanning device
Experiment Trigger	1 bit TTL TTL

Data Acquisition (FIFO / Time-Tag Mode)

Method	Time-tagging of individual photons and continuous writing to disk
Dead Time	100 ns
Output Data Format (ADC / Macrotime / Routing)	12 bit ADC / 12 bit macro time / 4 bit routing
Output Data Format for Scan Clock Markers (pxl, line, frame)	12 bit macro time / ppxl, line, frame
FIFO Buffer Capacity (photons and clock markers)	2 M
Macro Timer Resolution, internal clock	25 ns, 12 bit
Macro Timer Resolution, clock from SYNC input	10 ns to 100 ns, 12 bit
Curve Control (external Routing)	4 bit TTL
Count Enable Control	1 bit TTL

Operation Environment

Computer System	PC Pentium
Bus Connectors	PCI
Used PCI Slots	4
Power Consumption per TCSPC channel	approx. 60 W from +5V, 2.1 W from +12V
Power Consumption, total, all 4 TCSPC channels	approx. 15 W from +5V, 0.7 W from +12V
Dimensions	240 mm x 130 mm x 85 mm

Absolute Maximum Ratings (for all SPC modules)

Current into the SYNC and CFD inputs	100 mA (DC) 500 mA (pulse, <1us)
Voltage at the routing and control inputs / outputs	-0.5V ... +5.5 V
Currents at the	
+5V output	200 mA
-5V output	200 mA
+12V output	100 mA
-12V output	100 mA
Supply Voltage at the ISA Connector	
Vcc (+5V)	-0.5 ... +5.5 V
Vpp (+12V)	-0.5 ... +13 V
Signal Voltages at the ISA connector	-0.5 ... +5.5 V
Ambient temperature	0°C ... +40°C

References

1. M. Akatsu, Y. Enari, K. Hayasaka, T. Hokuue, T. Iijima, K. Inami, K. Itoh, Y. Kawakami, N. Kishimoto, T. Kubota, M. Kojima, Y. Kozakai, Y. Kuriyama, T. Matsuishi, Y. Miyabayashi, T. Ohshima, N. Sato, K. Senyo, A. Sugi, S. Tokuda, M. Tomita, H. Yanase, S. Yosino, MCP-PMT timing property for single photons, *Nucl. Instr. Meth. A* **528**, 763-775 (2004)
2. S.M. Ameer-Beg, N. Edme, M. Peter, P.R. Barber, T. Ng, B. Vojnovic, Imaging protein-protein interactions by multiphoton FLIM, *Proc. SPIE*, **5139**, 180-189 (2003)
3. S.M. Ameer-Beg, P.R. Barber, R. Locke, R.J. Hodgkiss, B. Vojnovic, G.M. Tozer, J. Wilson, Application of multiphoton steady state and lifetime imaging to mapping of tumor vascular architecture *in vivo*, *Proc. SPIE*, **4620**, 85-95 (2002)
4. R.M. Anderssen, K. Carlsson, A. Liljeborg, H. Brismar, Characterization of probe binding and comparison of its influence on fluorescence lifetime of two ph-sensitivity benzo[c]xantene dyes using intensity-modulated multiple-wavelength scanning technique, *Analytical Biochemistry* **283**, 104-110 (2000)
5. S.R. Arridge, Optical tomography in medical imaging, *Inverse Problems*, **15**, R41 (1999)
6. S.R. Arridge, M. Cope, D.T. Delpy, The theoretical basis for the determination of optical pathlengths in tissue, temporal and frequency analysis, *Phys. Med Biol.* **37**, 1531-1560 (1992)
7. S.R. Arridge, J.C. Hebden, M. Schweiger, F.E.W. Schmidt, M.E. Fry, E.M.C. Hillman, H. Dehghani, D.T. Delpy, A method for three-dimensional time-resolved optical tomography, *International Journal for Imaging systems and Technology* **11**, 2-11 (2000)
8. D. Axelrod, Fluorescence Polarisation Microscopy, D.L. Taylor, Y.-L. Wang (eds.), *Methods in Cell Biology*, Academic Press 1989
9. B. J. Bacskai, J. Skoch, G.A. Hickey, R. Allen, B.T. Hyman, Fluorescence resonance energy transfer determinations using multiphoton fluorescence lifetime imaging microscopy to characterize amyloid-beta plaques, *J. Biomed. Opt.* **8**, 368-375 (2003)
10. B. J. Bacskai, J. Skoch, G.A. Hickey, O. Berezovska, B.T. Hyman, Multiphoton imaging in mouse models of Alzheimer's disease, *Proc. SPIE*, **5323**, 71-76 (2004)
11. W.R.G. Baeyens, D. de Keukeleire, K. Korkidis, Luminescence techniques in chemical and biochemical analysis, M. Dekker, New York (1991)
12. K. Bahlmann, S.W. Hell, Deplorization by high aperture focusing, *Appl. Phys. Lett.* **77**, 612-614 (2000)
13. R.M. Ballew, J.N. Demas, An error analysis of the rapid lifetime determination method for the evaluation of single exponential decays, *Anal. Chem.* **61**, 30 (1989)
14. B.P. Barber, R.A. Hiller, R. Lofstedt, S.J. Puttermann, K.R. Weninger, Defining the unknowns of sonoluminescence, *Phys. Rep.* **281**, 65-143 (1997)
15. T. Basché, W.E. Moerner, M. Orrit, H. Talon, Photon antibunching in the fluorescence of a single dye molecule trapped in a solid, *Phys. Rev. Lett.* **69**, 1516 (1992)
16. A. Bassi, J. Swartling, C. D'Andrea, A. Pifferi, A. Torricelli, R. Cubeddu, Time-resolved spectrophotometer for turbid media based on supercontinuum generation in a photonic crystal fibre, *Opt. Lett.* **29**, 2405-2407 (2004)
17. Becker & Hickl GmbH, Routing modules for time-correlated single photon counting, manual, www.becker-hickl.com
18. Becker & Hickl GmbH, PML-16-C 16 channel detector head for time-correlated single photon counting. User handbook. Available on www.becker-hickl.com
19. Becker & Hickl GmbH, DCC-100 detector control module, manual, www.becker-hickl.com
20. Becker & Hickl GmbH, Modular FLIM systems for Zeiss LSM 510 laser scanning microscopes. User handbook. Available on www.becker-hickl.com
21. Becker & Hickl GmbH and Leica Microsystems, Leica MP-FLIM and D-FLIM Fluorescence Lifetime Microscopy Systems. User handbook. Available on www.becker-hickl.com
22. Becker & Hickl GmbH, Modular FLIM systems for Olympus laser scanning microscope FV1000. User handbook. Available on www.becker-hickl.com
23. Becker & Hickl GmbH, SPCImage Data Analysis Software for Fluorescence Lifetime Imaging Microscopy. User handbook. Available on www.becker-hickl.com
24. Becker & Hickl GmbH, MSA-200, MSA-300, MSA-1000 Photon counters / multiscalers, application manual. www.becker-hickl.com (2002)
25. Becker & Hickl GmbH, PMS-300, PMS-400 Gated photon counters and multiscalers, application manual. www.becker-hickl.com (2002)
26. Becker & Hickl GmbH, BDL-375-SMC, BDL-405-SPC, BDL-440-SMC, BDL-473-SMC NUV and blue picosecond diode lasers, www.becker-hickl.com
27. Becker & Hickl GmbH, BHL-600 and BHLP-700 Red and Near-Infrared Picosecond Diode Laser Modules, www.becker-hickl.com

28. W. Becker, A. Bergmann, Detectors for high-speed photon counting, Becker & Hickl GmbH, www.becker-hickl.com
29. W. Becker, A. Bergmann, Detector Assemblies for Picosecond Microscopy, Becker & Hickl GmbH, www.becker-hickl.com
30. W. Becker, H. Stiel, E. Klose, Flexible Instrument for time-correlated single photon counting, *Rev. Sci. Instrum.* **62**, 2991-2996 (1991)
31. W. Becker, Verfahren und Vorrichtung zur zeitkorrelierten Einzelphotonenzählung mit hoher Registrierrate, Patent DE 43 39 784 (1993)
32. W. Becker, Verfahren und Vorrichtung zur Messung von Lichtsignalen mit zeitlicher und räumlicher Auflösung, Patent DE 43 39 787 (1993)
33. W. Becker, H. Hickl, C. Zander, K.H. Drexhage, M. Sauer, S. Siebert, J. Wolfrum, Time-resolved detection and identification of single analyte molecules in microcapillaries by time-correlated single photon counting, *Rev. Sci. Instrum.* **70**, 1835-1841 (1999)
34. W. Becker, K. Benndorf, A. Bergmann, C. Biskup, K. König, U. Tirlapur, T. Zimmer, FRET measurements by TCSPC laser scanning microscopy, *Proc. SPIE* **4431**, 94-98 (2001)
35. W. Becker, A. Bergmann, K. König, U. Tirlapur, Picosecond fluorescence lifetime microscopy by TCSPC imaging, *Proc. SPIE* **4262**, 414-419 (2001)
36. W. Becker, A. Bergmann, H. Wabnitz, D. Grosenick, A. Liebert, High count rate multichannel TCSPC for optical tomography, *Proc. SPIE* **4431**, 249-245 (2001)
37. W. Becker, A. Bergmann, C. Biskup, T. Zimmer, N. Klöcker, K. Benndorf, Multi-wavelength TCSPC lifetime imaging, *Proc. SPIE* **4620** 79-84 (2002)
38. W. Becker, A. Bergmann, G. Weiss, Lifetime Imaging with the Zeiss LSM-510, *Proc. SPIE* **4620**, 30-35 (2002)
39. W. Becker, A. Bergmann, C. Biskup, L. Kelbauskas, T. Zimmer, N. Klöcker, K. Benndorf, High resolution TCSPC lifetime imaging, *Proc. SPIE* **4963**, 175-184 (2003)
40. W. Becker, A. Bergmann, M.A. Hink, K. König, K. Benndorf, C. Biskup, Fluorescence lifetime imaging by time-correlated single photon counting, *Micr. Res. Techn.* **63**, 58-66 (2004)
41. W. Becker, A. Bergmann, G. Biscotti, K. Koenig, I. Riemann, L. Kelbauskas, C. Biskup, High-speed FLIM data acquisition by time-correlated single photon counting, *Proc. SPIE* **5323**, 27-35 (2004)
42. W. Becker, A. Bergmann, G. Biscotti, A. Rück, Advanced time-correlated single photon counting technique for spectroscopy and imaging in biomedical systems, *Proc. SPIE* **5340**, 104-112 (2004)
43. W. Becker, A. Bergmann, E. Haustein, Z. Petrasek, P. Schwille, C. Biskup, T. Anhut, I. Riemann, K. Koenig, Fluorescence lifetime images and correlation spectra obtained by multi-dimensional TCSPC, *Proc. SPIE* **5700**, 144-152 (2005)
44. W. Becker, A. Bergmann, C. Biskup, D. Schweitzer, M. Hammer, Time- and Wavelength-Resolved Auto-fluorescence Detection by Multi-Dimensional TCSPC, *Proc. SPIE* **5862**, 58620S (2005)
45. W. Becker, A. Bergmann, E. Haustein, Z. Petrasek, P. Schwille, C. Biskup, L. Kelbauskas, K. Benndorf, N. Klöcker, T. Anhut, I. Riemann, K. König, Fluorescence lifetime images and correlation spectra obtained by multi-dimensional TCSPC, *Micr. Res. Tech.* **69**, 186-195 (2006)
46. W. Becker, Advanced time-correlated single-photon counting techniques. Springer, Berlin, Heidelberg, New York, 2005
47. J.M. Beechem, Picosecond fluorescence decay curves collected on millisecond time scale: direct measurement of hydrodynamic radii, local/global mobility, and intramolecular distances during protein-folding reactions. *Meth. Enzymol.* **278**, 24-49 (1997)
48. O. Berezovska, P. Ramdy, J. Skoch, M.S. Wolfe, B.J. Bacskai, B.T. Hyman, Amyloid precursor protein associates with a nicastrin-dependent docking site on the presenilin 1- γ -secretase complex in cells demonstrated by fluorescence lifetime imaging, *J. Neurosci.* **23**, 4560-4566 (2003)
49. O. Berezovska, B.J. Bacskai, B.T. Hyman, Monitoring Proteins in Intact Cells, *Science of Aging Knowledge Environment*, SAGE KE **14** (2003)
50. O. Berezovska, A. Lleo, L.D. Herl, M.P. Frosch, E.A. Stern, B.J. Bacskai, B.T. Hyman, Familial Alzheimer's disease presenilin 1 mutations cause alterations in the conformation of prenesilin and interactions with amyloid precursor protein, *J. Neurosci.* **25**, 3009-3017 (2005)
51. K.M. Berland, P.T.C. So, E. Gratton, Two-photon fluorescence correlation spectroscopy, Method and application to the intracellular environment, *Biophys. J.* **68**, 694-701 (1995)
52. R.A. Bhat, M. Miklis, E. Schmelzer, P. Schulze-Lefert, R. Panstruga, Recruitment and interaction dynamics of plant penetration resistance components in a plasma membrane microdomain. *PNAS* **102**, 3135-3140, 2005
53. O. Bilsel, C. Kayatekin, L.A. Wallace, C.R. Matthews, A microchannel solution mixer for studying microsecond protein folding reactions, *Rev. Sci. Instrum.* **76**, 014302 (2005)

54. D.J.S. Birch, R.E. Imhof, A. Dutch, Pulse fluorometry using simultaneous acquisition of fluorescence and excitation, *Rev. Sci. Instrum.* **55**, 1255-1264 (1984)
55. D.J.S. Birch, A.S. Holmes, R.E. Imhof, B.Z. Nadolski, K. Suhling, Multiplexed array fluorometry, *Journal of Phys. E. Sci Instrum.* **21**, 415 (1988)
56. D.K. Bird, K.W. Eliceiri, C-H. Fan, J.G. White, Simultaneous two-photon spectral and lifetime fluorescence microscopy, *Appl. Opt.* **43**, 5173-5182 (2004)
57. S. Bloch, F. Lesage, L. McIntosh, A. Gandjbakhche, K. Liang, S. Achilefu, Whole-body fluorescence lifetime imaging of a tumor-targeted near-infrared molecular probe in mice. *J. Biomed. Opt.* **10**, 054003-1 to -8
58. C. Biskup, A. Böhmer, R. Pusch, L. Kelbauskas, A. Gorshkov, I. Majoul, J. Lindenau, K. Benndorf, F-D. Böhmer, Visualization of SHP-1-target interaction, *J. Cell Sci.* **117**, 5155-5178 (2004)
59. C. Biskup, T. Zimmer, K. Benndorf, FRET between cardiac Na⁺ channel subunits measured with a confocal microscope and a streak camera, *Nature Biotechnology*, **22**(2), 220-224 (2004)
60. C. Biskup, L. Kelbauskas, T. Zimmer, K. Benndorf, A. Bergmann, W. Becker, J.P. Ruppertsberg, C. Stockklausner, N. Klöcker, Interaction of PSD-95 with potassium channels visualized by fluorescence lifetime-based resonance energy transfer imaging, *J. Biomed. Opt.* **9**, 735-759 (2004)
61. C. Biskup, L. Kelbauskas, Th. Zimmer, S. Dietrich, K. Benndorf, W. Becker, A. Bergmann, N. Klöcker, Spectrally resolved fluorescence lifetime and FRET measurements, *Proc. SPIE* **5700**, 188-196 (2005)
62. J.W. Borst, M.A. Hink, A. van Hoek, A.J.W.G. Visser, Multiphoton spectroscopy in living plant cells, *Proc. SPIE* **4963**, 231-238 (2003)
63. R. Brandenburg, K.V. Kozlov, P. Michel, H-E. Wagner, Diagnostics of the single filament barrier discharge in air by cross-correlation spectroscopy, 53-nd annual gaseous electronics conference, Houston (Texas) (2000)
64. D. Branning, A.L. Migdall, A.V. Sergienko, Simutaneous measurement of group and phase delay between photons, *Phys. Rev.* **62**, 063808-1 to -12 (2000)
65. R.P. Breault, Stray-light suppression, in W.L. Wolfe, Optical engineers's desk reference, OSA Optical society of America, SPIE The International Society for Optical Engineering (2003)
66. P.M. Brenner, S. Hilgenfeld, D. Lohse, Single-bubble sonoluminescence, *Rev. Mod. Phys.* **74**, 425-484 (2002)
67. S.Y. Breusegem, In vivo investigation of protein interactions in *C. Elegans* by Förster resonance energy transfer microscopy, University of Illinois at Urbana-Champaign (2002)
68. H. Brismar, B. Ulvhake, Fluorescence lifetime imaging measurements in confocal microscopy of neurons labeled with multiple fluorophores, *Nature Biotech.* **15**, 373-377 (1997)
69. I. Bugiel, K. König, H. Wabnitz, Investigations of cells by fluorescence laser scanning microscopy with subnanosecond time resolution, *Lasers in the Life Sciences* **3**(1), 47-53 (1989)
70. V. Calleja, S. Ameer-Beg, B. Vojnovic, R. Woscholski, J. Downwards, B. Larjani, Monitoring conformational changes of proteins in cells by fluorescence lifetime imaging microscopy, *Biochem. J.* **372**, 33-40 (2003)
71. S. Canonica, J. Forrer, U.P. Wild, Improved timing resolution using small side-on photomultipliers in single photon counting, *Rev. Sci. Instrum.* **56**, 1754-1758 (1985)
72. K. Carlsson, J.P. Philip, Theoretical investigation of the signal-to-noise ratio for different fluorescence lifetime imaging techniques, *Proc. SPIE* **4622**, 70-78 (2002)
73. B. Chan, K. Weidemaier, W-T. Yip, P.F. Barbara, K. Musier-Forsyth, Intra-tRNA distance measurements for nucleocapsid protein-dependent tRNA unwinding during priming of HIV reverse transcription, *PNAS* **96**, 459-464 (1999)
74. B. Chance, M. Cope, E. Gratton, N. Ramanujam, B. Tromberg, Phase measurement of light absorption and scatter in human tissue, *Rev. Sci. Instrum.* **69**, 3457-3481 (1998)
75. Y. Chen, J.D. Müller, P.T.C. So, E. Gratton, The Photon Counting Histogram in Fluorescence Fluctuation Spectroscopy, *Biophys. J.* **77**, 553-567 (1999)
76. Y. Chen, J.D. Müller, Q.Q. Ruan, E. Gratton, Molecular brightness characterization of EGFP in vivo by fluorescence fluctuation spectroscopy, *Biophys. J.* **82**, 133-144 (2002)
77. Y. Chen, A. Periasamy, Characterization of two-photon excitation fluorescence lifetime imaging microscopy for protein localization, *Microsc. Res. Tech.* **63**, 72-80 (2004)
78. Y. Chen, A. Periasamy, Two-photon FIM-FRET microscopy for protein localization, *Proc. SPIE* **5323**, 431-439 (2004)
79. W-F. Cheong, S.A. Prahl, A.J. Welch, A review of the optical properties of biological tissue, *IEEE Journal of Quantum Electronics* **26**, 2166-2185 (1990)
80. V. Chernomordik, D.W. Hattery, A.H. Gandjbakhche, A. Pifferi, P. Taroni, A. Torricelli, G. Valentini, R. Cubeddu, Quantification by random walk of the optical parameters of nonlocalized abnormalities embedded within tissuelike phantoms, *Opt. Lett.* **25**, 951-953 (2000)

81. V. Chernomordik, D.W. Hattery, D. Grosenick, H. Wabnitz, H. Rinneberg, K.T. Moesta, P.M. Schlag, A. Gandjbakhche, Quantification of optical properties of breast tumor using random walk theory, *J. Biomed. Opt.* **7** 80-87 (2002)
82. J. Christiansen, M. Mota, A high-resolution time interpolator based on a delay locked loop and an RC delay line, *IEEE Journal on solid state circuits* **34**, 1360-1366 (1999)
83. G.C. Cianci, K. Berland, Saturation in two-photon microscopy, *Proc. SPIE* **5323**, 128-135 (2004)
84. A.H.A. Clayton, Q.A. Hanley, D.J. Arndt-Jovin, V. Subramaniam, T.M. Jovin, Dynamic fluorescence anisotropy imaging microscopy in the frequency domain (FLIM), *Biophys. J.* **83**, 1631-1649 (2002)
85. P.B. Coates, The correction for photon ‘pile-up’ in the measurement of radiative lifetimes, *J. Phys. E. Sci. Instrum.* **1**, 878-879 (1968)
86. P.B. Coates, Pile-up corrections in the measurement of lifetimes, *J. Phys. E. Sci. Instrum.* **5**, 148-150 (1972)
87. P.B. Coates, Pile-up corrections in lifetime experiments, *Rev. Sci. Instrum.* **43**, 1855-1856 (1972)
88. M. Cotlet, J. Hofkens, S. Habuchi, G. Dirix, M. Van Guyse, J. Michels, J. Vanderleyden, F.C. De Schryver, Identification of different emitting species in the red fluorescent protein DsRed by means of ensemble and single molecule spectroscopy, *PNAS* **98**, 14398-5006 (2001)
89. M. Cotlet, J. Hofkens, M. Maus, T. Gensch, M. Van der Auweraer, J. Michels, G. Dirix, M. Van Guyse, J. Vanderleyden, A.J.W.G. Visser, F.C. De Schryver, Excited state dynamics in the green fluorescent protein mutant probed by picosecond time-resolved single-photon counting spectroscopy, *J. Phys. Chem.* **B105**, 4999-5006 (2001)
90. S. Cova, M. Bertolaccini, C. Bussolati, The measurement of luminescence waveforms by single-photon techniques, *Phys. Stat. Sol.* **18**, 11-61 (1973)
91. S. Cova, A. Longoni, G. Ripamonti, Active-quenching and gating circuits for single-photon avalanche diodes (SPADs), *IEEE Trans. Nucl. Sci.* **NS29**, 599-601 (1982)
92. S. Cova, G. Ripamonti, S. Lacaita, Avalanche semiconductor detector for single optical photons with a time resolution of 60 ps, *Nucl. Instr. Meth.* **A253**, 482-487 (1987)
93. S. Cova, S. Lacaita, M. Ghioni, G. Ripamonti, T.A. Louis, 20-ps timing resolution with single-photon avalanche photodiodes, *Rev. Sci. Instrum.* **60**, 1104-110 (1989)
94. S. Cova, M. Ghioni, A. Lacaita, C. Samori, F. Zappa, Avalanche photodiodes and quenching circuits for single-photon detection, *Appl. Opt.* **35**, 1954-1976 (1996)
95. S. Cova, M. Ghioni, A. Lotito, I. Rech, F. Zappa, Evolution and prospects for single-photon avalanche diodes and quenching circuits, *J. Mod. Opt.* **15**, 1267-1288 (2004)
96. R. Cubeddu, A. Pifferi, P. Taroni, A. Torricelli, G. Valentini, Time-resolved imaging on a realistic tissue phantom, μ_s and μ_a images versus time-integrated images, *Appl. Opt.* **35** 4533-4540 (1996)
97. R. Cubeddu, A. Pifferi, P. Taroni, A. Torricelli, G. Valentini, Imaging with diffusing light: an experimental study of the effect of background optical properties, *Appl. Opt.* **37**, 3564-3573 (1998)
98. R. Cubeddu, A. Pifferi, P. Taroni, A. Torricelli, G. Valentini, Compact tissue oximeter based on dual-wavelength multichannel time-resolved reflectance, *Appl. Opt.* **38**, 3670-3680 (1999)
99. R. Cubeddu, A. Pifferi, P. Taroni, A. Torricelli, G. Valentini, Noninvasive absorption and scattering spectroscopy of bulk diffuse media: An application to the optical characterization of human breast, *Appl. Phys. Lett.* **74**, 874-876 (1999)
100. R. Cubeddu, G. Canti, C. D’Andrea, A. Pifferi, P. Taroni, A. Torricelli, G. Valentini, Effects of photodynamic therapy on the absorption properties of disulphonated aluminum phthalocyanine in tumor-bearing mice, *Journal of Photochemistry and Photobiology B: Biology* **60**, 73-78 (2001)
101. R. Cubeddu, G. Biscotti, A. Pifferi, P. Taroni, A. Torricelli, M. Ferrari, V. Quaresima, Functional muscle studies by dual-wavelength, 8-channel time-resolved oximetry, *Proc. SPIE* **5138**, 29-34 (2003)
102. R. Cubeddu, G. M. Danesini, F. Messina, A. Pifferi, L. Spinelli, P. Taroni, A. Torricelli, Four-wavelength time-resolved optical mammograph, *Proc. SPIE* **4955**, 203-210 (2003)
103. W. Denk, J.H. Strickler, W.W.W. Webb, Two-photon laser scanning fluorescence microscopy, *Science* **248**, 73-76 (1990)
104. W. Denk, J. Strickler, W. Webb, Two-photon laser scanning microscopy, Patent WO 91/07651 (1991)
105. E. Deprez, P. Tauc, H. Leh, J-F. Mouscadet, C. Auclair, J-C. Brochon, Oligomeric states of the HIV-1 integrase as measured by time-resolved anisotropy, *Biochemistry* **39**, 9275-9284 (2000)
106. E. Deprez, P. Tauc, H. Leh, J-F. Mouscadet, C. Auclair, M.E. Hawkins, J-C. Brochon, DNA binding induces dissociation of the multimetric form of HIV-1 integrase: A time-resolved fluorescence anisotropy study, *PNAS* **98**, 10090-10095 (2001)
107. T. Desmettre, J.M. Devoiselle, S. Mordon, Fluorescence properties and metabolic features of indocyanine green (ICG) as related to angiography, *Surv. Ophthalmol.* **45**, 15-27 (2000)
108. A. Diaspro, Building a two-photon microscope using a laser scanning confocal architecture, in A. Periasamy (ed.), *Methods in Cellular Imaging*, Oxford University Press, 162-179 (2001)

109. A. Diaspro, M. Corosu, P. Ramoino, M. Robello, Adapting a compact confocal microscope system to a two-photon excitation fluorescence Imaging architecture, *Micr. Res. Tech.* **47**, 196–205 (1999)
110. Diaspro A. (ed.). Confocal and two-photon microscopy: Foundations, applications and advances. Wiley-Liss (2001)
111. M.E. Dickinson, C.W. Waters, G. Bearman, R. Wolleschensky, S. Tille, S.E. Fraser, Sensitive imaging of spectrally overlapping fluorochromes using the LSM 510 META, *Proc. SPIE*, **4620**, 123-136 (2002)
112. Y.T. Didenko, W.B. NCNamara, K.S. Suslick, Molecular emission from single-bubble sonoluminescence, *Nature* **407**, 877-879 (2000)
113. P.S. Dittrich, P. Schwille, Photobleaching and stabilization of fluorophores used for single-molecule analysis with one- and two-photon excitation, *Appl. Phys. B* **73**, 829-837 (2001)
114. L. Dougan, J. Crain, H. Vass, S.W. Magennis, Probing the liquid-state structure and dynamics od aqueous solutions by fluorescence spectroscopy, *J. Fluoresc.* **14**, 91-97 (2004)
115. R.R. Duncan, A. Bergmann, M.A. Cousin, D.K. Apps, M.J. Shipston, Multi-dimensional time-correlated single-photon counting (TCSPC) fluorescence lifetime imaging microscopy (FLIM) to deetct FRET in cells, *J. Microsc.* **215**, 1-12 (2004)
116. R.C. Dunn, Near-field scanning optical microscopy, *Chem. Rev.* **99**, 2891-2927 (1999)
117. T. Durduran, G. Yu, M.G. Burnett, J.A. Detre, J.H. Greenberg, J. Wang, C. Zhou, A. Yodh, Diffuse optical measurement of blood flow, blood oxygenation, and metabolism in a human brain during sensorimotor cortex activation, *Opt. Lett.* **29**, 1766-1768 (2004)
118. H-G. Eberle, J. Beuthan, M. Dierolf, D. Felsenberg, W. Gowin, G. Müller, Investigations of the application of a laser radar photogoniometer in the diagnosis of osteoporosis, *Proc. SPIE* **3259**, 144-153 (1998)
119. H-G. Eberle, J. Beuthan, G. Müller, The propagation of ps-laser-pulses through different bone structure, *Z. Med. Phys.* **10**, 177 (2000)
120. C. Eggeling, J.R. Fries, L. Brand, R. Günther, C.A.M. Seidel, Monitoring conformational dynamics of a single molecule by selective fluorescence spectroscopy, *PNAS* **95**, 1556-1561 (1998)
121. C. Eggeling, S. Berger, L. Brand, J.R. Fries, J. Schaffer, A. Volkmer, C.A. Seidel, Data registration and selective single-molecule analysis using multi-parameter fluorescence detection, *J. Biotechnol.* **86**, 163 (2001)
122. J.S. Eid, J.D. Müller, E. Gratton, Data acquisition card for fluctuation correlation spectroscopy allowing full access to the detected photon sequence, *Rev. Sci. Instrum.* **71**, 361-368 (2000)
123. P.A. Ekstrom, Triggered avalanche detection of optical photons, *J. Appl. Phys.* **52**, 6974-6979 (1981)
124. K.W. Eliceiri, C.H. Fan, G.E. Lyons, J.G. White, Analysis of histology specimens using lifetime multiphoton microscopy, *J. Biomed. Opt.* **8**, 376-380 (2003)
125. J. Enderlein, M. Sauer, Optimal algorithm for single molecule identification with time-correlated single photon counting, *J. Chem. Phys. A* **105**, 48-53 (2002)
126. T.J. Farrel, W.S. Patterson, Diffusion modeling of fluorescence in tissue, in M.-A. Mycek, B.W. Pogue (eds.), *Handbook of Biomedical Fluorescence*, Marcel Dekker Inc. New York, Basel, 29-60 (2003)
127. S. Felekyan, R. Kühnemuth, V. Kudryavtsev, C. Sandhagen, W. Becker, C.A.M. Seidel, Full correlation from picoseconds to seconds by time-resolved and time-correlated single photon detection, *Rev. Sci. Instrum.* **76**, 083104 (2005)
128. Th. Förster, Zwischenmolekulare Energiewanderung und Fluoreszenz, *Ann. Phys. (Serie 6)* **2**, 55-75 (1948)
129. M.A. Franceschini, S. Fantini, J.H. Thompson, J.P. Culver, D.A. Boas, Hemodynamic evoked response of the sensorimotor cortex measured noninvasively with near-infrared optical imaging, *Psychophysiology* **40**, 548-560 (2003)
130. M.A. Franceschini, V. Toronov, M.E. Filiaci, E. Gratton, S. Fantini, On-line optical imaging of the human brain with 160-ms temporal resolution, *Opt. Expr.* **6**, 49-57 (2000)
131. P. Gallant, A. Belenkova, G. Ma, F. Lesage, Y. Wang, D. Hall, L. McIntosh, A quantitative time-domain optical imager for small animals in vivo fluorescence studies, In OSA Biomedical Optics Topical Meetings on CD ROM (The Optical Society of America, Washington, DC,) WD2 (2004)
132. I. Gannot, I. Ron, F. Hekmat, V. Chernomordik, A. Ganjakhche, Functional optical detection based on pH dependent fluorescence lifetime, *Lasers in Surgery and Medicine* **35**, 342-348 (2004)
133. F. Gao, P. Poulet, Y. Yamada, Simultaneous mapping of absorption and scattering coefficients from a three-dimensional model of time-resolved optical tomography, *Appl. Opt.* **39**, 5898-5910 (2000)
134. S.V. Gaponenko, I.N. Germanenko, E.P. Petrov, Time-resolved spectroscopy of visibly emitting porous silicon, *Appl. Phys. Lett.* **64**, 85-87 (1994)
135. S.V. Gaponenko, V.K. Kononenko, E.P. Petrov, I.N. Germanenko, A.P. Stupak, Y.H. Xie, Polarization of porous silicon luminescence, *Appl. Phys. Lett.* **67**, 3019-3021 (1995)
136. S.V. Gaponenko, E.P. Petrov, U. Woggon, O. Wind, C. Klingshirn, Y.H. Xie, I.N. Germanenko, A.P. Stupak, Steady-state and time-resolved spectroscopy of porous silicon. *J. Luminesc.* **70**, 364-376 (1996)

137. C.D. Geddes, H. Cao, I. Gryczynski, J. Fang, J.R. Lakowicz, Metal-enhanced fluorescence (MEF) due to silver colloids on a planar surface: Potential applications of indocyanine green to in vivo imaging, *J. Phys. Chem. A* **107**, 3443-3449 (2003)
138. C.D. Geddes, H. Cao, I. Gryczynski, J. R. Lakowicz, Enhanced photostability of ICG in close proximity to gold colloids, *Spectrochimica Acta A* **59**, 2611-2617 (2003)
139. H.C. Gerritsen, M.A.H. Asselbergs, A.V. Agronskaia, W.G.J.H.M. van Sark, Fluorescence lifetime imaging in scanning microscopes: acquisition speed, photon economy and lifetime resolution, *J. Microsc.* **206**, 218-224 (2002)
140. M. Göppert-Mayer, Über Elementarakte mit zwei Quantensprüngen, *Ann. Phys.* **9**, 273-294 (1931)
141. B.R. Gompf, R. Gunther, G. Nick, R. Pecha, W. Eisenmenger, Resolving sonoluminescence pulse width with time-correlated single-photon counting, *Phys. Rev. Lett.* **79**, 1405-1408 (1997)
142. Govindjee, Sixty-three Years Since Kautsky: Chlorophyll α Fluorescence, *Aust. J. Plant Physiol.* **22**, 131-160 (1995)
143. Govindjee, M.J. Seufferheld, Non-photochemical quenching of chlorophyll α Fluorescence: Early history and characterization of two xanthophyll-cycle mutants of Chlamydomonas Reinhardtii, *Funct. Plant Biol.* **29**, 1141-1155 (2002)
144. E. Gratton, S. Breusegem, J. Sutin, Q. Ruan, N. Barry, Fluorescence lifetime imaging for the two-photon microscope: Time-domain and frequency domain methods, *J. Biomed. Opt.* **8**, 381-390 (2003)
145. D. Grosenick, H. Wabnitz, H. Rinneberg, Time-resolved imaging of solid phantoms for optical tomography, *Appl. Opt.* **36**, 221-231 (1997)
146. D. Grosenick, H. Wabnitz, H. Rinneberg, K.T. Moesta, P.M. Schlag, Development of a time-domain optical mammograph and first in-vivo applications, *Appl. Optics*, **38**, 2927-2943 (1999)
147. D. Grosenick, H. Wabnitz, R. MacDonald, H. Rinneberg, J. Mucke, C. Stroszynski, K.T. Moesta, P.M. Schlag, Determination of in vivo optical properties of breast tissue and tumors using a laser pulse mammograph, *Biomedical Topical Meetings, Technical Digest, OSA*, 459 (2002)
148. D. Grosenick, K.T. Moesta, H. Wabnitz, J. Mucke, C. Stroszynski, R. MacDonald, P.M. Schlag, H. Rinneberg, Time-domain optical mammography: initial clinical results on detection and characterization of breast tumors, *Appl. Opt.* **42**, 3170-3186 (2003)
149. D. Grosenick, H. Wabnitz, K.T. Moesta, J. Mucke, M. Möller, C. Stroszynski, J. Stössel, B. Wassermann, P.M. Schlag, H. Rinneberg, Concentration and oxygen saturation of haemoglobin of 50 breast tumours determined by time-domain optical mammography, *Physics in Medicine & Biology* **49**, 1165-1181 (2004)
150. A. Habenicht, J. Hjelm, E. Mukhtar, F. Bergström, L.B-A. Johansson, Two-photon excitation and time-resolved fluorescence: I. The proper response function for analysing single-photon counting experiments, *Chem. Phys. Lett.* **345**, 367-375 (2002)
151. S. Habuchi, M. Cotlet, J. Hofkens, G. Disix, J. Michiels, J. Vanderleyden, V. Subramaniam, F.C. De Schryver, Resonance Energy Transfer in a Calcium Concentration-Dependent Cameleon Protein, *Biophys. J.* **83**, 3499-3506 (2002)
152. S. Hackbarth, V. Horneffer, A. Wiehe, F. Hillenkamp, B. Röder, Photophysical properties of pheophorbide-a-substituted diaminobutane poly-propylene-imine dendrimer, *Chemical Physics* **269**, 339-346 (2001)
153. P. Hänninen, S. Hell, Luminescence scanning microscopy process and luminescence scanning microscope, Patent WO 95/30166 (1995)
154. Hamamatsu Photonics K.K., R7400 Series Metal package photomultiplier tube (2001)
155. Hamamatsu Photonics K.K., R3809U-50 series Microchannel plate photomultiplier tube (MCP-PMTs) (2001)
156. Hamamatsu Photonics K.K., R5900U-16 series Multianode photomultiplier tube (2001)
157. Hamamatsu Photonics K.K., H5773/H5783/H6779/H6780/H5784 Photosensor modules (2001)
158. Hamamatsu Photonics K.K., H7422 series Metal package PMT with cooler - photosensor modules (2003)
159. R. Hanbury-Brown, R.Q. Twiss, *Nature* **177**, 27-29 (1956)
160. K.M. Hanson, M.J. Behne, N.P. Barry, T.M. Mauro, E. Gratton, Two-photon fluorescence imaging of the skin stratum corneum pH gradient, *Biophys. J.* **83**, 1682-1690 (2002)
161. P.R. Hartig, K. Sauer, Measurement of very short fluorescence lifetimes by single photon counting, *Rev. Sci. Instrum.* **47**, 122 (1976)
162. W. Hartmann, F. Bernhard, *Fotovervielfacher und ihre Anwendung in der Kernphysik*, Akademie-Verlag Berlin (1957)
163. R.P. Haugland, Handbook of fluorescent probes and research chemicals, 7th Ed. Molecular Probes, Inc. (1999)

164. J.C. Hebden, E.W. Schmidt, M.E. Fry, M. Schweiger, E.M.C. Hillman, D.T. Delpy, Simultaneous reconstruction of absorption and scattering images by multichannel measurement of purely temporal data, *Opt. Lett.* **24**, 534-536 (1999)
165. J.C. Hebden, H. Veenstra, H. Dehghani, E.M.C. Hillman, M. Schweiger, S.R. Arridge, D.T. Delpy, Three-dimensional time-resolved optical tomography of a conical breast phantom, *Appl. Opt.* **40**, 3278-3287 (2001)
166. J.C. Hebden, A. Gibson, R.M. Yusof, N. Everdell, E.M.C. Hillman, D.T. Delpy, S.R. Arridge, T. Austin, J.H. Meek, J.S. Wyatt, Three-dimensional optical tomography of the premature infant brain, *Phys. Med. Biol.* **47**, 4155-4166 (2002)
167. J.C. Hebden, Advances in optical imaging of the newborn infant brain, *Psychophysiology* **40**, 501-510 (2003)
168. J.C. Hebden, A. Gibson, T. Austin, R.M. Yusof, N. Everdell, D.T. Delpy, S.R. Arridge, J.H. Meek, J.S. Wyatt, Imaging changes in blood volume and oxygenation in the newborn infant brain using three-dimensional optical tomography, *Phys. Med. Biol.* **49**, 1117-1130 (2004)
169. A.A. Heikal, S.T. Hess, G.S. Baird, R.Y. Tsien, W.W.W. Webb, Molecular spectroscopy and dynamics of intrinsically fluorescent proteins: Coral red (dsRed) and yellow (Citrine), *PNAS* **97**, 11996-12001 (2000)
170. A.A. Heikal, S.T. Hess, W.W.W. Webb, Multiphoton molecular spectroscopy and excited-state dynamics of enhanced green fluorescent protein (EGFP): acid-base specificity, *Chem. Phys.* **274**, 37-55 (2001)
171. S.T. Hess, E.D. Sheets, A. Wagenknecht-Wiesner, A.A. Heikal, Quantitative Analysis of the Fluorescence Properties of Intrinsically Fluorescent Proteins in Living Cells, *Biophys. J.* **85**, 2566 (2003)
172. R.A. Hiller, S.J. Puttermann, K.R. Weninger, Time-resolved spectra of sonoluminescence, *Phys. Rev. Lett.* **80**, 1090-1093 (1998)
173. E.M.C. Hillman, J.C. Hebden, M. Schweiger, H. Dehghani, F.E.W. Schmidt, D.T. Delpy, S.R. Arridge, Time resolved optical tomography of the human forearm, *Phys. Med. Biol.* **46**, 1117-1130 (2001)
174. M. Hof, V. Fidler, R. Hutterer, Basics of fluorescence in biosciences, in M. Hof, R. Hutterer, V. Fidler, *Fluorescence spectroscopy in biology*, Springer Verlag Berlin Heidelberg New York 1-29(2005)
175. J. Hofkens, M. Cotlet, T. Vosch, P. Tinnefeld, K.D. Weston, C. Ego, A. Grimsdale, K. Müllen, D. Beljonne, J.L. Bredas, S. Jordens, G. Schweitzer, M. Sauer, F.C. De Schryver, Revealing competitive Förster-type resonance energy-transfer pathways in single bichromophic molecules, *PNAS* **100**, 13146-13151 (2003)
176. A. Hopt, E. Neher, Highly nonlinear Photodamage in two-photon fluorescence microscopy, *Biophys. J.* **80**, 2029-2036 (2002)
177. D. Hu, M. Micic, N. Klymyshyn, Y.D. Suh, H.P. Lu, Correlated topographic and spectroscopic imaging beyond diffraction limit by atomic force microscopy metallic tip-enhanced near-field fluorescence lifetime microscopy, *Rev. Sci. Instrum.* **74**, 3347-3355 (2003)
178. M.K.Y. Hughes, S. Ameer-Beg, M. Peter, T. Ng, Use of acceptor fluorescence for determining FRET lifetimes, *Proc. SPIE* **5139**, 88-96 (2003)
179. id Quantique, id 100 single photon detection module, www.idquantique.com (2005)
180. J.C. Jackson, A.P. Morrison, D. Phelan, A. Mathewson, A novel silicon geiger-mode avalanche photodiode, *Proc. IEDM*, 32-2 (2002)
181. S. Jakobs, V. Subramaniam, A. Schönle, T. Jovin, S.W. Hell, EGFP and DsRed expressing cultures of *Escherichia coli* imaged by confocal, two-photon and fluorescence lifetime microscopy, *FEBS Letters* **479**, 131-135 (2002)
182. J. Kalisz, Review of methods for time interval measurements with picosecond resolution, *Metrologia* **41**, 17-32
183. H. Kaneko, I. Putzler, S. Frings, U. B. Kaupp, Th. Gensch, Chloride Accumulation in Mammalian Olfactory Sensory Neurons, *J. Neurosci.*, **24** 7931-7938 (2004)
184. C.N. Kästner, M. Prummer, B. Sick, A. Renn, U.P. Wild, P. Dimroth, The citrate carrier CitS probed by single molecule fluorescence spectroscopy, *Biophys. J.* **84**, 1651-1659 (2003)
185. P. Kask, K. Palo, D. Ullmann, K. Gall, Fluorescence-intensity distribution analysis and its application in bimolecular detection technology, *PNAS* **96**, 13756-13761 (1999)
186. P. Kask, K. Palo, N. Fay, L. Brand, Ü. Mets, D. Ullmann, J. Jungmann, J. Pschorr, K. Gall, Two-dimensional fluorescence intensity distribution analysis: theory and applications, *Biophys. J.* **78**, 1703-1713 (2000)
187. P. Kask, C. Eggeling, K. Palo, Ü. Mets, M. Cole, K. Gall, Fluorescence intensity distribution analysis(FIDA) and related fluorescence fluctuation techniques: theory and practice, in R. Kraayenhof, A.J.W.G. Visser, H.C. Gerritsen (eds.), *Fluorescence spectroscopy imaging and probes*, Springer Verlag Berlin Heidelberg New York, 153-181 (2000)
188. H. Kautsky, A. Hirsch, Neue Versuche zur Kohlensäureassimilation, *Naturwissenschaften* **19**, 964 (1931)

189. L. Kelbauskas, W. Dietel, Internalization of aggregated photosensitizers by tumor cells: Subcellular time-resolved fluorescence spectroscopy on derivates of pyropheophorbide-a ethers and chlorin e6 under femtosecond one- and two-photon excitation, *Photochem. Photobiol.* **76**, 686-694 (2002)
190. K. Kimura, Ultra fast luminescence in heavy-ion track-cores in insulators: Electron-hole plasma, *Nucl. Instr. Meth. Phys. Res.* **B191**, 48 (2002)
191. S. Kinoshita, T. Kushida, Subnanosecond fluorescence-lifetime measuring system using single photon counting method with mode-locked laser excitation, *Rev. Sci. Instrum.* **52**, 572-575 (1981)
192. S. Kinoshita, T. Kushida, High-performance, time-correlated single-photon counting apparatus using a side-on type photomultiplier, *Rev. Sci. Instrum.* **53**, 469-472 (1982)
193. N. Kitamura, N. Sakata, H-B. Kim, S. Habuchi, Energy gap dependence of the nonradiative decay rate constant of 1-anilino-8-naphthalene sulfonate in reverse micelles, *Analytical Sciences* **15**, 431-419 (1999)
194. J-P. Knemeyer, N. Marmé, M. Sauer, Probes for detection of specific DNA sequences at the single-molecule level, *Anal. Chem.* **72**, 3717-3724 (2002)
195. M. Köllner, J. Wolfrum, How many photons are necessary for fluorescence-lifetime measurements?, *Phys. Chem. Lett.* **200**, 199-204 (1992)
196. K. König, P.T.C. So, W.W. Mantulin, B.J. Tromberg, E. Gratton, Two-Photon excited lifetime imaging of autofluorescence in cells during UVA and NIR photostress, *J. Microsc.* **183**, 197-204 (1996)
197. K. König, Multiphoton microscopy in life sciences, *J. Microsc.* **200**, 83-104 (2000)
198. K. König, Laser tweezers and multiphoton microscopes on life science, *Histochem. Cell Biol.* **114**, 79-92 (2000)
199. K. König, Cellular Response to Laser Radiation in Fluorescence Microscopes, in A. Periasamy, *Methods in Cellular Imaging*, Oxford University Press, 236-254 (2001)
200. K. König, U. Wollina, I. Riemann, C. Peuckert, K-J. Halbhuber, H. Konrad, P. Fischer, V. Fuenfstueck, T.W. Fischer, P. Elsner, Optical tomography of human skin with subcellular resolution and picosecond time resolution using intense near infrared femtosecond laser pulses, *Proc. SPIE* **4620**, 191-202 (2002)
201. K. König, I. Riemann, High-resolution multiphoton tomography of human skin with subcellular spatial resolution and picosecond time resolution, *J. Biom. Opt.* **8**, 432-439 (2003)
202. K. König, I. Riemann, G. Ehrlich, V. Ulrich, P. Fischer, Multiphoton FLIM and spectral imaging of cells and tissue, *Proc. SPIE* **5323**, 240-251 (2004)
203. K. König, A. Ehlers, F. Stracke, I. Riemann, In vivo drug screening in human skin using femtosecond laser multiphoton tomography, *Skin Pharmacol Physiol* **19**, 78-88 (2006)
204. O. Korth, T. Hanke, B. Röder, Photophysical investigations of Langmuir-Blodgett mono- and multilayer films of pheophorbide-a, *Thin Solid Films* **320**, 305-315 (1998)
205. K.V. Kozlov, R. Brandenburg, H-E. Wagner, A.M. Morozov, P. Michel, Investigation of the filamentary and diffuse mode of barrier discharges in N₂/O₂ mixtures at atmospheric pressure by cross-correlation spectroscopy, *J. Phys. D: Appl. Phys.* **38**, 518-529 (2005)
206. K.V. Kozlov, V.V. Dobryakov, A.P. Monyakin, VG- Samoilovich, O.S. Shepelev, H-E. Wagner, R. Brandenburg, P. Michel, Cross-correlation spectroscopy in investigations of filamentary gas discharges at atmospheric pressure, *Proc. SPIE* **4460**, 165-176 (2002)
207. K.V. Kozlov, H-E. Wagner, R. Brandenburg, P. Michel, Spatio-temporally resolved spectroscopic diagnostics of the barrier discharge in air at atmospheric pressure, *J. Phys. D: Appl. Phys.* **34**, 3164-3176 (2001)
208. M. Kreiter, M. Prummer, B. Hecht, U.P. Wild, Orientation dependence of fluorescence lifetimes near an interface, *J. Chem. Phys.* **117**, 9430-9433 (2002)
209. R. Krause-Rehberger, H.S. Leipner, *Positron annihilation in semiconductors*, Springer Verlag Berlin Heidelberg New York, (1999)
210. R. Kühnemuth, C.A.M. Seidel, Principles of single molecule multiparameter fluorescence spectroscopy, *Single Molecules* **2**, 251-254 (2001)
211. H. Kume (ed.), *Photomultiplier Tube*, Hamamatsu Photonics K.K. (1994)
212. H. Kume, K. Koyama, N. Nakatsugawa, S. Suzuki, D. Fatlowitz, Ultrafast microchannel plate photomultipliers, *App. Opt.* **27**, 1170-1178 (1988)
213. C. Kurtsiefer, P. Zarda, S. Mayer, H. Weinfurter, The breakdown flash of Silicon Avalanche Photodiodes – backdoor for eavesdropper attacks?, *J. Mod. Opt.* **48**, 2039-2047 (2001)
214. E.S. Kwak, T.J. Kang, A.A. Vanden Bout, Fluorescence lifetime imaging with near-field scanning optical microscopy, *Anal. Chem.* **73**, 3257-3262 (2001)
215. P.G. Kwiat, A.M. Steinberg, R.Y. Chiao, P.H. Eberhard, M.D. Petroff, Absolute efficiency and time-response measurement of single-photon detectors, *Appl. Opt.* **33**, 1844-1853 (1994)
216. A. Lacaita, S. Cova, M. Ghioni, Four-hundred-picosecond single-photon timing with commercially available avalanche photodiodes, *Rev. Sci. Instrum.* **59**, 1115-1121 (1988)

217. L.H. Laiho, T.M. Hancewicz, P.D. Kaplan, P.T.C. So, Two-photon 3-D mapping of ex-vivo human skin endogenous fluorescence species based on fluorescence emission spectra. *J. Biomed. Opt.* **10**, 024016-1 to 10 (2005)
218. J.R. Lakowicz, I. Gryczynski, W. Wiczk, J. Kusba, M. Johnson, Correction for incomplete labeling in the measurement of distance distributions by frequency-domain fluorometry, *Anal. Biochem.* **195**, 243-254 (1991)
219. J.R. Lakowicz, H. Szmacinski, K. Nowaczyk, M.L. Johnson, Fluorescence lifetime imaging of free and protein-bound NADH, *PNAS* **89**, 1271-1275 (1992)
220. J.R. Lakowicz, Principles of Fluorescence Spectroscopy, 2nd edn., Plenum Press, New York (1999)
221. D.C. Lamb, A. Schenk, C. Röcker, C. Scalfi-Happ, G.U. Nienhaus, sensitivity enhancement in fluorescence correlation spectroscopy of multiple species using time-gated detection, *Biophys. J.* **79**, 1129-1138 (2000)
222. M. Lampton, R. Raffanti, A high-speed wide dynamic range time-to-digital converter, *Rev. Sci. Instrum.* **65**, 3577-3584 (1994)
223. B. Leskovar, C.C. Lo, Photon counting system for subnanosecond fluorescence lifetime measurements, *Rev. Sci. Instrum.* **47**, 1113-1121 (1976)
224. B. Leskovar, Nanosecond Fluorescence Spectroscopy, *IEEE Transactions on Nuclear Science*, **NS-32**, 1232-1241 (1985)
225. C. Lewis, W.R. Ware, The Measurement of Short-Lived Fluorescence Decay Using the Single Photon Counting Method, *Rev. Sci. Instrum.* **44**, 107-114 (1973)
226. L-Q. Li, L.M. Davis, Single photon avalanche diode for single molecule detection, *Rev. Sci. Instrum.* **64**, 1524-1529 (1993)
227. A Liebert, H. Wabnitz, J. Steinbrink, H. Obrig, M. Möller, R. Macdonald, H. Rinneberg, Intra- and extracerebral changes of hemoglobin concentrations by analysis of moments of distributions of times of flight of photons, *Proc. SPIE* **5138**, 126-130 (2003)
228. A. Liebert, H. Wabnitz, D. Grosenick, M. Möller, R. Macdonald, H. Rinneberg, Evaluation of optical properties of highly scattering media by moments of distributions of times of flight of photons, *Appl. Opt.* **42**, 5785-5792 (2003)
229. A. Liebert, H. Wabnitz, D. Grosenick, R. Macdonald, Fiber dispersion in time domain measurements compromising the accuracy of determination of optical properties of strongly scattering media, *J. Biomed. Opt.* **8**, 512-516 (2003).
230. A. Liebert, H. Wabnitz, M. Möller, A. Walter, R. Macdonald, H. Rinneberg, H. Obrig, I. Steinbrink, Time-resolved diffuse NIR-reflectance topography of the adult head during motor stimulation, In OSA Biomedical Optics Topical Meetings on CD ROM (The Optical Society of America, Washington, DC) WF34 (2004)
231. A. Liebert, H. Wabnitz, J. Steinbrink, H. Obrig, M. Möller, R. Macdonald, A. Villringer, H. Rinneberg, Time-resolved multidistance near-infrared spectroscopy at the human head: Intra- and extracerebral absorption changes from moments of distribution of times of flight of photons, *Appl. Opt.* **43**, 3037-3047 (2004)
232. A. Liebert, H. Wabnitz, J. Steinbrink, M. Möller, R. Macdonald, H. Rinneberg, A. Villringer, H. Obrig, Bed-side assessment of cerebral perfusion in stroke patients based on optical monitoring of a dye bolus by time-resolved diffuse reflectance, *NeuroImage* **24**, 426-435 (2005)
233. A. Lleo, O. Berezovska, L. Herl, S. Raju, A. Deng, B.J. Bacsikai, M.P. Frosch, M. Irizarry, B.T. Hyman, Nonsteroidal anti-inflammatory drugs lower $\text{A}\beta_{42}$ and change presenilin 1 conformation, *Nature Medicine* **10**, 1065-1066 (2004)
234. K. Määttä, J. Kostamovaara, A high precision time-to-digital converter for pulsed time-of-flight laser radar applications, *IEEE Transactions on Instrumentation and Measurement* **47**, 521-536 (1998)
235. D. Magde, E. Elson, W.W.W. Webb, Thermodynamic fluctuations in a reacting system - measurement by fluorescence correlation spectroscopy, *Phys. Rev. Lett.* **29**, 705-708 (1972)
236. C. Mangavel, R. Maget-Dana, P. Tauc, J-C. Brochon, D. Sy, J.A. Reynaud, Structural investigations of basic amphipatic model peptides in the presence of lipid vesicles studied by circular dichroism, fluorescence, monolayer and modeling, *Biochimica et Biophysica Acta* **1371**, 265-283 (1998)
237. J. Malicka, I. Gryczynski, C.D. Geddes, J.R. Lakowicz, Metal-enhanced emission from indocyanine green: a new approach to in vivo imaging, *J. Biomed. Opt.* **8**, 472-478 (2003)
238. J.S. Massa, G.S. Buller, A.C. Walker, S. Cova, M. Umasuthan, A.M. Wallace, Time-of-flight optical ranging system based on time-correlated single photon counting, *Appl. Opt.* **37**, 7298-7304 (1998)
239. J.S. Massa, G.S. Buller, A.C. Walker, G. Smith, S. Cova, M. Umasuthan, A.M. Wallace, Optical design and evaluation of a three-dimensional imaging and ranging system based on time-correlated single-photon counting, *Appl. Opt.* **41**, 1070-1063 (2002)
240. K. Maxwell, G.N. Johnson, Chlorophyll fluorescence - a practical guide, *Journal of Experimental Botany* **51**, 659-668 (2000)

241. T.O. McBride, B.W. Pogue, E.D. Gerety, S.B. Poplack, U.L. Österberg, K.D. Paulsen, Spectroscopic diffuse optical tomography for the quantitative assessment of hemoglobin concentration and oxygen saturation in breast tissue, *Appl. Opt.* **38**, 5480-5490 (1999)
242. W. Meiling, F. Stary, Nanosecond pulse techniques, Akademie-Verlag, Berlin (1963)
243. E.C. Meister, U.P. Wild, P. Klein-Böting, A.R. Holzwarth, Time response of small side-on photomultiplier tubes in time-correlated single-photon counting measurements, *Rev. Sci. Instrum.* **59**, 499-501 (1988)
244. J.S. Melinger, L.D. Davis, D. McMorrow, Y. Pan, Z. Peng, Photoluminescence properties of conjugated phenylacetylene monodendrons in thin films, *J. Fluoresc.* 105-112 (2004)
245. P. Michler, A. Imamoglu, M.D. Mason, P.J. Carson, G.F. Strouse, S.K. Buratto, Quantum correlation among photons from a single quantum dot at room temperature, *Nature* **406**, 968-970 (2000)
246. M. Micic, D. Hu, Y.D. Suh, G. Newton, M. Romine, H.P. Lu, Correlated atomic force microscopy and fluorescence lifetime imaging of live bacterial cells, *Colloids and Surfaces B, Biointerfaces* **34**, 205-212 (2004)
247. Micro Photon Devices, PDM Series photon counting modules, www.micro-photon-devices.com
248. K.D. Mielenz, E.D. Cehelink, R.L. McKenzie, Elimination of polarization bias in fluorescence intensity measurements, *J. Chem. Phys.* **62**, 370-374 (1976)
249. A. Migdall, Absolute quantum efficiency measurements using correlated photons: Toward a measurement protocol, *IEEE Trans. on Instrumentation and Measurement* **50**, 478-481 (2001)
250. A. Migdall, S. Castelletto, I.P. Degiovanni, M.L. Rastello, Intercomparison of a correlated-photon-based method to measure detector quantum efficiency, *Appl. Opt.* **41**, 2914-2922 (2002)
251. A.L. Migdall, R.U. Datla, A. Sergienko, J.S. Orszak, Y.H. Shih, Absolute detector quantum-efficiency measurements using correlated photons, *Metrologia* **32**, 479-483 (1995)
252. W. Min, G. Luo, B. J. Cherayil, S.C. Kou, X.S. Xie, Observation of a power-law memory kernel for fluctuations within a single protein molecule, *Phys. Chem. Lett.* 94 198302 (2005)
253. M. Minsky, Memoir on inventing the confocal microscope, *Scanning* **10**, 128-138 (1988)
254. K. Miyashita, S. Kuroda, S. Tajima, K. Takehira, S. Tobita, H. Kubota, Photoluminescence Study of Electron-Hole Recombination Dynamics in the Vacuum-Deposited SiO₂/TiO₂ Multilayer Film with Photo-Catalytic Activity, *Chem. Phys. Lett.* **369**, 225-231 (2003)
255. J. Mobley, T. Vo-Dinh, Optical properties of tissue, in T. Vo-Dinh (ed.) *Biomedical Photonics Handbook*, CRC Press, 53-1 to 53-48 (2003)
256. S. Mordon, J.M. Devoisselle, S. Soulie-Begu, Indocyanine Green: Physicochemical Factors Affecting Its Fluorescence in Vivo, *Microvascular Research* **55**, 146 (1998)
257. P.E. Morton, T.C. Ng, S.A. Roberts, B. Vojnovic, S.M. Ameer-Beg, Time resolved multiphoton imaging of the interaction between the PKC and NFkB signalling pathways, *Proc. SPIE* **5139**, 216-222 (2003)
258. J.D. Müller, Y. Chen, E. Gratton, Resolving Heterogeneity on the single molecular level with the photon-counting histogram, *Biophys. J.* **78**, 474-586 (2000)
259. R. Müller, C. Zander, M. Sauer, M. Deimel, D-S. Ko, S. Sieberte, J. Arden-Jacob, G. Deltau, N.J. Marx, K.H. Drexhage, J. Wolfrum, Time-resolved identification of single molecules in solution with a pulsed semiconductor diode laser, *Chem. Phys. Lett.* **262**, 716-722 (1996)
260. E. Nachliel, N. Pollak, D. Huppert, M. Gutman, Time-Resolved Study of the Inner Space of Lactose Permease, *Biophys. J.* **80**, 1498-1506 (2001)
261. V. Ntziachristos, X.H. Ma, B. Chance, Time-correlated single-photon counting imager for simultaneous magnetic resonance and near-infrared mammography, *Rev. Sci. Instrum.* **69**, 4221-4233 (1998)
262. V. Ntziachristos, X.H. Ma, A.G. Yodh, B. Chance, Multichannel photon counting instrument for spatially resolved near infrared spectroscopy, *Rev. Sci. Instrum.* **70**, 193-201 (1999)
263. V. Ntziachristos, A.G. Yodh, M. Schnall, B. Chance, Concurrent MRI and diffuse optical tomography of breast after indocyanine green enhancement, *PNAS* **97**, 2767-2772 (2000)
264. V. Ntziachristos, B. Chance, Accuracy limits in the determination of absolute optical properties using time-resolved NIR spectroscopy, *Med. Phys.* **28**, 1115-1124 (2001)
265. D.V. O'Connor, D. Phillips, Time-correlated single photon counting, Academic Press, London (1984)
266. B. Ohnesorge, R. Weigand, G. Bacher, A. Forchel, Minority-carrier lifetime and efficiency of Cu(In, Ga)Se₂ solar cells, *Appl. Phys. Lett.* **73**, 1224-1226 (1998)
267. K. Palo, L. Brand, C. Eggeling, S. Jäger, P. Kask, K. Gall, Fluorescence intensity and lifetime distribution analysis: Toward higher accuracy in fluorescence fluctuation spectroscopy, *Biophys. J.* **83**, 605-617 (2002)
268. K. Palo, Ü. Mets, S. Jäger, P. Kask, K. Gall, Fluorescence intensity multiple distribution analysis: concurrent determination of diffusion times and molecular brightness, *Biophys. J.* **79**, 2858-2866 (2000)

269. D.A. Parul, S.B. Bokut, A.A. Milyutin, E.P. Petrov, N.A. Nemkovich, A.N. Sobchuk, B.M. Dzhagarov, Time-resolved fluorescence reveals two binding sites of 1, 8-ANS in intact human oxyhemoglobin, *Journal of Photochemistry and Photobiology B: Biology* **58**, 156-162 (2000)
270. G.H. Patterson, D.W. Piston, Photobleaching in two-photon excitation microscopy, *Biophys. J.* **78**, 2159-2162 (2000)
271. M.S. Patterson, B. Chance, B.C. Wilson, Time-resolved reflectance and transmittance for the noninvasive measurement of tissue optical properties, *Appl. Opt.* **28**, 2331-2336 (1989)
272. R.J. Paul, H. Schneckenburger, Oxygen concentration and the oxidation-reduction state of yeast: Determination of free/bound NADH and flavins by time-resolved spectroscopy, *Naturwissenschaften* **83**, 32-35 (1996)
273. J. Pawley (ed.), *Handbook of biological confocal microscopy*, 2nd edn., Plenum Press, New York (1995)
274. S. Pelet, M.J.R. Previde, P.T.C. So, Comparing the quantification of Förster resonance energy transfer measurement accuracies based on intensity, spectral, and lifetime imaging. *J. Biomed. Opt.* 11 034017-1 to -11 (1006)
275. A. Periasamy, *Methods in Cellular Imaging*. Oxford University Press, Oxford New York (2001)
276. M.J.B. Pereira, D.A. Harris, D. Rueda, N.G. Walter, Reaction pathway of the trans-acting hepatitis delta virus ribozyme: A conformational change accompanies catalysis, *Biochemistry* **41**, 730-740 (2002)
277. M. Peter, S.M. Ameer-Beg, Imaging molecular interactions by multiphoton FLIM, *Biology of the Cell* **96**, 231-236 (2004)
278. M. Peter, S.M. Ameer-Beg, M.K.Y. Hughes, M.D. Keppler, S. Prag, M. Marsh, B. Vojnovic, T. Ng, Multiphoton-FLIM quantification of the EGFP-mRFP1 FRET pair for localization of membrane receptor-kinase interactions, *Biophys. J.* **88**, 1224-1237 (2005)
279. E.P. Petrov, J.V. Kruchenok, A.N. Rubinov, Effects of the external refractive index on fluorescence kinetics of perylene in human erythrocyte ghosts, *J. Fluoresc.* **9**, 111-121 (1999)
280. Perkin Elmer Optoelectronics, Single photon counting module, SPCM-AQR series.
www.perkinelmer.com
281. J.P. Philip and K. Carlsson, Theoretical investigation of the signal-to-noise ratio in fluorescence lifetime imaging, *J. Opt. Soc. Am. A* **20**, 368-379 (2003)
282. A. Pifferi, A. Torricelli, P. Taroni, R. Cubeddu, Reconstruction of absorber concentrations in a two-layer structure by use of multidistance time-resolved reflectance spectroscopy, *Opt. Lett.* **26**, 1963-1965 (2001)
283. A. Pifferi, P. Taroni, A. Torricelli, F. Messina, R. Cubeddu, Four-wavelength time-resolved optical mammography in the 680-980-nm range, *Opt. Lett.* **28**, 1138-1140 (2003)
284. A. Pifferi, A. Torricelli, P. Taroni, A. Bassi, E. Chikoidze, E. Gambatistelli, R. Cubeddu, Optical biopsy of bone tissue: A step toward the diagnosis of bone pathologies. *J. Biomed. Opt.* **9**, 474-480 (2004)
285. A. Pifferi, J. Swartling, E. Chikoidze, A. Torricelli, P. Taroni, A. Bassi, S. Andersson-Engels, R. Cubeddu, Spectroscopic time-resolved diffuse reflectance and transmittance measurements of the female breast at different interfibre distances, *J. Biomed. Opt.* **9**, 1143-1151
286. M. Prummer, C. Hübner, B. Sick, B. Hecht, A. Renn, U.P. Wild, Single-molecule identification by spectrally and time-resolved fluorescence detection, *Anal. Chem.* **72**, 433-447 (2000)
287. M. Prummer, B. Sick, A. Renn, U.P. Wild, Multiparameter microscopy and spectroscopy for single-molecule analysis, *Anal. Chem.* **76**, 1633-1640 (2004)
288. H. Qian, E.L. Elson, Distribution of molecular aggregation by analysis of fluctuation moments, *PNAS* **87**, 5479-5483 (1990)
289. V. Quaresima, M. Ferrari, A. Torricelli, L. Spinelli, A. Pifferi, R. Cubeddu, Bilateral prefocal cortex oxygenation responses to a verbal fluency task: a multichannel time-resolved near-infrared topography study, *J. Biomed. Opt.* 10 (2005), in press.
290. J.G. Rarity, K.D. Ridley, P.R. Tapster, Absolute measurement of detector quantum efficiency using parametric downconversion, *Appl. Opt.* **26**, 4616-4619 (1987)
291. I. Rech, G. Luo, M. Ghioni, H. Yang, X.S. Xie, S. Cova, Photon-timing detector module for single-molecule spectroscopy with 60-ps resolution, *IEEE Journal of selected topics in quantum electronics* **10**, 788-795 (2004)
292. B. Richards, E. Wolf, Electromagnetic diffraction in optical systems II. Structure of the image field in an aplanatic system, *Proc. Roy. Soc. A* **253**, 358-379 (1959)
293. I. Riemann, P. Fischer, M. Kaatz, T.W. Fischer, P. Elsner, E. Dimitrov, A. Reif, K. König, Optical tomography of pigmented human skin biopsies, *Proc. SPIE* **5312**, 24-34 (2004)
294. R. Rigler, E.S. Elson (eds), *Fluorescence Correlation Spectroscopy*, Springer Verlag Berlin, Heidelberg, New York (2001)
295. R. Rigler, Ü. Mets, J. Widengren, P. Kask, Fluorescence correlation spectroscopy with high count rate and low background: analysis of translational diffusion, *European Biophysics Journal* **22**, 169-175 (1993)
296. R. Rigler, J. Widengren, Ultrasensitive detection of single molecules by fluorescence correlation spectroscopy, *Bioscience* **3**, 180-183 (1990)

297. R. Richards-Kortum, R. Drezek, K. Sokolov, I. Pavlova, M. Follen, Survey of endogenous biological fluorophores. In M.-A. Mycek, B.W. Pogue (eds.), *Handbook of Biomedical Fluorescence*, Marcel Dekker Inc. New York, Basel, 237-264 (2003)
298. B. Riquelme, D. Dumas, J. Valverde, R. Rasia, J.F. Stoltz, Analysis of the 3D structure of agglutinated erythrocyte using CellScan and Confocal microscopy: Characterisation by FLIM-FRET, *Proc. SPIE* **5139**, 190-198 (2003)
299. L. Rovati, F. Docchio, Autofluorescence methods in ophthalmology, *J. Biomed. Opt.* **9**, 9-21 (2004)
300. A. Rück, F. Dolp, C. Happ, R. Steiner, M. Beil, Fluorescence lifetime imaging (FLIM) using ps-pulsed diode lasers in laser scanning microscopes, *Proc. SPIE* **4962**, 160-167 (2003)
301. A. Rück, F. Dolp, C. Happ, R. Steiner, M. Beil, Time-resolved microspectrofluorometry and fluorescence lifetime imaging using ps pulsed laser diodes in laser scanning microscopes, *Proc. SPIE* **5139**, 166-172 (2003)
302. A. Rück, F. Dolp, C. Hülshoff, C. Hauser, C. Scalfi-Happ, FLIM and SLIM for molecular imaging in PDT, *Proc. SPIE* **5700** (2005)
303. A. Rück, F. Dolp, C. Hülshoff, C. Hauser, C. Scalfi-Happ, Fluorescence lifetime imaging in PDT. An overview, *Medical Laser Application* **20**, 125-129 (2005)
304. R. Sanders, A. Draaijer, H.C. Gerritsen, P.M. Houpt, Y.K. Levine, Quantitative pH Imaging in cells using confocal fluorescence lifetime imaging microscopy, *Analytical Biochemistry* **227**, 302-308 (1995)
305. A. Saxena, J.B. Udgaonkar, G. Krishnamoorthy, Protein dynamics and protein folding revealed by time-resolved fluorescence, in M. Hof, R. Hutterer, V. Fidler, *Fluorescence spectroscopy in biology*, Springer Verlag Berlin Heidelberg New York 1-29(2005)
306. M. Sauer, C. Zander, R. Müller, B. Ullrich, S. Kaul, K.H. Drexhage, J. Wolfrum, Detection and identification of individual antigen molecules in human serum with pulsed semiconductor lasers, *Appl. Phys. B* **65**, 427-431 (1997)
307. J. Schaffer, A. Volkmer, C. Eggeling, V. Subramaniam, G. Striker, C.A.M. Seidel, Identification of single molecules in aqueous solution by time-resolved fluorescence anisotropy, *J. Phys. Chem. A* **103**, 331-336 (1999)
308. F.E.W. Schmidt, M.E. Fry, E.M.C. Hillman, J.C. Hebden, D.T. Delpy, A 32-channel time-resolved instrument for medical optical tomography, *Rev. Sci. Instrum.* **71**, 256-265 (2000)
309. A. Schönle, M. Glatz, S.W. Hell, Four-dimensional multiphoton microscopy with time-correlated single photon counting, *Appl. Opt.* **39**, 6306-6311 (2000)
310. R. Schuyler, I. Isenberg, A Monophoton Fluorometer with Energy Discrimination, *Rev. Sci. Instrum.* **42**, 813-817 (1971)
311. D. Schweitzer, A. Kolb, M. Hammer, E. Thamm, Tau-mapping of the autofluorescence of the human ocular fundus, *Proc. SPIE* **4164**, 79-89 (2000)
312. D. Schweitzer, A. Kolb, M. Hammer, Autofluorescence lifetime measurement in images of the human ocular fundus, *SPIE* **4432**, 29-39 (2001)
313. D. Schweitzer, A. Kolb, M. Hammer, E. Thamm, Basic investigations for 2-dimensional time-resolved fluorescence measurements at the fundus, *Int. Ophthalmol.* **23**, 399-404 (2001)
314. D. Schweitzer, A. Kolb, M. Hammer, R. Anders, Zeitaufgelöste Messung der Autofluoreszenz, *Ophthalmologe* **99**, 776-779 (2002)
315. D. Schweitzer, M. Hammer, F. Schweitzer, R. Anders, T. Doebbecke, S. Schenke, E. R. Gaillard, In vivo measurement of time-resolved autofluorescence at the human fundus, *J. Biomed. Opt.* **9**, 1214-1222 (2004)
316. D. Schweitzer, M. Hammer, F. Schweitzer, S. Schenke, E. Birckner, W. Becker, A. Bergmann, In vivo autofluorescence lifetime imaging at the fundus of the human eye. *Proc. SPIE* **6138** (2006)
317. P. Schwille, Cross-correlation analysis in FCS, in R. Rigler, E.S. Elson (eds.) *Fluorescence correlation spectroscopy*, Springer Verlag Berlin, Heidelberg, New York, 360-378 (2001)
318. P. Schwille, F.J. Meyer-Almes, R. Rigler, Dual-color fluorescence cross-correlation spectroscopy for multicomponent diffusional analysis in solution, *Biophys. J.* **72**, 1878-1886 (1997)
319. P. Schwille, U. Haupts, S. Maiti, W.W.W. Webb, Molecular Dynamics in Living Cells Observed by Fluorescence Correlation Spectroscopy with One- and Two-Photon Excitation, *Biophys. J.* **77**, 2251-2265 (1999)
320. P. Schwille, S. Kummer, A.H. Heikal, W.E. Moerner, W.W.W. Webb, Fluorescence correlation spectroscopy reveals fast optical excitation-driven intramolecular dynamics of yellow fluorescent proteins, *PNAS* **97**, 151-156 (2000)
321. SENSL Technologies Ltd., PCMPlus: Intelligent photon counting module, www.sensl.com
322. E.M. Sevick-Muraca, A. Godavarty, J.P. Houston, A.B. Thompson, R. Roy, Near-infrared imaging with fluorescence contrast agents. In M.-A. Mycek, B.W. Pogue (eds.), *Handbook of Biomedical Fluorescence*, Marcel Dekker New York, Basel, 445-527 (2003)

323. P.F. Sharp, A. Manivannan, H. Xu, J.V. Forrester, The scanning laser ophthalmoscope - a review of its role in bioscience and medicine, *Physics in Medicine & Biology* **49**, 1085 (2004)
324. S. Shiobara, R. Kamiyama, S. Tajima, H. Shizuka, S. Tobita, Excited-state proton transfer to solvent of protonated aniline derivatives in aqueous solution: a remarkable effect of ortho alkyl group on the proton-dissociation rate, *J. Photochem. Photobiol. A* **154**, 53-60 (2002)
325. S. Shiobara, S. Tajima, S. Tobita, Substituent effects on ultrafast excited-state proton transfer of protonated aniline derivatives in aqueous solution, *Chem. Phys. Lett.* **380**, 673-680 (2003)
326. B. Sick, B. Hecht, Orientation of single molecules by annular illumination, *Phys. Rev. Lett.* **85**, 4482-4485 (2000)
327. B. Sick, B. Hecht, U.P. Wild, L. Novotny, Probing confined fields with single molecules and vice versa, *J. Microsc.* **202**, 365-373 (2001)
328. M. Snippe, J.W. Borst, R. Goldbach, R. Kormelik, The use of fluorescence microscopy to visualise homotypic interactions of tomato spotted wilt virus nucleocapsid protein in living cells, *J. Vir. Meth.* **125**, 12-15 (2005)
329. P.T.C. So, K.H. Kim, L. Hsu, P. Kaplan, T. Hacewicz, C.Y. Dong, U. Greuter, N. Schlumpf, C. Buehler, Two-photon microscopy of tissues, in M.-A. Mycek, B.W. Pogue (eds.), *Handbook of Biomedical Fluorescence*, Marcel Dekker, New York, Basel, 181-208 (2003)
330. U. Solbach, C. Keilhauer, H. Knabben, S. Wolf, Imaging of retinal autofluorescence in patients with age-related macular degeneration, *Retina* **17**, 385-389 (1997)
331. R.D. Spencer, G. Weber, Influence of brownian rotations and energy transfer upon the measurement of fluorescence lifetime, *J. Chem. Phys.* **52** 1654-1663 (1970)
332. L. Spinelli, A. Torricelli, A. Pifferi, P. Taroni, R. Cubeddu, Experimental test of a perturbation model for time-resolved imaging in diffuse media, *Appl. Opt.* **42**, 3145-3153 (2003)
333. L. Spinelli, A. Torricelli, A. Pifferi, P. Taroni, R. Cubeddu, Bulk optical properties and tissue components in the female breast from multiwavelength time-resolved optical mammography, *J. Biomed. Opt.* **9**, 1137-1142 (2004)
334. J. Steinbrink, H. Wabnitz, H. Obrig, A. Villringer, H. Rinneberg, Determining changes in NIR absorption using a layered model of the human head, *Phys. Med. Biol.* **46**, 879-896 (2001)
335. C.D. Stubbs, S.W. Botchway, S.J. Slater, A.W. Parker, The use of time-resolved fluorescence imaging in the study of protein kinase C localisation in cells. *BioMed Central* 6:22 (2005), available on www.biomedcentral.com/1471-2121/6/22
336. K. Suhling, D. McLoskey, D.J.S. Birch, Multiplexed single-photon counting. II. The statistical theory of time-correlated measurements. *Rev. Sci. Instrum.* **67**, 2230-2246, (1996)
337. K. Suhling, D.M. Davis, Z. Petrasek, J. Siegel, D. Phillips, The influence of the refractive index on EGFP fluorescence lifetimes in mixtures of water and glycerol, *Proc. SPIE* **4259**, 91-101 (2001)
338. K. Suhling, J. Siegel, D. Phillips, P.M.W. French, S. Lévéque-Fort, S.E.D. Webb, D.M. Davis, Imaging the environment of green fluorescent protein, *Biophysical J.* **83**, 3589-3595 (2002)
339. S. Tajima, S. Shiobara, H. Shizuka, S. Tobita, Excited-state proton-dissociation of N-alkylated anilinium ions in aqueous solution studied by picosecond fluorescence measurements *Phys. Chem. Chem. Phys.* **4**, 3376-3382 (2002)
340. P. Taroni, G. Danesini, A. Torricelli, A. Pifferi, L. Spinelli, R. Cubeddu, Clinical trial of time-resolved scanning optical mammography at 4 wavelengths between 683 and 975 nm, *J. Biomed. Opt.* **9**, 464-473 (2004)
341. P. Taroni, A. Pifferi, A. Torricelli, L. Spinelli, G.M. Danesini, R. Cubeddu, Do shorter wavelength improve contrast in optical mammography?, *Phys. Med. Biol.* **49**, 1203-1215 (2004)
342. P. Tauc, C.R. Mateo, J-C. Brochon, Pressure effects on the lateral distribution of cholesterol in lipid bilayers: A time-resolved spectroscopy study, *Biophys. J.* **74**, 1864-1870 (1998)
343. P. Tauc, C.R. Mateo, J-C. Brochon, Investigation of the effect of high hydrostatic pressure on proteins in lipid membranes by dynamic fluorescence spectroscopy, *Biochim. Biophys. Acta* **1595**, 103-115 (2002)
344. P. Theer, M.T. Hasan, W. Denk, Multi-photon imaging using a Ti:sapphire regenerative amplifier, *Proc. SPIE* **5139**, 1-6 (2003)
345. N.L. Thomson, J.L. Mitchell, High order autocorrelation, in R. Rigler, E.S. Elson (eds.), *Fluorescence Correlation Spectroscopy*, Springer Verlag, Berlin, Heidelberg, New York 438-458 (2001)
346. R.M. Thompson, R.M. Stevenson, A.J. Shields, I. Farrer, C.J. Lobo, D.A. Ritchie, M.L. Leadbeater, M. Pepper, Single-photon emission from exciton complexes in individual quantum dots, *Physical Review B* **64**, 1-4 (2001)
347. P. Tinnefeld, V. Buschmann, D-P. Herten, K.T. Han, M. Sauer, Confocal fluorescence lifetime imaging microscopy (FLIM) at the single molecule level, *Single Mol.* **1**, 215-223 (2000)
348. U.K. Tirlapur, K. König, Targeted transfection by femtosecond laser, *Nature* **418**, 290-291 (2002)

349. V. Toronov, M.A. Franceschini, M. Filiaci, S. Fantini, M. Wolf, A. Michalos, E. Gratton, Near-infrared study of fluctuations in cerebral hemodynamics during rest and motor stimulation. *Med. Phys.* **27**, (801-815) (2000)
350. V. Toronov, A. Webb, J. H. Choi, M. Wolf, L. Safanova, U. Wolf, E. Gratton, Study of local cerebral hemodynamics by frequency-domain near-infrared spectroscopy and correlation with simultaneously acquired functional magnetic resonance imaging, *Opt. Expr.* **9**, 417-427 (2001)
351. A. Torricelli, A. Pifferi, P. Taroni, E. Giambattistelli, R. Cubeddu, In vivo optical characterization of human tissue from 610 to 1010 nm by time-resolved reflectance spectroscopy, *Phys. Med. Biol.* **46**, 2227-2237 (2001)
352. A. Torricelli, L. Spinelli, A. Pifferi, P. Taroni, R. Cubeddu, Use of a nonlinear perturbation approach for in vivo breast lesion characterization by multi-wavelength time-resolved optical mammography, *Opt. Expr.* **11**, 853-867 (2003)
353. A. Torricelli, V. Quaresima, A. Pifferi, G. Biscotti, L. Spinelli, P. Taroni, M. Ferrati, R. Cubeddu, Mapping of calf muscle oxygenation and haemoglobin content during dynamic plantrat flexion exercise by multi-channel time-resolved near-infrared spectroscopy, *Phys. Med. Biol.* **49**, 685-699 (2004)
354. B. Treanor, P.M.P. Lanigan, K. Suhling, T. Schreiber, I. Munro, M.A.A. Neil, D. Phillips, D.M. Davis, P.M.W. French, Imaging fluorescence lifetime heterogeneity applied to GFP-tagged MHC protein at an immunological synapse, *J. Microsc.* **217**, 36-43 (2005)
355. V. Ulrich, P. Fischer, I. Riemann, K. König, Compact multiphoton / single photon laser scanning microscope for spectral imaging and fluorescence lifetime imaging, *Scanning* **26**, 217-225 (2004)
356. G. Ulu, A.V. Sergienko, M.S. Ünlü, Influence of hot-carrier luminescence from avalanche photodiodes on time-correlated photon detection, *Opt. Lett.* **25**, 758-760 (2000)
357. M. Umasuthan, A.M. Wallace, J.S. Massa, G.S. Buller, A.C. Walker, Processing time-correlated single photon counting data to acquire range images, *IEEE Proc. Vis. Image Signal Process.* **145**, 237-243 (1998)
358. P.A.W. Van den Berg, A. van Hoek, C.D. Walentas, R.N. Perham, A.J.W.G. Visser, Flavin Fluorescence Dynamics and Photoinduced Electron Transfer in Escherichia coli Glutathione Reductase, *Biophys. J.* **74**, 2046-2058 (1998)
359. M.A.M.J. Van Zandvoort, C.J. de Grauw, H.C. Gerritsen, J.L.V. Broers, M.G.A. Egbrink, F.C.S. Ramaekers, D.W. Slaaf, Discrimination of DNA and RNA in cells by a vital fluorescent probe: Lifetime imaging of SYTO13 in healthy and apoptotic cells, *Cytometry* **47**, 226-232 (2002)
360. A. Volkmer, D.A. Hatruck, D.J.S. Birch, Time-resolved nonlinear fluorescence spectroscopy using femtosecond multiphoton excitation and single-photon timing, *Meas. Sci. Technol.* **8**, 1339-1349 (1997)
361. A. Volkmer, V. Subramaniam, D.J.S. Birch, T.M. Jovin, One- and two-photon excited fluorescence lifetimes and anisotropy decays of green fluorescent proteins, *Biophys. J.* **78**, 1589 (2000)
362. H. Wabnitz, H. Rinneberg, Imaging in turbid media by photon density waves: spatial resolution and scaling relations, *Appl. Opt.* **36**(1), 64-74 (1997)
363. H. Wabnitz, A. Liebert, M. Möller, D. Grosenick, R. Model, H. Rinneberg, Scanning laser-pulse mammography: matching fluid and off-axis measurements. *Biomedical Topical Meetings, Technical Digest, OSA* 686 (2002)
364. H. Wabnitz, D. Grosenick, M. Möller, J. Stössel, B. Wassermann, R. Macdonald, K.T. Moesta, H. Rinneberg, Scanning laser-pulse mammography: matching fluid and off-axis measurements, In *OSA Biomedical Optics Topical Meetings on CD ROM* (The Optical Society of America, Washington, DC) (2004)
365. H.E. Wagner, R. Brandenburg, K.V. Kozlov, Cross correlation emission spectroscopy: application to non-equilibrium plasma diagnostics, *Proceedings of Frontiers in Low Temperature Plasma Diagnostics V* (2003)
366. H.E. Wagner, R. Brandenburg, K.V. Kozlov, A. Sonnenfeld, P. Michel, J.F. Behnke, The barrier discharge: Basic properties and applications to surface treatment, *Vacuum* **71**, 417-436 (2003)
367. H.E. Wagner, R. Brandenburg, K.V. Kozlov, Progress in the visualisation of filamentary gas discharges, part1: Milestones and diagnostics of dielectric-barrier discharges by cross-correlation, *Journal of Advanced Oxidation Technologies* **7**, 11-19 (2004)
368. A.M. Wallace, G.S. Buller, A.C. Walker, 3D imaging and ranging by time-correlated single photon counting, *Computing & Control. IEE Computing and Control Engineering Journal* **12**, 157-168 (2001)
369. M. Ware, A. Migdall, Single-photon detector characterization using correlated photons: The march from feasibility to metrology, *Journal of Modern Optics* **51**, 1549-1557 (2004)
370. K.D. Weston, M. Dyck, P. Tinnefeld, C. Müller, D.P. Herten, M. Sauer, Measuring the number of independent emitters in single molecule fluorescence images and trajectories using coincident photons, *Anal. Chem.* **74**, 5342-5349 (2002)

371. R.W. Wijnaendts van Resandt, R.H. Vogel, S.W. Provencher, Double beam fluorescence lifetime spectrometer with subnanosecond resolution: Application to aqueous tryptophan, *Rev. Sci. Instrum.* **53**, 1392-1397 (1982)
372. O.M. Williams, W.J. Sandle, A 'pile-up' gate generator for removing distortion in multichannel delayed coincidence experiments, *Phys. Sci. Instrum.* **3**, 741-743 (1970)
373. B.C. Wilson, A.L. Jaques, Optical reflectance and transmittance of tissues: Principles and application, *IEEE Journal of Quantum Electronics* **26**, 2186-2199 (1990)
374. J.G. White, W.B. Amos, M. Fordham, An evaluation of confocal versus conventional imaging of biological structures by fluorescence light microscopy, *J. Cell Biol.* **105**, 41-48 (1987)
375. D. Wrobel, I. Hanyz, Charged porphyrin - dopa melanin interaction at varied pH: Fluorescence lifetime and photothermal studies, *J. Fluoresc.* **13**, 169-177 (2003)
376. Y. Wu, Y. Qu, Combined depth- and time-resolved autofluorescence spectroscopy of epithelial tissue, *Opt. Lett.* **31**, 1833-1835 (2006)
377. I. Yamazaki, N. Tamai, H. Kume, H. Tsuchiya, K. Oba, Microchannel-plate photomultiplier applicability to the time-correlated photon-counting, *Rev. Sci. Instrum.* **56**, 1187-1194 (1985)
378. H. Yang, X.S. Xie, Probing single-molecule dynamics photon by photon, *J. Chem. Phys.* **117**, 10965-10979 (2002)
379. J. Yguerabide, Nanosecond fluorescence spectroscopy of macromolecules, *Meth. Enzymol.* **26**, 498-578 (1972)
380. T. Yoshihara, H. Shimada, H. Shizuka, S. Tobita, Internal conversion of o-aminoacetophenone in solution, *Phys. Chem. Chem. Phys.* **3**, 4972-4978 (2001)
381. R. Yusada, C.D. Harvey, H. Zhong, A. Sobczyk, L. van Aelst, K. Svoboda, Supersensitive Ras activation in dendrites and spines revealed by two-photon fluorescence lifetime images, *Nature Neuroscience* **9** (2), 238-291 (2006)
382. K.S. Youngworth, T.G. Brown, Focusing of high numerical aperture cylindrical-vector beams, *Opt. Expr.* **7**, 77-87 (2000)
383. H. Yang, G. Luo, P. Karnchanaphanurach, T.-M. Louie, I. Rech, S. Cova, L. Xun, X.S. Xie, Protein conformational dynamics probed by single-molecule electron transfer, *Science* **302**, 262-266 (2003)
384. Z. Yuan, B. Kardynal, R.M. Stevenson, A.J. Shields, C.J. Lobo, K. Cooper, N.S. Beattie, D.A. Ritchie, M. Pepper, Electrically driven Single-Photon Source, *Science* **295**, 102-105 (2002)
385. C. Zander, M. Sauer, K.H. Drexhage, D-S. Ko, A. Schulz, J. Wolfrum, L. Brand, C. Eggeling, C.A.M. Seidel, Detection and characterisation of single molecules in aqueous solution, *Appl. Phys. B* **63**, 517-523 (1996)
386. C. Zander, K.H. Drexhage, K-T. Han, J. Wolfrum, M. Sauer, Single-molecule counting and identification in a microcapillary, *Chem. Phys. Lett.* **286**, 457-465 (1998)
387. V. Zwiller, H. Blom, P. Jonsson, N. Panev, S. Jeppesen, T. Tsegaye, E. Goobar, M.E. Pisto, L. Samuelson, G. Björk, Single quantum dots emit single photons at a time: Antibunching experiments, *Appl. Phys. Lett.* **78**, 2476-2478 (2001)

This page intentionally blank.

Index

- 2D Data Processing 324
- 2D Display Parameters 302
- 2D FIDA 223
- 3D Curve Display, display parameters) 303
- 3D curve mode 302, 325
- 3D Data Processing 328
- 3D Display 325
- 3D Display Parameters 302
- 3D display parameters, mode selection 304
- 3D display parameters, window selection 305
- 3D trace parameters 311
- Absorption coefficient 192
- Absorption of biological tissue 187
- Accumulate 257, 258, 260, 262, 265, 267, 271, 275, 279, 289
- Acquisition time
 - dynamic brain imaging 194
 - of TCSPC 19
 - of TCSPC FLIM 172
 - ophthalmic FLIM 201
 - scanning mammography 191
 - static brain imaging 192
- Active quenching of SPAD 53
- Adapters 13
- ADC 20, 36, 48
 - dither range 296
 - dithering 48
 - error correction 48
 - Resolution 49, 294
 - Zoom 294
 - zoom function 50
- Add / Sub Signal 290
- Adjust Parameters 321
- Afterpulsing, of PMTs 60, 139, 213
- Aggregates 164, 185
- Amplifiers
 - biased, in TAC 20
 - for detector signals 73
 - preamplifiers 11, 73
- Amplitude distribution 55, 120
 - of single photon pulses 55, 120
- Analog-to-digital conversion 48
- Analog-to-digital converter 20
- Anisotropy decay 144, 151
- Anisotropy, of fluorescence 154
- Anode luminous sensitivity 58
- Anti-bunching 203
 - by CW excitation 204
 - by pulsed excitation 204
 - technical aspects 205
- APD 205, 213
 - gain 52
 - geiger mode 52
 - light emission from 53
 - quenching 53
 - single-photon 52
- Aperture Stops 143
- A-PPI pulse inverter 13, 94, 95
- Assistance through bh 347
- Autocorrelation function, in FCS 207
- Autofluorescence 164
 - lifetime 183, 199
 - lifetime imaging 199
 - multi-wavelength measurement 199
- of tissue 183, 199
- single-point measurement 199
- two-photon excitation 199
- Autosave 255, 257, 258, 260, 262, 265, 267, 289
- Avalanche Photodiodes 69
- Background suppression 157
- Background, caused by afterpulsing 61
- Baffles 143
- Ballistic photons 187
- Banks, of memory 29, 40, 266, 267, 277
- Barrier discharges 226
- BCECF 177
- Beamsplitters, dichroic 152
- Biased amplifier 20
- BIFL 32, 219
- Block Info 241, 310
- Block mode, of 2D display 302, 307, 309
- Blocking filter, for 2p excitation 167, 169
- Brain imaging 187
- Brain imaging, dynamic 193
- Brain imaging, static 192
- Broken cables, electrical shock 76
- Cathode luminous sensitivity 58
- Cathode quantum efficiency 58
- Cathode radiant sensitivity 58
- CFD 42
 - cable length 124
 - configuration 118
 - delay lines 118
 - hold 292
 - limit high 292
 - limit low 292
 - parameters 292
 - positive input 119
 - pulse shaping 118
 - threshold 110, 120, 292
 - zero cross level 110, 122
 - Zero cross level 292
- CFD and SYNC circuits 35
- Channel PMT 51
- Channel register 37
- Chi Square 344
- Chlorophyll 158, 228
- Collection time 132, 253, 254, 255, 256, 258, 260, 262, 264, 266, 270, 272, 273, 278, 290, 350, 354
- Colour intensity mode 302, 303, 325
- Configuration file, for step motor 290
- Confocal detection 165, 167, 206
- Confocal microscope 164
- Constant Fraction Discriminator, see CFD 42
- Continuous flow mode 40
 - Banks and Autosave 267
 - curves 266
 - display 268
 - images 277
 - in DOT 194
 - multidetector operation 268
 - principle 29
 - recording of chlorophyll transients 159
 - single molecule detection 220
 - stopped flow 161
 - trigger 267
- Control Parameters 288
- Control Signals 348

Convert
 FIFO files 248
 into ASCII 247
 into EI format 247
 single traces 310

Cooling, of PMT 140

Corr Ovfl 288

Correlation
 down to picosecond scale 211
 FCS 206
 Hanbury-Brown-Twiss experiment 203
 of delayed detector signals 210
 of detector afterpulsing 60
 of fluorescence lifetimes 221
 online calculation 282

Count Increment 297

Count rate
 background by afterpulsing 139
 count rate display 238
 dark count rate of PMTs 59
 dependence on CFD threshold 120
 influence on IRF of H5773 66
 influence on IRF of R3809 63
 influence on IRF of SPADs 69
 influence on pile-up error 134
 maximum 132
 maximum useful 131
 multi-module FLIM 104
 of CFD 43, 44
 of MCP-PMT 63
 of multi-detector TCSPC 27
 of multi-module systems 33
 of SPADs 53
 of TCSPC 18
 of TCSPC in FIFO mode 42
 ophthalmic FLIM 201
 recorded vs. detected 131

Counting efficiency 18, 131
 of multi-detector TCSPC 26

Counting loss 123, 131
 in multi-detector TCSPC 27

Cross correlation of two TCSPC channels 211

Cross-correlation, in FCS 207

Cursors
 during measurement 236
 in 2D display 323
 in the display window 236
 in 3D display 327

Curve mode, of 2D display 302

Curve Mode, of 2D display 307

Curve mode, of 3D display 302, 303

Cycles 255, 257, 258, 260, 262, 265, 289

Damage
 by charged cables 77
 by electrostatic discharge 339
 by overvoltage 339
 how to avoid 339
 via routing connector 348

Dark count rate 59, 140

Data Analysis, of Scan mode data 13, 328

Data and Setup File Formats 241, 243

Data Blocks 333

Data file structure 331
 data blocks 333
 FIFO mode 335
 file header 331
 file info 332
 measurement description blocks 333

multi-SPC software 331
 setup section 332

Data Format
 FIFO Files SPC-134 337
 FIFO Files SPC-600/630 335
 FIFO Files SPC-830 337

Data Point, 2D display 324

Data Point, 3D display 327

Data Processing, 2D 324

Data Processing, 3D 328

DCC-100 169
 control of H7422 94
 control of PMC-100 94, 95
 control of R3809 94, 96
 Cooler Control 75
 cooling current 75
 cooling voltage 75
 detector gain control 75
 detector overload shutdown 75
 high-current switches 75
 parameters for startup 109
 peltier current 75
 peltier voltage 75
 shutter control 75

DCC-100 detector controller 11, 74, 105

Dead time 123, 129

Dead time compensation 47, 132, 292

Delay (Routing Signals) 298

Delay Lines, for SYNC and CFD 119

Delay of stop signal 91, 125

Delayed start-stop operation 91, 125

Depolarisation of fluorescence 144, 151, 154

Depth resolution
 by confocal pinhole 166

Depth resolution, by two-photon excitation 166

Descanned detection 165, 167

Detector Control 11, 74

Detector overload protection 168

Detector overload, by microscope lamp 168

Detector signal 93

Detectors
 16 channel 68
 for FCS 213
 for photon correlation 205
 for SPC modules 10, 11
 for TCSPC 51
 gain 54
 H5773, H5783 65
 H7421 68
 H7422 67
 H8632 67
 MCP PMTs 63
 PMC-100 66
 PMH-100 66
 PML-16 10, 68
 PML-SPEC 11
 PMTs 51
 R3809U 63
 R5600, R7400 64
 SER 54
 shutter assemblies 12
 side-window PMT 68
 SPADs 69

Device Driver 83

Device State 238

Dichroic beamsplitters 152

Differential Nonlinearity 128, 345

Diode laser 128

- connection to SPC 93, 95
 fast switching 159
 for microscopes 102
 noise radiation 128
 picosecond 9
 two-photon excitation 225
- Direct detection 166, 168
- Display
 2D curve display 323
 2D curve mode 323
 3D colour-intensity mode 302
 3D curve mode 302, 325
 3D display 325
 3D display parameters 304
 3D display parameters, mode selection 304
 3D display parameters, window selection 305
 after display time 291
 after each cycle 290
 after each step 290
 autoscale 302
 background colour 301
 block mode 302, 323
 colour intensity mode 302, 303, 325
 cursors in 2D display 323
 cursors in 3D display 327
 curve style 301
 data point in 3D display 327
 display parameters 301
 display routines 323
 display time 291
 display windows in main panel 233
 during measurement 237, 290
 FCS, off-line 283
 FCS, on-line 237, 282
 grid colour 302
 in scan modes 279
 multidimensional data 304
 multi-file show 246
 of curve maximum 236
 of first moment 236
 of FWHM 236
 of total counts 236
 OGL plot mode 302, 325
 parameters for different windows 306
 parameters, 2D 302
 parameters, 3D 302
 parameters, 3D curve mode 303
 Parameters, colour intensity mode 303
 parameters, OGL plot mode 303
 photon counting histograms, on-line 237, 282
 resizing of display window 236
 reverse axis 302
 scale 301
 zoom in 2D display 324
 zoom in 3D display 327
- Display time 253
- Distance Measurement 228
- Dither gain 321
- Dither range 296
- Dither Width 49
- Dithering 36, 48
- DLL Library, Installation 79
- DNL 128
- DOT 187
 detectors 197
 dynamic brain imaging 193
 exogenous absorbers 195
- fluorescence 196
 haemodynamic response 194
 moments of time-of-flight 194
 of muscles and bones 195
 optical fibres 197
 scanning mammography 190
 small animals 196
 static brain imaging 192
 technical aspects 197
 time-of-flight distribution 191, 192
 timing stability 197
- Download
 manual 80, 82
 Software 82
- Driver Information 83
- EEPROM Parameters 321
- Efficiency
 of multi-detector TCSPC 26
- Electrical shock, by broken cables, 76
- Energy transfer 164, 196
- Error correction, ADC 48
- Exit, the SPC software 330
- Experiment trigger 28, 30, 32, 98, 211, 271, 275, 279, 283, 289, 349, 352, 353
 input circuitry 98
- Export, ASCII data 247
- Export, Traces 310
- External Control 348
- External photoeffect 52
- f(t,EXT) mode 260
 accumulate 260
 autosave 260
 cycles 260
 display 261
 multidetector operation 261
 repeat 260
 steps 260
 trigger 261
- f(t,T) mode 258
 accumulate 258
 autosave 258
 cycles and autosave 258
 display 259
 multidetector operation 259
 Repeat 258
 steps 258
 trigger 258
- f(tx,y) mode 256
 accumulate 257
 autosave 257
 cycles 257
 display 257
 repeat 257
 stepping through pages 256
 trigger 257
- f(x,y) mode 99
- FBX 350, 354
- FBY 350, 354
- FCS 32, 206
 afterpulsing of detectors 213
 autocorrelation function 207
 background signals 214
 background suppression 218
 beam jitter 215
 clock from SYNC input 213
 combination with scanning 209
 correlation of delayed signals 210

- cross correlation 207, 214, 217
- cross correlation of two TCSPC channels 211
- CW operation, stop pulse for 212
- detectors 213
- FIFO Imaging mode 210
 - in cells 209
 - in solution 208, 215
 - main panel configuration 216, 235
 - matching of refractive index 215
 - off-line display 283
 - one-photon 206
 - on-line display 237, 282
 - optical aberrations 215
 - ps correlation times 211
 - sample volume 215
 - system parameters 216, 281
 - technical aspects 212
 - time-gated 218
 - two-photon 206, 217
 - with laser scanning microscopes 216
- fi(EXT) mode 264
 - accumulate 265
 - autosave 265
 - cycles 265
 - display 266
 - multidetector operation 265
 - repeat 265
 - steps 264
 - trigger 265
- fi(T) mode 262
 - accumulate 262, 267
 - autosave 262
 - cycles 262
 - display 263
 - multidetector operation 263
 - repeat 263
 - steps 262
 - trigger 263
- Fibres, optical 143
- FIDA 32, 223
- FIFO
 - buffer size 42, 355, 357, 358
 - FIFO files 248
 - FIFO imaging mode 285
 - FIFO mode 31, 41, 223
 - frame length 297
 - Overflow 239
- FIFO data, setup files 248
- FIFO Files
 - SPC-134 337
 - SPC-600/630 335
 - SPC-830 337
- FIFO mode 24, 31, 281
 - buffer size 42
 - count rate, burst 42
 - count rate, continuous 42
 - data file 281
 - data format selection 284
 - disk space 281
 - FIFO data, setup files 335
 - FIFO Files 335
 - FIFO imaging mode 209, 285
 - file structure 335
 - frame length 297
 - off-line display 283
 - on-line display 237, 282
 - software buffer 281
 - source of macro-time clock 213, 284
- synchronisation with scanners 286
- synchronisation with scanners 209
 - trigger 283
- FILDA 32, 223
- File Formats, Data and Setup 241, 243
- File Header (data files) 331
- File Info 241, 244
- File Info (data files) 332
- Files
 - conversion of FIFO files 248
 - convert into ASCII 247
 - exporting traces 310
 - FIFO 335
 - FIFO 248
 - loading of 241
 - multi-SPC software 331
 - of screen pattern 250
 - saving of 243
- Filters, absorptive 142
- Filters, interference 142
- First moment
 - display of 236
 - lifetime calculation 174
 - of IRF 197
 - of time-of-flight distribution 188, 193
- FLIM 164
 - acquisition time 172
 - adjusting of images 113
 - applications 177
 - autofluorescence of tissue 183, 199
 - confocal detection 167
 - DCC-100 detector controller 104, 105
 - descanned detection 167
 - detector options 103
 - direct detection 168
 - dual-detector systems 103
 - excitation sources 102
 - fluorescence quenching 177
 - FRET measurements 178
 - high-speed 171
 - in NSOMs 186
 - ion concentrations 177
 - main panel configuration 235
 - multi-exponential decay 175, 181, 183, 185
 - multi-module 104, 171
 - multiphoton 168
 - multi-wavelength 30, 31, 104, 169, 184
 - Non-descanned detection 168
 - ophthalmic imaging 200
 - parameters for startup 111
 - pH imaging 177
 - photosensitisers 185
 - recording of IRF 176
 - SHG imaging 184
 - shutter control 105
 - single PMC-100 detector 105
 - single-module systems 102
 - SPC modules for FLIM 104
 - system parameters 273
 - two H7422 detectors 106
 - two R3809 detectors 107
 - upgrading laser scanning microscopes 101
 - wiring diagrams of FLIM systems 105, 106, 107
- Fluorescence
 - anisotropy 144, 154
 - anisotropy decay 144, 151
 - depolarisation 144, 151, 154
 - fluorescence correlation spectroscopy 32

- fluorescence correlation, ps 203
 fluorescence decay 147
 Kautsky effect 158
 lifetime spectrometers 147
 of chlorophyll 158
 quenching 177
 re-absorption 145
 transient phenomena 158
 transients, of chlorophyll 158
- Fluorescence correlation spectroscopy 206
 Flyback X 270, 278, 350, 354
 Flyback Y 270, 278, 350, 354
 Förster resonance energy transfer 178
 Frame clock 30
 Freq Div (SYNC) 293
 FRET 178
 double-exponential 181
 single-exponential 180
 FRET Imaging 13, 328
 FRET, by double-exponential FLIM 179
 FWHM, display of 236
 G factor 154
 Gain
 of APDs 52
 of PMTs 54
 TAC gain 294
 Gain noise 17
 Geiger mode 52
 H5773 56, 65
 H5773, high count rates 66
 H5773, IRF 65
 H5783 65, 230
 H5783, high count rates 66
 H5783, IRF 65
 H7421 68
 H7422 55, 56, 67, 205, 213
 H7422, connection to SPC 94
 H8632 67
 Hanbury-Brown-Twiss experiment 203
 Hardware Test 84
 HFAC series preamplifiers 11, 73
 HFAH series preamplifiers 11, 73
 High voltage, for PMT 56, 76, 111
 High-current switches of DCC100 75
 Hold (CFD) 292
 Holdoff (SYNC) 293
 HRT series routers 12
 Hydrant 140
 ICG 195
 Imaging 164
 by multi-wavelength TCSPC 30
 control Signals 350, 353
 f(xyt) mode 99
 FIFO imaging mode 285
 imaging modes 270
 Scan Sync In mode 99
 Scan Sync Out mode 100
 Scan XY Out mode 101
 with scanning microscope 164
 Indocyanine green 195
 Initialisation Panel 84
 Input signals of SPC modules 89, 93
 Installation 79
 DCC-100 software 79
 device driver 83
 DLL Library 79
 download of manual 80
 hardware 83
 installation procedure 80
 Lab View Drivers 79
 licence number 80
 module test 85
 Multi SPC Software 79
 multi-module systems 84
 problems 86
 requirements to computer 79
 single SPC module 83
 Software 79
 software update 81
 SPC-134/144 84
 SPCImage 79
 uninstall 83
 update from the web 82
 Instrument Response Function 118, 138
 Internal photoeffect 52
 Interrupt, a measurement 329
 Inverters, APPI, for pulses 13
 Ion concentrations 177
 Ion feedback 139
 IRF 138
 H5773 65
 H5773, H5783 66
 H5783 65
 illuminated detector area 138
 of FLIM systems 176
 photosensor modules 65
 R3809U 63
 R5600 64
 R7400 64
 side-window PMTs 69
 SPCM-AQR 69
 stability vs. count rate 64, 66
 TO-8 PMTs 64
 two-photon 176
 voltage divider 138
 Jitter
 of pulse period 125
 of SER amplitude 55, 120, 141
 Kautsky effect 158
 Lab View Drivers, Installation 79
 Laser multiplexing 190
 Laser scanning microscopes, FLIM upgrade 101, 169
 Lenses 142
 Licence Number 80
 Lifetime Imaging, applications 177
 Lifetime spectrometers 147
 filter-based 150
 monochromators 147
 multi-wavelength 152
 time-resolved spectra 149
 Lifetime, of autofluorescence 183, 199
 Limit High (CFD) 292
 Limit High (TAC) 294
 Limit Low (TAC) 294
 Limit Low, CFD 292
 Line clock 30
 Line clock, double 114
 Load 241
 data files 241
 FIFO files 248
 File Formats 241
 files from older software versions 243
 predefined setups 245
 selected parts of a file 242

- setup files 241
- Lock-in SPC 157, 290
- Luminescence decay 147
- Luminous sensitivity 58
- Macro Timer Resolution 355
- Macro-time clock, synchronisation of 211, 213, 284
- Magic angle 145
- Main (in menu bar) 241
- Main Panel 233
 - configuration of 233
 - count rate display 238
 - cursors 236
 - device state 238
 - module select 238
 - trace statistics 236
- Mammography, optical 187
- Maximum Ratings 361
- MCP PMTs 63
- MCP, lifetime 138
- Measurement
 - dead time compensation 292
 - display during measurement 290, 291
 - imaging modes 299
 - lock-in TCSPC 157
 - multi-detector 298
 - normalisation to maximum 297
 - repeat 291
 - Stop T 254, 256, 260, 262, 264, 288, 290
- Measurement Description Blocks 333
- Measurement modes 253
 - continuous flow mode, curves 266
 - continuous flow mode, images 277
 - f(t,EXT) mode 260
 - f(t,T) mode 258
 - f(tx) Mode 256
 - fi(EXT) mode 264
 - fi(T) mode 262
 - FIFO mode 281
 - oscilloscope mode 255
 - Overview 2
 - Scan Sync In mode 273
 - Scan Sync Out mode 270
 - Scan XY Out mode 278
 - single mode 254
- Measurement System 35
- Measurement, Stop T 258
- Memory Banks 29, 40, 266, 277, 299
- Memory control 37
- Memory Control
 - Add/Sub 41
 - Count Enable 41
- Memory Offset 296
- Memory Page 298
- Memory swapping in TCSPC 29
- Microchannel PMT 51
- Microscope, confocal 164
- Mixing techniques 161
- Module Test 85
- Module types, SPC 3
- Molecular brightness 223
- Moments
 - fluorescence lifetime calculation 174
 - of time-of-flight distribution 188, 193
- Monochromators 143, 147
- More Parameters 299
- Multi SPC systems
 - equalize parameters 299
 - module select 238
- Module Select 299
- Parameters 299
- Multichannel scalers 9
- Multichannel System, pile-up 136
- Multi-detector operation 24
 - efficiency 26
 - in scanning systems 30
 - of TCSPC 23, 24
 - startup of systems 115
- Multi-detector Operation 256, 259, 261, 263, 265, 268, 271, 275
- Multidimensional data, display of subsets 304
- Multi-file view 246
- Multi-module TCSPC systems 5, 6, 33
- Multi-parameter TCSPC 24, 227
- Multiplexed TCSPC 27, 39, 190
- Multiplexing
 - in TCSPC 23
 - of lasers 190
- Multi-spectral FLIM 169
- Multi-spectral TCSPC 24
- Multi-wavelength detection 199
- Multi-wavelength operation
 - in scanning systems 30
- MW FLIM system 11, 170, 184
- NADH 185
- Nano particles 164
- Nano-particles, for IRF recording 177
- Near-Field Microscope 186
- NIM modules 21
- Noise in multi-detector systems 26
- Noise signals, effect of 129
- Non-descanned detection 166, 168
- NSOM 186
- OEM TCSPC boards 6
- Offset (TAC) 294
- OGL plot mode 325
- OGL plot mode 302
- OGL Plot, Display Parameters 303
- One-photon FCS 206
- Operating voltage, of PMT 56
- Operation Modes 253
 - continuous flow mode, curves 266
 - continuous flow mode, images 277
 - f(t,EXT) mode 260
 - f(t,T) mode 258
 - f(tx) Mode 256
 - fi(EXT) mode 264
 - fi(T) mode 262
 - FIFO Mode 281
 - oscilloscope mode 255
 - overview 2, 253
 - Scan Sync In mode 273
 - Scan Sync Out mode 270
 - Scan XY Out mode 278
 - single mode 254
- Ophthalmic Imaging 200
- Optical fibres 143, 197
- Optical reflections 144
- Optical System 142
- Optical System, influence on system response 142
- Optical tomography 187
- Optimising an SPC System 117
- Optimising the CFD Parameters 120
- Optimising the SYNC Parameters 123
- Optimising the TAC parameters 126
- Oscilloscope Mode 117, 255
 - application 230

- detectors 231
- multidetector operation 256
- trigger 256
- Out-of-focus suppression 166
- Overflow Handling 288
- Overflow, Correct 288
- Overflow, Stop 254, 256, 258, 260, 262, 264, 288
- Overload Flip-Flop of DCC-100 75
- Overload protection of detector 73, 168
- Overload shutdown of detector 75
- Overload Signal 75
- Overload, of PMT 140
- P box 105
- Page Control 298
- Page in memory 298
- Page stepping 255, 256, 271, 275, 279, 289
- Parametric downconversion, for QE measurement 230
- Passive quenching, of SPAD 53
- PCH 222
- Peltier Control 75
- Phosphorescence decay 162
- Photodiode Modules 12, 77, 90
- Photodynamic therapy 185
- Photomultiplier Tubes 51
- Photon correlation
 - anti-bunching 203
 - detectors 205
 - start-stop experiment 203
- Photon Counting Histograms 222
- Photon migration 187
- Photosensor modules 65
- Picosecond diode lasers 9
- Piezo stages 210
- Pile-up
 - at high rep rate 136
 - at low rep rate 135
 - classic 133
 - for laser multiplexing 137
 - in multi-detector systems 136
 - in multi-module systems 136
 - influence on recorded lifetime 134
 - inter-pulse 134
 - reduction of 135
- Pile-up effect 133
- Pinhole 206
- Pixel clock 30, 350, 353, 354
- PMC-100 detector 66
- PMC-100, connection to SPC 94, 95
- PMH-100 detector 66
- PMH-100, connection to SPC 93
- PML-16 detector 10, 68
- PML-SPEC spectral detection module 11
- PMT
 - afterpulsing 60, 139, 213
 - anode luminous sensitivity 58
 - background 139
 - cathode luminous sensitivity 58
 - cathode quantum efficiency 58
 - cathode radiant sensitivity 58
 - cooling 75, 140
 - dark count rate 59
 - focusing voltages 138
 - gain 54, 128
 - H5773, H5783 65
 - H7422 67
 - illuminated area 138
 - ion feedback 139
- measurement of quantum efficiency 230
- measurement of SER 140
- operating voltage 56, 76, 111
- optimisation 138
- overload 140
- overload protection 73
- PML-16 68
- pre-pulses 61, 65
- principle 51
- pulse amplitude distribution 55, 120
- pulse height spectrum 128
- quick test 141
- R3809U MCP PMT 63
- R5600, R7400 64
- recovery after overload 140
- Safety 76
- SER 54
- side-window 68
- single electron response 54
- single-photon pulses 15, 54
- timing stability 64, 66
- transit time 56
- transit time spread 57
- treatment for bad 140
- TTS 57
- voltage divider 138
- Polarisation, of fluorescence 154
- Polariser, in detection path 145
- Polariser, magic angle 145
- Polariser, rotating 156
- Polychromators 143, 152
- Positron Lifetime 227
- Power splitters 13
- Power Supply to external units 348
- Preamplifiers 73
 - detector overload detection 73
 - HFAC series 11, 73
 - HFAH series 11, 73
- Predefined Setups 245
- Pre-pulses, of PMT 61
- Print function 250
- Printing, into files 250
- Production Parameters 321
- Pulse amplitude distribution, of SER pulses 55, 120
- Pulse period jitter 125
- PxlClk 350, 353
- Quantum efficiency
 - of detectors 58
 - of photocathodes, measurement 230
- Quenching
 - of SPAD 53
- R3809U 63
 - connection to SPC 94, 96
 - IRF stability at high count rates 64
 - routing 96
 - transit time 56
- R5600 56, 64
- R7400 56, 64
- R928 56
- Radiant sensitivity, of photocathodes 58
- Random signals 92
- Range (TAC) 294
- Ranging Systems 228
- Rates 238
- Re-absorption 145
- Reference Photodiodes 12
- Reference signal

delay 125
 for reversed start-stop 125
Reflections
 in optical systems 118, 144
 on SYNC line 123
Repeat 255, 257, 258, 260, 263, 265, 271, 275, 289
Repeat time 253
Repeat Time 291
 Repetition Rate, measurement at low 91
Resizing Panels 236
Resolution
 ADC 49, 294
 Reversed start-stop 20, 36, 126
 Reference signal 125
 Rotational relaxation 154
Router
 for multi-anode PMTs 26
 noise accumulation 26
 principle 25
 routing devices 12
Routing 23, 24, 298, 348
 efficiency 26
 in scanning systems 30
Routing Channels X 298
Routing Channels Y 298
Routing devices 12
Routing Signals 348
Routing XY windows 315
Safety Recommendations 76
Sample rate 17, 230
Save 243
 data files 243
 file formats 243
 options 244
 selected data blocks 245
 setup files 243
Save, on exit 85
Save, screen pattern 250
Scan clocks 30
Scan Modes 299
Scan Pixels X 270, 273, 278, 299
Scan Pixels Y 270, 273, 278, 299
Scan stages 210
Scan Sync In mode 31, 99, 273, 350, 353
 accumulate 275
 autosave 275
 continuos flow operation 277
 cycles 275
 display 279
 multidetector operation 275
 stepping through pages 275
Scan Sync Out mode 30, 100, 270, 350, 354
 accumulate 271
 autosave 271
 cycles 271
 display 279
 multidetector operation 271
 repeat 271, 275
 stepping through pages 271
 trigger 271, 275
 use for fast sequential recording 272
Scan XY Out mode 30, 101, 278, 351
 accumulate 279
 autosave 279
 cycles 279
 display 279
 stepping through pages 279
 trigger 279
Scan XY windows 318
Scanning 24, 191
 by scan stages 210
Scanning interface 30
Scanning mammography 190
Scanning microscope 164
Scanning techniques for TCSPC 30
Scattering coefficient 187, 192
Second harmonic generation, for IRF recording 177
Secondary emission 54
Select-SPC Panel 238
Sequencer 24, 37
Sequential recording 24, 28, 39, 149, 158
 chlorophyll transients 159
 in DOT 194
 in single molecule spectroscopy 220
 phosphorescence decay 162
 stopped flow 161
SER 54
 amplitude jitter 55, 120, 141
 measurement of 140
 of PMT 140
Setup (data files) 332
SHG
 for IRF recording 177
 imaging 184
Shifting the Signal 124
Shutdown, of detectors 75
Shutter control, by DCC100 75
Shutters 12, 105, 169
Signal bandwidth 230
Simulation Mode 86
Single Electron Response 54
Single Mode 254
 cycles and autosave 255
 multidetector operation 255
 repeat 255
 stepping through pages 255
 trigger 255
Single molecule detection 203
Single-molecule spectroscopy 219
 BIFL 219
 correlation of lifetimes 221
 identification of molecules 222
 lifetime histogram 222
 photon counting histogram 222
Single-photon APD 52
Single-photon pulses 140
SLIM 31
Slow scan techniques 210
Small animal imaging 196
SNOM 186
Software 233
 2d trace parameters 307
 3D trace parameters 311
 conversion of files 247
 data file structures 331
 display parameters 301
 display routines 323
 Installation 79
 Loading of files 241
 Main 241
 Main panel 233
 operation modes 253
 predefined setups 245
 print function 250
 Saving of files 243
 simulation mode 86

- start 84
- start without module 86
- system parameters 253
- Update 81
- Update from the Web 82
- Window intervals 313
- SPADs 52, 205, 213
 - count-rate dependence of IRF 69
 - diffusion tail 71
 - id100-20 69
 - light emission from 53
 - PDM 50CT 69
 - quenching 53
 - SPCM-AQR 69
 - wavelength dependence of IRF 71
- SPC modules
 - adjusting FLIM systems 113
 - comparison of features 8
 - connection to diode laser 93, 95
 - control signals 348
 - delayed stop operation 91
 - detector signal 93
 - experiment trigger 98
 - FLIM systems 101
 - Imaging 99
 - input signals 89
 - installation 79
 - low repetition rates 91
 - module types 3
 - multi-module systems 5, 6
 - OEM boards 6
 - panel configuration for startup 108
 - random signals 92
 - routing signals 348
 - setup for H7422 94
 - setup for PMC-100 94
 - setup for PMH-100 93
 - setup for R3809 94
 - setup for several detectors 95
 - setup for several PMC-100 95
 - setup for several R3809 96
 - setup for single detector 93
 - setup for SPCM-AQR 95, 97
 - setup of FLIM systems 105
 - stand-alone systems 6
 - startup for FLIM systems 111
 - startup for multi-detector systems 115
 - startup of TCSPC systems 108
 - SYNC signal 89
 - system parameters for startup 108
- SPCImage Software 13, 328
- SPCM Software 233
- SPCM-AQR 69, 205, 213
 - IRF 69
 - several, connection to SPC 97
 - single, connection to SPC 95
 - timing stability 69
- Specification
 - Maximum Ratings 361
 - SPC-130/134 358
 - SPC-140/144 359, 360
 - SPC-150/154 360
 - SPC-600/630 355
 - SPC-700/730 356
 - SPC-830 357
- Spectra, recording in fi Modes 264
- Spectral lifetime imaging 31, 169
- Spectrum modes 262
- Stand-alone TCSPC systems 6
- Start, a measurement 329
- Start-Stop Time 129
- Start-stop, reversed 36
- Startup
 - DCC parameters 109
 - FLIM systems 111
 - FLIM, adjusting of images 113
 - multi-detector systems 115
 - panel configuration for 108
 - standard lifetime systems 109
 - system parameters for 108
- Step Motor 290
- Step Motor Controller 13
- Stepping Device 290
- Stepping through Pages 255, 256, 271, 275, 279, 289
- Steps 289
- Stop Condition 288
- Stop Ovfl 254, 256, 258, 260, 262, 264, 288
- Stop pulse, for CW FCS 212
- Stop signal
 - delay of stop pulses 125
 - for reversed start-stop 125
 - stop pulse from correct pulse period 125
- Stop T 254, 256, 258, 260, 262, 264, 288
- Stop, a measurement 329
- Stop, after collection time 254, 256, 258, 260, 262, 264, 288, 290
- Stop, on overflow 254, 256, 258, 260, 262, 264, 288
- Stopped flow techniques 161
- STP Config file 290
- Sub-D connector 348
- SYNC 44
 - cable length 124
 - configuration 118
 - configuring for input polarity 89
 - delay lines 118
 - frequency divider 293
 - frequency divider 36
 - generation of signal 89
 - Holdoff 293
 - No SYNC 239
 - parameters 292
 - pulse shaping 118
 - setting the SYNC parameters 123
 - SYNC OK 239
 - SYNC overload 239
 - threshold 293
 - ZC level 293
- Synchronisation
 - of macro-time clock 211
- Synchronisation Circuit 44
- Synchronisation signal 89, 117
 - delay 125
 - for reversed start-stop 125
- System Parameters 253
- System Response, Influence of optical system 142
- System Response, Measurement of 118
- System Response, PMT 138
- T Geometry 155
- TAC 20, 36, 46
 - architecture 46
 - biased amplifier 20
 - dead time 129
 - dead time compensation 47, 132
 - DNL 128

- linearity 128, 345
- optimising the TAC parameters 126
- overrange reset 47
- parameters 293
- recovery time 130
- reset time 130
- start-stop sime 129
- TAC Gain 127, 294
- TAC Limit High 294
- TAC Limit Low 294
- TAC Offset 126, 294
- TAC Range 127, 294
- TAC Window 47
- timing diagram 129
- Tail matching 154
- TCSPC 15
 - acquisition time 19, 172
 - architecture of bh SPC modules 35
 - channel register 37
 - classic architecture 19
 - continuous flow mode 29, 40, 220
 - count rate 18
 - counting efficiency 18, 131, 303
 - delayed stop 91
 - detectors 51
 - FIFO mode 24, 41
 - gain noise 17
 - general principle 15
 - memory control 37
 - memory swapping 29
 - multi-detector operation 23, 24, 38, 95
 - multi-dimensional 23
 - multi-module 33
 - multi-parameter 24, 227
 - multiplexed 23, 27, 39, 190
 - multiplexing 160
 - multi-spectral 24
 - multi-wavelength 152, 169
 - random signals 92
 - reversed start-stop 20
 - router 25
 - routing 24
 - sample rate 17
 - scanning techniques 24, 30, 40, 191
 - sensitivity 18
 - sequencer 37
 - sequential recording 24, 28, 39, 158
 - single molecule detection 203
 - time resolution 17
 - time-tag mode 24, 31, 41
- TCSPC Imaging 164
- TCSPC, Laser Scanning Microscope 164
- Telescope, measurement through 228
- Test
 - by test program 340
 - for basic function 340
 - for differential nonlinearity 340
 - for time resolution 341
 - of a PMT 141
- Thermoelectric cooling 75
- Threshold, CFD 36, 110, 120, 292
- Threshold, SYNC 36, 293
- Time per Channel 294, 295
- Time per Division 294
- Time resolution of TCSPC 17
- Time windows 313
- Time-correlated single photon counting, see TCSPC 15
- Time-of-flight distribution, in DOT 191, 192
- Time-resolved spectra 149
- Time-tag mode 24, 31, 41, 223, 281
- Time-tag mode, buffer size 42
- Time-to-amplitude converter 20, 46
- Timing Control Parameters 290
- Timing stability
 - H5773, H5783 66
 - MCP PMT 64
 - SPCM-AQR 69
- Tissue, autofluorescence 199
- Tomography, optical 187
- Trace parameters 307
 - block info 310
 - block mode 309
 - curve mode 307
 - export of traces 310
- Trace Statistics 236
- Traces 307
- Traces, export of 310
- Transit time of PMTs 56
- Transit time spread 57
- Trigger 28, 30, 32, 211, 255, 256, 257, 258, 261, 263, 265, 267, 271, 275, 279, 283, 289, 349, 352, 353
 - of sequence 28, 30
- Trigger Condition 289
- Trigger, to start a measurement 349, 352, 353
- Triggered sequential recording 28, 29
- Trouble Shooting 339
 - ADC rate problems 343
 - assistance through bh 347
 - bad system response 345
 - by test program 340
 - CFD problems 342
 - chi square 344
 - curves don't change 344
 - cuves shifted 346
 - differential nonlinearity 345
 - fan doesn't work 346
 - frequently encountered problems 341
 - high background count rate 345
 - module not found 341
 - no curves displayed 343
 - no TAC rate 343
 - noise or ripple 344
 - Premature stop of Scan Sync In 344
 - random data 344
 - Scan Sync In doesn't finish 344
 - Scan Sync In doesn't start 344
 - Sync problems 342
 - TAC problems 342
 - time resolution 344
- TTS 57
- Two-photon absorption 166
- Two-photon excitation 166, 225
- Two-photon FCS 206
- Two-photon microscope 164
- Uninstall SPC Software 83
- Window intervals 313
 - auto set sunction 319
 - routing XY windows 315
 - scan XY windows 318
 - time windows 313
- XP2020 56
- XSync 350, 353
- YSync 350, 353
- Zero cross level, CFD 110, 122, 292
- Zero cross level, SYNC 293
- Zoom

2D display 324
3D display 327

ADC 50, 294